

Intermediates in Iron Group Metal-Catalyzed Hydrogenation Reactions

Dissertation

zur Erlangung des Doktorgrades der Naturwissenschaften
Dr. rer. nat.
an der Fakultät für Chemie und Pharmazie der Universität
Regensburg



vorgelegt von

Sebastian Sandl

aus Riedenburg

Regensburg 2020

Der experimentelle Teil dieser Arbeit wurde in der Zeit zwischen November 2016 und Januar 2020 an der Universität Regensburg und Hamburg unter Anleitung von Prof. Dr. Axel Jacobi von Wangelin angefertigt.

Die Arbeit wurde angeleitet von: Prof. Dr. Axel Jacobi von Wangelin

Promotionsgesuch eingereicht am: 04.05.2020

Prüfungsausschuss:

Vorsitz	Prof. Dr. Alkwin Slenczka
Erstgutachter	Prof. Dr. Axel Jacobi von Wangelin
Zweitgutachter	Prof. Dr. Robert Wolf
Dritter Prüfer	Prof. Dr. Manfred Scheer

Meiner Familie

Life is a lot like jazz, it's best when you improvise.

George Gershwin

Prologue

The present thesis reports on the development of iron group metal-catalyzed hydrogenation reactions. Specifically, mechanistic investigations have been focused to develop better catalysts in future. *Chapter 1* advocates kinetic poisoning experiments for the distinction between homogeneous and heterogeneous catalysis with standard laboratory equipment. *Chapter 2* reviews dibenzo[a,e]cyclooctatetraene, a typical homogeneous catalyst poison. Simple cobalt catalysts for C=C, C=O, and C=N hydrogenations have been developed in *Chapter 3*: Olefinic substrates stabilize the reduction of cobalt salts to obtain cobalt nanoparticles. *Chapter 4* describes homogeneous hydrogenation catalysts for alkene and imine hydrogenation based on highly-reduced cobaltates. The redox-active ligand bis(imino)acenaphthene (BIAN) allowed the isolation and detailed mechanistic analyses of olefin cobaltate and hydride intermediates. Related cobaltate catalysts have been developed for amine-borane (de)hydrogenations and transfer hydrogenations to imines, chinolines and alkenes in *Chapter 5*. *Chapter 6* reports on the synthesis, characterization and catalysis of a dimeric iron ate complex with four bridging hydrides. In *Chapter 7*, olefin-stabilized nickel nanoparticle catalysts have been developed for alkene hydrogenation based on a nickel metalate. These catalysts exhibit a remarkable functional group tolerance. *Chapter 8* highlights recent studies by the groups of Bedford and Neidig for iron-catalyzed cross-coupling reactions by triorganoferrates as active species. *Chapter 9* summarizes the results of this thesis.

Prolog

Diese Dissertation handelt von der Erforschung neuer Hydrierkatalysatoren der Eisengruppe. Dabei wurde ein besonderer Fokus auf den Mechanismus gelegt, um zukünftig bessere Katalysatoren zu entwickeln. *Kapitel 1* berichtet über kinetische Vergiftungsstudien, um die Unterscheidung zwischen homogener und heterogener Katalyse mit möglichst einfachen Laborgeräten zu bewerkstelligen. *Kapitel 2* bietet einen Überblick über Dibenzo[a,e]cyclooctatetraene, ein typisches homogenes Vergiftungsreagenz. Ein möglichst einfacher Kobaltkatalysator für die Hydrierung von C=C-, C=O-, and C=N-Bindungen wurde in *Kapitel 3* entwickelt: Olefinische Substrate oder Anthracen stabilisieren die Reduktion von Kobaltsalzen, um Nanopartikel zu erhalten. Der redoxaktive Ligand Bis(imino)acenaphthen (BIAN) ermöglicht die in *Kapitel 4* beschriebene Stabilisierung von Olefin- und Hydridokobaltaten. Diese wurden in der katalytischen Hydrierung von Olefinen und Iminen unter milden Bedingungen eingesetzt. Weiterhin bietet die Isolierung dieser Modellkomplexe wertvolle Einblicke in die Identität des aktiven Katalysators. In *Kapitel 5* wurden verwandte Kobaltate in der katalytischen Dehydrierung von Amminboranen eingesetzt. Zudem konnten diese Katalysatoren für die Transferhydrierung von Iminen, Chinolinen und Alkenen eingesetzt werden. Präparativ konnte so auf Hochdruckapparaturen verzichtet werden. *Kapitel 6* beschreibt die Synthese eines Ferratdimers mit vier verbrückenden Hydridoliganden. Dieser Komplex konnte erfolgreich in der Hydrierung von anspruchsvollen Alkenen eingesetzt werden. In *Kapitel 7* wird die Entwicklung eines Hydrierkatalysators durch Hydrogenolyse eines Nickelmetallates beschrieben. Dieser verfügt über eine außerordentliche funktionelle Gruppentoleranz. *Kapitel 8* diskutiert eindrucksvolle Arbeiten über eisenkatalysierte Kreuzkupplungen der Gruppen Bedford und Neidig. Ihre Ergebnisse weisen auf Triorganoferrate als aktive Spezies in diesen Reaktionen hin. *Kapitel 9* fasst die Ergebnisse dieser Dissertation zusammen.

Table of Contents

1 Homogeneous vs. Heterogeneous: Insights into Iron Group Metal-Catalyzed Reduction Reactions from Kinetic Poisoning Experiments	1
1.1 Introduction.....	3
1.2 Distinction between Homogeneous and Heterogeneous Catalysis ..	4
1.3 Reaction Progress Analysis	6
1.3.1 Reaction progress analysis.....	6
1.3.2 Asymmetric catalysis.....	9
1.4 Kinetic Poisoning Studies.....	14
1.4.1 Quantitative poisoning experiments.....	14
1.4.2 The choice of the catalyst poison	18
1.4.3 The impact of the reaction conditions.....	20
1.4.4 Qualitative poisoning experiments	21
1.4.5 Mercury, a selective heterotopic catalyst poison	21
1.4.6 Dibenzo[a,e]cyclooctatetraene (dct), a selective homotopic catalyst poison.....	24
1.5 Conclusions	30
1.6 References	32
2 Dibenzo[a,e]cyclooctatetraene.....	37
2.1 General	38
2.2 Organic Transformations	39
2.3 Organometallic Synthesis.....	40
2.4 Catalysis ^[1]	42
2.5 References	44
3 Olefin-Stabilized Cobalt Nanoparticles for C=C, C=O and C=N Hydrogenations.....	47
3.1 Introduction.....	48
3.2 Results and Discussion	50
3.3 Conclusion	57
3.4 References	59

3.5	Supporting Information	62
3.5.1	General	62
3.5.2	Synthesis of catalysts, reagents, and starting materials	64
3.5.3	General procedures	80
3.5.4	Further optimization studies and mechanistic experiments.....	82
3.5.5	Selected NMR spectras of isolated products	103
4	Cobalt-Catalyzed Hydrogenations via Olefin Cobaltate and Hydride Intermediates	105
4.1	Introduction	107
4.2	Results and Discussion.....	109
4.2.1	Optimization and alkene hydrogenation	109
4.2.2	Methodology extension: Hydrogenation of imines.....	110
4.2.3	Mechanism	112
4.2.4	Complexes and catalyst intermediates.....	115
4.2.5	Hydrogenation Activities of Complexes 1-4 and Mechanistic Proposal.....	125
4.3	Conclusion.....	129
4.4	References	130
4.5	Supporting Information	141
4.5.1	General	141
4.5.2	Synthesis of precatalysts.....	145
4.5.3	Theoretical calculations of 4.....	189
4.5.4	Synthesis of Substrates and Hydrogenation products	194
4.5.5	General procedures	204
4.5.6	Optimization studies and catalytic application of complexes .	206
4.5.7	Mechanistic studies (ring-opening experiment, reaction of cobalt, <i>in-situ</i> ¹ H-NMR, LIFDI-MS).....	211
4.5.8	Kinetics & poisoning studies.....	218
5	Amine-Borane Dehydrogenation and Transfer Hydrogenation Catalyzed by α-Diimine Cobaltates	223
5.1	Introduction	225
5.2	Results and Discussion.....	227
5.3	Conclusions.....	241

5.4	Acknowledgements	241
5.5	References	243
5.6	Supporting Information	248
5.6.1	General information	248
5.6.2	Synthesis of starting materials	250
5.6.3	Synthesis of amine-boranes.....	255
5.6.4	Synthesis of deuterated amine-boranes	256
5.6.5	Synthesis of substrates	264
5.6.6	Synthesis of poisoning agents	265
5.6.7	Dehydrogenation reactions	267
5.6.8	Transfer hydrogenation reactions	277
5.6.9	Hydrogenation reactions (autoclave)	291
5.6.10	NMR spectra	294
5.6.11	References	301
6	A Dimeric Iron Ate Complex with Four Bridging Hydrides: Synthesis and Reactivity	303
6.1	Introduction.....	304
6.2	Results and Discussion	307
6.2.1	Synthesis and Crystallography.....	307
6.2.2	Reactivity	310
6.2.3	Catalysis.....	311
6.3	Conclusions	314
6.4	References	315
6.5	Supporting Information	318
6.5.1	General.....	318
6.5.2	Synthesis of complexes.....	320
6.5.3	Synthesis of substrates and hydrogenation products.....	342
6.5.4	General procedures	350
6.5.5	Optimization studies and catalytic application of complexes..	351
6.5.6	Mechanistic studies (ring-opening experiment, LIFDI-MS).....	352
6.5.7	Reaction progress analyses.....	357
7	Heterogeneous Olefin Hydrogenation Enabled by a Highly-Reduced Nickel(–II) Catalyst Precursor	359

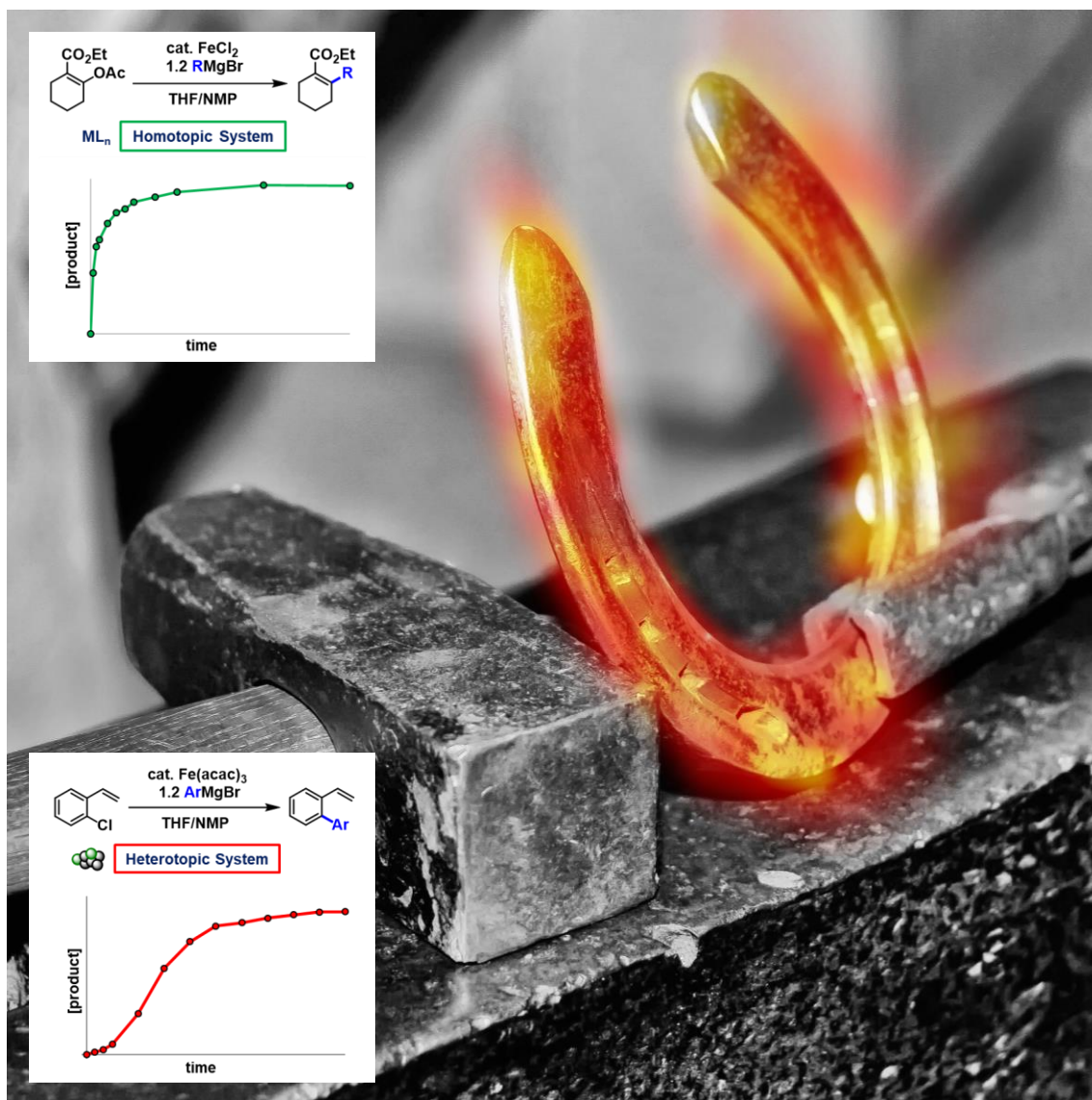
Table of Contents

7.1	Introduction	360
7.2	Results & Discussion.....	363
7.3	Conclusion.....	371
7.4	References.....	372
7.5	Supporting Information	376
7.5.1	General information.....	376
7.5.2	Synthesis of $[\text{Li}_2(\text{thf})_4\{\text{Ni}(\eta^4\text{-cod})(\eta^2\text{-cod})\}]$ (1).....	377
7.5.3	Hydrogenation reactions.....	378
7.5.4	Hydrogenation products: NMR spectra	384
7.5.5	Hydrogenation products: GC-FID analyses.....	391
7.5.6	Isomerization of olefins.....	393
7.5.7	Ring-opening experiment with α -cyclopropylstyrene	395
7.5.8	Kinetic investigations.....	395
7.5.9	Determination of turnover frequencies (TOFs) for selected reactions	396
7.5.10	Poisoning experiments	397
7.5.11	Deuterium labeling experiments.....	398
7.5.12	Mechanism: Stoichiometric NMR experiments	403
7.5.13	Mechanism: GC analyses.....	406
7.5.14	Mechanism: Cyclic voltammetry	410
7.5.15	Mechanism: UV-vis spectroscopy.....	412
7.5.16	Nanoparticle TEM analysis.....	413
7.5.17	References.....	413
8	The Role of Organoferrates in Iron-Catalyzed Cross-Couplings	415
8.1	Introduction	416
8.2	Triorganoferrates as Active Cross-Coupling Catalysts.....	418
8.3	Conclusion.....	422
8.4	References.....	423
9	Summary.....	425
10	List of Abbreviations.....	432
11	Acknowledgments.....	433

12 Curriculum Vitae.....	435
13 Eidesstattliche Versicherung	439

Table of Contents

1 Homogeneous vs. Heterogeneous: Insights into Iron Group Metal-Catalyzed Reduction Reactions from Kinetic Poisoning Experiments[†]



Author contribution:

D. Gärtner:[†] Initial manuscript preparation, see D. Gärtner, *Dissertation*, Universität Regensburg, **2016**.

S. Sandl:[†] Completion of the manuscript.

[†] These authors contributed equally.

A. Jacobi von Wangelin: Corresponding author.

1 Homogeneous vs. Heterogeneous: Insights into Iron Group Metal-Catalyzed Reduction Reactions from Kinetic Poisoning Experiments

Abstract: Iron group metal catalysts constitute a promising alternative to well-established noble metal catalysts in reduction reactions. However, the development of effective 3d metal catalysts has largely been hampered by their distinct coordination properties, their higher lability toward ligand exchange, redox reactions, and rapid aggregation to larger particles. The facile transition from homogeneous to heterogeneous catalysts under reducing conditions has been a major challenge in method optimization and mechanistic understanding. While ex-situ-analyses of catalyst derivatives can be achieved by various spectroscopic techniques, their results have only limited value for the different conditions, concentrations, and complex kinetics of a real catalytic system. On the other hand, in-situ-tools usually require highly sophisticated setups aiming at the detection of fleeting intermediates. This review advocates the use of kinetic poisoning experiments which can be easily performed in a standard laboratory and enable the distinction between homotopic and heterotopic catalysis mechanisms.



1.1 Introduction

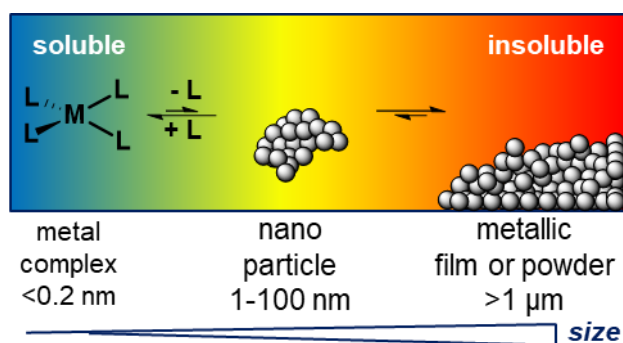
Transition metal-catalyzed reactions that operate under reducing conditions - such as reductions, hydrogenations, isomerizations, cycloadditions, and cross-couplings - constitute key methods for the synthesis of pharmaceuticals, fine and bulk chemicals.^{[1],[2]} Despite the great versatility and high selectivity of precious metal catalysts such as Ru, Rh, Pd, recent environmental and economic concerns have stimulated intensive research into the use of their lighter congeners, the iron group metals Fe, Co, and Ni.^{[3],[4]} In the past decade, numerous iron-, cobalt- and nickel-based catalysts have been developed that exhibited high activity and selectivity in organic reactions under reductive conditions.^[5] Despite the great progress in the field of catalysis with late earth abundant metals, the transition from the heavier 4d and 5d metals to 3d transition metals entails several mechanistic distinctions and synthetic limitations. Generally, 3d metal complexes exhibit a smaller ligand field splitting in comparison to their heavier congeners. The metal-ligand bond strength tends to be stronger for the latter which can be merely explained by the greater spatial overlap of the metal and ligand orbitals. Consequently, a vivid coordination behavior and population of various spin states is observed. Complexes with paramagnetic spin states (i. e. metalloradicals) tend to undergo rapid one-electron transfer reactions and hamper the analysis of the reaction mixture by nuclear magnetic resonance spectroscopy (NMR). Moreover, reduced metal complexes are less stable and thus require stronger reducing reagents to access low oxidation states. These intrinsic properties of 3d metal catalysts may limit the observed selectivity of catalytic reactions, favor unwanted side reactions, and result in the decomposition of the catalyst species. The observation of heterogeneity problems under operationally homogeneous conditions of reductive late 3d metal catalysis has been a topic of intensive speculation and several mechanistic studies.^[6] While several techniques became well-established for precious metals, most of these methods are poorly developed for 3d metals.^{[6]-[9]} On the contrary, investigations of similar mechanisms of heavier transition metal catalysts have had a much longer history. A very instructive example is the rhodium-catalyzed hydrogenation of benzene with $[\text{RhCp}^*\text{Cl}_2]_2$ ($\text{Cp}^* = [\eta^5\text{-C}_5\text{Me}_5]$). More than 30 years have elapsed since the first postulation of a homogeneous mechanism based on light scattering experiments

(1977). Deeper insights were gained from the study of metal precipitates and polymer-supported catalysts (1984), preliminary analytical studies including poisoning experiments and TEM measurements (2005), and the comprehensive analytical report including EXAFS, kinetic poisoning studies and the resultant formulation of $\text{Cp}^*_{2.4}\text{Rh}_4\text{Cl}_4\text{H}_c$ cluster catalysts (2011).^[10]

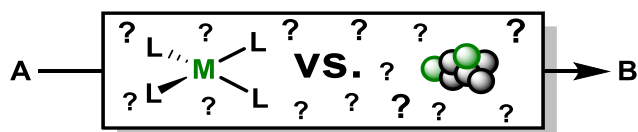
1.2 Distinction between Homogeneous and Heterogeneous Catalysis

It is important to note that the classical Ostwald definition of the terms “homogeneous” and “heterogeneous”, where the catalyst is either in the same phase with the substrate or not, is not entirely suited to address the true nature of the catalytic mechanism. Ostwald’s definition is imprecise for contemporary standards as even nanoparticles (NPs) and colloids can be highly dispersible in substrate solutions, despite the formal heterogeneity between solution and catalysts (Scheme 1.1).^[11] Schwartz therefore introduced a new definition that is not based on the physical appearance of the catalyst but instead on the catalytic mechanism being operative.^{[6],[12]} According to Schwartz’s definition, a homogeneous catalyst has a single active site, whereas heterogeneous catalysts have multiple active sites. It should be mentioned, that authors generally do not clearly differentiate between Ostwald’s and Schwartz’s definition. To avoid this definition conflict, Crabtree suggested the use of the “topicity” terminology, i.e. homotopic vs. heterotopic.^[6] Although we have multiple techniques at hand to characterize well-defined metal complexes, nanoparticles, and colloids, the identification of the true active catalyst in a reaction is still a challenging task given the general difficulties of bulk spectroscopic ex-situ analyses to detect fleeting kinetic species within the complex setting of reaction conditions. Notably, there is not a single fully conclusive test that can unambiguously distinguish between homotopic or heterotopic catalysis. Hence, a multi-technique approach is essential which many chemical practitioners shy away from.^[13]

1 Homogeneous vs. Heterogeneous: Insights into Iron Group Metal-Catalyzed Reduction Reactions from Kinetic Poisoning Experiments



Scheme 1.1. Correlation between size and solubility of different metal conditions.



Scheme 1.2. Distinction between homotopic and heterotopic catalysis.

In general, reaction analysis can be classified into *in operando* techniques (in-situ) which are conducted during the reaction, and *post operando* techniques (ex-situ) that involve additional steps such as sample preparation, dilution, elimination of other reagents etc. (Scheme 1.2). It is obvious that *in operando* measurements lead to more instructive data for the discussed problem, since any catalyst solution manipulation may lead to an entirely different thermodynamic and kinetic scenario.^[6] The arsenal of available spectroscopic tools for *in operando* studies of catalytic species mostly involve highly sophisticated instrumentation that are beyond the reach of a standard chemical laboratory. However, there are a handful of operationally facile methods that enable a rapid and reliable insight into the catalytic mechanism. Below, we wish to discuss some of the most reliable and powerful *in operando* techniques that have been applied to modern iron-, cobalt- and nickel-catalyzed reactions. A special focus is placed on catalyst development at the fine borderline of homotopic and heterotopic reaction mechanisms.

1.3 Reaction Progress Analysis

The prime characteristic of a catalytic reaction is its kinetic control. The determination of various kinetic data from the reaction under investigation is a key to the understanding of the catalyst species. Therefore, reaction progress analyses, i.e. the determination of substrate conversions and product formations over time, are very powerful techniques in many cases where reliable quantification of reagents by nuclear magnetic resonance (^1H or other nuclei), chromatography (GC-FID, HPLC), or optical spectroscopy (IR, UV-Vis) is available. Additional kinetic experiments such as the use of selective additives (i.e. poisons, ligands) and the determination of reaction orders provide a wider picture of the operating mechanism.^{[6],[14]}

Kinetic data that are highly reproducible are already a first indication of homotopic catalyst species under operationally homogeneous conditions.^[7] On the contrary, a much lower reproducibility is often observed for heterotopic catalysts. This is a direct consequence of the interference of particle growth and catalytic activity of metal NPs, the high sensitivity of *in situ* formed NPs to the reaction conditions, local concentrations, impurities etc.^[13] However, high reproducibility must not always be associated with homotopic catalysis, and has also been observed with nanoparticles.^[15]

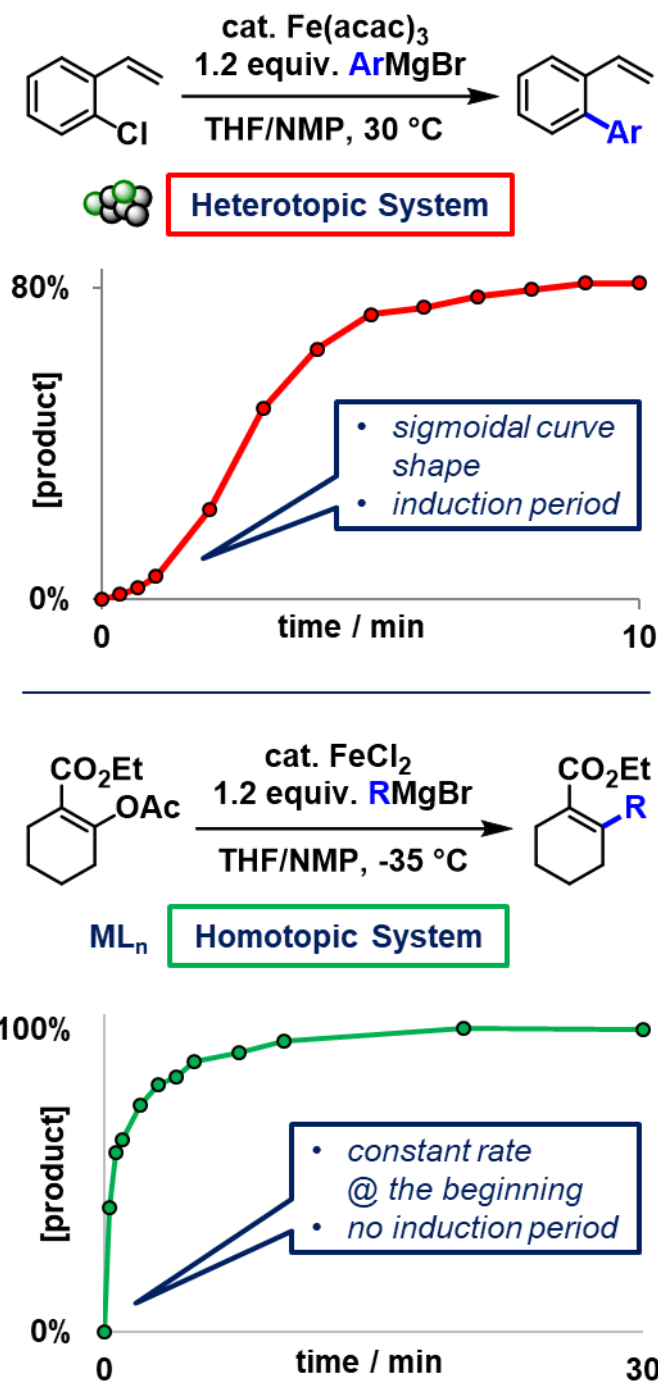
1.3.1 Reaction progress analysis

The curvature of the conversion-vs.-time and product formation-vs.-time can constitute further important indicators of the underlying catalytic mechanism (Scheme 1.3). In most protocols, a convenient and stable source of the metal catalyst is employed which undergoes transformation to the active catalyst species under the reaction conditions, often by metal salt reduction, ligand substitution, or ligand dissociation.^[13] Therefore, careful analysis of the initial reaction phase can assist in the interpretation of catalyst formation events. In Scheme 1.3 left, the reaction progress curve consists of three distinct intervals: (i) initiation, (ii) steady conversion and (iii) completion. Contrary to this curvature, a steady conversion without any detectable induction period was observed in a very similar cross-coupling reaction in Scheme 1.3 right. Both protocols operate in the absence of

strong-field ligands so that the reducing conditions of the Grignard reagents are very likely to effect pre-catalyst reduction and/or ligand substitution. The lability of all ligands present in the reaction mixture may lead to the formation of reduced iron species that undergo nucleation and growth to larger aggregates and particles. Such behavior would ultimately result in prolonged induction periods of the catalytic reaction if a heterotopic catalyst was operative. The activation and/or generation of active homotopic catalysts is usually a faster process.^[16] Hence, the former case of Scheme 1.3, left, may indicate the slow formation of a heterotopic catalyst.^{[17],[18]} The latter cross-coupling reaction may involve homotopic catalysts such as triorganoferrates.^[10] The same outcome was independently proven by poisoning experiments (*vide infra*).^{[17],[18]} The determination of different catalytic mechanism in these two reactions is especially interesting as both cross-couplings employ very similar pre-catalysts, reagents, and conditions: (i) Fe salts as pre-catalysts, (ii) organomagnesium halides as nucleophiles, (iii) THF/NMP as solvent mixture, and (iv) no further ligands.

Ligands play a key role in the formation and stabilization of active catalyst species, both in homotopic and heterotopic mechanisms. There are many examples where the addition of strong ligands to a soluble metal pre-catalyst resulted in the formation of an operationally homogeneous catalyst, yet a heterotopic mechanism appeared to operate. In heterogeneous species, ligands may trigger the formation of low-valent metal species that are prone to aggregation or act as surfactants that enhance catalytic activity of the catalyst surface or inhibit further particle growth.^{[6],[7]}

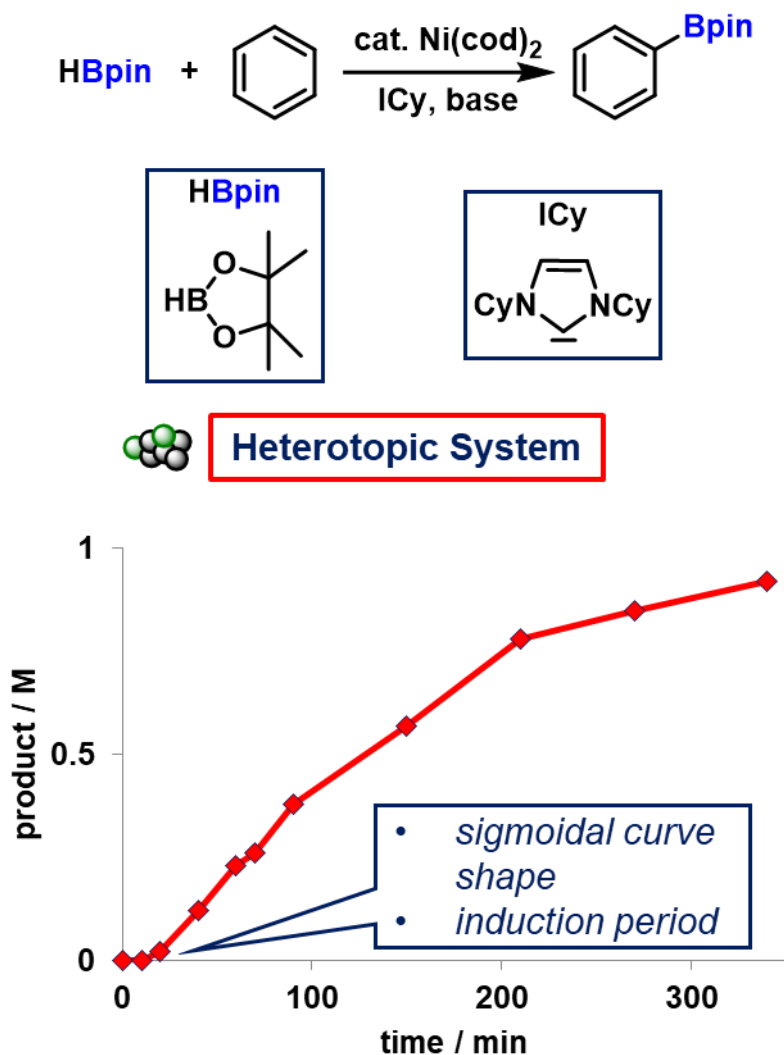
1 Homogeneous vs. Heterogeneous: Insights into Iron Group Metal-Catalyzed Reduction Reactions from Kinetic Poisoning Experiments



Scheme 1.3. Iron-catalyzed cross-coupling of 2-chlorostyrene (left, heterotopic)^[17] and alkenyl acetates (right, homotopic).^[18]

An interesting example is the nickel-catalyzed borylation of arenes reported by the Chatani group (Scheme 1.4). A sigmoidal curvature and an induction period were observed in the reaction progress analysis. Note, that the reaction mixture involves the ligands 1,3-di(cyclohexyl)imidazolylidene (ICy) and 1,5-cyclooctadiene. The presence of a heterotopic catalyst was further supported by a mercury test (*vide*

infra).^[20]



Scheme 1.4. Ni-catalyzed borylation of benzene according to Chatani et al.^[20]

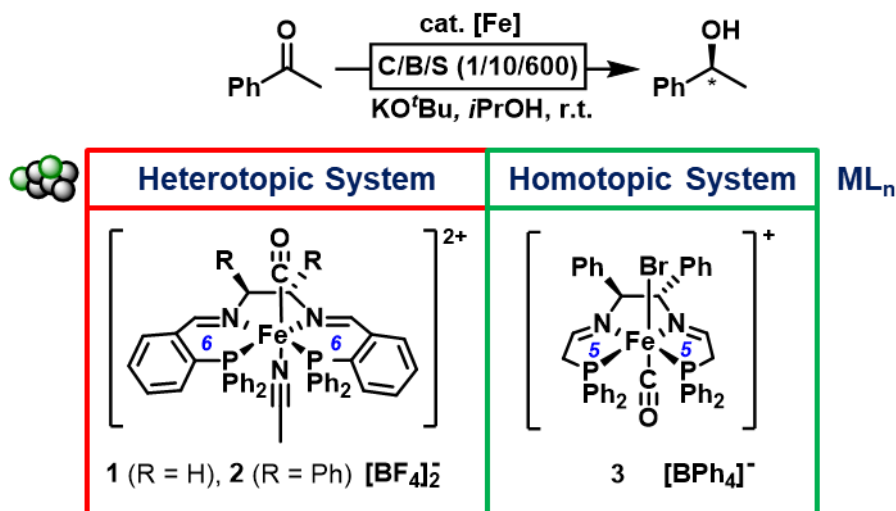
1.3.2 Asymmetric catalysis

High levels of asymmetric induction in chemical reactions has mostly been attributed to homotopic catalysis mechanisms where the metal is coordinated by the chiral ligand. However, great care should be taken as chiral ligand-modified metal surfaces can indeed act as chiral catalysts in heterotopic mechanisms.^[21]

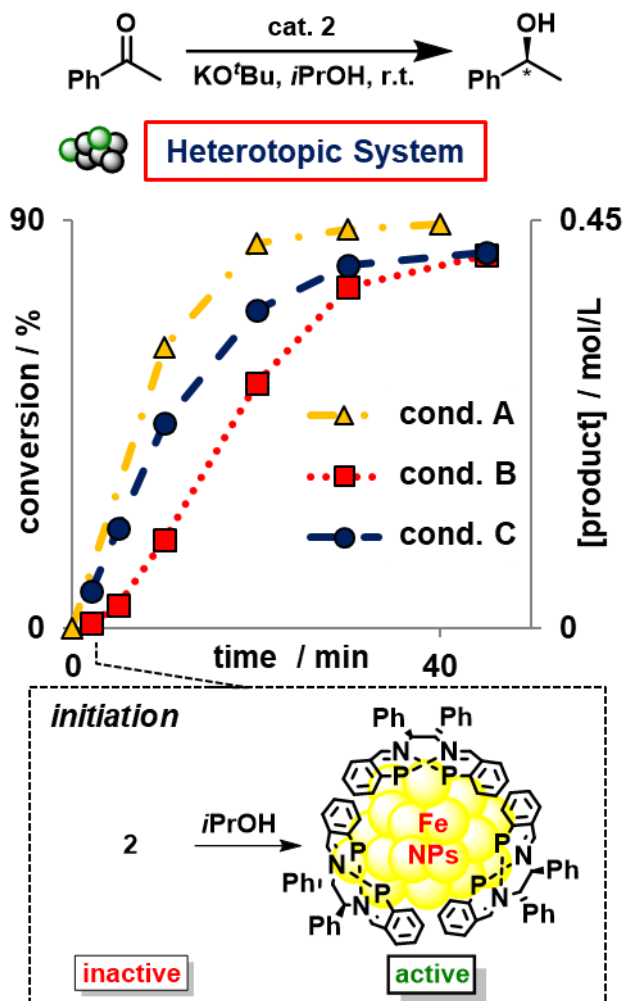
In general, the determination of reaction progress curves from quantified substrate conversion and product formation is an indirect tool to ascertain induction periods or a change of mechanism during turnover. However, the choice of collected data

points and their interpretation can still be misleading if the operating effects are small or the distinction between homogeneous and heterogeneous catalysis blurred by similar reaction rates, rapid aggregation processes or the presence of fast equilibria between the two catalyst phases.^[9] A highly insightful example that gained great attention in the literature is the iron-catalyzed reduction of ketones reported by Morris and coworkers. Fe^{II}-*PNNP* complexes were employed as well-defined pre-catalysts in the asymmetric transfer hydrogenation (ATH, Scheme 1.5)).^{[13],[16],[22],[23]} Later, careful mechanistic studies allowed the differentiation of these similar catalysts into homotopic and heterotopic. The originally anticipated homotopic catalysis was only found complex **3**.^[16] Employment of the related complexes **1** and **2** under the very same conditions lead to a heterotopic reaction pathway catalyzed by metal particles (Scheme 1.5). Note, that the complexes merely differ in their N-Fe-P ring size (6 atoms for **1** and **2** and 5 atoms for **3**).^{[13],[22],[23]} The initial study published in 2009 reported a steady conversion of ketone with catalytic **2** without any detectable induction period (Scheme 1.6, A).^[23] However, the data points were unsuitable for a thorough investigation of the catalytic onset: The first sample was taken after 10 min at a conversion of more than 60% of starting material (Scheme 1.8, A). The trend line suggested an immediate onset of catalytic activity which apparently did not require any preceding transformation of the pre-catalyst to an active catalyst species. A renewed attempt with pre-catalyst **2** in 2012 indeed revealed a significant initiation phase (Scheme 1.6, B). This study B was based on product formation instead of substrate consumption to determine the reaction progress.^[22] Notably, substrates can be involved in the catalyst formation, especially when bearing fairly reactive functional groups.^[24] The authors demonstrated that treatment of **2** with base and *i*PrOH afforded an active catalyst that showed steady product formation without any detectable induction period (Scheme 1.6, C). The presence of ligand-stabilized metal NPs was supported by EDX, SQUID, STEM and XPS analysis (Scheme 1.6, bottom).^[22]

1 Homogeneous vs. Heterogeneous: Insights into Iron Group Metal-Catalyzed Reduction Reactions from Kinetic Poisoning Experiments



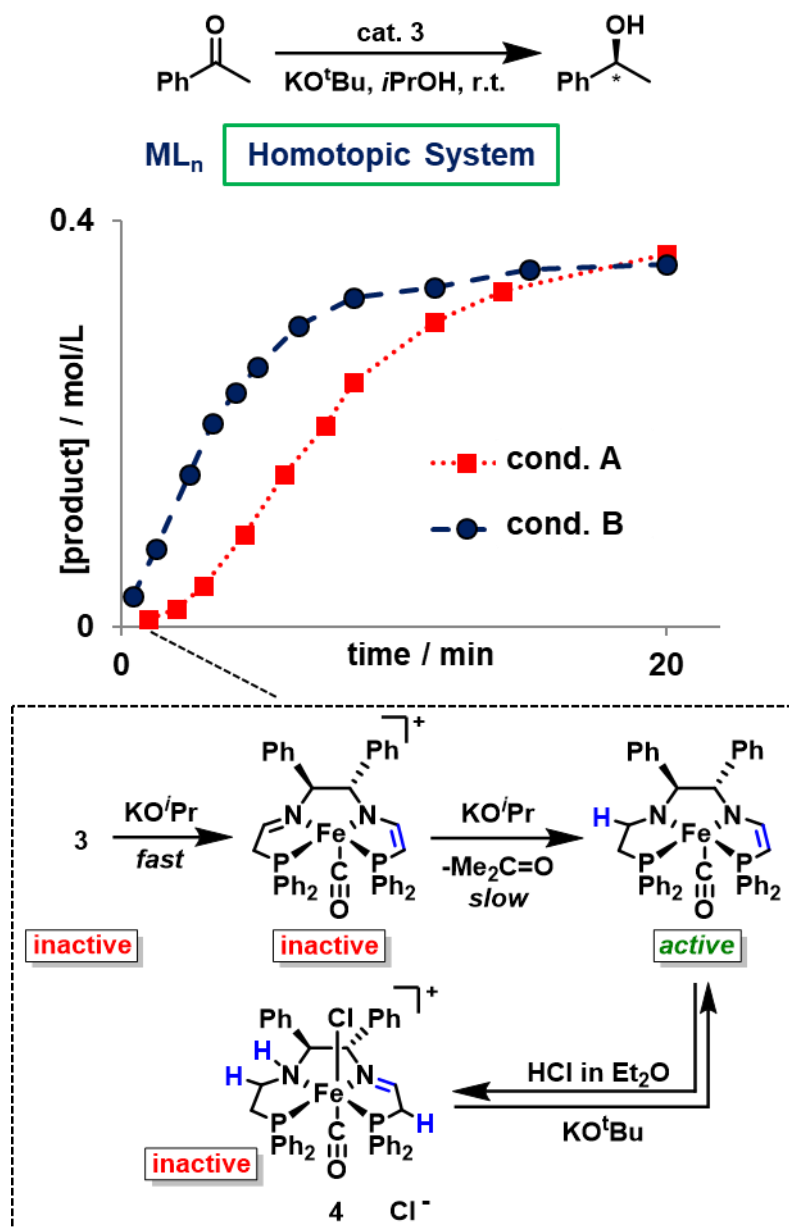
Scheme 1.5. Fe^{II} -PNNP complexes in the asymmetric transfer hydrogenation by Morris et al.; C/B/S: molar ratio of complex (C), KO^tBu (B) and substrate (S).^{[16],[22]}



Scheme 1.6. Asymmetric transfer hydrogenation. Conditions: A, B: substrate in $i\text{PrOH}$ was added to solid **2** and KO^tBu ; C: preformation of catalyst prior to substrate addition; Ph substituents of P-ligand omitted for clarity.^{[22],[23]}

Kinetic studies on the topicity of the ATH with complex **3** revealed an unexpected induction period (Scheme 1.7, A) despite some examples of similarly long initiation phases of molecular catalysts under similar conditions.^{[25],[26]} Prior treatment of **3** with *i*-PrOH and KO^tBu resulted in a steady conversion without any induction period (Scheme 1.7, B). This indicated that the employment of **3** involves slow formation of the active catalyst in the presence of solvent and base. Deactivation and reactivation experiments supported a homotopic catalysis: Treatment of the active catalyst with hydrochloric acid immediately inhibited catalyst activity which was rapidly re-established by addition of base. Further preparative efforts allowed the isolation of a related chloridoiron complex **4** which exhibited superior activity in the ATH of ketones. Hence, the induction period can be interpreted as ligand reduction.^{[13],[16]} Importantly, analogous treatment of **2** with HCl led to irreversible decomposition to catalytically inactive nanoparticles.^{[13],[22]}

1 Homogeneous vs. Heterogeneous: Insights into Iron Group Metal-Catalyzed Reduction Reactions from Kinetic Poisoning Experiments



Scheme 1.7. ATH of acetophenone using complex **3**. Conditions: A: substrate in iPrOH added to solid **3** and KO^tBu; B: preformation of catalyst with KO^tBu / iPrOH prior addition of substrate.^[16]

1.4 Kinetic Poisoning Studies

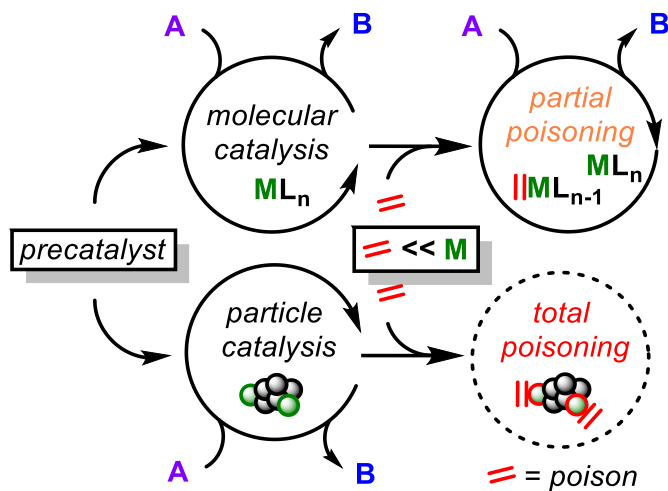
Catalyst deactivation is usually undesired, and the replacement of inactive catalysts is a major cost driver in technical processes. Deactivation processes are manifold and can involve redox or acid-base reactions, ligand exchange, aggregation, or active site blockage. The latter case is especially frequent and difficult to ascertain. Strong and irreversible chemisorption of substrates, additives, co-catalysts or impurities on the active site may lead to catalyst poisoning.^{[27],[28],[29]} The same strong binding of poisons can be beneficially used for the modulation of catalyst. For example, desired poisoning has been used in the stereoselective semi-hydrogenation of alkynes by lead-poisoned palladium catalysts (Lindlar catalyst).^{[30],[31]} Furthermore, the interaction of catalyst species with selective poisons can provide deep insight into the topicity of a catalyst and the number of active sites. Such kinetic poisoning studies can be performed by addition of a poison into a running catalytic reaction at low conversions where an interaction of the poison with the catalyst site competes with the conversion of substrates. The distinction between homotopic and heterotopic catalysts may be complemented with other analytical tools (electron microscopy (TEM), X-ray methods (EXAFS, EDX, SAXS, XPS), spectroscopy (IR, EPR, NMR, UV-VIS, Mößbauer), dynamic light scattering (DLS), magnetometry (SQUID), etc).^[6]

1.4.1 Quantitative poisoning experiments

Quantitative poisons act as strongly metal-binding ligands and react with both homotopic and heterotopic catalysts. The topicity of the catalyst is determined based on the amount of the poison (quantity) rather than on the selectivity of a poison (quality, *vide infra*).^[7] The topicity of the catalyst is determined based on the amount of the poison (quantity) rather than on the selectivity of a poison (quality, *vide infra*). Common quantitative poisons are phosphines, thiophenes, and CS₂.^[32] Especially useful insight into the number of active catalyst sites can be gained from partial poisoning experiments (Scheme 1.8).^[31] As most heterotopic catalysts are composed of compact particles, only a small fraction of active metal atoms reside on the surface while most of the metals form the bulk heterogeneous inner core. Therefore, the addition of sub-stoichiometric amounts of a metal-binding poison

1 Homogeneous vs. Heterogeneous: Insights into Iron Group Metal-Catalyzed Reduction Reactions from Kinetic Poisoning Experiments

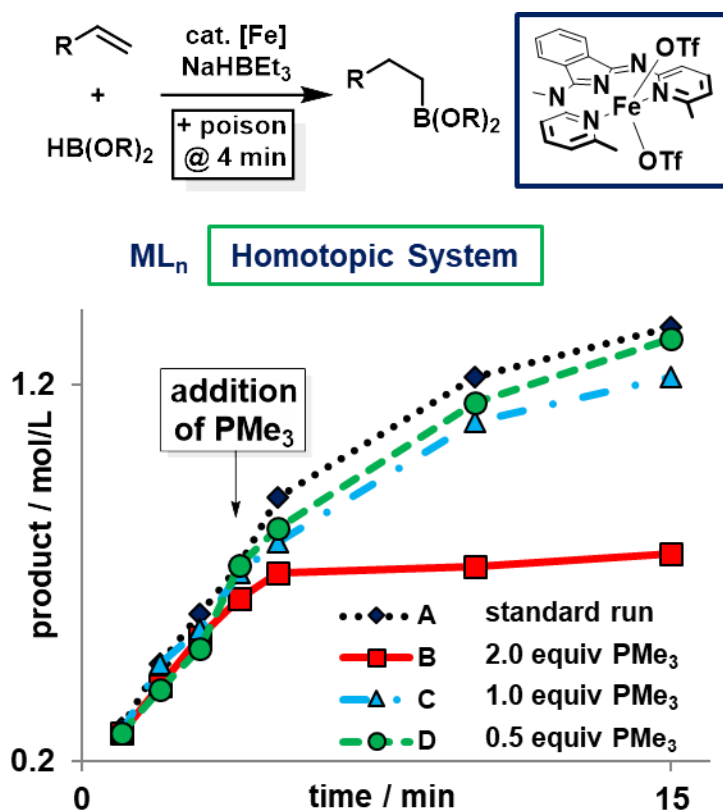
per metal already leads to complete catalyst inhibition (i. e. sub-catalytic). On the contrary, molecular catalysts containing a single metal ion in its active structure will require at least stoichiometric amounts of poison per metal ion.^{[25],[26]}



Scheme 1.8. Partial poisoning of molecular and particle catalysts.

Szymczak and coworkers studied the iron-catalyzed hydroboration of alkenes which exhibited complete catalyst inhibition when 2 equiv. PMe₃ per Fe were added. This observation was interpreted as indication that a homotopic catalyst with two vacant coordination sites per Fe atom was operating under the reaction conditions (Scheme 1.9).^[15]

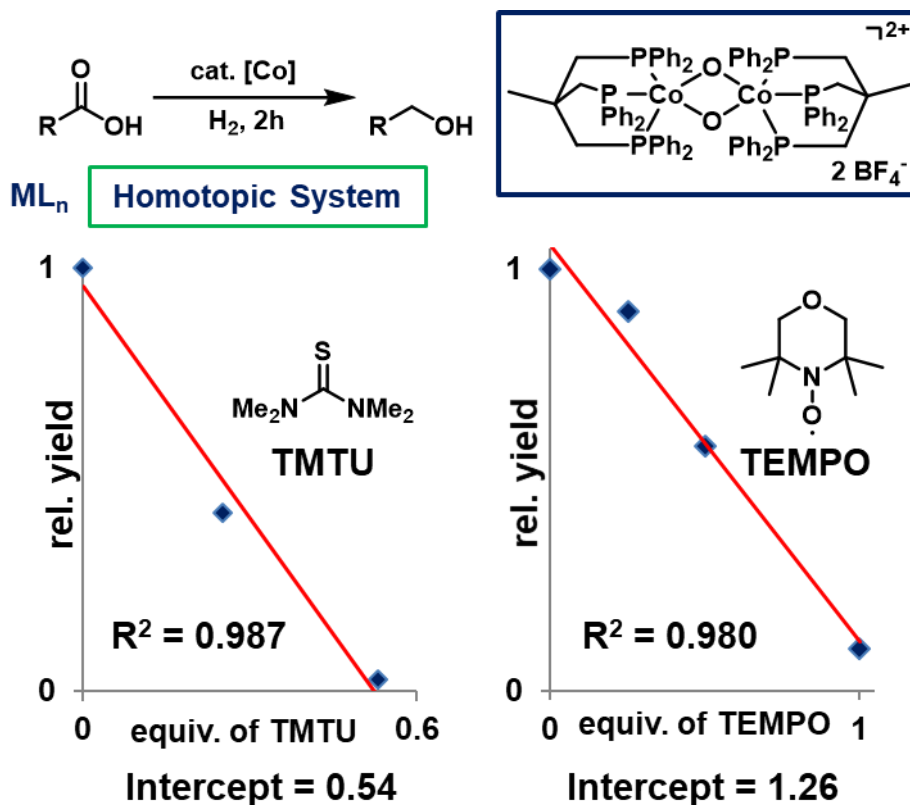
1 Homogeneous vs. Heterogeneous: Insights into Iron Group Metal-Catalyzed Reduction Reactions from Kinetic Poisoning Experiments



Scheme 1.9. Iron-catalyzed hydroboration of olefins.^[15]

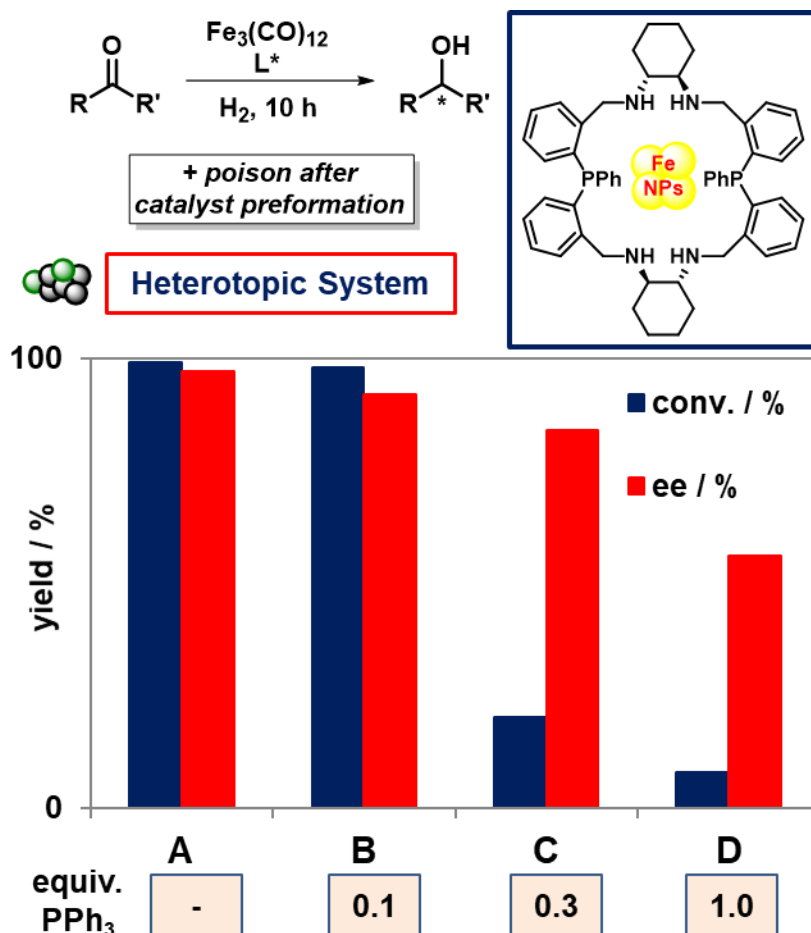
There are few cases where less than one equivalent of poison can inhibit homotopic catalysts. Recently, the group of de Bruin reported the cobalt-catalyzed hydrogenation of carboxylic acids (Scheme 1.10). Partial kinetic poisoning studies revealed that two active cobalt centers could be inhibited by one molecule of tetramethylthiourea (TMTU), while only 1 equiv. of 2,2,6,6-tetramethyl-piperidin-1-oxyl (TEMPO) gave total inhibition.^[33]

1 Homogeneous vs. Heterogeneous: Insights into Iron Group Metal-Catalyzed Reduction Reactions from Kinetic Poisoning Experiments



Scheme 1.10. Carboxylate hydrogenation by *de Bruin et al.*^[33]

In rare cases or when very small discrete clusters operate as catalysts, unusually high concentrations of a poisonous additive may be required for the modulation of heterotopic catalysts. Gao and coworkers studied the effect of triphenylphosphine onto the iron-catalyzed asymmetric hydrogenation (AH) of ketones (Scheme 1.11).^[34] Under standard conditions, full conversions and high stereocontrol (98% ee) were observed. The addition of 0.1 equiv. PPh₃ showed a negligible effect, while >0.3 equiv. PPh₃ resulted in a sharp loss of catalytic activity and stereoselectivity (Scheme 1.11, C). However, the analysis of the reaction rates for these experiments are not available from the publication.^[34]



Scheme 1.11. Asymmetric hydrogenation of ketones according to Gao et al.^[34]

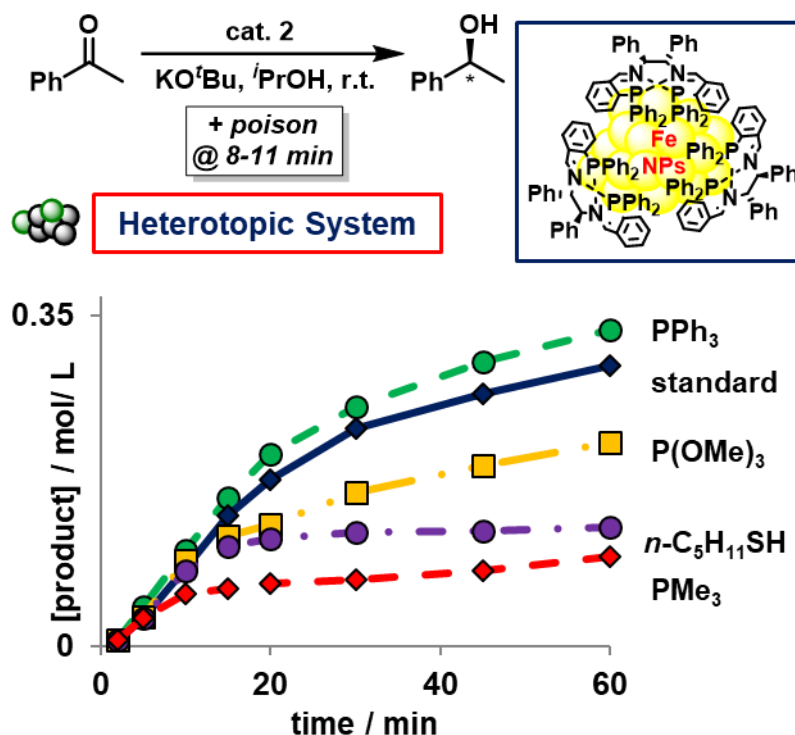
1.4.2 The choice of the catalyst poison

Successful poisoning of a metal catalyst is considered as an irreversible complexation of a metal with a poison (i.e. ligand). Hence, strong-field ligands are used in order to give a stable binding. Additional stability of the metal-ligand complex can be achieved by chelating ligands. Moreover, the choice of the catalyst poison strongly depends on the metal and its oxidation state (i.e. electron-rich metal for reduced late 3d metal catalysts). The steric bulk of the ligand can be further used for the distinction of homotopic and heterotopic catalysis (*vide infra*).

Morris and co-workers investigated the effect of various additives onto the iron-catalyzed asymmetric transfer hydrogenation of ketones. Amines, phosphines, phosphites, or thiols were evaluated as selective catalyst poisons (Scheme 1.12).^{[13],[22]} Very little alteration of catalyst activities was observed with amine

1 Homogeneous vs. Heterogeneous: Insights into Iron Group Metal-Catalyzed Reduction Reactions from Kinetic Poisoning Experiments

additives such as 1,4-diazabicyclo[2.2.2]octane (DABCO) or ethylene-1,2-diamine. Addition of only 0.15 equiv. *n*-pentyl-mercaptan led to complete inhibition. The complexity of selective catalyst poisoning is illustrated by phosphine additives: 0.2 equiv. of the phosphines PCy₃ or PPh₃ enhanced the catalyst activity without any loss of selectivity. This may indicate that bulky phosphines effectively stabilize the nanoparticulate catalyst against agglomeration or deactivation. On the contrary, 0.1 equiv. of the less bulky PMe₃ or PPhMe₂ showed complete inhibition of catalyst activity which suggests quantitative poisoning. Upon addition of the electron-poor phosphine P(OMe)₃ (0.2 equiv.), the rate of catalytic turnover was merely slowed down, which may be indicative of reversible poison adsorption to the catalyst surface.^{[13],[22]} In other cases, low concentrations of P(OMe)₃ (0.1-0.2 equiv.) have also been reported to effect higher reaction rates.^[35] Depending on the nature and topology of the catalyst, even PMe₃ can be an inefficient poison due to undesired side reactions.^{[16],[36],[37]} These issues of poor efficacies of poisonous additives requires the study of alternative reagents: 1,10-Phenanthroline^[34] and pivalonitrile, ^tBuCN,^[37] showed in two specific cases superior poisoning profiles than the commonly employed trimethylphosphine, PMe₃. 1,10-Phenanthroline has been used as effective catalyst poison in hydrogenation reactions that proceed under relatively harsh conditions (≥ 100 °C, ≥ 50 bar H₂).^[38]

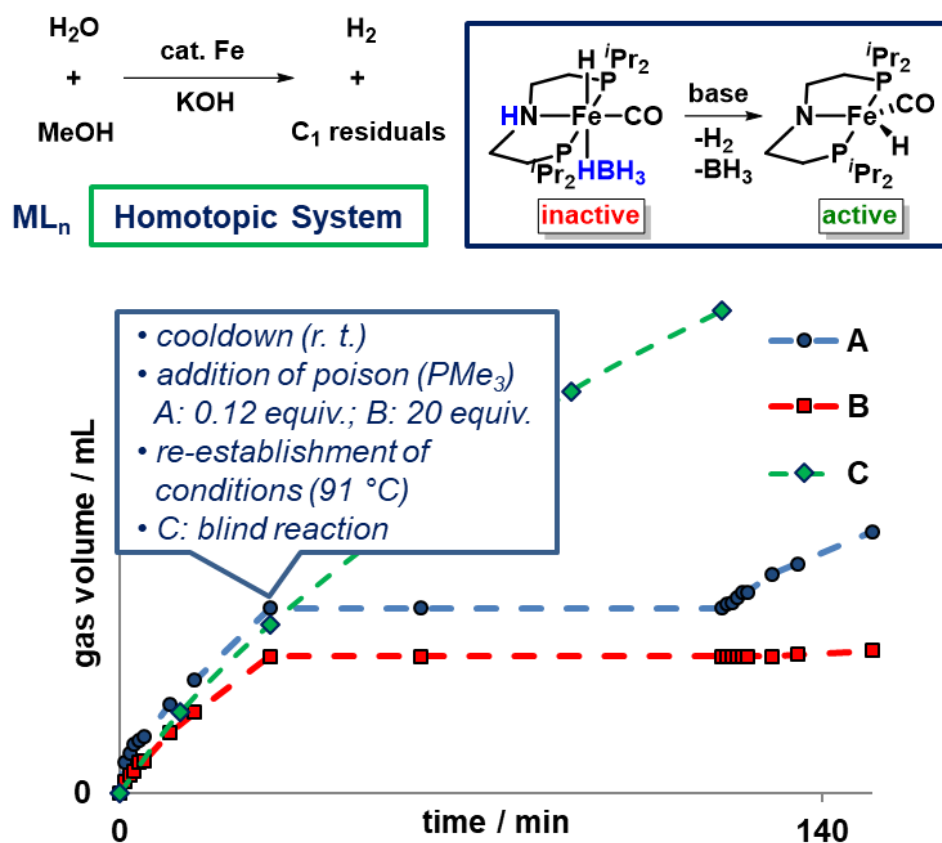


Scheme 1.12. Comparison of poisoning reagents in the ATH of acetophenone.^[22]

1.4.3 The impact of the reaction conditions

The complex kinetic and thermodynamic aspects of metal-catalyzed reactions – which mostly involve mechanisms via multiple elemental steps – are sensitive to the employed reaction conditions. Most of the successful poisoning experiments were performed at low or near ambient temperatures (mostly $<50\text{ }^{\circ}\text{C}$) as elevated temperatures are likely to result in reversible binding of the poisons, catalyst decomposition, or surface leaching.^[39] Direct insight into the modulation of catalyst activity by poison addition requires addition of the latter under reaction conditions. However, technical issues (reagent inlet, volatility, safety etc.) may prohibit this so that thermal modifications of the standard reaction may overlay with the poisoning effect. Beller and coworkers performed poisoning experiments in iron-catalyzed dehydrogenation of methanol (Scheme 1.13).^[40] Before addition of trimethylphosphine as potential poison of the homogeneous iron-pincer catalyst, substrate conversion was stopped by lowering the reaction temperature (bp. of $\text{PMe}_3 = 37.5\text{ }^{\circ}\text{C}$).^[41] Sub-stoichiometric addition of 0.12 equiv. PMe_3 had a minimal influence on the dehydrogenation activity when the standard reaction temperature was restored, whereas 20 equiv. PMe_3 gave complete inhibition.^[40]

1 Homogeneous vs. Heterogeneous: Insights into Iron Group Metal-Catalyzed Reduction Reactions from Kinetic Poisoning Experiments



Scheme 1.13. Dehydrogenation of methanol by an iron-*PNP*-catalyst; Reaction progress of poisoned reaction under temperature change.^[40]

1.4.4 Qualitative poisoning experiments

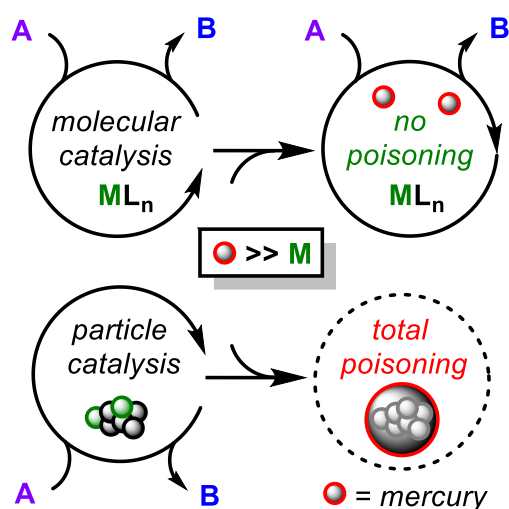
Qualitative poisons selectively interact with either a homotopic or a heterotopic catalyst. A handful of common poisons have been validated mostly for 4d- and 5d-transition metal catalysts.^{[6],[7]} However, the rapid progress in the field of 3d transition metal catalysis has led to several applications of such qualitative poisonous reagents to the lighter homologues.

1.4.5 Mercury, a selective heterotopic catalyst poison

The mercury test is a prominent example of a qualitative heterotopic poisoning of metal catalysts by adsorption or amalgamation. Metal-ligand complexes do not show this behavior so that little to no influence of Hg addition is expected (Scheme 1.14).^[32] Although mercury poisoning has been widely used for iron and cobalt catalysts, the validity of this test is still under dispute.^[42] The incorporation of mercury is hindered by the low solubility of iron, cobalt, and nickel in mercury (for

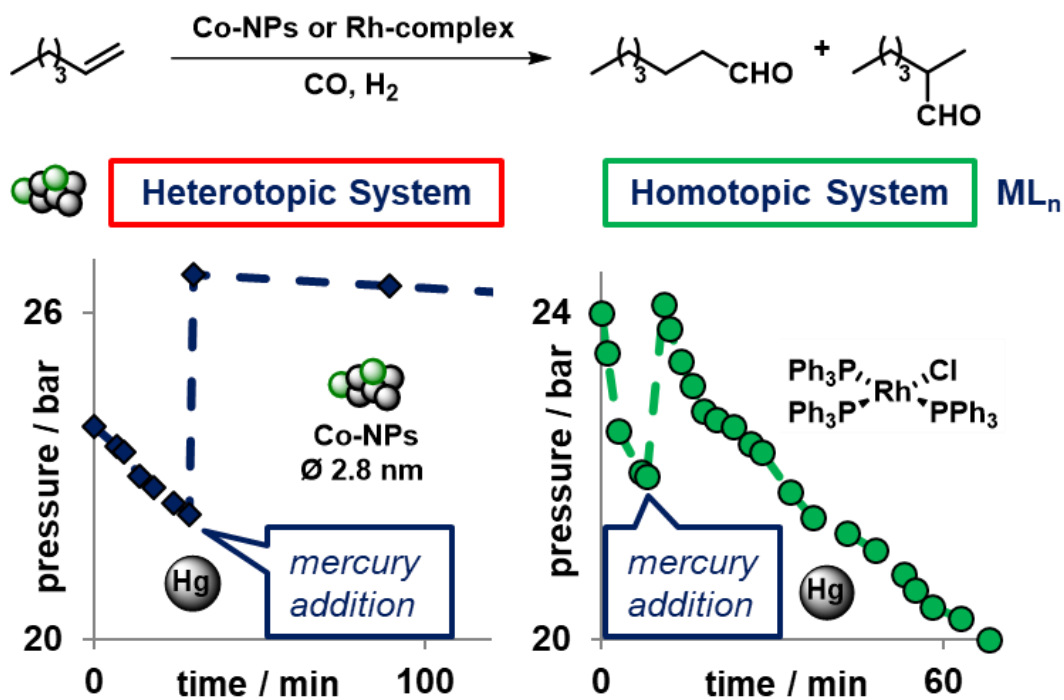
1 Homogeneous vs. Heterogeneous: Insights into Iron Group Metal-Catalyzed Reduction Reactions from Kinetic Poisoning Experiments

Fe and Co $<10^{-5}$ wt%).^[43] However, the commonly investigated noble catalyst metals Ru, Rh, and Ir where the Hg test was proposed to be selective, have equally low solubilities in Hg.^[44] Most reports use a large excess of Hg; >500 equiv. Hg for Ni, Pd, Pt and even more for Fe and Co.^[43] Furthermore, Fe and Co form metastable alloys with mercury which may lead to catalyst metal release under the reaction conditions.^{[45],[46]} Careful analysis of the reaction progress is advised to observe indications of partial or reversible catalyst poisoning. The crucial parameters of effective Hg poisoning are long lifetimes, irreversibility of amalgam formation, and high concentrations of added mercury. Despite some literature precedents of Fe, Co, and Ni poisoning by Hg,^{[34],[47]–[51]} many heterotopic catalysts of these metals were not affected by the addition of Hg. Kou and coworkers reported the hydroformylation of alkenes catalyzed by Co nanoparticle (Scheme 1.15). Injection of Hg to the reaction after 30 min resulted in an inactive catalyst. The truly homogeneous Wilkinson catalyst remained active under the same conditions.^[48]



Scheme 1.14. Hg addition to molecular and particle catalysts.

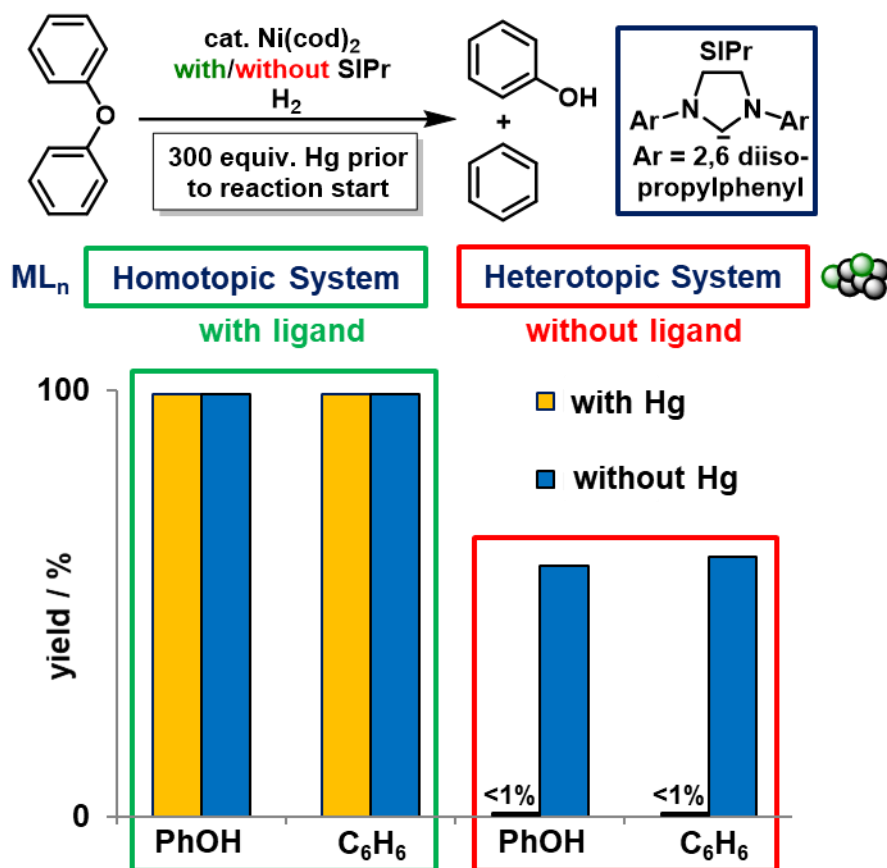
1 Homogeneous vs. Heterogeneous: Insights into Iron Group Metal-Catalyzed Reduction Reactions from Kinetic Poisoning Experiments



Scheme 1.15. Hg poisoning of Co NPs vs. the Rh-complex-catalyzed reaction.^[48]

The significance of ligand binding to homotopic catalysts was illustrated by a poisoning study of the Ni-catalyzed hydrogenolysis of diarylethers by Hartwig and coworkers (Scheme 1.16). Reactions with catalytic $\text{Ni}(\text{cod})_2$ and no additional ligands were apparently heterotopic as indicated by the effective Hg poisoning. Addition of 4,5-dihydro-1,3-bis(2,6-diisopropylphenyl) imidazolylidene (SIPr) resulted in a homotopic catalyst which was inert toward Hg addition.^{[50],[52]}

1 Homogeneous vs. Heterogeneous: Insights into Iron Group Metal-Catalyzed Reduction Reactions from Kinetic Poisoning Experiments



Scheme 1.16. Hg poisoning in the Ni-catalyzed hydrogenolysis of diarylethers.^{[50],[52]}

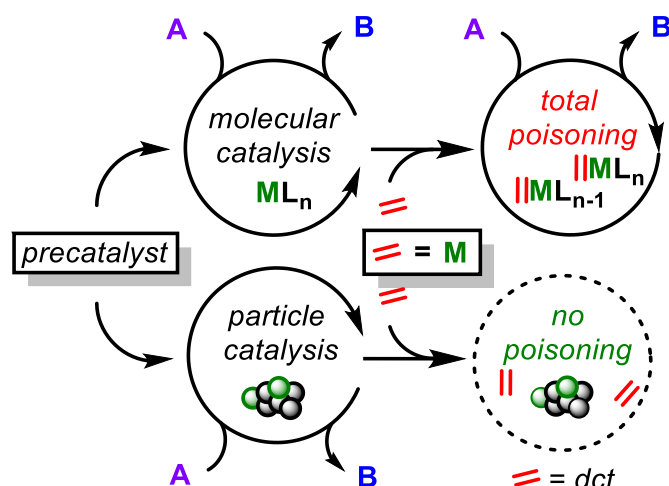
There are some reported cases where mercury underwent chemical reactions with molecular complexes that resulted in unwanted side reactions or even gave improved product yields.^{[7],[6],[13],[53]} This may be a direct consequence of the modulation of ligand dissociation equilibria that may lead to the leaching of homeopathic metal species into the solution.^{[6],[9],[54]} Nevertheless, mercury poisoning experiments have been demonstrated to be an operationally facile and meaningful tool for catalyst characterization, especially for late transition metals. However, the results should be interpreted with great care and complemented with other available tests.^{[55],[56]}

1.4.6 Dibenzo[*a,e*]cyclooctatetraene (dct), a selective homotopic catalyst poison

Homotopic catalyst poisons selectively bind to the active site of a molecular ligand-

1 Homogeneous vs. Heterogeneous: Insights into Iron Group Metal-Catalyzed Reduction Reactions from Kinetic Poisoning Experiments

metal complex but do not strongly bind to metal surfaces. The major difference of both coordination environments is steric in nature. Molecular complexes may provide multiple neighboring coordination sites to a strongly binding (chelate) ligand, whereas metal surfaces have large flat surfaces that occupy sterical volumes of around 180° . Common homotopic poisons are phosphines,^[57] thiols^[58] or pyridines^{[6],[59]} that are anchored on polymers or silica supports to provide high steric hindrance. Active sites of heterotopic catalysts should be inaccessible due to the bulkiness of the high-molecular weight poisons. However, in some cases homotopic catalysts have remained active despite the coordination of potential poisons which may indicate reversible binding (*vide supra*).^{[57],[60]} Alternatively, matrix-bound poisons were observed to leach from the support materials under certain reaction conditions.^[58]

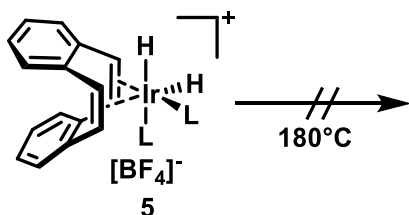


Scheme 1.17. Selective homotopic catalyst poisoning by dct.

A highly effective homotopic poisoning test for coinage metals is the method of dibenzo[*a,e*]cyclooctatetraene (dct) addition by Crabtree and coworkers.^{[61],[62]} Dct is a rigid, tub-like diene that adopts a twisted conformation so that the inner side of the diene pocket can accommodate single metal ions from molecular complexes. This bonding motif results in poor π -binding character and rather can be characterized as an electron-withdrawing σ -type bonding. Hence, a strongly electrophilic character of dct-complexes is observed, which is in the range of phosphites.^{[61],[63]} The nearly parallel orientation of the alkenes makes coordination to surfaces much less effective due to repulsion from the vinyl-H atoms.^{[61],[64]} The

1 Homogeneous vs. Heterogeneous: Insights into Iron Group Metal-Catalyzed Reduction Reactions from Kinetic Poisoning Experiments

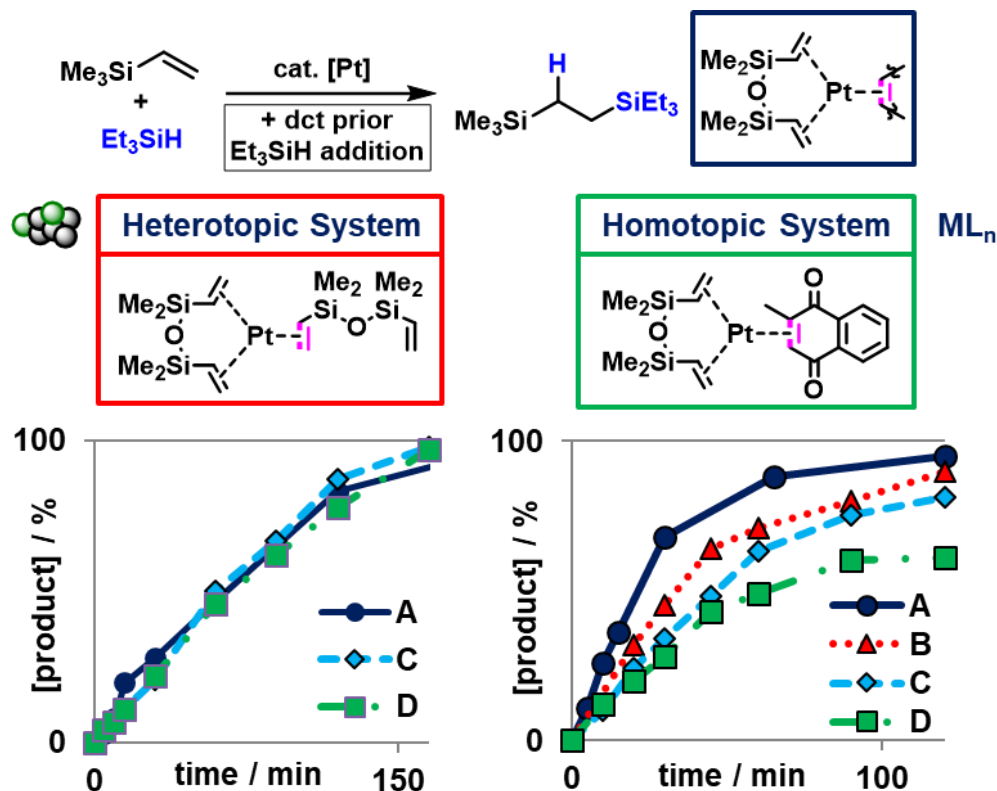
thermal stability of the (dct)Ir dihydride complex **5** represents the poisoned catalyst species formed in the Ir-catalyzed hydrogenation (Scheme 1.18).^[63]



Scheme 1.18. Stable (dct)(bishydrido)Iridium complex.

Dct has mostly been employed as effective poison of low-valent platinum group metal catalysts.^{[66],[67]} Fisher and coworkers applied dct to Pt-catalyzed hydrosilylations of alkenes. Addition of 5 equiv. dct per Pt (1 h prior to substrate addition!) inhibited catalyst turnover while lower poison loadings showed only partial inhibition (Scheme 1.19). On the other hand, dct had no effect on the hydrosilylation reaction with the Karstedt catalyst which acts as precursor to a heterotopic catalyst species that is formed by hydrosilylation of the alkene ligands and dissociation of the resultant alkylsilanes. For the complexation of dct to platinum group metals in reactions of alkenes as substrates, competing coordination of dct and substrates may require long reaction times until effective poisoning is observed. A rhodium-catalyzed hydrogenation showed activity shutdown when stirring dct with Wilkinson's catalyst for 2 h prior to catalysis.^[61] The degree of dct coordination can very well be monitored by ¹H-NMR spectroscopy if the metal forms diamagnetic complexes as with most of the 4d and 5d platinum group metals.^{[68],[69]} In contrast to the rich literature precedents of 4d and 5d metal catalyst poisoning by dct, there are only very few examples of related studies with 3d transition metals. In general, alkene complexes of the 3d row metals are substitutionally more labile than their heavier congeners.

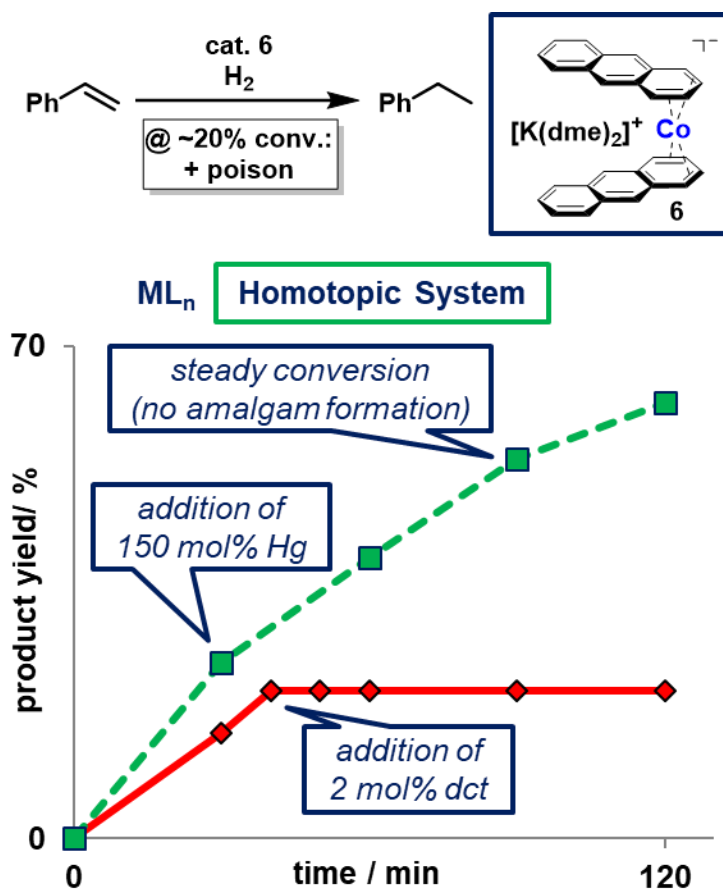
1 Homogeneous vs. Heterogeneous: Insights into Iron Group Metal-Catalyzed Reduction Reactions from Kinetic Poisoning Experiments



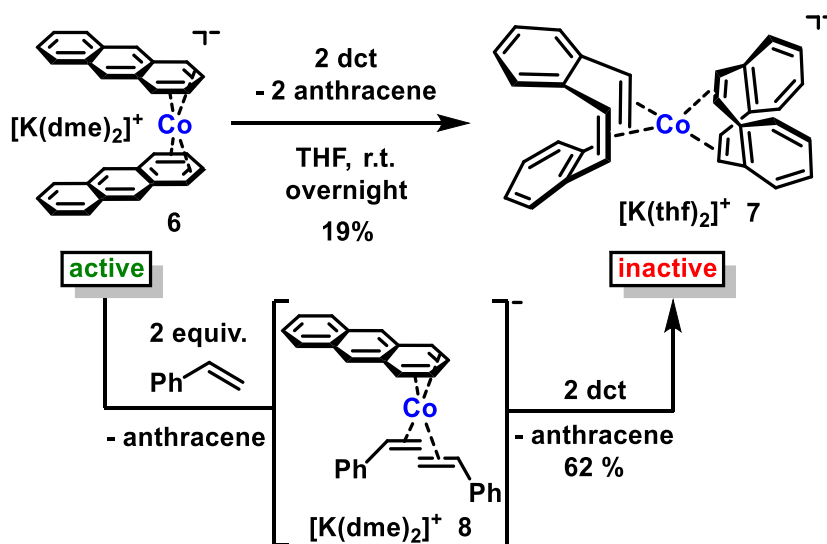
Scheme 1.19. Poisoning studies by dct-addition to pre-catalyst solutions 1 h prior to silane addition. A: without dct; B: 1 equiv.; C: 2 equiv.; D: 5 equiv. dct.^[66]

The utility of dct as effective poison for low-valent iron and cobalt catalysts has only recently been emphasized by the groups of Wolf and Jacobi von Wangelin.^{[18],[51],[68]-[72]} The complementary Hg and dct tests established the homotopic nature of the hydrogenation catalyst that formed under hydrogenation conditions from the pre-catalyst potassium bis(anthracene)cobaltate **6** (Scheme 1.20). No Hg poisoning was observed but complete inhibition by 2 equiv. dct per Co. The kinetic poisoning studies were corroborated by preparative studies: Treatment of **6** with 2 equiv. dct led to the isolation of the poisoned catalyst species, the homoleptic bis(dct)cobaltate complex **7** in 19% yield (Scheme 1.21). Notably, addition of 2 equiv. styrene allowed the isolation of **7** in 62% yield, which might proceed through an intermediary bis(styrene) complex **8**. Employment of catalytic amounts of **7** in the alkene hydrogenation gave no conversion.^[69]

1 Homogeneous vs. Heterogeneous: Insights into Iron Group Metal-Catalyzed Reduction Reactions from Kinetic Poisoning Experiments



Scheme 1.20. Hg and dct poisoning in Co-catalyzed alkene hydrogenations.^[69]

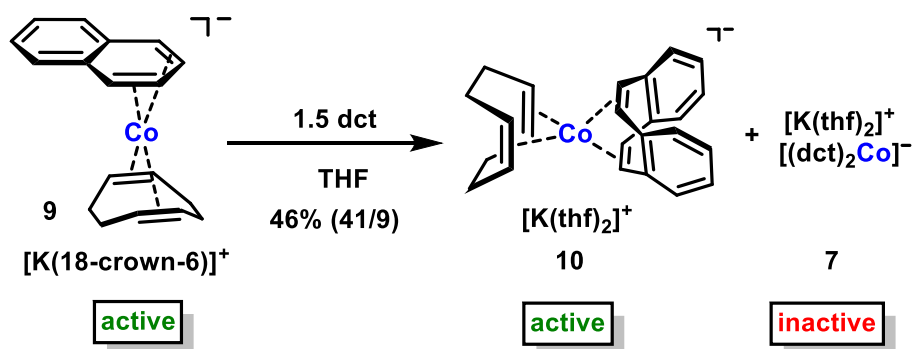


Scheme 1.21. Formation of bis(dct)cobaltate **7**.^[69]

However, in hydrogenation reactions with the related pre-catalyst (naphthalene)(cod)cobaltate **9**, only partial catalyst inhibition was recorded when

1 Homogeneous vs. Heterogeneous: Insights into Iron Group Metal-Catalyzed Reduction Reactions from Kinetic Poisoning Experiments

adding dct to the reaction. This observation was supported by the isolation of the mono(dct) complex **10** as major product from the reaction of **9** with dct (41%), alongside minor amounts of the homoleptic bis(dct) complex **7** (5%, Scheme 1.22). Indeed, **10** was an active hydrogenation catalyst, possibly due to rapid exchange of the cod ligand with the alkene substrates.^{[69],[73]}



Scheme 1.22. Formation of (dct)(cod)cobaltate **10**.^[69]

It is important to note that highly active heterotopic Fe and Co catalysts were shown to hydrogenate dct even under very mild conditions (r.t., 1 bar H₂), possibly by rapid leaching of metal (ions) into the bulk solution phase.^{[68],[70],[71]} These observations may interfere two commonly accepted principles of qualitative poisoning: dct is a poor ligand for metal particle catalysts, and dct hydrogenation is very slow in comparison with other alkenes. Likewise, partial poisoning of a homotopic catalyst and partial hydrogenation of dct under related conditions was observed.^[72] Dct is now commercially available but robust syntheses have been reported.^{[73],[74]} Despite several successful applications of dct as selective homotopic poison, issues of concern include the sometimes long poisoning times^[61] and the formation of catalytically active dct-metal complexes.^{[69],[73]} It is therefore advisable to couple the dct test with complementary poisoning. Overall, a multi-technique approach is desirable including *in operando* and *post operando* studies to understand the mechanism being operative.

1.5 Conclusions

The development of sustainable catalytic processes has become increasingly important in the past decades. Especially, catalysts based on abundant 3d metals such as Fe, Co and Ni constitute interesting alternatives to well-established noble metal catalysts. However, several constraints such as short lifetimes, low selectivities and activities, and little mechanistic insights may limit their implementation into lab-scale and technical syntheses. Mechanistic understanding is the key to catalyst optimizations and method development. The distinct catalytic mechanisms of 3d transition metals may prohibit the application of common analytical tools that have proven successful with heavier 4d and 5d metal complexes. Beyond the arsenal of sophisticated spectroscopic techniques, a small set of operationally facile kinetic studies may be consulted as *in operando* techniques to ascertain the catalytic mechanism and nature of the operating catalyst. This review has summarized key reports that utilized reaction progress analyses and kinetic poisoning experiments as analytical tools to distinguish between homotopic and heterotopic iron group metal catalysts. The application of quantitative poisoning with sub-catalytic amounts of PMe_3 has decisively enabled the elucidation of a heterotopic mechanism such as in the iron-catalyzed ATH by Morris and coworkers.^{[13],[22]} Contrarily, stoichiometric poisoning by PMe_3 indicated a homotopic mechanism in the iron-catalyzed hydroboration by Szymczak and coworkers.^[15] The former also displays a very insightful reaction progress analysis consisting of an induction period.^{[13],[22]} Lastly, qualitative poisons have been used such as the heterotopic poison Hg for cobalt-catalyzed hydroformylation by Kou and coworkers.^[48] The homotopic poison *dct* has been successfully applied by Wolf, Jacobi von Wangelin and coworkers in cobalt-catalyzed hydrogenation reactions.^[69] These experiments can be complemented with other techniques such as (hot) filtration tests, three-phase tests, spectroscopic or spectrometric methods.^{[6]-[9]} Future studies should not only focus on the clear distinction of homotopic and heterotopic catalysts but should also consider dynamic ‘cocktails’ of catalysts.^[9] Currently, there is only a small set of poisons available, mostly for the study of late transition metals in low oxidation states. The development of an even wider variety of selective poisonous ligands and the detailed understanding of their coordination abilities is certainly desirable in order to finely match the properties of the potential catalyst species in terms of size, oxidation state, and

1 Homogeneous vs. Heterogeneous: Insights into Iron Group Metal-Catalyzed Reduction Reactions from Kinetic Poisoning Experiments

coordination properties. Furthermore, the development of combined analytical tools comprising kinetic studies coupled to online spectroscopic methods may enhance the quality of mechanistic data.

Acknowledgement

This work was funded by the Deutsche Forschungsgemeinschaft (DFG, JA 1107/6-1) and by the European Research Council (ERC) through a Consolidator grant (683150).

Keywords: homogeneous catalysis · heterogeneous catalysis · reaction mechanism · iron · reductions

1.6 References

- [1] a) *The Handbook of Homogeneous Hydrogenation*, (Eds. J. G. de Vries, C. J. Elsevier), Wiley, Weinheim, **2007**; b) *Metal-Catalyzed Cross-Coupling Reactions and More* (Eds.: A. de Meijere, S. Bräse, M. Oestreich), Wiley, Weinheim, **2014**.
- [2] a) *Catalysis Without Non-Precious Metals* (Ed.: R. M. Bullock), Wiley, Weinheim, **2010**. b) *Non-Noble Metal Catalysis* (Eds.: R. J. M. Klein Gebbink, M.-E. Moret), Wiley, Weinheim, **2018**; c) *Homogeneous Hydrogenation with Non-Precious Catalysts* (Ed.: J. F. Teichert), Wiley, Weinheim, **2019**.
- [3] P. Chirik, R. Morris, *Acc. Chem. Res.* **2015**, *48*, 2495.
- [4] a) *Handbook on the Toxicology of Metals*, (Eds.: G. Nordberg, B. A. Fowler, M. Nordberg), Academic Press, Amsterdam, **2014**; b) K. S. Egorova, V. P. Ananikov, *Angew. Chem. Int. Ed.* **2016**, *55*, 12150; c) K. S. Egorova, V. P. Ananikov, *Organometallics* **2017**, *36*, 4071.
- [5] a) I. Bauer, H.-J. Knölker, *Chem. Rev.* **2015**, *115*, 3170; b) G. Cahiez, A. Moyeux, *Chem. Rev.* **2010**, *110*, 1435; c) P. Röse, G. Hilt, *Synthesis* **2016**, *48*, 463–492; d) A. Mukherjee, D. Milstein, *ACS Catal.* **2018**, *8*, 11435; e) W. Ai, R. Zhong, X. Liu, Q. Liu, *Chem. Rev.* **2019**, *119*, 2876; f) D. Wei, C. Darcel, *Chem. Rev.* **2019**, *119*, 2550; g) L. Alig, M. Fritz, S. Schneider, *Chem. Rev.* **2019**, *119*, 2681; h) T. Irrgang, R. Kempe, *Chem. Rev.* **2019**, *119*, 2524; i) D. Formenti, F. Ferretti, F. K. Scharnagl, M. Beller, *Chem. Rev.* **2019**, *119*, 2611.
- [6] R. H. Crabtree, *Chem. Rev.* **2012**, *112*, 1536.
- [7] J. A. Widegren, R. G. Finke, *J. Mol. Catal. A* **2003**, *198*, 317.
- [8] J. J. Stracke, R. G. Finke, *ACS Catal.* **2014**, *4*, 909.
- [9] D. B. Eremin, V. P. Ananikov, *Coord. Chem. Rev.* **2017**, *346*, 2.
- [10] a) M. J. Russell, C. White, P. M. Maitlis, *J. Chem. Soc., Chem. Commun.* **1977**, 427; b) J. P. Collman, K. M. Kosydar, M. Bressan, W. Lamanna, T. Garrett, *J. Am. Chem. Soc.* **1984**, *106*, 2569; c) C. M. Hagen, J. A. Widegren, P. M. Maitlis, R. G. Finke, *J. Am. Chem. Soc.* **2005**, *127*, 4423; d) E. Bayram, J. C. Linehan, J. L. Fulton, J. A. S. Roberts, N. K. Szymczak, T. D. Smurthwaite, S. Özkar, M. Balasubramanian, R. G. Finke, *J. Am. Chem. Soc.* **2011**, *133*, 18889; e) E. Bayram, J. C. Linehan, J. L. Fulton, N. K. Szymczak, R. G. Finke, *ACS Catal.* **2015**, *5*, 3876; f) S. Kim, F. Loose, M. J. Bezdek, X. Wang, P. J. Chirik, *J. Am. Chem. Soc.* **2019**, *141*, 17900.

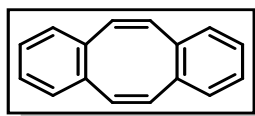
- [11] a) D. Astruc, F. Lu, J. R. Aranzaes, *Angew. Chem. Int. Ed.* **2005**, *44*, 7852; b) A. Roucoux, J. Schulz, H. Patin, *Chem. Rev.* **2002**, *102*, 3757; c) B. Chaudret, *Top. Organomet. Chem.* **2005**, *16*, 234; d) D. Astruc, *Nanoparticles and Catalysis*, Wiley, Weinheim, **2008**; e) D. Wang, D. Astruc, *Chem. Soc. Rev.* **2017**, *46*, 816.
- [12] J. Schwartz, *Acc. Chem. Res.* **1985**, *18*, 302.
- [13] J. F. Sonnenberg, R. H. Morris, *Catal. Sci. Technol.* **2014**, *4*, 3426.
- [14] a) D. G. Blackmond, *Angew. Chem. Int. Ed.* **2005**, *44*, 4302; b) D. G. Blackmond, *J. Am. Chem. Soc.* **2015**, *137*, 10852; c) J. Burés, *Angew. Chem. Int. Ed.* **2016**, *55*, 2028.
- [15] K.-N. T. Tseng, J. W. Kampf, N. K. Szymczak, *ACS Catal.* **2015**, *5*, 411.
- [16] A. A. Mikhailine, M. I. Maishan, A. J. Lough, R. H. Morris, *J. Am. Chem. Soc.* **2012**, *134*, 12266.
- [17] E. Reyes-Rodriguez, *Master Thesis*, University of Regensburg, **2014**.
- [18] D. Gärtner, A. L. Stein, S. Grupe, J. Arp, A. Jacobi von Wangelin, *Angew. Chem. Int. Ed.* **2015**, *54*, 10545.
- [19] a) S. B. Muñoz, S. L. Daifuku, J. D. Sears, T. M. Baker, S. H. Carpenter, W. W. Brennessel, M. L. Neidig, *Angew. Chem. Int. Ed.* **2018**, *57*, 6496; b) J. D. Sears, S. B. Muñoz, S. L. Daifuku, A. A. Shaps, S. H. Carpenter, W. W. Brennessel, M. L. Neidig, *Angew. Chem. Int. Ed.* **2019**, *58*, 2769; c) S. Sandl, A. Jacobi von Wangelin, *Angew. Chem. Int. Ed.* **2020**, 10.1002/anie.201914844.
- [20] T. Furukawa, M. Tobisu, N. Chatani, *Chem. Commun.* **2015**, *51*, 6508.
- [21] a) M. Heitbaum, F. Glorius, I. Escher, *Angew. Chem. Int. Ed.* **2006**, *45*, 4732; b) *Handbook of Asymmetric Heterogeneous Catalysis*, (Eds.: K. Ding and Y. Uozumi), Wiley-VCH, Weinheim, **2008**.
- [22] J. F. Sonnenberg, N. Coombs, P. A. Dube, R. H. Morris, *J. Am. Chem. Soc.* **2012**, *134*, 5893.
- [23] N. Meyer, A. J. Lough, R. H. Morris, *Chem. Eur. J.* **2009**, *15*, 5605.
- [24] S. Gülak, O. Stepanek, J. Malberg, B. R. Rad, M. Kotorá, R. Wolf, A. Jacobi von Wangelin, *Chem. Sci.* **2013**, *4*, 776.
- [25] R. Imayoshi, H. Tanaka, Y. Matsuo, M. Yuki, K. Nakajima, K. Yoshizawa, Y. Nishibayashi, *Chem. Eur. J.* **2015**, *21*, 8905.

- [26] a) R. Spogliarich, J. Kašpar, M. Graziani, F. Morandini, *J. Organomet. Chem.* **1986**, 306, 407; b) M. C. Carrión, F. Sepúlveda, F. A. Jalón, B. R. Manzano, A. M. Rodríguez, *Organometallics* **2009**, 28, 3822.
- [27] R. H. Crabtree, *Chem. Rev.* **2015**, 115, 127.
- [28] W. M. Alley, I. K. Hamdemir, K. A. Johnson, R. G. Finke, *J. Mol. Catal. A* **2010**, 315, 1.
- [29] C. H. Bartholomew, *Appl. Catal. A* **2001**, 212, 17.
- [30] H. Lindlar, *Helv. Chim. Acta* **1952**, 35, 446.
- [31] R. M. Drost, V. Rosar, S. D. Marta, M. Lutz, N. Demitri, B. Milani, B. de Bruin, C. J. Elsevier, *ChemCatChem* **2015**, 7, 2095.
- [32] V. Artero, M. Fontecave, *Chem. Soc. Rev.* **2013**, 42, 2338.
- [33] T. J. Korstanje, J. Ivar van der Vlugt, C. J. Elsevier, B. de Bruin, *Science* **2015**, 350, 298.
- [34] Y. Li, S. Yu, X. Wu, J. Xiao, W. Shen, Z. Dong, J. Gao, *J. Am. Chem. Soc.* **2014**, 136, 4031.
- [35] C. Lichtenberg, M. Adelhardt, T. L. Gianetti, K. Meyer, B. de Bruin, H. Grützmacher, *ACS Catal.* **2015**, 5, 6230.
- [36] R. E. Cowley, M. R. Golder, N. A. Eckert, M. H. Al-Afyouni, P. L. Holland, *Organometallics* **2013**, 32, 5289.
- [37] R. B. Siedschlag, V. Bernales, K. D. Vogiatzis, N. Planas, L. J. Clouston, E. Bill, L. Gagliardi, C. C. Lu, *J. Am. Chem. Soc.* **2015**, 137, 4638.
- [38] E. Bayram, J. C. Linehan, J. L. Fulton, J. A. S. Roberts, N. K. Szymczak, T. D. Smurthwaite, S. Özkar, M. Balasubramanian, R. G. Finke, *J. Am. Chem. Soc.* **2011**, 133, 18889.
- [39] M. R. Eberhard, *Org. Lett.* **2004**, 6, 2125.
- [40] E. Alberico, P. Sponholz, C. Cordes, M. Nielsen, H.-J. Drexler, W. Baumann, H. Junge, M. Beller, *Angew. Chem. Int. Ed.* **2013**, 52, 14162.
- [41] W. J. Bailey, S. A. Buckler, *J. Am. Chem. Soc.* **1957**, 79, 3567.
- [42] a) P. Bhattacharya, J. A. Krause, H. Guan, *J. Am. Chem. Soc.* **2014**, 136, 11153; b) P. J. Dyson, *Dalton Trans.* **2003**, 2964.
- [43] a) *Metals in Mercury* (Eds.: A. S. Kertes, C. Hirayama, Z. Galus, C. Guminski), Pergamon Press, New York, USA, **1986**; b) P. Paklepa, J. Woroniecki, P. Wrona, *J. Electroanal. Chem.* **2001**, 498, 181.
- [44] C. Gumiński, *J. Mater. Sci.* **1989**, 24, 3285.

- [45] H. R. Kirchmayr, *Monatshefte Chem.* **1964**, *95*, 1479.
- [46] a) C. Guminski, *J. Phase Equilibria* **1993**, *14*, 643; b) S. Mørup, S. Linderroth, J. Jacobsen, M. Holmblad, *Hyperfine Interact.* **1992**, *69*, 489; c) S. Linderroth, S. Morup, *J. Phys.: Condens. Matter* **1992**, *4*, 8627.
- [47] C. Chen, T. R. Dugan, W. W. Brennessel, D. J. Weix, P. L. Holland, *J. Am. Chem. Soc.* **2014**, *136*, 945.
- [48] Z. Cai, H. Wang, C. Xiao, M. Zhong, D. Ma, Y. Kou, *J. Mol. Catal. A* **2010**, *330*, 94.
- [49] Y. Ren, M. Yan, J. Wang, Z. C. Zhang, K. Yao, *Angew. Chem. Int. Ed.* **2013**, *52*, 12674.
- [50] A. G. Sergeev, J. D. Webb, J. F. Hartwig, *J. Am. Chem. Soc.* **2012**, *134*, 20226.
- [51] P. Büschelberger, E. Reyes-Rodriguez, C. Schöttle, J. Treptow, C. Feldmann, A. Jacobi von Wangelin, R. Wolf, *Catal. Sci. Technol.* **2018**, *8*, 2648.
- [52] A. G. Sergeev, J. F. Hartwig, *Science* **2011**, *332*, 439.
- [53] a) R. A. Jones, F. M. Real, G. Wilkinson, A. M. R. Galas, M. B. Hursthouse, *J. Chem. Soc., Dalton Trans.* **1981**, 126; b) G. M. Whitesides, M. Hackett, R. L. Brainard, Lavalleye, Jean Paul P. M., A. F. Sowinski, A. N. Izumi, S. S. Moore, D. W. Brown, E. M. Staudt, *Organometallics* **1985**, *4*, 1819; c) V. M. Chernyshev, A. V. Astakhov, I. E. Chikunov, R. V. Tyurin, D. B. Eremin, G. S. Ranny, V. N. Khrustalev, V. P. Ananikov, *ACS Catal.* **2019**, *9*, 2984.
- [54] a) A. H. M de Vries, J. M. C. A. Mulders, J. H. M. Mommers, H. J. W. Henderickx, J. G. de Vries, *Org. Lett.* **2003**, *5*, 3285; b) M. T. Reetz, E. Westermann, R. Lohmer, G. Lohmer, *Tetrahedron Lett.* **1998**, *39*, 8449; c) C. Deraedt, D. Astruc, *Acc. Chem. Res.* **2014**, *47*, 494.
- [55] S. Chakraborty, W. W. Brennessel, W. D. Jones, *J. Am. Chem. Soc.* **2014**, *136*, 8564.
- [56] S. Chakraborty, P. O. Lagaditis, M. Förster, E. A. Bielinski, N. Hazari, M. C. Holthausen, W. D. Jones, S. Schneider, *ACS Catal.* **2014**, *4*, 3994.
- [57] B. H. Lipshutz, S. Tasler, W. Chrisman, B. Spliethoff, B. Tesche, *J. Org. Chem.* **2003**, *68*, 1177.
- [58] L. Huang, T. P. Ang, Z. Wang, J. Tan, J. Chen, P. K. Wong, *Inorg. Chem.* **2011**, *50*, 2094.
- [59] J. M. J. Fréchet, M. V. de Meftahi, *Brit. Poly. J.* **1984**, *16*, 193.

- [60] *Palladium-Catalyzed Coupling Reactions. Practical Aspects and Future Developments* (Ed.: Á. Molnár), Wiley-VCH, Weinheim, **2013**.
- [61] D. R. Anton, R. H. Crabtree, *Organometallics* **1983**, *2*, 855.
- [62] S. Sandl, A. Jacobi von Wangelin, *Dibenzo[a,e]cyclooctatetraene* in *Encyclopedia of Organic Reagents*, John Wiley & Sons, New York, **2019**.
- [63] D. R. Anton, R. H. Crabtree, *Organometallics* **1983**, *2*, 621.
- [64] L. N. Lewis, *Chem. Rev.* **1993**, *93*, 2693.
- [65] T. C. Mak, H. N. Wong, K. Hung Sze, L. Book, *J. Organomet. Chem.* **1983**, *255*, 123.
- [66] P. Steffanut, J. A. Osborn, A. DeCian, J. Fisher, *Chem. Eur. J.* **1998**, *4*, 2008.
- [67] a) S. G. Harsy, *Tetrahedron* **1990**, *46*, 7403; b) X. L. Luo, R. H. Crabtree, *J. Am. Chem. Soc.* **1989**, *111*, 2527.
- [68] S. Sandl, F. Schwarzhuber, S. Pöllath, J. Zweck, A. Jacobi von Wangelin, *Chem. Eur. J.* **2018**, *24*, 3403.
- [69] a) D. Gärtner, A. Welther, B. R. Rad, R. Wolf, A. Jacobi von Wangelin, *Angew. Chem. Int. Ed.* **2014**, *53*, 3722; b) P. Büschelberger, D. Gärtner, E. Reyes-Rodriguez, F. Kreyenschmidt, K. Koszinowski, A. Jacobi von Wangelin, R. Wolf, *Chem. Eur. J.* **2017**, *23*, 3139.
- [70] T. N. Gieshoff, M. Villa, A. Welther, M. Plois, U. Chakraborty, R. Wolf, A. Jacobi von Wangelin, *Green Chem.* **2015**, *17*, 1408.
- [71] T. N. Gieshoff, U. Chakraborty, M. Villa, A. Jacobi von Wangelin, *Angew. Chem. Int. Ed.* **2017**, *56*, 3585.
- [72] S. Sandl, T. M. Maier, N. P. van Leest, S. Kröncke, U. Chakraborty, S. Demeshko, K. Koszinowski, B. de Bruin, F. Meyer, M. Bodensteiner, C. Herrmann, R. Wolf, A. Jacobi von Wangelin, *ACS Catal.* **2019**, *9*, 7596.
- [73] a) S. Spiess, C. Welter, G. Franck, J.-P. Taquet, G. Helmchen, *Angew. Chem. Int. Ed.* **2008**, *47*, 7652; b) W. Chen, J. F. Hartwig, *J. Am. Chem. Soc.* **2013**, *135*, 2068; c) Y. Hiroi, N. Komine, S. Komiya, M. Hirano, *Organometallics* **2014**, *33*, 6604.
- [74] G. Franck, G. Helmchen, *Org. Synth.* **2020**, *97*, 66.

2 Dibenzo[a,e]cyclooctatetraene



Abstract: Dibenzo[a,e]cyclooctatetraene (dct) is a non-conjugated cyclic diene that finds widespread use as ligand in transition metal coordination chemistry. Most notably, dct has been used as selective poisoning ligand for homogeneous monometal complexes where the metal exists in low oxidation states.^{11,[1]}

[262-89-5] C₁₆H₁₂ (MW 204.27)

(olefins, heteroatom-free ligands, kinetic poisoning experiments, topicity, homogeneous catalysis)^[2]

¹¹ Reproduced with permission from: S. Sandl, A. Jacobi von Wangelin, *Dibenzo[a,e]cyclooctatetraene* in *Encyclopedia of Organic Reagents*, John Wiley & Sons, New York, **2019**. Copyright 2019 John Wiley & Sons, New York, schemes, figures and text may differ from published version.

Author contribution:

S. Sandl: Manuscript preparation.

A. Jacobi von Wangelin: Corresponding author.

2.1 General

Alternate Names: Dibenzo[a,e]cyclooctatetraene, dct, dbcot

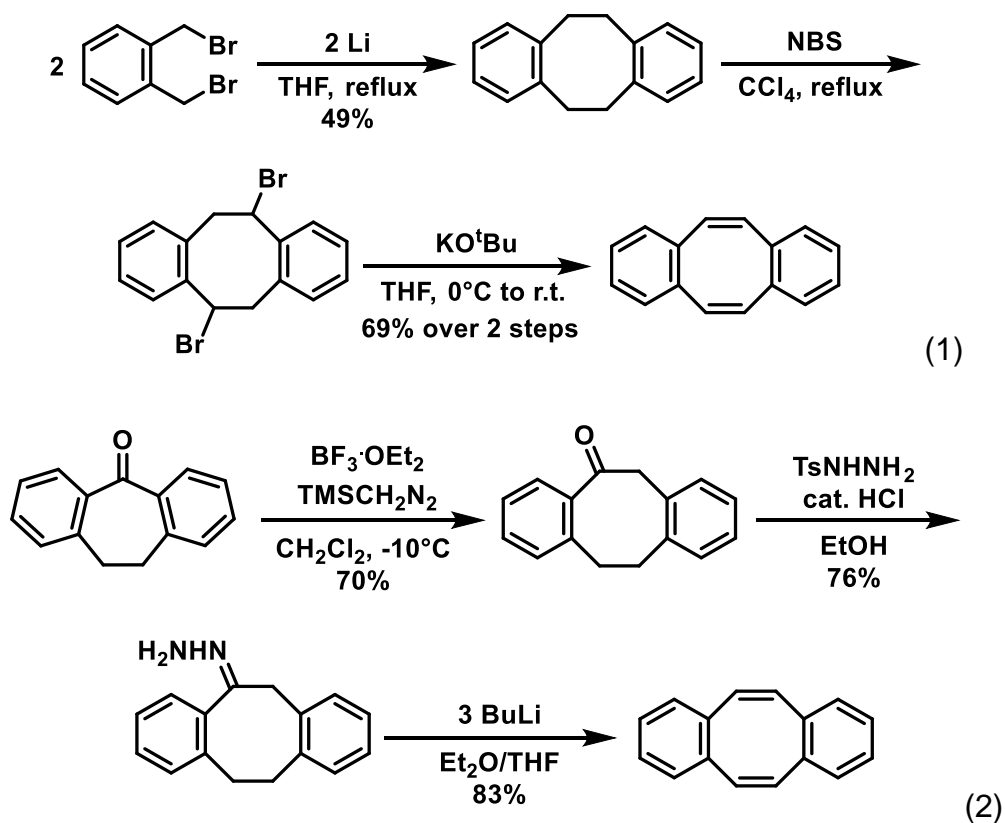
Physical data: mp 108.5-109.2 °C;^[3]

Appearance: Colorless plates;^{[1]b}

Solubility: THF; Et₂O, petrol ether (35 – 60°C);^{[1]b}

Analysis of reagent purity: ¹H NMR (CDCl₃, 300.13 MHz) δ 6.72 (s, 4 H, CH), 7.02–7.11 (m, 8 H, Ar-H); ¹³C NMR (CDCl₃, 100 MHz) δ 126.76 (d, CH), 129.03, 133.18 (2 d, C-Ar), 137.00 (s, C_{quart.}-Ar); IR (KBr): 3054, 3010, 1922, 1815, 1650, 1490, 1432, 1400, 1153, 1088, 1039 cm⁻¹; Anal. Calcd. for C₁₆H₁₂: C, 94.08; H, 5.92. Found C, 94.14; H, 6.14. HRMS: Calcd. for C₁₆H₁₃: 205.1017. Found: 205.1017. MS (EI, 70 eV): 204 (79), 203 (100), 202 (63), 176 (5); 150 (4), 101 (30), 88 (10), 76 (7).^{[1]b}

Preparative Methods: Commercially available in small quantities; synthesis of choice (i) by reductive coupling of α,α'-dibromo-*o*-xylene with lithium, subsequent bromination and elimination (eq 1)^{[1]b} or (ii) from 5-dibenzosuberone by homologation and elimination (eq 2).^[4]



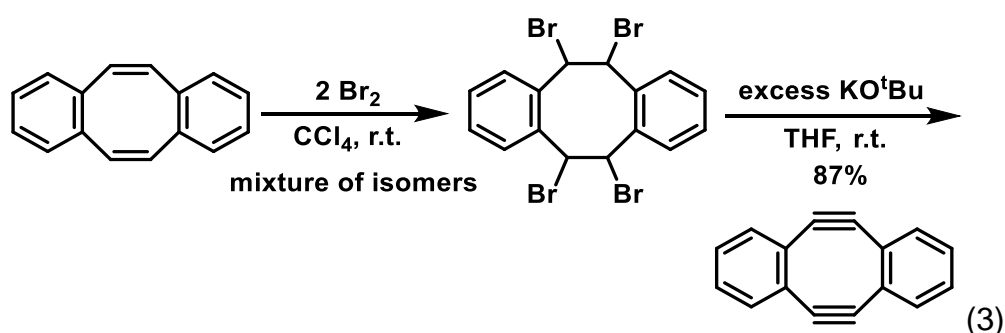
First synthesis was developed by Fieser and Pechet in 1946.^{[1]a} Other approaches involve the Wittig reaction;^[5] decarboxylation;^[6] usage of Ni(CO)₄ and mercury amalgam;^[7] or photoisomerization.^[8]

Purification: Kugelrohr distillation or column chromatography (petrol ether (35 – 60°C)).^{[1]b}

Handling, Storage, and Precautions: Air-, moisture-stable; Caution: α,α'-dibromo-o-xylene in organic solvents is lachrymatory. CCl₄ is toxic.

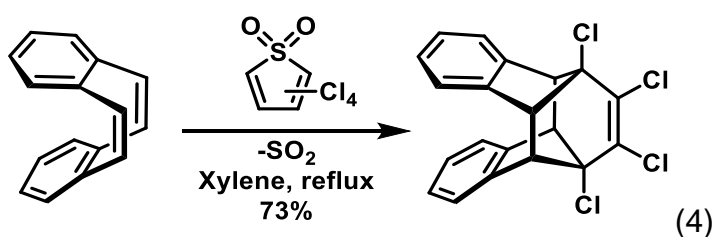
2.2 Organic Transformations

Electrophilic addition. Dct has been used to obtain the corresponding cyclooctadiyne derivative (eq 3).^{[4]a}



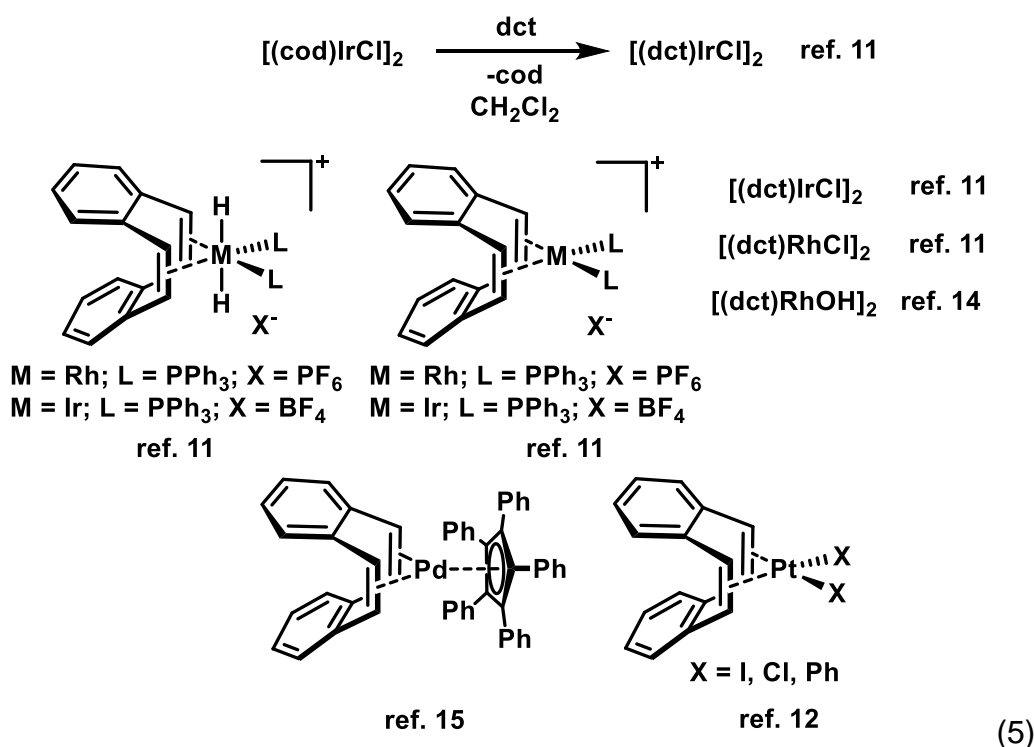
Epoxidation. Heterogeneous Ti catalysts enabled the epoxidation of dct.^[9]

Cycloaddition. Dct has been employed in consecutive [2+4]-cycloadditions (eq 4).^[10]

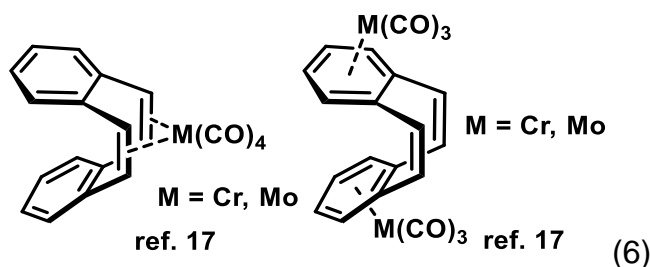


2.3 Organometallic Synthesis

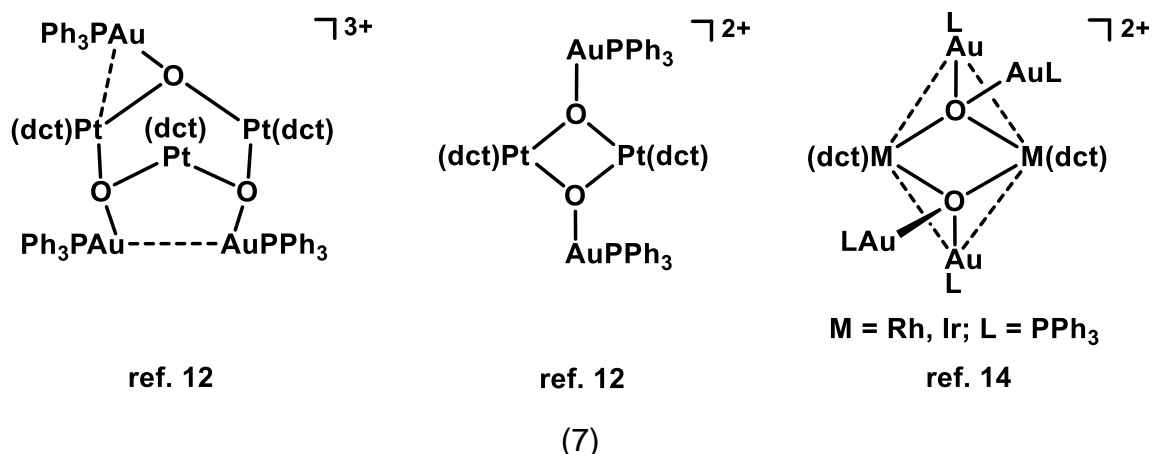
General considerations. As in most of its transition metal complexes, free dct adopts a rigid tub shaped C_{2v} configuration. The twisted orientation of the (non-conjugated) aryl substituents prohibit effective π -donation, but an electron-withdrawing σ -type donation of the alkene units is possible. Hence, dct binds more strongly to metals than cod and ligand exchange is facile (eq 5).^{[1],[11]} However, in case of Pt^{II} , competition experiments suggested that cod is the stronger ligand.^[12] A highly electrophilic character of dct-metal complexes was proposed based on Tolman-type electronic parameters for $L_2Mo(CO)_4$.^[11] Metal coordination can be monitored by a significant high-field shift of the olefinic protons in 1H -NMR spectra.^{[1],[13]} Various **coinage metal** complexes have been synthesized (eq 5).^{[11],[12],[14],[15],[12]}



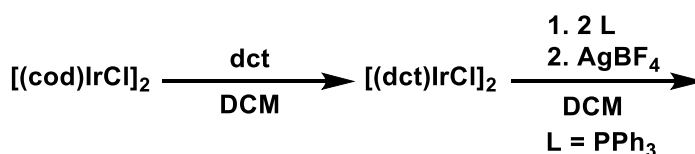
Group 6. The distinct stereo-electronic properties of dct allowed the isolation of highly unusual alkene complexes of group 6 metals, such as chromium or molybdenum (eq 6).^[11]

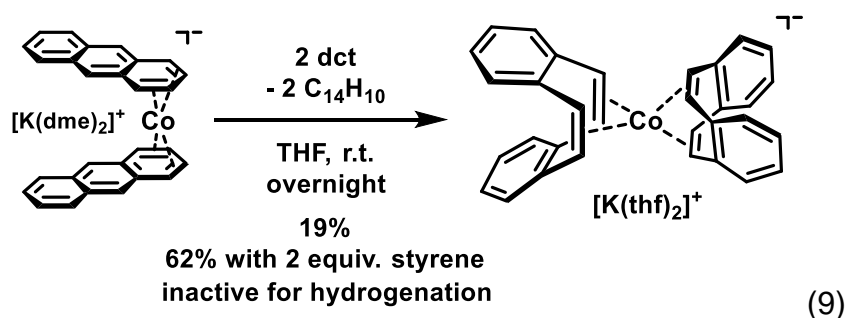
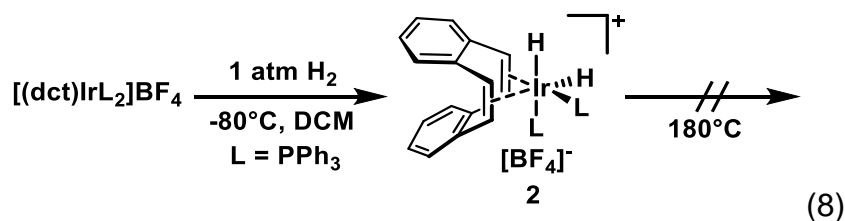


Heterometallic complexes have been synthesized with coinage metals, such as palladium, platinum and gold (eq 7).^{[12],[14]}



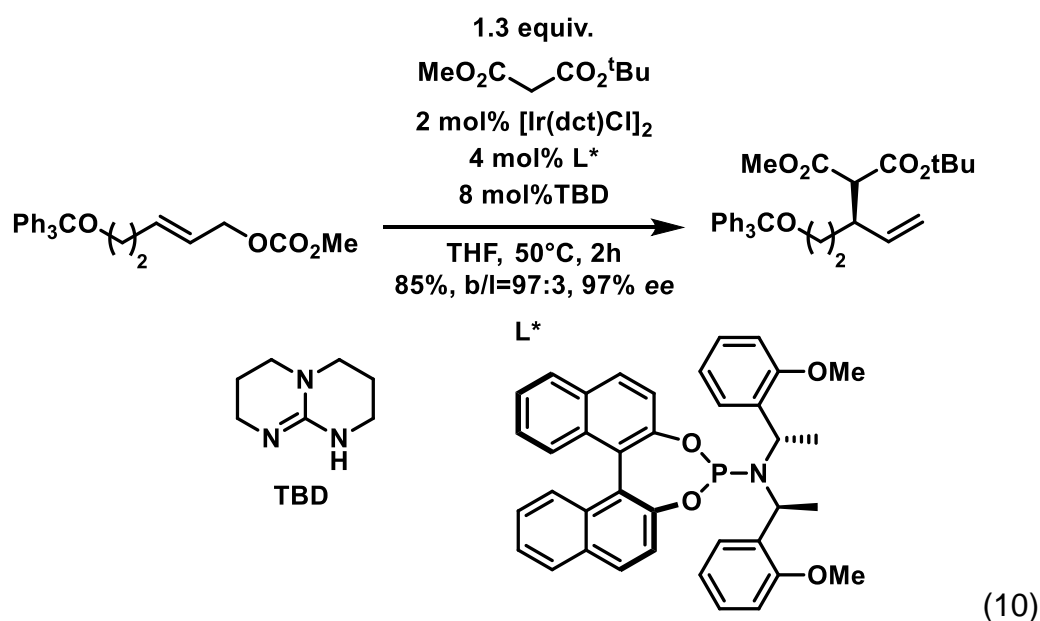
Crabtree's poisoning test. Due to its strong binding character,^{[1],[11]} dct has been used to determine the topicity of platinum group catalysts. Successful poisoning of catalysis by dct indicates a homotopic catalyst being operative, even though additional experiments, such as reaction progress analysis and a complementary heterotopic kinetic poisoning test, may prove beneficial.^[2] The thermal stability of **2** illustrates the poisoning effect of dct in its corresponding Ir-catalyzed hydrogenation reaction (eq 8).^[2] Recently, the validity of the dct test was also indicated for 3d metals in catalytic olefin hydrogenation reactions by catalytic and preparative studies by Jacobi von Wangelin, Wolf and coworkers (eq 9).^[18] Heterotopic hydrogenation catalysts have been shown to hydrogenate dct.^{[13],[19]}





2.4 Catalysis^[1]

Helmchen and coworkers developed an Ir-catalyzed **asymmetric allylic substitution** reaction. The air-stable catalyst consists of dct and phosphoramidites. Dct leads in contrast to the related cod-based catalyst to higher air stability and regioselectivity in the allylic substitution.^{[20],[4]b} The catalyst was applied to the **total synthesis** of (+)-cryptocaryone and (+)-infectocaryone (eq 10).^[21]



Polymerization. Dct has been used as ligand in Rh-catalyzed polymerization of acetylene.^[22]

Asymmetric Catalysis. Chiral substituted dct derivatives were employed in Rh/Ir-catalyzed **enantioselective hydroborations** of ketones,^[23] asymmetric Rh-catalyzed **1,2- and 1,4-hydroarylations**,^[24] and Rh-catalyzed **[5+2]-cycloadditions**.^[25] A racemic dct derivative was kinetically resolved by organometallic complexation.^[23]

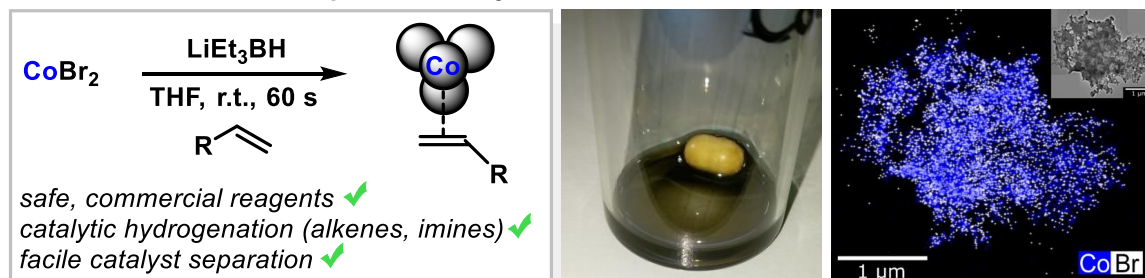
2.5 References

- [1] (a) L. F. Fieser, M. M. Pechet, *J. Am. Chem. Soc.* **1946**, *68*, 2577–2580; (b) G. Franck, M. Brill, G. Helmchen, *Org. Synth.* **2012**, *89*, 55; (c) J. B. Johnson, T. Rovis, *Angew. Chem. Int. Ed.* **2008**, *47*, 840–871; (d) C. Defieber, H. Grützmacher, E. M. Carreira, *Angew. Chem. Int. Ed.* **2008**, *47*, 4482–4502.
- [2] a) J. A. Widegren, R. G. Finke, *J. Mol. Catal. A* **2004**, *198*, 317–341; b) D. Astruc, F. Lu, J. R. Aranzaes, *Angew. Chem. Int. Ed.* **2005**, *44*, 7852–7872; c) R. H. Crabtree, *Chem. Rev.* **2012**, *112*, 1536–1554; d) D. R. Anton, R. H. Crabtree, *Organometallics* **1983**, *2*, 855–859.
- [3] G. Wittig, H. Tenhaeff, W. Schoch, G. Koenig, *Liebigs Ann. Chem.* **1951**, *572*, 1–22.
- [4] a) S. Chaffins, M. Brettreich, F. Wudl, *Synthesis* **2002**, 1191–1194; b) W. Chen, J. F. Hartwig, *J. Am. Chem. Soc.* **2013**, *135*, 2068–2071.
- [5] C. E. Griffin, J. A. Peters, *J. Org. Chem.* **1963**, *28*, 1715–1716.
- [6] A. C. Cope, S. W. Fenton, *J. Am. Chem. Soc.* **1951**, *73*, 1668–1673.
- [7] M. Avram, D. Dinu, G. Mateescu, C. D. Nenitzescu, *Chem Ber.* **1960**, *93*, 1789–1794.
- [8] a) P. W. Rabideau, J. B. Hamilton, L. Friedman, *J. Am. Chem. Soc.* **1968**, *90*, 4465–4466; b) X. M. Wang, X. Hou, Z. Zhou, T. C. W. Mak, H. N. C. Wong, *J. Org. Chem.* **1993**, *58*, 7498–7506.
- [9] I. Mandache, V. I. Parvulescu, A. Popescu, L. Pârvulescu, M. D. Banciu, P. Amoros, D. Beltran, D. T. On, S. Kaliaguine, *Microporous Mesoporous Mater.* **2005**, *81*, 115–124.
- [10] W.-D. Fessner, G. Sedelmeier, L. Knothe, H. Prinzbach, G. Rihs, Z.-Z. Yang, B. Kovac, E. Heilbronner, *Helv. Chim. Acta* **1987**, *70*, 1816–1842.
- [11] D. R. Anton, R. H. Crabtree, *Organometallics* **1983**, *2*, 621–627.
- [12] a) S. Shekhar, J. F. Hartwig, *J. Am. Chem. Soc.* **2004**, *126*, 13016–13027; b) A. Singh, P. R. Sharp, *Organometallics* **2006**, *25*, 678–683.
- [13] S. Sandl, F. Schwarzhuber, S. Pöllath, J. Zweck, A. Jacobi von Wangelin, *Chem. Eur. J.* **2018**, *24*, 3403–3407.
- [14] A. Singh, P. R. Sharp, *Inorg. Chim. Acta* **2008**, *361*, 3159–3164.
- [15] J. A. DeGray, W. E. Geiger, G. A. Lane, P. H. Rieger, *Inorg. Chem.* **1991**, *30*, 4100–4102.
- [16] G. Wittig, H. Eggers, P. Duffner, *Liebigs Ann. Chem.* **1958**, *619*, 10–27.

- [17] a) J. Müller, P. Göser, M. Elia, *Angew. Chem. Int. Ed.* **1969**, *8*, 374–375; b) M. Brown, J. D. Zubkowski, E. J. Valente, G. Yang, W. P. Henry, *J. Organomet. Chem.* **2000**, *613*, 111–118.
- [18] a) D. Gärtner, A. Welther, B. R. Rad, R. Wolf, A. Jacobi von Wangelin, *Angew. Chem. Int. Ed.* **2014**, *53*, 3722–3726; b) P. Büschelberger, D. Gärtner, E. Reyes-Rodriguez, F. Kreyenschmidt, K. Koszinowski, A. Jacobi von Wangelin, R. Wolf, *Chem. Eur. J.* **2017**, *23*, 3139–3151.
- [19] a) T. N. Gieshoff, M. Villa, A. Welther, M. Plois, U. Chakraborty, R. Wolf, A. Jacobi von Wangelin, *Green Chem.* **2015**, *17*, 1408–1413; b) T. N. Gieshoff, U. Chakraborty, M. Villa, A. Jacobi von Wangelin, *Angew. Chem. Int. Ed.* **2017**, *56*, 3585–3589; c) U. Chakraborty, E. Reyes-Rodriguez, S. Demeshko, F. Meyer, A. Jacobi von Wangelin, *Angew. Chem. Int. Ed.* **2018**, *57*, 4970–4975; d) T. M. Maier, S. Sandl, I. G. Shenderovich, A. Jacobi von Wangelin, J. J. Weigand, R. Wolf, *Chem. Eur. J.* **2019**, 238–245.
- [20] S. Spiess, C. Welter, G. Franck, J.-P. Taquet, G. Helmchen, G., *Angew. Chem. Int. Ed.* **2008**, *47*, 7652–7655.
- [21] G. Franck, K. Brödner, G. Helmchen, G., *Org. Lett.* **2010**, *12*, 3886–3889.
- [22] P. Zhang, H. Wang, X. Shi, X. Yan, X. Wu, S. Zhang, B. Yao, X. Feng, J. Zhi, X. Li, et al., *J. Polym. Sci. A* **2017**, *55*, 716–725.
- [23] F. Läng, F. Breher, D. Stein, H. Grützmacher, *Organometallics* **2005**, *24*, 2997–3007.
- [24] M.-C. Melcher, T. Ivšić, C. Olagnon, C. Tenten, A. Lützen, D. Strand, *Chem. Eur. J.* **2018**, *24*, 2344–2348.
- [25] P. A. Wender, A. B. Lesser, L. E. Sirois, *Angew. Chem. Int. Ed.* **2012**, *51*, 2736–2740; (b) X. Xu, P. Liu, A. Lesser, L. E. Sirois, P. A. Wender, K. N. Houk, *J. Am. Chem. Soc.* **2012**, *134*, 11012–11025.

3 Olefin-Stabilized Cobalt Nanoparticles for C=C, C=O and C=N Hydrogenations^{III}

Olefin-stabilized Co nanoparticle catalysts



Abstract: The development of cobalt catalysts that combine easy accessibility and high selectivity constitutes a promising approach to the replacement of noble metal catalysts in hydrogenation reactions. This report introduces a user-friendly protocol that avoids complex ligands, hazardous reductants, special reaction conditions, and the formation of highly unstable pre-catalysts. Reduction of CoBr_2 with LiEt_3BH in the presence of alkenes led to the formation of hydrogenation catalysts which effected clean conversions of alkenes, carbonyls, imines, and heteroarenes at mild conditions (3 mol% cat., 2-10 bar H_2 , 20-80 °C). Poisoning studies and nanoparticle characterization by TEM, EDX, and DLS supported the notion of a heterotopic catalysis mechanism.

^{III} Reproduced with permission from: S. Sandl, F. Schwarzhuber, S. Pöllath, J. Zweck, A. Jacobi von Wangelin, *Chem. Eur. J.* **2018**, *24*, 3403–3407. Copyright 2018 WILEY-VCH Verlag GmbH & Co. KGaA, Weinheim; schemes, figures and text may differ from published version.

Author contribution:

S. Sandl: Development of the catalytic reaction conditions (Table 3.1, Scheme 3.2); investigation of the reaction mechanism (Scheme 3.5); investigation of the substrate scope with technical assistance by H. Sterzel and M. Eisenhofer (Scheme 3.3 / 3.4); manuscript preparation.

F. Schwarzhuber and S. Pöllath: TEM and EDX measurements (Figure 3.1).

J. Zweck and A. Jacobi von Wangelin: Corresponding authors.

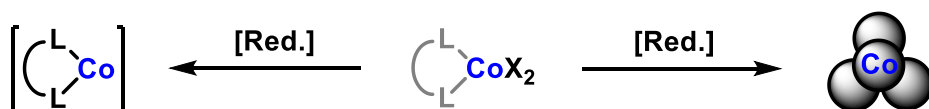
3.1 Introduction

The rational design of ligands holds the key to the development of efficient metal-catalyzed transformations and their mechanistic understanding.^[1] Special attention has been directed at the stabilization of coordinatively unsaturated low-valent metal catalysts to prevent ligand dissociation and catalyst aggregation to larger inactive particles.^[1] Most protocols utilize organic ligands with heteroatom donor functions such as amines and phosphines. Simple alkenes are a highly under-utilized class of ligands for low-valent metal species, despite their wide availability, high modularity, and well-established coordination chemistry. In the context of catalytic hydrogenations, labile π -coordination of olefins to homogeneous and heterogeneous catalysts could enable steric and/or electronic stabilization of dormant catalyst sites, prevent aggregation to larger inactive species, and undergo rapid exchange with the reaction substrates.^[3] Low-valent metal-olefin complexes such as $\text{Ni}(\text{cod})_2$ ^[4], $[\text{Pd}_2(\text{dba})_3]$,^[5] $[\text{Pt}_2(\text{dvds})_3]$ have been frequently employed as pre-catalysts (cod = 1,5-cyclooctadiene, dba = dibenzylidene acetone, dvds = divinyltetramethyl disiloxane).^[3] Several homogeneous and heterogeneous cobalt catalysts have recently been developed for alkene hydrogenations; yet olefin-cobalt catalysts have seen only very few applications.^{[6],[7],[8]} Efficient molecular Co catalysts bearing amine, phosphine, and *N*-heterocyclic carbene ligands were reported by the groups of Beller, Chirik, Fout, Hanson, Kempe, and others.^{[9],[10]} Heterogeneous^[11] Co catalysts formed from the reduction of cobalt(II) salts exhibited equally good catalytic activities in hydrogenations of alkenes and polar C=X bonds. However, the reduction of Co(II) precursors by strong reductants such as organometallics or hydrides has often led to ill-defined, highly sensitive, and rapidly ageing catalyst species. An early example from Takegami et al. used a $\text{CoCl}_2/\text{LiAlH}_4$ catalyst for hydrogenations of a few internal olefins, but the scope and experimental details were scarce.^[12] Recently, similar procedures were reported with heterogeneous catalysts prepared by chemical reduction, solvothermal or pyrolytic syntheses.^{[9],[13]} We envisioned the formation of active cobalt catalysts by the reduction of Co salts with a simple reductant in the presence of an olefin co-catalyst that acts as a placeholder for vacant coordination sites during catalyst operation. Here, we report the synthesis of olefin-stabilized Co nanoparticles and their application to catalytic hydrogenations of alkenes,

3 Olefin-Stabilized Cobalt Nanoparticles for C=C, C=O and C=N Hydrogenations

carbonyls, and imines. This catalytic system presents tangible advances over current protocols: *i)* the active catalyst is prepared from commercial reagents; *ii)* an inexpensive olefin is employed, instead of a complex ligand, which is traceless when being consumed under the hydrogenation conditions, *iii)* the complete consumption of all unsaturated components at the end of the reaction triggers catalyst aggregation and allows facile catalyst separation (Scheme 3.1).^[14]

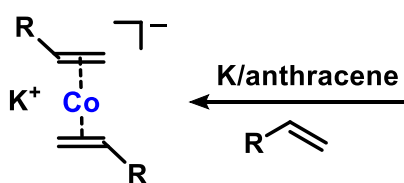
Homogeneous & heterogeneous Co catalysts:



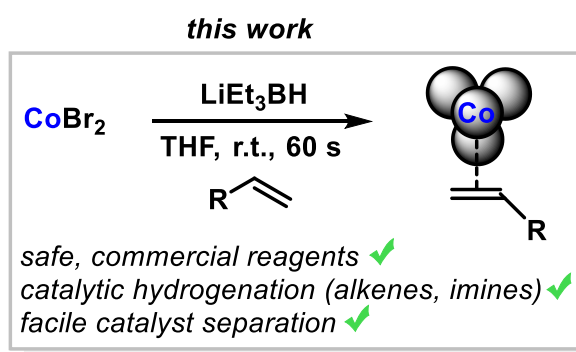
few recent reports: ref. [10]

several reports: ref. [13],[14]

Olefin-stabilized Co catalysts:



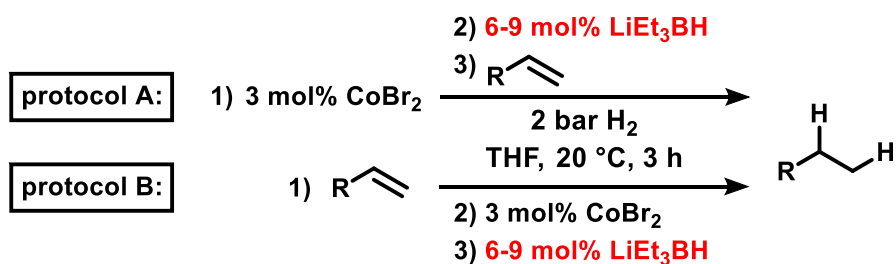
Wolf, Jacobi von Wangelin:
ref. [8]

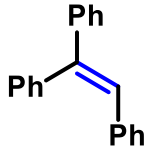



Scheme 3.1. Cobalt catalysts for hydrogenation reactions.

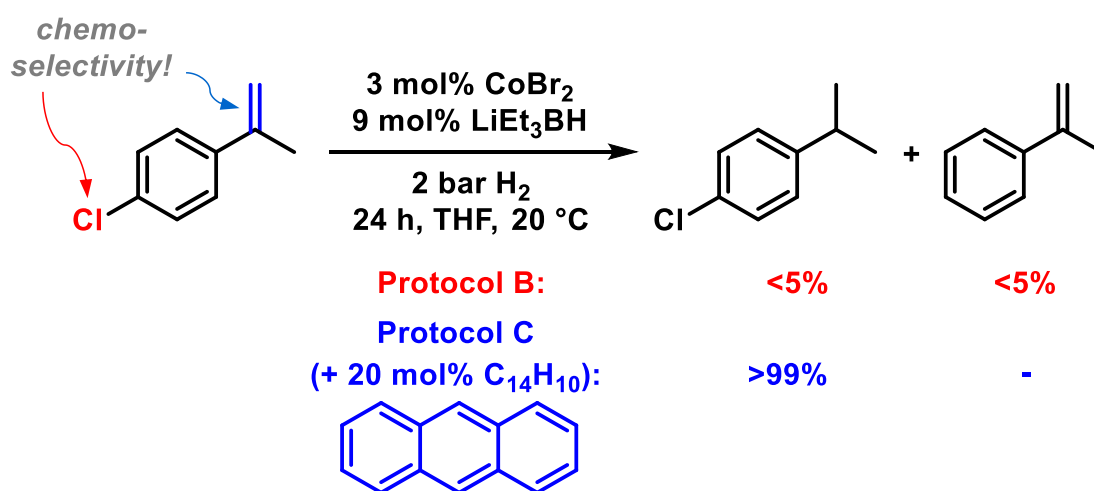
3.2 Results and Discussion

We initiated our investigations with the simple pre-catalyst mixture of CoBr_2 and LiEt_3BH (lithium triethylborohydride) and three model substrates: 4-octene, triphenylethylene, and the bifunctional alkene 4-chloro- α -methylstyrene (Table 3.1).^[15] The order of reagent additions was crucial to the catalytic activity. Reductive catalyst formation from CoBr_2 and LiEt_3BH (ratio 1:2) resulted in low catalytic activity due to catalyst precipitation (protocol A: entries 1, 4, 5). A higher reductant concentration was required for effective hydrogenation of 4-octene at 2 bar H_2 and 20 °C (entry 2). An alternative protocol involved pre-catalyst reduction in the presence of the olefinic substrate to prevent rapid catalyst ageing. The resultant black solution gave clean hydrogenation of 4-octene and the challenging triphenylethylene in excellent yields (protocol B: entries 3, 7).^[16] The addition of the hydride reagent^[17] to the solution of CoBr_2 and alkene might give rise to selectivity issues if the alkene itself was sensitive to reduction. Indeed, hydrogenation of 4-chloro- α -methylstyrene was inhibited under the conditions of protocol B. Therefore, we developed a protocol where anthracene was employed as additive during the pre-catalyst reduction step to stabilize vacant coordination sites and prevent catalyst aggregation (protocol C).^[8] Naphthalene and toluene were no competent surfactants but led to catalyst precipitation. Addition of the bifunctional 4-chloro- α -methylstyrene^[18] to a solution containing anthracene, CoBr_2 , and LiEt_3BH resulted in a dark solution that underwent clean hydrogenation of the alkene. Hydrodechlorination was not observed (Scheme 3.2). The operational simplicity and unprecedentedly mild conditions make protocol B the most effective heterogeneous cobalt-catalyzed olefin hydrogenation reported.^{[12],[13]}

Table 3.1. Optimization experiments.

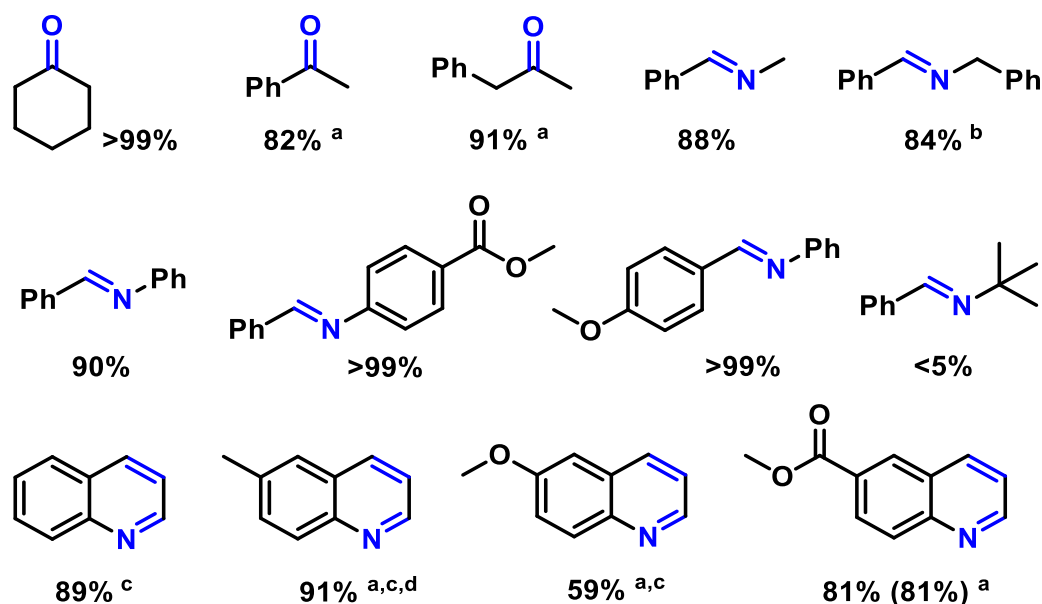
Entry	Alkene	Protocol	mol% LiEt ₃ BH	Yield [%]
1	4-octene	A	6	0 (8) ^a
2		A	9	94 ^a
3		B	6	98 ^a
4		A	6	0 (15) ^a
5		A	9	24 (35) ^a
6		B	6	71 (74)
7		B	9	>99 ^b
8		B	9	<5 (<5)

Conditions: 0.2 mmol (0.2 M) alkene in THF, 3 mol% CoBr₂, 6-9 mol% LiEt₃BH, 2 bar H₂, 20 °C, 3 h. Yields (GC-FID vs. internal *n*-pentadecane); conversions in parentheses if <90%. ^a catalyst precipitation. ^b 1 h.

**Scheme 3.2.** High chemoselectivity toward alkene hydrogenation (protocol C).

3 Olefin-Stabilized Cobalt Nanoparticles for C=C, C=O and C=N Hydrogenations

The optimized conditions of protocol B (for unfunctionalized alkenes) and protocol C (for alkenes with reduction-sensitive functions) were applied to various unsaturated substrates (Scheme 3.3). Mono-, di-, and tri-substituted alkenes were cleanly reacted at 2 bar H₂ and room temperature. The mild conditions of protocol C tolerated chloride, bromide, imide, hydroxyl, ether, and ester functions (Scheme 3.3, bottom).^[19] The catalyst solution obtained from anthracene, CoBr₂, and LiEt₃BH proved to be very stable and showed no loss of catalytic activity after storage for several hours at room temperature. Extensions of this methodology to the hydrogenation of polar C=X bonds such as ketones,^{[8],[13]c} imines,^[8] and quinolines^{[13]b,e} resulted in very good yields of the desired alcohols and amines (Scheme 3.4). While the activity of the ternary catalyst mixture anthracene/CoBr₂/LiEt₃BH is comparable to recent literature methods, this protocol exhibits much higher operational simplicity as no complex ligand or pre-catalyst is required and the catalyst preparation operates in situ by simple mixing of the components at room temperature prior to hydrogenation. To the best of our knowledge, this catalyst system constitutes the most active heterogeneous cobalt catalyst for ketone hydrogenation reactions^[13] which is equally active to our recently reported homogeneous bis(anthracene)cobaltate(-I).^[8] At the start of our studies, no heterogeneous Co catalyst was known for imine hydrogenations.^[13]



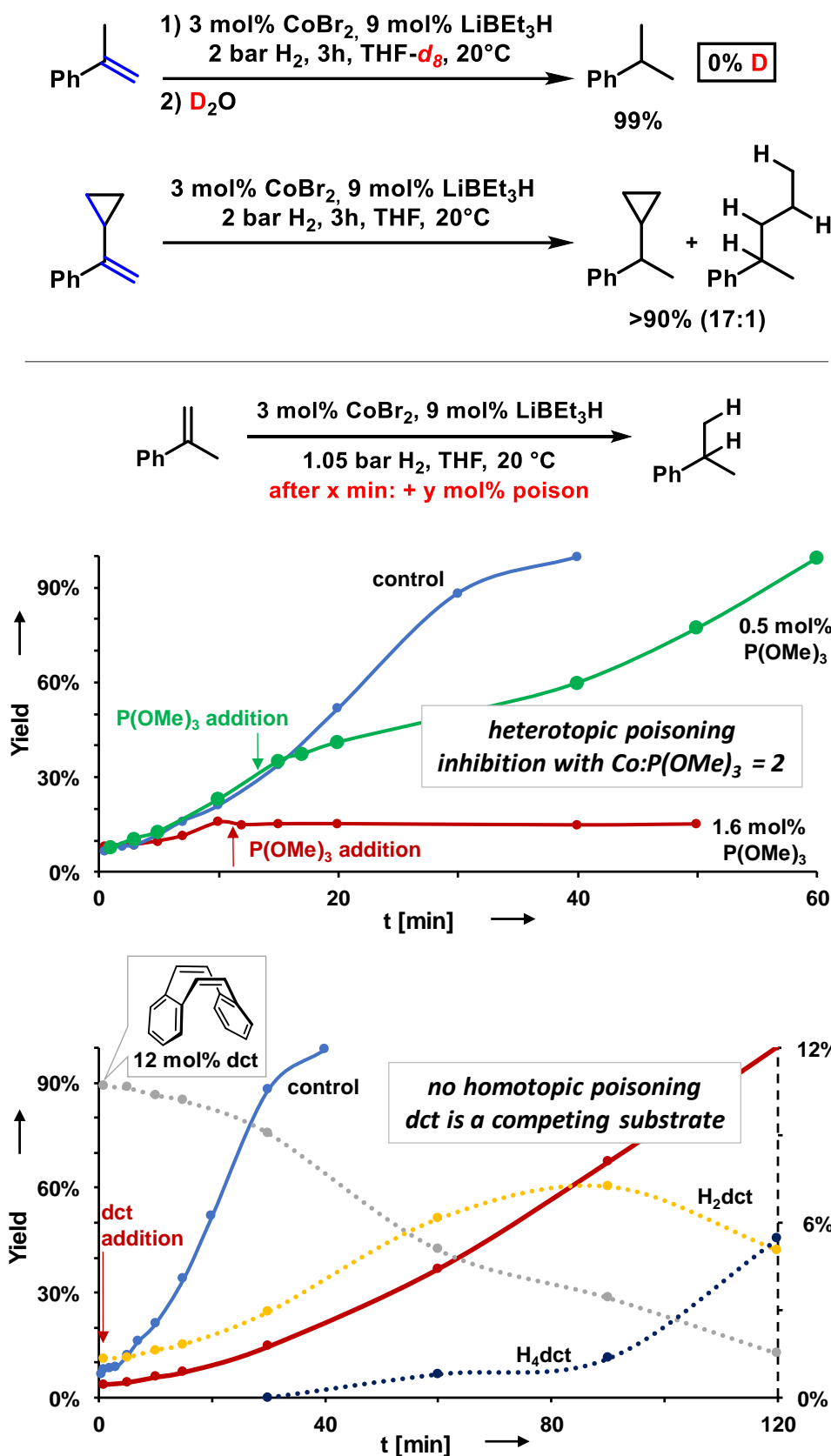
Scheme 3.4. Hydrogenation of ketones, imines, and quinolines. Blue bonds indicate the site of hydrogenation. Conditions: 0.2 mmol (0.2 M) substrate in THF, 3 mol% CoBr₂, 12 mol% anthracene, 9 mol% LiEt₃BH, 10 bar H₂, 60 °C, 24 h. GC-FID yields vs. internal *n*-pentadecane; conversions in parentheses if <90%. ^a 80 °C. ^b 30 mol% anthracene. ^c Protocol B. ^d traces of 6-methyl-5,6,7,8-tetrahydroquinoline.

Mechanistic studies were directed at the potential intermediacy of radical species and the nature of the active catalyst (Scheme 3.5). Reactions in THF-*d*₈ and work-up with D₂O afforded no deuterated products (Scheme 5, top). Only minimal ring-opening was obtained in the hydrogenation of the radical probe 1-cyclopropyl-1-phenyl-ethylene. Kinetic poisoning studies were performed to ascertain the topicity of the operating catalyst species (Scheme 3.5).^[20] Reaction progress analyses documented significant induction periods and a sigmoidal behaviour of product formation which is characteristic of nanocluster nucleation. This is in full agreement with poisoning studies that were performed with selective metal scavengers. Addition of “sub-catalytic” amounts of trimethyl-phosphite, P(OMe)₃, resulted in complete catalyst inhibition already at a catalyst/poison ratio of 2/1 (Scheme 5, middle, red curve).^{[8],[20]} The selective homogeneous catalyst poison dibenzo[*a,e*]cycloocta-tetraene^[21] (dct, 4 equiv. per Co) showed only a slight deceleration of *i*-propylbenzene formation (Scheme 3.5, bottom, red curve) and competing hydrogenation of dct (dotted lines).^[8] Based on these instructive experiments, we postulate a heterotopic mechanism that involves initial reduction

3 Olefin-Stabilized Cobalt Nanoparticles for C=C, C=O and C=N Hydrogenations

of CoBr_2 by LiEt_3BH and rapid aggregation of the resulting low-valent cobalt complexes to nano-particles (for further details, see the Supporting Information).^[22] The intermediacy of low-valent cobalt complexes from the reaction of CoBr_2 with LiBEt_3H (3 equiv.) and *dct* (10 equiv.) in THF was supported by $^1\text{H-NMR}$ experiments at low temperature. Clean formation of a molecular diamagnetic olefin-cobalt complex, very similar to the earlier reported bis(*dct*)cobaltate, was observed (see Supporting Information).^[8] The anthracene-stabilized Co nanoparticles were studied by transmission electron microscopy (TEM, Figure 3.1).^[22] Particle accumulations in the sub-10 μm range (Figure 3.1A) with high Co concentrations (from energy dispersive X-ray spectroscopy, EDX, Figure 3.1B) were observed. Co was exclusively detected within or at the periphery of the larger accumulations which accounts for >90% of total Co content. The Co concentration varied across the agglomerate, presumably due to particle stacking as a consequence of their inherent attractive magnetic moment and the evaporation of the organic solvent during the sample preparation (see Supporting Information). The grainy texture, visibility of crystalline structures as well as Moiré patterns with a size in the order of individual particles (*vide infra*) indicated that the accumulations mainly consist of individual Co particles (see Supporting Information). The presence of Br most likely originates from residual LiBr. High-resolution (HR)-TEM images showed well-separated particles in the sub-10 nm range at the periphery of the larger accumulations (Figure 3.1C). The upper panel of Figure 1D displays an image of two nanoparticles with crystalline structures which are also indicated by the distinct symmetrical spots in the diffractogram (see inset). The lattice constant was $\sim 2.5 \text{ \AA}$. The analysis of 124 individual nanoparticles at the periphery of larger accumulations showed an average particle size of 5.6 nm with a standard deviation of 1.7 nm (Figure 3.1C). The EDX spectrum of isolated particles displayed high Co concentration and very low Br content (Figure 3.1D).^[23]

3 Olefin-Stabilized Cobalt Nanoparticles for C=C, C=O and C=N Hydrogenations



Scheme 4.5. Key mechanistic experiments. Top: Deuteration and radical clock reactions. Bottom: Poisoning studies with trimethylphosphite (P(OMe)₃) and dibenzo[a,e]cyclooctatetraene (dct). Product yields of *i*PrPh on the left axis.

Dynamic light scattering (DLS) measurements with filtered solutions (through 450 nm filters) of the freshly prepared Co catalyst suspension documented the presence of polydisperse particles. Low-dispersion particles were observed after filtration through a 100 nm filter (Z-average: 142 nm, see Supporting Information). The obtained Z-average value is most likely a result of aggregation after filtration. The generally broad ^1H NMR resonances of the catalyst solutions further indicated the presence of particles.^[8]

3.3 Conclusion

In summary, we have developed an operationally simple cobalt-catalyzed hydrogenation of alkenes, ketones, imines, and hetero-arenes that does not require the presence of complex ligands or the elaborate synthesis of molecular pre-catalysts. The reaction operates at mild conditions with a catalyst that was prepared *in situ* from the three commercial reagents anthracene, CoBr_2 , and LiEt_3BH . The substrates or anthracene acted as π -ligands that stabilize the low-valent Co catalyst species and prevent the formation of higher aggregates. Poisoning studies indicated the formation of a hetero-topic catalyst which was characterized by TEM, EDX, and DLS. This protocol constitutes the most practical Co-catalyzed hydro-genation method of C=C and C=X bonds. We currently investigate applications of this catalyst to related reductive transformations.^[24]

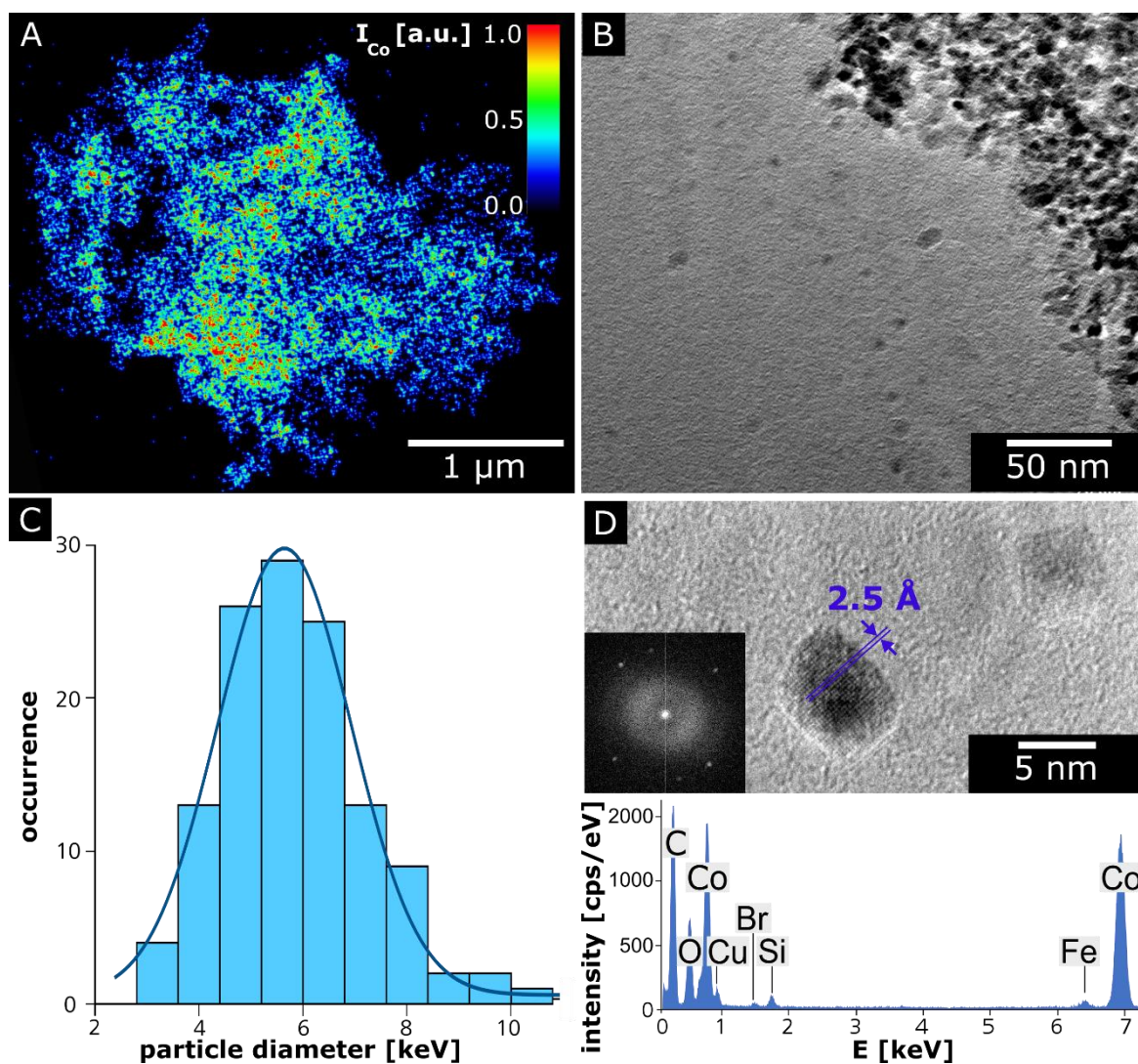


Figure 3.1. TEM measurements. A: Relative Co amount of particle accumulations by scanning EDX (color bars indicate relative Co abundance and scales with Co content per irradiated volume element, a.u. = arbitrary units). B: HR-TEM of separated particles at accumulation edges. C: Size distribution of 124 particles. D, top: Atomically resolved HR-TEM image of two crystalline particles with corresponding diffractogram (inset). D, bottom: EDX spectrum of single particles.

3.4 References

- [1] a) *The Handbook of Homogeneous Hydrogenation* (Eds.: J. G. de Vries, C. J. Elsevier), Wiley-VCH, Weinheim, **2007**; b) *Catalysis without Precious Metals* (Ed.: R. M. Bullock), Wiley-VCH, Weinheim, **2010**; c) *Metal-Catalyzed Cross-Coupling Reactions and More* (Eds.: A. de Meijere, S. Bräse, M. Oestreich), Wiley-VCH, Weinheim, **2014**.
- [2] a) B. E. Mann, A. Musco, *J. Chem. Soc., Dalton Trans.* **1975**, 1673; b) H. Urata, H. Suzuki, Y. Morooka, T. Ikawa, *J. Organomet. Chem.* **1989**, 364, 235; c) V. V. Grushin, C. Bensimon, H. Alper, *Organometallics* **1995**, 14, 3259; d) J. F. Hartwig, *Synlett* **1997**, 329; e) A. F. Littke, C. Dai, G. C. Fu, *J. Am. Chem. Soc.* **2000**, 122, 4020.
- [3] Olefin ligands in catalysis: a) J. B. Johnson, T. Rovis, *Angew. Chem. Int. Ed.* **2008**, 47, 840; b) C. Defieber, H. Grützmacher, E. M. Carreira, *Angew. Chem. Int. Ed.* **2008**, 47, 4482; c) B. M. Trost, M. C. Ryan, *Angew. Chem. Int. Ed.* **2017**, 56, 2862; d) M. Nagamoto, T. Nishimura, *ACS Catal.* **2017**, 7, 833.
- [4] a) G. Wilke, *Angew. Chem. Int. Ed.* **1988**, 27, 185; b) J. Montgomery, *Angew. Chem. Int. Ed.* **2004**, 43, 3890; c) S. Z. Tasker, E. A. Standley, T. F. Jamison, *Nature* **2014**, 299.
- [5] a) C. Amatore, A. Jutand, *Coord. Chem. Rev.* **1998**, 178–180, 511; b) I. J. S. Fairlamb, A. R. Kapdi, A. F. Lee, G. P. McGlacken, F. Weissburger, A. H. M. de Vries, L. Schmieder-van de Vondervoort, *Chem. Eur. J.* **2006**, 12, 8750.
- [6] Olefin/arene Fe and Co complexes: a) J. E. Ellis, *Inorg. Chem.* **2006**, 45, 3167; b) A. Fürstner, R. Martin, H. Krause, G. Seidel, R. Goddard, C. W. Lehmann, *J. Am. Chem. Soc.* **2008**, 130, 8773; c) K. Weber, E. M. Schnöckelborg, R. Wolf, *ChemCatChem* **2011**, 3, 1572; d) W. W. Brennessel, J. E. Ellis, *Inorg. Chem.* **2012**, 51, 9076.
- [7] a) S. Gülak, A. Jacobi von Wangelin, *Angew. Chem Int. Ed.* **2012**, 51, 1357; b) S. Gülak, T. N. Gieshoff, A. Jacobi von Wangelin, *Adv. Synth. Catal.* **2013**, 355, 2197; c) S. Gülak, O. Stepanek, J. Malberg, B. R. Rad, M. Kotorá, R. Wolf, A. Jacobi von Wangelin, *Chem. Sci.* **2013**, 4, 776.
- [8] a) D. Gärtner, A. Welther, B. R. Rad, R. Wolf, A. Jacobi von Wangelin, *Angew. Chem. Int. Ed.* **2014**, 53, 3722; b) P. Büschelberger, D. Gärtner, E. Reyes-Rodriguez, F. Kreyenschmidt, K. Koszinowski, A. Jacobi von Wangelin, R. Wolf, *Chem. Eur. J.* **2017**, 23, 3139.

- [9] a) W. Hess, J. Treutwein, G. Hilt, *Synthesis* **2008**, *40*, 3537; b) M. S. Holzwarth, B. Plietker, *ChemCatChem* **2013**, *5*, 1650; c) P. Gandeepan, C. H. Cheng, *Acc. Chem. Res.* **2015**, *48*, 1194; d) P. Röse, G. Hilt, *Synthesis* **2016**, *48*, 463.
- [10] Recent examples: a) G. Zhang, B. L. Scott, S. K. Hanson, *Angew. Chem. Int. Ed.* **2012**, *51*, 12102; b) R. P. Yu, J. M. Darmon, C. Milsman, G. W. Margulieux, S. C. E. Stieber, S. Debeer, P. J. Chirik, *J. Am. Chem. Soc.* **2013**, *135*, 13168; c) S. Rösler, J. Obenauf, R. Kempe, *J. Am. Chem. Soc.* **2015**, *137*, 7998; d) K. Tokmic, C. R. Markus, L. Zhu, A. R. Fout, *J. Am. Chem. Soc.* **2016**, *138*, 11907; e) R. Adam, J. R. Cabrero-Antonino, A. Spannenberg, K. Junge, R. Jackstell, M. Beller, *Angew. Chem. Int. Ed.* **2017**, *56*, 3216.
- [11] S. Nishimura, *Handbook of Heterogeneous Catalytic Hydrogenation for Organic Synthesis*; Wiley, New York, **2001**.
- [12] Y. Takegami, T. Ueno, T. Fujii, *Bull. Chem. Soc. Jpn.* **1965**, *38*, 1279.
- [13] Selected examples: a) F. K. Schmidt, Y. Titova, L. B. Belykh, V. A. Umanets, S. S. Khutsishvili, *Russ. J. Gen. Chem.* **2012**, *82*, 1334; b) F. Chen, A.-E. Surkus, L. He, M.-M. Pohl, J. Radnik, C. Topf, K. Junge, M. Beller, *J. Am. Chem. Soc.* **2015**, *137*, 11718; c) F. Chen, C. Topf, J. Radnik, C. Kreyenschulte, H. Lund, M. Schneider, A. E. Surkus, L. He, K. Junge, M. Beller, *J. Am. Chem. Soc.* **2016**, *138*, 8781; d) T. Schwob, R. Kempe, *Angew. Chem. Int. Ed.* **2016**, *55*, 15175; e) Z. Wei, Y. Chen, J. Wang, D. Su, M. Tang, S. Mao, Y. Wang, *ACS Catal.* **2016**, *6*, 5816; f) R. V. Jagadeesh, K. Murugesan, A. S. Alshammari, H. Neumann, M.-M. Pohl, J. Radnik, M. Beller, *Science* **2017**, *358*, 326.
- [14] Nanoparticles from $\text{Co}(\eta^3\text{-C}_8\text{H}_{13})(\eta^4\text{-C}_8\text{H}_{12})$: J. Osuna, D. De Caro, C. Amiens, B. Chaudret, E. Snoeck, M. Respaud, J.-M. Broto, A. Fert, *J. Phys. Chem.* **1996**, *100*, 14571.
- [15] a) B. A. F. Le Bailly, M. D. Greenhalgh, S. P. Thomas, *Chem. Commun.* **2012**, *48*, 1580; b) T. S. Carter, L. Guiet, D. J. Frank, J. West, S. P. Thomas, *Adv. Synth. Catal.* **2013**, *355*, 880; c) J. H. Docherty, J. Peng, A. P. Dominey, S. P. Thomas, *Nat. Chem.* **2017**, *9*, 595.
- [16] a) $\text{CoBr}_2/\text{LiEt}_3\text{BH}$, THF: H. Bönemann, W. Brijoux, R. Brinkmann, R. Fretzen, T. Jousen, R. Köppler, B. Korall, P. Neiteler, J. Richter, *J. Mol. Catal.* **1994**, *86*, 129; b) $\text{MX}_2 \cdot \text{THF}/\text{KEt}_3\text{BH}$: H. Bönemann, G. Braun, W. Brijoux, R. Brinkmann, A. S. Tilling, K. Seevogel, K. Siepen, *J. Organomet. Chem.* **1996**,

- 520, 143; c) $\text{CoBr}_2/\text{NR}_4\text{Et}_3\text{BH}$: H. Bönemann, W. Brijoux, R. Brinkmann, E. Dinjus, T. Joußen, B. Korall, *Angew. Chem. Int. Ed.* **1991**, *30*, 1312; d) $\text{CoBr}_2/\text{pyridine}/\text{LiEt}_3\text{BH}$, toluene: T. Andou, Y. Saga, H. Komai, S. Matsunaga, M. Kanai, *Angew. Chem. Int. Ed.* **2013**, *52*, 3213.
- [17] a) H. C. Brown, S. C. Kim, S. Krishnamurthy, *J. Org. Chem.* **1980**, *45*, 1; b) S. Krishnamurthy, H. C. Brown, *J. Org. Chem.* **1983**, *48*, 3085.
- [18] a) Minimal hydrodehalogenation was observed when the alkene was reduced in the presence of CoBr_2 (Table 1, entry 9); see Supporting Information for further optimization studies.
- [19] α -Methylstyrene was hydrogenated in the presence of functional additives (1 equiv., protocol C, 3 h, 20 °C, 1 mL THF): Catalyst activity was unaffected by added aniline, 2-phenylpyridine, and ethyl benzoate, respectively. Slightly lower catalyst activities were observed in the presence of isopulegol, phenol, acetanilides, and benzophenone, respectively. Addition of benzonitrile and benzaldehyde, respectively, inhibited the alkene hydrogenation. See Supporting Information.
- [20] a) J. A. Widegren, R. G. Finke, *J. Mol. Catal. A* **2003**, *198*, 317; b) D. Astruc, F. Lu, J. Ruiz Aranzaes, *Angew. Chem. Int. Ed.* **2005**, *44*, 7852; c) R. H. Crabtree, *Chem. Rev.* **2012**, *112*, 1536.
- [21] a) D. R. Anton, R. H. Crabtree, *Organometallics* **1983**, *2*, 855; b) G. Franck, M. Brill, G. Helmchen, *Org. Synth.* **2012**, *89*, 55.
- [22] a) D. Astruc, *Nanoparticles and Catalysis*, Wiley-VCH, Weinheim, **2008**; b) B. Chaudret, *Top. Organomet. Chem.* **2005**, *16*, 234.
- [23] The C, O, Cu, Si and Fe artefacts also showed up in blank experiments with unloaded support and grid materials (see Supporting Information).
- [24] a) M. Mayer, W. M. Czaplik, A. Jacobi von Wangelin, *Synlett* **2009**, 2919; b) W. M. Czaplik, M. Mayer, A. Jacobi von Wangelin, *Synlett* **2009**, 2931.

3.5 Supporting Information

3.5.1 General

Analytical Thin-Layer Chromatography: TLC was performed using aluminium plates with silica gel and fluorescent indicator (Merck, 60, F254). Thin layer chromatography plates were visualized by exposure to ultraviolet light (366 or 254 nm) or by immersion in a staining solution of molybdato-phosphoric acid in ethanol or potassium permanganate in water.

Column Chromatography: Flash column chromatography with silica gel 60 from KMF (0.040-0.063 mm). Mixtures of solvents used are noted in brackets.

Chemicals and Solvents: Commercially available olefins were distilled under reduced pressure prior use. Solvents (THF, Et₂O, n-hexane, toluene) were distilled over sodium and benzophenone and stored over molecular sieves (4 Å) under argon. Solvents used for column chromatography were distilled under reduced pressure prior use (ethyl acetate). Anthracene was sublimed prior use and stored under argon. LiEt₃BH (1 M in THF) was used as received from SigmaAldrich or diluted before use.

High Pressure Reactor: Hydrogenation reactions were carried out in 160 and 300 mL high pressure reactors (Parr™) in 4 mL glass vials. The reactors were loaded under argon, purged with H₂ (1 min), sealed and the internal pressure was adjusted. Hydrogen (99.9992%) was purchased from Linde.

¹H- und ¹³C-NMR-Spectroscopy: Nuclear magnetic resonance spectra were recorded on a Bruker Avance 300 (300 MHz) and Bruker Avance 400 (400 MHz). ¹H-NMR: The following abbreviations are used to indicate multiplicities: s = singlet; d = doublet; t = triplet, q = quartet; m = multiplet, dd = doublet of doublet, dt = doublet of triplet, dq = doublet of quartet. Chemical shift δ is given in ppm relative to tetramethylsilane.

Gas chromatography with FID (GC-FID): HP6890 GC-System with injector 7683B and Agilent 7820A System. Column: HP-5, 19091J-413 (30 m × 0.32 mm × 0.25 μm), carrier gas: N₂. GC-FID was used for reaction control and catalyst screening.

3 Olefin-Stabilized Cobalt Nanoparticles for C=C, C=O and C=N Hydrogenations

Calibration with internal standard *n*-pentadecane and analytically pure samples. Non-commercial authentic samples were prepared by hydrogenation with Pd/C/H₂.

Gas chromatography with mass-selective detector (GC-MS): Agilent 6890N Network GC-System, mass detector 5975 MS. Column: HP-5MS (30m × 0.25 mm × 0.25 μm, 5% phenylmethylsiloxane, carrier gas: H₂. Standard heating procedure: 50 °C (2 min), 25 °C/min -> 300 °C (5 min).

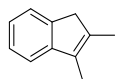
Dynamic Light Scattering: Zetasizer Nano ZS (Malvern Instruments, UK), 173° backward scatter and the general-purpose mode with automatic measurement position and attenuator selection at a temperature of 25°C was used. The maximum peak of the intensity distribution was stated / Z-Average values of the intensity distribution were stated.

TEM: (S)TEM FEI Tecnai F30 ST equipped with Bruker Quantax EDX System (AXS X-Flash detector 530) for both high-resolution imaging of particles with atomic resolution and spatially resolved element distribution (elemental mapping). Special vacuum transfer holder (Gatan) for specimen transfer to the microscope without exposure to ambient atmosphere. Reference spectra were taken close to, but apart from the Co particles to determine the spurious contributions of C, O, Cu, Si and Fe, which stem from the specimen support grid (holey carbon grid) and the microscope's pole pieces. EDX spectra and elemental map signals are on a relative scale.

3.5.2 Synthesis of catalysts, reagents, and starting materials

2,3-Dimethyl-1*H*-indene

Synthesis was performed by Gieshoff, Tim, *Dissertation 2017*, Regensburg, following the procedure described by M. V. Troutman, D. H. Appella, S. L. Buchwald, *J. Am. Chem. Soc.* **1999**, *121*, 4916–4917.

C₁₁H₁₂

144.22 g/mol

Appearance

colorless liquid

Yield

1.49 g, 10.3 mmol (69%)

TLC*R_f* = 0.66 (SiO₂, *n*-pentane)**¹H-NMR**

(300 MHz, CDCl₃) δ 7.37 (dp, *J* = 7.3, 0.9 Hz, 1H), 7.31 – 7.21 (m, 2H), 7.12 (td, *J* = 7.2, 1.5 Hz, 1H), 3.31 – 3.21 (m, 2H), 2.07 (q, *J* = 1.0 Hz, 3H), 2.04 (tq, *J* = 2.1, 1.1 Hz, 3H).

¹³C-NMR

(75 MHz, CDCl₃) δ 126.05, 123.55, 122.97, 117.91, 42.46, 13.95, 10.17.

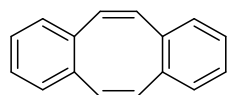
GC-MS

t_R = 6.77 min, (EI, 70 eV): *m/z* = 144 [M⁺], 129, 115, 89, 77, 63, 51.

Analytical data were in full agreement with M. G. Schrems, E. Neumann, A. Pfaltz, *Angew. Chem. Int. Ed.* **2007**, *46*, 8274–8276.

Dibenzo[*a,e*]cyclooctatetraene (dct)

Synthesis was performed by Gieshoff, Tim, *Dissertation 2017*, Regensburg., following the procedure described by G. Franck, M. Brill, G. Helmchen, *Org. Synth.* **2012**, *89*, 55-65.

C₁₆H₁₂

204.27 g/mol

Appearance

colorless solid

Yield

912 mg, 4.46 mmol (47%)

TLC*R_f* = 0.46 (SiO₂, hexanes)**¹H-NMR**

(300 MHz, CDCl₃): δ 7.19–7.13 (m, 4H), 7.10–7.02 (m, 4H), 6.76 (s, 4H).

¹³C-NMR (75 MHz, CDCl₃): δ 137.1, 133.3, 129.1, 126.8.

GC-MS *t_R* = 9.35 min, (EI, 70 eV): *m/z* = 204 [M⁺].

Analytical data were in full agreement with G. Franck, M. Brill, G. Helmchen, *Org. Synth.* **2012**, *89*, 55-65.

1-Phenyl-1-cyclopentene

Synthesis was performed by Schachtner, Josef, *Dissertation* **2016**, Regensburg., following the procedure described by G. Hu, J. Xu, P. Li, *Org. Lett.* **2014**, *16*, 6036–6039.



C₁₁H₁₂

144.22 g/mol

Appearance colorless liquid

Yield 1.99 g, 13.8 mmol (69%)

TLC *R_f* = 0.66 (SiO₂, hexanes)

¹H-NMR (300 MHz, CDCl₃) δ 7.48 – 7.42 (m, 2H), 7.36 – 7.27 (m, 2H), 7.25 – 7.18 (m, 1H), 6.19 (h, *J* = 2.1 Hz, 1H), 2.82 – 2.61 (m, 2H), 2.54 (tq, *J* = 7.6, 2.5 Hz, 2H), 2.15 – 1.93 (m, 2H).

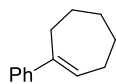
¹³C-NMR (75 MHz, CDCl₃) δ 128.29, 128.27, 127.60, 126.82, 126.12, 125.91, 125.54, 66.45, 33.37, 33.18, 28.91, 28.08, 23.37, 19.35.

GC-MS *t_R* = 6.94 min, (EI, 70 eV): *m/z* = 144 [M]⁺, 129, 115, 103, 91, 77, 63, 51.

Analytical data were in full agreement with W. Su, S. Urgaonkar, P. A. McLaughlin, J. G. Verkade, *J. Am. Chem. Soc.* **2004**, *126*, 16433–16439.

1-Phenyl-1-cycloheptene

Synthesis following a procedure by Schachtner, Josef, *Dissertation* **2016**, Regensburg., following the procedure described by G. Hu, J. Xu, P. Li, *Org. Lett.* **2014**, *16*, 6036–6039.



C₁₃H₁₆

172.27 g/mol

Appearance colorless liquid

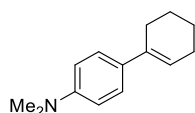
3 Olefin-Stabilized Cobalt Nanoparticles for C=C, C=O and C=N Hydrogenations

Yield	2.89 g, 16.8 mmol (84%)
TLC	$R_f = 0.69$ (SiO ₂ , hexanes)
¹H-NMR	(300 MHz, CDCl ₃) δ 7.42 – 7.16 (m, 5H), 6.13 (td, $J = 6.8, 1.3$ Hz, 1H), 2.75 – 2.52 (m, 2H), 2.43 – 2.25 (m, 2H), 1.94 – 1.80 (m, 2H), 1.74 – 1.50 (m, 4H).
¹³C-NMR	(75 MHz, CDCl ₃) δ 144.99, 130.45, 128.13, 126.26, 125.67, 32.86, 32.82, 28.92, 26.98, 26.85.
GC-MS	$t_R = 7.97$ min, (EI, 70 eV): $m/z = 172$ [M ⁺], 157, 144, 129, 115, 104, 91, 77, 63, 51.

Analytical data were in full agreement with G. Baddeley, J. Chadwick, H. T. Taylor, *J. Chem. Soc.* **1956**, 451.

4-(Cyclohex-1-enyl)-*N,N*-dimethylaniline

Synthesis was performed by Schachtner, Josef, *Dissertation* **2016**, Regensburg., following the procedure described by G. Hu, J. Xu, P. Li, *Org. Lett.* **2014**, *16*, 6036–6039.



	C ₁₄ H ₁₉ N
	201.31 g/mol
Appearance	colorless liquid
Yield	1.65 g, 8.20 mmol (82%)
TLC	$R_f = 0.82$ (SiO ₂ , hexanes)
¹H-NMR	(300 MHz, CDCl ₃) δ 7.41 – 7.19 (m, 2H), 6.76 (ddd, $J = 13.1, 6.8, 2.8$ Hz, 2H), 6.06 – 6.00 (m, 1H), 2.96 (d, $J = 2.8$ Hz, 6H), 2.35 – 2.49 (m, 2H), 2.27 – 2.14 (m, 2H), 1.87 – 1.73 (m, 2H), 1.61 – 1.72 (m, 2H).
¹³C-NMR	(75 MHz, CDCl ₃) δ 149.4, 136.0, 129.1, 125.6, 121.7, 116.7, 112.7, 112.6, 40.8, 40.7, 27.4, 25.9, 23.2, 22.4.
GC-MS	$t_R = 9.59$ min, (EI, 70 eV): $m/z = 202$ [M] ⁺ , 180, 157, 129, 101, 77, 51.

3 Olefin-Stabilized Cobalt Nanoparticles for C=C, C=O and C=N Hydrogenations

Analytical data were in full agreement with K. Ishiuka, H. Seike, T. Hatakeyama, M. Nakamura, *J. Am. Chem. Soc.* **2010**, *132*, 13117-13119.

(1-Cyclopropylvinyl)benzene

Synthesis was performed by Gieshoff, Tim, *Dissertation* **2017**, Regensburg.

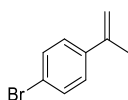


	C ₁₁ H ₁₂
	144.22 g/mol
Appearance	colorless liquid
Yield	1.27 g, 8.8 mmol (80%)
TLC	R _f = 0.53 (SiO ₂ , hexanes)
¹H-NMR	(300 MHz, CDCl ₃) δ 7.67 – 7.57 (m, 2H), 7.42 – 7.26 (m, 3H), 5.30 (d, J=1.0, 1H), 4.95 (t, J=1.2, 1H), 1.67 (ttt, J=8.3, 5.4, 1.2, 1H), 0.92 – 0.79 (m, 2H), 0.61 (ddd, J=6.4, 5.4, 4.1, 2H).
¹³C-NMR	(75 MHz, CDCl ₃) δ 149.47, 141.75, 128.28, 127.58, 126.25, 109.15, 77.58, 77.16, 77.16, 76.74, 15.78, 6.83.
GC-MS	t _R = 6.31 min, (EI, 70 eV): m/z = 144 [M ⁺], 129, 115, 103, 91, 77, 63, 51.

Analytical data were in full agreement with C. Chatalova-Sazepin, Q. Wang, G. M. Sammis, J. Zhu, *Angew. Chem. Int. Ed.* **2015**, *54*, 5443–5446.

4-Bromo- α -methylstyrene

Synthesis following a modified procedure by A. O. Terent'Ev, O. M. Mulina, D. A. Pirgach, D. V. Demchuk, M. A. Syroeshkin, G. I. Nikishin, *RSC Adv.* 2016, *6*, 93476.



	C ₉ H ₉ Br
	197.08 g/mol
Appearance	colorless oil
Yield	3.44 g, 17.5 mmol (83%)
TLC	R _f = 0.67 (SiO ₂ , n-pentane)

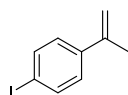
3 Olefin-Stabilized Cobalt Nanoparticles for C=C, C=O and C=N Hydrogenations

¹H-NMR	(400 MHz, CDCl ₃) δ 7.50-7.40 (m, 2H), 7.36-7.28 (m, 2H), 5.39 – 5.32 (m, 1H), 5.14 – 5.07 (m, 1H), 2.13 (s, 3H).
¹³C-NMR	(101 MHz, CDCl ₃) δ 142.2, 140.1, 131.3, 127.2, 121.3, 113.1, 21.7.
GC-MS	<i>t</i> _R = 6.01 min, (EI, 70 eV): <i>m/z</i> = 197 [M ⁺], 183, 171, 156, 115, 102, 91, 75, 63, 51.

Analytical data were in full agreement with T. Taniguchi, A. Yajima, H. Ishibashi, *Adv. Synth. Catal.* **2011**, 353, 2643–2647.

4-Iodo- α -methylstyrene

Synthesis was performed by T. N. Gieshoff, U. Chakraborty, M. Villa, A. Jacobi von Wangelin, *Angew. Chem. Int. Ed.* **2017**, 56, 3585.

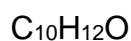


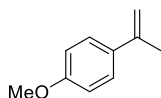
	C ₉ H ₉ I
	244.08 g/mol
Appearance	colorless solid
Yield	1.21 g, 4.96 mmol (71%)
TLC	<i>R</i> _f = 0.84 (SiO ₂ , <i>n</i> -pentane)
¹H-NMR	(300 MHz, CDCl ₃) δ 7.70 – 7.59 (m, 2H), 7.24 – 7.15 (m, 2H), 5.40 – 5.33 (m, 1H), 5.12 – 5.07 (m, 1H), 2.14 – 2.09 (m, 3H).
¹³C-NMR	(75 MHz, CDCl ₃) δ 142.28, 140.70, 137.27, 134.97, 127.41, 113.15, 92.88, 21.62.
GC-MS	<i>t</i> _R = 7.14 min, (EI, 70 eV): <i>m/z</i> = 244 [M ⁺], 127, 115, 102, 91, 75, 63, 50.

Analytical data were in full agreement with G. B. Bachman, C. L. Carlson, M. Robinson, *J. Am. Chem. Soc.* **1951**, 73, 1964–1965.

4-Methoxy- α -methylstyrene

Synthesis following a modified procedure by A. O. Terent'Ev, O. M. Mulina, D. A. Pirgach, D. V. Demchuk, M. A. Syroeshkin, G. I. Nikishin, *RSC Adv.* **2016**, 6, 93476.





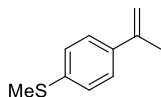
148.20 g/mol

Appearance	colorless liquid
Yield	3.91 g, 26.4 mmol (88 %)
TLC	$R_f = 0.27$ (SiO ₂ , <i>n</i> -pentane)
¹H-NMR	(300 MHz, CDCl ₃) δ 7.42 (m, 2H), 6.87 (m, 2H), 5.29 (m, 1H), 5.00 (m, 1H), 3.81 (s, 3H), 2.14 (s, 3H).
¹³C-NMR	(75 MHz, CDCl ₃) δ 159.0, 142.5, 133.7, 126.6, 113.5, 110.7, 55.3, 21.9.
GC-MS	$t_R = 6.48$ min, (EI, 70 eV): $m/z = 148$ [M ⁺], 127, 133, 115, 105, 89, 77, 63, 51.

Analytical data were in full agreement with A. Fryszkowska, K. Fisher, J. M. Gardiner, G. M. Stephens, *J. Org. Chem.* **2008**, *73*, 4295-4298.

Methyl(4-(prop-1-en-2-yl)phenyl)sulfane

Synthesis was performed by T. N. Gieshoff, U. Chakraborty, M. Villa, A. Jacobi von Wangelin, *Angew. Chem. Int. Ed.* **2017**, *56*, 3585.



C₁₀H₁₂S

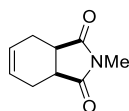
164.27 g/mol

Appearance	colorless solid
Yield	1.09 g, 6.63 mmol (33%)
TLC	$R_f = 0.44$ (SiO ₂ , <i>n</i> -pentane)
¹H-NMR	(300 MHz, CDCl ₃) δ 7.45 – 7.35 (m, 2H), 7.25 – 7.18 (m, 2H), 5.36 (dq, $J=1.6, 0.8$, 1H), 5.06 (dq, $J=1.5, 1.5$, 1H), 2.49 (s, 3H), 2.14 (dd, $J=1.5, 0.8$, 3H).
¹³C-NMR	(75 MHz, CDCl ₃) δ 142.51, 138.01, 137.49, 126.37, 125.90, 111.96, 21.75, 15.91.
GC-MS	$t_R = 7.38$ min, (EI, 70 eV): $m/z = 164$ [M ⁺], 149, 134, 115, 102, 91, 77, 69, 51.

Analytical data were in full agreement with G. Fraenkel, J. M. Geckle, *J. Am. Chem. Soc.* **1980**, *102*, 2869–2880.

N-Methyl-1,2,3,6-tetrahydrophthalimide

Synthesis was performed by Schachtner, Josef, *Dissertation* **2016**, Regensburg.



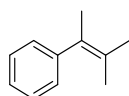
$C_9H_{11}NO_2$
165.19 g/mol

Appearance	colorless solid
Yield	5.7 g, 34.5 mmol (70%)
TLC	$R_f = 0.42$ (SiO ₂ , hexanes/ethyl acetate 2/1)
¹H-NMR	(400 MHz, CDCl ₃): δ 5.92-5.85 (m, 2H), 3.12-3.05 (m, 2H), 2.96 (s, 3H), 2.64-2.58 (m, 2H), 2.27-2.19 (m, 2H).
GC-MS	$t_R = 7.58$ min (EI, 70 eV): $m/z = 165$ [M ⁺], 150, 136, 107, 80, 65, 57, 51.

Analytical data were in full agreement with E. Schefczik, *Chem. Ber.* **1965**, *98*, 1270–1281.

(3-methylbut-2-en-2-yl)benzene

Synthesis was performed by Gieshoff, Tim, *Dissertation* **2017**, Regensburg, following the procedure by W. Adam, M. A. Arnold, M. Grüne, W. M. Nau, U. Pischel, C. R. Saha-Möller, *Organic Letters* **2002**, *4*, 537-540.



$C_{11}H_{14}$
146.23 g/mol

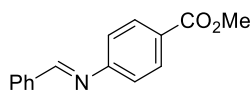
Appearance	colorless liquid
Yield	850 mg, 5.8 mmol (39%)
¹H-NMR	(300 MHz, CDCl ₃) δ 7.36 – 7.13 (m, 5H), 1.99 (m, 3H), 1.84 (m, 3H), 1.62 (m, 3H).
¹³C-NMR	(75 MHz, CDCl ₃) δ 145.35, 130.00, 128.44, 127.94, 127.23, 125.73, 22.11, 20.85, 20.59.
GC-MS	$t_R = 5.62$ min, (EI, 70 eV): $m/z = 146$ [M ⁺], 131, 115, 103, 91, 77, 65, 51.

Analytical data were in full agreement with W. Adam, M. A. Arnold, M. Grüne, W. M. Nau, U. Pischel, C. R. Saha-Möller, *Org. Lett.* **2002**, *4*, 537-540.

Methyl 4-(benzylideneamino)benzoate

Synthesis was performed by Gärtner, Dominik, *Dissertation* **2016**, Regensburg, following a modified procedure by K. Taguchi, F. H. Westheimer, *J. Org. Chem.* **1971**, *36*, 1570-1572.

3 Olefin-Stabilized Cobalt Nanoparticles for C=C, C=O and C=N Hydrogenations



C₁₅H₁₃NO₂

239.27 g/mol

Appearance

Pale yellow solid

¹H-NMR

(300 MHz, CDCl₃) δ 8.44 (s, 1H), 8.08 (m, 2H), 7.9 (m, 2H), 7.49 (m, 3H), 7.2 (m, 2H), 3.93 (s, 3H).

¹³C-NMR

(75 MHz, CDCl₃) δ 161.7, 156.3, 135.8, 130.9, 129.1, 128.9, 127.3, 120.7, 52.1.

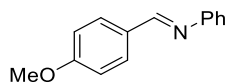
GC-MS

t_R = 10.78 min, (EI, 70 eV): *m/z* = 239 [M⁺].

Analytical data were in full agreement with B. B.-N. Ben-Aroya, M. Portnoy, *Tetrahedron* **2002**, 58, 5147-5158.

N-(4-Methoxybenzylidene)aniline

Synthesis was performed by Gärtner, Dominik, *Dissertation* **2016**, Regensburg, following a modified procedure by K. Taguchi, F. H. Westheimer, *J. Org. Chem.* **1971**, 36, 1570-1572.



C₁₄H₁₃NO

211.26 g/mol

Appearance

Colorless solid

¹H-NMR

(300 MHz, CDCl₃) δ 8.38 (s, 1H), 7.87-7.84 (m, 2H), 7.417.36 (m, 2H), 7.23-7.18 (m, 3H), 6.99-6.97 (m, 2H), 3.87 (s, 3H).

¹³C-NMR

(75 MHz, CDCl₃) δ 162.3, 159.8, 152.4, 130.5, 129.3, 129.1, 125.6, 120.9, 114.2, 55.5.

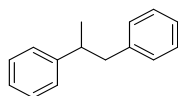
GC-MS

t_R = 10.09 min, (EI, 70 eV): *m/z* = 211 [M⁺].

Analytical data were in full agreement with N. M. O'Boyle, M. Carr, L. M. Greene, O. Bergin, S. M. Nathwani, T. McCabe, D. G. Lloyd, D. M Zisterer, M. J. Meegan, *J. Med. Chem.* **2010**, 53, 8569–8584.

Hydrogenation products

Propane-1,2-diylidibenzene



C₁₅H₁₆

196,29 g/mol

¹H-NMR

(300 MHz, CDCl₃) δ 7.44 – 7.10 (m, 10H), 3.17 – 2.95 (m, 2H), 2.91 – 2.78 (m, 1H), 1.31 (d, J = 6.8 Hz, 3H).

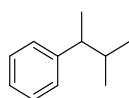
3 Olefin-Stabilized Cobalt Nanoparticles for C=C, C=O and C=N Hydrogenations

¹³C-NMR (75 MHz, CDCl₃) δ 147.05, 140.88, 129.23, 128.37, 128.17, 127.11, 126.09, 125.91, 45.13, 41.96, 21.23.

GC-MS $t_R = 8,24$ min, (EI, 70 eV): $m/z = 196$ [M⁺], 178, 165, 152, 139, 128, 115, 105, 91, 77, 65, 51.

Analytical data were in full agreement with C. Metallinos, J. Zaifman, L. Van Belle, L. Dodge, M. Pilkington, *Organometallics* **2009**, 28, 4534-4543.

(3-methylbutan-2-yl)benzene



C₁₁H₁₆

148,28 g/mol

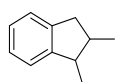
¹H-NMR (300 MHz, CDCl₃) δ 7.35 – 7.14 (m, 5H), 2.42 (m, 1H), 1.77 (m, 1H), 1.24 (m, 3H), 0.94 (d, $J = 6.7$ Hz, 3H), 0.76 (d, $J = 6.7$ Hz, 3H).

¹³C-NMR (75 MHz, CDCl₃) δ 147.10, 128.02, 127.65, 125.68, 46.88, 34.45, 21.20, 20.20, 18.78.

GC-MS $t_R = 5,41$ min, (EI, 70 eV): $m/z = 148$ [M⁺], 131, 115, 105, 77, 65, 51.

Analytical data were in full agreement with V. Jurčík, S. P. Nolan, C. S. J. Cazin, *Chem. Eur. J.* **2009**, 15, 2509-2511.

1,2-dimethyl-2,3-dihydro-1H-indene



C₁₁H₁₄

146.23 g/mol

¹H-NMR (400 MHz, CDCl₃) δ 7.23 – 7.10 (m, 4H), 3.17 (p, $J = 7.1$ Hz, 1H), 3.04 – 2.92 (m, 1H), 2.63 – 2.53 (m, 2H), 1.15 (d, $J = 7.2$ Hz, 3H), 0.99 (d, $J = 6.8$ Hz, 3H).

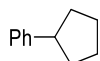
¹³C-NMR (75 MHz, CDCl₃) δ 148.81, 142.95, 126.10, 126.04, 124.48, 123.59, 42.39, 39.39, 37.84, 15.20, 14.67.

GC-MS $t_R = 6.03$ min, (EI, 70 eV): $m/z = 146$ [M⁺], 131, 115, 103, 91, 77, 63, 51.

3 Olefin-Stabilized Cobalt Nanoparticles for C=C, C=O and C=N Hydrogenations

Analytical data were in full agreement with R. P. Yu, J. M. Darmon, J. M. Hoyt, G. W. Margulieux, Z. R. Turner, P. J. Chirik, *ACS Catal.* **2012**, 2, 1760–1764.

Phenylcyclopentane



C₁₁H₁₄

146.23 g/mol

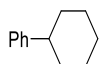
¹H-NMR (300 MHz, CDCl₃) δ 7.34 – 7.12 (m, 5H), 3.09 – 2.91 (m, 1H), 2.18 – 1.98 (m, 2H), 1.92 – 1.48 (m, 6H).

¹³C-NMR (75 MHz, CDCl₃) δ 146.5, 128.2, 127.1, 125.7, 46.0, 34.6, 25.5.

GC-MS *t_R* = 6.94 min, (EI, 70 eV): *m/z* = 143 [M⁺], 128, 115, 101, 89, 77, 63, 58.

Analytical data were in full agreement with A. Paul, M. D. Smith, A. K. Vannucci, *J. Org. Chem.* **2017**, 82, 1996–2003.

Phenylcyclohexane



C₁₂H₁₆

160.26 g/mol

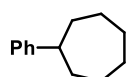
¹H-NMR (300 MHz, CDCl₃) δ 7.34 – 7.25 (m, 2H), 7.24 – 7.14 (m, 3H), 2.60 – 2.39 (m, 1H), 2.00 – 1.79 (m, 4H), 1.80 – 1.73 (m, 1H), 1.51 – 1.19 (m, 5H).

¹³C-NMR (75 MHz, CDCl₃) δ 148.1, 128.3, 126.5, 125.8, 44.7, 34.52, 27.0, 26.2.

GC-MS *t_R* = 7.30 min, (EI, 70 eV): *m/z* = 160 [M⁺], 143, 129, 115, 102, 91, 77, 63, 51.

Analytical data were in full agreement with W. M. Czaplik, M. Mayer, A. Jacobi von Wangelin, *Angew. Chem. Int. Ed.* **2009**, 48, 607–610.

Phenylcycloheptane



C₁₃H₁₈

174.29 g/mol

3 Olefin-Stabilized Cobalt Nanoparticles for C=C, C=O and C=N Hydrogenations

¹H-NMR	(300 MHz, CDCl ₃) δ 7.35 – 7.11 (m, 5H), 2.76 – 2.56 (m, 1H), 2.00 – 1.75 (m, 4H), 1.74 – 1.49 (m, 8H).
¹³C-NMR	(75 MHz, CDCl ₃) δ 150.0, 128.3, 126.7, 125.5, 47.1, 36.8, 28.0, 27.3.
GC-MS	<i>t_R</i> = 7.80 min, (EI, 70 eV): <i>m/z</i> = 174 [M ⁺], 117, 104, 91, 78, 65, 55.

Analytical data were in full agreement with S. Kawamura, K. Ishizuka, H. Takaya, M. Nakamura, *Chem. Commun.* **2010**, 46, 6054–6056.

1,1-Diphenylethane



C₁₄H₁₄

182.27 g/mol

¹H-NMR	(300 MHz, CDCl ₃) δ 7.35 – 7.11 (m, 10H), 4.15 (q, <i>J</i> =7.1, 1H), 1.63 (d, <i>J</i> =7.2, 3H).
GC-MS	<i>t_R</i> = 7.97 min, (EI, 70 eV): <i>m/z</i> = 182 [M ⁺], 167, 152, 139, 128, 115, 103, 89, 77, 63, 51.

Analytical data were in full agreement with F. Schoenebeck, J. A. Murphy, S.-z. Zhou, Y. Uenoyama, Y. Miclo, T. Tuttle, *J. Am. Chem. Soc.* **2007**, 129, 13368–13369.

1-Cyclopropyl-1-phenylethane



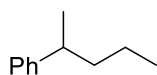
C₁₁H₁₄

146.23 g/mol

¹H-NMR	(300 MHz, CDCl ₃) δ 7.41 – 7.26 (m, 4H), 7.25 – 7.17 (m, 1H), 1.99 (dq, <i>J</i> = 9.2, 7.0 Hz, 1H), 1.35 (d, <i>J</i> = 7.0 Hz, 3H), 1.00 – 0.90 (m, 1H), 0.65 – 0.36 (m, 2H), 0.27 – 0.09 (m, 2H).
¹³C-NMR	(75 MHz, CDCl ₃) δ 147.38, 128.23, 127.00, 125.89, 44.67, 21.62, 18.56, 4.64, 4.34.
GC-MS	<i>t_R</i> = 5.87 min, (EI, 70 eV): <i>m/z</i> = 146 [M ⁺], 131, 117, 105, 91, 77, 65, 51.

Analytical data were in full agreement with T. N. Gieshoff, M. Villa, A. Welther, M. Plois, U. Chakraborty, R. Wolf, A. Jacobi von Wangelin, *Green Chem* **2015**, 17, 1408–1413.

2-Pentylbenzene



$C_{11}H_{16}$

148.25 g/mol

1H -NMR

(300 MHz, $CDCl_3$) δ 7.34 – 7.26 (m, 2H), 7.22 – 7.14 (m, 3H), 2.70 (sextet, $J = 7.0$ Hz, 1H), 1.65 – 1.45 (m, 2H), 1.35 – 1.10 (m, 5H), 0.87 (t, $J = 7.3$ Hz, 3H).

^{13}C -NMR

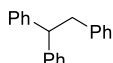
(75 MHz, $CDCl_3$) δ 147.9, 128.3, 127.0, 125.7, 40.7, 39.7, 22.3, 20.8, 14.2.

GC-MS

$t_R = 5.51$ min, (EI, 70 eV): $m/z = 148$ [M^+], 131, 115, 105, 91, 77, 65, 51.

Analytical data were in full agreement with R. B. Bedford, P. B. Brenner, E. Carter, T. W. Carvell, P. M. Cogswell, T. Gallagher, J. N. Harvey, D. M. Murphy, E. C. Neeve, J. Nunn, D. R. Pye, *Chem. Eur. J.* **2014**, *20*, 7935–7938.

Ethane-1,1,2-triyltribenzene



$C_{20}H_{18}$

258.36 g/mol

1H -NMR

(300 MHz, $CDCl_3$) δ 7.30 – 7.09 (m, 13H), 7.05 – 6.95 (m, 2H), 4.24 (t, $J = 7.8$ Hz, 1H), 3.37 (d, $J = 7.8$ Hz, 2H).

^{13}C -NMR

(75 MHz, $CDCl_3$) δ 144.45, 140.26, 129.08, 128.34, 128.05, 126.19, 125.88, 53.11, 42.11.

GC-MS

$t_R = 10.67$ min, (EI, 70 eV): $m/z = 258$ [M^+], 167, 152, 139, 128, 115, 102, 91, 77, 65, 51.

Analytical data were in full agreement with T. C. Fessard, H. Motoyoshi, E. M. Carreira, *Angew. Chem. Int. Ed.* **2007**, *46*, 2078–2081.

Pinane

Mixture of diastereomers.



$C_{10}H_{18}$

138.25 g/mol

1H -NMR

mixture of isomers

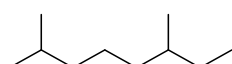
3 Olefin-Stabilized Cobalt Nanoparticles for C=C, C=O and C=N Hydrogenations

¹³C-NMR (75 MHz, CDCl₃) δ 67.98, 65.88, 48.07, 47.62, 41.35, 40.88, 39.49, 38.82, 35.95, 33.96, 29.35, 28.30, 26.84, 26.54, 25.63, 24.61, 23.93, 23.83, 23.22, 23.04, 22.90, 21.61, 20.09, 15.29.

GC-MS t_R = 4.67 min, (EI, 70 eV): m/z = 138 [M⁺], 123, 95, 81, 67, 55.

Analytical data were in full agreement with A. Stolle, B. Ondruschka, W. Bonrath, T. Netscher, M. Findeisen, M. M. Hoffmann, *Chemistry* **2008**, *14*, 6805–6814.

2,6-Dimethyloctane



C₁₀H₂₂

142.29 g/mol

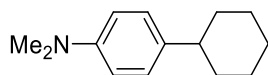
¹H-NMR (300 MHz, CDCl₃) δ 1.76 – 1.45 (m, 2H), 1.41 – 0.98 (m, 8H), 0.95 – 0.71 (m, 12H).

¹³C-NMR (75 MHz, CDCl₃) δ 39.4, 36.9, 34.4, 29.5, 28.0, 24.8, 22.7, 22.6, 19.2, 14.0, 11.4.

GC-MS t_R = 3.99 min, (EI, 70 eV): m/z = 142 [M⁺], 127, 113, 98, 85, 71, 57.

Analytical data were in full agreement with M. G. Speziali, F. C. C. Moura, P. A. Robles-Dutenhefner, M. H. Araujo, E. V. Gusevskaya, E. N. dos Santos, *J. Mol. Catal. A Chem.* **2005**, *239*, 10–14.

4-Cyclohexyl-*N,N*-dimethylaniline



C₁₄H₂₁N

203.33 g/mol

¹H-NMR (300 MHz, CDCl₃) δ 7.15 – 7.07 (m, 2H), 6.77 – 6.72 (m, 2H), 2.93 (s, 6H), 2.52 – 2.38 (m, 1H), 1.94 – 1.80 (m, 4H), 1.78 – 1.70 (m, 1H), 1.48 – 1.34 (m, 4H), 1.34 – 1.25 (m, 1H).

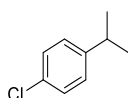
3 Olefin-Stabilized Cobalt Nanoparticles for C=C, C=O and C=N Hydrogenations

¹³C-NMR (75 MHz, CDCl₃) δ 127.34, 113.11, 43.53, 41.06, 34.75, 27.05, 26.26.

GC-MS *t_R* = 9.30 min, (EI, 70 eV): *m/z* = 203, 160, 146, 134, 118, 103, 91, 77, 65, 55.

Analytical data were in full agreement with Z. Li, H.-M. Sun, Q. Shen, *Org. Biomol. Chem.* **2016**, *14*, 3314–3321.

1-Chloro-4-isopropylbenzene



C₉H₁₁Cl

154.64 g/mol

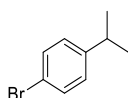
¹H-NMR (300 MHz, CDCl₃) δ 7.25 (m, 2H), 7.21–7.09 (m, 2H), 2.89 (m, 1H), 1.23 (d, *J* = 6.9 Hz, 6H).

¹³C-NMR (75 MHz, CDCl₃) δ 142.3, 131.3, 128.4, 127.8, 33.6, 23.9.

GC-MS *t_R* = 5.37 min, (EI, 70 eV): *m/z* = 154 [M⁺], 139, 125, 119, 105, 89, 77, 63, 51.

Analytical data were in full agreement with S. S. Kim, C. S. Kim, *J. Org. Chem.* **1999**, *64*, 9261–9264.

1-Bromo-4-isopropylbenzene



C₉H₁₁Br

199.09 g/mol

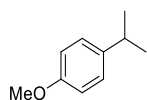
¹H-NMR (300 MHz, CDCl₃) δ 7.47 – 7.36 (m, 2H), 7.15 – 7.04 (m, 2H), 2.87 (hept, *J* = 6.9 Hz, 1H), 1.23 (d, *J* = 6.9 Hz, 6H).

¹³C-NMR (101 MHz, CDCl₃) δ 147.8, 131.3, 128.2, 119.3, 33.7, 30.9, 23.8.

GC-MS *t_R* = 6.16 min, (EI, 70 eV): *m/z* = 198 [M⁺], 185, 169, 158, 143, 119, 104, 91, 77, 63, 51.

Analytical data were in full agreement with M. A. Hall, J. Xi, C. Lor, S. Dai, R. Pearce, W. P. Dailey, R. G. Eckenhoff, *J. Med. Chem.* **2010**, *53*, 5667–5675.

1-Isopropyl-4-methoxybenzene



C₁₀H₁₄O

180.24 g/mol

¹H-NMR

(300 MHz, CDCl₃) δ 7.20 – 7.10 (m, 2H), 6.88 – 6.80 (m, 2H), 3.80(s, 3H), 2.95 – 2.78 (hept, *J* = 6.9 Hz 1H), 1.23 (d, *J* = 6.8 Hz, 6H).

¹³C-NMR

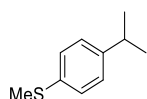
(75 MHz, CDCl₃) δ 157.6, 141.1, 127.3, 113.7, 55.3, 33.3, 24.2.

GC-MS

t_R = 5.93 min, (EI, 70 eV): *m/z* = 150 [M⁺], 120, 105, 91, 77, 65, 51.

Analytical data were in full agreement with Cahiez, G.; Foulgoc, L.; Moyeux, A. *Angew. Chem. Int. Ed.* **2009**, *48*, 2969–2972.

Methyl(4-(prop-2-yl)phenyl)sulfane



C₁₀H₁₄S

166.28 g/mol

¹H-NMR

(300 MHz, CDCl₃) δ 7.26 – 7.19 (m, 2H), 7.19 – 7.13 (m, 2H), 2.88 (p, *J* = 6.9 Hz, 1H), 2.48 (s, 3H), 1.24 (d, *J* = 6.9 Hz, 6H).

¹³C-NMR

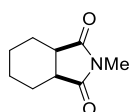
(75 MHz, CDCl₃) δ 146.1, 135.1, 127.2, 127.0, 77.5, 77.0, 76.6, 33.7, 24.0, 16.4.

GC-MS

t_R = 7.20 min, (EI, 70 eV): *m/z* = 166 [M⁺], 151, 136, 104, 91, 77, 51.

Analytical data were in full agreement with X.-m. Wu, J.-m. Lou, G.-b. Yan, *Synlett* **2016**, *27*, 2269–2273.

2-Methylhexahydro-1*H*-isoindole-1,3(2*H*)-dione



C₉H₁₃NO₂

167.21 g/mol

¹H-NMR

(300 MHz, CDCl₃) δ 2.97 (s, 3H), 2.85 (td, *J* = 4.5, 2.2 Hz, 2H), 1.98 – 1.80 (m, 2H), 1.80 – 1.68 (m, 2H), 1.53 – 1.35 (m, 4H).

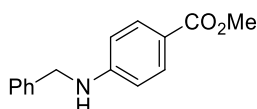
3 Olefin-Stabilized Cobalt Nanoparticles for C=C, C=O and C=N Hydrogenations

¹³C-NMR (75 MHz, CDCl₃) δ 180.0, 77.5, 77.0, 76.62, 39.8, 24.7, 23.7, 21.6.

GC-MS $t_R = 7.77$ min, (EI, 70 eV): $m/z = 167$ [M⁺], 138, 113, 82, 67, 54.

Analytical data were in full agreement with B. Bailey, R. D. Haworth, J. McKenna, *J. Chem. Soc.* **1954**, 967.

Methyl 4-(benzylamino)benzoate



C₁₅H₁₅NO₂

241.29 g/mol

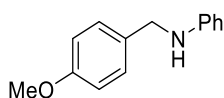
¹H-NMR (300 MHz, CDCl₃) δ 7.87 (d, $J = 8.8$ Hz, 2H), 7.41 – 7.27 (m, 5H), 6.61 (d, $J = 8.8$ Hz, 2H), 4.81 (br s, 1H), 4.39 (s, 2H), 3.85 (s, 3H).

¹³C-NMR (75 MHz, CDCl₃) δ 167.4, 151.6, 138.3, 131.7, 128.9, 127.7, 127.6, 119.0, 112.0, 51.7, 48.0.

GC-MS $t_R = 11.24$ min, (EI, 70 eV): $m/z = 241$ [M⁺], 210, 180, 164, 151, 135, 119, 104, 91, 77, 51.

Analytical data were in full agreement with L. Fan, J. Jia, H. Hou, Q. Lefebvre, M. Rueping, *Chem. Eur. J.* **2016**, 22, 16437.

N-(4-Methoxybenzyl)aniline



C₁₄H₁₅NO

213.28 g/mol

¹H-NMR (300 MHz, CDCl₃) δ 7.34-7.30 (m, 2H), 7.25-7.19 (m, 2H), 6.94-6.90 (m, 2H), 6.80-6.74 (m, 1H), 6.69-6.66 (m, 2H), 4.28 (s, 2H), 3.98 (bs, 1H), 3.83 (s, 3H).

¹³C-NMR (75 MHz, CDCl₃) δ 158.9, 148.3, 131.5, 129.3, 128.9, 117.5, 114.1, 112.9, 55.3, 47.8.

GC-MS $t_R = 10.15$ min, (EI, 70 eV): $m/z = 213$ [M⁺].

Analytical data were in full agreement with M. Zhang, H. Yang, Y. Zhang, C. Zhu, W. Li, Y. Cheng, H. Hu, *Chem. Commun.* **2001**, 47, 6605-6607.

3.5.3 General procedures

General method for catalytic hydrogenation: Particle stabilization by the substrate (Protocol B)

In an argon-filled glovebox a flame-dried 4 mL reaction vial was charged with CoBr_2 (0.006 mmol), the substrate (0.2 mmol), THF (1 mL) and *n*-pentadecane as internal reference for GC-FID quantification (0.2 mmol). The resulting pale blue solution was reduced by dropwise addition of LiEt_3BH (0.018 mmol, 1 M, THF) with a Hamilton® syringe during which the colour changed to black. After 10 minutes stirring, the reaction vial was transferred to a high-pressure reactor which was sealed and removed from the glovebox. The reactor was purged with H_2 (3×3 bar) and the reaction pressure and temperature were set. After the indicated reaction time, the vial was retrieved and hydrolyzed with a saturated aqueous solution of NH_4Cl (1 mL) or NaHCO_3 (1 mL) for alkene or ketones and imines, respectively. The reaction mixture was extracted with ethyl acetate (3×1 mL), dried over sodium sulfate and analyzed by GC-FID and GC-MS. For product isolation, 1 mmol of the starting material was used (Scale-up: 5x). After quenching, the product was extracted with ethyl acetate (3×10 mL), washed with brine (30 mL), dried over sodium sulfate and filtered over a pad of silica. Removal of the solvent at reduced pressure afforded the product in high purity.



Figure 3.5.2. Magnetic separation of Co Particles (left); Co precipitate after reduction in absence of substrate / anthracene (right).

General method for catalytic hydrogenation: Particle stabilization by additional anthracene (Protocol C)

In an argon-filled glovebox a flame-dried 4 mL reaction vial was charged with CoBr_2 (0.006 mmol), anthracene (0.06 mmol), THF (1 mL) and *n*-pentadecane as internal reference for GC-FID quantification (0.2 mmol). The resulting pale blue solution was reduced by dropwise addition of LiEt_3BH (0.018 mmol, 1 M, THF) with a Hamilton® syringe during which the colour changed to black. After 10 minutes stirring, the substrate was added and the reaction vial was transferred to a high-pressure reactor which was sealed and removed from the glovebox. See protocol A for hydrogenation and work-up. For product isolation, 1 mmol of the starting material was used (Scale-up: 5x). The crude mixture was purified by flash-chromatography (SiO_2 , pentane / ethyl acetate).



Figure 3.5.3. Anthracene-stabilized Co Particles.

General method for kinetic examination in catalytic hydrogenation and poisoning experiments

In an argon-filled glovebox a flame-dried 10 mL Schlenk tube was charged with CoBr_2 (0.015 mmol), the substrate (0.5 mmol), THF (2.5 mL) and *n*-pentadecane as internal reference for GC-FID quantification (0.2 mmol). The tube was closed with a rubber septum and connected to a Vacuum/ H_2 Schlenk line. After saturating the solution by a flow of H_2 (needle, 5 min), the solution was reduced by dropwise addition of LiEt_3BH (0.045 mmol, 1 M, THF) with a Hamilton® syringe during which the colour changed from pale blue to black. After defined time fractions, aliquots

3 Olefin-Stabilized Cobalt Nanoparticles for C=C, C=O and C=N Hydrogenations

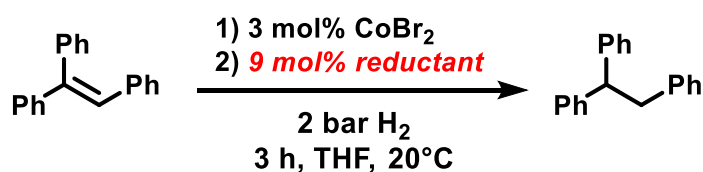
(500 μL) were taken, quenched by filtration over a pad of silica (+ethyl acetate wash) and analyzed by GC-FID and GC-MS.

For poisoning studies a solution of the poison in THF (50-500 μL) was added to the reaction solution after a defined time.

3.5.4 Further optimization studies and mechanistic experiments

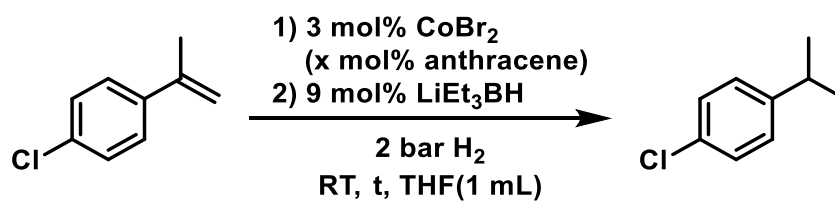
Optimization studies

Table 3.5.2. Additional optimization experiments of protocol B.



Entry	reductant	colour	Yield [%]
1	$(\text{EtO})_3\text{SiH}$	blue	0 (<5)
2	$(\text{EtO})_3\text{SiH} + 18 \text{ mol\% KO}^t\text{Bu}$	brown	0 (<5)
3	HBpin	blue	0 (<5)
4	HBpin + 18 mol% KO^tBu	brown	53 (55)
5	18 mol% KO^tBu	violet	0 (<5)
6	MeMgCl (3 M, THF)	black	<5 (5)
7	NaEt_3BH	black	97
8	LiEt_3BH	black	95 ^a
9	LiEt_3BH	black	61 (66) ^{a,b}
10	LiEt_3BH	black	37 (38) ^c

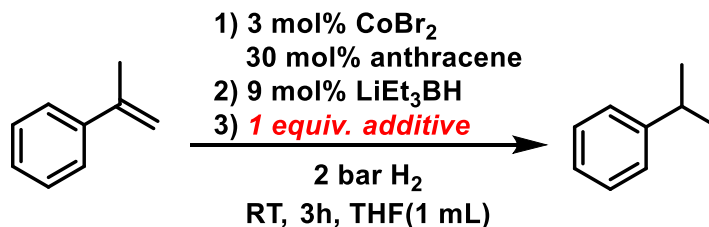
Conditions: 0.2 mmol (0.2 M) alkene in THF, 3 mol% CoBr_2 , 9 mol% reductant, 2 bar H_2 , 20 °C. Yields were determined by quantitative GC-FID vs. internal *n*-pentadecane. Conversions are given in parentheses if <90%; Reduction in presence of the substrate (protocol B); ^a 1h; ^b 1 mol% CoBr_2 ; ^c Protocol C: Reduction in presence of 30 mol% anthracene prior to substrate addition.

Table 3.5.3. Optimization of protocol C.

Entry	time	Anthracene	Yield [%]
1	3 h	-	<5 (7) ^a
2		-	5 (6)
3		-	- (<5) ^b
4		100 mol%	31 (32)
5		As entry 4	26 (26) ^b
6	24 h	3 mol%	63 (65)
7		6 mol%	69 (69)
8		15 mol%	85 (86)
9		30 mol%	>99

Conditions: 0.2 mmol (0.2 M) alkene in THF, 3 mol% CoBr₂, 9 mol% LiEt₃BH, 2 bar H₂, 20 °C. Yields were determined by quantitative GC-FID vs. internal *n*-pentadecane. Conversions are given in parentheses if <90%; Reduction in presence of x mol% anthracene prior to substrate addition; ^aReduction in presence of the substrate (protocol B); Traces of hydrodehalogenation ^b 6 mol% LiEt₃BH;

External functional group tolerance (protocol C)

Table 3.5.4. External functional group tolerance (protocol C).

Entry	additive	Cumene yield [%]	Cumene yield [%] after 16 h
1	PhCN	0 (<5)	
2	PhC(O)H	0 (<5) ^a	
3	PhC(O)Ph	11 (11) ^a	
4	PhOH	24 (24)	71 (75)
5	PhNHAc	82 (82)	85
6	PhCOOEt	>99	
7	2-Ph-pyridine	98	
8	PhNH ₂	>99	
9	Isopulegol (ROH)	62 (62)	86

Conditions: 0.2 mmol (0.2 M) alkene in THF, 0.2 mmol additive, 3 mol% CoBr₂, 9 mol% LiEt₃BH, 2 bar H₂, 20 °C. Yields were determined by quantitative GC-FID vs. internal *n*-pentadecane. Conversions are given in parentheses if <90%; Reduction in presence of 30 mol% anthracene prior to substrate addition; ^aTraces: Corresponding alcohol.

Isomerization

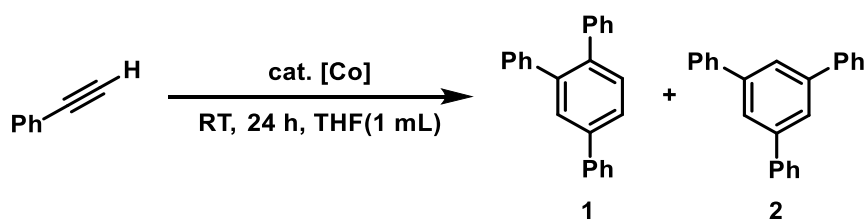
Table 3.5.5. Isomerization of 1-octene
$$\text{1-octene} \xrightarrow[\text{RT, 3 h, THF(1 mL)}]{\text{cat. [Co]}} \text{octene isomers}$$

Entry	Protocol	Octene yield [%]				
		1	(E)- 2	(E)- 3	(E)- 4	others
1	B	-	43	37	9	10
2	C	78	14	-	-	8

Conditions: 0.2 mmol (0.2 M) alkene in THF, 3 mol% CoBr₂, 9 mol% LiEt₃BH, 2 bar H₂, 20 °C. Yields were determined by rel. peak areas of GC-FID. Reduction in presence of the substrate (protocol B); Reduction in presence of 30 mol% anthracene prior to substrate addition (protocol C);

Isomerization reactions were performed according to the general procedures (protocol B & C) in absence of a H₂ atmosphere.

Cyclotrimerization

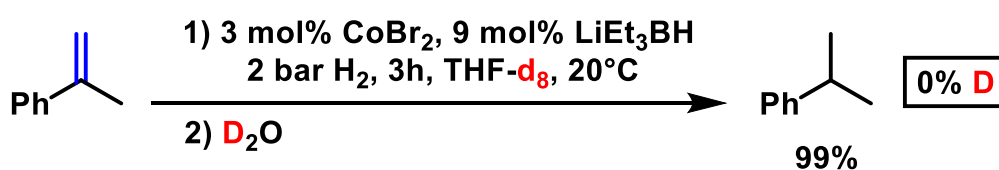
Table 3.5.6. Cyclotrimerization of Phenylacetylene.

Entry	Protocol	Yield [%]		Conversion [%]
		1	2	
1	B	23	8	55
2	C	<5	-	6

Conditions: 0.2 mmol (0.2 M) alkyne in THF, 3 mol% CoBr₂, 9 mol% LiEt₃BH, 2 bar H₂, 20 °C. Yields were determined by quantitative GC-FID vs. internal *n*-pentadecane. Reduction in presence of the substrate (protocol B); Reduction in presence of 30 mol% anthracene prior to substrate addition (protocol C);

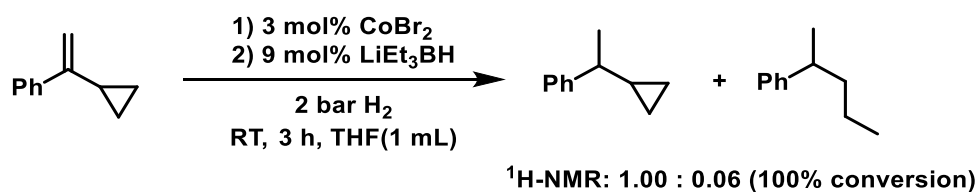
Cyclotrimerization reactions were performed according to the general procedures (protocol B & C) in absence of a H₂ atmosphere.

Deuterium labeling experiment

**Scheme 3.5.6.** Deuterium labeling experiment with α -methylstyrene.

The hydrogenation reaction was performed according to the general procedure protocol B using THF-d₈ as solvent and D₂O for the quench. No deuterium-incorporation was observed by ²D-NMR and GC-MS.

Ring opening experiment with (1-Cyclopropylethyl)benzene



Scheme 3.5.7. Ring opening experiment with (1-cyclopropylethyl)benzene.

The hydrogenation reaction was performed according to the general procedure protocol B.

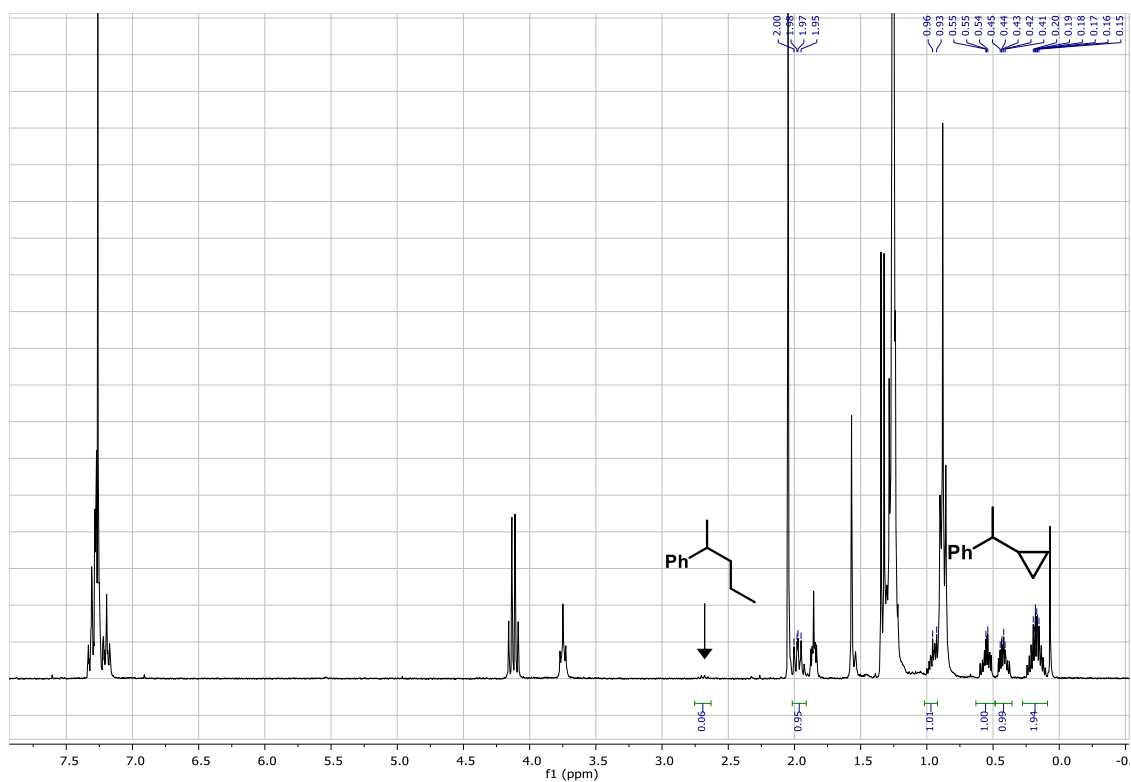


Figure 3.5.4. ¹H-NMR of the hydrogenation reaction of (1-cyclopropylethyl)benzene.

3 Olefin-Stabilized Cobalt Nanoparticles for C=C, C=O and C=N Hydrogenations

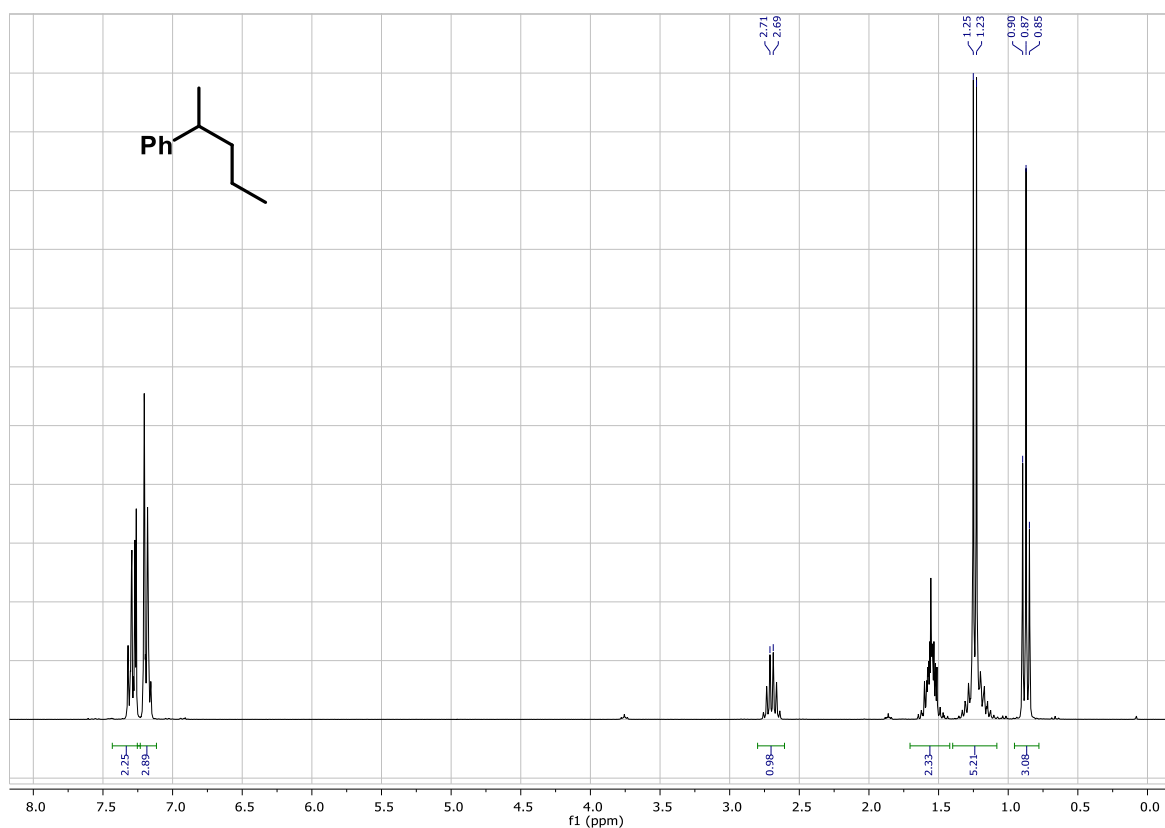


Figure 3.5.5. $^1\text{H-NMR}$ of 2-pentylbenzene.

Poisoning studies: DCT

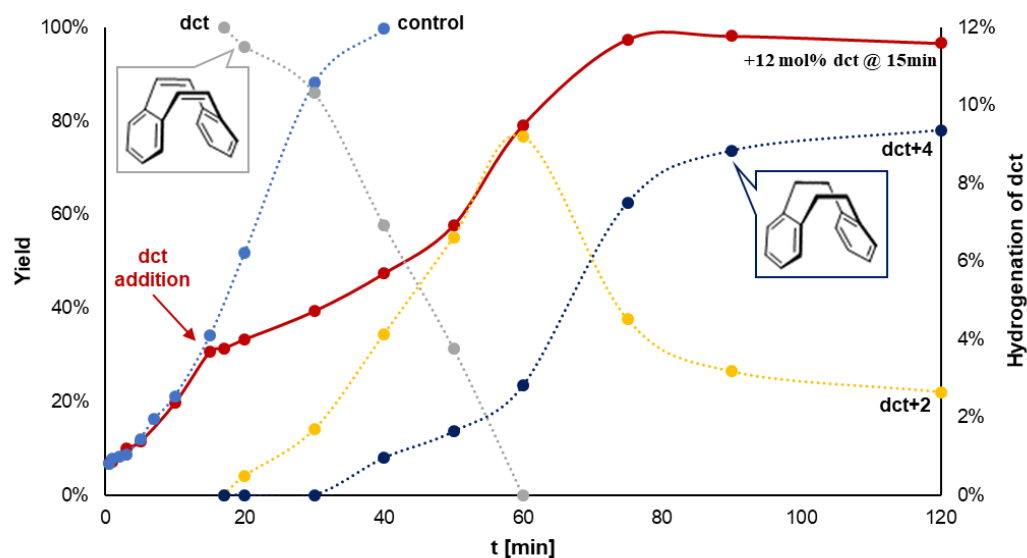


Figure 3.5.6. Poisoning studies with dibenzo[a,e]cyclooctatetraene (dct). Cumene yields were determined by quantitative GC-FID vs. *n*-pentadecane. Hydrogenation of dct was determined by relative peak areas of GC-FID.

DCT addition before reduction and hydrogenation reaction (Scheme 3.5, communication):

In an argon-filled glovebox a flame-dried 10 mL Schlenk tube was charged with CoBr_2 (0.015 mmol), the substrate (0.5 mmol), DCT (0.06 mmol), THF (2.5 mL) and *n*-pentadecane as internal reference for GC-FID quantification (0.2 mmol). The tube was closed with a rubber septum and connected to a Vacuum/ H_2 Schlenk line. After saturating the solution by a flow of H_2 (needle, 5 min), the solution was reduced by dropwise addition of LiEt_3BH (0.045 mmol, 1 M, THF) with a Hamilton® syringe during which the colour changed from pale blue to clear brown. After defined time fractions, aliquots (500 μL) were taken, quenched by filtration over a pad of silica (+ethyl acetate wash) and analyzed by GC-FID and GC-MS.

Low-temperature $^1\text{H-NMR}$ studies: 2 anthracene/ $\text{CoBr}_2/3 \text{LiEt}_3\text{H}$

In an argon-filled glovebox, a screw-capped NMR tube was filled with a solution of CoBr_2 (33.3 μmol) and anthracene (67.3 μmol , Co/anthracene ratio = 1/2) in THF-d_8 (0.6 mL) and closed with a septum. After removal of the sample from the glovebox, the mixture was cooled to $-80\text{ }^\circ\text{C}$ and reduced by dropwise addition of LiEt_3BH (0.1 mL) during which the pale blue colour turned black. The temperature-dependent $^1\text{H-NMR}$ was measured subsequently.

Very broad $^1\text{H-NMR}$ signals of the reaction mixture suggest formation of Co particles even at 193 K.

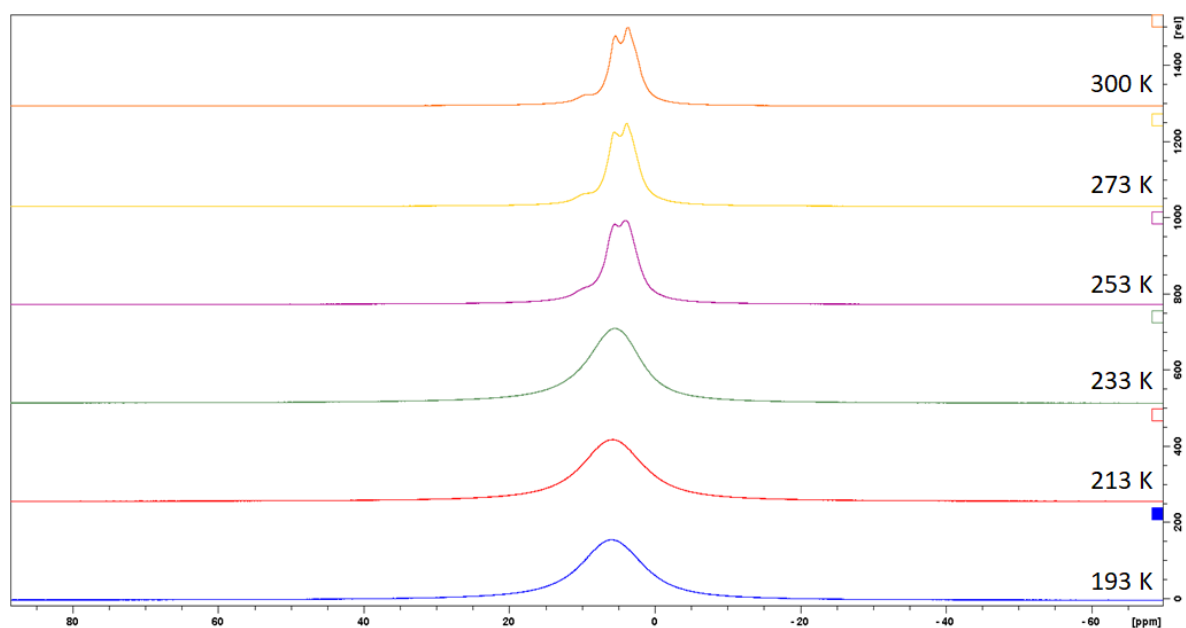


Figure 3.5.7. Low-temperature ¹H-NMR studies: Anthracene-stabilized Co Particles.

Low-temperature ¹H-NMR studies: 10 anthracene/CoBr₂/3 LiEt₃H

In an argon-filled glovebox, a screw-capped NMR tube was filled with a solution of CoBr₂ (0.006 mmol) and anthracene (0,06 mmol, Co/anthracene ratio = 1/10) in THF-d₈ (0.6 mL) and closed with a septum. After removal of the sample from the glovebox, the mixture was cooled to -50 °C and reduced by dropwise addition of LiEt₃BH (0.011 μL, THF, 1.1M) during which the pale blue color turned to a dark brown solution. The ¹H-NMR was measured subsequently.

Broad ¹H-NMR signals of the reaction mixture suggest formation of Co particles.

3 Olefin-Stabilized Cobalt Nanoparticles for C=C, C=O and C=N Hydrogenations

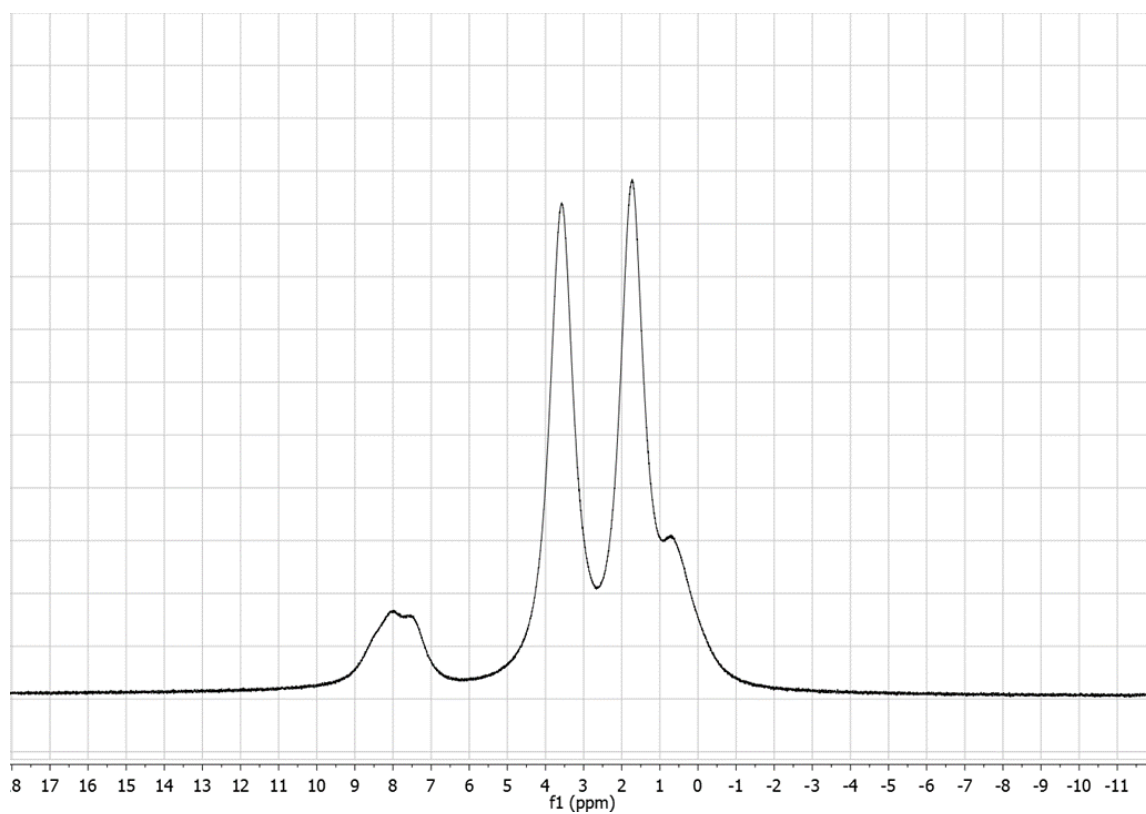


Figure 3.5.8. Low-temperature ¹H-NMR studies: 10 anthracene/CoBr₂/3 LiBEt₃H measured at 223 K.

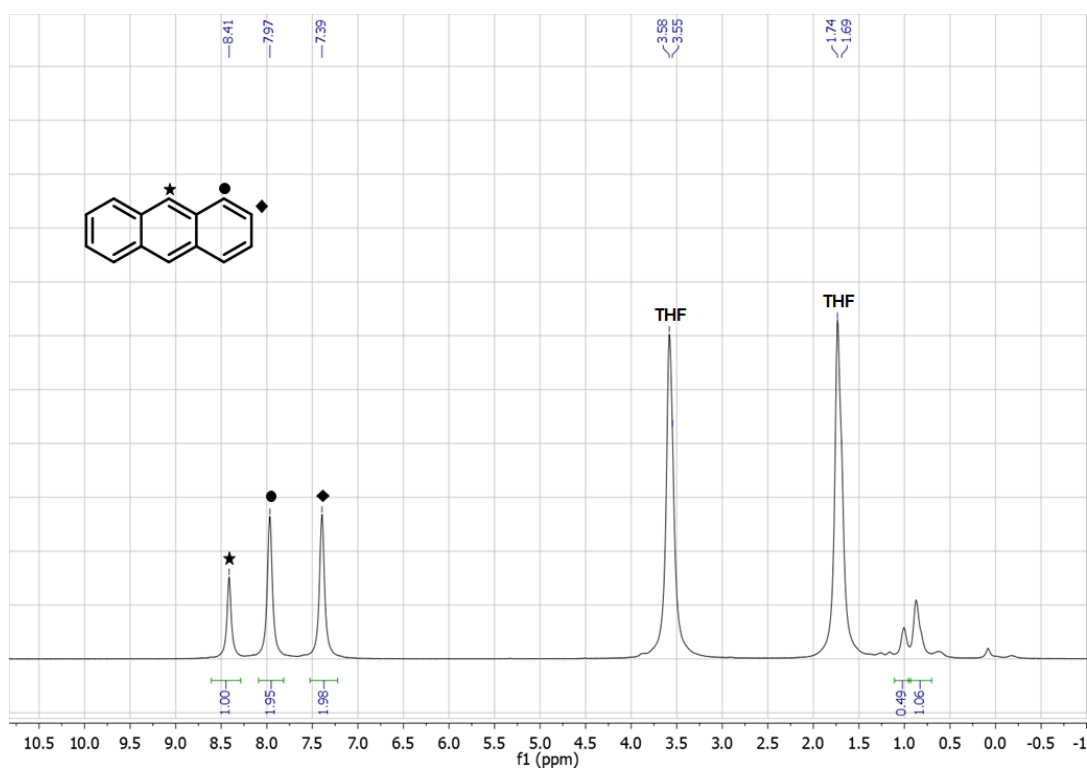


Figure 4.9. ¹H-NMR studies: 10 anthracene/CoBr₂/3 LiBEt₃H measured at 300 K.

Low-temperature $^1\text{H-NMR}$ studies: 10 dct/CoBr₂/3 LiEt₃BH

A similar approach to the catalytic studies was chosen:

In an argon-filled glovebox, a screw-capped NMR tube was filled with a solution of CoBr₂ (0.006 mmol) and dct (0.06 μmol , Co/dct = 1/10) in THF-d₈ (0.6 mL) and closed in a Schlenk tube. After removal of the sample from the glovebox, the mixture was cooled to -80 °C and reduced by dropwise addition of LiEt₃BH (0.011 μL , THF, 1.1M) during which the pale blue colour turned to clear dark brown. The temperature-dependent $^1\text{H-NMR}$ was measured subsequently.

A high-field shift of the dct signals indicate the formation of a molecular diamagnetic Li[(dct)₂Co] complex. Spectroscopic yield: 71% (related to free dct). The observed signal at 3.31/3.15 could not unambiguously assigned. However, the observed set of signals is comparable to a reported [K(thf)₂][Co(dct)₂] derivative. $^1\text{H NMR}$ (400 MHz, 213 K, THF-d₈): δ = 7.20 – 6.96 (m, 16H, free dct), 6.56 – 6.40 (m, 16H, dct Ar-H), 3.61 (m, THF), 3.31 or 3.15 (s, 8H, dct CH), 1.77 (m, THF).

[K(thf)₂][Co(dct)₂]: $^1\text{H NMR}$ (400 MHz, THF-d₈): δ = 6.58-6.45 (m, 16H, Ar-H), 3.45 (s, 8H, CH); Lit.: P. Büschelberger, D. Gärtner, E. Reyes-Rodriguez, F. Kreyenschmidt, K. Koszinowski, A. Jacobi von Wangelin, R. Wolf, *Chem. Eur. J.* **2017**, *23*, 3139).

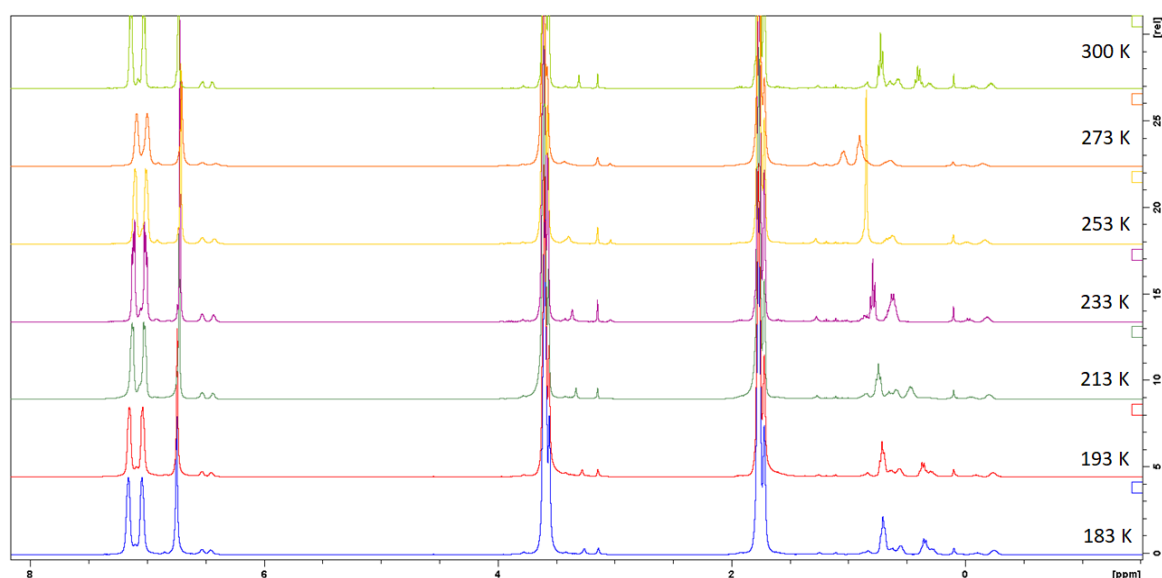


Figure 3.5.10. Low-temperature $^1\text{H-NMR}$ studies: Mixture of 10 dct/CoBr₂/3 LiEt₃BH.

3 Olefin-Stabilized Cobalt Nanoparticles for C=C, C=O and C=N Hydrogenations

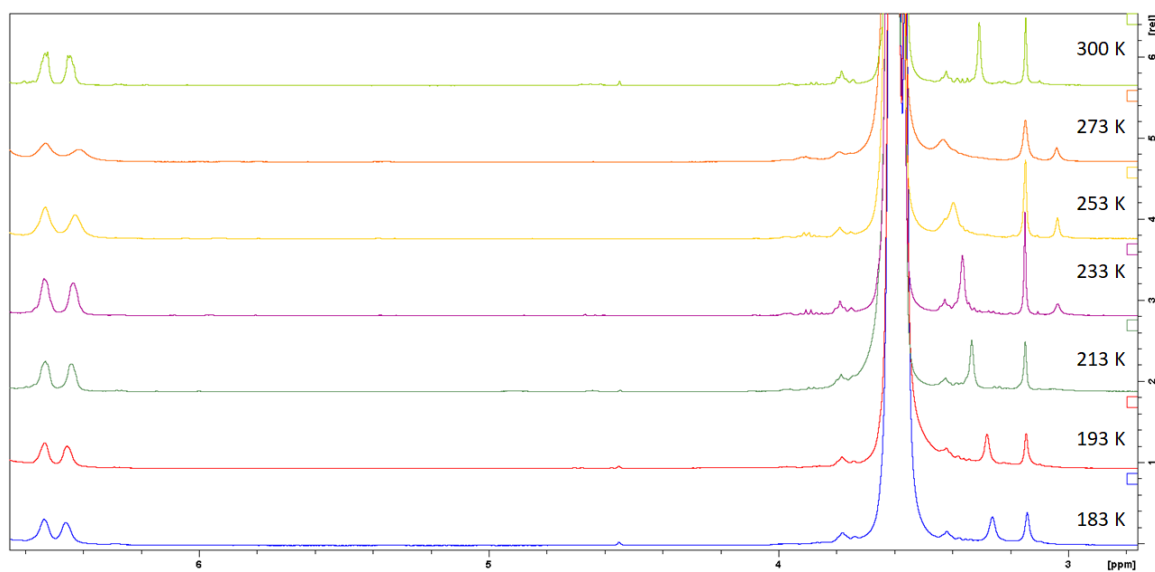


Figure 3.5.11. Low-temperature $^1\text{H-NMR}$ studies: Mixture of 10 dct/CoBr₂/3 LiBEt₃H; zoom.

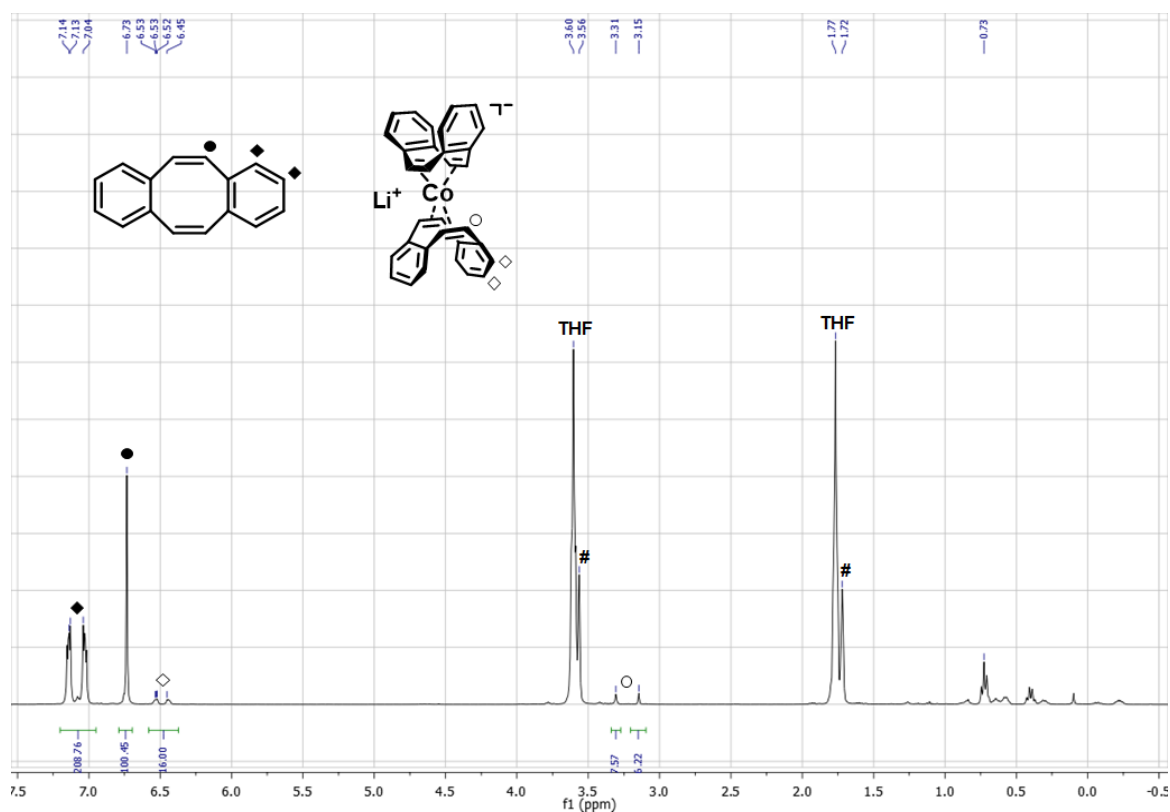
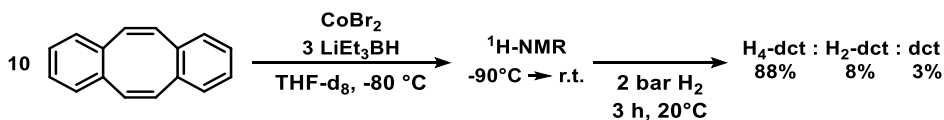


Figure 3.5.12. Low-temperature $^1\text{H-NMR}$ studies: Mixture of 10 dct/CoBr₂/3 LiBEt₃H measured at 213 K (THF-d₈: #).

3 Olefin-Stabilized Cobalt Nanoparticles for C=C, C=O and C=N Hydrogenations

Importantly, the NMR sample was found to be active in hydrogenation. After the reaction, partial catalyst precipitation was observed consistent with the hydrogenated substrate.



Scheme 3.5.8. Hydrogenation of the mixture 10 dct/CoBr₂/3 LiEt₃H.

¹H-NMR studies: 2 dct/CoBr₂/3 LiEt₃H

In an argon-filled glovebox, a screw-capped NMR tube was filled with a solution of CoBr₂ (0.006 mmol) and dct (0.012 μmol, Co/dct = 1/2) in THF-d₈ (1 mL) and closed in a Schlenk tube. After removal of the sample from the glovebox, the mixture was cooled to -80 °C and reduced by dropwise addition of LiEt₃BH (0.011 μL, THF, 1.1M) during which the pale blue colour turned to clear dark brown. The sample was warmed up to 300 K and the ¹H-NMR was measured subsequently.

Broad ¹H-NMR signals of the reaction mixture suggest formation of Co particles.

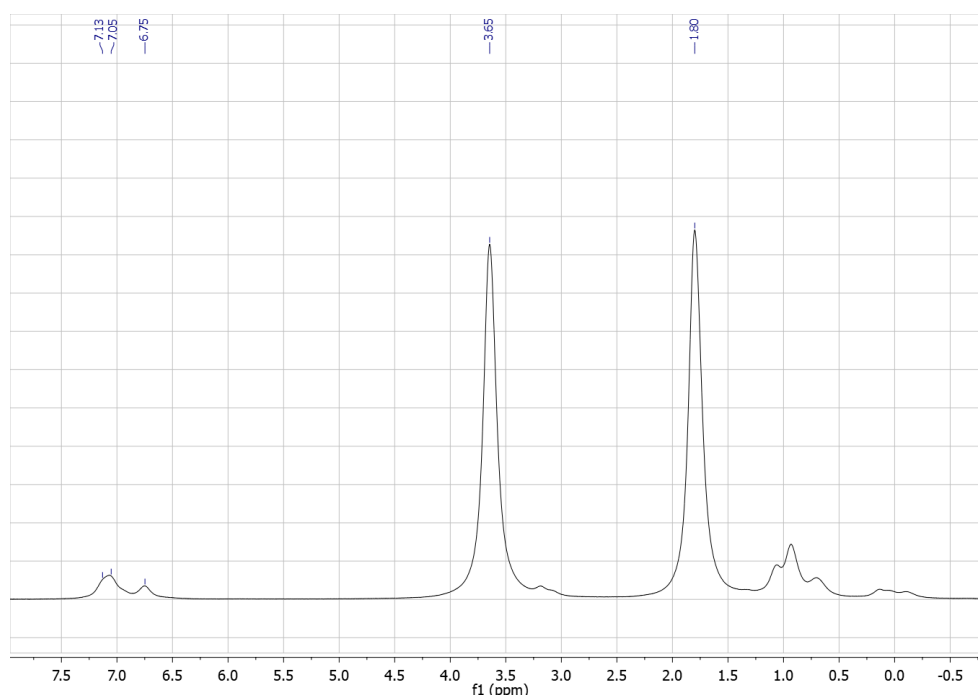


Figure 3.5.13. ¹H-NMR studies: Mixture of 2 dct/CoBr₂/3 LiEt₃H measured at 300 K (THF-d₈).

DLS studies: Anthracene-stabilized Co Particles (Protocol C)

A similar approach to the catalytic studies was chosen:

In an argon-filled glovebox a flame-dried 4 mL reaction vial was charged with CoBr_2 (0.006 mmol), anthracene (0.06 mmol) and THF (1 mL). The resulting pale blue solution was reduced by dropwise addition of LiEt_3BH (0.18 mmol, 1 M, THF) with a Hamilton® syringe during which the colour changed to black. After 10 minutes stirring, the solution was diluted to achieve the desired concentration ($[\text{c}(\text{Co})] = 0.00006 \text{ M}$, THF) and filtered (PTFE filter, Sample A: 450 nm, Sample B: 100 nm). The sample was filled into a Quartz cuvette (10.00 mm) and measured after ageing for 30 minutes.

Mean particle sizes:

Sample A: Too polydisperse

Sample B (two independent experiments):

Z-Average (d.nm): 143 Pdl: 0.143 Peak 1 (d.nm): 162 (± 61).

Z-Average (d.nm): 141 Pdl: 0.094 Peak 1 (d.nm): 156 (± 51).

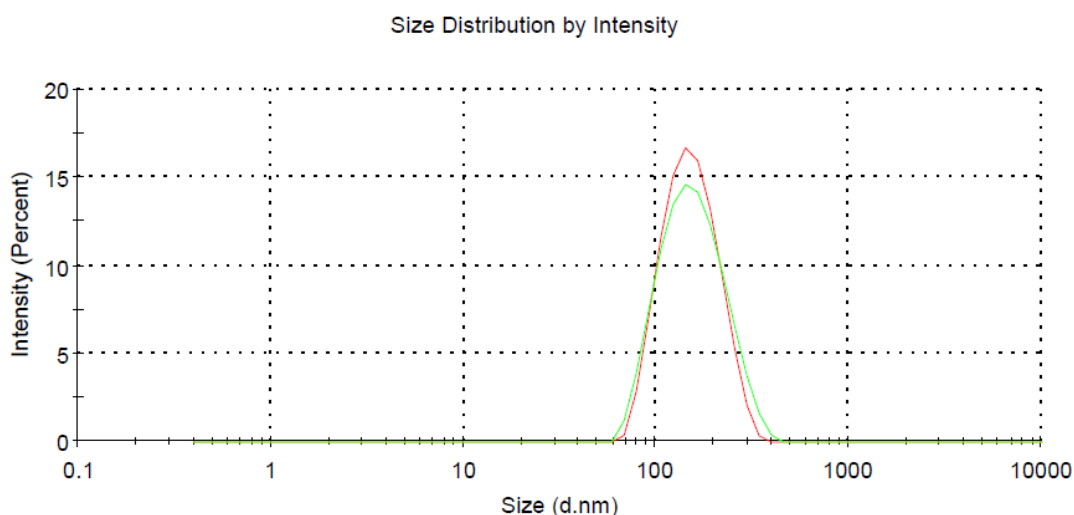


Figure 3.5.14. DLS studies: Anthracene-stabilized Co Particles; Size distribution by intensity.

3 Olefin-Stabilized Cobalt Nanoparticles for C=C, C=O and C=N Hydrogenations

Sample B undiluted ($[c(\text{Co})] = 0.006 \text{ M}$, THF): Absorbance too high (coloured sample).

Monodispersed particles were obtained after filtration (100 nm) of bigger aggregates. The measured particles probably aggregated after the filtration to the measured size as the pores of the filter are smaller than the measured value.

It is important to note that the manipulation by filtration or dilution prior to measurement has a big influence for the particle size / distribution. This step is essential for obtaining good measurement results by DLS.

TEM studies: Anthracene-stabilized Co Particles (Protocol C)

A similar approach to the catalytic studies was chosen:

In an argon-filled glovebox a flame-dried 4 mL reaction vial was charged with CoBr_2 (0.006 mmol), anthracene (0.06 mmol) and THF (1 mL). The resulting pale blue solution was reduced by dropwise addition of LiEt_3BH (0.18 mmol, 1 M, THF) with a Hamilton® syringe during which the colour changed to black. After 10 minutes stirring, the solution was diluted to achieve the desired concentration ($[c(\text{Co})] = 0.0002 \text{ M}$, THF). A droplet was placed on a holey carbon grid, supported by a Cu mesh and the solvent evaporated (assistance: filter paper). The grid was placed in a Gatan vacuum transfer sample holder, sealed and set *in vacuo* to maintain inert conditions during the transport to the microscope. After removing the sample holder from the glovebox and insertion into the TEM, the particles were measured subsequently.

The transmission electron microscope measurements (HRTEM and STEM) were conducted with an FEI Tecnai F30 ST microscope operated at 300 kV acceleration voltage. The Energy dispersive X-ray spectra were acquired in standard TEM and STEM mode with a Bruker AXS X-Flash detector 530. The quantitative evaluation of the X-ray spectra was performed with the software Bruker Esprit (v 1.9). The TEM column pressure during the measurements was $9\text{e-}8 \text{ hPa}$. The measurements were performed on four subsequent days, during which the sample remained stable.

3 Olefin-Stabilized Cobalt Nanoparticles for C=C, C=O and C=N Hydrogenations

Additional cubic objects were observed during the TEM study. EDX measurements reveal a large Br content of these objects, while Co is absent (Figure 3.5.16). Therefore we assume these particles to be LiBr crystals, which may form as reaction side product. The objects were sensitive to beam irradiation as it can be expected for halogenides in general.

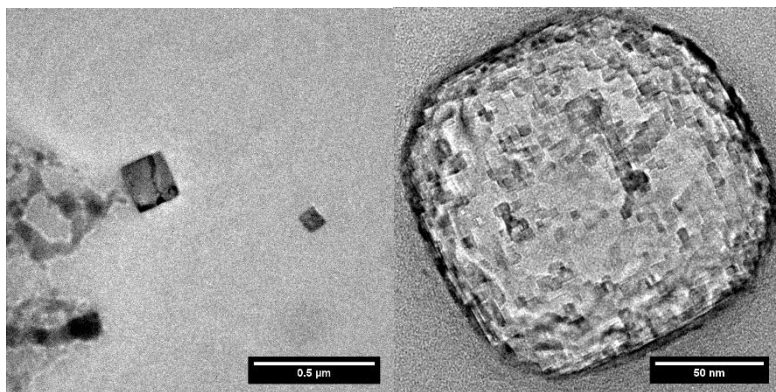
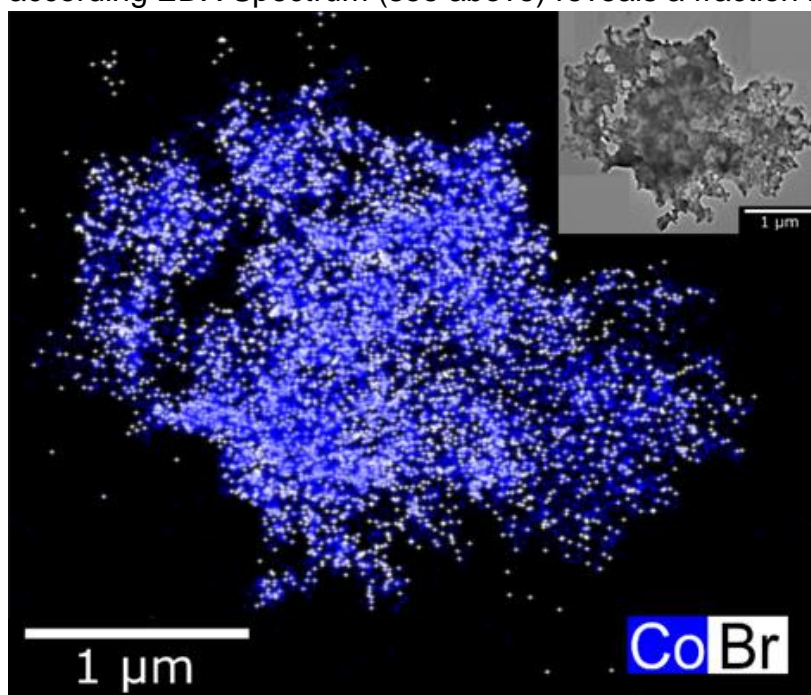


Figure 3.5.15. TEM studies: Anthracene-stabilized Co Particles; LiBr. Left: Initial shape, sharp edges. Right: After irradiation by the electron beam, rounded edges, multi-facetting and voids due to electron beam etching of Br.

The distribution of Co (indicated in blue) and Br (indicated in white) in the large particle accumulations was investigated by scanning EDX measurements (Figure 3.5.17). Both elements occur across the accumulation. The evaluation of the according EDX Spectrum (see above) reveals a fraction between Co and Br of



approximately 2 to 1, with a relative Co concentration of 68 \pm 3 % and a Br concentration of 32 \pm 1 %.

Figure 3.5.16. Scanning EDX measurement of a large particle accumulation. The inset shows the corresponding HRTEM measurement.

Background EDX spectrum (Figure 3.5.18) of the same specimen of a particle-free region in the illuminated area and hence acts as reference to the presented spectrum in the main part of this publication. In comparison, the dominant Co and Br peaks are missing. The occurrence of Co in this measurement can be attributed to the objective lens pole piece of the microscope, which equally consists of Co and Fe, whereas the small Br peak may be detected due to Br particles on the edges of the illuminated area. The presence of C, O, Cu and Si can be attributed to the sample holder and the carbon mounting grid (see above). The C peak was cut off for a better visual representation.

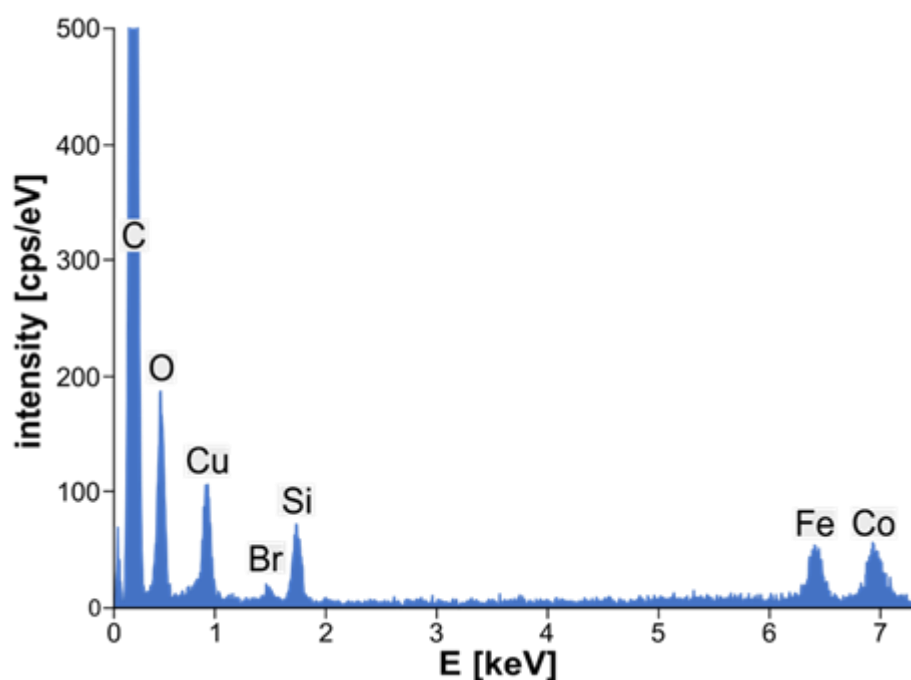


Figure 3.5.17. EDX spectrum of the same specimen but of a region without any visible particles.

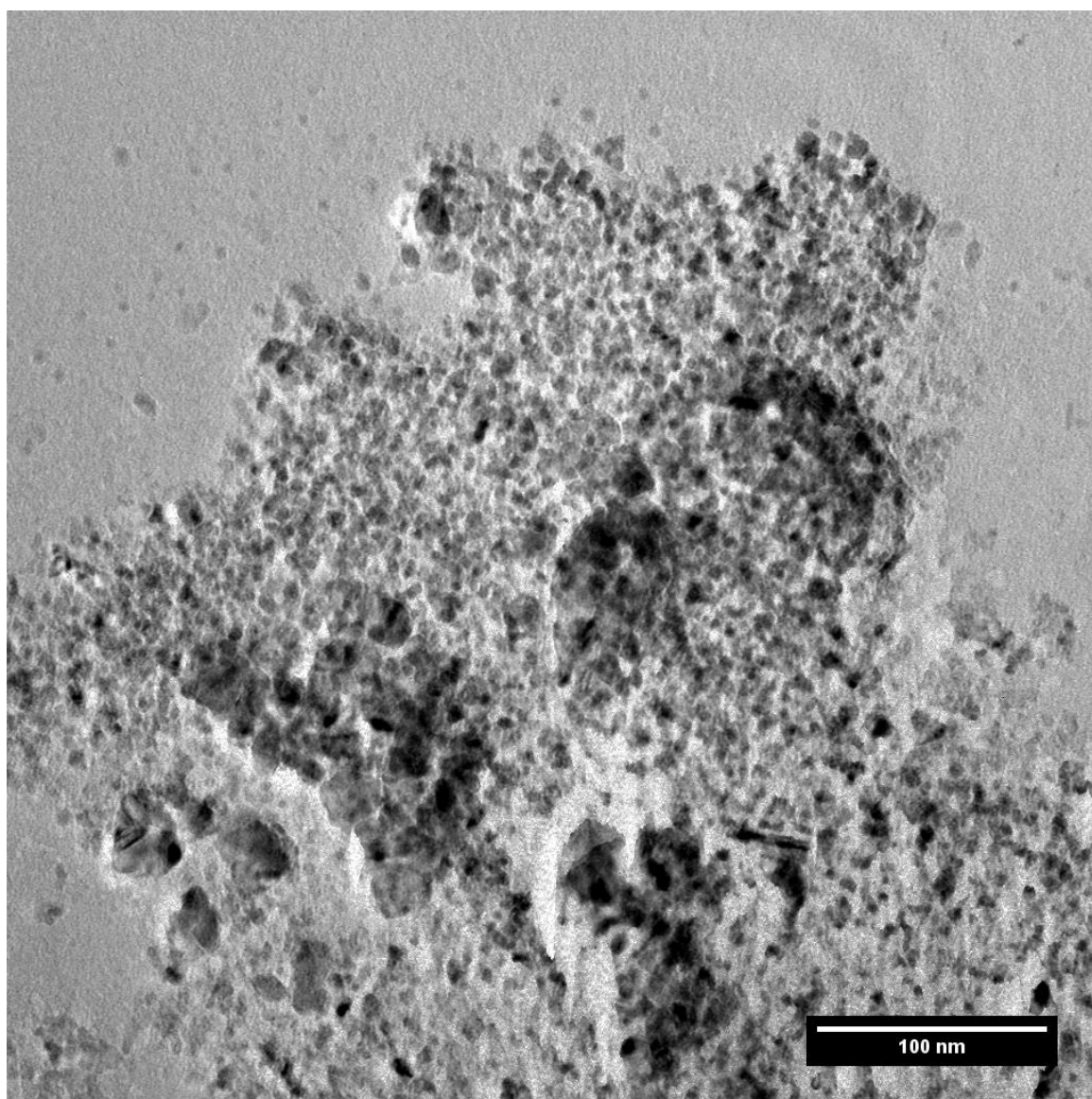


Figure 3.5.18. HR-TEM of Co accumulations showing its grainy texture.

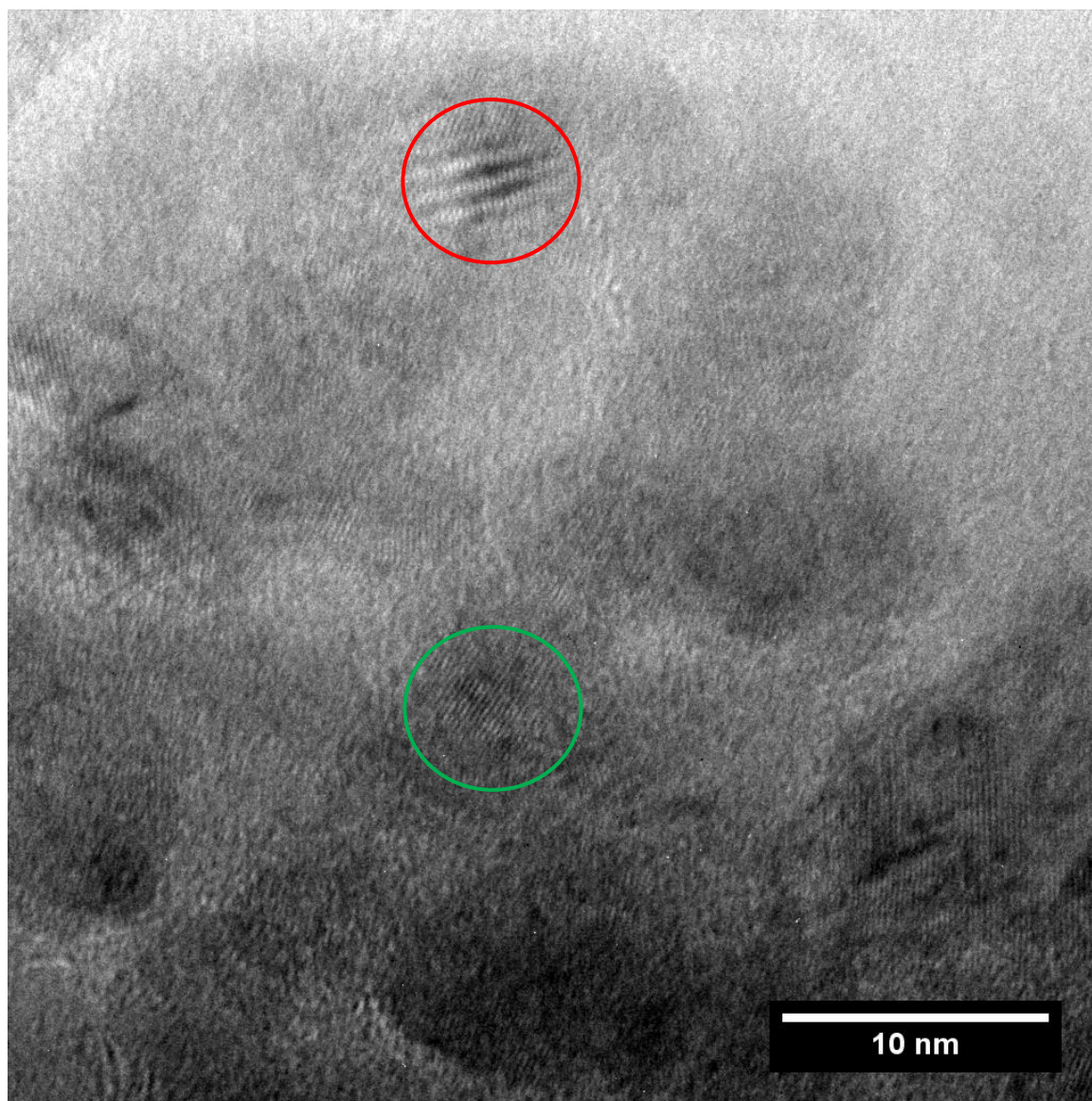


Figure 3.5.19. HR-TEM of Co accumulations showing crystalline structures (green) as well as Moiré patterns (red) with a size in the order of the described individual particles.

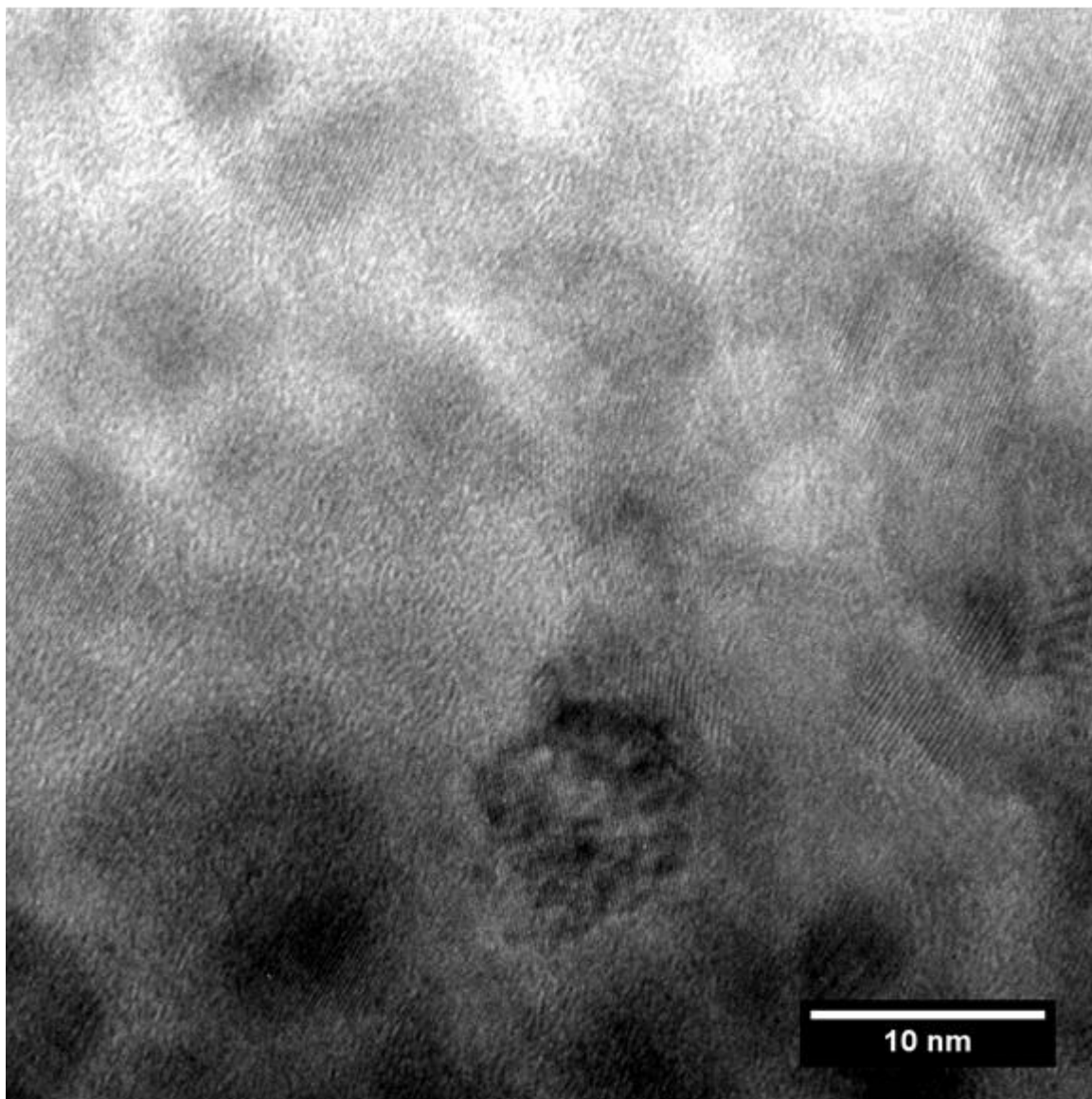


Figure 3.5.20. HR-TEM of Co accumulations showing crystalline structures with a size in the order of the described individual particles.

ICP-OES studies

Five stock solutions of CoCl_2 in HNO_3 (35%) were prepared and a calibration curve was measured by integration of the emission signal of cobalt at 230.786 nm. Each data point corresponds to the mean value of three consecutive measurements corrected by the observed background signals.

Sample A (hydrogenation reaction, protocol B):

α -Methylstyrene was hydrogenated according to the general procedure protocol A. After the reaction, the cobalt precipitate was separated by a magnet and an aliquot (0.5 mL) was taken from the reaction solution. The solvent was removed under reduced pressure and the residue was solubilized in HNO_3 (5 mL, 20% w/w, water). After filtration, the concentration of cobalt was measured by ICP-OES.

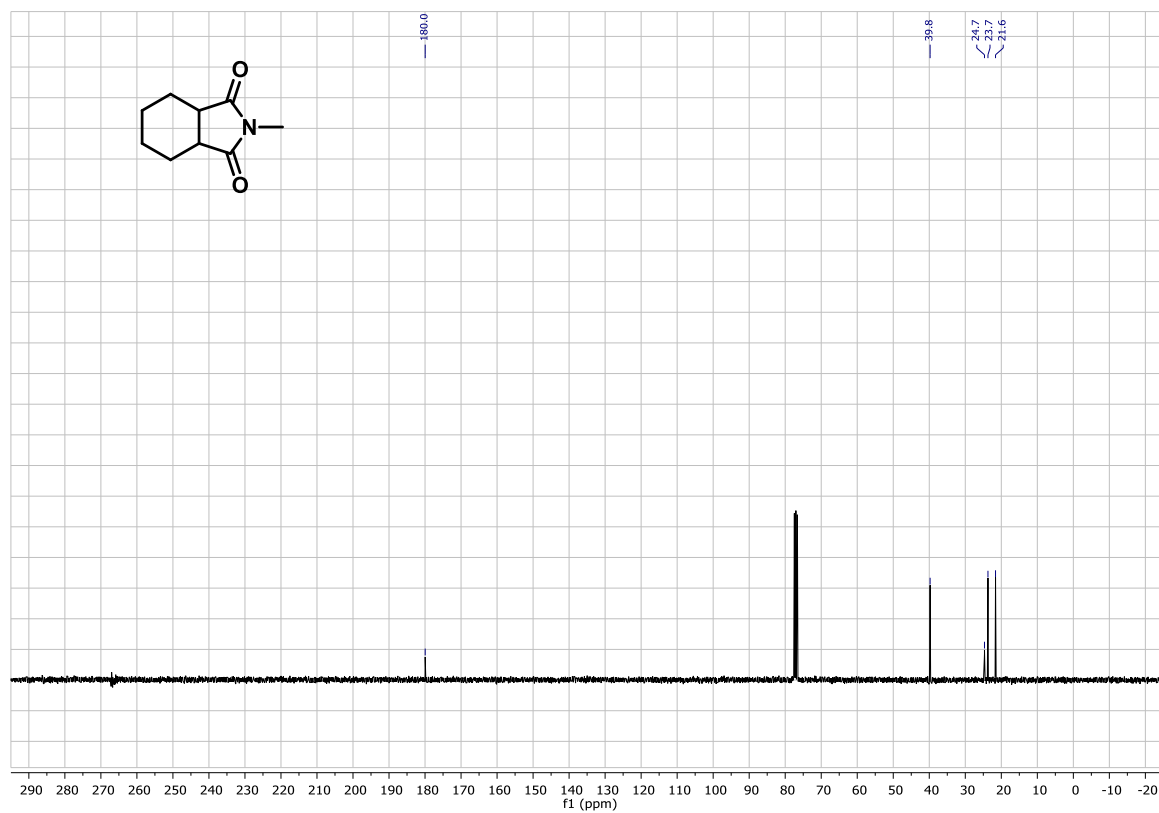
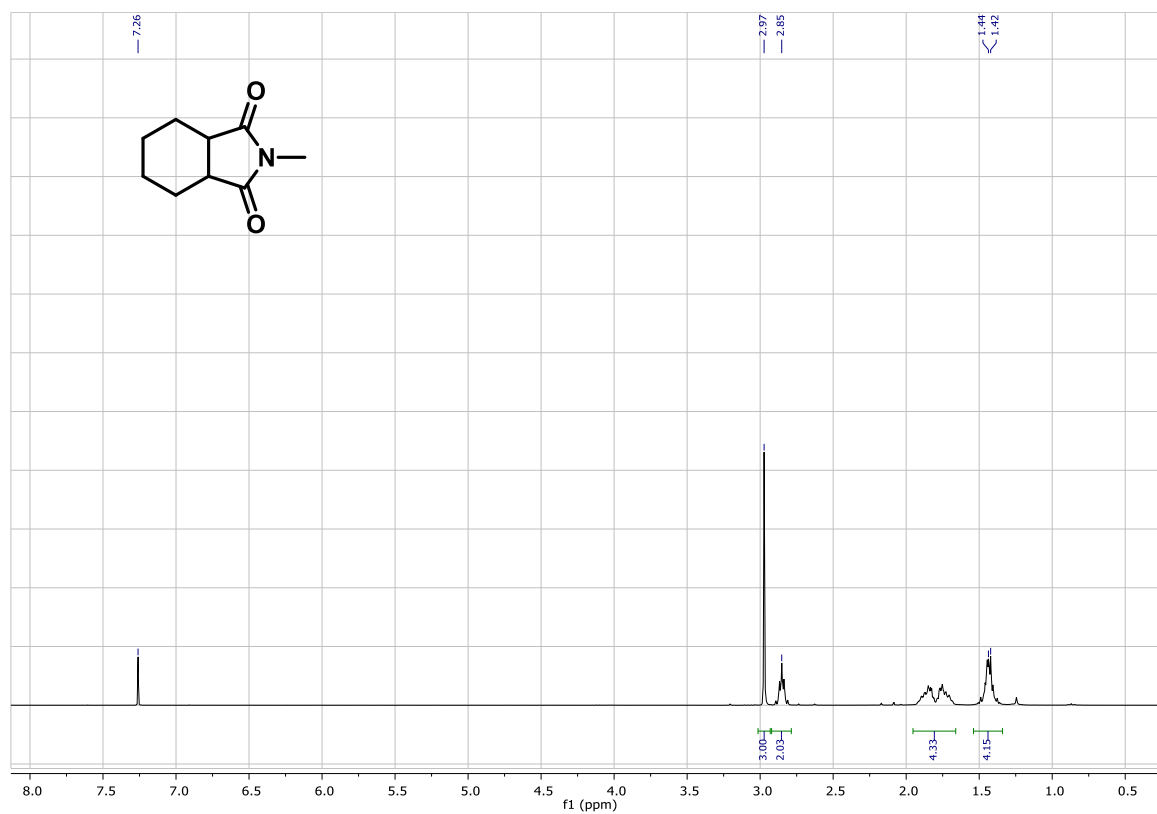
$[\text{c}(\text{Co})] = 0.0043(1)$ mM, which is equivalent to <0.8 % of the initial $[\text{c}(\text{Co})]$.

Sample B (Anthracene-stabilized particles):

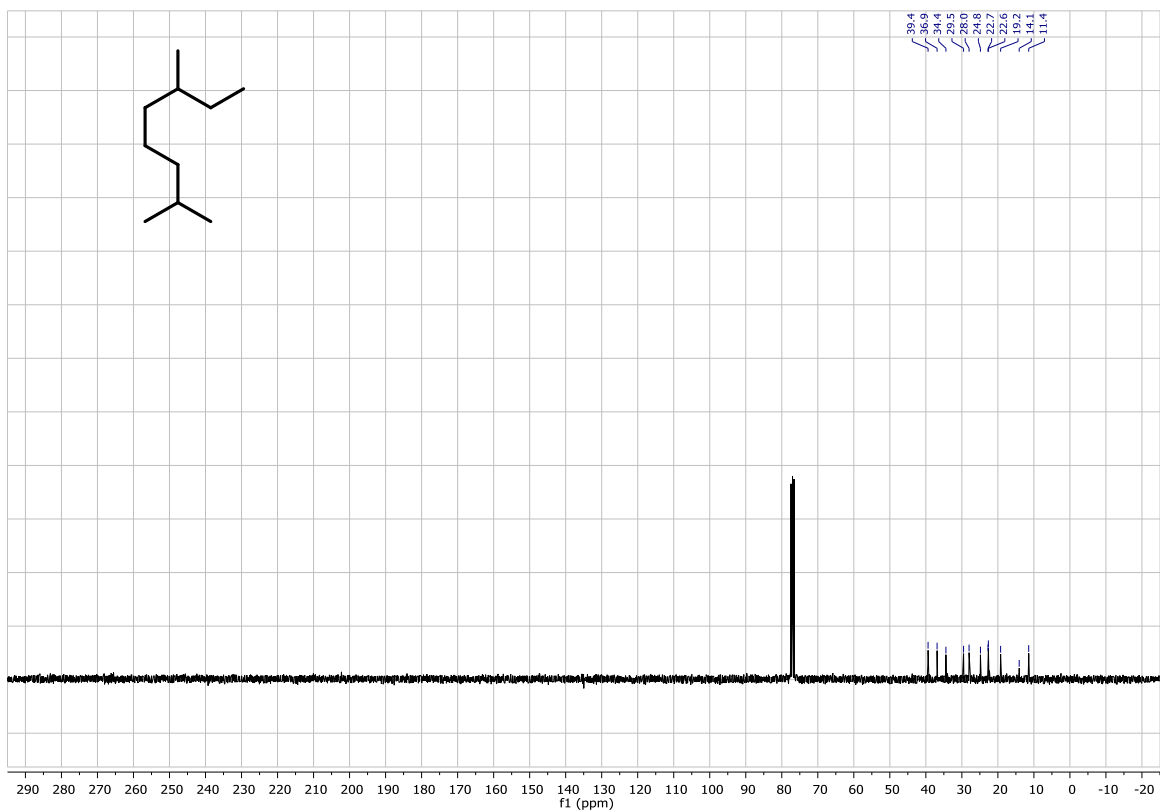
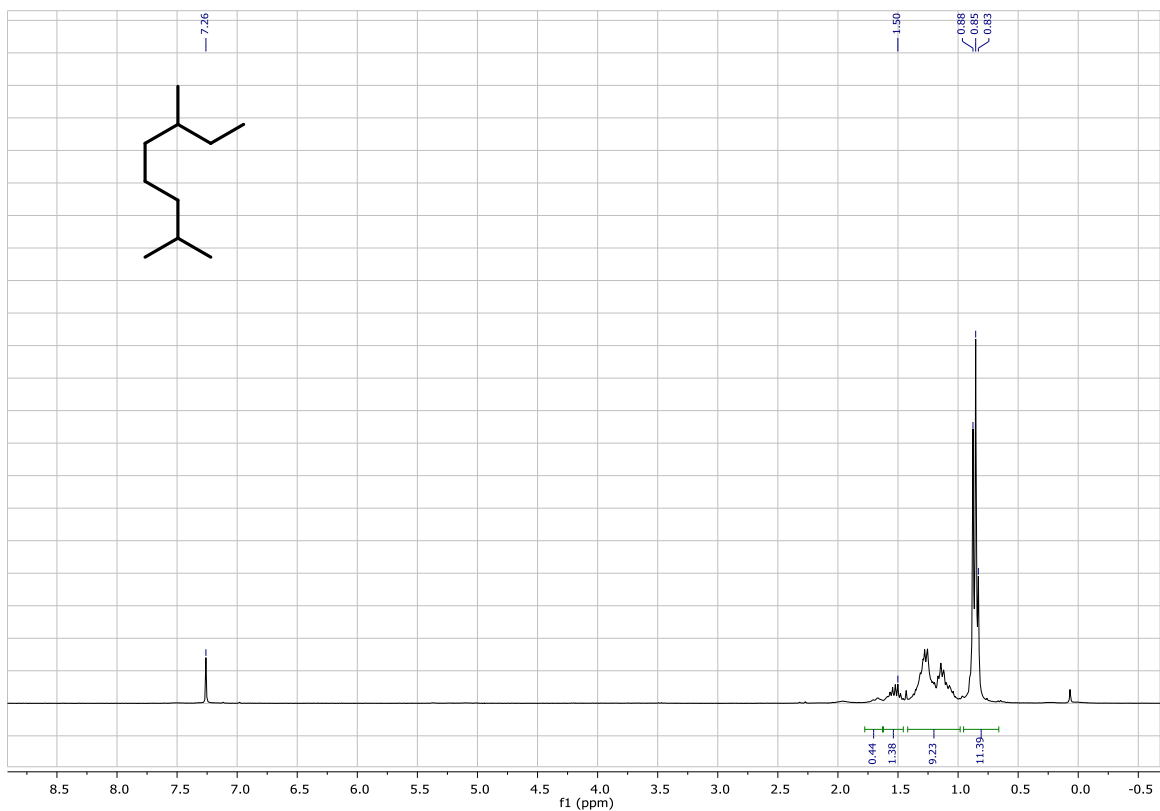
In an argon-filled glovebox a flame-dried 4 mL reaction vial was charged with CoBr_2 (0.006 mmol), anthracene (0.06 mmol) and THF (1 mL). The resulting pale blue solution was reduced by dropwise addition of LiEt_3BH (0.018 mmol, 1 M, THF) with a Hamilton® syringe during which the colour changed to black. After 10 h stirring, the suspension was removed from the glovebox and the particles were separated by a magnet. An aliquot (0.5 mL) was taken from the reaction solution and the solvent was removed under reduced pressure. The residue was solubilized in HNO_3 (5 mL, 20% w/w, water). After filtration, the concentration of cobalt was measured by ICP-OES.

$[\text{c}(\text{Co})] = 0.0060(1)$ mM, which is equivalent to 1 % of the initial $[\text{c}(\text{Co})]$.

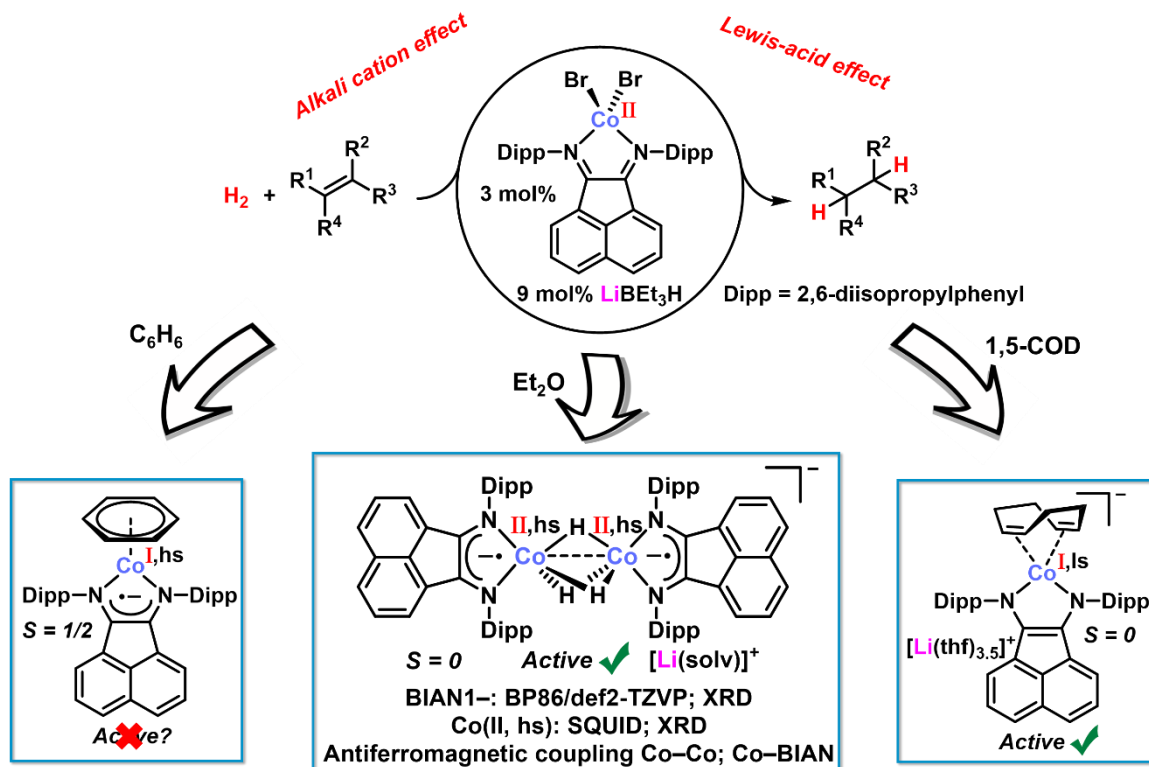
3.5.5 Selected NMR spectras of isolated products



3 Olefin-Stabilized Cobalt Nanoparticles for C=C, C=O and C=N Hydrogenations



4 Cobalt-Catalyzed Hydrogenations via Olefin Cobaltate and Hydride Intermediates^{IV}



^{IV} Reproduced with permission from: S. Sandl, T. M. Maier, N. P. van Leest, S. Kröncke, U. Chakraborty, S. Demeshko, K. Koszinowski, B. de Bruin, F. Meyer, M. Bodensteiner, C. Herrmann, R. Wolf, A. Jacobi von Wangelin, *ACS Catal.* **2019**, 9, 7596–7606. Copyright 2019 ACS, Washington; schemes, figures and text may differ from published version.

Author contribution:

S. Sandl: Development of catalytic reaction conditions (Table 4.1); investigation of the reaction mechanism (Scheme 4.3, Table 4.2); syntheses and characterization of **3**, **4a** and **4b** (Scheme 4.5, Figure 4.2/4.5); reactivity of **1**, **2** and **4b** with technical assistance by U. Otterpohl (Scheme 4.6); manuscript preparation.

S. Sandl and T. Maier: Substrate scope (Scheme 4.1/4.2).

T. Maier: Syntheses and characterization of **1** and **2** (Scheme 4.5, Figure 4.2); gas evolution measurement (Figure 4.5.31) and amine-borane dehydrogenation of **4a** (Figure 4.5.32); reaction progress analyses with technical assistance by F. Seeberger (Scheme 4.4); UV-vis spectroscopy and CV analyses of **3**, **4a** and **4b**.

N. P. van Leest and B. de Bruin: EPR experiments (Figure 4.3).

S. Kröncke and C. Herrmann: DFT experiments (Figure 4.7).

U. Chakraborty and M. Bodensteiner: Technical assistance for crystallographic experiments. S. Demeshko and F. Meyer: SQUID experiments (Figure 4.6).

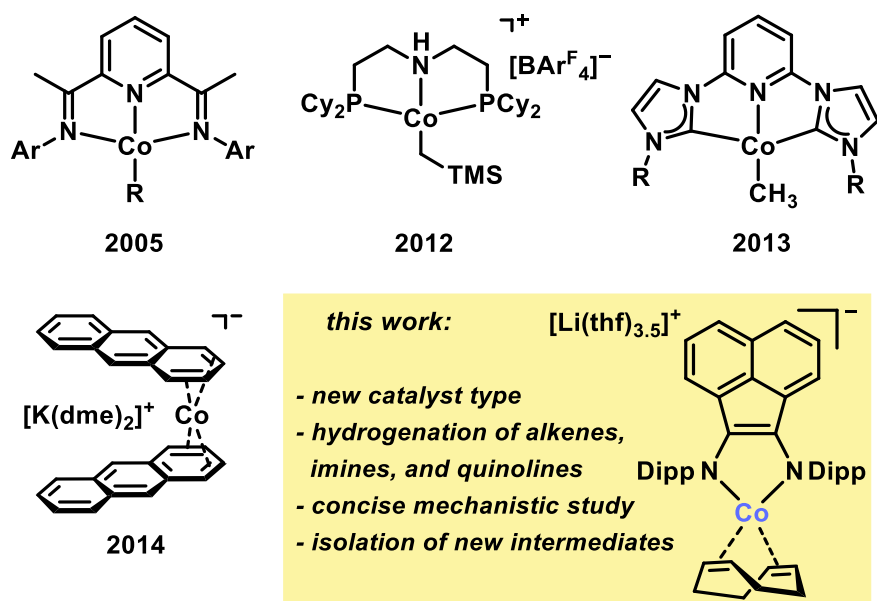
K. Koszinowski: ESI-MS experiments (Figure 4.4).

R. Wolf and A. Jacobi von Wangelin: Corresponding authors.

Abstract: Redox non-innocent ligands are a promising tool to moderate electron transfer processes within base-metal catalysts. This report introduces bis(imino)acenaphthene (BIAN) cobaltate complexes as hydrogenation catalysts. Sterically hindered tri-substituted alkenes, imines, and quinolines underwent clean hydrogenation under mild conditions (2-10 bar, 20-80°C) by use of the stable catalyst precursor $[(\text{Dipp})\text{BIAN}]\text{CoBr}_2$ and the co-catalyst LiEt_3BH . Mechanistic studies support the notion of a homogeneous catalysis pathway involving alkene and hydrido cobaltates as active catalyst species. Further, considerable reaction acceleration by alkali cations and Lewis acids was observed. The first cobaltate with bridging hydrides was isolated and fully characterized.

4.1 Introduction

Metal-catalyzed hydrogenations of alkenes constitute one of the key chemical transformations with numerous applications to lab-scale syntheses and industrial manufacture.^[1] The elucidation of the underlying catalytic mechanisms by Eisenberg, Halpern, Tolman, and others were major scientific milestones toward the understanding of catalytic elemental steps and the rational design of more active and selective catalysts.^{[1],[2]} Very recently, the dominance of hydrogenation catalysts based on the noble metals Rh, Ru, Ir, Pd, and Pt has been challenged by the development of highly active 3d transition metals.^[3] While the use of more abundant, cheaper, and often less toxic base metals constitutes an important contribution to a more sustainable chemistry, their distinct reactivity and selectivity was often plagued by undesirable destructive side reactions.^[4] Recently, elaborate ligand design enabled the development of highly active cobalt catalysts by the groups of Beller, Budzelaar, Chirik, Hanson, Elsevier, de Bruin, and others (Figure 4.1).^{[5],[6],[7],[8]} In most of the recent literature works, the implementation of pincer ligands (e.g. *NNN*; *PNP*; *CNC*) proved pivotal to the control of high activity and selectivity.^[9] Following our previous work on metalates with redox non-innocent arene ligands,^{[10],[11]} we believed that an efficient 3d metal catalyst for hydrogenation reactions would fulfill the following criteria: *i*) facilitation of redox steps at the metal by a redox-active ligand; *ii*) modular ligand design that allows for convenient synthesis and easy catalyst tuning; *iii*) stabilization of reduced forms of the catalyst by the ligand, and *iv*) broad scope of hydrogenations of unsaturated C=C and C=X.

Figure 4.1. Homogeneous cobalt catalysts for hydrogenations.^{[8]a,b,c,[8]}

Imine-based ligand architectures constitute a privileged class of ligands as evidenced by the numerous applications to catalytic reactions.^[7] Simple α -diimine catalysts were first introduced by *tom Dieck* and co-workers in 1977.^[12] Pincer-type motifs such as pyridinediimines^[13] (PDI) have recently received great attention. Bis(imino)acenaphthenes^{[14],[15]} (BIANs) are another class of ligands that fulfill the aforementioned criteria: BIANs can be rapidly assembled from commercial precursors on multi-gram scales and are highly redox-active as they can harbor up to four electrons.^{[14]b} There are eight reports of (BIAN)cobalt complexes with five applications to catalysis.^[16] On this basis, we investigated combinations of BIAN ligands and cobalt salts toward their ability to form active hydrogenation catalysts. Documented herein are the benefits of using this simple catalytic system that presents tangible advances over the current state-of-the-art that could not have been predicted: Clean hydrogenations of challenging alkenes (e.g. tetra-substituted), imines, and heteroarenes proceeded under mild conditions. New mechanistic insight was gained from the isolation of structurally novel olefin and hydride complexes as potential catalyst intermediates that are distinct from those of the traditional noble metal catalysts (Figure 4.1, bottom).

4.2 Results and Discussion

4.2.1 Optimization and alkene hydrogenation

Initially, we probed the feasibility of $(^{\text{Dipp}}\text{BIAN})\text{Co}^{\text{II}}\text{Br}_2$ to act as pre-catalyst for the hydrogenation of the model substrate triphenylethylene under very mild conditions (Dipp = 2,6-diiso-propylphenyl). High conversion was observed with lithium superhydride (LiEt_3BH) as co-catalyst at 2 bar H_2 and room temperature with only 3 mol% $(^{\text{Dipp}}\text{BIAN})\text{CoBr}_2$ (Table 4.1, procedure A). The presence of olefins during the reduction proved beneficial for the high catalyst activity, possibly due to transient olefin coordination and stabilization of the low-valent catalyst.^{[6]d,[17],[3]} The significantly lower activity of NaEt_3BH suggests a considerable alkali-cation effect (entry 5).^{†,[19]} Mono-, di- and tri-substituted alkenes were cleanly hydrogenated under 2-10 bar H_2 pressure at room temperature (Scheme 4.1).^[19] The high efficacy of the developed protocol was demonstrated in the hydrogenation of challenging tri- and tetra-substituted alkenes such as myrcene, α -pinene, and α,β,β -trimethylstyrene under mild conditions (Scheme 4.2). Under standard conditions, the hydrogenation of α -methylstyrene exhibited a turnover frequency (TOF) of 780 h^{-1} (Supporting Information). To the best of our knowledge, this protocol involves one of the most active homogeneous Co catalysts for alkene hydrogenations.^[8] Reduction-sensitive functional groups in the alkenes required a different protocol involving addition of the hydride co-catalyst prior to the alkene (protocol B, see Table 4.1, entry 2 and Scheme 4.2, right). This alternative protocol B was tolerant to chloride, bromide, ether, and ester functions.

Table 4.1. Selected optimization experiments.

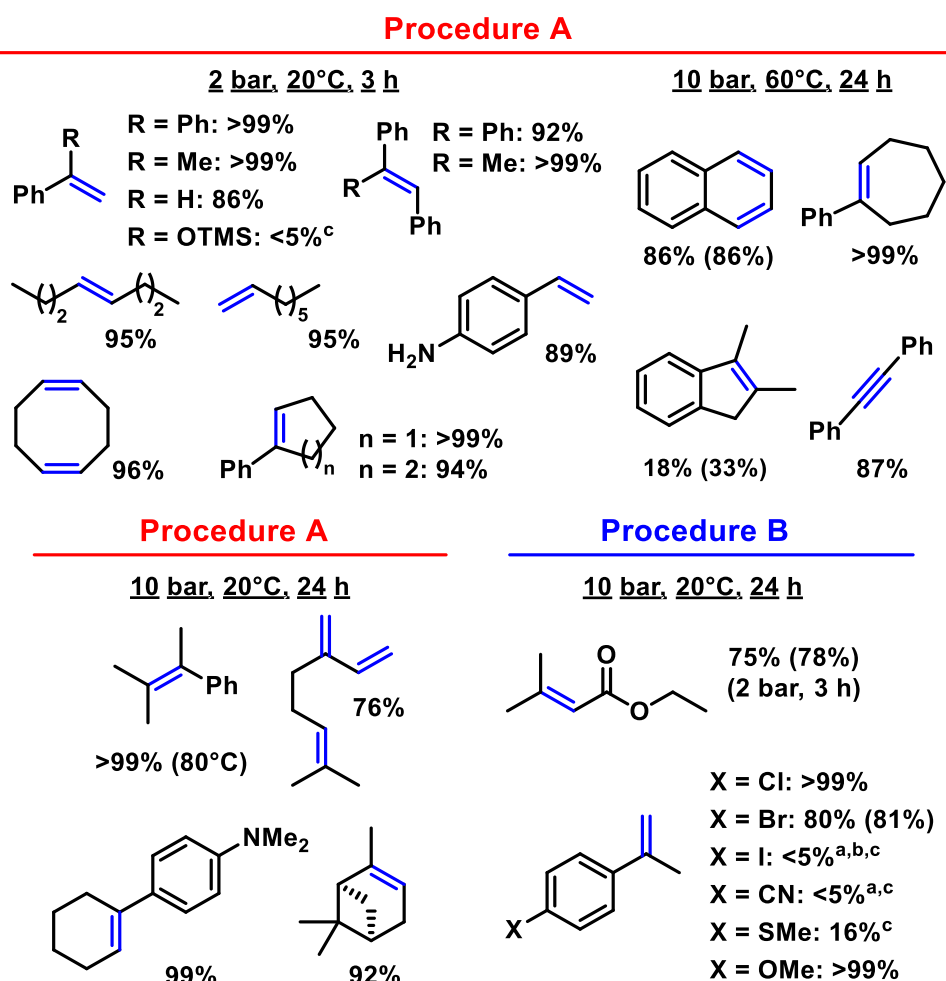
Entry	Deviation from standard conditions	Yield (%) ^a
1	A: reduction in presence of the substrate	92 (93)
2	B: substrate addition after reductant	41 (50)
3	A: 6 mol% LiEt ₃ BH	75 (75)
4	A: 6 mol% NaEt ₃ BH	23 (33)
5	A: 9 mol% NaEt ₃ BH	64 (65)
6	A: 9 mol% HBpin + 9 mol% KOtBu	1 (12)
7	A: (DippBIAN)CoCl ₂	72 (72)
8	A: CoCl ₂ + 2 DippBIAN	25 (35)
9	A: w/o reductant	<1 (9)

Conditions: 0.2 mmol alkene (1 M, THF), 9 mol% LiEt₃BH (1 M, THF), 3 mol% (DippBIAN)CoBr₂, 2 bar H₂; ^a Yields determined by quantitative GC-FID vs. internal *n*-pentadecane; conversions in parentheses.

4.2.2 Methodology extension: Hydrogenation of imines

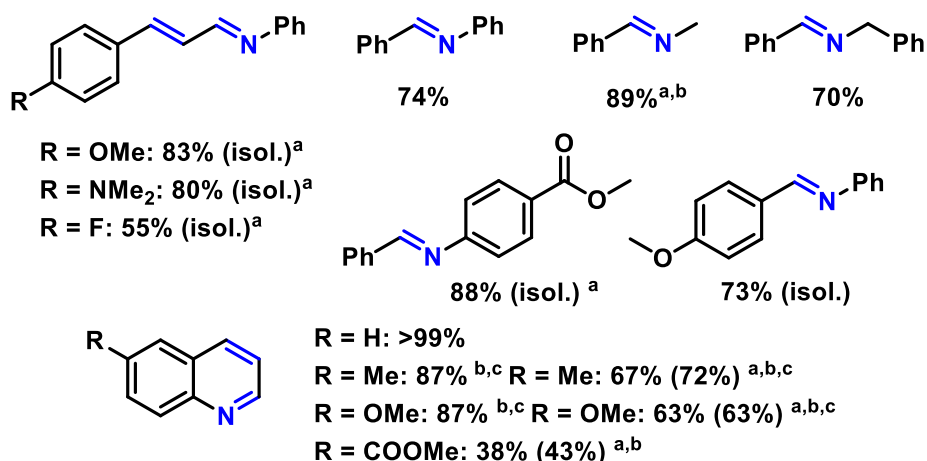
Despite being an atom-economic route to amines and tetrahydroquinolines that are often present in natural products and pharmaceuticals, homogeneous cobalt-catalyzed hydrogenation of imines^{[8]b,[10]} and quinolines^{[8]f,h} is still rather in its infancy. One possible implication of such reactions is catalyst poisoning by the substrate and product.^[21] Gratifyingly, our developed cobalt catalyst was also active in the hydrogenation of unsaturated C=N bonds.

Scheme 4.1. Substrate scope of cobalt-catalyzed hydrogenation of alkenes.



Bonds in blue indicate the site of complete π -bond hydrogenation. Standard conditions: 0.2 mmol alkene/alkyne (1 M, THF), 3 mol% (DippBIAN)CoBr₂, 9 mol% LiEt₃BH (1 M, THF). Yields were determined by quantitative GC-FID vs. *n*-pentadecane. Conversions are given in parentheses if <90%. **Procedure A:** Catalyst reduction in the presence of substrate. **Procedure B:** Catalyst reduction in the absence of substrate. ^a Traces of α -methylstyrene formed. ^b Traces of cumene formed. ^c Conversion <20%.

Scheme 4.2. Hydrogenation of imines and quinolines. Blue bonds indicate the sites of double bond hydrogenation. Conditions: Procedure A, 0.2 mmol substrate (1 M, THF), 3 mol% (Dipp)BIAN)CoBr₂, 9 mol% LiEt₃BH (1 M, THF); 10 bar H₂, 60 °C, 24 h. GC-FID yields vs. internal *n*-pentadecane; conversions in parentheses if <90%. ^a Procedure B. ^b 80 °C. ^c traces of the 5,6,7,8-tetrahydroquinoline derivative.



Very good conversions were observed under comparably mild conditions to the reported catalysts (10 bar H₂ and 60°C, Scheme 5.2).^{[8]b,f,h,[8]}

4.2.3 Mechanism

The advent of powerful 3d transition metal catalysts has gone hand in hand with the utilization of redox-active ligands that profoundly influence the electronic properties at the metal ions and enable redox reactivity patterns that are distinct from those of noble metals catalysts.^[9] The reaction mechanisms of catalytic alkene hydrogenations with 2nd and 3rd row transition metals (Rh, Ru, Ir, Pd, Pt) are very well understood. For the classical Rh-catalyzed hydrogenation, alkene and hydride complexes have been determined as key catalyst intermediates and the elemental reaction steps to involve two electron redox events at the metal.^{[1],[2],[7],[8]} There is much less insight into the hydrogenation mechanisms of first row transition metals; the nature of the key catalyst intermediates are still largely unexplored. Chirik and coworkers reported on a bis(aryl-imidazol-2-ylidene)pyridine cobalt hydride complex and a radical pathway that operate in cobalt-catalyzed alkene hydrogenations.^{[8]c} In this work, we aimed at a concise

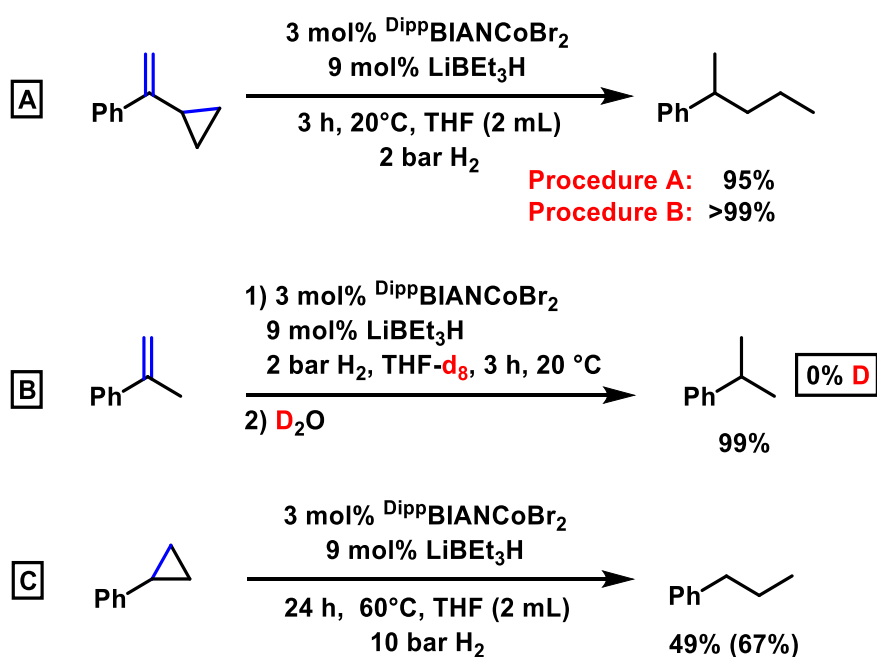
mechanistic study of Co-BIAN catalysts in alkene hydrogenations that would address the following questions: Is the BIAN ligand redox-active under the reaction conditions?^[9] Are radical pathways operating?^[7] To what extent are heterogeneous catalyst species involved?^[22] Do alkene and hydride intermediates play a similarly important role as with 4d and 5d metal catalysts?

We commenced our mechanistic studies with a set of key experiments that addressed the operation of radical mechanisms and the topicity of the active catalysts species. Initially, radical probes were evaluated. α -Cyclopropyl styrene underwent dual alkene hydrogenation and hydrogenative ring-opening to give 2-phenylpentane in excellent yields following protocol A or B, respectively (Scheme 4.3, A). This might be indicative of a mechanism involving hydrogen atom transfer (HAT).^[23] Furthermore, this is in full accord with our observations that non-styrenic olefins (i.e. alkenes without aryl substituents that could stabilize potential radical intermediates in benzyl positions) constitute more difficult substrates under the standard conditions. Hydrogen atom transfer from the solvent is rather unlikely as no deuterium incorporation could be determined from reactions in THF- d_8 (Scheme 4.3, B). The high activity of the catalyst was further demonstrated by the challenging hydrogenation of a σ -bond in cyclopropylbenzene (Scheme 4.3, C). In the absence of H_2 , 1-octene rapidly isomerized to a mixture of octene regioisomers and stereoisomers. With the terminal alkyne phenylacetylene, slow cyclotrimerization to triphenylbenzene was observed in low yield (see Supporting Information).^[24]

The clear distinction between homogeneous and heterogeneous catalyst species is intricate,^[22] yet our observations are consistent with a homogeneous mechanism. Reaction progress analyses documented an immediate onset of catalytic activity and steady conversion, which indicates a zero order for the substrate in the rate law (Scheme 4.4, red curve). Thus, the rate-determining step presumably does not include olefin coordination. A plot of the initial rates versus catalyst concentrations showed a first order rate in cobalt.[†] The absence of any sigmoidal curvature argues clearly against initial pre-catalyst nucleation and particle formation.^[6] However, an induction period might be not visible due to the experimental setup (Procedure B, substrate conversion determined by gas-uptake).[†] Kinetic poisoning studies are a competent tool to ascertain the topicity of the operating catalyst species.^[22] The attempted amalgamation of the catalyst with

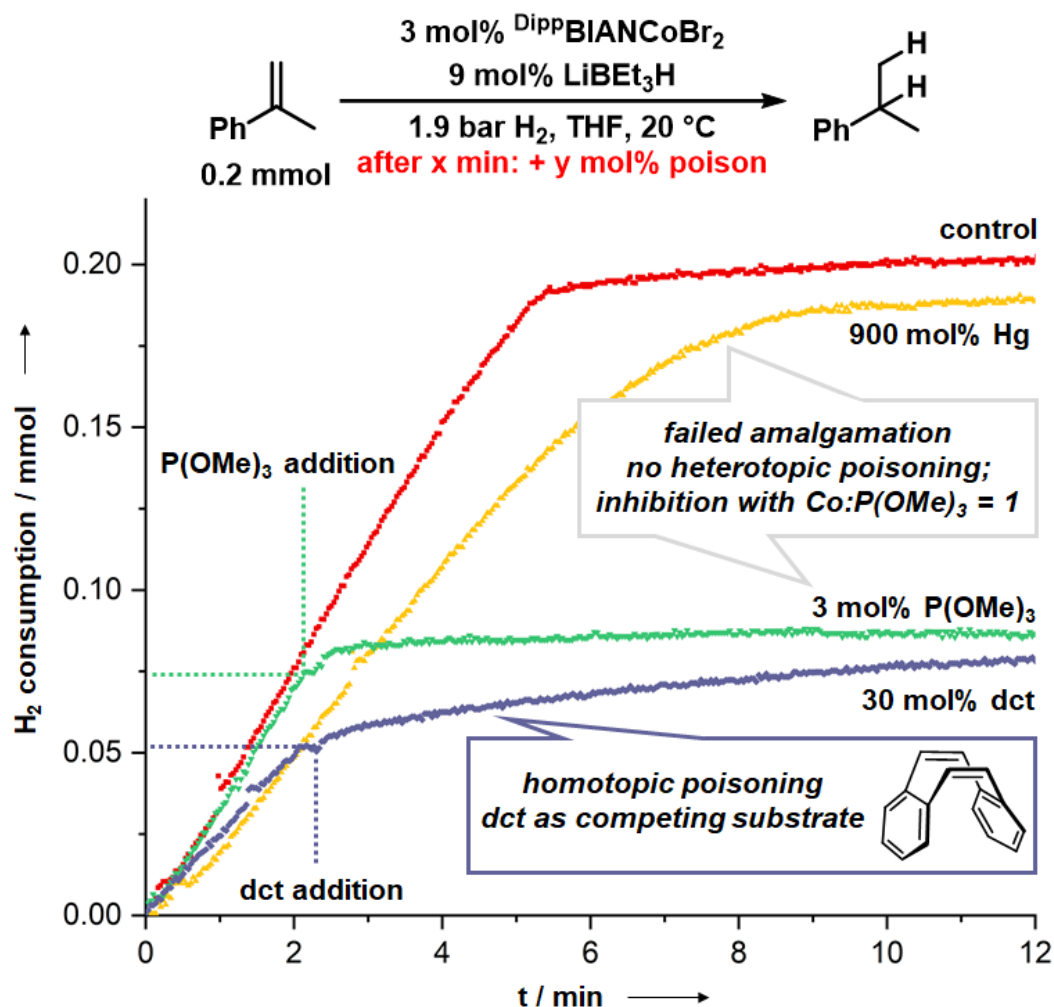
300 equiv. Hg had only a minimal effect on the reaction rate. Upon addition of sub-catalytic amounts of trimethylphosphite ($\text{P}(\text{OMe})_3$, 0.3 mol%), partial catalyst inhibition was recorded. Complete inhibition was achieved at a catalyst/poison ratio of 1:1 which is consistent with a homotopic catalyst (Scheme 4, green curve). The selective homotopic catalyst poison dibenzo[*a,e*]cycloocta-tetraene^[21] (dct, 10 equiv. per Co) resulted in catalyst inhibition which was slightly diminished by the concomitant hydrogenation of dct as a competing substrate (Scheme 4.4, violet curve, 31% conversion of dct).[†] The lower efficacy of dct as poison is presumably a consequence of the lower stability of 3d olefin complexes vs. their heavier congeners.^[3]

Scheme 4.3. Key mechanistic experiments.



Scheme 4.4. Catalyst poisoning studies with P(OMe)₃, Hg, and dct.

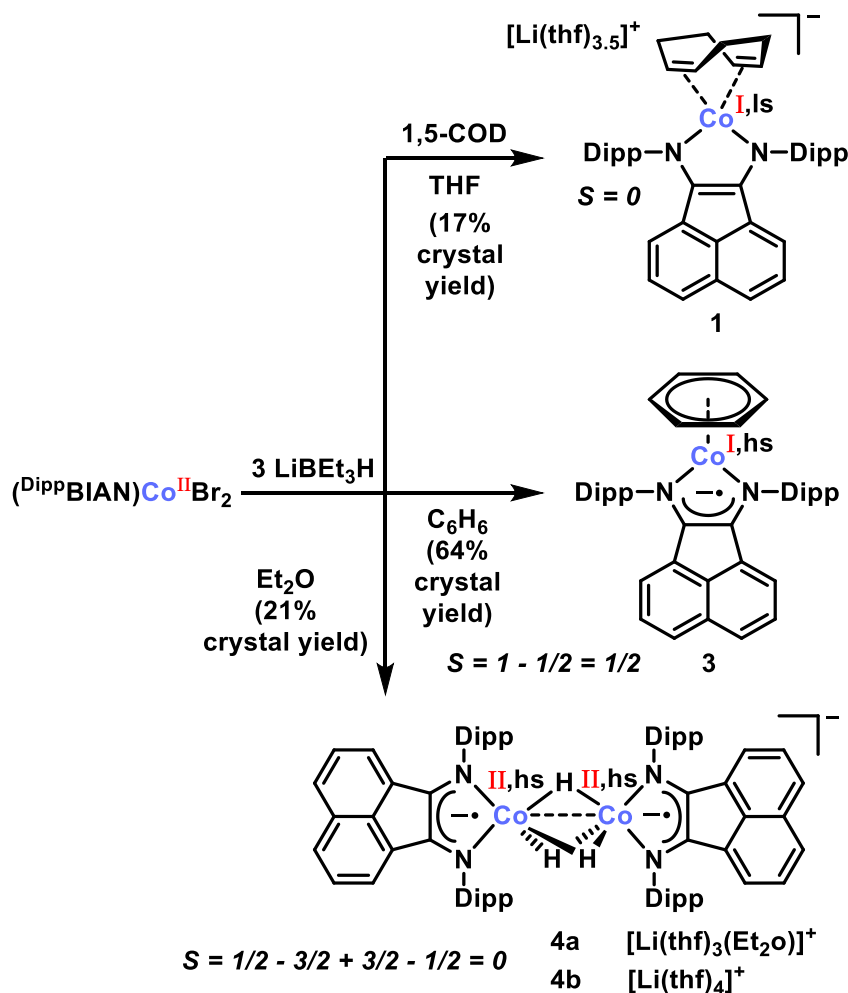
Procedure B. Substrate conversion determined by gas-uptake and quantitative GC-FID vs. *n*-pentadecane.



Based on the initial mechanistic experiments, we postulate a homotopic mechanism by molecular cobalt catalysts. The distinct electronic properties of 3d transition metals vs. their heavier congeners might also entail the participation of catalyst structures that are different from the Rh(I) catalysts of hydrogenation reactions. While the operation of alkene and hydride pathways has been intensively studied in rhodium-catalyzed hydrogenations, the knowledge of related catalyst intermediates with cobalt is still rather in its infancy. In an effort to identify potential catalyst species, we investigated reactions of (Dip^PBIAN)CoBr₂ with 3

equiv. LiEt_3BH in THF solution (Scheme 4.5). LIFDI-MS (liquid injection field desorption mass spectrometry) analyses of the crude catalyst mixture displayed the formation of the low-valent dimer $[(^{\text{Dipp}}\text{BIAN})\text{Co}]_2$ which is structurally related to a complex with two direct cobalt-arene bonding interactions prepared by Yang and coworkers using a different diimine.^[26] In an effort to prepare the reduced $(^{\text{Dipp}}\text{BIAN})\text{Co}$ unit, we employed several arenes and olefins as labile coordination placeholders to obtain structurally related intermediates. Reduction of $^{\text{Dipp}}\text{BIANCoBr}_2$ in THF with 3 equiv. LiEt_3H and excess amounts of 1,5-cyclooctadiene (cod) led to the formation of $[\text{Li}(\text{thf})_{3.5}\{(^{\text{Dipp}}\text{BIAN})\text{Co}(\text{cod})\}]$ (**1**) which was isolated after recrystallization in 17 % yield.^{[27],[16]c} This complex is the corresponding Li salt to our previously described potassium cobaltate (**2**) and shows similar ^1H and ^{13}C spectra.^{[16]c} Based on literature precedents, the oxidation level of BIAN in **1** can be assigned as 2– from the crystallographic bond distances (C-C: 1.389(4) Å; C-N: 1.383(3) Å; Figure 4.2).^{[28],[29]} In comparison, $^{\text{Dipp}}\text{BIANCoBr}_2$ consists of a neutral BIAN (C-C: 1.513(7) and 1.521(6) Å; C-N: 1.277(7)–1.286(8) Å).^{[16]b,[28],[29]}

Scheme 4.5. Cobalt complexes **1**, **3** and **4** that were isolated from reactions of $(\text{DippBIAN})\text{CoBr}_2$ and LiEt_3H .



The analogous reduction of $(\text{DippBIAN})\text{CoBr}_2$ with 3 equiv. LiEt_3BH in benzene furnished the neutral complex $[(\text{DippBIAN})\text{Co}(\eta^6\text{-C}_6\text{H}_6)]$ (**3**) as dark red single crystals in 64 % yield.^[30] Single crystal structure analysis suggests a radical anion state of the BIAN ligand (C-C: 1.433(2) Å; C-N: 1.3246(19) Å and 1.3224(19) Å, Figure 4.2), which was further investigated by EPR.^{[28],[29]} The X-band spectrum of **3** in toluene glass at 20 K (Figure 4.3) shows a rhombic symmetry and was simulated in accordance with an unpaired electron coupled to a spin 7/2 nucleus. We attribute this signal to a cobalt-centered radical.[†] Inclusion of the Euler angles $[-2.0, +90.0, 0]$ proved to be necessary to align the g and A_{Co} tensors and provided a more satisfactory simulation of the measured spectrum. Some linear and quadratic A -strain parameters have been included to simulate the final line shape.[†]

Some remaining slight deviations in the line shapes between simulation and experiment can be attributed to non-perfect glass formation. The provided simulation allowed for accurate determination of the g and A_{Co} tensors (MHz): [2.013, 2.145, 2.134] and [+185.0, +406.0, 198.4], respectively. These results are in agreement with an effective magnetic moment μ_{eff} of $1.9 \mu_{\text{B}}$ (Evans method, C_6D_6), which is only slightly higher than the spin-only value for an $S = \frac{1}{2}$ system ($\mu_{\text{eff}} = 1.7 \mu_{\text{B}}$).

Figure 4.2. Molecular structures of 1, 3 and 4. Thermal ellipsoids at the 50% probability level; minor disordered parts, non-coordinated solvents, and selected H atoms were omitted for clarity.

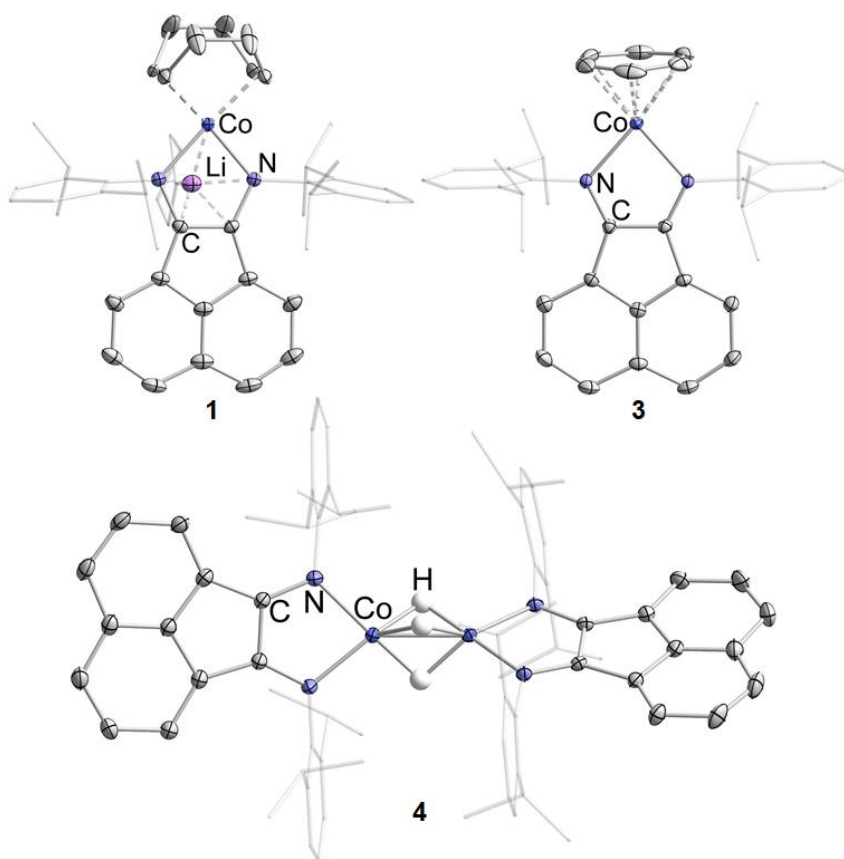
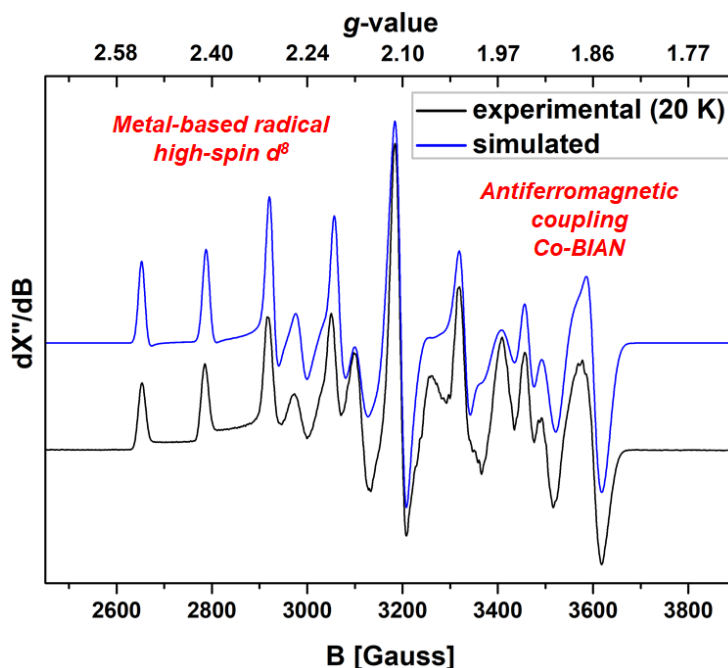


Figure 4.3. Simulated (blue) and experimental (black) X-band EPR spectrum of **3.** In toluene glass at 20 K. $\nu = 9.389494$ GHz, microwave power = 1.002 mW, mod. amp. = 1.000 G.



Further analysis of **3** included elemental analysis, LIFDI-MS ($m/z = 637.2781$), cyclic voltammetry (CV, one reversible reduction, $E = -2.3$ V vs. Fc/Fc^+) and UV-VIS (C_6H_6 , $\nu_{max} = 481$ nm, $\epsilon_{max} = 14300$ mol $^{-1}$ cm $^{-1}$ L). The combined data point to a highly unusual electronic structure of complex **3** which is described as a $[(BIAN^-)Co^I(\eta^6-C_6H_6)]$ complex that contains a very rare high-spin Co(I) center.^[31] The BIAN radical anion is (strongly) antiferromagnetically coupled to the $S = 1$ Co(I) ion, thus resulting in an effective $S = \frac{1}{2}$ system with the unpaired electron being primarily located at Co (as detected by EPR). The cobalt-arene coordination in **3** is not only relevant for the catalysis protocol, as it is structurally related to $[(Dipp)BIAN)Co]_2$. Moreover, substrates may coordinate in a similar way, as most substrates involve a phenyl ring. **3** also co-crystallized in a benzene-free synthesis of **1**, which might be a consequence of a solvent impurity.

Transition metal hydrides are key intermediates in many synthetic^[32] and biological^[33] processes. The largest industrial catalytic processes are hydrogenation reactions that operate via metal hydride species. Since the landmark studies of homogeneous Rh-catalyzed hydrogenations,^[2] extensive knowledge of hydridorhodium complexes has been collected whereas very little is

known about the nature and catalytic role of related intermediates in Co-catalyzed reactions. From a reaction of $(\text{DippBIAN})\text{CoBr}_2$ with 3 equiv. LiEt_3BH in Et_2O in a closed reaction vessel, we isolated a structurally unusual cobalt hydride complex.[†][34] Effervescence was observed during the reduction, presumably by formation of H_2 . Extraction with *n*-heptane and Et_2O afforded the anionic hydridocobaltate $[\text{Li}(\text{thf})_3(\text{Et}_2\text{O})\{(\text{DippBIAN})\text{Co}\}_2(\mu\text{-H})_3]$ (**4a**) as dark green microcrystals in 23 % yield (Figure 4.2).^[35] X-ray diffraction analysis revealed three hydride ligands (located in the electron density Fourier map) that bridge two $(\text{DippBIAN})\text{Co}$ units (Figure 4.2). The lithium counter-ion is solvent-separated,^{[14]b} **4** crystallizes as $[\text{Li}(\text{thf})_3(\text{Et}_2\text{O})]^+$ (**4a**) and $[\text{Li}(\text{thf})_4]^+$ (**4b**) solvate depending on the crystallization method. The molecular structure contains a very short Co-Co distance presumably due to the presence of three bridging hydrides: 2.2640(5) Å and 2.2426(3) for **4a** and **4b**, respectively. *To the best of our knowledge, the latter is the shortest $\text{Co}(\mu\text{-H})_n\text{Co}$ motif known to date* (2nd shortest: 2.249(1) Å).^{[35]b} The Co-H bond distances are between 1.51(2) and 1.63(5) Å. The twist angle between the two CoN_2 planes is 54.94(7)°. The NCCN bond lengths of BIAN are slightly shorter than in **3** (Figure 4.1; C-N: 1.333(3)–1.349(3) Å, C-C: 1.412(3)–1.419(3) Å), yet are in good agreement with the monoanionic BIAN in the complex $[(\text{DippBIAN})_2\text{Fe}]$ (C-N: 1.3367(15) and 1.3393(15) Å, C-C: 1.4234(18) Å) which contains a high-spin Fe^{2+} that is antiferromagnetically coupled to BIAN.^[36] Accordingly, the observed bond lengths of the BIAN ligands in **4** suggest a radical anion state of BIAN which is supported by theoretical studies (*vide infra*).^{[28],[29],[37]} The sum formula of **4** was further verified by negative-ion mode ESI mass spectrometry (Figure 5.4, $m/z = 1121.4$). The compound proved highly sensitive as unsealed THF solutions decomposed in an argon-filled glovebox within several hours to a red-brown paramagnetic mixture presumably by formation of H_2 . Direct evidence of such decomposition came from the gas-phase fragmentation of the mass-selected anionic component of **4** in ESI-MS. Apart from dissociation into its monomeric subunit $[(\text{DippBIAN})\text{CoH}_2]^-$, the dinuclear cobaltate readily underwent dehydrogenation (Figures 4.5.25 and 4.5.26). Remarkably, multiple dehydrogenation steps were operative (≥ 7). Most likely, the released H-atoms originated from the bridging hydrides and from the isopropyl groups of the DippBIANs . The $^1\text{H-NMR}$ spectrum of **4a** displayed a characteristic singlet resonance for the three bridging hydrides at -75.21 ppm (see supporting

information for 2D NMR analyses). This remarkable high-field shift may indicate an open-shell structure which was further investigated by temperature-dependent ^1H -NMR studies.^[38] The observed non-Curie behavior indeed points to an antiferromagnetic coupling of the cobalt centers with the diamagnetic ground state at low temperatures. Signal fitting provided a ratio of the coexisting configurations. Hence, the paramagnetic configurations are 27% of the singlet at 293 K (Figure 4.5).[†]^[39] The ratio decreased to 0.3 % at 193 K ($\Delta E_{\text{triplet-singlet}} = 21.4 \text{ kJ/mol}$). An effective magnetic moment $\mu_{\text{eff}} = 2.1 \mu_{\text{B}}$ was determined in solution at 293 K (Evans method, THF- d_8).

Figure 4.4. ESI-MS of 4a. Negative-ion mode ESI mass spectrum of **4a** (5 mM in THF). Inset: Experimental (black) and simulated (blue line) isotope pattern of $[\{(\text{DippBIAN})\text{Co}\}_2\text{H}_3]^-$.

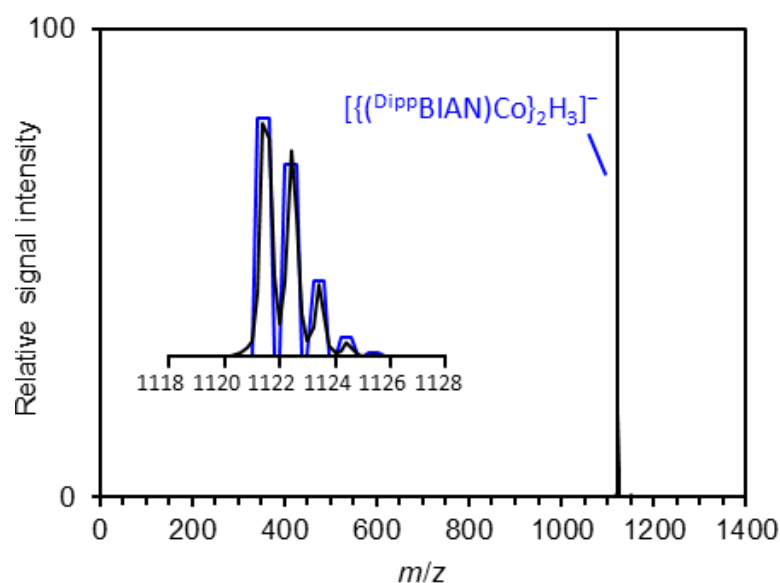
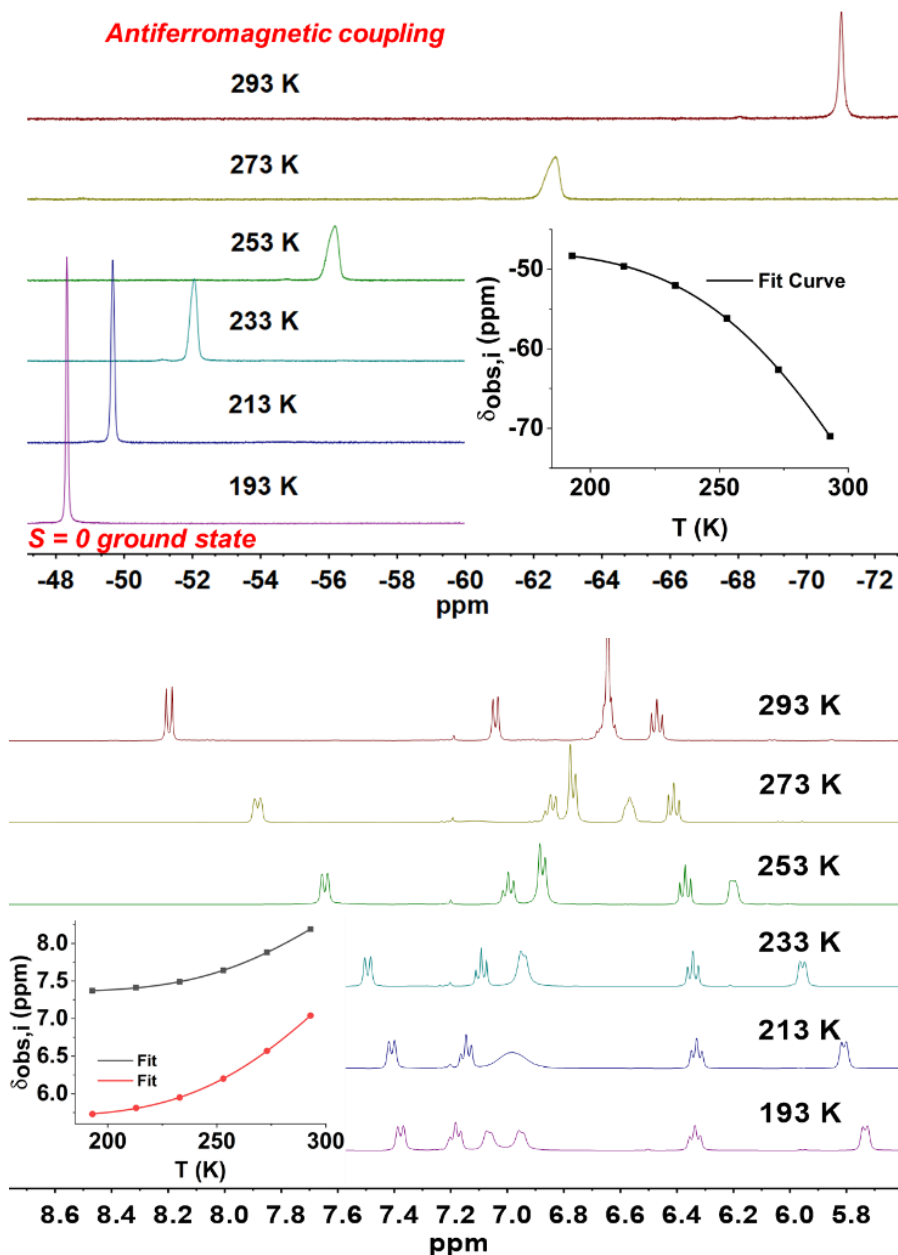


Figure 4.5. Variable temperature $^1\text{H-NMR}$ spectrum of **4a**.

The solid-state magnetic behaviour of **4b** was investigated in the 2–250 K range by SQUID magnetometry (Figure 4.6). The $\chi_{\text{M}}T$ product was $1.76 \text{ cm}^3\text{mol}^{-1}\text{K}$ (or $3.75 \mu_{\text{B}}$) at 250 K and decreased to almost zero by lowering the temperature, indicating overall antiferromagnetic coupling and a diamagnetic ground state of **4b**. The best fit was achieved using a model of four antiferromagnetically coupled centers: two BIAN radical anions with $S = \frac{1}{2}$ and two $S = \frac{3}{2}$ cobalt(II) ions. The best fit parameters were: $g(\text{BIAN}) = 2.0$ (fixed), $g(\text{Co(II)}) = 2.08$, $J(\text{BIAN-Co}) = -427 \text{ cm}^{-1}$ and $J(\text{Co-Co}) = -17 \text{ cm}^{-1}$.

Figure 4.6. Temperature-dependence of the product $\chi_M T$ of 4b.

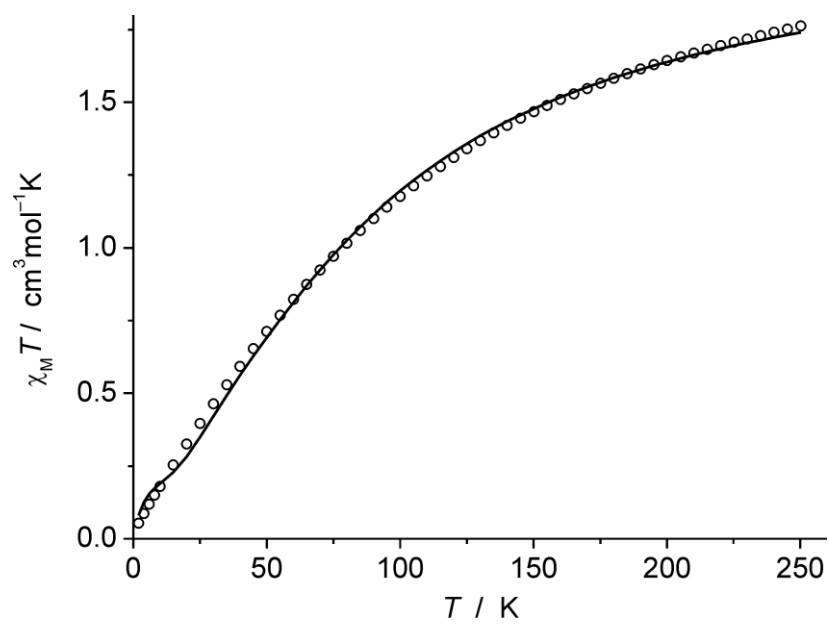
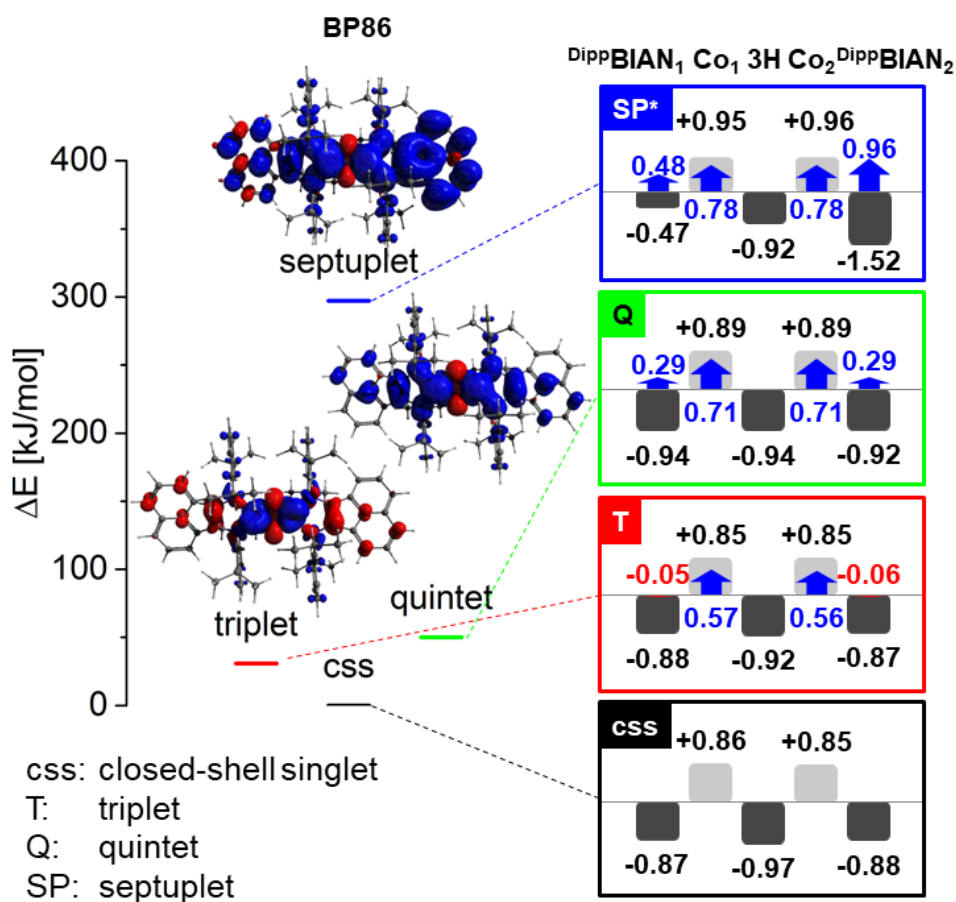


Figure 4.7. Energy diagram of 4 in various spin states. Anion optimized with BP86/def2-TZVP. Left: Spin density (isosurface value: 0.001) of the corresponding spin state. Right: Local charges (light/dark grey: positive/negative) and spins (blue/red: α/β) on specific fragments of the molecule in different spin states. A local spin of $\frac{1}{2}$ corresponds to one unpaired electron. * From single-point calc. on optimized mol. structure in css state (BP86/def2-TZVP).



Additional analyses of the cobaltate **4** include elemental analysis (EA), UV-VIS spectroscopy (C_6H_6 , $\lambda_{max}=474$ nm, $\epsilon_{max}=1200$ mol⁻¹cm⁻¹L), and CV (one reversible reduction, $E = -2.4$ V vs. Fc/Fc⁺). The combined data are strongly indicative of a highly unusual electronic structure of the trihydridodicobaltate **4**. The compound is best described as $[\{(DippBIAN^-)Co^{II}\}_2(\mu-H)_3]^{-1}$, assuming that DippBIAN and each bridging hydride atom are singly negatively charged, respectively. DFT calculations suggest a charge of 0.33– for each of the hydrides and of 0.85 for each of the cobalt centres (Figure 4.7). Since charge distributions are typically less polarized

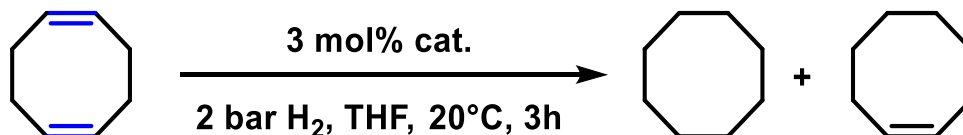
than formal oxidation numbers suggest, this is compatible with a Co^{II} assignment, even though it does not exclude Co^{I} . Importantly, DFT confirms the singlet ground state, this state being both lowest in energy and showing the best agreement with the X-ray crystallographic structure.^[37]

4.2.5 Hydrogenation Activities of Complexes 1-4 and Mechanistic Proposal

We evaluated the catalytic activities of the isolated cobalt complexes **1-4** and various pre-catalyst mixtures in a hydrogenation model reaction (Table 4.2). The cobaltate complex $[\text{Li}(\text{thf})_{3.5}\{\text{DippBIAN}\}\text{Co}(\text{cod})]$ **1** was found to be active for the hydrogenation of 1,5-cyclooctadiene (cod), albeit exhibiting slightly lower activity than the *in situ* formed catalyst (entry 2). Interestingly, **1** could be further activated by addition of 3 equiv. Et_3B (entry 5), which may indicate Lewis acid-assisted catalysis.^[40] The borane could facilitate the cleavage of H_2 as demonstrated by Peters and coworkers with a borylcobalt complex.^{[40]a} The catalytic inactivity of the corresponding potassium derivative $[\text{K}(\text{thf})\{\text{DippBIAN}\}\text{Co}(\text{cod})]$ **2** (Table 4.2, entry 6) manifested the observed alkali cation effect during our preliminary optimization experiments (Table 5.1, entries 1 and 5).^{†.[19]} One possible explanation for this effect is a cation– π interaction. It describes the attractive force between a cation and a π system and is one of the strongest non-covalent interactions. As mainly electrostatic interaction, the association free enthalpy (ΔH°) for the alkali metals with benzene follows the trend: $\text{Li}^+ > \text{Na}^+ > \text{K}^+$. Hence, the alkali cation can stabilize transition-states in the present catalysis or bind substrates (i.e. alkenes and/or arenes) in proximity to the catalyst.^[19] Moreover, alkali metals are able to tune the redox-activity of the ligand. Mazzanti and coworkers reported on ligand- or metal-based reduction of cobalt salophen complexes dependent on the alkali metal.^{[19]f} The group of Holland reported on reduced iron dimers with redox-active formazanate ligands. The dimer, which is stabilized by cation– π interactions, rearranged in THF solution to form a five-membered metallacycle with a reactivity order of $\text{Na}^+ > \text{K}^+ < \text{Rb}^+ < \text{Cs}^+$.^{[19]h}

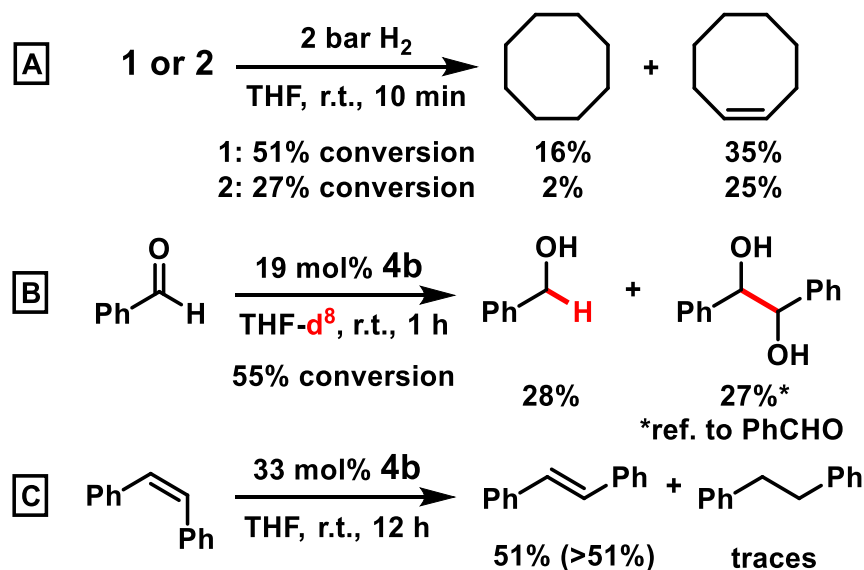
The neutral (benzene)cobalt complex $[(\text{DippBIAN})\text{Co}(\eta^6\text{-C}_6\text{H}_6)]$ **3** was only active after additional reduction with LiEt_3BH (Table 4.2, entry 16). Notably, the related 17-VE-complex $[(\text{dppe})\text{Co}(\text{cod})]$ bearing a redox-innocent ligand is indeed an

active pre-catalyst for hydrogenations.^{[7]d} The hydridocobaltate [Li(thf)₃(Et₂O){(DippBIAN)Co}₂(μ-H)₃] **4a** showed moderate hydrogenation activity which was significantly enhanced by further reduction with 0.5 equiv. of LiEt₃BH (entries 12 and 14). It may be speculated that **4** (or related derivatives) act as catalyst reservoirs for mononuclear hydrides as indicated by *in situ* NMR studies.[†] A catalytic mechanism via multinuclear metal complexes can be ruled out since the rate law includes the cobalt concentration in first order.^{†,[41]} Based on the collected synthetic, spectroscopic, and theoretical data, we propose a homotopic reaction mechanism that involves cobaltate complexes as active catalyst species. Rate acceleration by Lewis acids and an alkali-cation effect were observed.

Table 4.2. Hydrogenations with isolated complexes and pre-catalyst mixtures.

Entry	Catalyst mixture	Yields ^a	
1 ^b	(^{Dipp} BIAN)CoBr ₂ + 9 mol% LiBEt ₃ H	96 %	1 %
2	[Li(thf) _{3.5} { ^{Dipp} BIAN)Co(cod)}] 1	5 %	61 %
3	1 + 3.5 mol% 12-crown-4	4 %	44 %
4	1 + 3 mol% [Fc]PF ₆	2 %	17 %
5	1 + 9 mol% BEt ₃	66 %	33 %
6	[K(thf){(^{Dipp} BIAN)Co(cod)}] 2	-	1 %
7	2 + 3 mol% [Fc]PF ₆	1 %	-
8	2 + 30 mol% LiBr + [2.2.2]Cryptand	-	2 %
9	2 + 30 mol% LiCl + 3 mol% 18-crown-6	-	1 %
10	2 + 9 mol% BEt ₃	1 %	1 %
11	2 + 9 mol% BEt ₃ + 30 mol% LiBr	3 %	38 %
12 ^b	[Li(thf) ₃ (Et ₂ O){(^{Dipp} BIAN)Co} ₂ (μ ² -H) ₃] 4a	6 %	7 %
13 ^b	4a + 3 mol% Et ₃ B	22 %	22 %
14 ^b	4a + 1.5 mol% LiEt ₃ BH	57 %	43 %
15	[(^{Dipp} BIAN)Co(η ⁶ -C ₆ H ₆)] 3	-	-
16 ^c	3 + 9 mol% LiBEt ₃ H	4 %	29 %

Conditions: 0.2 mmol alkene, 0.1 M in THF, 3 mol% cat., 2 bar H₂. ^a Yields determined by quantitative GC-FID vs. internal *n*-pentadecane; ^b 1.5 mol% **4a**; ^c Reduction in presence of the substrate.

Scheme 4.6. Related Reactivity of **1**, **2** and **4**.

The observed alkali cation effect was also evident in a stoichiometric hydrogenation of **1** being readily reduced in contrast to **2** (Scheme 4.6, A). Preliminary explorations of the reactivity of relevant hydrides were performed with **4** as model compound: Protolysis occurred with the strong Brønsted acid HCl in dioxane to give H₂ evolution (2.3 ± 0.1 eq. H₂). In the presence of benzaldehyde, **4b** reacted to give 28% benzyl alcohol and 27% pinacol coupling product (Scheme 4.6, B). This may indicate the competing operation of hydride transfer and single-electron transfer processes from **4b**. In the absence of dihydrogen, incomplete isomerization of (*Z*)-stilbene to (*E*)-stilbene was observed (51%, Scheme 4.6, C). **4** represents a conceivable intermediate in our recently published (BIAN)Co-catalyzed amine-borane dehydrogenation reaction as it affords the same reaction products (borazine, cyclotriaminoborane, cyclodiaminoborane, H₃BNH₂-cyclo-B₃N₃H₁₁, polyborazine and polyaminoborane, Scheme 4.6, D).^[16]

4.3 Conclusion

In summary, this report has established reduced cobalt complexes as competent catalysts in a user-friendly hydrogenation protocol for challenging alkenes under mild conditions. The obtained reactivity suggests bidentate BIANs as interesting alternatives to well-established pincer-type motifs possessing comparably high activities in cobalt-catalyzed alkene and imine hydrogenations. Mechanistic studies revealed considerable alkali cation and Lewis-acid effects. Synthetic, kinetic, and spectroscopic experiments indicate a mechanism involving homotopic cobaltate catalysts. Catalytically relevant cobalt complexes were isolated that document the redox non-innocence of the BIAN ligand. Especially, the isolation of the hydridocobaltate **4** represents a tangible advance over the current state-of-the-art of transition metal hydrides. It contains the shortest $\text{Co}(\mu_2\text{-H})_n\text{Co}$ moiety known to date and represents the first reported cobaltate with bridging hydrides. In contrast to the vast majority of reported transition metal hydrides bearing multidentate phosphines, cyclopentadienyl, or carbonyl ligands, the high electron density in this complex is stabilized by the redox non-innocent BIAN. It is reasonable to assume that **4** constitutes a catalytically competent off-cycle intermediate of (BIAN)Co-catalyzed (de)hydrogenation reactions.^{[16]e}

Associated content

Crystal data for $(\text{D}^{\text{iPP}}\text{BIAN})\text{CoBr}_2$, **1**, **3**, **4a**, **4b** with CCDC 1909828, 1909827, 1909829, 1909830, 1909831, respectively (CIF).

Acknowledgment

This work was financed by the Deutsche Forschungsgemeinschaft (DFG, JA 1107/6-1, WO 1496/6-1, KK 2875/8-1), the European Research Council (ERC, CoG 683150) and the Fonds der Chemischen Industrie (T.M.M.)

4.4 References

- [1] (a) Nishimura, S. *Handbook of Heterogeneous Catalytic Hydrogenation for Organic Synthesis*; Wiley: New York, **2001**. (b) *The Handbook of Homogeneous Hydrogenation*. de Vries, J. G.; Elsevier, C.J., Eds.; Wiley-VCH: Weinheim, **2007**.
- [2] (a) Meakin, P.; Jesson, J. P.; Tolman, C. A. The Nature of Chlorotris(Triphenylphosphine)Rhodium in Solution and Its Reaction with Hydrogen. *J. Am. Chem. Soc.* **1972**, *94*, 3240–3242; (b) Tolman, C. A.; Meakin, P. Z.; Lindner, D. L.; Jesson, J. P. Triarylphosphine, Hydride, and Ethylene Complexes of Rhodium(I) Chloride. *J. Am. Chem. Soc.* **1974**, *96*, 2762–2774; (c) Halpern, J. Mechanistic Aspects of Homogeneous Catalytic Hydrogenation and Related Processes. *Inorg. Chim. Acta* **1981**, *50*, 11–19; (d) Halpern, J. Mechanism and Stereoselectivity of Asymmetric Hydrogenation. *Science* **1982**, *217*, 401–407; (e) Duckett, S. B.; Newell, C. L.; Eisenberg, R. Observation of New Intermediates in Hydrogenation Catalyzed by Wilkinson's Catalyst, RhCl(PPh₃)₃, Using Parahydrogen-Induced Polarization. *J. Am. Chem. Soc.* **1994**, *116*, 10548–10556.
- [3] Bullock, R. M. *Catalysis without Precious Metals*, Wiley-VCH, Weinheim, Germany, **2010**.
- [4] (a) Hess, W.; Treutwein, J.; Hilt, G. Cobalt-Catalysed Carbon-Carbon Bond-Formation Reactions. *Synthesis* **2008**, *40*, 3537–3562; (b) Holzwarth, M. S.; Plietker, B. Biorelevant Metals in Sustainable Metal Catalysis-A Survey. *ChemCatChem* **2013**, *5*, 1650–1679; (c) Röse, P.; Hilt, G. Cobalt-Catalysed Bond Formation Reactions; Part 2. *Synthesis* **2016**, *48*, 463–492.
- [5] *Non-Noble Metal Catalysis: Molecular Approaches and Reactions*. Klein Gebbink, R. J. M.; Moret, M.-E., Eds.; Wiley-VCH: Weinheim, Germany, **2019**.
- [6] Efficient heterogeneous Co catalysts have been prepared by chemical reduction, pyrolysis, or solvothermal synthesis: (a) Chen, F.; Topf, C.; Radnik, J.; Kreyenschulte, C.; Lund, H.; Schneider, M.; Surkus, A. E.; He, L.; Junge, K.; Beller, M. Stable and Inert Cobalt Catalysts for Highly Selective and Practical Hydrogenation of C≡N and C=O Bonds. *J. Am. Chem. Soc.* **2016**, *138*, 8781–8788; (b) Wei, Z.; Chen, Y.; Wang, J.; Su, D.; Tang, M.; Mao, S.; Wang, Y. Cobalt Encapsulated in N-Doped Graphene Layers: An Efficient and Stable Catalyst for Hydrogenation of Quinoline Compounds. *ACS Catal.* **2016**,

- 6, 5816–5822; (c) Jagadeesh, R. V.; Murugesan, K.; Alshammari, A. S.; Neumann, H.; Pohl, M.-M.; Radnik, J.; Beller, M. MOF-Derived Cobalt Nanoparticles Catalyze a General Synthesis of Amines. *Science* **2017**, *358*, 326–332; (d) Sandl, S.; Schwarzhuber, F.; Pöllath, S.; Zweck, J.; Jacobi von Wangelin, A. Olefin-Stabilized Cobalt Nanoparticles for C=C, C=O, and C=N Hydrogenations. *Chem. Eur. J.* **2018**, *24*, 3403–3407; (e) Büschelberger, P.; Reyes-Rodriguez, E.; Schöttle, C.; Treptow, J.; Feldmann, C.; Jacobi von Wangelin, A.; Wolf, R. Recyclable Cobalt(0) Nanoparticle Catalysts for Hydrogenations. *Catal. Sci. Technol.* **2018**, *8*, 2648–2653.
- [7] Reviews: (a) Chirik, P. J. Iron- and Cobalt-Catalyzed Alkene Hydrogenation: Catalysis with Both Redox-Active and Strong Field Ligands. *Acc. Chem. Res.* **2015**, *48*, 1687–1695; (b) Zell, T.; Langer, R. From Ruthenium to Iron and Manganese—A Mechanistic View on Challenges and Design Principles of Base-Metal Hydrogenation Catalysts. *ChemCatChem* **2018**, *10*, 1930–1940; (c) Mukherjee, A.; Milstein, D. Homogeneous Catalysis by Cobalt and Manganese Pincer Complexes. *ACS Catal.* **2018**, *8*, 11435–11469; (d) Papa, V.; Junge, K.; Beller, M. Cobalt-Pincer Complexes in Catalysis. *Chem. Eur. J.* **2019**, *25*, 122–143; (e) Alig, L.; Fritz, M.; Schneider, S. First-Row Transition Metal (De)Hydrogenation Catalysis Based On Functional Pincer Ligands. *Chem. Rev.* **2019**, *119*, 2681–2751; (f) Ai, W.; Zhong, R.; Liu, X.; Liu, Q. Hydride Transfer Reactions Catalyzed by Cobalt Complexes. *Chem. Rev.* **2019**, *119*, 2876–2953.
- [8] Selected examples: (a) Knijnenburg, Q.; Horton, A. D.; Van Der Heijden, H.; Kooistra, T. M.; Hetterscheid, D. G. H.; Smits, J. M. M.; De Bruin, B.; Budzelaar, P. H. M.; Gal, A. W. Olefin Hydrogenation Using Diimine Pyridine Complexes of Co and Rh. *J. Mol. Catal. A Chem.* **2005**, *232*, 151–159; (b) Zhang, G.; Scott, B. L.; Hanson, S. K. Mild and Homogeneous Cobalt-Catalyzed Hydrogenation of C=C, C=O, and C=N Bonds. *Angew. Chem., Int. Ed.* **2012**, *51*, 12102–12106; (c) Yu, R. P.; Darmon, J. M.; Milsmann, C.; Margulieux, G. W.; Stieber, S. C. E.; Debeer, S.; Chirik, P. J. Catalytic Hydrogenation Activity and Electronic Structure Determination of Bis(Arylimidazol-2-Ylidene)Pyridine Cobalt Alkyl and Hydride Complexes. *J. Am. Chem. Soc.* **2013**, *135*, 13168–13184; (d) Friedfeld, M. R.; Margulieux, G. W.; Schaefer, B. A.; Chirik, P. J. Bis(Phosphine)Cobalt Dialkyl Complexes

- for Directed Catalytic Alkene Hydrogenation. *J. Am. Chem. Soc.* **2014**, *136*, 13178–13181; (e) Rösler, S.; Obenauf, J.; Kempe, R. A Highly Active and Easily Accessible Cobalt Catalyst for Selective Hydrogenation of C=O Bonds. *J. Am. Chem. Soc.* **2015**, *137*, 7998–8001; (f) Xu, R.; Chakraborty, S.; Yuan, H.; Jones, W. D. Acceptorless, Reversible Dehydrogenation and Hydrogenation of N-Heterocycles with a Cobalt Pincer Catalyst. *ACS Catal.* **2015**, *5*, 6350–6354; (g) Korstanje, T.J.; van der Vlugt, J.I.; Elsevier, C.J.; de Bruin, B. Hydrogenation of Carboxylic Acids with a Homogeneous Cobalt Catalyst. *Science* **2015**, *350* (6258), 298-302; (h) Adam, R.; Cabrero-Antonino, J. R.; Spannenberg, A.; Junge, K.; Jackstell, R.; Beller, M. A General and Highly Selective Cobalt-Catalyzed Hydrogenation of N-Heteroarenes under Mild Reaction Conditions. *Angew. Chem., Int. Ed.* **2017**, *56*, 3216–3220.
- [9] (a) Lyaskovskyy, V.; de Bruin, B. Redox Non-Innocent Ligands: Versatile New Tools to Control Catalytic Reactions. *ACS Catal.* **2012**, *2* 270–279; (b) Luca, O. R.; Crabtree, R. H. Redox-Active Ligands in Catalysis. *Chem. Soc. Rev.* **2013**, *42*, 1440–1459.
- [10] (a) Gärtner, D.; Welther, A.; Rad, B. R.; Wolf, R.; Jacobi von Wangelin, A. Heteroatom-Free Arene-Cobalt and Arene-Iron Catalysts for Hydrogenations. *Angew. Chem., Int. Ed.* **2014**, *53*, 3722–3726; (b) Büschelberger, P.; Gärtner, D.; Reyes-Rodriguez, E.; Kreyenschmidt, F.; Koszinowski, K.; Jacobi von Wangelin, A.; Wolf, R. Alkene Metalates as Hydrogenation Catalysts. *Chem. Eur. J.* **2017**, *23*, 3139–3151.
- [11] Schnöckelborg, E. M.; Khusniyarov, M. M.; De Bruin, B.; Hartl, F.; Langer, T.; Eul, M.; Schulz, S.; Pöttgen, R.; Wolf, R. Unraveling the Electronic Structures of Low-Valent Naphthalene and Anthracene Iron Complexes: X-Ray, Spectroscopic, and Density Functional Theory Studies. *Inorg. Chem.* **2012**, *51*, 6719–6730.
- [12] tom Dieck, H.; Bruder, H. Bis(Diazadiene)Iron Complexes, $(R^1N=CR^2-CR^2=NR^1)_2Fe$. *J. Chem. Soc., Chem. Commun.* **1977**, *0*, 24–25.
- [13] Flisak, Z.; Sun, W. H. Progression of Diiminopyridines: From Single Application to Catalytic Versatility. *ACS Catal.* **2015**, *5*, 4713–4724.
- [14] (a) Hill, N. J.; Vargas-Baca, I.; Cowley, A. H. Recent Developments in the Coordination Chemistry of Bis(Imino)Acenaphthene (BIAN) Ligands with s-

- and p-Block Elements. *Dalton Trans.* **2009**, 0, 240–253; (b) Fedushkin, I. L.; Skatova, A. A.; Chudakova, V. A.; Fukin, G. K. Four-Step Reduction of Dpp-Bian with Sodium Metal: Crystal Structures of the Sodium Salts of the Mono-, Di-, Tri- and Tetraanions of Dpp-Bian. *Angew. Chem., Int. Ed.* **2003**, *42*, 3294–3298.
- [15] Selected examples of hydrogenations with BIAN: (a) van Asselt, R.; Elsevier, C. J. Homogeneous Catalytic Hydrogenation of Alkenes by Zero-Valent Palladium Complexes of Cis-Fixed Dinitrogen Ligands. *J. Mol. Catal.* **1991**, *65*, L13–L19; (b) Van Laren, M. W.; Elsevier, C. J. Selective Homogeneous Palladium(0)-Catalyzed Hydrogenation of Alkynes to (Z)-Alkenes. *Angew. Chem., Int. Ed.* **1999**, *38* (24), 3715–3717; (c) Villa, M.; Miesel, D.; Hildebrandt, A.; Ragaini, F.; Schaarschmidt, D.; Jacobi von Wangelin, A. Synthesis and Catalysis of Redox-Active Bis(Imino)Acenaphthene (BIAN) Iron Complexes. *ChemCatChem* **2017**, *9*, 3203–3209.
- [16] Selected (BIAN)Co reports: (a) Khusniyarov, M. M.; Harms, K.; Burghaus, O.; Sundermeyer, J. Molecular and Electronic Structures of Homoleptic Nickel and Cobalt Complexes with Non-Innocent Bulky Diimine Ligands Derived from Fluorinated 1,4-Diaza-1,3-Butadiene (DAD) and Bis(Arylimino)Acenaphthene (BIAN). *Eur. J. Inorg. Chem.* **2006**, 2985–2996; (b) Rosa, V.; Carabineiro, S. A.; Avilés, T.; Gomes, P. T.; Welter, R.; Campos, J. M.; Ribeiro, M. R. Synthesis, Characterisation and Solid State Structures of α -Diimine Cobalt(II) Complexes: Ethylene Polymerisation Tests. *J. Organomet. Chem.* **2008**, *693*, 769–775; (c) Pelties, S.; Maier, T.; Herrmann, D.; De Bruin, B.; Rebreyend, C.; Gärtner, S.; Shenderovich, I. G.; Wolf, R. Selective P 4 Activation by a Highly Reduced Cobaltate: Synthesis of Dicobalt Tetraphosphido Complexes. *Chem. - A Eur. J.* **2017**, *23*, 6094–6102. (d) Formenti, D.; Ferretti, F.; Topf, C.; Surkus, A.-E.; Pohl, M.-M.; Radnik, J.; Schneider, M.; Junge, K.; Beller, M.; Ragaini, F. Co-Based Heterogeneous Catalysts from Well-Defined α -Diimine Complexes: Discussing the Role of Nitrogen. *J. Catal.* **2017**, *351*, 79–89; (e) Maier, T. M.; Sandl, S.; Shenderovich, I. G.; Jacobi von Wangelin, A.; Weigand, J. J.; Wolf, R. Amine-Borane Dehydrogenation and Transfer Hydrogenation Catalyzed by α -Diimine Cobaltates. *Chem. – A Eur. J.* **2019**, *25*, 238–245; (f) Ziegler, C. G. P.; Maier, T. M.; Pelties, S.; Taube, C.; Hennersdorf, F.; Ehlers, A. W.; Weigand, J. J.;

- Wolf, R. Construction of Alkyl-Substituted Pentaphosphido Ligands in the Coordination Sphere of Cobalt. *Chem. Sci.* **2019**, *10*, 1302–1308.
- [17] Recent studies from our group showing the beneficial effect of olefins: (a) Gülak, S.; Jacobi von Wangelin, A. Chlorostyrenes in Iron-Catalyzed Biaryl Coupling Reactions. *Angew. Chem., Int. Ed.* **2012**, *51*, 1357–1361; (b) Gülak, S.; Gieshoff, T. N.; Jacobi von Wangelin, A. Olefin-Assisted Iron-Catalyzed Alkylation of Aryl Chlorides. *Adv. Synth. Catal.* **2013**, *355*, 2197–2202; (c) Gülak, S.; Stepanek, O.; Malberg, J.; Rad, B. R.; Katora, M.; Wolf, R.; Jacobi von Wangelin, A. Highly Chemoselective Cobalt-Catalyzed Biaryl Coupling Reactions. *Chem. Sci.* **2013**, *4*, 776–784.
- [18] (a) Johnson, J. B.; Rovis, T. More than Bystanders: The Effect of Olefins on Transition-Metal-Catalyzed Cross-Coupling Reactions. *Angew. Chem., Int. Ed.* **2008**, *47*, 840–871; (b) Defieber, C.; Grützmacher, H.; Carreira, E. M. Chiral Olefins as Steering Ligands in Asymmetric Catalysis. *Angew. Chem., Int. Ed.* **2008**, *47*, 4482–4502.
- [19] Cation effects: (a) Collman, J. P.; Finke, R. G.; Cawse, J. N.; Brauman, J. I. Lewis Acid Catalyzed [RFe(CO)₄]⁻ Alkyl Migration Reactions. A Mechanistic Investigation. *J. Am. Chem. Soc.* **1978**, *100*, 4766–4772; (b) Hartmann, R.; Chen, P. Noyori's Hydrogenation Catalyst Needs a Lewis Acid Cocatalyst for High Activity. *Angew. Chem., Int. Ed.* **2001**, *40*, 3581–3585. (c) Macchioni, A. Ion Pairing in Transition-Metal Organometallic Chemistry. *Chem. Rev.* **2005**, *105*, 2039–2073; (d) Kennedy, C. R.; Lin, S.; Jacobsen, E. N. The Cation- π Interaction in Small-Molecule Catalysis. *Angew. Chemie Int. Ed.* **2016**, *55*, 12596–12624; (e) Kita, M. R.; Miller, A. J. M. An Ion-Responsive Pincer-Crown Ether Catalyst System for Rapid and Switchable Olefin Isomerization. *Angew. Chem., Int. Ed.* **2017**, *56*, 5498–5502; (f) Andrez, J.; Guidal, V.; Scopelliti, R.; Pécaut, J.; Gambarelli, S.; Mazzanti, M. Ligand and Metal Based Multielectron Redox Chemistry of Cobalt Supported by Tetradentate Schiff Bases. *J. Am. Chem. Soc.* **2017**, *139*, 8628–8638; (g) Neel, A. J.; Hilton, M. J.; Sigman, M. S.; Toste, F. D. Exploiting Non-Covalent π Interactions for Catalyst Design. *Nature* **2017**, *543*, 637–646; (h) Broere, D. L. J.; Mercado, B. Q.; Bill, E.; Lancaster, K. M.; Sproules, S.; Holland, P. L. Alkali Cation Effects on Redox-Active Formazanate Ligands in Iron Chemistry. *Inorg. Chem.* **2018**, *57*, 9580–9591; (i) Yamada, S. Cation- π Interactions in Organic Synthesis. *Chem. Rev.*

- 2018**, *118*, 11353–11432; (j) Mahmudov, K. T.; Gurbanov, A. V.; Guseinov, F. I.; Guedes da Silva, M. F. C. Noncovalent Interactions in Metal Complex Catalysis. *Coord. Chem. Rev.* **2019**, *387*, 32–46.
- [20] α -Methylstyrene was hydrogenated under standard conditions in the presence of various functional additives (1 equiv., protocol B, 3 h, 20 °C, THF (2 mL)): No decrease in hydrogenation activity was observed with added PhNH₂, whereas reduced activity was observed with 4-Tol-CH₂OH, PhC(O)Ph, respectively. No conversion was obtained in the presence of PhCN, PhC(O)H, PhNO₂, respectively.[†]
- [21] (a) Giustra, Z. X.; Ishibashi, J. S. A.; Liu, S.-Y. Homogeneous Metal Catalysis for Conversion between Aromatic and Saturated Compounds. *Coord. Chem. Rev.* **2016**, *314*, 134–181; (b) Seo, C. S. G.; Morris, R. H. Catalytic Homogeneous Asymmetric Hydrogenation: Successes and Opportunities. *Organometallics* **2019**, *38*, 47–65; (c) Muthukrishnan, I.; Sridharan, V.; Menéndez, J. C. Progress in the Chemistry of Tetrahydroquinolines. *Chem. Rev.* **2019**, *119*, 5057–5191.
- [22] (a) Widegren, J. A.; Finke, R. G. A review of the problem of distinguishing true homogeneous catalysis from soluble or other metal-particle heterogeneous catalysis under reducing conditions. *J. Mol. Catal. A* **2003**, *198*, 317–341; (b) Astruc, D.; Lu, F.; Aranzaes, J. R. Nanoparticles as Recyclable Catalysts: The Frontier between Homogeneous and Heterogeneous Catalysis. *Angew. Chem., Int. Ed.* **2005**, *44*, 7852–7872; (c) Crabtree, R. H., Resolving Heterogeneity Problems and Impurity Artifacts in Operationally Homogeneous Transition Metal Catalysts. *Chem. Rev.* **2012**, *112*, 1536–1554. (d) Drost, R.M.; Rosar, V.; Dalla Marta, S.; Lutz, M.; Demitri, N.; Milani, B.; de Bruin, B.; Elsevier, C.J., Pd-Catalyzed Z-Selective Semihydrogenation of Alkynes: Determining the Type of Active Species. *ChemCatChem*, **2015**, *7*, 2095–2107.
- [23] (a) Kinetics and mechanism of the hydrogenation of α -cyclopropylstyrene: Rate constant of the ring-opening rearrangement of the corresponding radical: $3.6 \times 10^5 \text{ s}^{-1}$ at 22 °C in hexane solution: Bullock, M. R.; Samsel, E. G. Hydrogen Atom Transfer Reactions of Transition-Metal Hydrides by Metal Carbonyl Hydrides. *J. Am. Chem. Soc.* **1990**, *112*, 6886–6898; (b) Choi, J.; Tang, L.; Norton, J. R. Kinetics of Hydrogen Atom Transfer from (η^5 -

- $C_5H_5)Cr(CO)_3H$ to Various Olefins: Influence of Olefin Structure. *J. Am. Chem. Soc.* **2007**, *129*, 234–240. (c) de Bruin, B.; Dzik, W.I.; Li, S.; Wayland, B.B. Hydrogen-Atom Transfer in Reactions of Organic Radicals with $[Co^{II}(por)]$. (por=Porphyrinato) and in Subsequent Addition of $[Co(H)(por)]$ to Olefins. *Chem. Eur. J.* **2009**, *15*, 4312–4320.
- [24] Brenna, D.; Villa, M.; Gieshoff, T. N.; Fischer, F.; Hapke, M.; Jacobi von Wangelin, A. Iron-Catalyzed Cyclotrimerization of Terminal Alkynes by Dual Catalyst Activation in the Absence of Reductants. *Angew. Chem., Int. Ed.* **2017**, *56*, 8451–8454.
- [25] (a) Anton, D. R.; Crabtree, R. H. Dibenzo[a,e]cyclooctatetraene in a Proposed Test for Heterogeneity in Catalysts formed from Soluble Platinum-group Metal Complexes. *Organometallics* **1983**, *2*, 855–859; (b) Franck, G.; Brill, M.; Helmchen, G. Dibenzo[a,e]cyclooctene: Multi-gram Synthesis of a Bidentate Ligand. *Org. Synth.* **2012**, *89*, 55–65; (c) Sandl, S.; Jacobi von Wangelin, A. *Dibenzo[a,e]cyclooctatetra-ene* in *Encyclopedia of Organic Reagents*. John Wiley & Sons, New York, USA, **2019**.
- [26] Yang, X.-J.; Fan, X.; Zhao, Y.; Wang, X.; Liu, B.; Su, J.-H.; Dong, Q.; Xu, M.; Wu, B. Synthesis and Characterization of Cobalt Complexes with Radical Anionic α -Diimine Ligands. *Organometallics* **2013**, *32*, 6945–6949.
- [27] Examples of α -diimine cobaltates: (a) $Li[(\alpha\text{-diimine})Co(cod)]$: Döring, M.; Uhlig, E.; Taldbach, T. Zur Reaktion von $[Li(TMED)_2][Co(COD)_2]$ mit π -Akzeptorliganden. *Z. Anorg. Allg. Chem.* **1991**, *600*, 163–167; (b) $K[(bipy)Co(cod)]$: Brennessel, W. W.; Ellis, J. E. Naphthalene and Anthracene Cobaltates(1-): Useful Storable Sources of an Atomic Cobalt Anion. *Inorg. Chem.* **2012**, *51*, 9076–9094; (c) $Na/Co/\alpha\text{-diimine/polyarene}$ complexes: Wang, X.; Zhao, Y.; Gong, S.; Liu, B.; Li, Q.-S.; Su, J.-H.; Wu, B.; Yang, X.-J. Mono- and Dinuclear Heteroleptic Cobalt Complexes with α -Diimine and Polyarene Ligands. *Chem. Eur. J.* **2015**, *21*, 13302–13310.
- [28] Ray, K.; Petrenko, T.; Wieghardt, K.; Neese, F. Joint Spectroscopic and Theoretical Investigations of Transition Metal Complexes Involving Non-Innocent Ligands. *Dalton Trans.* **2007**, 1552–1566.
- [29] For average bond distances of BIAN from the literature, see ref. [16]c: $BIAN^0$: C–N 1.28, C–C 1.49; $BIAN^{1-}$: C–N 1.34, C–C 1.44; $BIAN^{2-}$: C–N 1.39, C–C 1.40.

- [30] Similar (η^6 -arene)Co complexes: (a) [(NacNac)Co(arene)]: Dai, X.; Kapoor, P.; Warren, T. H. [Me₂NN]Co(η^6 -Toluene): O=O, N=N, and O=N Bond Cleavage Provides β -Diketiminato Cobalt μ -Oxo and Imido Complexes. *J. Am. Chem. Soc.* **2004**, *126*, 4798–4799; (b) [(α -diimine)Co(arene)] and [(α -diimine)Co]₂: see ref. [26]; (c) Cobalt α -diimine and polyarene complexes: see ref.: [27]c; (d) [(NacNac)Co(arene)]: Chen, C.; Hecht, M. B.; Kavara, A.; Brennessel, W. W.; Mercado, B. Q.; Weix, D. J.; Holland, P. L. Rapid, Regioconvergent, Solvent-Free Alkene Hydrosilylation with a Cobalt Catalyst. *J. Am. Chem. Soc.* **2015**, *137*, 13244–13247; (e) [(α -diimine)Fe(arene)] complexes as inactive olefin hydrogenation precatalysts: Bart, S. C.; Hawrelak, E. J.; Lobkovsky, E.; Chirik, P. J. Low-Valent α -Diimine Iron Complexes for Catalytic Olefin Hydrogenation. *Organometallics* **2005**, *24*, 5518–5527.
- [31] Krzystek, J.; Ozarowski, A.; Zvyagin, S.A.; Telser, J. High Spin Co(I): High-Frequency and -Field EPR Spectroscopy of CoX(PPh₃)₃ (X = Cl, Br). *Inorg. Chem.*, **2012**, *51*, 4954–4964.
- [32] Reviews: (a) Moore, D. S.; Robinson, S. D. Hydrido Complexes of the Transition Metals. *Chem. Soc. Rev.* **1983**, *12*, 415–452; (b) Darensbourg, M. Y.; Ash, C. E. Anionic Transition Metal Hydrides. *Adv. Organomet. Chem.* **1987**, *27*, 1–50; (c) Robinson, S. J. C.; Heinekey, D. M. Hydride & Dihydrogen Complexes of Earth Abundant Metals: Structure, Reactivity, and Applications to Catalysis. *Chem. Commun.* **2017**, *53*, 669–676.
- [33] Reviews: (a) Lubitz, W.; Ogata, H.; Rüdiger, O.; Reijerse, E. Hydrogenases. *Chem. Rev.* **2014**, *114*, 4081–4148; (b) Schilter, D.; Camara, J. M.; Huynh, M. T.; Hammes-Schiffer, S.; Rauchfuss, T. B. Hydrogenase Enzymes and Their Synthetic Models: The Role of Metal Hydrides. *Chem. Rev.* **2016**, *116*, 8693–8749.
- [34] It is notable, that it is necessary to perform the reaction in a closed reaction vessel as reported by Finke and co-workers: Laxson, W. W.; Özkar, S.; Folkman, S.; Finke, R. G. The Story of a Mechanism-Based Solution to an Irreproducible Synthesis Resulting in an Unexpected Closed-System Requirement for the LiBEt₃H-Based Reduction: The Case of the Novel Subnanometer Cluster, [Ir(1,5-COD)(μ -H)]₄, and the Resulting Improved, Independently Repeatable, Reliable Synthesis. *Inorg. Chim. Acta* **2015**, *432*, 250–257.

- [35] Related hydrides: (a) Fryzuk, M. D.; Ng, J. B.; Rettig, S. J.; Huffman, J. C.; Jonas, K. Nature of the Catalytically Inactive Cobalt Hydride Formed upon Hydrogenation of Aromatic Substrates. Structure and Characterization of the Binuclear Cobalt Hydride $[\{^i\text{Pr}_2\text{P}(\text{CH}_2)_3\text{P}^i\text{Pr}_2\}\text{Co}]_2(\text{H})(\mu\text{-H})_3$. *Inorg. Chem.* **1991**, *30*, 2437–2441; (b) $[\{(\text{Cp}^*)\text{Co}\}_2(\mu^2\text{-H})_3]$: Kersten, J. L.; Rheingold, A. L.; Theopold, K. H.; Casey, C. P.; Widenhoefer, R. A.; Hop, C. E. C. A. “[Cp*Co=CoCp*]” Is a Hydride. *Angew. Chem., Int. Ed.* **1992**, *31*, 1341–1343; (c) $[(\text{NacNac})\text{Co}(\mu^2\text{-H})]_2$ and $\text{K}_2[(\text{NacNac})\text{Co}(\mu\text{-H})]_2$: Ding, K.; Brennessel, W. W.; Holland, P. L. Three-Coordinate and Four-Coordinate Cobalt Hydride Complexes That React with Dinitrogen. *J. Am. Chem. Soc.* **2009**, *131*, 10804–10805; (d) $\text{LiEt}_3\text{BH}\cdot[(\text{dippe})\text{Rh}(\mu^2\text{-H})]_2$: Swartz, B. D.; Ateşin, T. A.; Grochowski, M. R.; Oster, S. S.; Brennessel, W. W.; Jones, W. D. Unusual Lithium Coordinated Platinum and Rhodium Hydride Dimers. *Inorg. Chim. Acta* **2010**, *363*, 517–522.
- [36] Fedushkin, I. L.; Skatova, A. A.; Khvoynova, N. M.; Lukoyanov, A. N.; Fukin, G. K.; Ketkov, S. Y.; Maslov, M. O.; Bogomyakov, A. S.; Makarov, V. M. New High-Spin Iron Complexes Based on Bis(Imino)Acenaphthenes (BIAN): Synthesis, Structure, and Magnetic Properties. *Russ. Chem. Bull.* **2013**, *62*, 2122–2131.
- [37] Based on molecular structure optimizations of the anion with the BP86 functional and Ahlrichs’ def2-TZVP basis set, the closed-shell singlet (css) represents the lowest energy state, with the triplet (t) being the next highest in energy ($\Delta E(\text{t-css}) = 30.8$ kJ/mol), followed by the quintet state (q) ($\Delta E(\text{q-css}) = 50.2$ kJ/mol).[†] Single-point energy calculations of the open-shell singlet state (oss) on the triplet molecular structure converged to the closed-shell singlet state (css). The highest energy state is the septuplet (sp) ($\Delta E(\text{sp-css}) = 297.2$ kJ/mol), which due to convergence issues is evaluated as a single-point energy calculation on the optimized molecular structure of the css. Molecular structure optimizations with the TPSSH functional and Ahlrichs’ def2-TZVP basis set predict the triplet state to be the lowest energy state ($\Delta E(\text{t-css}) = 22.5$ kJ/mol), followed by the quintet state ($\Delta E(\text{q-css}) = 10.7$ kJ/mol).[†] From local charges and spins obtained from BADER population analysis, the cobalt ions in **4** are predicted to be singly positively charged for both the BP86 and TPSSH functional.[†] The three bridging hydrides summed

up are singly negatively charged in total for either functional. The oxidation state of the BIAN core remains ambiguous, as its charge ranges between –1.15 (css) and –2.23 (t), and between –2.19 (oss) and –2.85 (t) for the BP86 and the TPSSH functional, respectively. However, the overall ligand fragment [DippBIAN] turns out to be roughly singly negatively charged in all cases except for the septuplet.

- [38] Knijnenburg, Q.; Hetterscheid, D.; Martijn Kooistra, T.; Budzelaar, P. H. M. The Electronic Structure of (Diiminopyridine)Cobalt(I) Complexes. *Eur. J. Inorg. Chem.* **2004**, 1204–1211.
- [39] Bachmann, B.; Hahn, F.; Heck, J.; Wünsch, M. Cooperative Effects In π -Ligand Bridged Binuclear Complexes. 8. Cyclic Voltammetric, NMR, and ESR Spectroscopic Studies of Electron-Poor Synfacial Bis((H₅-Cyclopentadienyl)Metal) μ -Cyclooctatetraene Complexes of Chromium and Vanadium. *Organometallics* **1989**, *8*, 2523–2543.
- [40] Lewis-acid effects in hydrogenation reactions: (a) Lin, T.-P.; Peters, J. C. Boryl-Mediated Reversible H Activation at Cobalt: Catalytic Boryl-Mediated Reversible H₂ Activation at Cobalt: Catalytic Hydrogenation, Dehydrogenation, and Transfer Hydrogenation. *J. Am. Chem. Soc.* **2013**, *135*, 15310–15313; (b) Maity, A.; Teets, T. S. Main Group Lewis Acid-Mediated Transformations of Transition-Metal Hydride Complexes. *Chem. Rev.* **2016**, *116*, 8873–8911; (c) Tokmic, K.; Jackson, B. J.; Salazar, A.; Woods, T. J.; Fout, A. R. Cobalt-Catalyzed and Lewis Acid-Assisted Nitrile Hydrogenation to Primary Amines: A Combined Effort. *J. Am. Chem. Soc.* **2017**, *139*, 13554–13561; (d) Léonard, N. G.; Chirik, P. J. Air-Stable α -Diimine Nickel Precatalysts for the Hydrogenation of Hindered, Unactivated Alkenes. *ACS Catal.* **2018**, *8*, 342–348.
- [41] (a) Oro, L. A.; Sola, E. *Mechanistic Aspects of Dihydrogen Activation and Catalysis by Dinuclear Complexes in Recent Advances in Hydride chemistry*; Peruzzini, M.; Poli, R., Eds.; Elsevier Science Ltd, Amsterdam, Netherlands, **2001**; pp 299–327; (b) Siedschlag, R. B.; Bernales, V.; Vogiatzis, K. D.; Planas, N.; Clouston, L. J.; Bill, E.; Gagliardi, L.; Lu, C. C. Catalytic Silylation of Dinitrogen with a Dicobalt Complex. *J. Am. Chem. Soc.* **2015**, *137*, 4638–4641; (c) Gieshoff, T. N.; Chakraborty, U.; Villa, M.; Jacobi von Wangelin, A. Alkene Hydrogenations by Soluble Iron Nanocluster Catalysts. *Angew.*

Chem., Int. Ed. **2017**, *56*, 3585–3589; (d) Powers, I. G.; Uyeda, C. Metal-Metal Bonds in Catalysis. *ACS Catal.* **2017**, *7*, 936–958; (e) Chakraborty, U.; Reyes-Rodriguez, E.; Demeshko, S.; Meyer, F.; Jacobi von Wangelin, A. A Manganese Nanosheet: New Cluster Topology and Catalysis. *Angew. Chem., Int. Ed.* **2018**, *57*, 4970–4975.

4.5 Supporting Information

4.5.1 General

Analytical Thin-Layer Chromatography: TLC was performed using aluminium plates with silica gel and fluorescent indicator (Merck, 60, F254). Thin layer chromatography plates were visualized by exposure to ultraviolet light (366 or 254 nm) or by immersion in a staining solution of molybdato-phosphoric acid in ethanol or potassium permanganate in water.

Column Chromatography: Flash column chromatography with silica gel 60 from KMF (0.040-0.063 mm). Mixtures of solvents used are noted in brackets.

Chemicals and Solvents: Commercially available olefins were distilled under reduced pressure before use. Solvents (THF, Et₂O, *n*-hexane, toluene) were distilled over sodium and benzophenone and stored over molecular sieves (3 Å) under argon. Solvents used for column chromatography were distilled under reduced pressure prior use (ethyl acetate). LiBEt₃H (1 M in THF) was used as received from SigmaAldrich or diluted before use.

Cyclic voltammetry: Cyclic voltammetry experiments were performed in a single-compartment cell inside a nitrogen-filled glovebox using a CH Instruments CH1600E potentiostat. The cell was equipped with a platinum disc working electrode (1 mm diameter) polished with 0.05 μm alumina paste, a platinum wire counter electrode and a silver wire pseudoreference electrode. The supporting electrolyte, tetra-*n*-butylammonium hexafluorophosphate, was dried in vacuo at 110 °C overnight. All redox potentials are reported versus the ferrocenium/ferrocene (Fc⁺/Fc) couple. The scan rate is $v = 100 \text{ mV}\cdot\text{s}^{-1}$ unless stated otherwise.

Electronic paramagnetic resonance spectroscopy (EPR): The experimental X-band EPR spectrum of **1** was recorded on a Bruker EMX spectrometer (Bruker BioSpin Rheinstetten) equipped with a He temperature control cryostat system (Oxford Instruments). The spectra were simulated using the W95EPR program of Prof. F. Neese.

High Pressure Reactor: Hydrogenation reactions were carried out in 160 and 300 mL high pressure reactors (ParrTM) in 4 mL glass vials. The reactors were loaded

under argon, purged with H₂ (1 min), sealed and the internal pressure was adjusted. Hydrogen (99.9992%) was purchased from Linde.

¹H- und ¹³C-NMR-Spectroscopy: Nuclear magnetic resonance spectra were recorded on a Bruker Avance 300 (300 MHz) and Bruker Avance 400 (400 MHz). ¹H-NMR: The following abbreviations are used to indicate multiplicities: s = singlet; d = doublet; t = triplet, q = quartet; m = multiplet, dd = doublet of doublet, dt = doublet of triplet, dq = doublet of quartet, ddt = doublet of doublet of quartet. Chemical shift δ is given in ppm to tetramethylsilane.

Gas chromatography with FID (GC-FID): HP6890 GC-System with injector 7683B and Agilent 7820A System. Column: HP-5, 19091J-413 (30 m \times 0.32 mm \times 0.25 μ m), carrier gas: N₂. GC-FID was used for reaction control and catalyst screening. Calibration with internal standard *n*-pentadecane and analytically pure samples. Non-commercial authentic samples were prepared by hydrogenation with Pd/C/H₂.

Gas chromatography with mass-selective detector (GC-MS): Agilent 6890N Network GC-System, mass detector 5975 MS. Column: HP-5MS (30m \times 0.25 mm \times 0.25 μ m, 5% phenylmethylsiloxane, carrier gas: H₂. Standard heating procedure: 50 °C (2 min), 25 °C/min \rightarrow 300 °C (5 min).

Gas-uptake reaction monitoring: Gas-uptake was monitored with a *Man On the Moon X201* kinetic system to maintain a constant reaction pressure. The system was purged with hydrogen prior use. Reservoir pressure was set to about 9 bar H₂. H₂ consumption was related to final yields by GC-FID vs. *n*-pentadecane.

Gas evolution measurements: Gas evolution was monitored with a *Man on the Moon X103* kit. Manipulations were performed under inert conditions. The volume of the reaction vessel was determined by protic hydrolysis of different amounts of zinc. The evolved hydrogen amount was calculated using the ideal gas law.

Magnetic moment: Magnet susceptibility χ_M was determined by performing a NMR experiment following the procedure of *Evans*. (D. F. Evans, *J. Chem. Soc.* **1959**, 2003.)

UV-Vis-spectroscopy: UV-vis spectra of investigated solutions were recorded on a Varian Cary 50 spectrophotometer in quartz cuvettes with a layer thickness of 1 cm and a concentration of 10^{-4} to 10^{-6} mol·L⁻¹ at room temperature.

X-ray crystallography: The single crystal X-ray diffraction data were recorded on an Agilent or Rigaku GV 50 with a Titan S2 CCD detector (**1**, **4a**) and on an Agilent SuperNova with an Atlas CCD detector (**3**, ^{Dipp}BIANCoBr₂) with microfocus Cu K_α radiation ($\lambda = 1.54184$ Å). Empirical multi-scan and analytical absorption corrections were applied to the data.

CrysAlisPro 1.171.38.43, CrysAlisPro Software System, Rigaku Oxford Diffraction, (2015).

In case of **4b**, X-ray diffraction data was recorded on an Bruker APEX-II CCD diffractometer with microfocus Mo K_α radiation ($\lambda = 0.71073$ Å). Data reduction, scaling and absorption corrections were performed using SAINT (Bruker, V8.34A, after 2013). Multi-scan absorption correction was performed using SADABS-2012/1 (Bruker, 2012).

The structures were solved with SHELXT and least-square refinements on F^2 were carried out with SHELXL.

O.V. Dolomanov and L.J. Bourhis and R.J. Gildea and J.A.K. Howard and H. Puschmann, Olex2: A complete structure solution, refinement and analysis program, *J. Appl. Cryst.*, (2009), **42**, 339-341.

Sheldrick, G.M., Crystal structure refinement with ShelXL, *Acta Cryst.*, (2015), **C27**, 3-8.

Sheldrick, G.M., ShelXT-Integrated space-group and crystal-structure determination, *Acta Cryst.*, (2015), **A71**, 3-8.

High resolution mass spectrometry (HRMS): The spectra were recorded by the Central Analytics Lab at the Department of Chemistry, University of Regensburg, on a MAT SSQ 710 A from Finnigan.

Liquid injection field desorption mass spectrometry (LIFDI-MS): The spectra were recorded by the Central Analytics Lab at the Department of Chemistry, University

of Regensburg, on a LIFDI-MS from Linden connected to an AccuTOF GCX from Jeol.

Computational Methodology: KS—DFT calculations were performed by using the GAUSSIAN 09⁽¹⁾ package, where the initial geometry was obtained from X-ray crystallographic data. In the molecular structure optimizations and single-point energy calculations, the BP86⁽²⁾ and the TPSSH⁽³⁾ exchange—correlation functional were employed together with Ahlrichs' def2-TZVP⁽⁴⁾ basis set. The convergence criterion in the self-consistent field (SCF) algorithm was set 10^{-7} hartree for the change of the energy in all calculations and to 10^{-4} a.u. for the gradient in molecular structure optimizations. BADER⁽⁵⁾ population analyses were performed with the code from the Henkelman group. Molecular structures and spin densities (isosurface value: 0.001) were visualized with the AVOGADRO⁽⁶⁾ editor.

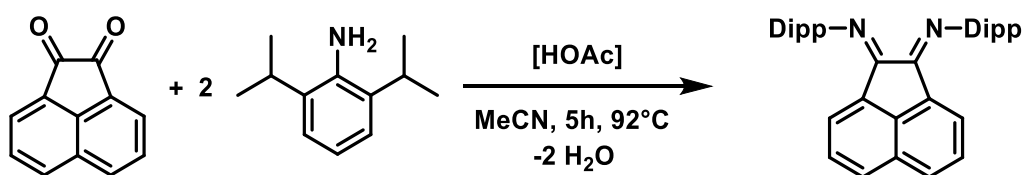
- (1) Frisch, M. J. et al. "Gaussian 09 Revision A.1.", software, Gaussian Inc. Wallingford CT, 2009.
- (2) a) Becke, A. D. Density-functional exchange-energy approximation with correct asymptotic-behavior. *Phys Rev A* **1988**, 38, 3098-3100; b) Perdew, J. P. Density-functional approximation for the correlation energy of the inhomogeneous electron gas. *Phys. Rev. B* **1986**, 33, 8822.
- (3) a) J. M. Tao, J. P. Perdew, V. N. Staroverov, and G. E. Scuseria, "Climbing the density functional ladder: Nonempirical meta-generalized gradient approximation designed for molecules and solids," *Phys. Rev. Lett.* **2003**, 91, 146401; b) V. N. Staroverov, G. E. Scuseria, J. Tao and J. P. Perdew, "Comparative assessment of a new nonempirical density functional: Molecules and hydrogen-bonded complexes," *J. Chem. Phys.* **2003**, 119, 12129.
- (4) Weigend, F.; Ahlrichs, R. Balanced basis sets of split valence, triple zeta valence and quadruple zeta valence quality for h to rn: Design and assessment of accuracy. *Phys. Chem. Chem. Phys.* **2005**, 7, 3297-305.
- (5) Tang, W.; Sanville, E.; Henkelman, G. A grid-based Bader analysis algorithm without lattice bias. *J. Phys.: Condens. Matter* **2009**, 21, 084204.

- (6) Hanwell, M.; Curtis, D.; Lonie, D.; Vandermeersch, T.; Zurek, E.; Hutchison, G. Avogadro: an advanced semantic chemical editor, visualization, and analysis platform. *J. Cheminf.* **2012**, *4*, 1-17.

4.5.2 Synthesis of precatalysts

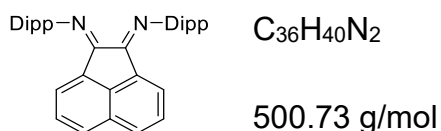
Synthesis of Bis[*N,N'*-(2,6-diisopropylphenyl)imino]acenaphthene (DippBIAN)

Synthesis was performed following a procedure by A. Paulovicova, U. El-Ayaan, K. Shibayama, T. Morita, Y. Fukuda, *Eur. J. Inorg. Chem.* **2001**, *2001*, 2641–2646.



Scheme 4.5.1. Synthesis DippBIAN.

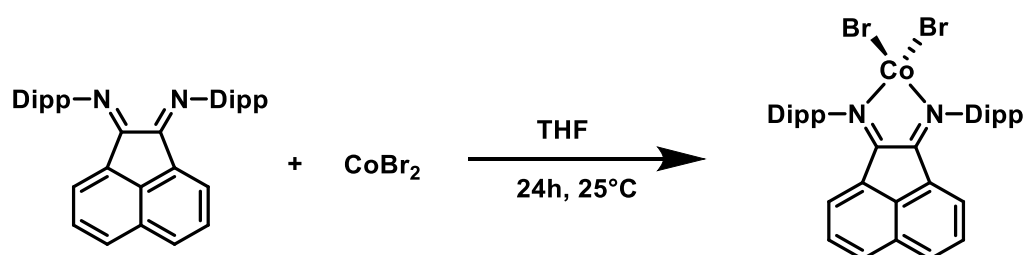
Acenaphthenquinone (3.50 g, 19.2 mmol, 1.00 equiv.) was suspended in acetonitrile (125 mL) and refluxed at 90 °C for 1 h. After addition of 35 mL acetic acid the reaction mixture was stirred for further 30 min. During this time acenaphthenquinone was almost dissolved with a yellow to orange color. 2,6-diisopropylaniline (8.15 g, 46.0 mmol, 2.40 equiv.) was added dropwise during which a color change to red-orange was observed. The solution was heated under reflux for 5.5 h. A yellow-orange solid was formed, filtered at room temperature and washed with *n*-pentane (5 x 20 mL). The raw material was dissolved in chloroform (300 mL), filtered and the solvent was removed under reduced pressure. After washing with *n*-pentane (2 x 100 mL) bis[*N,N'*-(2,6-diisopropylphenyl)imino]acenaphthene was isolated by drying in vacuo as orange-yellow powder.



Appearance	Yellow to orange solid
Yield	7.5 g, 1.9 mmol (49%)
¹H-NMR	(300 MHz, CDCl ₃): δ 7.88 (d, <i>J</i> = 8.3 Hz, 2H, CH _{BIAN}), 7.36 (t, <i>J</i> = 7.6 Hz, 2H, CH _{BIAN}), 7.27 (m, 6H, CH _{Dipp}), 6.63 (d, <i>J</i> = 7.2 Hz, 2H, CH _{BIAN}), 3.03 (sept, <i>J</i> = 6.8 Hz, 4H, CH(CH ₃) ₂), 1.23 (d, <i>J</i> = 6.8 Hz, 12H, CH(CH ₃) ₂), 0.97 (d, <i>J</i> = 6.8 Hz, 12H, CH(CH ₃) ₂)

DippBIANCoBr₂

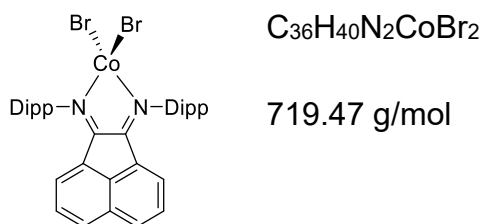
Synthesis was performed following an adapted procedure by V. Rosa, P. J. Gonzales, T. Aviles, P. T. Gomes, R. Welter, A. C. Rizzi, M. C. G. Passeggi, C. D. Brondino, *Eur. J. Inorg. Chem.* **2006**, 4761–4769.



Scheme 4.5.2. Synthesis of (DippBIAN)CoBr₂.

CoBr₂ (2.1 g, 9.5 mmol, 1.0 equiv.) and DippBIAN (5.0 g, 10 mmol, 1.1 equiv.) were mixed as solids and dissolved in THF (120 mL). An immediate color change to red occurred. The reaction mixture was stirred for 24 h and the solvent was removed under reduced pressure. The crude product was washed with toluene (40 mL), dissolved in DCM (150 mL) and filtered over a P3-frit. After reducing the solvent to 100 mL, the concentrated solution was layered with 70 mL *n*-hexane. Black needles were formed after storing at room temperature in 3 days. They were isolated by decanting the solvent and washing the crystals with toluene (3 x 15 mL).

4 Cobalt-Catalyzed Hydrogenations via Olefin Cobaltate and Hydride Intermediates



Appearance Brown needles

Yield 7.5 g, 1.9 mmol (49%)

1H -NMR (400 MHz, THF- d_8) δ 28.99 (s), 7.40 – 6.77 (m), 4.18 (s), 3.99 (s), 3.35 (s), 1.22 (s), 1.06 (s), -2.39 (s), -21.26 (s)

Elemental Analysis Found (calc.): C: 60.16 (60.16); H: 5.48 (5.60); N: 3.77 (3.89)

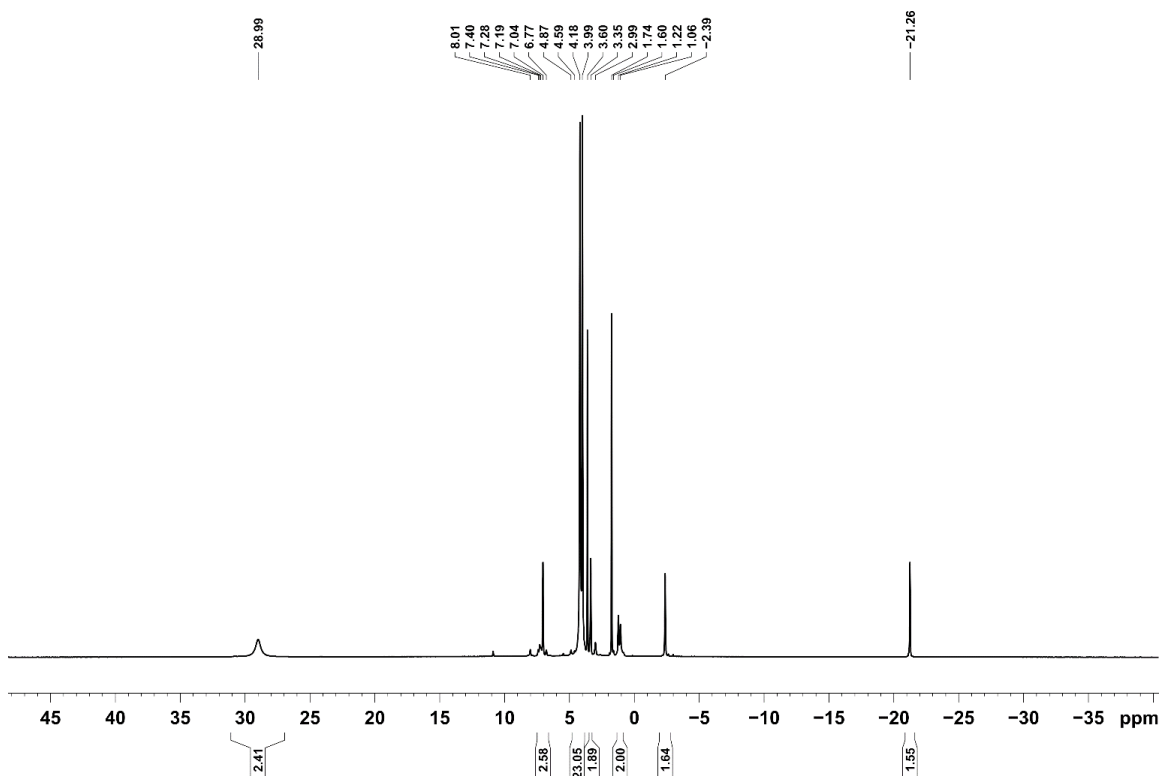


Figure 4.5.1. 1H -NMR spectrum of $(DippBIAN)CoBr_2$ (400.13 MHz, THF- d_8 , 300K).

Crystal structure

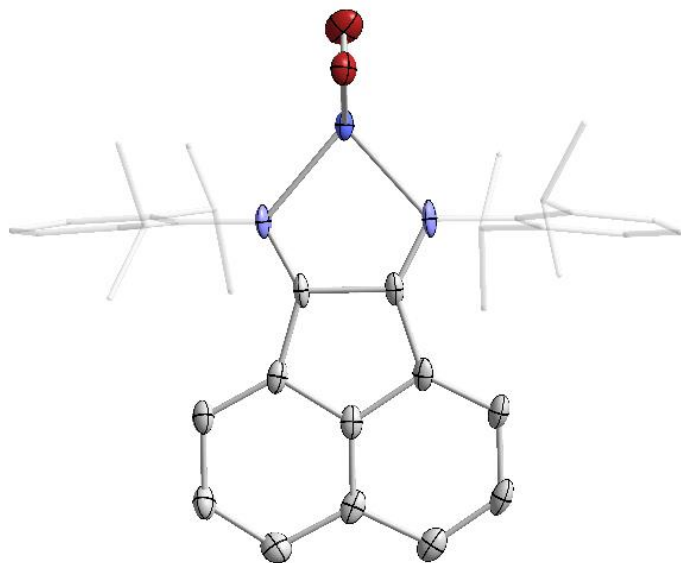


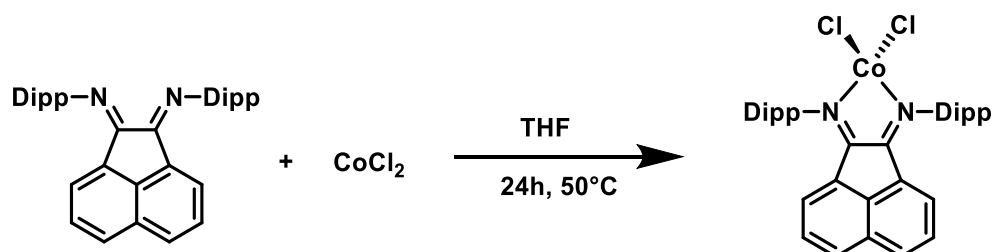
Figure 4.5.2. Solid-state molecular structure of DippBIANCoBr_2 . One of two molecules in the asymmetric unit shown. Thermal ellipsoids are drawn at the 50% probability level; hydrogen atoms are omitted for clarity.

Table 4.5.1. Crystal data and structure refinement for DippBIANCoBr_2 .

Formula	$\text{C}_{36}\text{H}_{40}\text{Br}_2\text{CoN}_2$
$D_{\text{calc.}}/\text{g cm}^{-3}$	1.401
μ/mm^{-1}	6.871
Formula Weight	719.45
Colour	black
Shape	block
Size/ mm^3	0.76x0.29x0.21
T/K	123(1)
Crystal System	monoclinic
Space Group	$P2_1/c$
$a/\text{\AA}$	27.0266(7)
$b/\text{\AA}$	12.0329(2)
$c/\text{\AA}$	22.8033(6)
α°	90
β°	113.047(3)
γ°	90
$V/\text{\AA}^3$	6823.9(3)
Z	8
Z'	2
Wavelength/ \AA	1.54184
Radiation type	$\text{CuK}\alpha$
$\Theta_{\text{min}}^\circ$	3.554
$\Theta_{\text{max}}^\circ$	73.616
Measured Refl.	24613
Independent Refl.	13116
Reflections with $I > 2(I)$	12117
R_{int}	0.0735
Parameters	755
Restraints	0
Largest Peak	1.801
Deepest Hole	-1.563
GooF	1.057
wR_2 (all data)	0.2404
wR_2	0.2360
R_1 (all data)	0.0892
R_1	0.0857

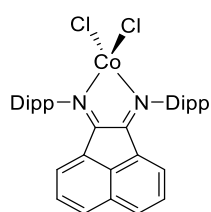
DippBIANCoCl₂

Synthesis was performed following an adapted procedure by V. Rosa, P. J. Gonzales, T. Aviles, P. T. Gomes, R. Welter, A. C. Rizzi, M. C. G. Passeggi, C. D. Brondino, *Eur. J. Inorg. Chem.* **2006**, 4761–4769.



Scheme 4.5.3. Synthesis of (DippBIAN)CoCl₂.

Cobalt(II)-chloride (0.82 g, 6.3 mmol, 1.0 equiv.) and DippBIAN (3.5 g, 7.0 mmol, 1.1 equiv.) were mixed as solids and dissolved in THF (120 mL). An immediate color change to red occurred. The reaction mixture was stirred for 24 h at 50°C and the solvent was removed under reduced pressure. The crude product was washed with toluene (30 mL), dissolved in DCM (70 mL) and filtered over a P3-frit. After reducing the solvent to 40 mL, the concentrated solution was layered with *n*-hexane (40 mL). Black needles were formed after storing at room temperature. They were isolated by decanting the solvent, washing the crystals with toluene (2 x 20 mL) and drying *in vacuo*.



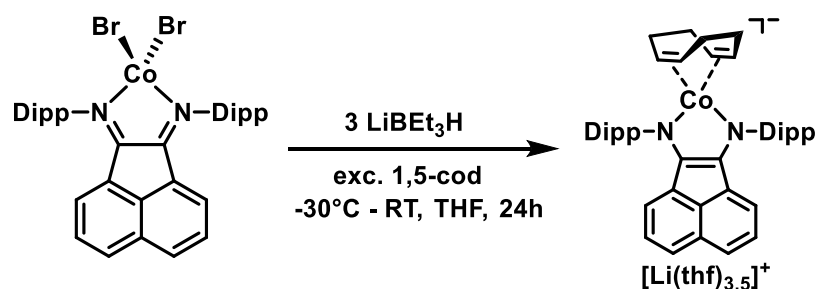
C₃₆H₄₀N₂CoCl₂

630.56 g/mol

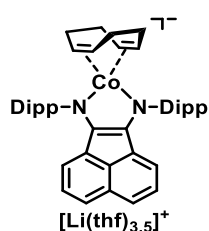
Appearance	Brown solid
Yield	245 g, 3.9 mmol (61%)
Elemental Analysis	Found (calc.): C: 68.75 (68.57); H: 6.29 (6.39); N: 4.39 (4.44)

[Li(thf)_{3.5}{(Dipp)BIAN}Co(cod)] (1)

DippBIANCoBr₂ (2.0 g, 2.8 mmol, 1.0 equiv.) was dissolved in 30 mL THF and 1,5-COD (2.0 mL, 16 mmol, 6.0 equiv.) was added to the solution. The reaction mixture was cooled to -30°C and a solution of LiEt₃BH (1 M in THF, 8.3 mL, 3 equiv.) was added dropwise. The solution was warmed to room temperature and stirred for further 24 h. The solvent was removed under reduced pressure and the residue was washed with 60 mL *n*-hexane. Extraction with 80 mL diethylether and filtration lead to a yellow-green solution which was reduced to 1/3 and layered with 20 mL *n*-hexane. After a few days, dark crystals were obtained and isolated by decanting the solution and drying crystals in vacuo. For analytics and catalytic test reactions an aliquot of this product was recrystallized from THF/*n*-hexane (2.5:1) at -30°C.



Scheme 4.5.4. Synthesis of Li(thf)_{3.5}{(Dipp)BIAN}Co(cod)].



C₅₈H₈₀N₂CoLiO_{3.5}

927.16 g/mol

Appearance

Dark black crystals

Yield

443 mg, 0.48 mmol (17%)

¹H-NMR

(400 MHz, THF-d₈) δ 7.06 – 6.99 (m, 6H, CH_{Ar}), 6.24 (m, 4H, CH_{BIAN}), 4.93 (m, 2H, CH_{BIAN}), 4.51 (m, 4H, CH_{Dipp}), 2.89 (m, 4H, cod-CH), 2.32 (m, 4H, cod-CH₂), 1.37 (d, 12H, CH_{3(Dipp)}), 1.03 (m, 4H, cod-CH₂), 0.95 (d, 12H, CH_{3(Dipp)})

$^{13}\text{C}\{^1\text{H}\}$ -NMR (101 MHz, THF- d_8) δ 154.6, 145.7, 127.2, 123.0, 122.9, 118.9, 114.5, 64.3, 32.9, 28.2, 26.0 (two quaternary C-atom could not be detected due to low solubility)

Elemental analysis Found (calc. for $[\text{Li}(\text{thf})_{3.5}\{\text{DippBIAN}\}\text{Co}(\text{cod})]$): C: 74.28 (74.82); H: 8.43 (8.70); N: 2.91 (3.02).
Elemental analysis is not in agreement with calculated values, which is presumably due to LiBr residue.

NMR spectra

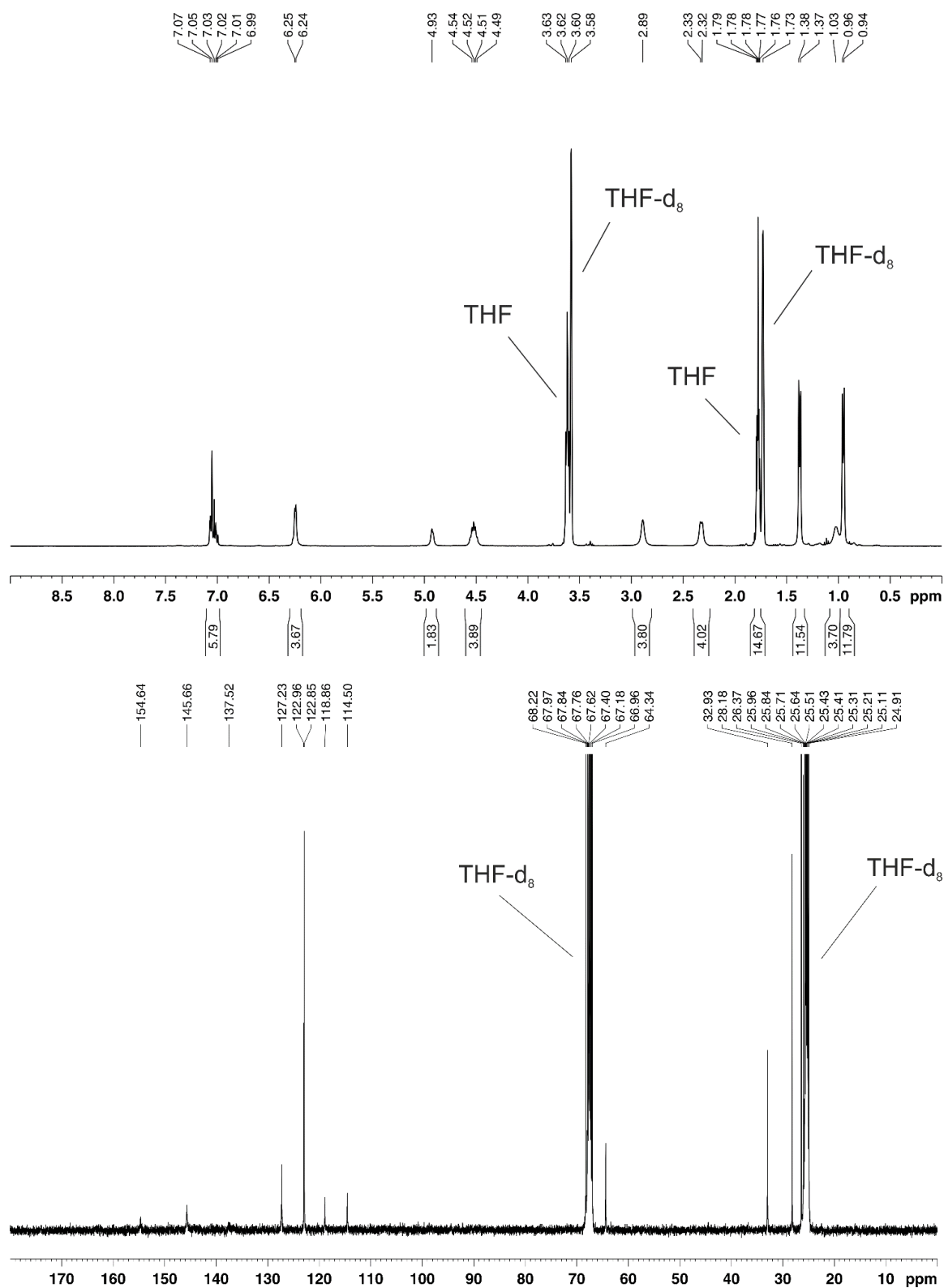


Figure 4.5.3. ¹H (top) and ¹³C{¹H} NMR spectra (bottom) of **1** (400.13/100.61 MHz, THF-d₈, 300K).

Crystal structure

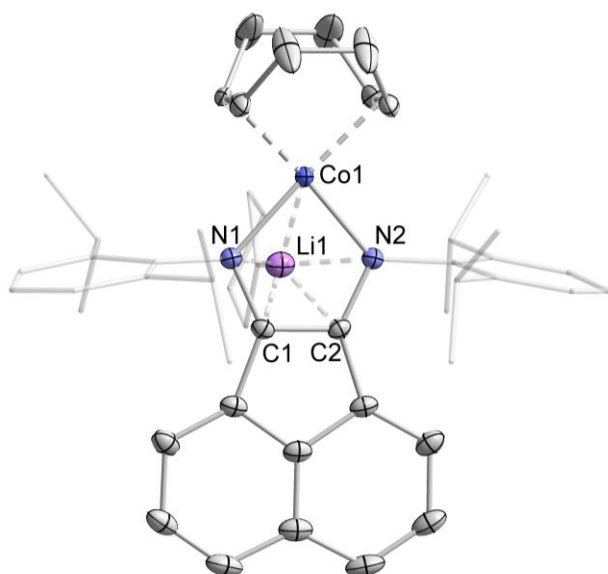


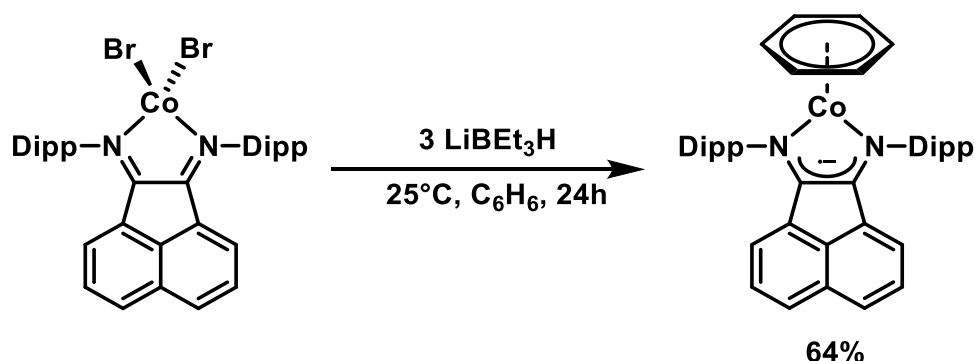
Figure 4.5.4. Solid-state molecular structure of [Li(thf){(Dipp)BIAN}Co(1,5-cod)]. Thermal ellipsoids are drawn at the 50% probability level; Minor disordered parts and hydrogen atoms are omitted for clarity.

Table 4.5.2. Crystal data and structure refinement for **1**.

4 Cobalt-Catalyzed Hydrogenations via Olefin Cobaltate and Hydride Intermediates

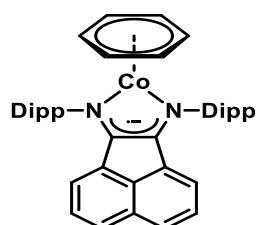
Formula	C ₄₈ H ₆₀ CoLiN ₂ O
<i>D</i> _{calc.} / g cm ⁻³	1.226
μ/mm ⁻¹	3.600
Formula Weight	746.85
Colour	black
Shape	plate
Size/mm ³	0.35×0.19×0.09
<i>T</i> /K	123.00(10)
Crystal System	orthorhombic
Flack Parameter	-0.021(3)
Hooft Parameter	-0.0301(14)
Space Group	<i>Pmn</i> 2 ₁
<i>a</i> /Å	17.4715(2)
<i>b</i> /Å	10.54720(10)
<i>c</i> /Å	10.97630(10)
α°	90
β°	90
γ°	90
<i>V</i> /Å ³	2022.66(4)
<i>Z</i>	2
<i>Z</i> '	0.5
Wavelength/Å	1.54184
Radiation type	CuK _α
Θ _{min} °	4.192
Θ _{max} °	73.654
Measured Refl.	14345
Independent Refl.	3823
Reflections with <i>I</i> > 2(<i>I</i>)	3744
<i>R</i> _{int}	0.0328
Parameters	286
Restraints	1
Largest Peak	0.197
Deepest Hole	-0.414
GooF	1.057
<i>wR</i> ₂ (all data)	0.0801
<i>wR</i> ₂	0.0791
<i>R</i> ₁ (all data)	0.0317
<i>R</i> ₁	0.0307

[(^{Dipp}BIAN)Co(η^6 -C₆H₆)] (3)



Scheme 4.5.5. Synthesis of [(^{Dipp}BIAN)Co(η^6 -C₆H₆)].

A suspension of ^{Dipp}BIANCoBr₂ (0.70 mmol) in benzene (15 mL) was reduced by dropwise addition of LiBEt₃H (2.09 mmol, 1.1M, THF) during which a color change from pale brown to dark red and solubilization was observed. After filtration over neutral alumina, the solvent was removed under reduced pressure and extracted with 30 mL hexane. Single crystals were grown by cooling to -35 °C (3 days), isolated by decanting the solution and in vacuo.



C₄₂H₄₆CoN₂
637.78 g/mol

Appearance

Dark red crystals

Yield

282 mg, 0.44 mmol (64%)

¹H-NMR

(400 MHz, C₆D₆) δ 17.47 (br), 6.23 (br), 1,71 (br), 1.24 (s), 0.89 (s), -0.32 (br)

UV-VIS

(C₆H₆, λ_{max} / nm (ϵ_{max} / L mol⁻¹ cm⁻¹): 481 (14300).

CV

E = -2.3 V vs. Fc/Fc⁺ in THF

Elemental analysis	Found (calc. for $[(\text{DippBIAN})\text{Co}(\eta^6\text{-C}_6\text{H}_6)]$): C: 79.20 (79.10); H: 7.36 (7.27); N: 4.03 (4.39).
Melting point:	230 °C (decomposition)
Determination of magnetic moment (Evans)	$\mu_{\text{eff}} (\text{C}_6\text{D}_6) = 1.9 \mu_{\text{B}}$
LIFDI-MS (FD+)	Calc. for $\text{C}_{42}\text{H}_{46}\text{CoN}_2$: $m/z = 637.2988$. Found: $m/z = 637.2781$ $[\text{M}^+]$ (100%), 638.2819 (49%), 639.2834 (13%), 640.2625 (3%).

NMR spectra

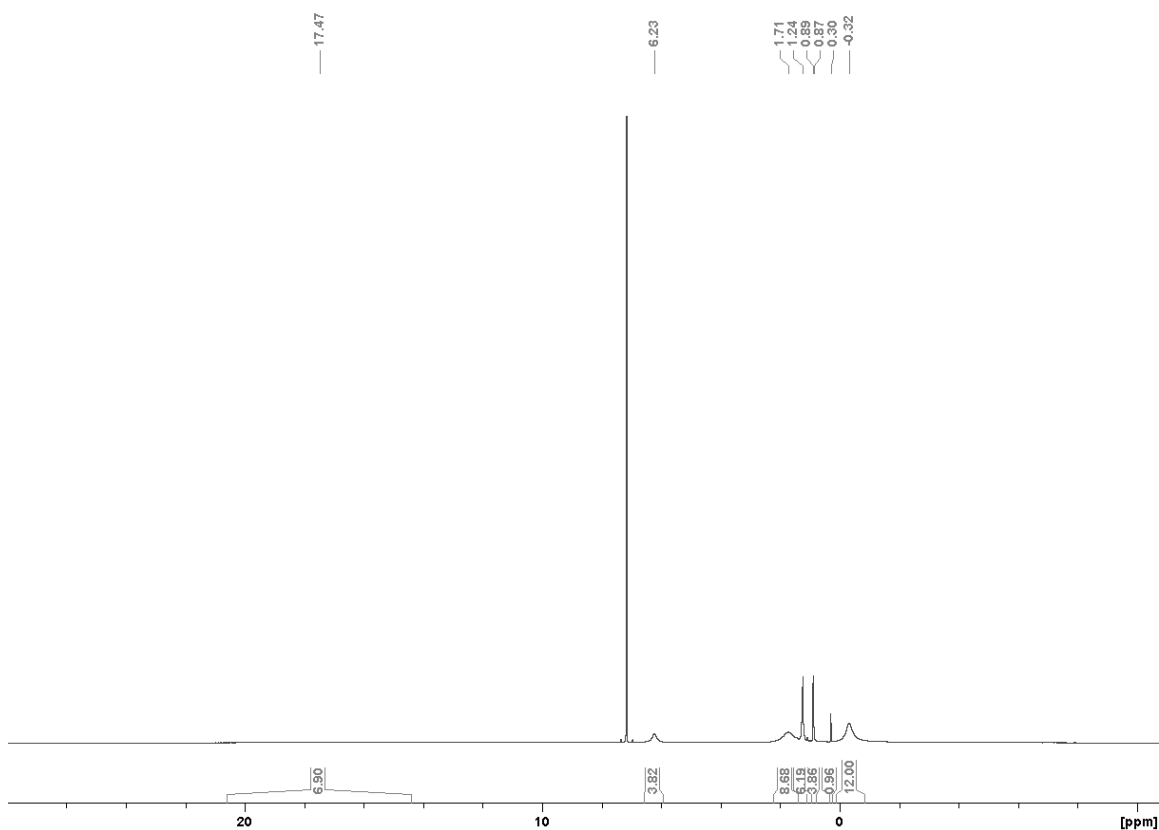


Figure 4.5.5. ^1H NMR spectra of **3** (400.13 MHz, C_6D_6 , 300K).

Cyclic voltammetry

Complex **3** was electrochemically investigated by means of cyclic voltammetry. One reversible reduction at -2.3 V and one irreversible oxidation at -0.9 V was observed.

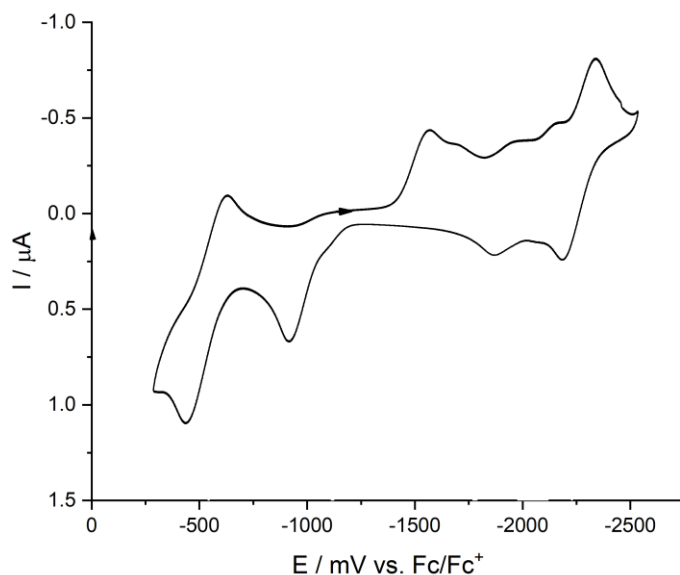


Figure 4.5.6. Cyclovoltammogram of $[(\text{DippBIAN})\text{Co}(\eta^6\text{-C}_6\text{H}_6)]$.

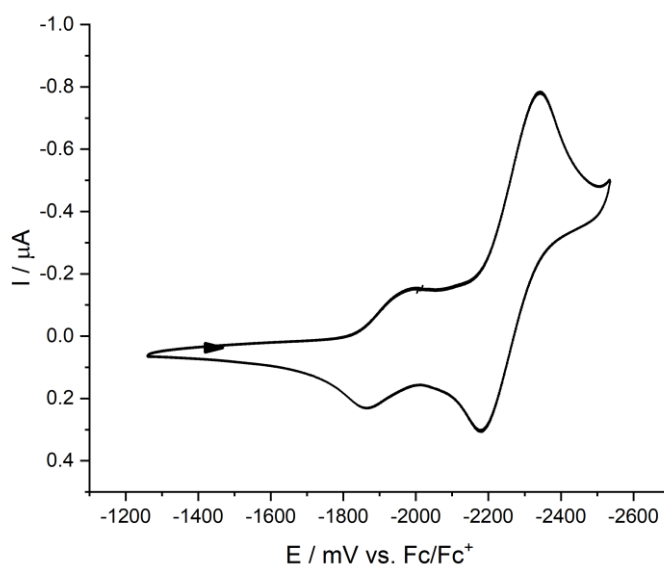


Figure 4.5.7. Cyclovoltammogram of $[(\text{DippBIAN})\text{Co}(\eta^6\text{-C}_6\text{H}_6)]$.

UV-vis spectroscopy

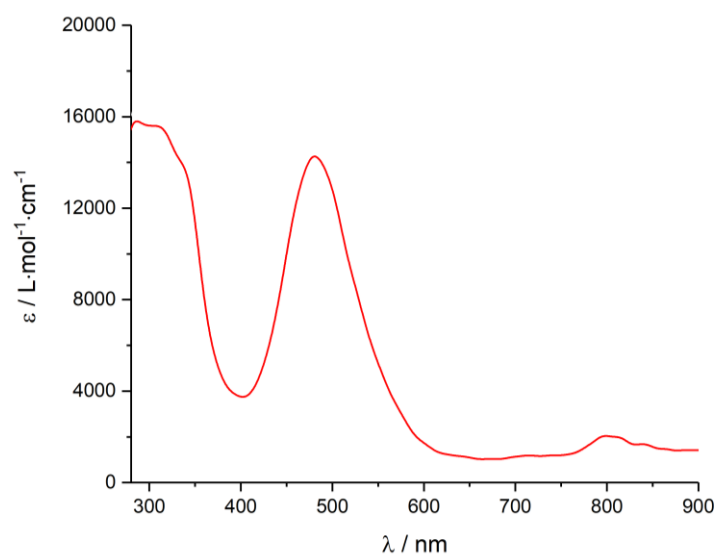


Figure 4.5.8. UV-VIS of $[(\text{DippBIAN})\text{Co}(\eta^6\text{-C}_6\text{H}_6)]$.

EPR

Room temperature X-Band EPR spectrum of $[(\text{DippBIAN})\text{Co}(\eta^6\text{-C}_6\text{H}_6)]$ in toluene (Figure 4.5.9 and Table 4.5.3). The experimental spectrum was simulated in accordance with an unpaired electron showing coupling to a spin 7/2 nucleus, which we attribute to a cobalt-centred doublet at $g_{\text{iso}} = 2.080$ and cobalt hyperfine interaction ($A^{\text{Co}_{\text{iso}}} = +254.5$ MHz). Manual introduction of minor g strain along g_x , g_y and g_z and linear A strain (E) along the x , y and z axis proved necessary for the final line-shape optimization of the simulated spectrum (see Table 4.5.3).

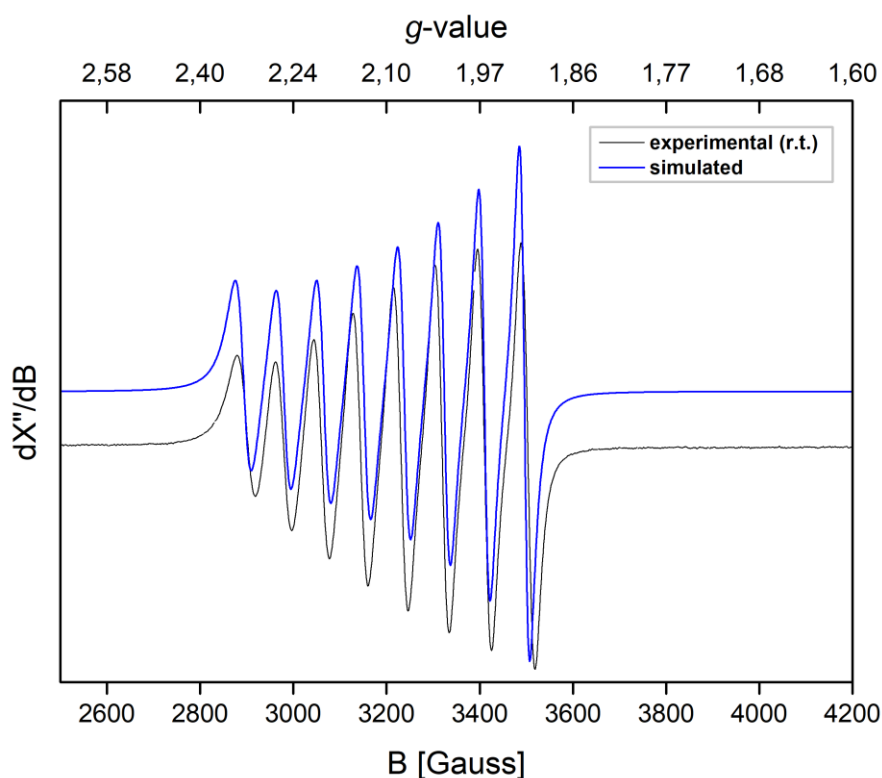


Figure 4.5.9. Simulated (blue) and experimental (black) X-band EPR spectrum of $[(\text{DippBIAN})\text{Co}(\eta^6\text{-C}_6\text{H}_6)]$ in toluene at room temperature.

Table 4.5.3. g and A values for the isotropic EPR spectrum of $[(\text{DippBIAN})\text{Co}(\eta^6\text{-C}_6\text{H}_6)]$ in toluene. $\nu = 9.389121$ GHz, power = 0.6325 mW, modulation amplitude = 4.000 G. E = linear A strain.

g_{iso}	$A^{\text{Co}_{\text{iso}}} \text{ (MHz)}$	E
2.080 (g_x 2.085, g_y 2.080, g_z 2.075)	+254.5	$E_x = E_y = E_z = 0.009$

X-Band EPR spectrum of $[(\text{DippBIAN})\text{Co}(\eta^6\text{-C}_6\text{H}_6)]$ measured in a toluene-glass at 20 K is shown in Figure 4.5.10. The rhombic experimental spectrum was simulated in accordance with an unpaired electron showing coupling to a spin 7/2 nucleus (Figure 4.5.10 and Table 4.5.4). We attribute this signal to a cobalt-centred radical (see Table 4.5.4 for g and A^{Co} values along x , y and z direction). The g and A^{Co} tensors are not aligned along the same direction, as consideration of the Euler angles provided a more satisfactory simulation of the measured spectrum. Linear and quadratic A -strain have been included to simulate the final line shape. Some remaining slight deviations in the line shapes comparing the simulated and experimental spectra can be attributed to non-perfect glass formation. The provided simulation allowed for accurate determination of the g and A^{Co} values: [2.013, 2.145, 2.134] and [185, 406, 198].

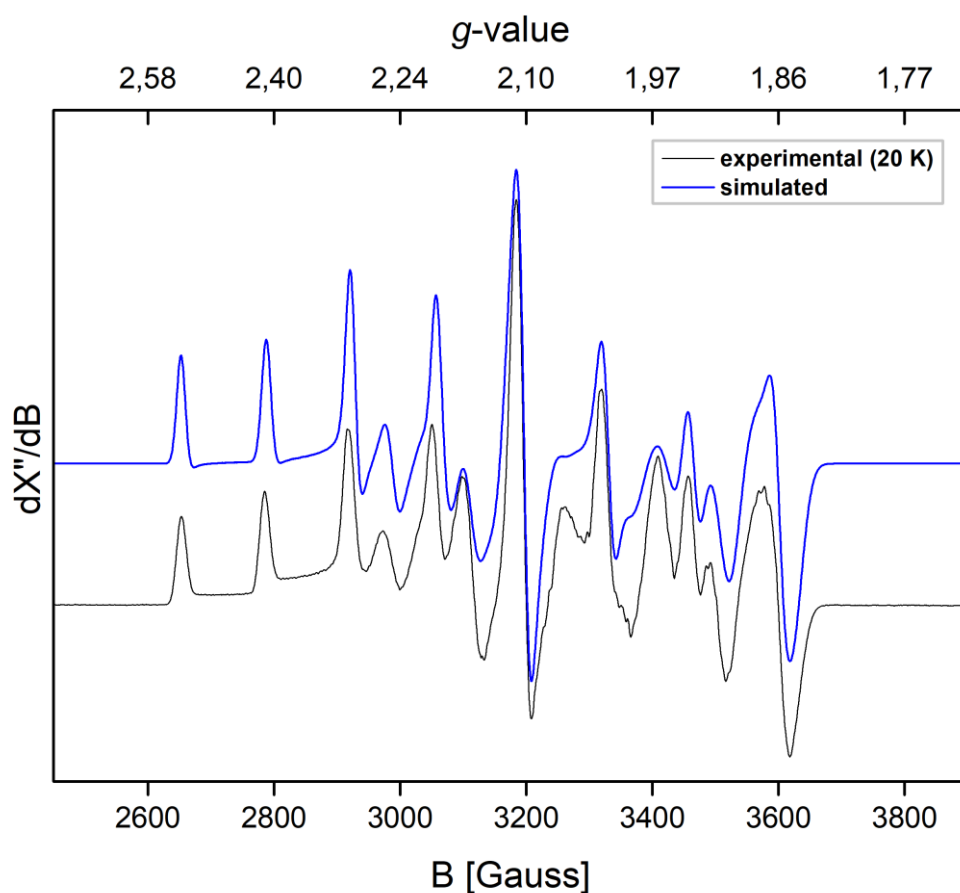


Figure 4.5.10. Simulated (blue) and experimental (black) X-band EPR spectrum of $[(\text{DippBIAN})\text{Co}(\eta^6\text{-C}_6\text{H}_6)]$ in a toluene glass at 20 K. $\nu = 9.389494$ GHz, microwave power = 1.002 mW, mod. amp. = 1.000 G.

Table 4.5.4. *g* and *A* tensor values for the rhombic EPR spectrum of [(^{Dipp}BIAN)Co(η^6 -C₆H₆)] in a toluene glass at 20 K. *E* = linear *A* strain, *C* = quadratic *A*-strain.

	<i>g</i> value	<i>A</i> ^{Co} (MHz)	<i>E</i>	<i>C</i>	<i>Euler angle</i>
x-axis	2.0125	+185.0	-0.00460	-0.003816	-2.0
y-axis	2.1450	+406.0	-0.001	-0.001	+90.0
z-axis	2.1340	+198.4	-0.006	-0.006	0.0

Crystal structure

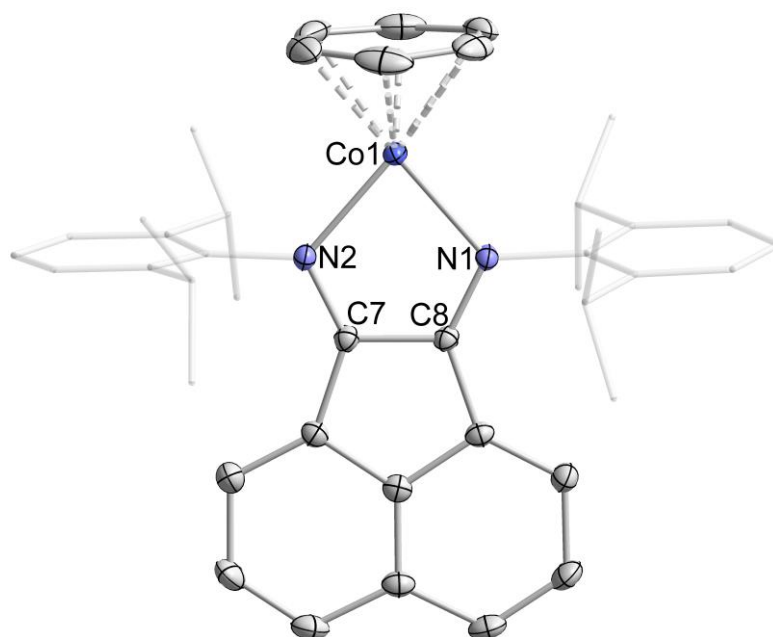


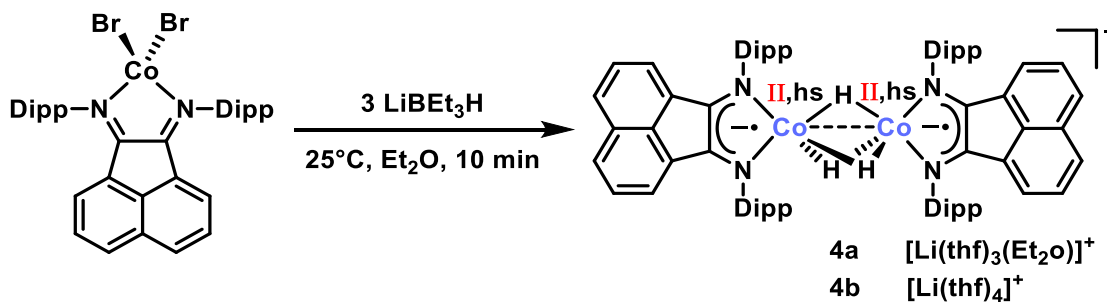
Figure 4.5.11. Solid-state molecular structure of [(^{Dipp}BIAN)Co(η^6 -C₆H₆)]. Thermal ellipsoids are drawn at the 50% probability level; non-coordinated solvents and hydrogen atoms are omitted for clarity.

Table 4.5.5. Crystal data and structure refinement for **3**.

4 Cobalt-Catalyzed Hydrogenations via Olefin Cobaltate and Hydride Intermediates

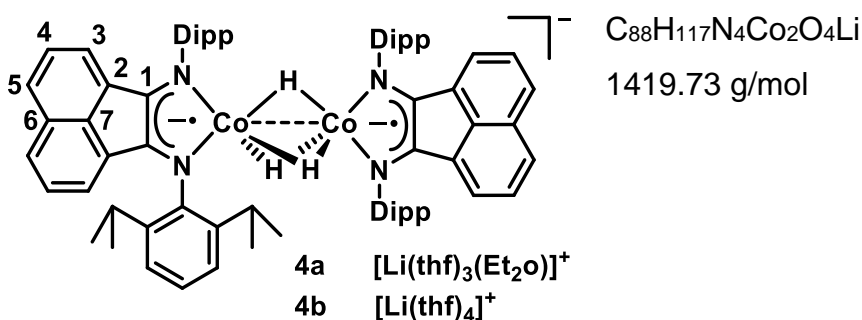
Formula	C ₄₅ H ₅₃ CoN ₂
<i>D</i> _{calc.} / g cm ⁻³	1.177
<i>m</i> /mm ⁻¹	3.731
Formula Weight	680.82
Color	clear dark red
Shape	block
Size/mm ³	0.29x0.20x0.07
<i>T</i> /K	123.0
Crystal System	triclinic
Space Group	P-1
<i>a</i> /Å	12.3103(3)
<i>b</i> /Å	12.6855(3)
<i>c</i> /Å	13.5302(4)
<i>α</i> °	69.519(2)
<i>β</i> °	77.844(2)
<i>γ</i> °	79.251(2)
<i>V</i> /Å ³	1920.22(9)
<i>Z</i>	2
<i>Z</i> '	1
Wavelength/Å	1.54184
Radiation type	CuK _α
<i>Θ</i> _{min} °	3.531
<i>Θ</i> _{max} °	66.545
Measured Refl.	41777
Independent Refl.	6603
Reflections Used	6358
<i>R</i> _{int}	0.0613
Parameters	442
Restraints	0
Largest Peak	0.232
Deepest Hole	-0.513
GooF	1.038
<i>wR</i> ₂ (all data)	0.0824
<i>wR</i> ₂	0.0813
<i>R</i> ₁ (all data)	0.0335
<i>R</i> ₁	0.0320

[Li(thf)₃(Et₂O)]{(DippBIAN)Co}₂(μ-H)₃ (4a)



Scheme 4.5.6. Synthesis of $[\text{Li}(\text{thf})_3(\text{Et}_2\text{O})]\{(\text{DippBIAN})\text{Co}\}_2(\mu\text{-H})_3$.

In an argon-filled glovebox, a Schlenk flask was equipped with a suspension of DippBIANCoBr_2 (1.39 mmol) in Et_2O (20 mL) and closed with a septum. After cooling to -35°C , the flask was taken out of the freezer and LiBEt_3H (3 equiv., 1.1M, THF) was added dropwise during which a color change from pale brown to dark green, effervescence and solubilization was observed. It is very important to create an overpressure in the flask in order to obtain the product. After 10 minutes stirring, heptane (8 mL) was added and the mixture was filtered through a closed Schlenk frit (P4, gravitation). The filter cake was washed with hexane (3 x 2 mL), and Et_2O (4 x 2 mL) to obtain the microcrystalline product in high purity. For the isolation of single crystals, hexane was used instead of heptane. After filtration, the crystals were grown from the filtrate by slow evaporation at 20°C . $[\text{Li}(\text{thf})_4]\{(\text{DippBIAN})\text{Co}\}_2(\mu\text{-H})_3$ (**4b**) was obtained in an analogous procedure: The microcrystals were recrystallized from a solution of $\text{thf}:\text{hexane} = 1:1$ at -35°C to obtain single crystals.



Appearance

Black micro-crystals

Yield	228.4 mg, 0.16 mmol, (23%).
¹H-NMR	(400 MHz, THF-d ₈) δ 8.37 – 8.32 (d, <i>J</i> = 8.2 Hz, 4H), 7.29 – 7.24 (d, <i>J</i> = 7.0 Hz, 4H), 6.58 (s, 12H), 6.50 (dd, <i>J</i> = 8.1 Hz, <i>J</i> = 7.0 Hz, 4H), 3.50 – 3.32 (br, 8H, CH _{Dipp}), 0.88 (d, <i>J</i> = 4.61 Hz, 24H, CH _{3(Dipp)}), 0.05 (m, 24H, CH _{3(Dipp)}), -75.20 (s, 3H, CoHCo).
¹³C-NMR	(101 MHz, THF-d ₈) δ 169.1 (<i>ipso</i> -C _{Ar}), 155.7 (C _{6,BIAN,q}), 152.4 (C _{1,BIAN,q}), 139.9 (C _{2,BIAN,q}), 134.5 (<i>ortho</i> -C _{Ar,q}), 134.3 (C _{4,BIANH}) 133.8 (C _{7,BIAN,q}), 127.0 (C _{ArH}), 119.8 (C _{ArH}), 116.1 (C _{5,BIANH}), 112.1 (C _{3,BIANH}), 68.2 (thf), 66.3 (Et ₂ O), 27.5 (CH _{Dipp}), 26.4 (thf), 24.7 (CH _{3Dipp}), 15.7 (Et ₂ O).
UV-VIS	(THF, I _{max} / nm (ε _{max} / L mol ⁻¹ cm ⁻¹): 474 (1200).
CV	E = -2.4 V vs. Fc/Fc ⁺ in THF
m.p.	260 °C (decomposition).
Determination of magnetic moment (Evans)	μ _{eff} (THF-d ₈ , 293 K) = 2.1 μ _B .
Negative ion-mode ESI-MS	Calc. for C ₇₂ H ₈₃ Co ₂ N ₄ : <i>m/z</i> = 1121.4. Found: <i>m/z</i> = 1121.4 [M] ⁻ (100%), 1122.4 (88%), 1123.4 (31%), 1124.4 (6%) (see below).

Elemental analysis

Found (calc. for
[Li(thf)₃(Et₂O){(DⁱppBIAN)Co}₂(μ²-H)₃):
C: 74.66 (74.45); H: 8.29 (8.31); N:
3.82 (3.95).

NMR spectra

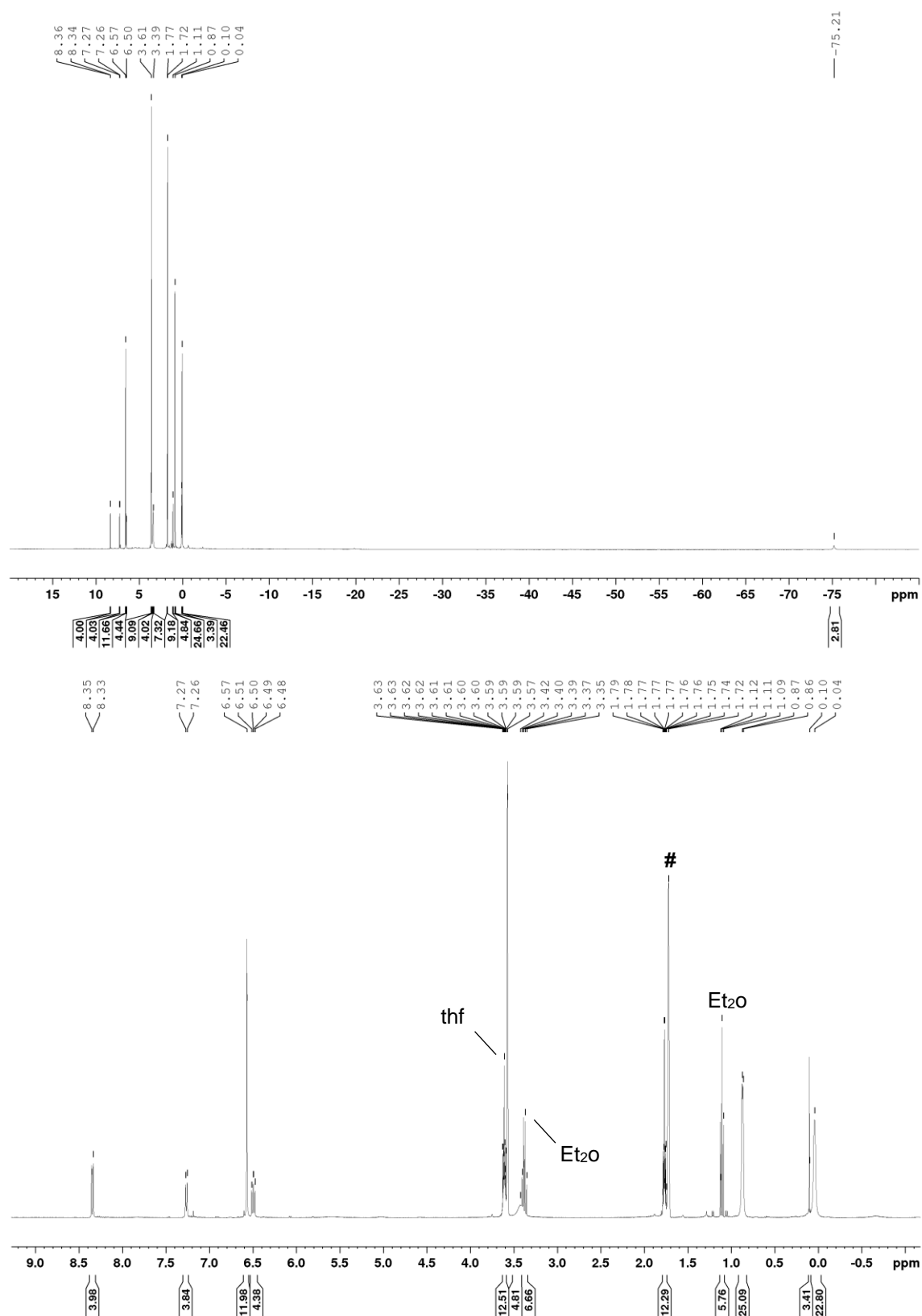


Figure 4.5.12. ^1H NMR spectra of **4a** (400.13 MHz, THF- d_8 , 300K).

4 Cobalt-Catalyzed Hydrogenations via Olefin Cobaltate and Hydride Intermediates

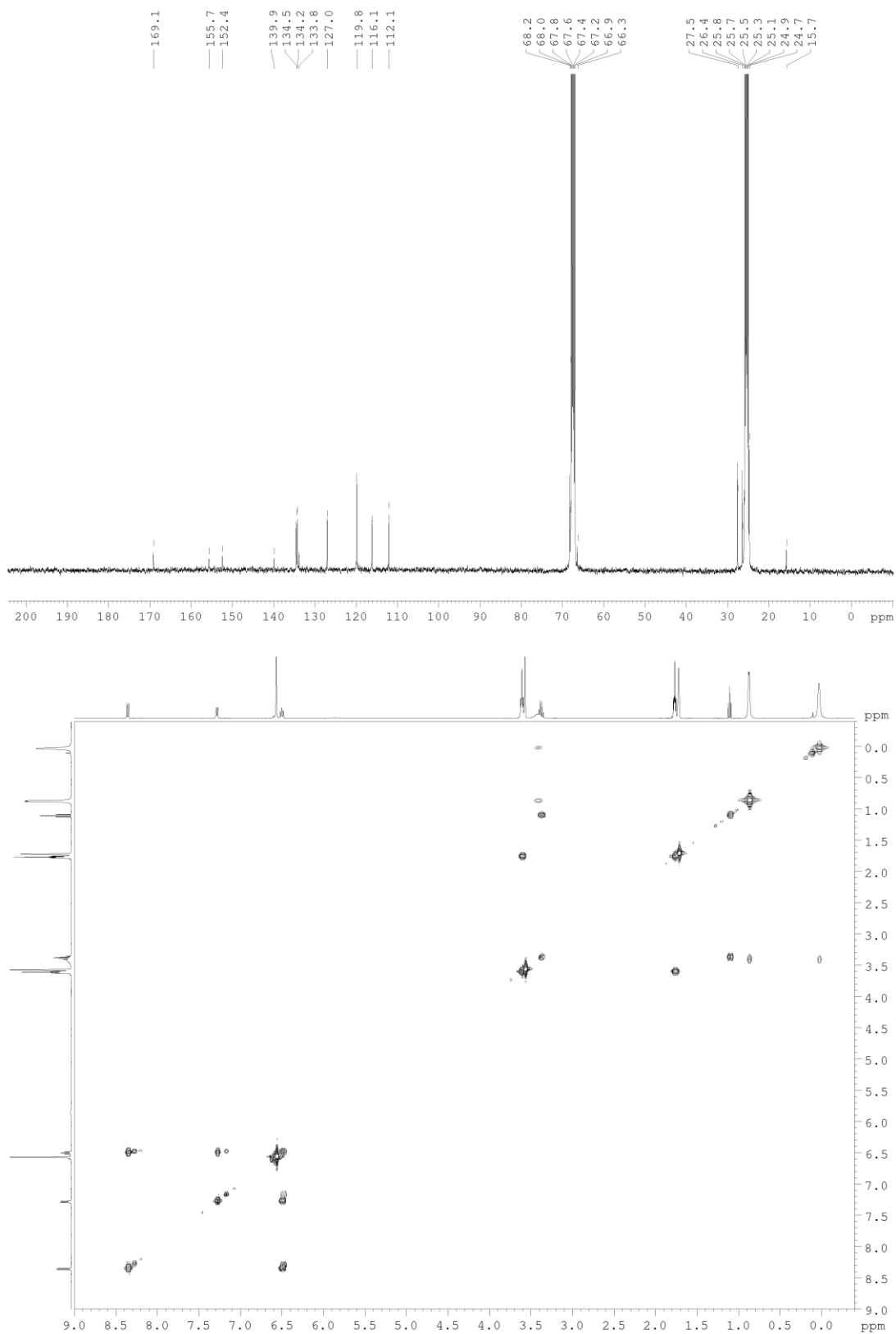


Figure 4.5.13. $^{13}\text{C}\{^1\text{H}\}$ (top) and $^1\text{H}-^1\text{H}$ -COSY NMR spectra (bottom) of **4a** (400.13/100.61 MHz, THF- d_8 , 300K).

4 Cobalt-Catalyzed Hydrogenations via Olefin Cobaltate and Hydride Intermediates

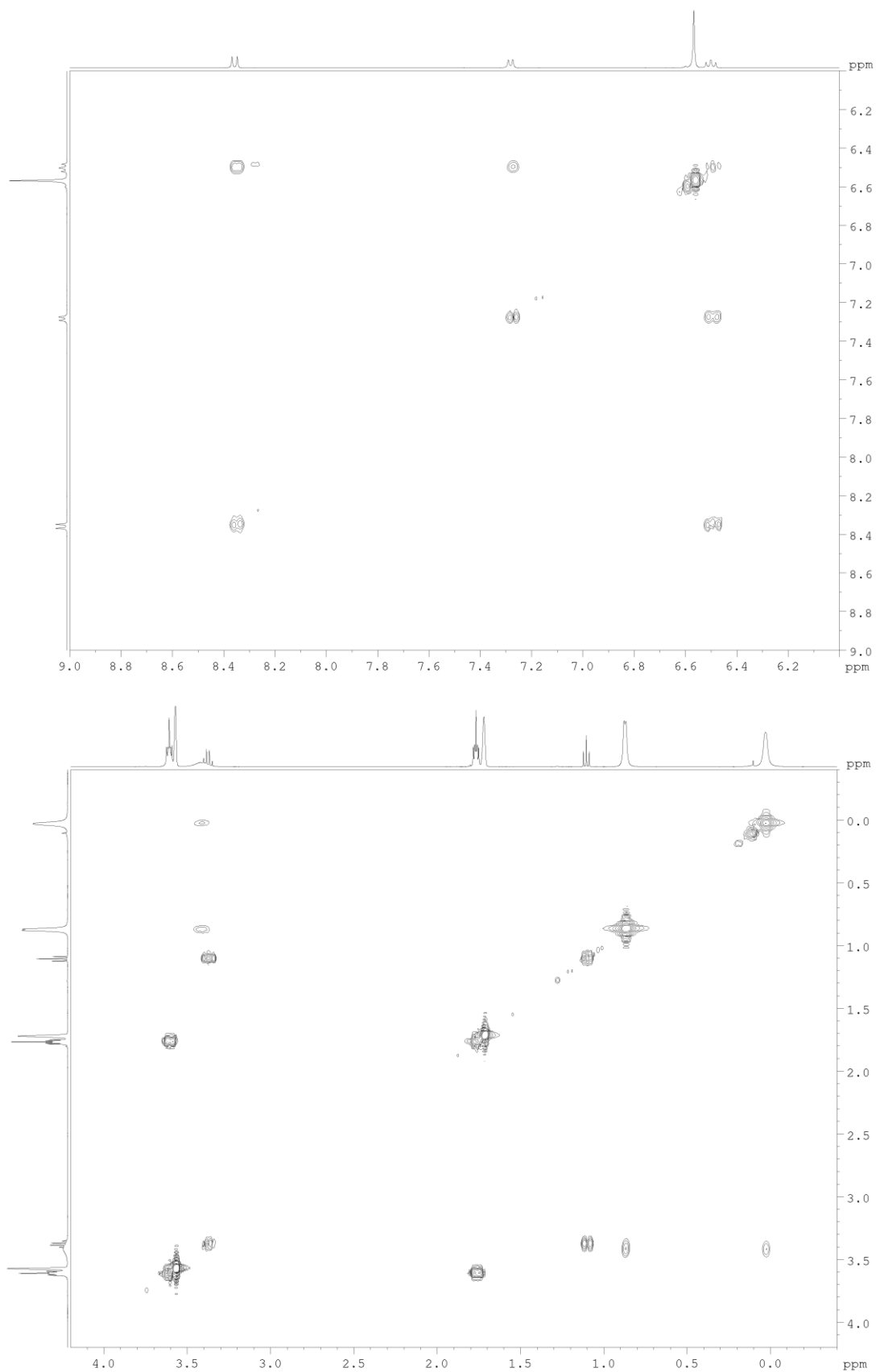


Figure 4.5.14. ^1H - ^1H -COSY NMR spectra (bottom) of **4a** (400.13 MHz, THF- d_8 , 300K).

4 Cobalt-Catalyzed Hydrogenations via Olefin Cobaltate and Hydride Intermediates

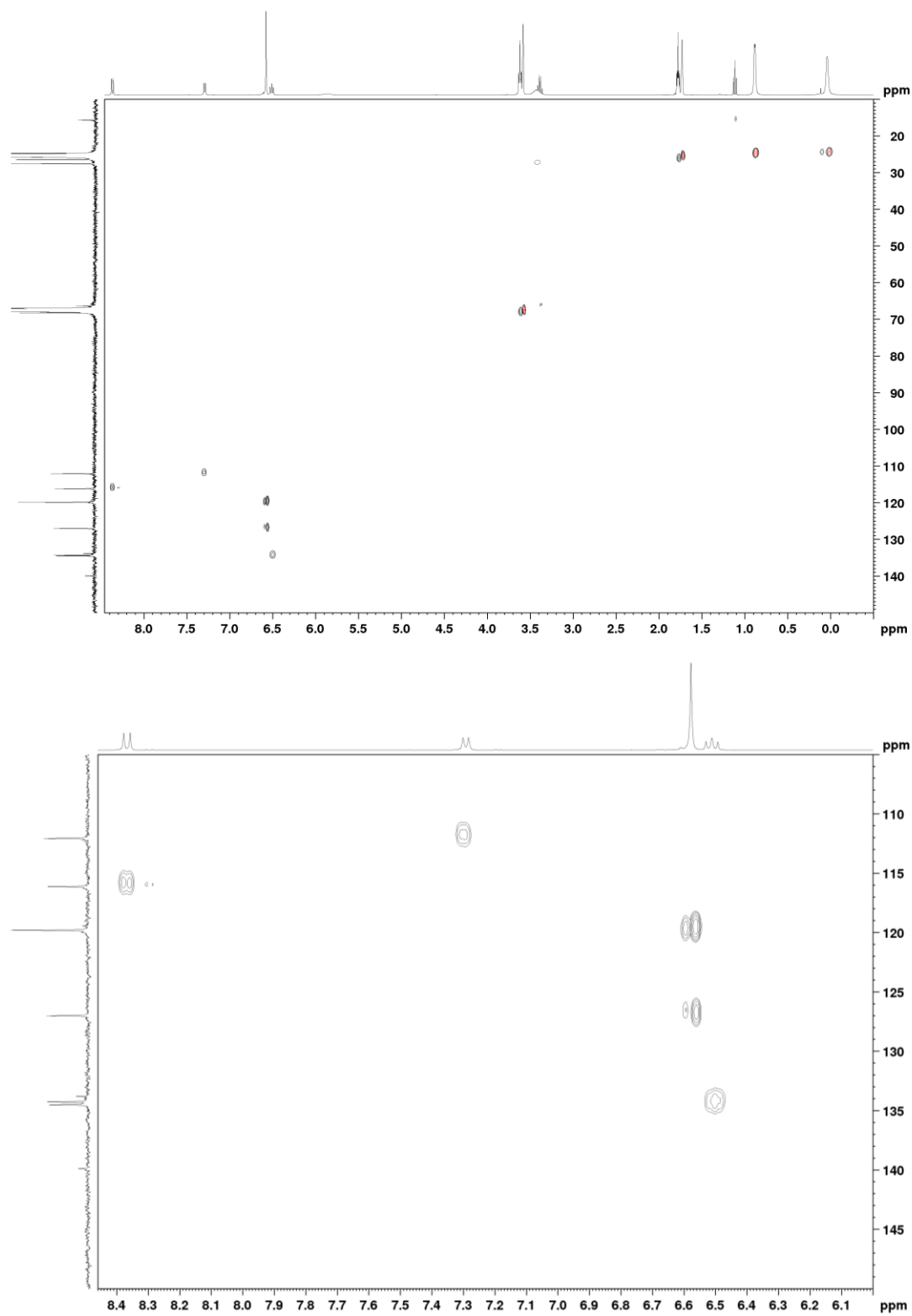


Figure 4.5.15. ^1H - $^{13}\text{C}\{^1\text{H}\}$ -HSQC NMR spectra (bottom) of **4a** (400.13/100.61 MHz, THF-d_8 , 300K).

4 Cobalt-Catalyzed Hydrogenations via Olefin Cobaltate and Hydride Intermediates

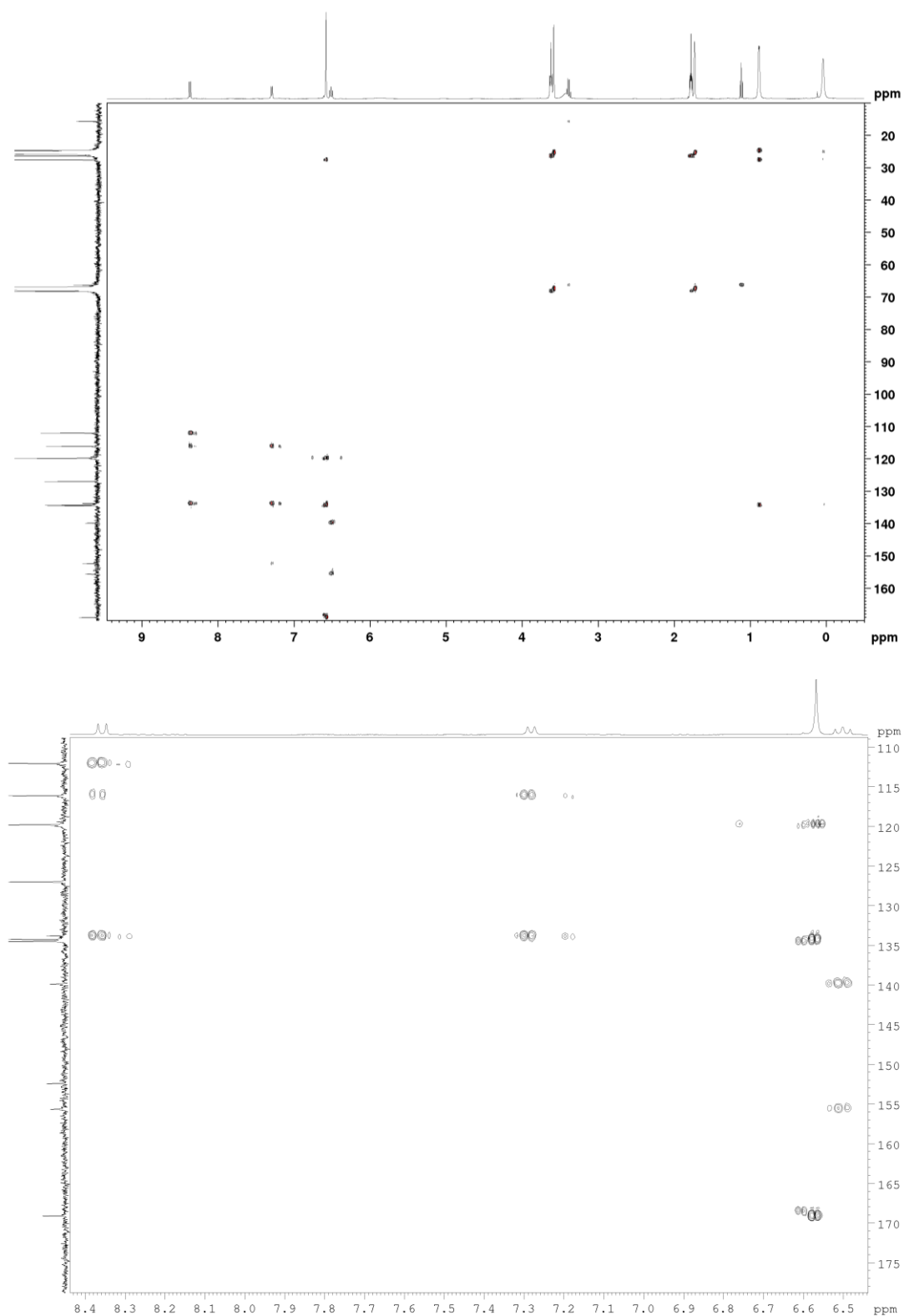


Figure 4.5.16. ^1H - $^{13}\text{C}\{^1\text{H}\}$ -HMBC NMR spectra of **4a** (400.13/100.61 MHz, THF-d_8 , 300K).

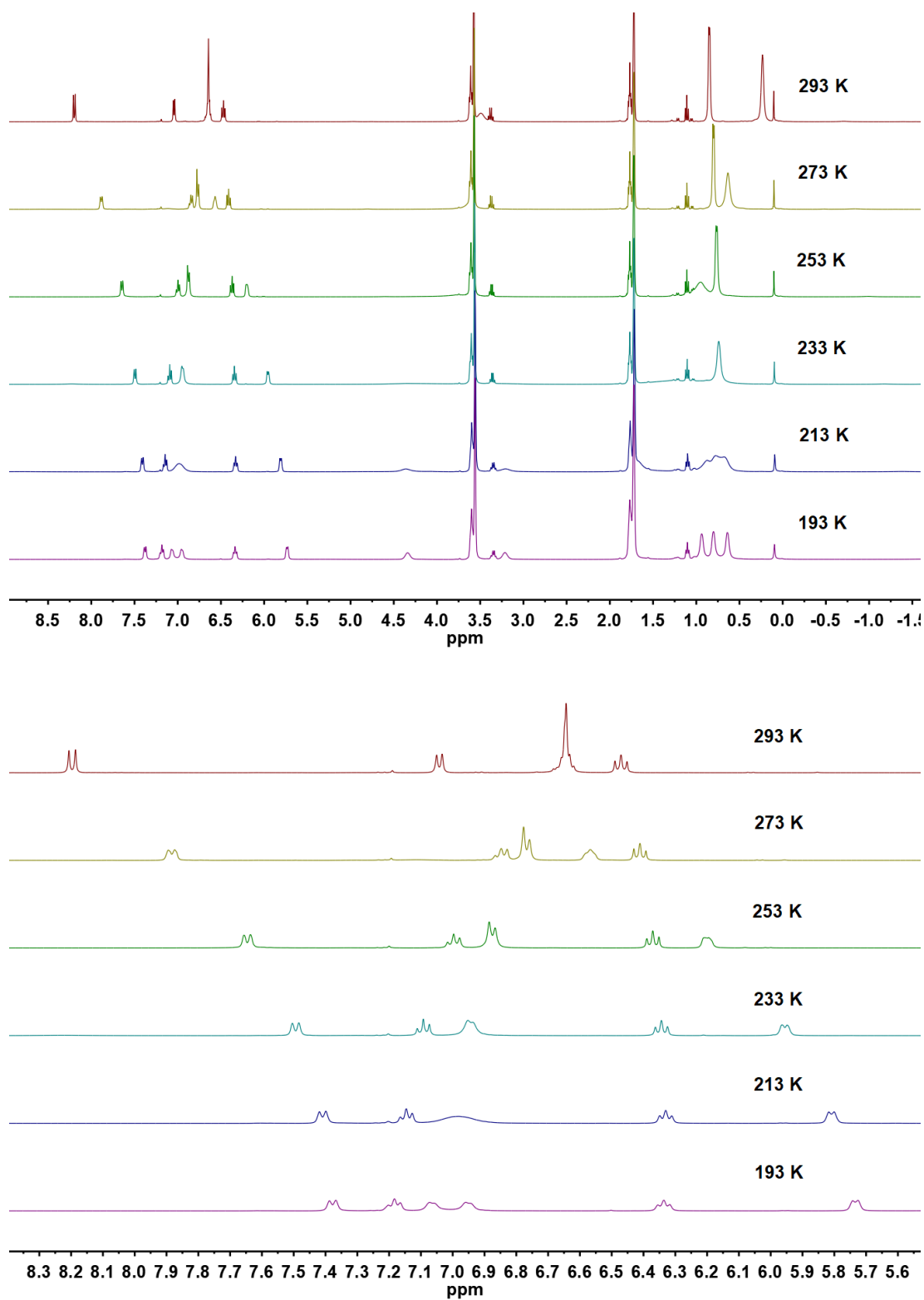


Figure 4.5.17. Variable-temperature $^1\text{H-NMR}$ spectra of **4a** (400.13 MHz, THF-d_8 , 193-293K).

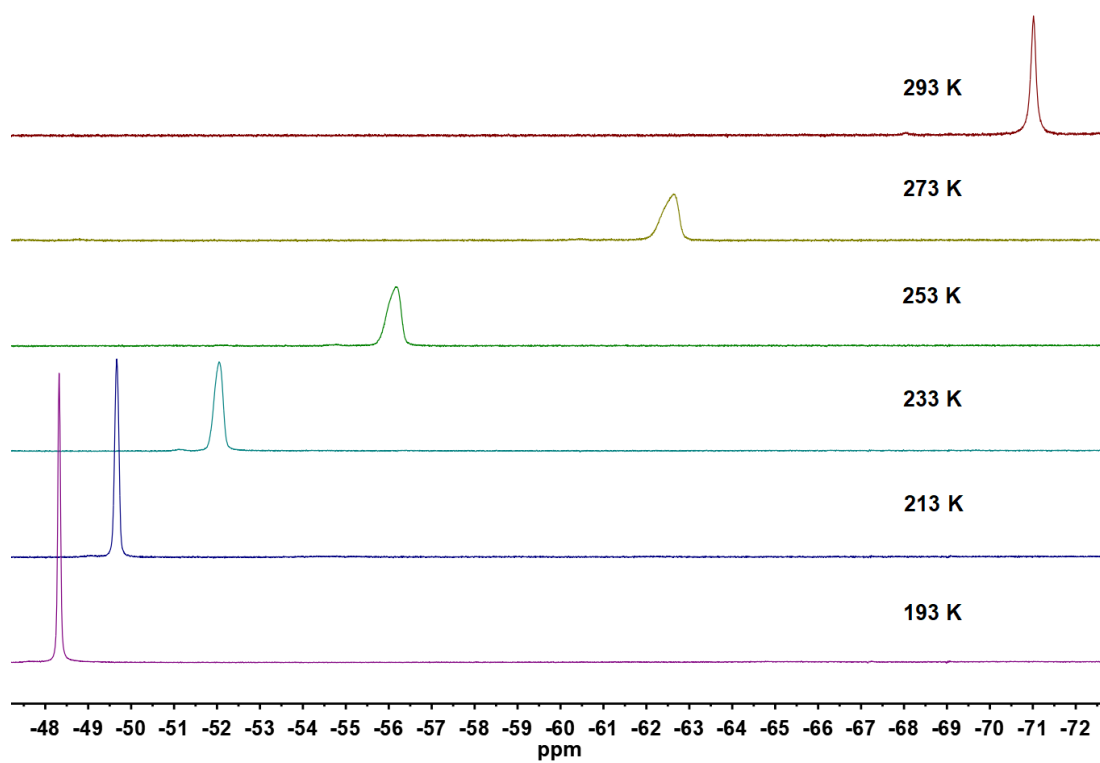


Figure 4.5.18. Variable-temperature ¹H-NMR spectra of **4a** (400.13 MHz, THF-d₈, 193-293K).

Fitting of variable-temperature ^1H -NMR spectra of **4a**.

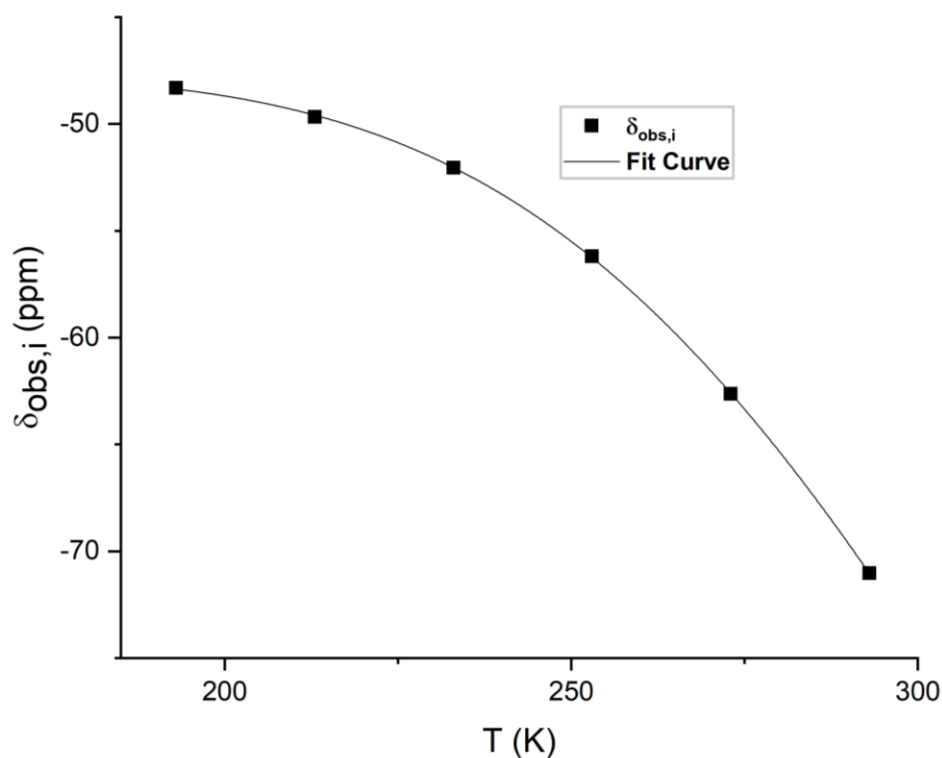


Figure 4.5.19. Hydride ^1H -NMR shift of **4a** vs. T with fit curve (400.13 MHz, THF-d_8 , 193-293K).

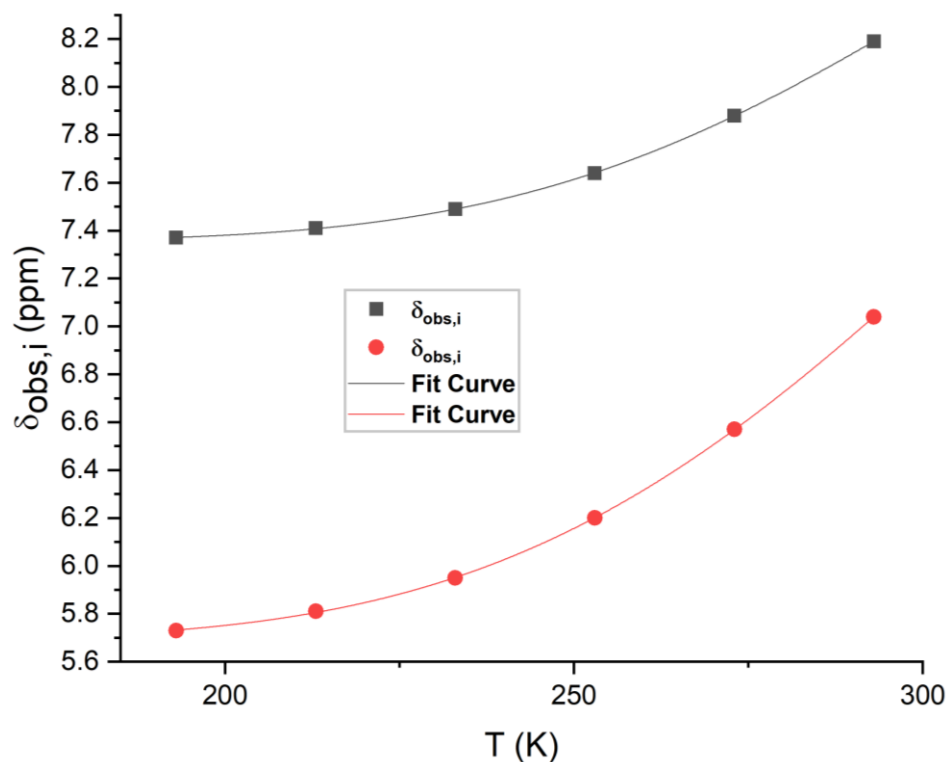


Figure 4.5.20. BIAN ^1H -NMR shift of **4a** vs. T with fit curve (400.13 MHz, THF-d_8 , 193-293K).

Fitting was performed for protons showing a significant temperature dependence according to B. Bachmann, F. Hahn, J. Heck, M. Wünsch, *Organometallics* **1989**, *8*, 2523 with

$$K = \exp\left(-\frac{\Delta G}{RT}\right)$$

and

$$\delta_{i,obs} = \delta_{i,dia} + \delta_{i,para}$$

and

$$\delta_{i,para} = \frac{C_i}{T} \left[1 + \exp\left(\frac{\Delta G}{RT}\right)\right]^{-1}$$

and

$$C_i = a_i \frac{\gamma_e g \beta S(S+1)}{\gamma_h 6SK}$$

with a_i = isotropic hfcc of the the nucleus (here proton); γ_e and γ_h are the magnetogyric ratios of the electron and proton, respectively; g = isotropic g value and S = spin state of the paramagnetic form, β = Bohr magneton, K = Boltzmann factor.

Dipolar shift was neglected due to small spin-orbit coupling for Cobalt.

Table 4.5.6. Fitting data for variable-temperature $^1\text{H-NMR}$ spectra of **4a** (400.13 MHz, THF- d_8 , 193-293K).

$\delta_{dia} / \text{ppm}$		C / K		$\Delta H / \text{kJ mol}^{-1}$		$\Delta S / \text{J mol}^{-1} \text{K}^{-1}$		Reduced Chi-Sqr.	Adj. R- Square
Value	SD ^a	Value	SD ^a	Value	SD ^a	Value	SD ^a		
7.35	0.003	1147	168	21.4	0.7	62.2	3.7	5.70E-06	0.99994
5.69	0.007	2329	526	19.2	0.7	52.5	4.5	1.76E-05	0.99993
-47.67	0.154	-55853	23191	19.1	0.9	48.8	6.7	0.00797	0.9999

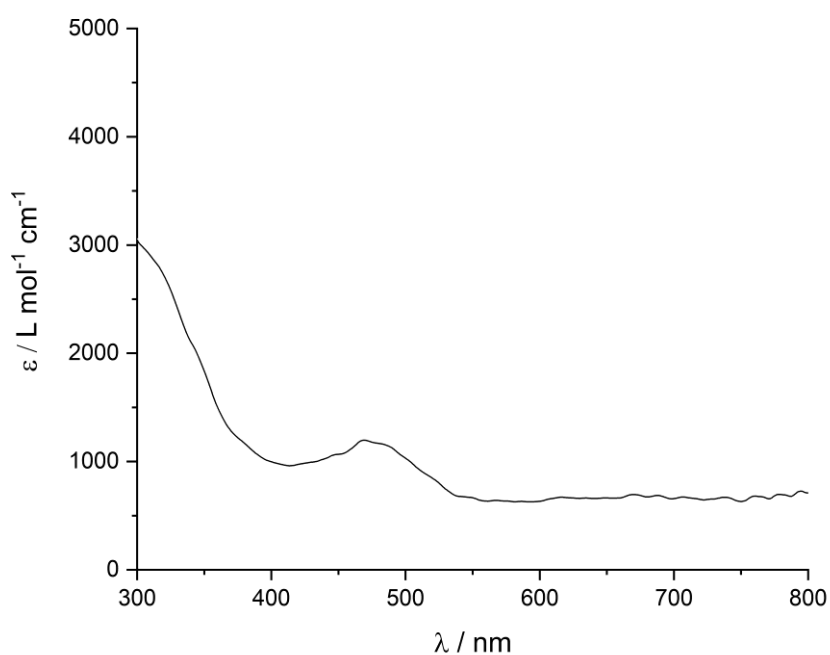
^a standard deviation.

Table 4.5.7. Spin equilibrium data from fitting data for variable-temperature ^1H -NMR spectra of **4a** (400.13 MHz, THF- d_8 , 193-293K).

T / K	$\Delta G / \text{kJ mol}^{-1}$	$\Delta G / \text{kJ mol}^{-1}$	$\Delta G / \text{kJ mol}^{-1} \text{ K}$	K	K	K
$\delta_{\text{dia}} / \text{ppm}$	7.35	5.69	-47.67	7.35	5.69	-47.67
193	9.40	9.11	9.67	0.003	0.003	0.002
213	8.15	8.06	8.70	0.010	0.011	0.007
233	6.91	7.02	7.72	0.028	0.027	0.019
253	5.67	5.97	6.75	0.068	0.059	0.040
273	4.42	4.92	5.77	0.143	0.115	0.079
293	3.18	3.87	4.80	0.271	0.204	0.140
296	2.99	3.71	4.65	0.297	0.221	0.151

Presumably, the true K value is similar to the value obtained for the fitting of $\delta_{\text{dia}} = 7.35$ ppm as the peaks show little chemical dynamics.

UV-Vis spectra

**Figure 4.5.21.** UV-VIS of **4a**.

Cyclovoltammetry

Complex **4a** was electrochemically investigated by means of cyclovoltammetry. One reversible process at -2.4 was observed. Reversibility was proved by measuring with different rates from 20 mV s^{-1} to 200 mV s^{-1} . Plotting current vs. square root of scan rate gave a linear correlation, which is an indication for reversibility.

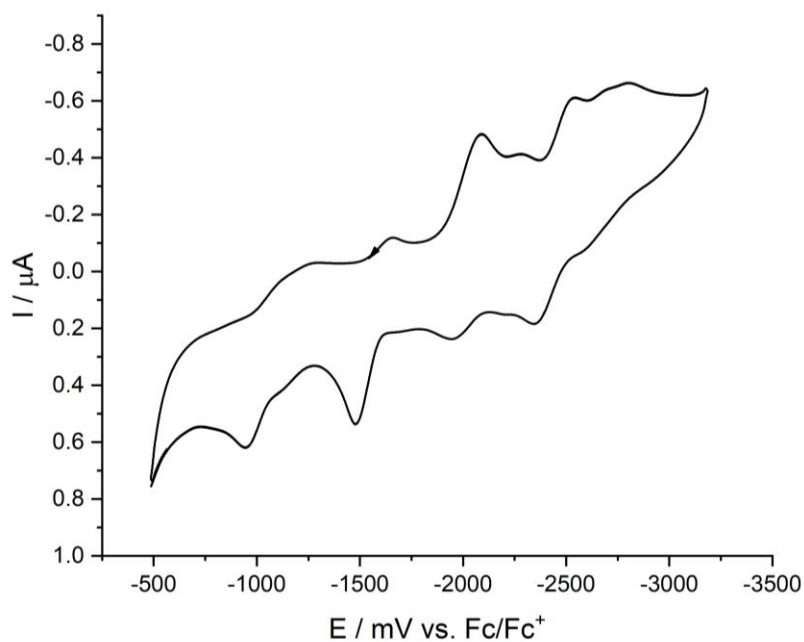


Figure 4.5.22. CV of **4a**.

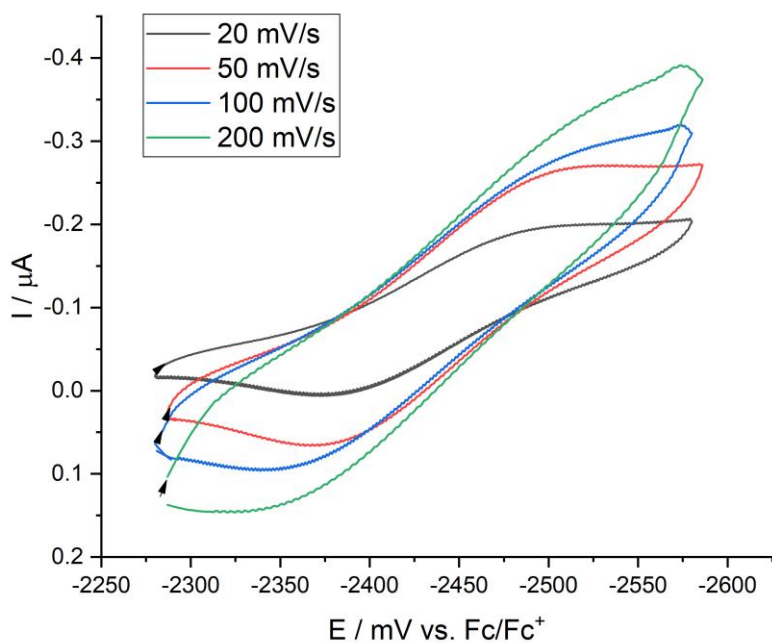


Figure 4.5.23. CV of 4a.

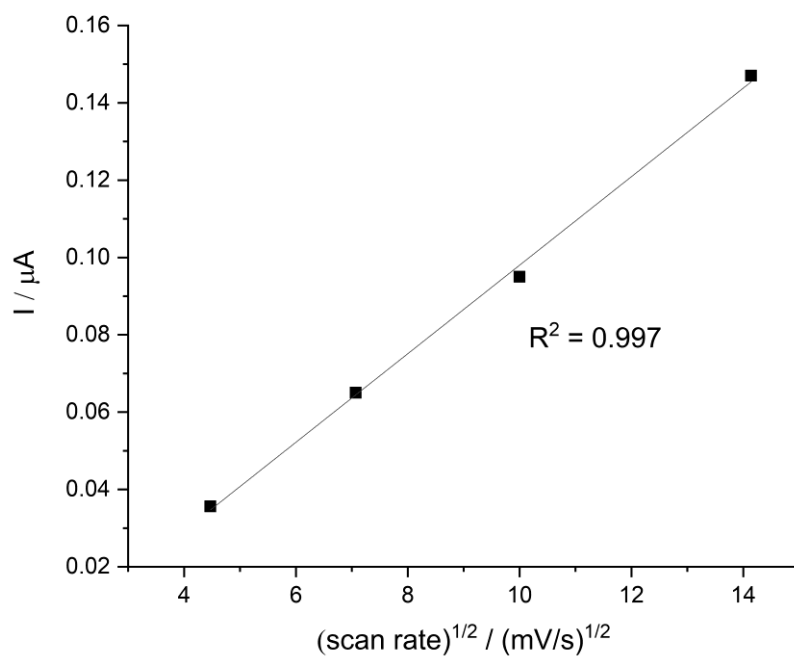


Figure 4.5.24. Plot current vs. square root of the scan rate of 4a.

ESI-mass spectrometric experiments

For the measurement of ESI mass spectra, solutions of **4a** in carefully dried THF were injected into the ESI source of an HCT quadrupole-ion trap mass spectrometer (Bruker Daltonik) at a flow rate of $13 \mu\text{L min}^{-1}$. The ESI source was operated at a voltage of 3.0 kV with nitrogen as nebulizer gas (0.7 bar) and drying gas (5 L min^{-1} , 333 K). The ions were then transferred into the helium-filled ion trap, which was operated at a trap drive of 60. Mass spectra were recorded over an m/z range from 50 to 1400. For gas-phase fragmentation experiments, the dinuclear cobaltate ion was mass-selected (isolation width of 4 u), subjected to excitation voltages of amplitudes V_{exc} , and allowed to collide with helium atoms for 40 ms. Isotope patterns were simulated with the Compass software package (Bruker Daltonik).

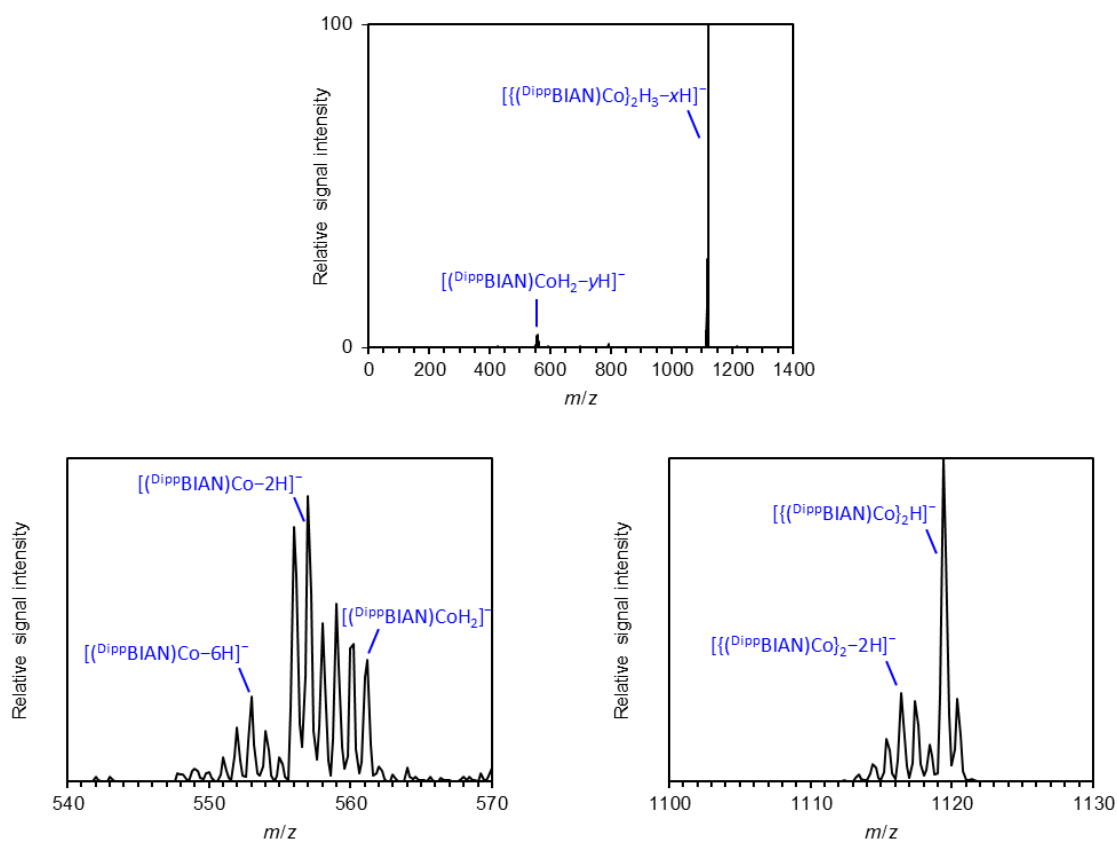


Figure 4.5.25. Mass spectrum of mass-selected $[\{(\text{DippBIAN})\text{Co}\}_2(\mu\text{-H})_3]^-$ and its fragment ions produced upon collision-induced dissociation with an excitation voltage of the amplitude of $V_{\text{exc}} = 0.4 \text{ V}$ (low collision energy). Top: overview, bottom: sections from the spectrum.

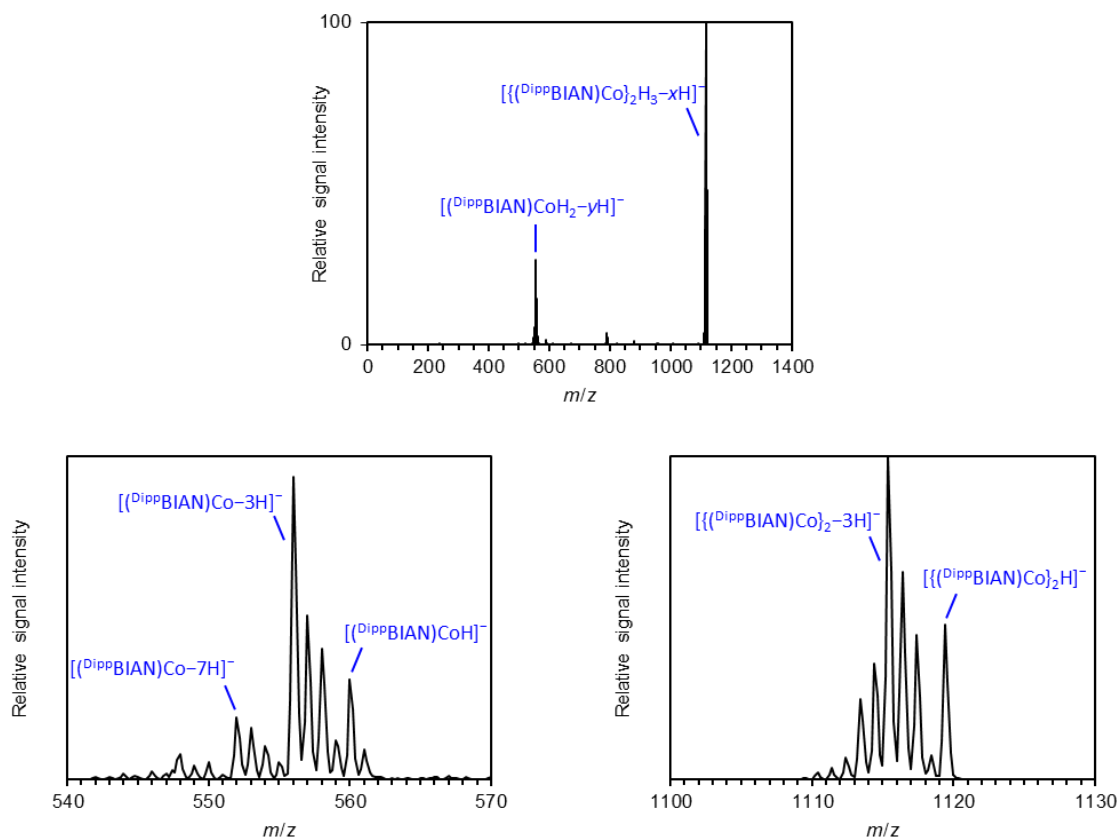


Figure 4.5.26. Mass spectrum of mass-selected $[\{(\text{DippBIAN})\text{Co}\}_2(\mu\text{-H})_3]^-$ and its fragment ions produced upon collision-induced dissociation with an excitation voltage of the amplitude of $V_{\text{exc}} = 0.7$ V (high collision energy). Top: overview, bottom: sections from the spectrum.

Crystal structure

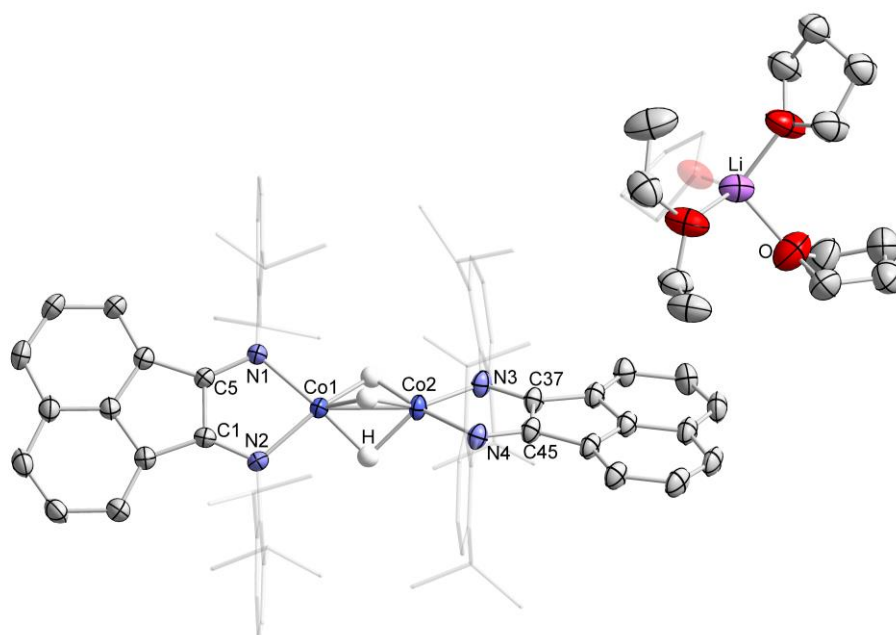


Figure 4.5.27. Solid-state molecular structure of **4a**. Minor disordered parts, non-coordinated solvents and selected hydrogen atoms are omitted for clarity. Thermal ellipsoids are drawn at the 50% probability level.

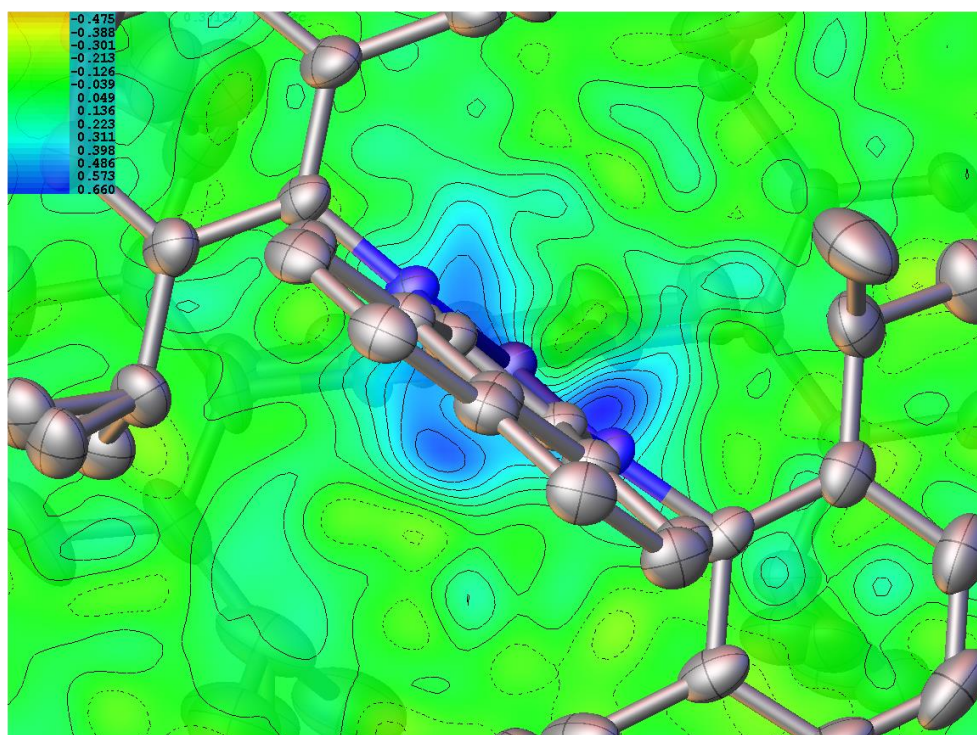


Figure 4.5.28. Residual electron density from the difference Fourier map, rendered at 0.1 Å resolution for **4a** (hydrides removed).

Table 4.5.8. Crystal data and structure refinement for **4a**.

Formula	C ₉₀ Co ₂ H ₁₂₁ LiN ₄ O _{4.5}
<i>D</i> _{calc.} / g cm ⁻³	1.169
<i>μ</i> /mm ⁻¹	3.532
Formula Weight	1455.70
Colour	dark green
Shape	block
Size/mm ³	0.31×0.24×0.16
<i>T</i> /K	138.2(6)
Crystal System	orthorhombic
Space Group	<i>Pbca</i>
<i>a</i> /Å	25.0102(2)
<i>b</i> /Å	21.4146(2)
<i>c</i> /Å	30.8908(3)
<i>α</i> /°	90
<i>β</i> /°	90
<i>γ</i> /°	90
<i>V</i> /Å ³	16544.6(3)
<i>Z</i>	8
<i>Z'</i>	1
Wavelength/Å	1.54184
Radiation type	CuK _α
<i>Θ</i> _{min} /°	2.861
<i>Θ</i> _{max} /°	74.682
Measured Refl.	126831
Independent Refl.	16725
Reflections with <i>I</i> > 2(<i>I</i>)	14835
<i>R</i> _{int}	0.0511
Parameters	1175
Restraints	686
Largest Peak	1.419
Deepest Hole	-0.609
GooF	1.020
<i>wR</i> ₂ (all data)	0.1864
<i>wR</i> ₂	0.1797
<i>R</i> ₁ (all data)	0.0690
<i>R</i> ₁	0.0623

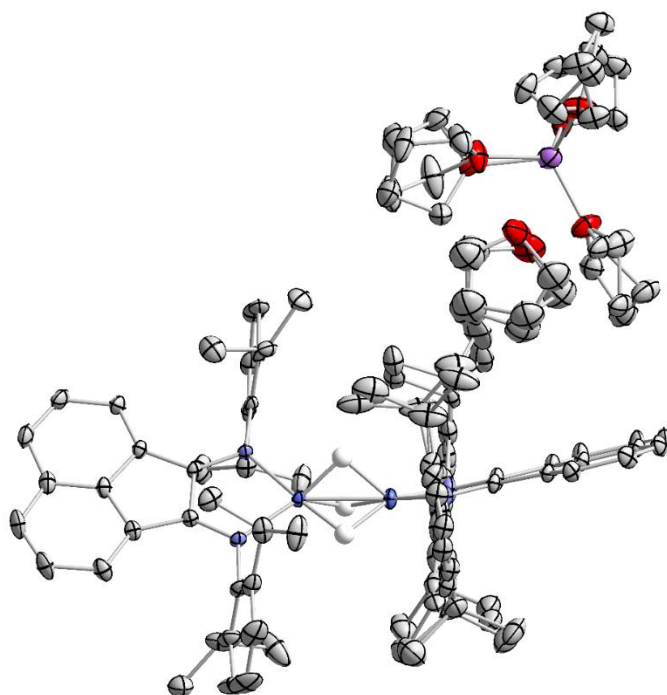


Figure 4.5.29. Solid-state molecular structure of **4b**. Minor disordered parts, non-coordinated solvents and selected hydrogen atoms are omitted for clarity. Thermal ellipsoids are drawn at the 50% probability level.

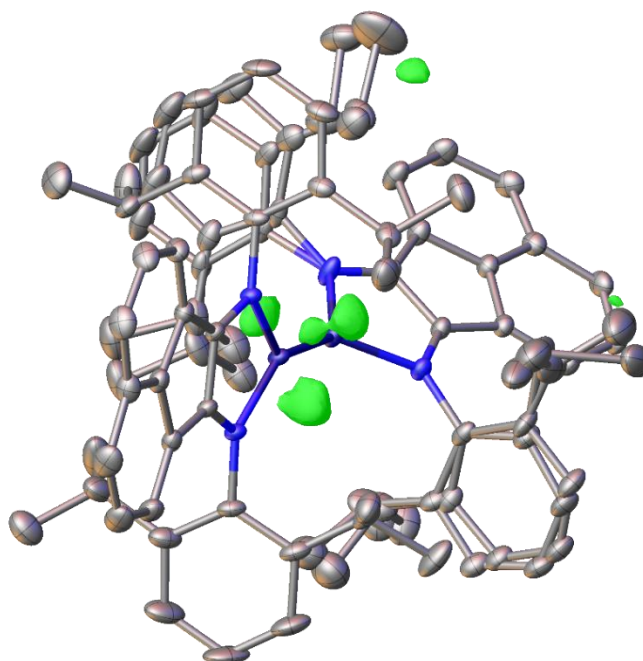


Figure 4.5.30. Residual electron density from the difference Fourier map, rendered at 0.1 Å resolution and at 0.6 e/Å³ for **4b** (hydrides removed).

Table 4.5.9. Crystal data and structure refinement for **4b** solvate.

Formula	C ₉₂ H ₁₂₃ Co ₂ LiN ₄ O ₅
<i>D</i> _{calc.} / g cm ⁻³	1.201
<i>μ</i> /mm ⁻¹	0.456
Formula Weight	1489.74
Color	metallic dark green
Shape	block
Size/mm ³	0.23×0.16×0.07
<i>T</i> /K	100
Crystal System	monoclinic
Space Group	<i>P</i> 2 ₁ / <i>n</i>
<i>a</i> /Å	21.4917(16)
<i>b</i> /Å	13.0279(10)
<i>c</i> /Å	29.987(2)
<i>α</i> °	90
<i>β</i> °	101.0860(10)
<i>γ</i> °	90
<i>V</i> /Å ³	8239.5(11)
<i>Z</i>	4
<i>Z</i> '	1
Wavelength/Å	0.710730
Radiation type	MoK _α
<i>Θ</i> _{min} °	1.291
<i>Θ</i> _{max} °	28.906
Measured Refl.	125720
Independent Refl.	20508
Reflections with <i>I</i> > 2(<i>I</i>)	15724
<i>R</i> _{int}	0.0433
Parameters	1478
Restraints	1020
Largest Peak	0.604
Deepest Hole	-0.469
GooF	1.030
<i>wR</i> ₂ (all data)	0.1100
<i>wR</i> ₂	0.0994
<i>R</i> ₁ (all data)	0.0650
<i>R</i> ₁	0.0432

Magnetic susceptibility measurements of 4b

Temperature-dependent magnetic susceptibility measurements were carried out with a *Quantum-Design* MPMS-XL-5 SQUID magnetometer equipped with a 5 Tesla magnet in the range from 2 to 250 K at a magnetic field of 0.5 T. The powdered sample was contained in a Teflon bucket and fixed in a non-magnetic sample holder. Each raw data file for the measured magnetic moment was corrected for the diamagnetic contribution of the Teflon bucket. The molar susceptibility data were corrected for the diamagnetic contribution.

Experimental data for **4** were modelled by using a fitting procedure to the appropriate Heisenberg-Dirac-van-Vleck (HDvV) spin Hamiltonian for isotropic exchange coupling and Zeeman splitting, equation (1).

$$\hat{H} = -2J_{Co-Co}\hat{S}_2\hat{S}_3 - 2J_{Bian-Co}(\hat{S}_1\hat{S}_2 + \hat{S}_3\hat{S}_4) + g\mu_B\vec{B}\sum\vec{S}_i \quad (1)$$

A Curie-behaved paramagnetic impurity ($PI = 7.5\%$ per cobalt center, $S = 3/2$) was included according to $C_{calc} = (1 - PI) \cdot C + PI \cdot C_{mono}$.

Simulation of the experimental magnetic data was performed with the *julX* program (E. Bill: Max-Planck Institute for Chemical Energy Conversion, Mülheim/Ruhr, Germany).

Gas evolution measurement

In an argon-filled glovebox, **4a** (16.1 mg, 0.0113 mmol) was dissolved in 1.2 mL THF, transferred outside of the glovebox and added to the Man on the moon gas evolution apparatus by syringe. During the introduction of a solution of HCl in dioxane (4 M) gas evolution was monitored, which corresponds to 2.3 ± 0.1 eq. H₂ per cobalt dimer.

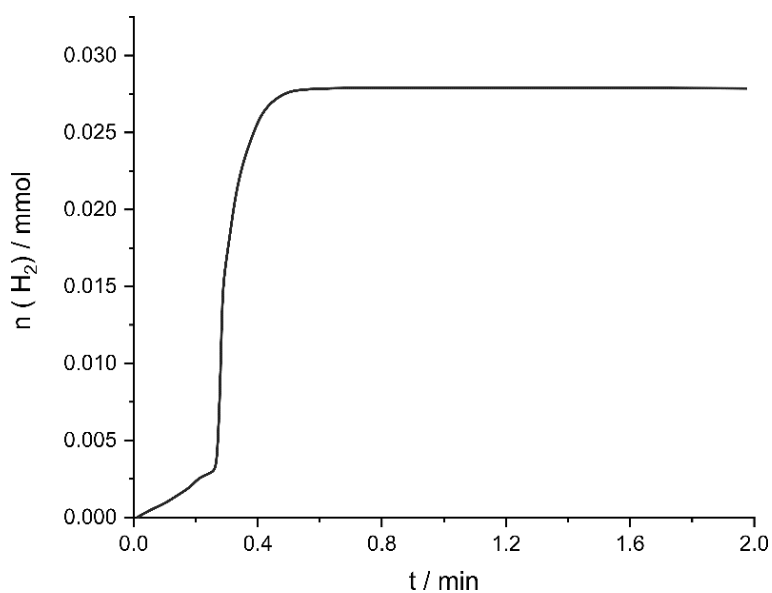


Figure 4.5.31. Gas evolution measurement of with **4a**.

Amine-borane dehydrogenation

In an argon-filled glovebox, **4a** (8.0 mg, 0.006 mmol) was dissolved in THF (0.4 mL). The resulting solution was added dropwise to a solution of NH_3BH_3 (6.4 mg, 0.22 mmol) during which the color changed from dark green to dark violet. After 17 h, the dark violet solution was filtered from the white precipitate and investigated by ^{11}B -NMR.

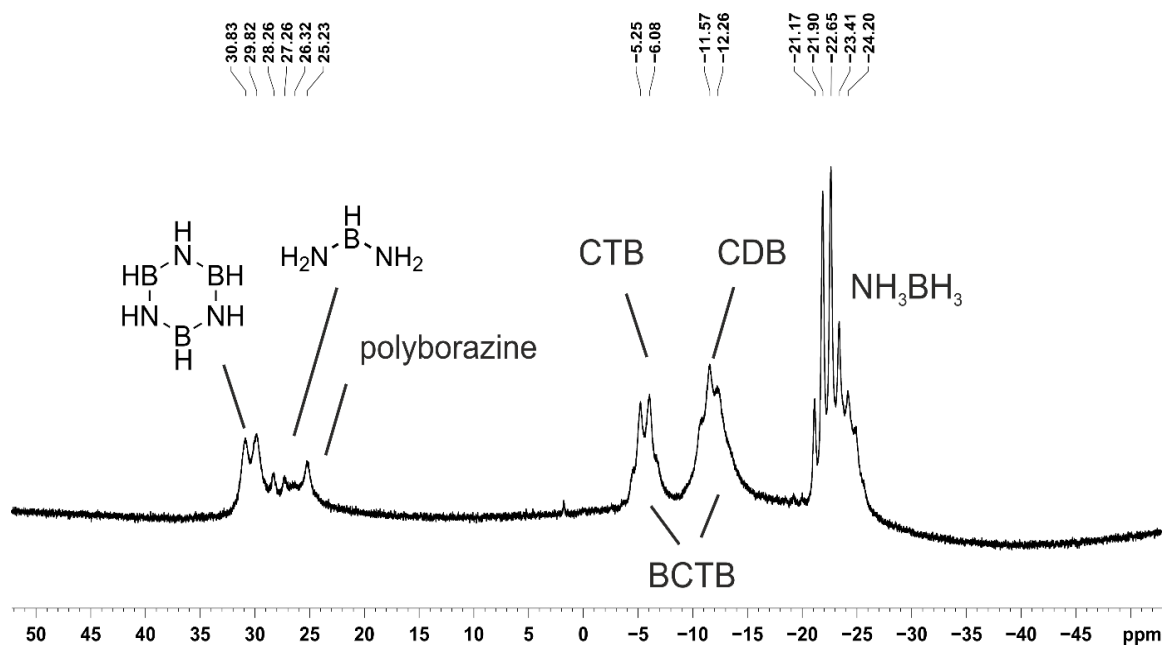


Figure 4.5.32. ^{11}B -NMR spectrum of NH_3BH_3 dehydrogenation catalyzed by **4a** after 17h (CTB = cyclo-triaminoborane, CDB = cyclo-diaminoborane, BCTB = H_3BNH_2 -cyclo- $\text{B}_3\text{N}_3\text{H}_{11}$)

Indication of the formation of hydride species in a related procedure using THF

In an argon-filled glovebox, a Schlenk flask was equipped with a suspension of $\text{Dipp}^{\text{pp}}\text{BIANCoBr}_2$ (0.18 mmol) in THF (5 mL) and closed with a septum. After cooling to $-35\text{ }^\circ\text{C}$, the flask was taken out of the freezer and subsequently reduced by dropwise addition of LiEt_3H (3 equiv., 1.1M, THF) during which a color change from pale brown to dark green and solubilization was observed. After 10 minutes stirring, hexane (10 mL) was added and the mixture was filtered through a closed Schlenk frit (P4, gravitation). The filter cake was washed with hexane (3 x 1 mL) and the solvent of the combined fractions was slowly evaporated (RT, 2 days) during which a phase separation occurred. The upper red-brown fraction was removed by pipette leaving a dark green suspension which was decanted. The precipitate was washed with hexane (3 x 1 mL) and diluted in thf-d^8 (0.5 mL). After filtration, the $^1\text{H-NMR}$ was measured subsequently. High-field shifted signals similar to the hydride shift of **4** indicate the formation of related hydride species in a reaction solution using THF as solvent.

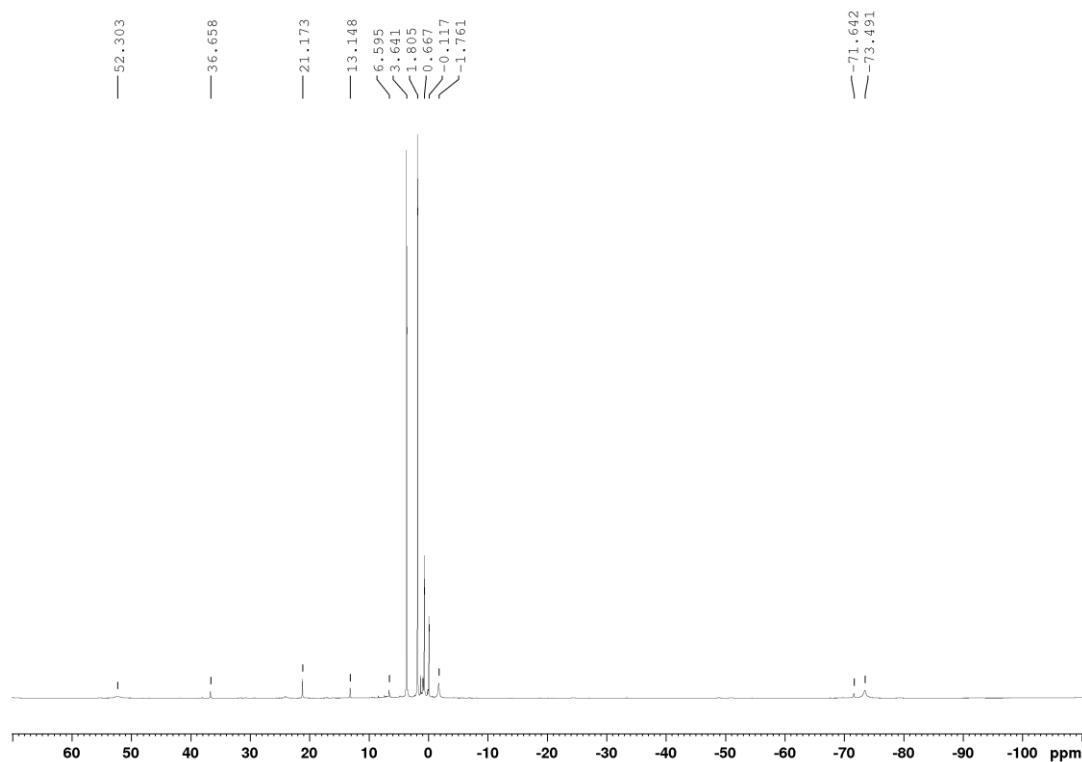
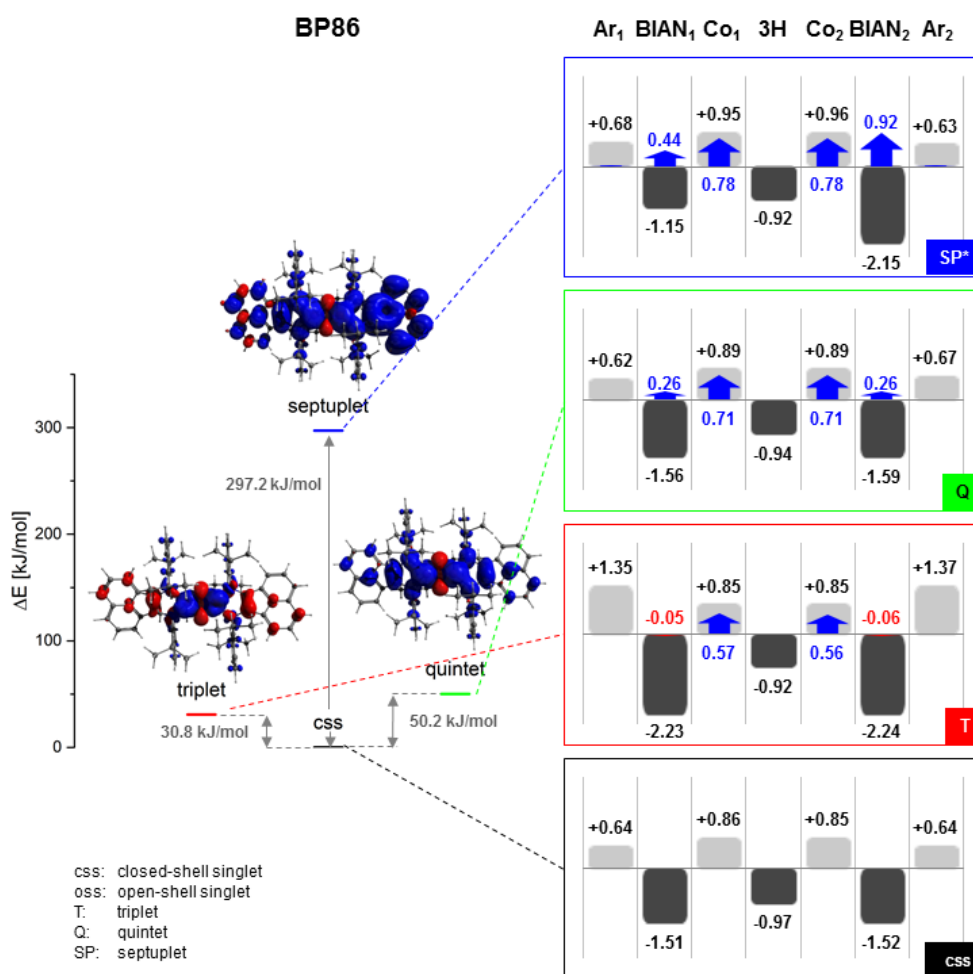


Figure 4.5.33. $^1\text{H-NMR}$ of crude product from a synthesis in THF (400.13 MHz, THF-d_8 , 193-293K).

4.5.3 Theoretical calculations of 4

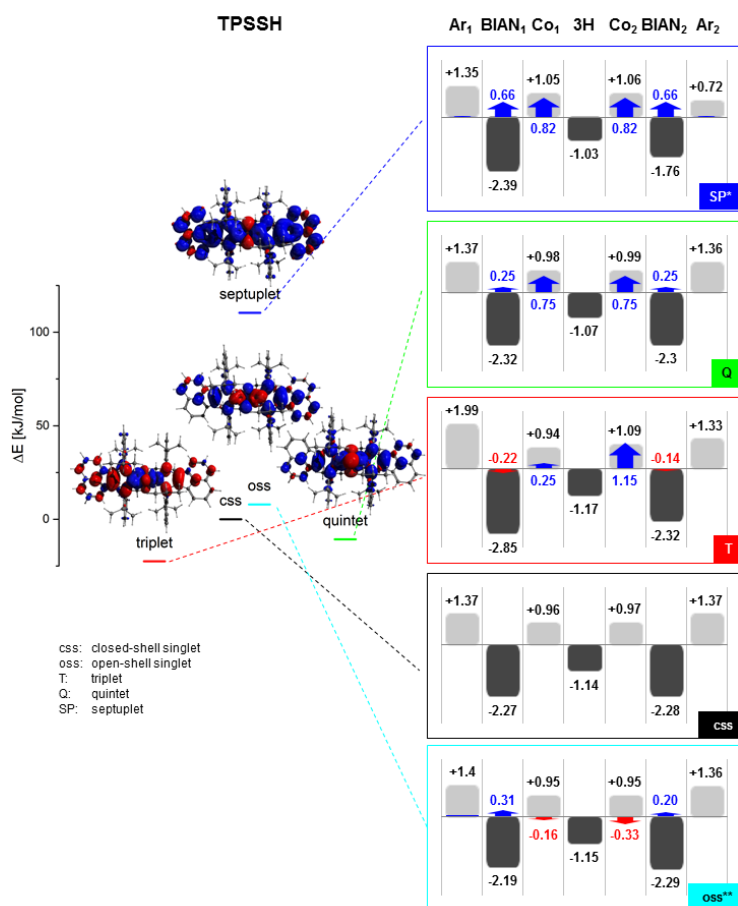
Figure 4.5.34. Energy diagram of **4** in various spin states; anion optimized with BP86 functional and Ahlrichs' def2-TZVP basis set. Left: Spin density (isosurface value: 0.001) of the corresponding spin state. Right: Local charges (light / dark grey: positive/ negative) and spins (blue/ red: α/β) on specific fragments of the molecule in different spin states. A local spin of $\frac{1}{2}$ corresponds to one unpaired electron. Reference (36) in the main manuscript.



* From single-point calc. on optimized mol. structure in css state (BP86/def2-TZVP)

From molecular structure optimizations with the TPSSH functional (*Figure 4.5.35*), higher spin states are predicted to be energetically below the closed-shell singlet state. The single-point energy of the open-shell singlet state based on the triplet molecular structure is 7.9 kJ/mol above the closed-shell singlet state. However, since no molecular structure optimization was performed due to convergence issues, the open-shell singlet may even be energetically more favored than the triplet and thus may possibly represent the ground state. As it was the case for the BP86 functional, based on single-point calculations the septuplet represents the highest energy state ($\Delta E_{SP-CSS} = 110.4$ kJ/mol).

Figure 4.5.35. Energy diagram of **4** in various spin states, anion optimized with the TPSSH functional and Ahlrichs' def2-TZVP basis set. Left: Spin density (isosurface value: 0.001) of the corresponding spin state. Right: Local charges (light / dark grey: positive/ negative) and spins (blue/ red: α/β) on specific fragments of the molecule in different spin states. A local spin of $\frac{1}{2}$ corresponds to one unpaired electron.



* From single-point calc. on optimized mol. structure in CSS state (BP86/def2-TZVP)

** From single-point calc. on optimized mol. structure in T state (TPSSH/def2-TZVP)

Table 4.5.10. Total energies of **4** in various spin states from molecular structure optimizations and single-point energy calculations with the BP86 and TPSSH functional and Ahlrichs' def2-TZVP basis set. Energies are given relative to the closed-shell structures in kJ/mol.

Functional	$\Delta E(\text{oss-css})$	$\Delta E(\text{T-css})$	$\Delta E(\text{Q-css})$	$\Delta E(\text{SP-css})$
BP86	-	30.8	50.2	297.2*
TPSSH	7.9**	-22.5	-10.7	110.4*

* SP: From single-point energy calculation on optimized mol. structure in closed-shell singlet state (BP86/def2-TZVP)

**TPSSH oss: From single-point energy calculation on optimized mol. structure in triplet state (TPSSH/def2-TZVP)

Table 4.5.11. Local charges and spins from BADER atoms-in-molecules analysis for **4** in various spin states, resulting from molecular structure optimizations and single-point energy calculations with the BP86 and TPSSH functional and Ahlrich's def2-TZVP basis set. Charges and spins are summed over specific fragments with the local spins given in parentheses, where a value of $\frac{1}{2}$ refers to one electron.

css	Ar ₁	BIAN ₁	Co ₁	3H	Co ₂	BIAN ₂	Ar ₂
BP86	+0.64	-1.51	+0.86	-0.97	+0.85	-1.52	+0.64
TPSSH	+1.37	-2.27	+0.96	-1.14	+0.97	-2.28	+1.37
oss							
TPSSH**	+1.40 (0.01)	-2.19 (0.31)	+0.95 (- 0.16)	-1.15 (- 0.04)	+0.95 (- 0.33)	-2.29 (0.20)	+1.36 (0.00)
T							
BP86	+1.35 (0.00)	-2.23 (- 0.05)	+0.85 (0.57)	-0.92 (0.00)	+0.85 (0.56)	-2.24 (- 0.06)	+1.37 (0.00)
TPSSH	+1.99 (- 0.03)	-2.85 (- 0.22)	+0.94 (0.25)	-1.17 (0.00)	+1.09 (1.15)	-2.32 (- 0.14)	+1.33 (- 0.02)
Q							
BP86	+0.62 (0.03)	-1.56 (0.26)	+0.89 (0.71)	-0.97 (0.00)	+0.89 (0.71)	-1.59 (0.26)	+0.67 (0.03)
TPSSH	+1.37 (0.00)	-2.32 (0.25)	+0.98 (0.75)	-1.07 (0.00)	+0.99 (0.75)	-2.30 (0.25)	+1.36 (0.00)
SP							
BP86*	+0.68 (0.04)	-1.15 (0.44)	+0.95 (0.78)	-0.92 (0.00)	+0.96 (0.78)	-2.15 (0.92)	+0.63 (0.04)
TPSSH*	+1.35 (0.02)	-2.39 (0.66)	+1.05 (0.82)	-1.03 (0.00)	+1.06 (0.82)	-1.76 (0.66)	+0.72 (0.02)

* From single-point energy calculation on optimized mol. structure in closed-shell singlet state (BP86/def2-TZVP)

** From single-point energy calculation on optimized mol. structure in triplet state (TPSSH/def2-TZVP)

Table 4.5.12. Top: Selected bond lengths of **4** in Å in various spin states, resulting from molecular structure optimizations with the BP86 and TPSSH functional and Ahlrichs' def2-TZVP basis set. Middle/bottom: Differences between bond lengths of **4** from molecular structure optimizations and from X-ray crystallographic data of **4a** and **4b** next to the average bond length deviation.

Selected bond lengths from optimized molecular structures													
BP86	C _{SS} ^{a,b}		T ^{a,b}		Q ^{a,b}		TPSSH	C _{SS} ^{a,b}		T ^{a,b}		Q ^{a,b}	
d _(C-C)	1.426	1.426	1.432	1.432	1.43	1.43	d _(C-C)	1.409	1.409	1.412	1.428	1.418	1.417
d _{(N-C)₁}	1.352	1.352	1.352	1.352	1.351	1.351	d _{(N-C)₁}	1.352	1.352	1.356	1.339	1.345	1.345
d _{(N-C)₂}	1.346	1.346	1.343	1.343	1.349	1.349	d _{(N-C)₂}	1.339	1.339	1.339	1.335	1.345	1.345
d _{(N-Co)₁}	1.908	1.908	1.968	1.967	1.964	1.964	d _{(N-Co)₁}	1.914	1.914	1.944	2.021	1.97	1.97
d _{(N-Co)₂}	1.894	1.894	1.928	1.927	1.964	1.964	d _{(N-Co)₂}	1.875	1.875	1.905	2.016	1.956	1.955
d _(Co-Co)	2.282		2.335		2.364		d _(Co-Co)	2.258		2.316		2.354	
Comparison of bond lengths from molecular structure optimizations and XRD 4a													
BP86	C _{SS} ^{a,b}		T ^{a,b}		Q ^{a,b}		TPSSH	C _{SS} ^{a,b}		T ^{a,b}		Q ^{a,b}	
$\bar{\delta}_{(C-C)}$	0.014	0.007	0.02	0.013	0.018	0.011	$\bar{\delta}_{(C-C)}$	0.003	0.01	0	0.009	0.006	0.002
$\bar{\delta}_{(N-C)1$	0.013	0.003	0.013	0.003	0.012	0.002	$\bar{\delta}_{(N-C)1$	0.013	0.003	0.017	0.01	0.006	0.004
$\bar{\delta}_{(N-C)2$	0.013	0.006	0.01	0.003	0.016	0.009	$\bar{\delta}_{(N-C)2$	0.006	0.001	0.006	0.005	0.012	0.005
$\bar{\delta}_{(N-Co)1$	0.005	0.001	0.065	0.058	0.061	0.055	$\bar{\delta}_{(N-Co)1$	0.011	0.005	0.041	0.112	0.067	0.061
$\bar{\delta}_{(N-Co)2$	0.002	0.009	0.032	0.024	0.068	0.061	$\bar{\delta}_{(N-Co)2$	0.021	0.028	0.009	0.113	0.06	0.052
$\bar{\delta}_{(Co-Co)}$	0.018		0.071		0.1		$\bar{\delta}_{(Co-Co)}$	0.006		0.052		0.09	
$\bar{\delta}$	0.008		0.028		0.038		$\bar{\delta}$	0.010		0.034		0.033	
Comparison of bond lengths from molecular structure optimizations and XRD 4b .													
BP86	C _{SS} ^{a,b}		T ^{a,b}		Q ^{a,b}		TPSSH	C _{SS} ^{a,b}		T ^{a,b}		Q ^{a,b}	
$\bar{\delta}_{(C-C)}$	0.013	0.009	0.019	0.015	0.017	0.013	$\bar{\delta}_{(C-C)}$	0.004	0.008	0.001	0.011	0.005	0
$\bar{\delta}_{(N-C)1$	0.007	0.01	0.007	0.01	0.006	0.009	$\bar{\delta}_{(N-C)1$	0.007	0.01	0.011	0.003	0	0.003
$\bar{\delta}_{(N-C)2$	0.009	0.01	0.006	0.007	0.012	0.013	$\bar{\delta}_{(N-C)2$	0.002	0.003	0.002	0.001	0.008	0.009
$\bar{\delta}_{(N-Co)1$	0.01	0.014	0.07	0.073	0.066	0.07	$\bar{\delta}_{(N-Co)1$	0.016	0.02	0.046	0.127	0.072	0.076
$\bar{\delta}_{(N-Co)2$	0.005	0.001	0.039	0.034	0.075	0.071	$\bar{\delta}_{(N-Co)2$	0.014	0.018	0.016	0.123	0.067	0.062
$\bar{\delta}_{(Co-Co)}$	0.039		0.092		0.121		$\bar{\delta}_{(Co-Co)}$	0.015		0.073		0.111	
$\bar{\delta}$	0.012		0.034		0.043		$\bar{\delta}$	0.011		0.038		0.038	

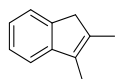
^{a,b} Fragment ^aAr₁—BIAN₁—Co₁ and ^bAr₂—

BIAN₂—Co₂

4.5.4 Synthesis of Substrates and Hydrogenation products

2,3-Dimethyl-1*H*-indene

Synthesis was performed by Gieshoff, Tim, *Dissertation* **2017**, Regensburg, following the procedure described by M. V. Troutman, D. H. Appella, S. L. Buchwald, *J. Am. Chem. Soc.* **1999**, *121*, 4916–4917.



C₁₁H₁₂

144.22 g/mol

Appearance

colorless liquid

Yield

1.49 g, 10.3 mmol (69%)

TLC

R_f = 0.66 (SiO₂, *n*-pentane)

¹H-NMR

(300 MHz, CDCl₃) δ 7.37 (dp, *J* = 7.3, 0.9 Hz, 1H), 7.31 – 7.21 (m, 2H), 7.12 (td, *J* = 7.2, 1.5 Hz, 1H), 3.31 – 3.21 (m, 2H), 2.07 (q, *J* = 1.0 Hz, 3H), 2.04 (tq, *J* = 2.1, 1.1 Hz, 3H).

¹³C-NMR

(75 MHz, CDCl₃) δ 126.05, 123.55, 122.97, 117.91, 42.46, 13.95, 10.17.

GC-MS

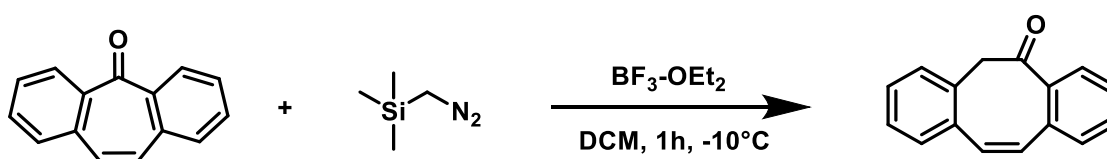
t_R = 6.77 min, (EI, 70 eV): *m/z* = 144 [M⁺], 129, 115, 89, 77, 63, 51.

Analytical data were in full agreement with M. G. Schrems, E. Neumann, A. Pfaltz, *Angew. Chem. Int. Ed.* **2007**, *46*, 8274–8276.

Dibenzo[*a,e*]cyclooctatetraene (dct)

Dibenzo[*a,e*]cyclooctatetraene was synthesized in 3 steps according to S. Chaffins, M. Brettreich, F. Wudl, *Synthesis* **2002**, *9*, 1191-1194. (step 1) and W. Chen, J. F. Hartwig, *J. Am. Chem. Soc.* **2013**, *135*, 2068 (step 2 & 3)

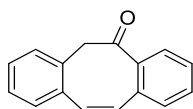
Step 1:



Scheme 5.5.7. Dct synthesis; step 1.

4 Cobalt-Catalyzed Hydrogenations via Olefin Cobaltate and Hydride Intermediates

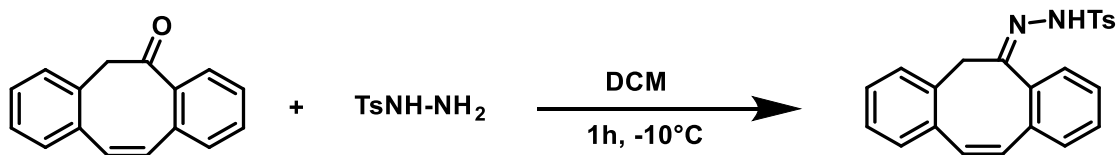
5-Dibenzosuberone (2.91 g, 14.1 mmol, 1.0 equiv.) was dissolved in 20 mL DCM in a 2-necked flask containing a nitrogen bubbler and a dropping funnel. Boron trifluoride etherate complex (2.67 mL, 21.0 mmol, 1.5 equiv.) was added at -10 °C to the solution, which lead to an immediate color change to yellow. Trimethylsilyldiazomethane (2.0 M in diethylether, 105 mL, 21.0 mmol, 1.5 equiv.) was dissolved in DCM (25 mL) and added dropwise over 1 h at -10 °C. The reaction mixture was stirred for additional 2 h at -10 °C. The mixture was poured into ice and the organic phase was separated. The aqueous phase was extracted twice with DCM (100 mL) and the organic phases were combined. After washing with brine (80 mL), the organic phase was dried over MgSO₄. The solvent was evaporated and a yellow oil was obtained. The crude product was purified by column chromatography (SiO₂ (20 cm); *n*-hexane/ethylacetate 10:1; R_f = 0.4). 6*H*-Dibenzo[*a,e*]cyclooctatrien-5-on was obtained as white to light yellow solid.



C₁₆H₁₂O
220.27 g/mol

Appearance	Colorless to light yellow solid
Yield	1.60 g, 7.3 mmol (52%)
TLC	R _f = 0.4 (SiO ₂ , <i>n</i> -hexane/ethylacetate 10:1)
¹H-NMR	(300 MHz, CDCl ₃): δ 78.29 (dd, <i>J</i> = 8.0 Hz, 1.0 Hz, 1H), 7.53-7.20 (m, 7H, CH _{Ar}), 7.05 (d, <i>J</i> = 2.8 Hz, 2H), CH _{alkene}), 4.08 (s, 2H, CH ₂)

Step 2:

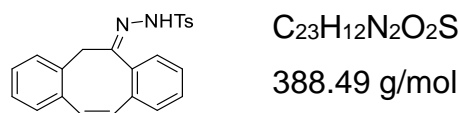


Scheme 4.5.8. Dct synthesis; step 2.

6*H*-Dibenzo[*a,e*]cyclooctatrien-5-on (0.55 g, 2.4 mmol, 1.0 equiv.) and tosylhydrazine (0.49 g, 2.6 mmol, 1.1 equiv.) were dissolved in ethanol (15 mL).

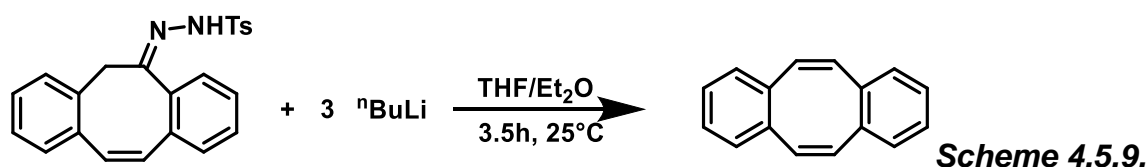
4 Cobalt-Catalyzed Hydrogenations via Olefin Cobaltate and Hydride Intermediates

After addition of 3 drops of concentrated hydrochloric acid, the suspension was stirred for 22 h. A white solid was received after filtration and dried in vacuo. This compound was used in the next step without further purification.



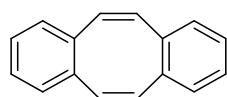
Appearance Colorless solid
Yield (crude) 0.74 g, 1.9 mmol (80%)

Step 3:



Dct synthesis; step 3.

The corresponding hydrazone (1.5 g, 3.9 mmol, 1.0 equiv.) was suspended in a mixture of THF/Et₂O (100 mL, 1:3). *n*-Butyllithium (2.5 M in hexane; 4.6 mL, 11.6 mmol, 3.0 equiv.) was added dropwise. The reaction mixture turned red and was stirred for 3.5 h (product formation was checked via TLC). A saturated solution of ammonium chloride (15 mL) was added to the solution, which led to a yellow solution. After phase separation, the aqueous phase was washed with ethylacetate (2x15 mL). The organic phases were combined and dried over Na₂SO₄. A yellow oil was obtained after evaporation of the solvent. The crude product was purified by column chromatography (SiO₂ (20 cm); *n*-hexane; R_f = 0.25). Dibenzo[*a,e*]cyclooctatetraene was obtained as a white solid



$C_{16}H_{12}$
204.27 g/mol
Appearance colorless solid
Yield 380 mg, 1.9 mmol (49%)

TLC	$R_f = 0.25$ (SiO ₂ , <i>n</i> -hexane)
¹H-NMR	(300 MHz, CDCl ₃): δ 7.17 (m, 4H, CH _{Ar}), 7.08 (m, 1H, CH _{Ar}), 6.77 (s, 1H CH _{alkene})

1-Phenyl-1-cyclopentene

Synthesis was performed by Schachtner, Josef, *Dissertation 2016*, Regensburg., following the procedure described by G. Hu, J. Xu, P. Li, *Org. Lett.* **2014**, *16*, 6036–6039.



	C ₁₁ H ₁₂ 144.22 g/mol
Appearance	colorless liquid
Yield	1.99 g, 13.8 mmol (69%)
TLC	$R_f = 0.66$ (SiO ₂ , hexanes)
¹H-NMR	(300 MHz, CDCl ₃) δ 7.48 – 7.42 (m, 2H), 7.36 – 7.27 (m, 2H), 7.25 – 7.18 (m, 1H), 6.19 (h, $J = 2.1$ Hz, 1H), 2.82 – 2.61 (m, 2H), 2.54 (tq, $J = 7.6, 2.5$ Hz, 2H), 2.15 – 1.93 (m, 2H).
¹³C-NMR	(75 MHz, CDCl ₃) δ 128.29, 128.27, 127.60, 126.82, 126.12, 125.91, 125.54, 66.45, 33.37, 33.18, 28.91, 28.08, 23.37, 19.35.
GC-MS	$t_R = 6.94$ min, (EI, 70 eV): $m/z = 144$ [M] ⁺ , 129, 115, 103, 91, 77, 63, 51.

Analytical data were in full agreement with W. Su, S. Urgaonkar, P. A. McLaughlin, J. G. Verkade, *J. Am. Chem. Soc.* **2004**, *126*, 16433–16439.

1-Phenyl-1-cycloheptene

Synthesis following a procedure by Schachtner, Josef, *Dissertation 2016*, Regensburg., following the procedure described by G. Hu, J. Xu, P. Li, *Org. Lett.* **2014**, *16*, 6036–6039.



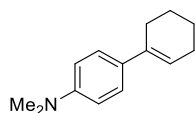
C ₁₃ H ₁₆ 172.27 g/mol

Appearance	colorless liquid
Yield	2.89 g, 16.8 mmol (84%)
TLC	$R_f = 0.69$ (SiO ₂ , hexanes)
¹H-NMR	(300 MHz, CDCl ₃) δ 7.42 – 7.16 (m, 5H), 6.13 (td, $J = 6.8, 1.3$ Hz, 1H), 2.75 – 2.52 (m, 2H), 2.43 – 2.25 (m, 2H), 1.94 – 1.80 (m, 2H), 1.74 – 1.50 (m, 4H).
¹³C-NMR	(75 MHz, CDCl ₃) δ 144.99, 130.45, 128.13, 126.26, 125.67, 32.86, 32.82, 28.92, 26.98, 26.85.
GC-MS	$t_R = 7.97$ min, (EI, 70 eV): $m/z = 172$ [M ⁺], 157, 144, 129, 115, 104, 91, 77, 63, 51.

Analytical data were in full agreement with G. Baddeley, J. Chadwick, H. T. Taylor, *J. Chem. Soc.* **1956**, 451.

4-(Cyclohex-1-enyl)-*N,N*-dimethylaniline

Synthesis was performed by Schachtner, Josef, *Dissertation* **2016**, Regensburg., following the procedure described by G. Hu, J. Xu, P. Li, *Org. Lett.* **2014**, *16*, 6036–6039.



C₁₄H₁₉N
201.31 g/mol

Appearance	colorless liquid
Yield	1.65 g, 8.20 mmol (82%)
TLC	$R_f = 0.82$ (SiO ₂ , hexanes)
¹H-NMR	(300 MHz, CDCl ₃) δ 7.41 – 7.19 (m, 2H), 6.76 (ddd, $J = 13.1, 6.8, 2.8$ Hz, 2H), 6.06 – 6.00 (m, 1H), 2.96 (d, $J = 2.8$ Hz, 6H), 2.35 – 2.49 (m, 2H), 2.27 – 2.14 (m, 2H), 1.87 – 1.73 (m, 2H), 1.61 – 1.72 (m, 2H).
¹³C-NMR	(75 MHz, CDCl ₃) δ 149.4, 136.0, 129.1, 125.6, 121.7, 116.7, 112.7, 112.6, 40.8, 40.7, 27.4, 25.9, 23.2, 22.4.
GC-MS	$t_R = 9.59$ min, (EI, 70 eV): $m/z = 202$ [M] ⁺ , 180, 157, 129, 101, 77, 51.

Analytical data were in full agreement with K. Ishiuka, H. Seike, T. Hatakeyama, M. Nakamura, *J. Am. Chem. Soc.* **2010**, *132*, 13117-13119.

(1-cyclopropylvinyl)benzene

Synthesis was performed by Gieshoff, Tim, *Dissertation 2017*, Regensburg.



C₁₁H₁₂

144.22 g/mol

Appearance

colorless liquid

Yield

1.27 g, 8.8 mmol (80%)

TLC

R_f = 0.53 (SiO₂, hexanes)

¹H-NMR

(300 MHz, CDCl₃) δ 7.67 – 7.57 (m, 2H), 7.42 – 7.26 (m, 3H), 5.30 (d, *J*=1.0, 1H), 4.95 (t, *J*=1.2, 1H), 1.67 (tt, *J*=8.3, 5.4, 1.2, 1H), 0.92 – 0.79 (m, 2H), 0.61 (ddd, *J*=6.4, 5.4, 4.1, 2H).

¹³C-NMR

(75 MHz, CDCl₃) δ 149.47, 141.75, 128.28, 127.58, 126.25, 109.15, 77.58, 77.16, 77.16, 76.74, 15.78, 6.83.

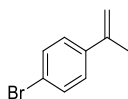
GC-MS

t_R = 6.31 min, (EI, 70 eV): *m/z* = 144 [M⁺], 129, 115, 103, 91, 77, 63, 51.

Analytical data were in full agreement with C. Chatalova-Sazepin, Q. Wang, G. M. Sammis, J. Zhu, *Angew. Chem. Int. Ed.* **2015**, *54*, 5443–5446.

4-Bromo- α -methylstyrene

Synthesis following a modified procedure by A. O. Terent'Ev, O. M. Mulina, D. A. Pirgach, D. V. Demchuk, M. A. Syroeshkin, G. I. Nikishin, *RSC Adv.* 2016, *6*, 93476.



C₉H₉Br

197.08 g/mol

Appearance

colorless oil

Yield

3.44 g, 17.5 mmol (83%)

TLC

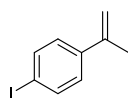
R_f = 0.67 (SiO₂, *n*-pentane)

¹H-NMR	(400 MHz, CDCl ₃) δ 7.50-7.40 (m, 2H), 7.36-7.28 (m, 2H), 5.39 – 5.32 (m, 1H), 5.14 – 5.07 (m, 1H), 2.13 (s, 3H).
¹³C-NMR	(101 MHz, CDCl ₃) δ 142.2, 140.1, 131.3, 127.2, 121.3, 113.1, 21.7.
GC-MS	<i>t</i> _R = 6.01 min, (EI, 70 eV): <i>m/z</i> = 197 [M ⁺], 183, 171, 156, 115, 102, 91, 75, 63, 51.

Analytical data were in full agreement with T. Taniguchi, A. Yajima, H. Ishibashi, *Adv. Synth. Catal.* **2011**, 353, 2643–2647.

4-Iodo- α -methylstyrene

Synthesis was performed by T. N. Gieshoff, U. Chakraborty, M. Villa, A. Jacobi von Wangelin, *Angew. Chem. Int. Ed.* **2017**, 56, 3585.

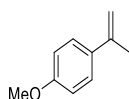


	C ₉ H ₉ I
	244.08 g/mol
Appearance	colorless solid
Yield	1.21 g, 4.96 mmol (71%)
TLC	<i>R</i> _f = 0.84 (SiO ₂ , <i>n</i> -pentane)
¹H-NMR	(300 MHz, CDCl ₃) δ 7.70 – 7.59 (m, 2H), 7.24 – 7.15 (m, 2H), 5.40 – 5.33 (m, 1H), 5.12 – 5.07 (m, 1H), 2.14 – 2.09 (m, 3H).
¹³C-NMR	(75 MHz, CDCl ₃) δ 142.28, 140.70, 137.27, 134.97, 127.41, 113.15, 92.88, 21.62.
GC-MS	<i>t</i> _R = 7.14 min, (EI, 70 eV): <i>m/z</i> = 244 [M ⁺], 127, 115, 102, 91, 75, 63, 50.

Analytical data were in full agreement with G. B. Bachman, C. L. Carlson, M. Robinson, *J. Am. Chem. Soc.* **1951**, 73, 1964–1965.

4-Methoxy- α -methylstyrene

Synthesis following a modified procedure by A. O. Terent'Ev, O. M. Mulina, D. A. Pirgach, D. V. Demchuk, M. A. Syroeshkin, G. I. Nikishin, *RSC Adv.* **2016**, 6, 93476.



C₁₀H₁₂O

148.20 g/mol

Appearance

colorless liquid

Yield

3.91 g, 26.4 mmol (88 %)

TLC

R_f = 0.27 (SiO₂, *n*-pentane)

¹H-NMR

(300 MHz, CDCl₃) δ 7.42 (m, 2H), 6.87 (m, 2H), 5.29 (m, 1H), 5.00 (m, 1H), 3.81 (s, 3H), 2.14 (s, 3H).

¹³C-NMR

(75 MHz, CDCl₃) δ 159.0, 142.5, 133.7, 126.6, 113.5, 110.7, 55.3, 21.9.

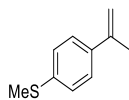
GC-MS

t_R = 6.48 min, (EI, 70 eV): *m/z* = 148 [M⁺], 127, 133, 115, 105, 89, 77, 63, 51.

Analytical data were in full agreement with A. Fryszkowska, K. Fisher, J. M. Gardiner, G. M. Stephens, *J. Org. Chem.* **2008**, 73, 4295-4298.

Methyl(4-(prop-1-en-2-yl)phenyl)sulfane

Synthesis was performed by T. N. Gieshoff, U. Chakraborty, M. Villa, A. Jacobi von Wangelin, *Angew. Chem. Int. Ed.* **2017**, 56, 3585.



C₁₀H₁₂S

164.27 g/mol

Appearance

colorless solid

Yield

1.09 g, 6.63 mmol (33%)

TLC

R_f = 0.44 (SiO₂, *n*-pentane)

¹H-NMR

(300 MHz, CDCl₃) δ 7.45 – 7.35 (m, 2H), 7.25 – 7.18 (m, 2H), 5.36 (dq, *J*=1.6, 0.8, 1H), 5.06 (dq, *J*=1.5, 1.5, 1H), 2.49 (s, 3H), 2.14 (dd, *J*=1.5, 0.8, 3H).

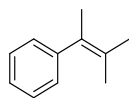
¹³C-NMR (75 MHz, CDCl₃) δ 142.51, 138.01, 137.49, 126.37, 125.90, 111.96, 21.75, 15.91.

GC-MS t_R = 7.38 min, (EI, 70 eV): m/z = 164 [M⁺], 149, 134, 115, 102, 91, 77, 69, 51.

Analytical data were in full agreement with G. Fraenkel, J. M. Geckle, *J. Am. Chem. Soc.* **1980**, *102*, 2869–2880.

(3-methylbut-2-en-2-yl)benzene

Synthesis was performed by Gieshoff, Tim, *Dissertation 2017*, Regensburg, following the procedure by W. Adam, M. A. Arnold, M. Grüne, W. M. Nau, U. Pischel, C. R. Saha-Möller, *Organic Letters* **2002**, *4*, 537-540.



C₁₁H₁₄

146.23 g/mol

Appearance colorless liquid

Yield 850 mg, 5.8 mmol (39%)

¹H-NMR (300 MHz, CDCl₃) δ 7.36 – 7.13 (m, 5H), 1.99 (s, 3H), 1.84 (s, 3H), 1.62 (s, 3H).

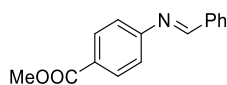
¹³C-NMR (75 MHz, CDCl₃) δ 145.35, 130.00, 128.44, 127.94, 127.23, 125.73, 22.11, 20.85, 20.59.

GC-MS t_R = 5.62 min, (EI, 70 eV): m/z = 146 [M⁺], 131, 115, 103, 91, 77, 65, 51.

Analytical data were in full agreement with W. Adam, M. A. Arnold, M. Grüne, W. M. Nau, U. Pischel, C. R. Saha-Möller, *Org. Lett.* **2002**, *4*, 537-540.

Methyl (E)-4-(benzylideneamino)benzoate

Synthesis was performed by Gärtner, Dominik, *Dissertation 2016*, Regensburg, following the procedure by K. Taguchi, F. H. Westheimer, *J. Org. Chem.* **1971**, *36*, 1570-1572.



C₁₁H₁₄

146.23 g/mol

Appearance colorless liquid

Yield 850 mg, 5.8 mmol (39%)

4 Cobalt-Catalyzed Hydrogenations via Olefin Cobaltate and Hydride Intermediates

¹H-NMR	(300 MHz, CDCl ₃) δ 7.36 – 7.13 (m, 5H), 1.99 (s, 3H), 1.84 (s, 3H), 1.62 (s, 3H).
¹³C-NMR	(75 MHz, CDCl ₃) δ 145.35, 130.00, 128.44, 127.94, 127.23, 125.73, 22.11, 20.85, 20.59.
GC-MS	<i>t_R</i> = 5.62 min, (EI, 70 eV): <i>m/z</i> = 146 [M ⁺], 131, 115, 103, 91, 77, 65, 51.

Analytical data were in full agreement with W. Adam, M. A. Arnold, M. Grüne, W. M. Nau, U. Pischel, C. R. Saha-Möller, *Org. Lett.* **2002**, *4*, 537-540.

4.5.5 General procedures

General method for catalytic hydrogenation: Olefin-stabilized BIAN Cobalt catalysts (Procedure A)

In an argon-filled glovebox, a flame-dried 4 mL reaction vial was charged with DippBIANCoBr_2 (0.006 mmol), the substrate (0.2 mmol), THF (2 mL) and *n*-pentadecane as internal reference for GC-FID quantification (0.2 mmol). The pale brown solution was reduced by dropwise addition of LiBEt_3H (0.018 mmol, 1 M, THF) with a Hamilton® syringe during which the color changed to red or brown depending on the substrate. After 10 minutes stirring, the reaction vial was transferred to a high-pressure reactor which was sealed and removed from the glovebox. The reactor was purged with H_2 (3 × 3 bar) and the reaction pressure and temperature were set. After the indicated reaction time, the vial was retrieved and hydrolyzed with a saturated aqueous solution of NH_4Cl (1 mL). The reaction mixture was extracted with ethyl acetate (3 × 1 mL), dried over sodium sulfate and analyzed by GC-FID and GC-MS.

General method for catalytic hydrogenation: Reduced Cobalt catalysts in absence of substrate (Procedure B)

In an argon-filled glovebox a flame-dried 4 mL reaction vial was charged with DippBIANCoBr_2 (0.006 mmol), THF (1 mL) and *n*-pentadecane as internal reference for GC-FID quantification (0.2 mmol). The resulting pale brown solution was reduced by dropwise addition of LiBEt_3H (0.018 mmol, 1 M, THF) with a Hamilton® syringe during which the color changed to brown. After 10 minutes stirring, the substrate was added and the reaction vial was transferred to a high-pressure reactor which was sealed and removed from the glovebox. See protocol A for hydrogenation and work-up.

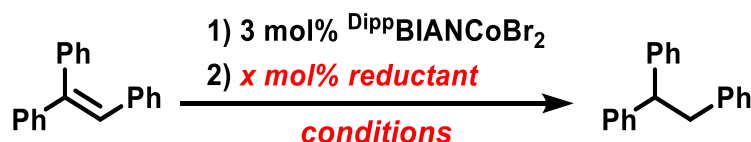
General method for kinetic examination in catalytic hydrogenation and poisoning experiments (Procedure B)

A flame-dried 10 mL two-necked flask was connected to a *Man on the Moon X201* gas-uptake system with a reservoir pressure of 9 bar H₂ and a constant reaction pressure of 1.9 bar H₂. After purging with H₂, the freshly prepared catalyst solution (reduction of ^{Dipp}BIANCoBr₂ (0.006 mmol) with LiBEt₃H (0.018 mmol)) was transferred with a syringe. The hydrogen uptake started with the addition of α -methylstyrene (0.2 mmol). After two minutes, the poisoning agent (for dct and trimethylphosphite) was added by Hamilton syringe. In the case of mercury, the reduced precatalyst was stirred over mercury for two, respectively 30 minutes before addition of the substrate. After the reaction, the mixture was treated with a saturated aqueous solution of NH₄Cl and ethyl acetate. The organic phase was separated and filtered over a plug of silica and analyzed by quantitative GC-FID analysis vs. internal standard (*n*-pentadecane). The monitored hydrogen consumption was related to the yield of cumene, which was determined by GC-FID. An induction period may be not detectable since the addition by syringe through the septum creates a temporary leakage.

4.5.6 Optimization studies and catalytic application of complexes

Optimization studies

Table 4.5.13. Additional optimization experiments and counterion effect of procedure A.

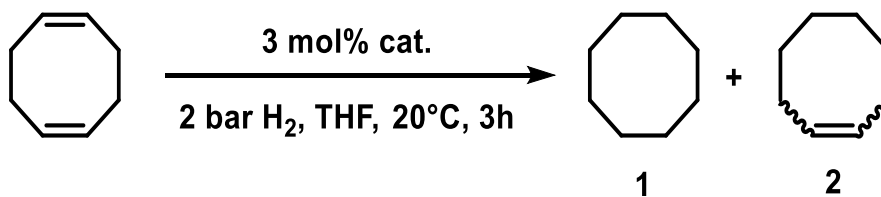


Entry	Reductant (mol%)	Conditions	Yield [%]
1	HBpin (9)	20 bar H ₂ , 60°C, 24 h	0 (12)
2	DiBAIH (9)	As entry 1	50 (57)
3	NaBEt ₃ H (9)	As entry 1	>99
4	LiBEt ₃ H (9)	As entry 1	>99
5	LiAlH ₄ (6)	2 bar H ₂ , 20°C, 3 h	0 (11)
6	HBpin (9) + KO ^t Bu (9)	As entry 5	<5 (12)
7	K-Selectride (6)	As entry 5	<5 (14)
8	N-Selectride (6)	As entry 5	<5 (14)
9	N-Selectride (9)	As entry 5	8 (15)
10	Li-Selectride (6)	As entry 5	6 (20)
11	Li-Selectride (9)	As entry 5	37 (43)
12	NaBEt ₃ H (6)	As entry 5	23 (33)
13	NaBEt ₃ H (9)	As entry 5	64 (65)
14	LiBEt ₃ H (6)	As entry 5	73 (75)
15	LiBEt ₃ H (9)	As entry 5	92
16	LiBEt ₃ H (12)	As entry 5	78 (78)

Conditions: 0.2 mmol (0.1 M) alkene in THF, 3 mol% DippBIANCoBr₂.

Yields were determined by quantitative GC-FID vs. internal *n*-pentadecane. Conversions are given in parentheses if <90%;

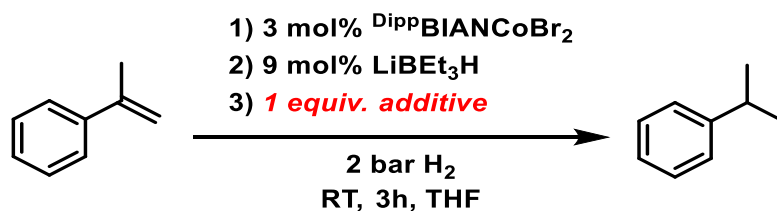
Reduction in presence of the substrate (protocol A);

Table 4.5.14. Catalytic studies with BIAN Co model complexes.

Entry	cat.	1^a	2^a
1 ^b	(^{Dipp} BIAN)CoBr ₂ + 9 mol% LiBEt ₃ H	96 %	1 %
2	[Li(thf) _{3.5} { ^{Dipp} BIAN}Co(cod)] 1	5 %	61 %
3	1 + 3.5 mol% 12crown4	4 %	44 %
4	1 + 3 mol% [Fc]PF ₆	2 %	17 %
5	1 + 9 mol% BEt ₃	66 %	33 %
6	1 + 9 mol% BEt ₃ + 30 mol% LiBr	46 %	53 %
7	[K(thf){(^{Dipp} BIAN)Co(cod)}] 2	-	1 %
8	2 + 3 mol% [Fc]PF ₆	1 %	-
9	2 + 30 mol% LiCl	1 %	3 %
10	2 + 30 mol% LiBr	2 %	4 %
11	2 + 30 mol% LiBr + [2.2.2]Cryptand	-	2 %
12	2 + 30 mol% LiCl + 3 mol% 18-crown-6	-	1 %
13	2 + 9 mol% BEt ₃	1 %	1 %
14	2 + 9 mol% BEt ₃ + 30 mol% LiBr	3 %	38 %
15 ^b	[Li(thf) ₃ (Et ₂ O){(^{Dipp} BIAN)Co} ₂ (μ-H) ₃] 4a	6 %	7 %
16 ^b	4a + 3 mol% Et ₃ B	22 %	22 %
17 ^b	4a + 1.5 mol% LiEt ₃ BH	57 %	43 %
18	[(^{Dipp} BIAN)Co(η ⁶ -C ₆ H ₆)] 3	-	-
19 ^c	3 + 9 mol% LiBEt ₃ H	4 %	29 %

Conditions: 0.2 mmol alkene, 0.1 M in THF, 3 mol% cat., 2 bar H₂. ^a Yields determined by quantitative GC-FID vs. internal *n*-pentadecane; ^b 1.5 mol% **4a**; ^c Reduction in presence of the substrate.

External functional group tolerance (procedure A)

Table 4.5.15. External functional group tolerance (procedure A).

Entry	Additive	Cumene yield [%]	Cumene yield [%] after 24 h, 10 bar
1	PhCN	<5 (7)	<5 (<5)
2	PhC(O)H	<5 (<5)	<5 (<5)
3	PhC(O)Ph	16 (18)	69 (69)
4	4-Tol-CH ₂ OH	6 (9)	9 (9)
5	PhNO ₂	5 (<5)	
6	PhNH ₂	>99	>99

Conditions: 0.2 mmol (0.1 M) alkene in THF, 0.2 mmol additive, 3 mol% DippBIANCoBr_2 , 9 mol% LiEt_3H , 2 bar H_2 , 20 °C. Yields were determined by quantitative GC-FID vs. internal *n*-pentadecane. Conversions are given in parentheses if <90%; Substrate addition prior to reduction (procedure A).

Isomerization

Table 4.5.16. Isomerization of 1-octene.

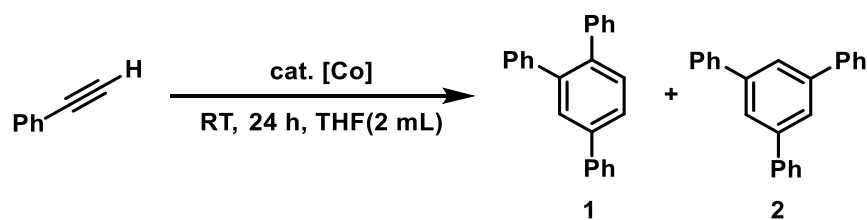


Entry	Procedure	Octene yield [%]				
		1	(E)-2	(E)-3	(E)-4	others
1	A	3	71	22	4	0
2	B	31	39	8	1	20

Conditions: 0.2 mmol (0.1 M) alkene in THF, 3 mol% ^{Dipp}BIANCoBr₂. Yields were determined by rel. peak areas of GC-FID. Reduction in presence of the substrate (procedure A); Substrate addition after reduction (procedure B).

Isomerization reactions were performed according to the general procedures in absence of a H₂ atmosphere.

Cyclotrimerization

Table 4.5.17. Cyclotrimerization of Phenylacetylene.

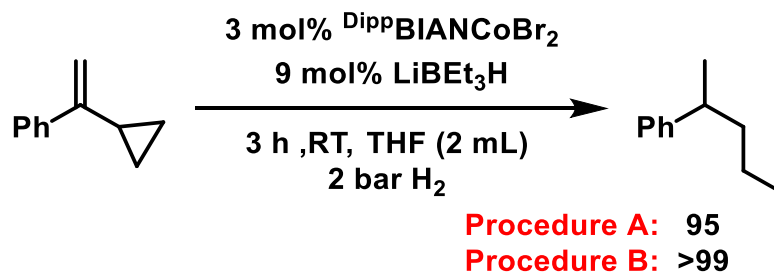
Entry	Procedure	Yield [%]		Conversion [%]
		1	2	
1	A	20	9	38
2	B	26	14	54

Conditions: 0.2 mmol (0.1 M) alkene in THF, 3 mol% DippBIANCoBr_2 . Yields were determined by rel. peak areas of GC-FID. Reduction in presence of the substrate (procedure A); Substrate addition after reduction (procedure B).

Cyclotrimerization reactions were performed according to the general procedures in absence of a H_2 atmosphere.

4.5.7 Mechanistic studies (ring-opening experiment, reaction of cobalt, *in-situ* $^1\text{H-NMR}$, LIFDI-MS)

Ring opening experiment with (1-Cyclopropylethyl)benzene



Scheme 4.5.10. Ring opening experiment with (1-cyclopropylethyl)benzene. Yields were determined by quantitative GC-FID vs. internal n-pentadecane.

The hydrogenation reaction was performed according to general procedures.

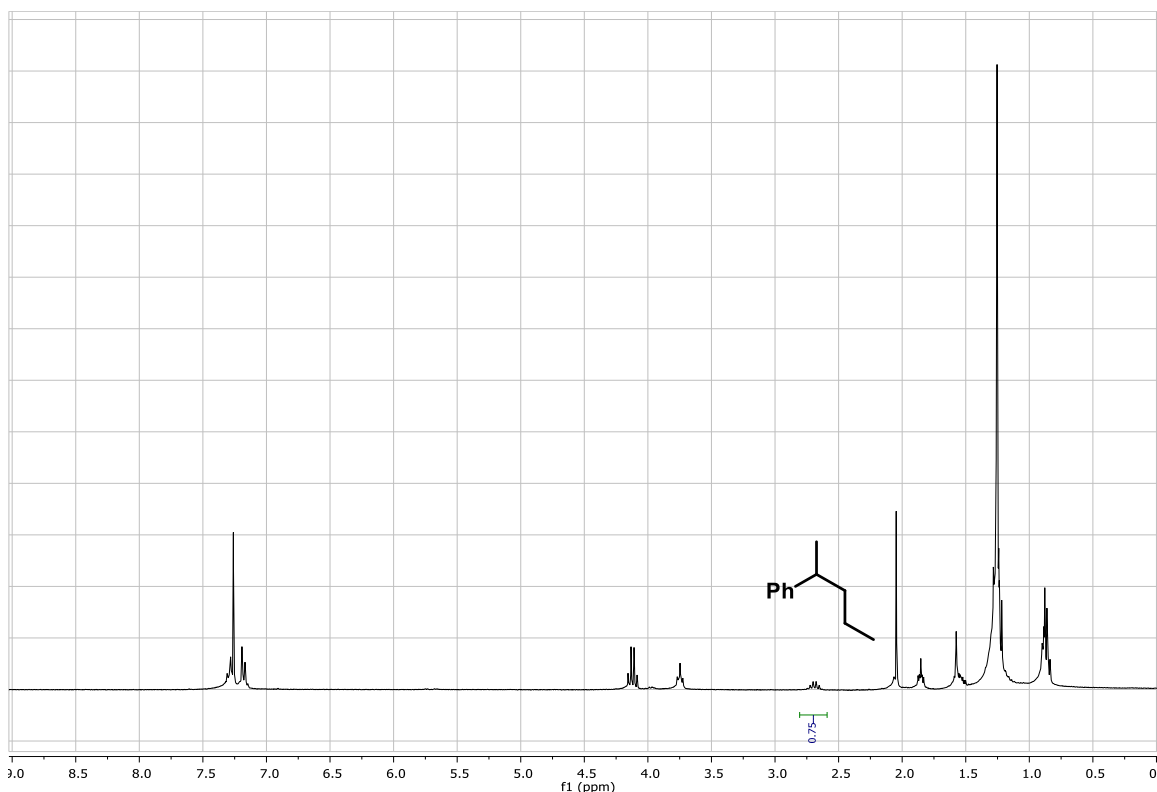


Figure 4.5.36. $^1\text{H-NMR}$ of the hydrogenation reaction of (1-cyclopropylethyl)benzene after work-up (Procedure A).

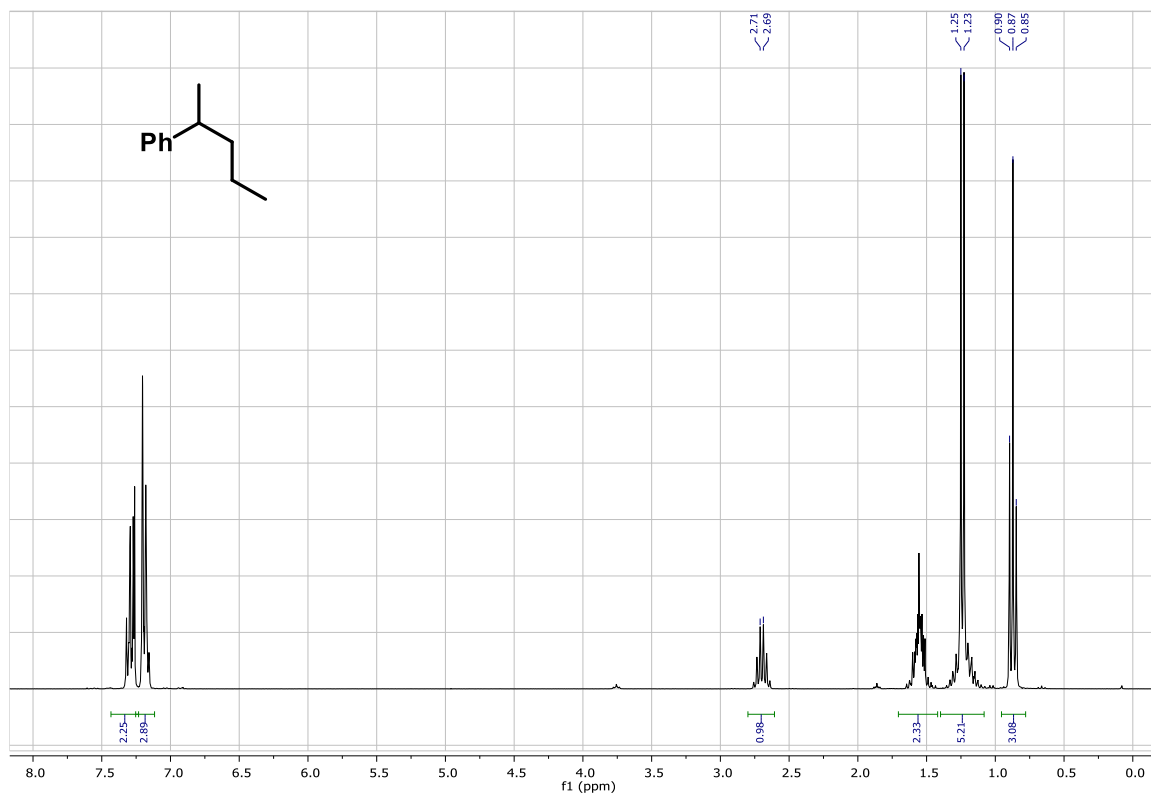


Figure 4.5.37. $^1\text{H-NMR}$ of 2-pentylbenzene.

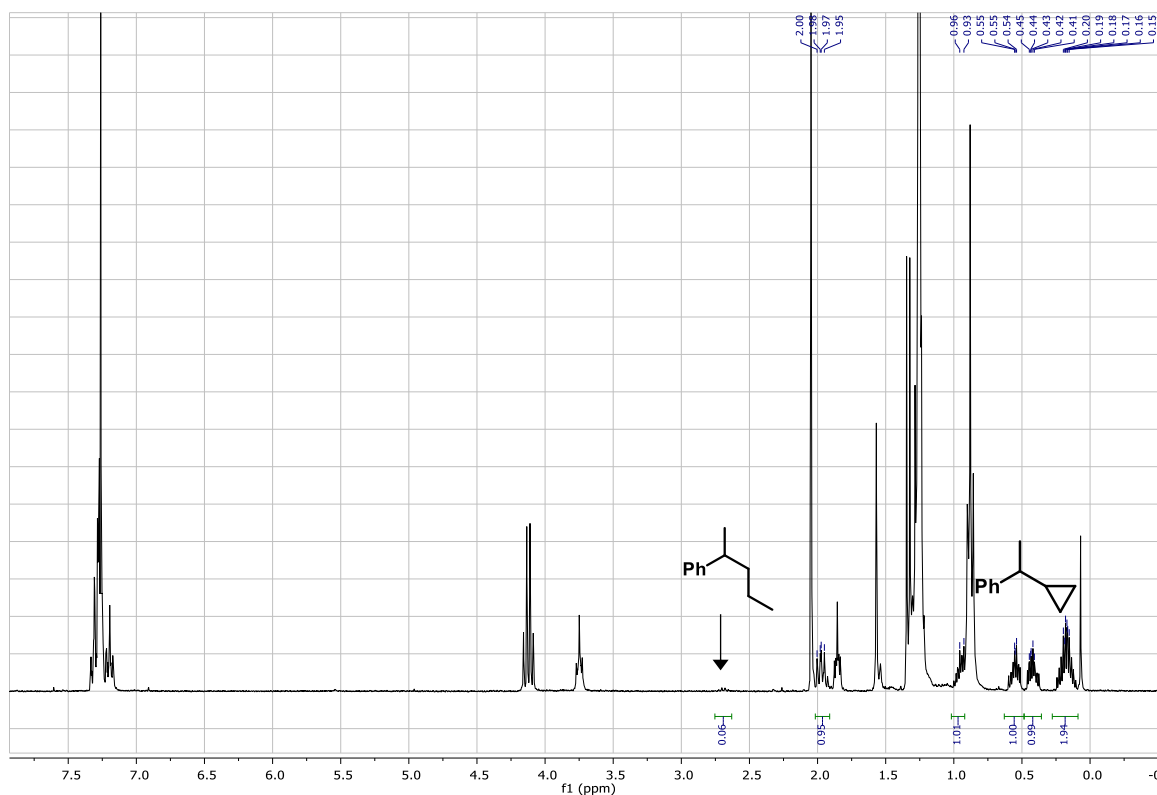
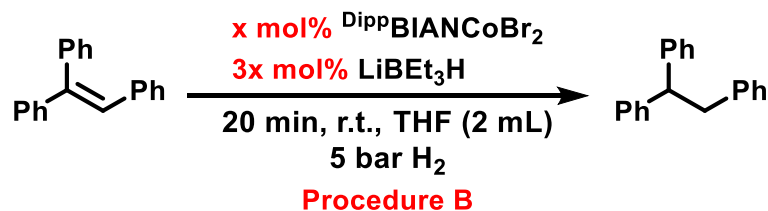


Figure 4.5.38. $^1\text{H-NMR}$ of the hydrogenation reaction of (1-cyclopropylethyl)benzene with a catalyst possessing traces of ring-opening product.

Reaction order of cobalt in the catalytic hydrogenation

For the determination of the reaction order in cobalt, varying catalyst loadings have been tested in the catalytic hydrogenation in a parallel setup (autoclave).



Scheme 4.5.11. Method of initial rates for determination of the reaction order of cobalt. Yields were determined by quantitative GC-FID vs. internal n-pentadecane.

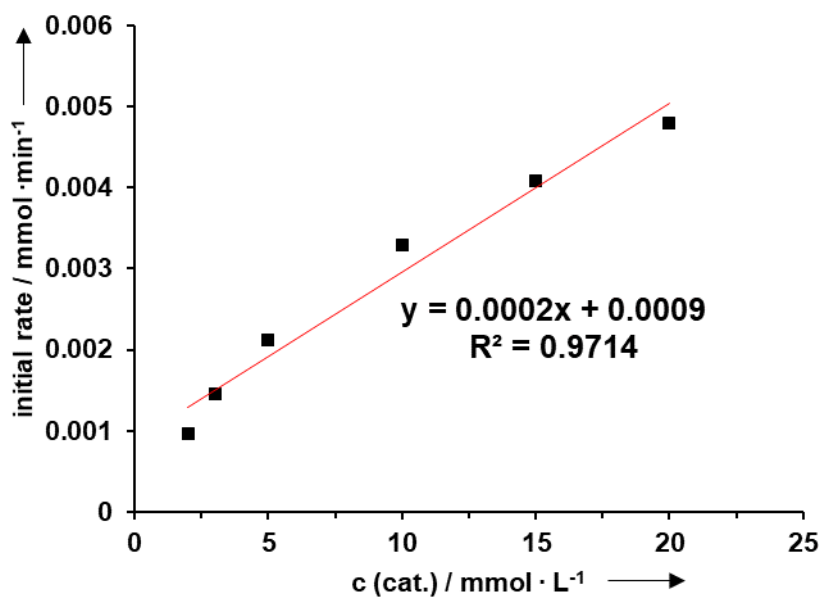


Figure 4.5.39. Method of initial rates for determination of the reaction order of cobalt.

$^1\text{H-NMR}$ of $\text{DippBIANCoBr}_2 + 3 \text{LiEt}_3\text{H}$ in THF.

In an argon-filled glovebox, a 4 mL reaction vial was charged with DippBIANCoBr_2 (0.025 mmol) and THF- d^8 (1 mL). The resulting pale brown solution was reduced by dropwise addition of LiEt_3H (0.075 mmol, 1 M, THF) with a Hamilton® syringe during which the color changed to brown. After 10 minutes stirring, the mixture was filled in a screw capped NMR tube and the $^1\text{H-NMR}$ was measured subsequently. The presence of high-field-shifted signals indicates related hydride species as observed for the synthesis of **4** (*vide supra*). Further analysis was hampered by the presence of paramagnetic species.

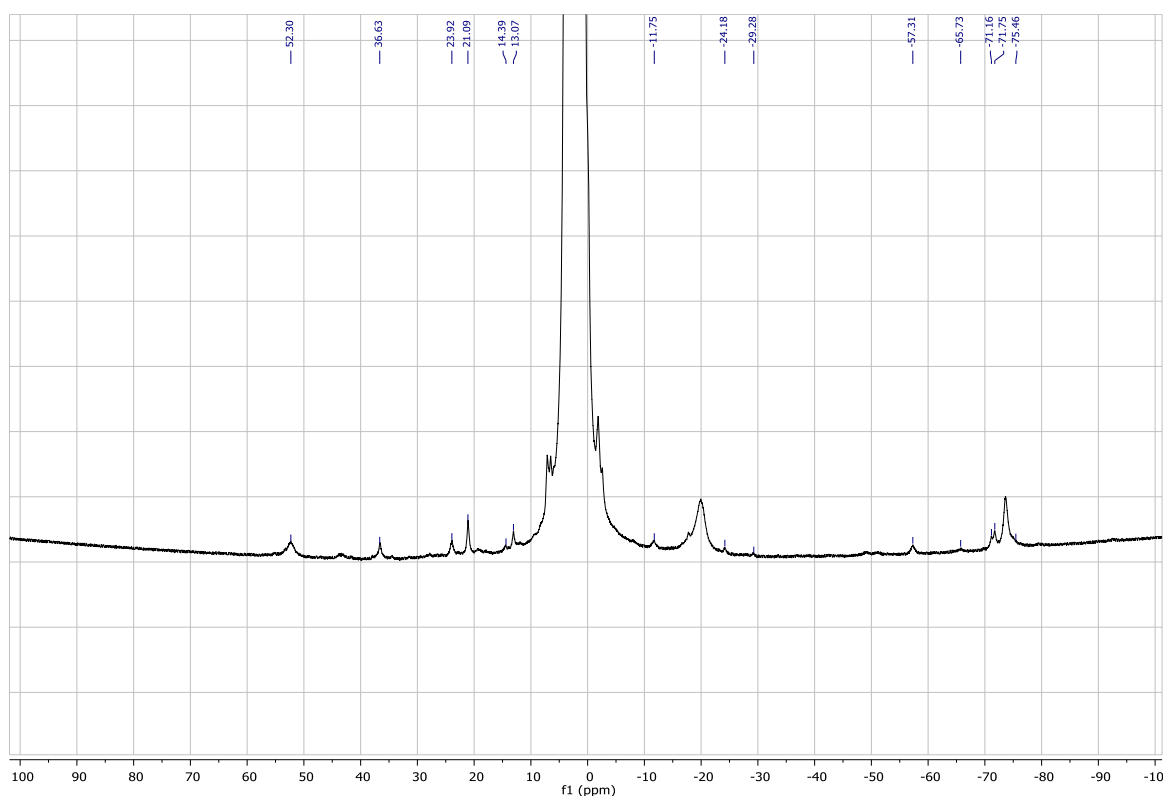


Figure 4.5.40. $^1\text{H-NMR}$ of $\text{DippBIANCoBr}_2 + 3 \text{LiEt}_3\text{H}$ in THF.

LIFDI-MS of ^{Dipp}BIANCoBr₂ + 3 LiBEt₃H in THF.

In an argon-filled glovebox, a 4 mL reaction vial was charged with ^{Dipp}BIANCoBr₂ (0.1 mmol) and THF (1 mL). The resulting pale brown solution was reduced by dropwise addition of LiBEt₃H (0.3 mmol, 1 M, THF) with a Hamilton® syringe during which the color changed to brown. After 10 minutes stirring, the vial was closed with a septum und removed from the glovebox. The LIFDI-MS was subsequently measured by injection through a cannula in quasi-inert conditions (vacuum).

Table 4.5.18. LIFDI of ^{Dipp}BIANCoBr₂ + 3 LiBEt₃H in THF.

$$[\text{DippBIANCoBr}_2] + 3 \text{LiBEt}_3\text{H (1M, THF)} \xrightarrow{\text{THF}}$$

Entry	Mass found	Mass calc.	Formula
2	507.3477		LLi
3	1059.6067	1059.571	L2Co
4	1118.5419	1118.5042	L2Co2

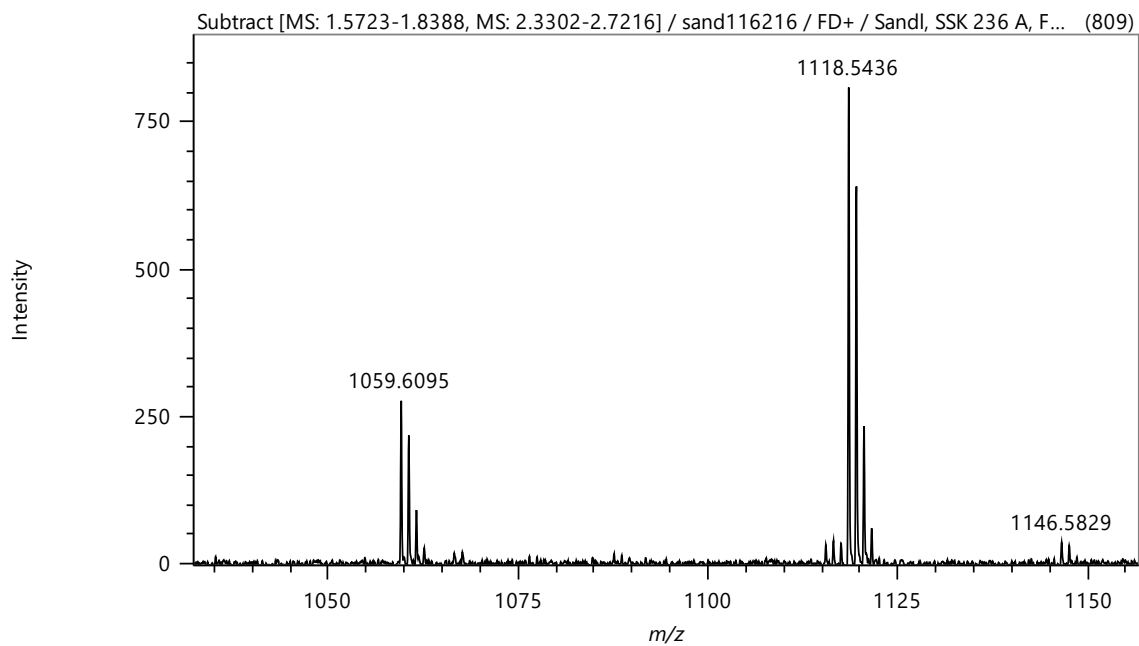


Figure 4.5.41. LIFDI-MS of $\text{DippBIANCoBr}_2 + 3 \text{LiBEt}_3\text{H}$ in THF; Zoom.

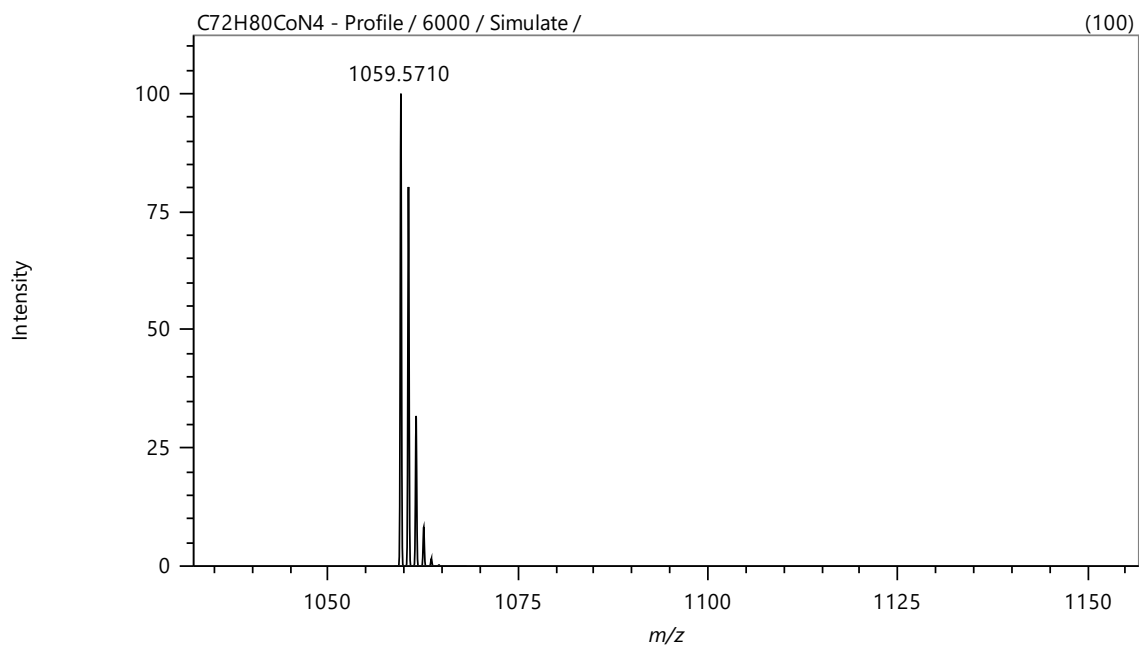


Figure 4.5.42. MS simulation of $\text{C}_{72}\text{H}_{80}\text{CoN}_4$.

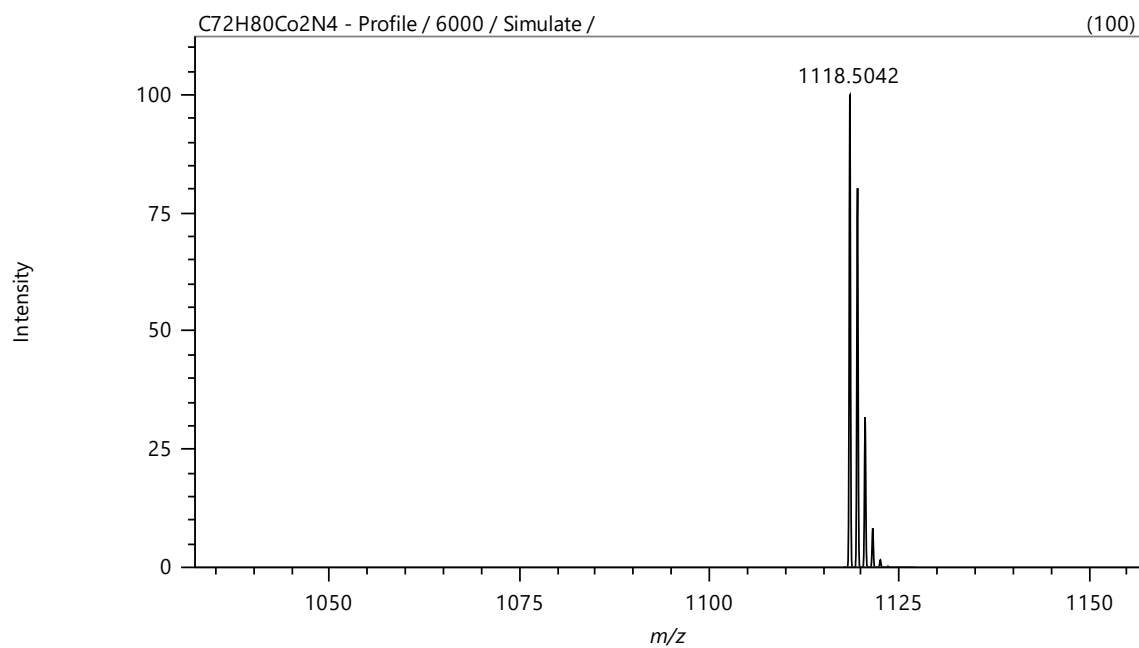


Figure 4.5.43. MS simulation of C₇₂H₈₀Co₂N₄.

4.5.8 Kinetics & poisoning studies

Reaction progress analyses: Procedure A vs. Procedure B

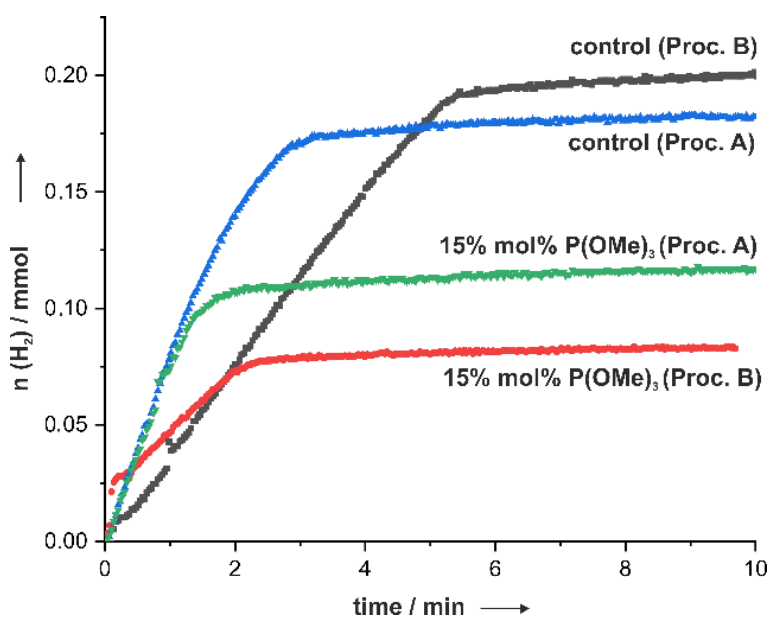


Figure 4.5.44. Reaction progress analyses: Procedure A vs. Procedure B. Cumene yields determined by hydrogen consumption related to final quantitative GC-FID vs. n-pentadecane.

After a reaction time of 5, minutes a turnover frequency (TOF) of 370 h^{-1} at a catalyst loading of 3 mol% was measured (procedure B). For procedure A, a TOF of 780 h^{-1} after a reaction time of 2 minutes at a catalyst loading of 3 mol% was measured.

Mercury (Hg)

As described in the general information, mercury (0.27 mL, 3000 equiv.) was added to the freshly prepared catalyst solution. The reaction mixture was stirred for two, respectively 30 minutes before addition of α -methylstyrene. In both cases steady conversion was observed.

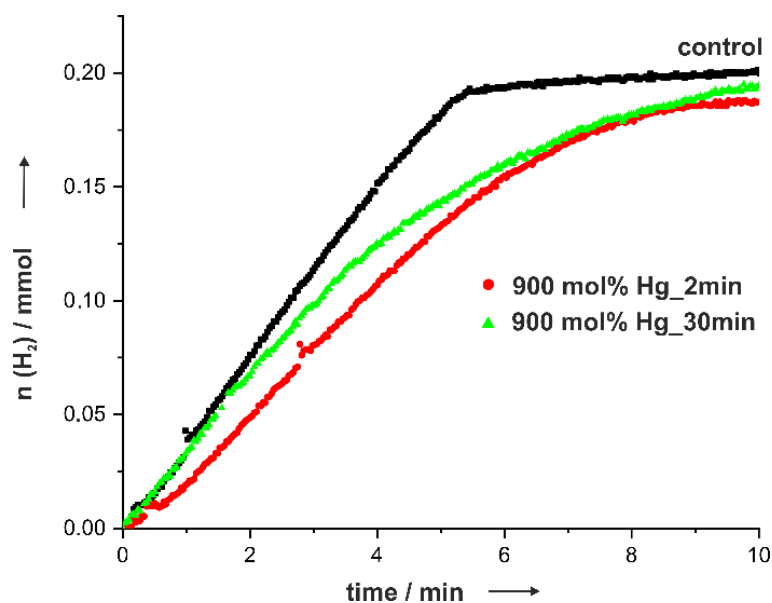


Figure 4.5.45. Poisoning studies with mercury. Cumene yields determined by hydrogen consumption related to final quantitative GC-FID vs. *n*-pentadecane.

Trimethylphosphite ($\text{P}(\text{OMe})_3$)

A defined volume of a standardized solution of trimethylphosphite in THF was added to the freshly prepared catalyst solution with a Hamilton syringe two minutes after addition to the substrate.

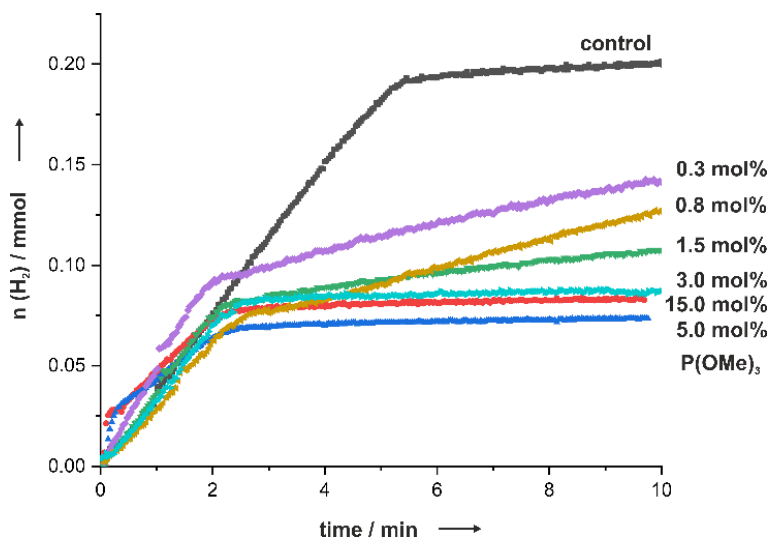


Figure 4.5.46. Poisoning studies with trimethylphosphite. Cumene yields determined by hydrogen consumption related to final quantitative GC-FID vs. *n*-pentadecane.

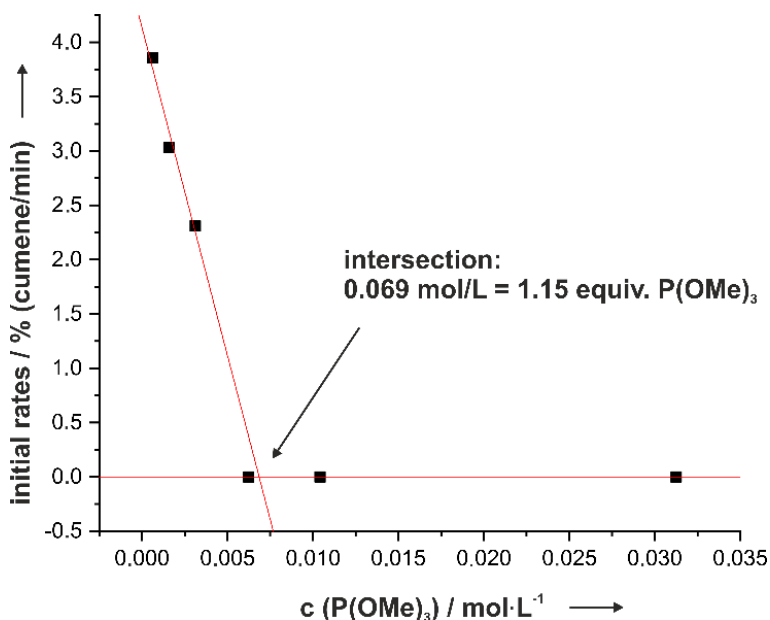


Figure 4.5.47. Poisoning studies with trimethylphosphite. Method of initial rates.

The initial rates of $\text{P}(\text{OMe})_3$ poisoning reactions were determined as linear plot of the first two minutes after addition of trimethylphosphite.

Dibenzo[*a,e*]cyclooctatetraene (dct)

A defined volume of a standardized solution of dct in THF was added to the freshly prepared catalyst solution with a Hamilton syringe two minutes after addition to the substrate.

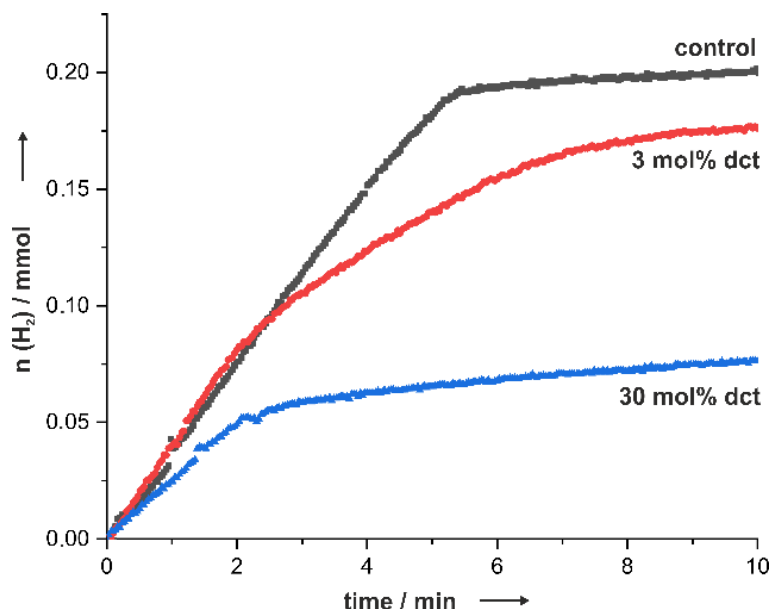
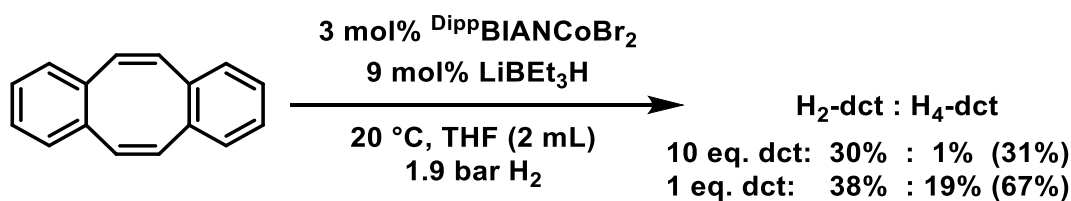
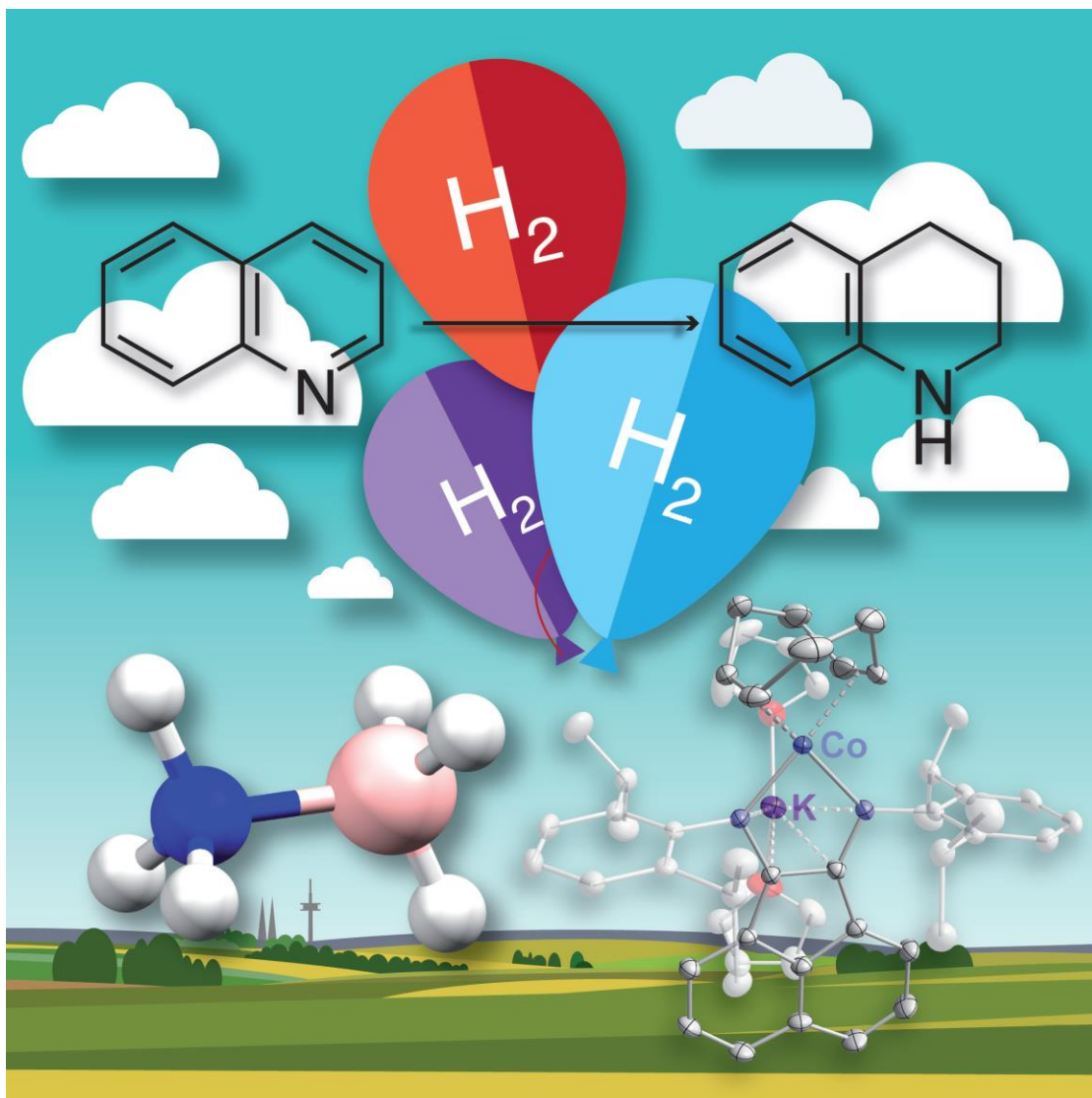


Figure 4.5.48. Poisoning studies with dibenzo[*a,e*]cyclooctatetraene (dct). Cumene yields determined by hydrogen consumption related to final quantitative GC-FID vs. *n*-pentadecane.



Scheme 4.5.12. Poisoning studies with dibenzo[*a,e*]cyclooctatetraene (dct). dct yields were determined by rel. peak areas of GC-FID; Conversion in parentheses.

5 Amine-Borane Dehydrogenation and Transfer Hydrogenation Catalyzed by α -Diimine Cobaltates^V



^V Reproduced with permission from: T. M. Maier, S. Sandl, I. G. Shenderovich, A. Jacobi von Wangelin, J. J. Weigand, R. Wolf, *Chem. Eur. J.* **2019**, *25*, 2 and 238–245. Copyright 2019 Wiley-VCH, Weinheim, schemes, figures and text may differ from published version.

Author contribution:

S. Sandl: Development of catalytic hydrogenation reaction conditions (Table 5.1); substrate scope for autoclave reactions (Figure 5.11).

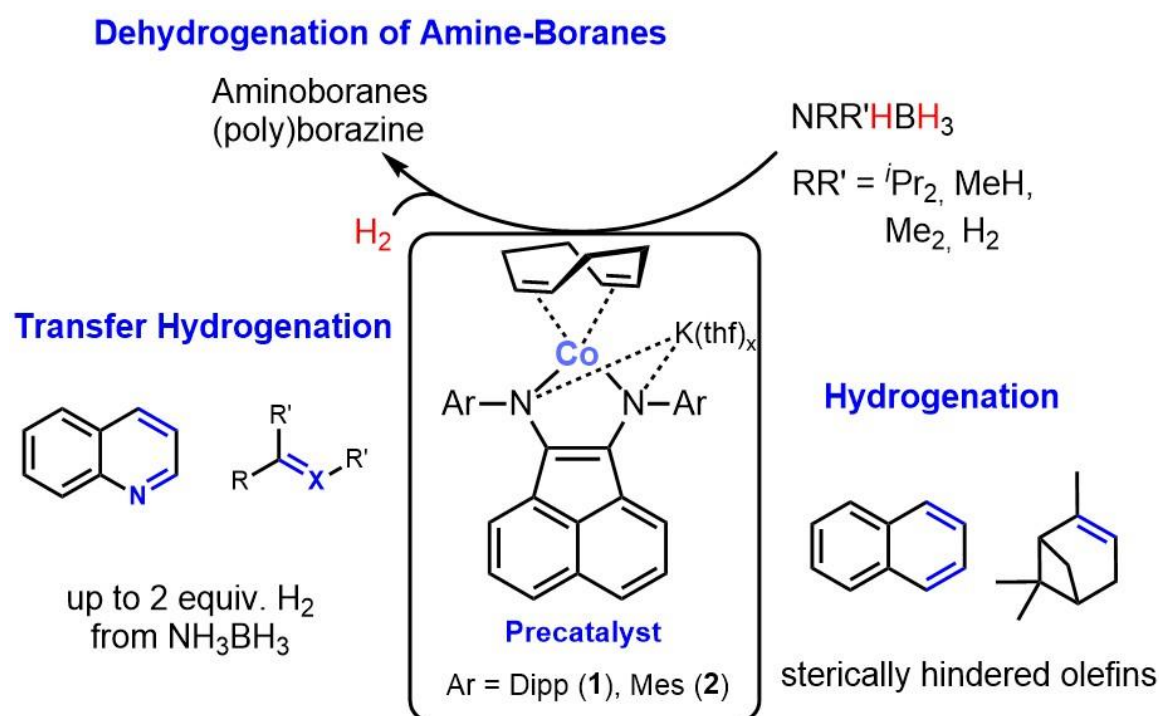
T. Maier: Synthesis of **1**; amine-borane dehydrogenations: substrate scope and mechanism (Figure 5.2 – 5.7); catalytic transfer hydrogenation: substrate scope and mechanism (Figure 5.8 – 5.10); manuscript preparation.

I. G. Shenderovich: ¹¹B-MAS NMR analyses (Figure 5.4).

J. J. Weigand: Assistance with ¹¹B NMR in solution.

R. Wolf: Corresponding author.

Abstract: Anionic α -diimine cobalt complexes such as $[\text{K}(\text{thf})_{1.5}\{(\text{Dipp})\text{BIAN}\}\text{Co}(\eta^4\text{-cod})]$ (**1**, cod = 1,5-cyclooctadiene) catalyze the dehydrogenation of several amine-boranes. Based on the excellent catalytic properties, an especially effective transfer hydrogenation protocol for challenging olefins, imines, and N-heteroarenes has been developed. NH_3BH_3 was used as dihydrogen surrogate, which transferred up to two equiv. H_2 per NH_3BH_3 . Detailed spectroscopic and mechanistic studies are presented, which document the rate determination by acidic protons in the amine-borane.



Mechanistic Studies: Kinetic and Poisoning Studies,
Deuterium Experiments, Characterization of Dehydrogenation
Products

5.1 Introduction

Transition metal-catalyzed dehydrogenations of amine-boranes have attracted great attention as a potentially versatile method of hydrogen storage and B-N materials synthesis.^{[1]–[3]} Amine-boranes can serve as solid hydrogen surrogates in transfer hydrogenations.^[4] Various dehydrogenation and transfer hydrogenation protocols have been developed with precious metal catalysts, and the underlying mechanisms have been thoroughly studied.^[5] By contrast, dehydrogenations are far less advanced with the abundant and cheaper late 3d metals, despite the recent progress with Ti, Mn, Fe, Co, and Ni catalysts.^{[7]–[12]} While a number of iron catalysts for amine-borane dehydrogenations have been studied recently,^[8] effective cobalt catalysts are scarce.^{[9]–[11]} To our knowledge, only three well-defined molecular cobalt catalysts have been reported to date (Figure 5.1). *Peters* and co-workers reported bis(phosphino)boryl (PBP) cobalt catalysts (Figure 5.1) for the dehydrogenation of dimethylamine-borane (DMAB)^[9] and applications to the transfer hydrogenation of styrene. *Waterman* and co-workers reported that the cyclopentadienylcobalt complexes $\text{Cp}^{\text{R}}\text{Co}(\text{CO})_2\text{I}$ (R= H, Me, Figure 5.1) catalyze ammonia borane (AB) dehydrogenation at elevated temperatures (65°C).^[10] The authors performed catalytic transfer hydrogenations with styrenes, alkynes, and olefins with an excess (8 equiv.) of AB at 65°C within 6 h. Tripodal polyphosphine cobalt(I) hydrides (Figure 5.1) recently reported by *Shubina* and co-workers exhibited similar activity in the AB-dehydrogenation.^[11] A mechanism was proposed based on DFT calculations.

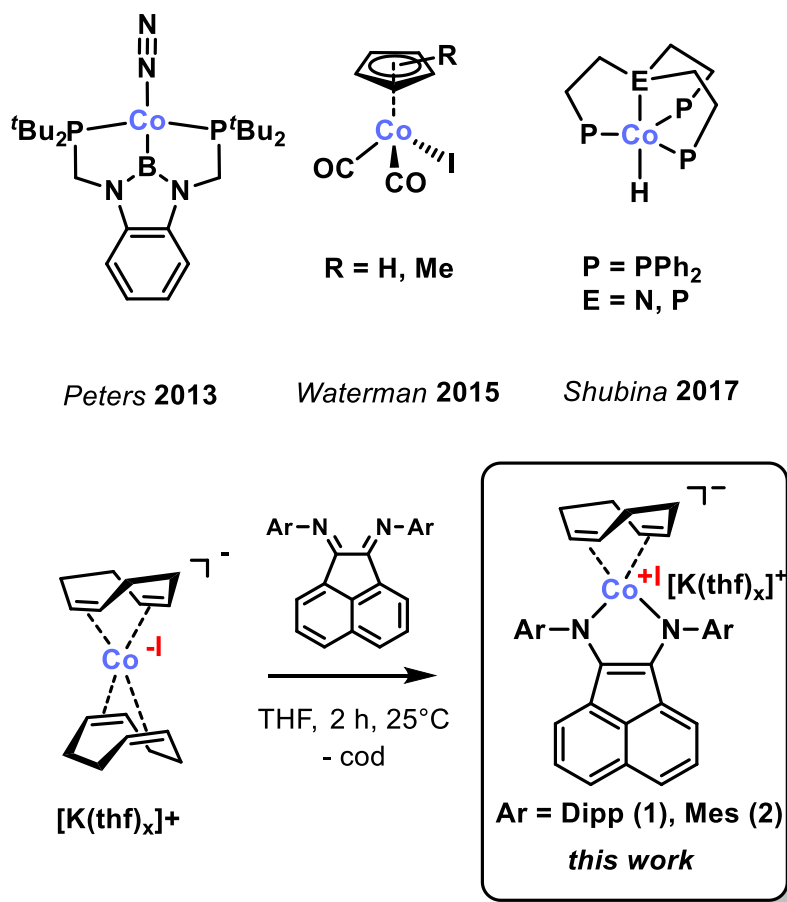


Figure 5.1. Homogeneous cobalt catalysts for amine-borane dehydrogenation (Dipp = 2,6-diisopropylphenyl, Mes = 2,4,6-trimethylphenyl, cod = 1,5-cyclo-octadiene).

The paucity of cobalt-based amine-borane dehydrogenation and transfer hydrogenation catalysts^{[9]-[11]} prompted us to investigate the efficacy of complexes containing redox-active bis(iminoacenaphthene)diimine (BIAN) ligands.^[13] This ligand class was deemed particularly suitable because it offers a convenient synthesis from commercial precursors (>60 g scales), redox-activity, modular structure, and a persistent ligand backbone.^[13] BIANs have mainly been exploited in noble metal catalysis so far,^[14] while applications to 3d metal catalysis have only been reported very sporadically; systematic investigations are still in their infancy.^[15]

5.2 Results and Discussion

Key discoveries and model reactions. We previously investigated the catalytic properties of low-valent ferrate and cobaltate anions in the hydrogenation of olefins, ketones, and imines.^[16] The pre-catalysts $[\text{K}([\text{18}]\text{crown-6})(\text{thf})_2][\text{M}(\eta^4\text{-anthracene})_2]$ ($\text{M} = \text{Fe}, \text{Co}$)^[17] and $[\text{K}(\text{thf})_x][\text{Co}(\eta^4\text{-cod})_2]$ ^{[18],[19]} ($\text{cod} = 1,5\text{-cyclooctadiene}$) enabled the hydrogenation of disubstituted alkenes, ketones and imines. Poor activities were observed for the hydrogenation of tri-substituted alkenes and dehydrogenations of amine-boranes.^[19] We therefore set out to manipulate the stereoelectronic properties of the catalysts by incorporation of redox-active bis(imino)acenaphthene ligands. The synthesis of $[\text{K}(\text{thf})_{1.5}\{\text{DippBIAN}\}\text{Co}(\eta^4\text{-cod})]$ (**1**) ($\text{Dipp} = 2,6\text{-diisopropylphenyl}$; $\text{cod} = 1,5\text{-cyclooctadiene}$ BIAN = bisaryl-(imino)acenaphthene, Figure 5.1) was recently reported.^[20] **1** and the closely related mesityl-derivative $[\text{K}(\text{thf})\{\text{MesBIAN}\}\text{Co}(\eta^4\text{-cod})]$ (**2**) ($\text{Mes} = 2,4,6\text{-trimethylphenyl}$, see the SI for details) were readily accessible in high yields from a straightforward ligand exchange reaction of $[\text{K}(\text{thf})_x][\text{Co}(\eta^4\text{-cod})_2]$ with ArBIAN ($\text{Ar} = \text{Dipp}$ or Mes). The redox-active BIAN moiety in **1** and **2** may facilitate metal-centered redox processes by its ability to accommodate two electrons, while cod can serve as a placeholder for vacant coordination sites. We commenced our studies with dimethylamine-borane (NHMe_2BH_3 , DMAB, Scheme 5.1 and Figure 5.2) as model substrate and monitored its consumption by ^{11}B -NMR spectroscopy. With 5 mol% catalyst loading of **1** at 25°C , DMAB was completely consumed within 34 h. The formation of two main products, tetramethyl-1,3-diaza-2,4-diboretane (74%) and N,N' -dimethylaminoborane (22%), and one minor BH_3 -containing compound (quartet at -9.5 ppm, $^1J_{\text{B-H}} = 134$ Hz) was observed. The less bulky pre-catalyst **2** was far less selective as illustrated by the observation of significant quantities of N,N' -dimethylaminoborane (19%) and unknown BH_3 -containing species (17%). We therefore employed pre-catalyst **1** for further dehydrogenation studies. A kinetic analysis by ^{11}B -NMR spectroscopy showed that the reaction likely proceeded through a stepwise mechanism involving the linear intermediate **B** ($\text{Me}_2\text{N-BH}_2\text{-NMe}_2\text{-BH}_3$) and the unsaturated intermediate **C** ($\text{Me}_2\text{N}=\text{BH}_2$) (Scheme 5.1). As proposed by *Schneider* and co-workers for dehydrogenations catalyzed by a Ru-amido pincer complex and by *Weller* and co-workers with a cationic Rh-phosphine complex,^[21] the loss of two molecules dihydrogen operates

over two steps when the reaction proceeds through **B**. In case of **C**, both dihydrogen molecules are eliminated in the first step and a cycloaddition gives the terminal product **D**. We cannot rule out that **B** was also converted into **D** by the loss of one molecule H_2 . The side product $HB(NMe)_2$ was reported for many catalytic DMAB hydrogenations in the literature.^{[5],[8],[9]} Monitoring the time-dependent H_2 formation (see the SI) revealed an induction period of approx. 1 min (SI, Figure 5.6.13). A comparison of the initial rates indicates that the catalytic dehydrogenation activity of **2** is five times higher than that of **1** (SI, Figure 5.6.13).

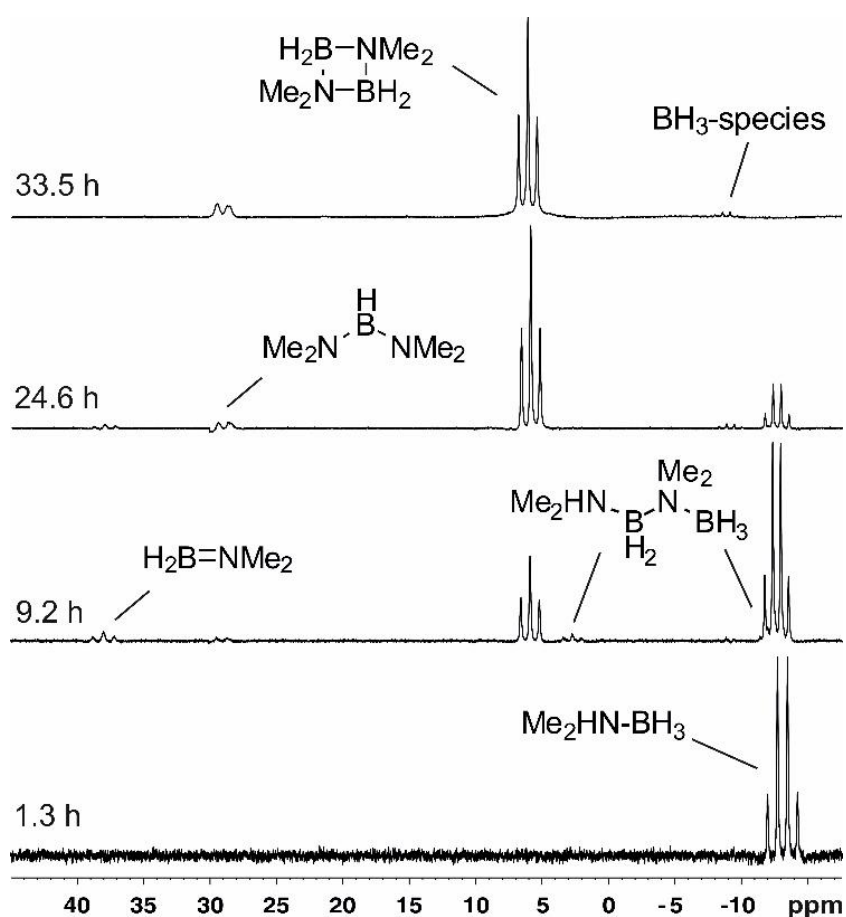
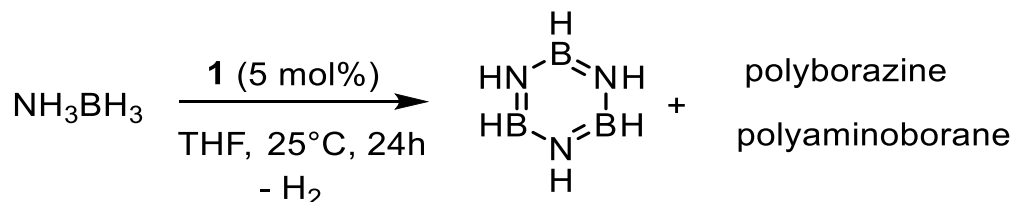


Figure 5.2. Time-dependent ^{11}B -NMR spectra (160.4 MHz, 300K, C_6D_6 -capillary) of the DMAB-dehydrogenation with catalyst **1** (0.2 mmol DMAB in 2.5 mL THF).

Figures 5.6.19-S21). ^{11}B -NMR spectra recorded in THF displayed a broad triplet at -4.8 ppm with the typical line broadening of $^1J_{\text{BH}} = 106$ Hz. Significantly broader peaks are expected for a polymer (Figure 5.3, bottom).^[23]



Scheme 5.3. Dehydrogenation of AB catalyzed by **1** (5 mol%).

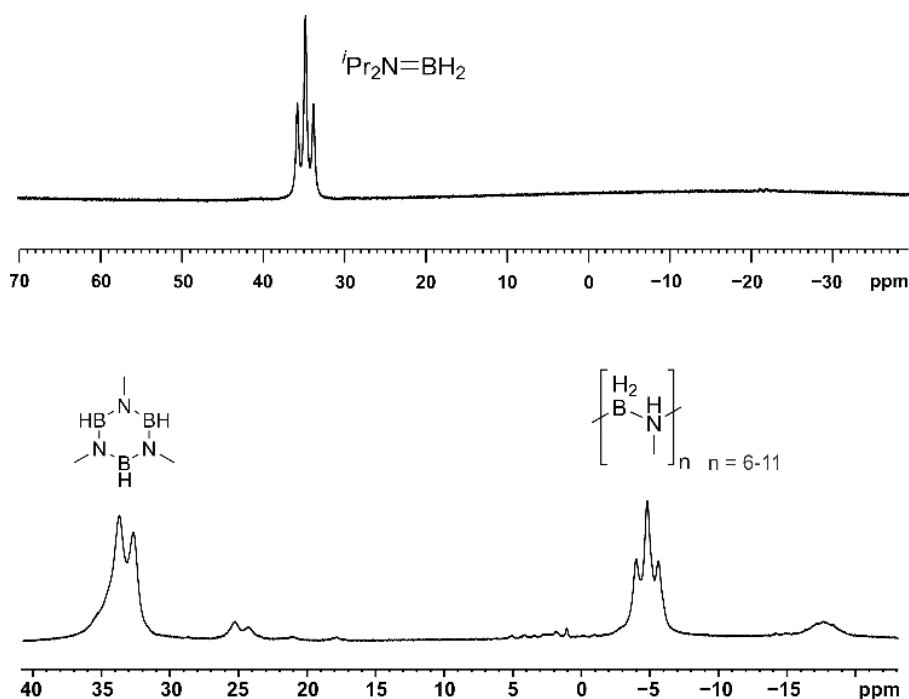


Figure 5.3. $^{11}\text{B}\{^1\text{H}\}$ -NMR (128.4 MHz, 300K, C_6D_6) of dehydrogenation products of diisopropylamine-borane- (top) and *N*-methylamine-borane (bottom) in THF.

The dehydrogenation of ammonia borane (AB) is of particular interest due its high hydrogen content of 19.6 wt%.^[1] The cyclopentadienyl carbonyl cobalt and tripodal phosphine cobalt complexes reported by the groups of *Waterman* and *Shubina*,^[8b,c] respectively, are the only previously reported molecular cobalt catalysts for the AB-dehydrogenation (Figure 5.1).^[9] Hence, we sought to compare the properties of pre-catalyst **1** with these benchmark systems that both operate at elevated temperature (65°C). When **1** (5 mol%) was added to a solution of AB in

THF, the evolution of H₂ commenced immediately. This indicates a rapid onset of catalytic dehydrogenation already at ambient temperature. The characterization of reaction intermediates (Scheme 5.3) was performed by ¹¹B-NMR spectroscopy. The starting material AB was completely consumed after 24 h. Borazine (30 ppm) and polyborazine (26 ppm) were identified as the two main soluble products. However, it is noteworthy that a white precipitate formed during the reaction in THF. This solid was studied by magic angle spinning (MAS) ¹¹B NMR spectroscopy with proton decoupling and cross-polarization (¹¹B-CPMAS-NMR) as well as without cross-polarization from protons and with proton coupling. The ¹¹B MAS NMR spectrum of this material showed two signals at 2 ppm and -19 ppm (Figure 5.4). Proton decoupling (¹¹B{¹H} MAS NMR) reduced the linewidth of the -19 ppm resonance while it did not affect the signal at -2 ppm. The intensity of the former signal was strongly enhanced in the ¹¹B{¹H} CPMAS spectrum. Thus, this signal should be assigned to a boron atom bonded to hydrogen(s). In contrast, the signal at -2 ppm may be assigned to a boron atom bearing no H atoms. We believe that this solid is polyaminoborane for which similar solid-state NMR data, particularly similar chemical shifts, were reported by *Schneider* and co-workers.^[8]

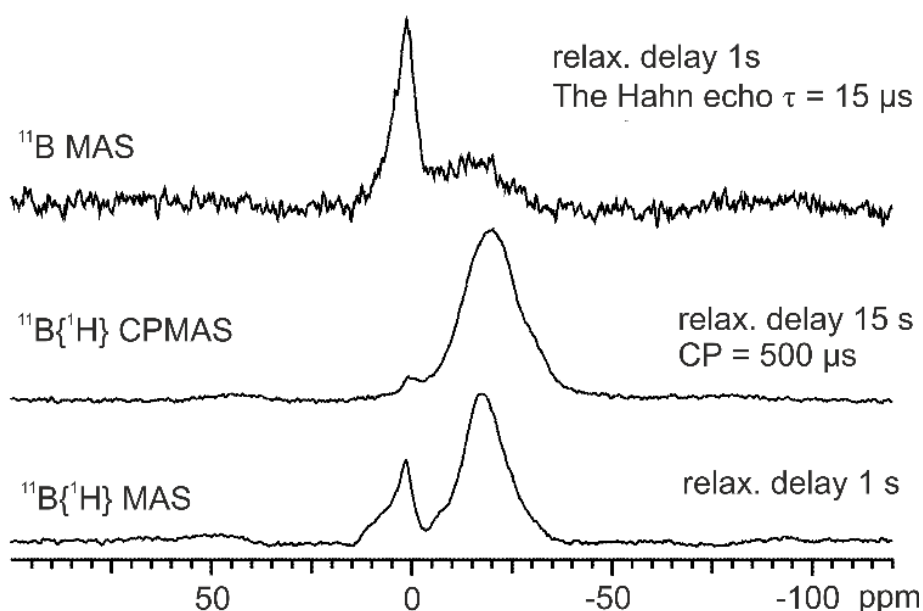


Figure 5.4. ¹¹B-NMR spectra at 300 K of polyaminoborane; MAS at 6 kHz; relax = relaxation.

Mechanistic studies of dehydrogenation. AB dehydrogenation was directly monitored by H₂ evolution at 1-12.5 mol% catalyst loading (Figure 5.5). An induction period was apparent at low catalyst concentrations, indicating that **1** might act as a pre-catalyst that is converted to the active catalyst species under reaction conditions. The formation of 0.5 equivalents H₂ per AB was observed within the first 2 min with 5 mol% (10 mM) catalyst. Subsequently, the reaction became much slower, indicating catalyst deactivation and possibly a change in the reaction mechanism. A plot of the initial rates vs. catalyst concentrations (SI, Figure 5.6.16) showed a 2nd order rate in catalyst. A linear relationship between reaction rate and substrate concentration from 50 – 200 mM was established from dehydrogenations with different AB concentrations and constant catalyst concentration (SI, Figure 5.6.18). Higher substrate concentrations afforded no significant enhancement of the initial rate constant. Based on these data, the following rate law can be formulated:

$$d(\text{H}_2)/dt = k \cdot [\text{catalyst } \mathbf{1}]^2 \cdot [\text{NH}_3\text{BH}_3] \quad (1)$$

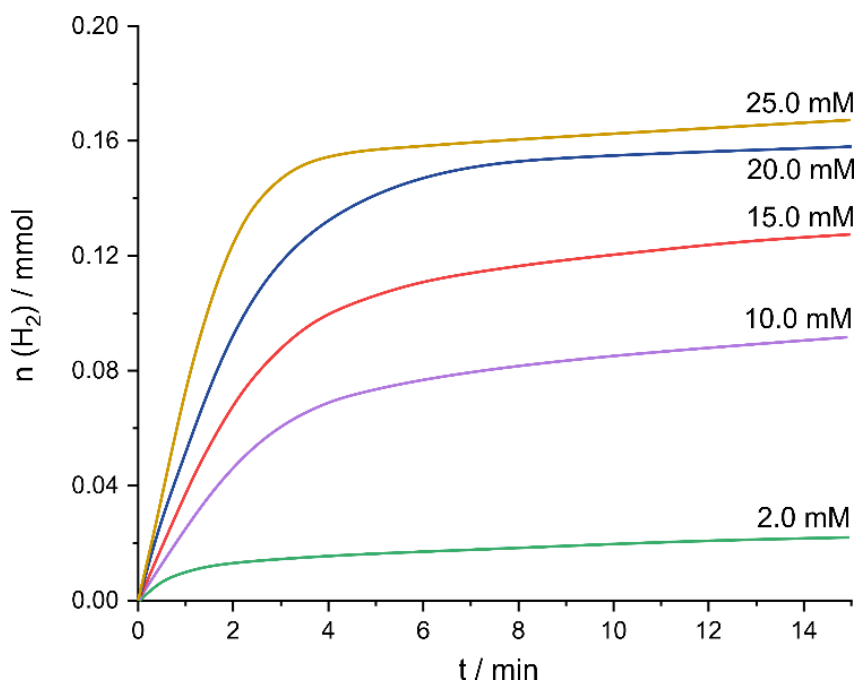


Figure 5.5. Dehydrogenation of AB catalyzed with different catalyst loading of **1**. Reaction conditions: 0.2 mmol AB in THF (1 mL) at 25°C.

Further mechanistic evidence was gathered from GC-MS investigations of the reaction mixtures, which documented the formation of cyclooctene and cyclooctane arising from (partial) hydrogenation of the 1,5-cyclooctadiene ligand in **1**. No H₂ formation was observed in control experiments with NMe₃BH₃ and NH₃BEt₃. A crossover experiment with a substrate mixture of NMe₃BH₃ and NH₃BEt₃ did not result in any H₂ formation. Consistently, no dehydrogenation products were observed by ¹¹B-NMR. These results proved that the presence of H-N *and* H-B entities within one molecule are required to enable dehydrogenation of amine-boranes. In an effort to gain more insight into the operating reaction mechanism, we performed dehydrogenations of the deuterated species ND₃BH₃, NH₃BD₃, and ND₃BD₃. Experiments with 5 mol% catalyst **1** and ND₃BH₃ revealed a kinetic isotope effect (KIE) $k(\text{NH}_3\text{BH}_3) / k(\text{ND}_3\text{BH}_3) = 1.6$ (2° KIE), while with NH₃BD₃ a negligible KIE $k(\text{NH}_3\text{BH}_3) / k(\text{NH}_3\text{BD}_3)$ of 0.9 was observed. This is strongly indicative of a participation of a protic H-N in the rate determining step. Fully deuterated ammonia borane (ND₃BD₃) showed a strong KIE $k(\text{NH}_3\text{BH}_3) / k(\text{ND}_3\text{BH}_3)$ of 2.0 (Figure 5.6). Complementing the kinetic studies, we conducted poisoning experiments in order to study the nature of the catalytically active species.^[24] The analysis of changes of catalyst activity by the presence of selective catalyst poisons is an instructive tool for the distinction between homotopic and heterotopic catalysis pathways.^{[19],[25]} Mercury (675 equiv. per [Co]) and P(OMe)₃ (0.2 equiv. per catalyst) barely had an influence on the overall reaction rate (5 mol% catalyst, see Figure 5.7). Both additives are known to selectively poison heterogeneous catalysts.^{[19],[24],[25]} A complementary experiment was performed with the strong π -ligand dibenzo[*a,e*]cyclooctatetraene (dct), which selectively deactivates soluble metal complexes in low oxidation states and therefore is a powerful poison of homogeneous catalysts.^{[19],[24]-[26]} Addition of AB to a solution of the catalyst (5 mol% **1**) and dct (2 equiv. per [Co]) significantly slowed down the reaction. The inhibition was not complete as dct underwent partial hydrogenation to *E/Z*-dibenzocyclooctene and dibenzocyclooctane (GC-MS). These poisoning studies support the notion of a homotopic reaction mechanism.

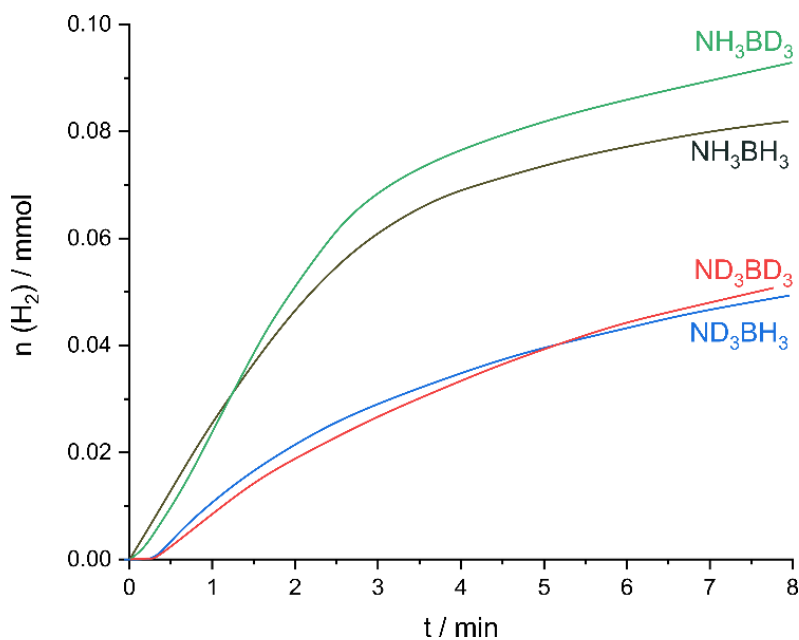


Figure 5.6. Observation of kinetic isotope effects in the dehydrogenation of ammonia borane. Reaction conditions: 5 mol% **1**, 0.2 mmol AB, THF (1 mL), 25°C.

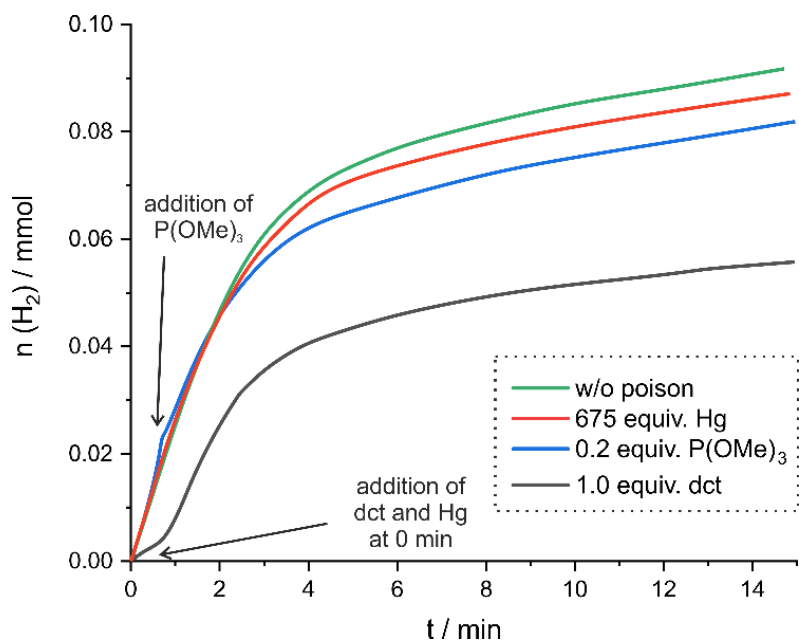
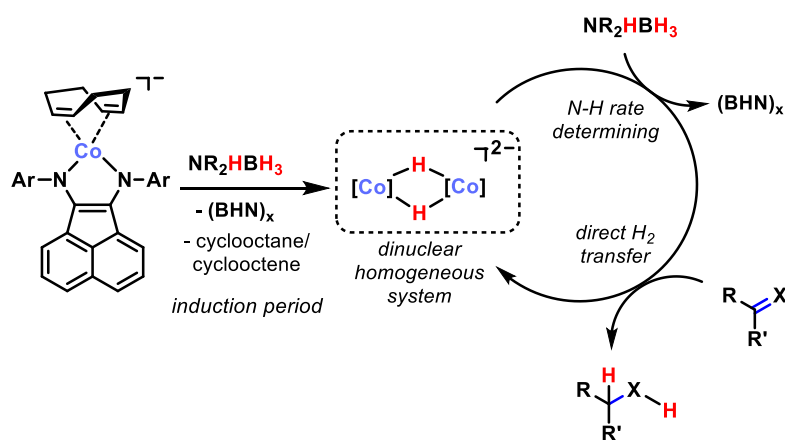


Figure 5.7. Poisoning experiments in the dehydrogenation of AB. Reaction conditions: 5 mol% **1**, 0.2 mmol AB, THF (1 mL), 25°C.

The insight gained by these studies can be summarized in a tentative mechanistic scheme (Scheme 5.3). Catalysis is initiated by the (partial) hydrogenation the cyclooctadiene ligand. This results in an induction period observed in the reaction-

time profiles at low catalyst concentrations. The poisoning studies indicate that a homogeneous (molecular) catalyst is operative, while the 2nd order rate law with respect to cobalt suggests that the rate-determining step involves two cobalt atoms. While the exact structure of the active species still remains obscure presently, it should be noted that numerous transition metal hydrides catalyze amine-borane dehydrogenation,^[1] and there is literature precedent for dinuclear cobalt hydride complexes.^[32] A dinuclear cobalt hydride species thus might be a plausible on-cycle intermediate. The basic nature of the hydride ligands might explain why N-H transfer appears to be rate determining in this case.



Scheme 5.3. Summary of the mechanistic information gained for amine-borane dehydrogenation and transfer transfer hydrogenation ($X = CR_2, NHR''$).

Scope of transfer hydrogenations. Next, we expanded the catalytic applications of **1** and **2** to transfer hydrogenations of C=C and C=N bonds using AB as formal hydrogen donor. Only a few molecular cobalt catalysts are known to be competent in transfer hydrogenations of olefins and imines (Figure 5.1).^[9] We performed initial studies with the combination of NH_3BH_3 and α -methylstyrene (SI, Table 5.6.1). Pre-catalysts **1** and **2** gave similar results. Optimizations with **1** showed best activities and full conversion at 5 mol% catalyst loading and equimolar concentrations of alkene and AB (0.2 mol L^{-1} in THF, see SI: Table 5.6.1). Allylbenzene, linear α -olefins, and 4-octene were successfully hydrogenated under these conditions (Figure 5.8). Complete hydrogenation of 1,1-diphenylethylene proceeded within 40 h at ambient temperature. The reaction conditions were compatible with ethers, esters, amines, CF_3 , F, and free alcohols (Figure 5.8). Minor dehydrohalogenation (3%) was observed for 4-chloro- α -methylstyrene. Alkyl

5 Amine-Borane Dehydrogenation and Transfer Hydrogenation Catalyzed by α -Diimine Cobaltates

cinnamates underwent competitive carbonyl hydrogenation to give 3-phenyl-1-propanol. Challenging trisubstituted olefins such as 1-phenylcyclopentene, 1-phenylcyclohexene, and 1,1',2-triphenylethylene as well as arene moieties remained untouched even at elevated temperatures and with an excess of AB. Hydrogenation of such unsaturated functions could be realized by applying external H₂ pressure (*vide infra*). The scope of transfer hydrogenations was extended to imines and quinoline derivatives (Figure 5.9). Hydrogenations of quinolines are of particular interest due to the formation of 1,2,3,4-tetrahydroquinolines, which constitute key motifs of several bioactive compounds.^{[29],[30]}

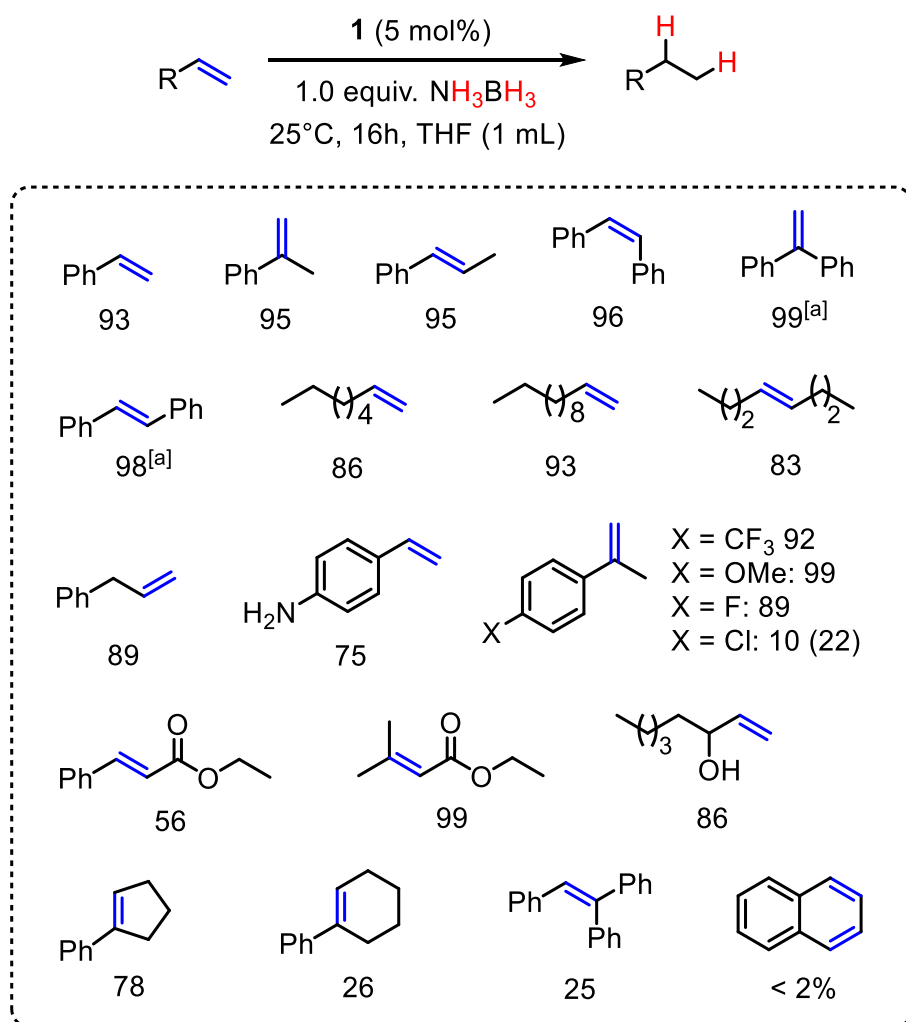


Figure 5.8. Transfer hydrogenation of alkenes with **1** (5 mol%). Standard conditions: alkene and AB (each 0.2 mmol), THF (1 mL); yields were determined by quantitative GC vs. internal *n*-pentadecane. ^[a] 40 h.

Very few heterogeneous catalysts for the transfer hydrogenation of quinolines and related *N*-heterocycles were described by *Beller* and co-workers,^[27] while molecular catalysts are also scarce.^[29] Using catalyst **1**, various quinolines was hydrogenated to 1,2,3,4-tetra-hydroquinolines at room temperature within 16 h. The equimolar stoichiometry of quinolines and AB underlines the high efficacy of catalyst **1** as 2 equiv. H₂ per AB are being transferred. Quinoxaline containing two C=N bonds was fully hydrogenated.

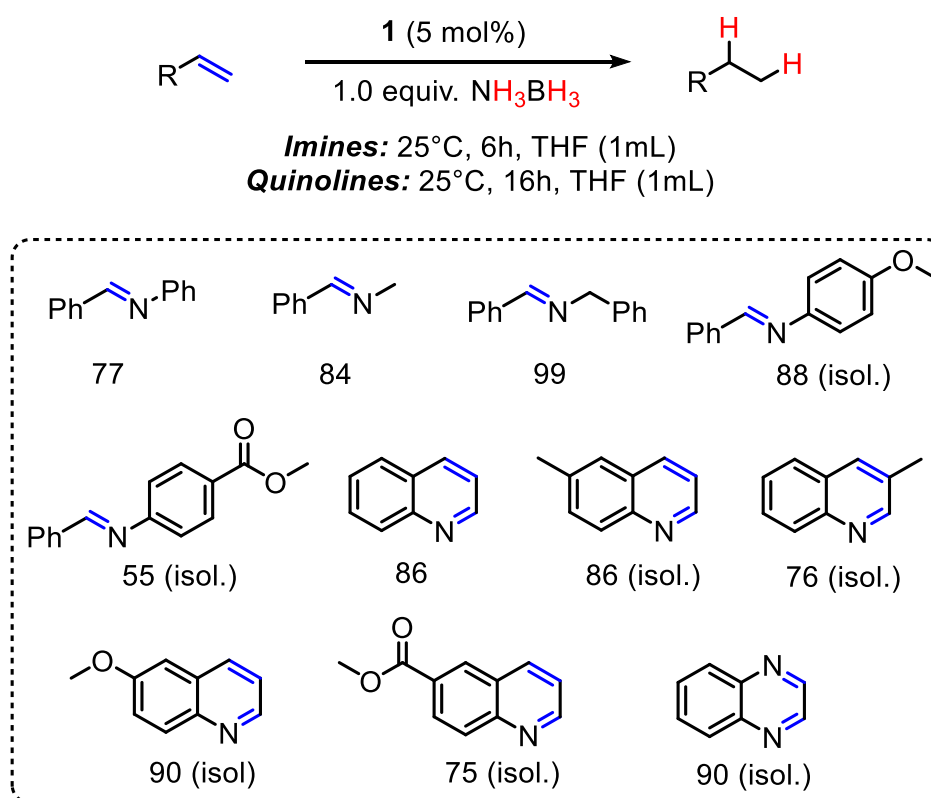


Figure 5.9. Transfer hydrogenation of imines. Standard conditions: substrate (0.2 mmol), THF (1 mL); yields were determined by quantitative GC vs. internal *n*-pentadecane. Conditions for isolated (isol.) substrates: substrate (0.4 mmol), THF (2 mL).

Mechanistic studies of transfer hydrogenation. We investigated the reaction-time profile of the hydrogenation of α -methyl-styrene (blue curve in Figure 5.10). The reaction onset is very fast (50% conversion after 3 min) and very similar to the dehydrogenation of AB (Figure 5.5). The reaction between α -methyl-styrene and AB under an atmosphere of 1 bar D₂ showed no deuterium incorporation after 5

min (GC-MS, SI, Figure 5.6.31). This indicates a direct (i.e. intramolecular) hydrogen

transfer from AB to the alkene (Scheme 5.3) which is orders of magnitude faster than the reduction of the alkene by D_2 . Furthermore, this observation argues against a stepwise mechanism involving H_2 formation from AB followed by cobalt-catalyzed hydrogenation of the alkene. Deuterated cumenes (appr. 15-20%, mostly cumene- d_1 , little cumene- d_{2-7}) were only observed after long reaction times (16 h, GC-MS, SI, Figures 5.6.30 and 5.6.32).^[31] Catalyst poisoning studies with dct suggested that the reaction follows a homotopic mechanism. The reaction was immediately inhibited after dct addition at 50% conversion (1.0 equiv. per [Co], Figure 5.10). The partial hydrogenation of the catalyst poison dct to a mixture of dibenzocyclooctene and dibenzocyclooctane resulted in the recovery of low catalyst activity after a few minutes (GC-MS).

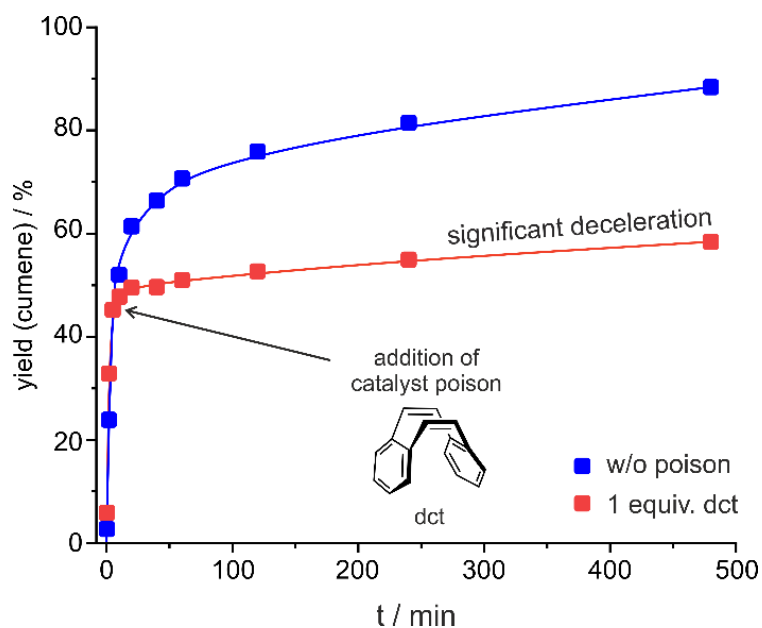
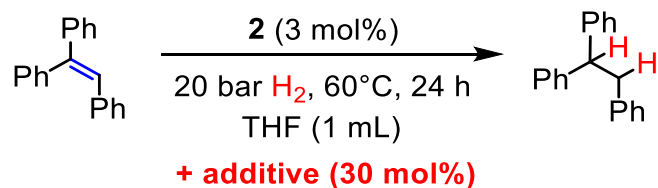


Figure 5.10. Catalyst poisoning in the transfer hydrogenation with **1**.

Hydrogenation of alkenes. The inefficacy of the transfer hydrogenation protocol for sterically hindered and some functionalized substrates prompted us to develop a hydrogenation protocol that would combine the rapid catalyst activation mechanism by catalytic amounts of AB with a hydrogenation mechanism in the presence of (super)stoichiometric amounts of H_2 gas (Table 5.1).^{[33],[34]} Pre-catalyst **2** proved slightly more active than **1** in the hydrogenation of the model

substrate 1,1',2-triphenylethylene. With 3 mol% of **2**, the hydrogenation proceeded cleanly at 20 bar H₂ and 60°C in the presence of several amine-boranes as catalyst activators. Amines and BH₃·THF were unreactive; NMe₂HBH₃ fared much poorer than AB.

Table 5.1. Screening of different additives in the hydrogenation of 1,1',2-triphenylethylene with catalyst **2**.



Additive	Yield (conversion) in [%]
w/o	0 (0)
NMe ₂ HBH ₃	92
NH ₃ BH ₃	> 99
NH ₃ BH ₃ ^[b]	> 99
NEt ₃	0 (13)
Pyridine	1 (14)
Piperidine	0 (12)
BH ₃ ·(THF)	2 (52) ^[c]

^[a] Standard conditions: **2** (3 mol%), substrate (0.2 mmol) in THF (1 mL). Yields of hydrogenated products were determined by quantitative GC vs. internal *n*-pentadecane. ^[b] catalyst **1** instead of **2**. ^[c] possibly due to hydroboration of triphenylethylene.

The general conditions were applied to a series of trisubstituted olefins (Figure 5.11). It is noteworthy that, unlike the transfer hydrogenation protocol, no dehalogenation was observed for 4-halo- α -methylstyrenes (X = Cl, Br) under these hydrogenation conditions. Naphthalene and pinene were hydrogenated at elevated temperature.

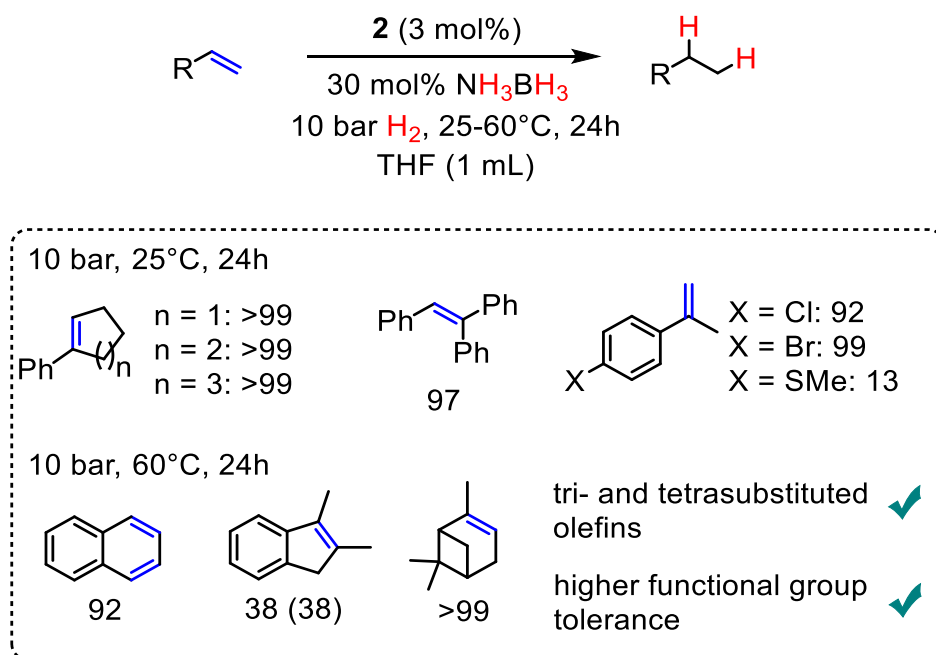


Figure 5.11. Substrate scope of alkene hydrogenations involving AB-mediated catalyst activation. Bonds in blue indicate sites of π -bond hydrogenation. Standard conditions: 0.2 mmol alkene, THF (1 mL). Yields determined by quantitative GC-FID vs. internal *n*-pentadecane; conversions given in parentheses if <90%.

5.3 Conclusions

We have shown that for the first time that highly reduced cobalt anions such as $[\text{K}(\text{thf})_{1.5}\{\text{DippBIAN}\}\text{Co}(\eta^4\text{-cod})]$ (**1**) can be used as active catalysts for the dehydrogenation of ammonia borane (AB) and related amine-boranes under mild conditions. The activity of **1** surpasses that of other molecular cobalt catalysts by *Waterman*^[10] and *Shubina*^[11] (Figure 5.1), which require elevated temperatures for an effective dehydrogenation reaction. Pre-catalyst **1** displayed a similar activity as *Peter's* PBP pincer complex^[9] for the dehydrogenation of DMAB. A mixture of polyaminoborane, borazine, polyborazine was obtained using catalyst **1**, indicating that >1 equiv. H₂ was released from AB. Reaction monitoring and poisoning experiments strongly indicate the operation of a homotopic catalyst. Transfer hydrogenation of olefins, imines, and quinolines have attracted increased only recently.^{[27],[28]} Catalyst **1** is also able to catalyze such transformations effectively, which involved the transfer of up to 2 equiv. H₂ from AB. Mechanistic studies documented that the rate-determining step likely involves proton transfer from the amine-borane, while the rate law suggested that more than one Co atom may be involved. Poisoning experiments again supported a homogeneous mechanism. $[\text{K}(\text{thf})\{\text{MesBIAN}\}\text{Co}(\eta^4\text{-cod})]$ (**2**) exhibited similarly good catalytic activity in the transfer hydrogenation reaction between AB and alkenes/imines. A related protocol was used for the hydrogenation of challenging trisubstituted olefins which involved catalyst activation by AB and subsequent hydrogenation under 10 bar H₂. This initial study demonstrates the significant potential of highly reduced α -diimine cobaltate for (de)hydrogenation reactions for the first time. The results have direct ramifications for the development of related reductive transformations and H₂ storage processes under base metal catalysis, which are the subject of on-going investigation in our laboratories.

5.4 Acknowledgements

We thank the mass spectrometry department of the University of Regensburg for ESI-MS analysis, Matthew J. Margeson (University of Regensburg) for experimental assistance, and Dr. Daniel J. Scott (University of Regensburg) for valuable comments on the manuscript. Financial support by the Fonds der

5 Amine-Borane Dehydrogenation and Transfer Hydrogenation Catalyzed by α -Diimine Cobaltates

Chemischen Industrie (fellowship to T.M.M.), the Deutsche Forschungsgemeinschaft (JA 1107/6-1, WO 1496/6-1), and the European Research Council (CoG 683150) is gratefully acknowledged.

Keywords: cobalt • catalysis • amine-boranes • transfer hydrogenation • dehydrogenation

5.5 References

- [1] a) A. Staubitz, A. P. M. Robertson, I. Manners, *Chem. Rev.* **2010**, *110*, 4079–4124. b) A. Rossin, M. Peruzzini, *Chem. Rev.* **2016**, *116*, 8848–8872.
- [2] a) F. H. Stephens, V. Pons, R. T. Baker, *Dalton Trans.* **2007**, *0*, 2613–2626. b) N. C. Smythe, J. C. Gordon, *Eur. J. Inorg. Chem.* **2010**, *2010*, 509–521
- [3] a) A. Staubitz, A. Presa Soto, I. Manners, *Angew. Chem. Int. Ed.* **2008**, *47*, 6212–6215; *Angew. Chem.* **2008**, *120*, 6308–6311. b) A. Ledoux, P. Larini, C. Boisson, V. Monteil, J. Raynaud, E. Lacôte, *Angew. Chem. Int. Ed.* **2015**, *54*, 15744–15749; *Angew. Chem.* **2015**, *127*, 15970–15975. c) E. M. Leitaó, T. Jurca, I. Manners, *Nature Chem.* **2013**, *5*, 817–829.
- [4] a) S. Fu, N.-Y. Chen, X. Liu, Z. Shao, S.-P. Luo, Q. Liu, *J. Am. Chem. Soc.* **2016**, *138*, 8588–8594. b) E. Korytiaková, N. O. Thiel, F. Pape, J. F. Teichert, *Chem. Commun.* **2017**, *53*, 732–735.
- [5] Selected examples for Ru, Pd, Rh, and Ir: a) C. A. Jaska, K. Temple, A. J. Lough, I. Manners, *Chem. Commun.* **2001**, 962–963. b) A. Staubitz, A. Presa Soto, I. Manners, *Angew. Chem. Int. Ed.* **2008**, *47*, 6212–6215; *Angew. Chem.* **2008**, *120*, 6308–6311. c) N. Blaquiere, S. Diallo-Garcia, S. I. Gorelsky, D. A. Black, K. Fagnou, *J. Am. Chem. Soc.* **2008**, *130*, 14034–14035. d) A. Friedrich, M. Drees, S. Schneider, *Chem. Eur. J.* **2009**, *15*, 10339–10342. e) T. M. Douglas, A. B. Chaplin, A. S. Weller, X. Yang, M. B. Hall, *J. Am. Chem. Soc.* **2009**, *131*, 15440–15456. f) A. Rossin, G. Bottari, A. M. Lozano-Vila, M. Paneque, M. Peruzzini, A. Rossi, F. Zanobini, *Dalton Trans.* **2013**, *42*, 3533–3541. f) E. H. Kwan, H. Ogawa, M. Yamashita, *ChemCatChem* **2017**, *9*, 2457–2462.
- [6] a) A. Staubitz, M. E. Sloan, A. P. M. Robertson, A. Friedrich, S. Schneider, P. J. Gates, J. Schmedt auf der Günne, I. Manners, *J. Am. Chem. Soc.* **2010**, *132*, 13332–13345. b) T. Jurca, T. Dellermann, N. E. Stubbs, D. A. Resendiz-Lara, G. R. Whittell, I. Manners, *Chem. Sci.* **2018**, *9*, 3360.
- [7] a) T. Kakizawa, Y. Kawano, K. Naganeyama, M. Shimoi, *Chem. Lett.* **2011**, *40*, 171–173. b) S. Muhammad, S. Moncho, E. N. Brothers, A. A. Bengali, *Chem. Commun.* **2014**, *50*, 5874–5877. c) M. Gediga, C. M. Feil, S. H. Schlindwein, J. Bender, M. Nieger, D. Gudat, *Chem. Eur. J.* **2017**, *23*, 11560–11569. d) H. R. Sharpe, A. M. Geer, T. J. Blundell, F. R. Hastings, M. W. Fay,

- G. A. Rance, W. Lewis, A. J. Blake, D. L. Kays, *Catal. Sci. Technol.* **2018**, *8*, 229–235.
- [8] a) J. R. Vance, A. P. M. Robertson, K. Lee, I. Manners, *Chem. Eur. J.* **2011**, *17*, 4099–4103. b) R. T. Baker, J. C. Gordon, C. W. Hamilton, N. J. Henson, P.-H. Lin, S. Maguire, M. Murugesu, B. L. Scott, N. C. Smythe, *J. Am. Chem. Soc.* **2012**, *134*, 5598–5609. c) P. Bhattacharya, J. A. Krause, H. Guan, *J. Am. Chem. Soc.* **2014**, *136*, 11153–11161. d) J. R. Vance, A. Schäfer, A. P. M. Robertson, K. Lee, J. Turner, G. R. Whittell, I. Manners, *J. Am. Chem. Soc.* **2014**, *136*, 3048–3064. e) A. Glüer, M. Förster, V. R. Celinski, J. Schmedt auf der Günne, M. C. Holthausen, S. Schneider, *ACS Catal.* **2015**, *5*, 7214–7217. f) C. Lichtenberg, M. Adelhardt, T. L. Gianetti, K. Meyer, B. de Bruin, H. Grützmacher, *ACS Catal.* **2015**, *5*, 6230–6240. g) C. Lichtenberg, L. Viciu, M. Adelhardt, J. Sutter, K. Meyer, B. de Bruin, H. Grützmacher, *Angew. Chem. Int. Ed.* **2015**, *54*, 5766–5771; *Angew. Chem.* **2015**, *127*, 5858–5863. h) A. M. Lunsford, J. H. Blank, S. Moncho, S. C. Haas, S. Muhammad, E. N. Brothers, M. Y. Darensbourg, A. A. Bengali, *Inorg. Chem.* **2016**, *55*, 964–973. i) N. T. Coles, M. F. Mahon, R. L. Webster, *Organometallics* **2017**, *36*, 2262–2268. j) U. Chakraborty, S. Demeshko, F. Meyer, C. Rebreyend, B. de Bruin, M. Atanasov, F. Neese, B. Mühldorf, R. Wolf, *Angew. Chem. Int. Ed.* **2017**, *56*, 7995–7999; *Angew. Chem.* **2017**, *129*, 8107–8112. k) F. Anke, D. Han, M. Klahn, A. Spannenberg, T. Beweries *Dalton Trans.* **2017**, *46*, 6843–6847, l) J. Turner, N. F. Chilton, A. Kumar, A. L. Colebatch, G. R. Whittell, H. A. Sparkes, A. S. Weller, I. Manners, *Chem. Eur. J.* **2018**; DOI: 10.1002/chem.201705316.
- [9] a) T.-P. Lin, J. C. Peters, *J. Am. Chem. Soc.* **2013**, *135*, 15310–15313. b) G. Ganguly, T. Malakar, A. Paul, *ACS Catal.* **2015**, *5*, 2754–2769.
- [10] J. K. Pagano, J. P. W. Stelmach, R. Waterman, *Dalton Trans.* **2015**, *44*, 12074–12077.
- [11] S. Todisco, L. Luconi, G. Giambastiani, A. Rossin, M. Peruzzini, I. E. Golub, O. A. Filippov, N. V. Belkova, E. S. Shubina, *Inorg. Chem.* **2017**, *56*, 4296–4307.
- [12] a) R. J. Keaton, J. M. Blacquiere, R. T. Baker, *J. Am. Chem. Soc.* **2007**, *129*, 1844–1845. b) M. Vogt, B. de Bruin, H. Berke, M. Trincado, H. Grützmacher, *Chem. Sci.* **2011**, *2*, 723–727. c) A. P. M. Robertson, R. Suter, L. Chabanne, G. R. Whittell, I. Manners, *Inorg. Chem.* **2011**, *50*, 12680–12691. d) S.-K. Kim,

- S.-A. Hong, H.-J. Son, W.-S. Han, A. Michalak, S.-J. Hwang, S. O. Kang, *Dalton Trans.* **2015**, *44*, 7373–7381.
- [13] reviews on properties of BIAN derivatives and their coordination chemistry with s- and p-block elements: a) N. J. Hill, I. Vargas-Baca, A. H. Cowley, *Dalt. Trans.* **2009**, 9226, 240; b) I. L. Fedushkin, A. A. Skatova, V. A. Chudakova, G. K. Fukin, *Angew. Chem. Int. Ed.* **2003**, *42*, 3294; *Angew. Chem.* **2003**, *115*, 3416–3420.
- [14] Selected examples of (BIAN)Pd(olefin)-catalyzed hydrogenations: a) R. van Asselt, C. J. Elsevier, *J. Mol. Catal. A* **1991**, *65*, L13–L19. b) R. van Asselt, C. J. Elsevier, W. J. J. Smeets, A. L. Spek, R. Benedix, *Recl. Trav. Chim. Pays-Bas* **1994**, *113*, 88–98. c) M. W. Van Laren, C. J. Elsevier, *Angew. Chem. Int. Ed.* **1999**, *38*, 3715–3717; *Angew. Chem.* **1999**, *11*, 3926–3929.
- [15] a) F. S. Wekesa, R. Arias-Ugarte, L. Kong, Z. Sumner, G. P. McGovern, M. Findlater, *Organometallics* **2015**, *34*, 5051–5056; b) M. J. Supej, A. Volkov, L. Darko, R. A. West, J. M. Darmon, C. E. Schulz, K. A. Wheeler, H. M. Hoyt, *Polyhedron* **2016**, *114*, 403–414; c) M. Villa, D. Miesel, A. Hildebrandt, F. Ragaini, D. Schaarschmidt, A. Jacobi von Wangelin, *ChemCatChem* **2017**, *9*, 3203–3209.
- [16] Review on metalate anions highlighting the pioneering work of Jonas and Ellis: J. E. Ellis, *Inorg. Chem.* **2006**, *45*, 3167–3186.
- [17] a) W. W. Brennessel, J. Young Victor G., J. E. Ellis, *Angew. Chem. Int. Ed.* **2002**, *41*, 1211–1215; *Angew. Chem.* **2002**, *114*, 1259–1263. b) W. W. Brennessel, R. E. Jilek, J. E. Ellis, *Angew. Chem. Int. Ed.* **2007**, *46*, 6132–6136; *Angew. Chem.* **2007**, *119*, 6244–6248.
- [18] a) K. Jonas, R. Mynott, C. Krüger, J. C. Sekutowski, Y.-H. Tsay, *Angew. Chem. Int. Ed. Engl.* **1976**, *15*, 767–768; *Angew. Chem.* **1976**, *88*, 808–809.
- [19] a) D. Gärtner, A. Welther, B. R. Rad, R. Wolf, A. Jacobi von Wangelin, *Angew. Chem. Int. Ed.* **2014**, *53*, 3722–3726; *Angew. Chem.* **2014**, *126*, 3796–3800. b) P. Büschelberger, D. Gärtner, E. Reyes-Rodriguez, F. Kreyenschmidt, K. Koszinowski, A. Jacobi von Wangelin, R. Wolf, *Chem. Eur. J.* **2017**, *23*, 3139–3151.
- [20] S. Pelties, T. Maier, D. Herrmann, B. de Bruin, C. Rebreyend, S. Gärtner, I. G. Shenderovich, R. Wolf, *Chem. Eur. J.* **2017**, *23*, 6094–6102.

- [21]a) A. Friedrich, M. Drees, S. Schneider, *Chem. Eur. J.* **2009**, *15*, 10339–10342.
b) L. J. Sewell, G. C. Lloyd-Jones, A. S. Weller, *J. Am. Chem. Soc.* **2012**, *134*, 3598–3610.
- [22]Dehydrogenation of diisopropylamino borane: a) C. A. De Albuquerque Pinheiro, C. Roiland, P. Jehan, G. Alcaraz, *Angew. Chem. Int. Ed.* **2018**, *57*, 1519; *Angew. Chem.* **2018**, *130*, 1535. b) ref. [11c].
- [23]Selected examples for dehydrogenation of methylamine-borane to poly-*N*-methylaminoborane or [MeHN-BH₂]₃: a) A. Staubitz, A. Presa Soto, I. Manners, *Angew. Chem. Int. Ed.* **2008**, *47*, 6212–6215; *Angew. Chem.* **2008**, *120*, 6308–6311. b) Y. Kawano, M. Uruichi, M. Shimoi, S. Taki, T. Kawaguchi, T. Kakizawa, H. Ogino, *J. Am. Chem. Soc.* **2009**, *131*, 14946–14957. c) T. Kakizawa, Y. Kawano, K. Naganeyama, M. Shimoi, *Chem. Lett.* **2011**, *40*, 171–173. e) G. M. Adams, A. L. Colebatch, J. T. Skornia, A. I. McKay, H. C. Johnson, G. C. Lloyd Jones, S. A. Macgregor, N. A. Beattie, A. S. Weller, *J. Am. Chem. Soc.* **2018**, *140*, 1481. f) see also ref. [6a], [7k].
- [24]Selected reviews on homotopic vs. heterotopic catalysis: a) R. H. Crabtree, *Chem. Rev.* **2012**, *112*, 1536–1554. b) V. Artero, M. Fontecave, *Chem. Soc. Rev.* **2013**, *42*, 2338–2356. c) J. F. Sonnenberg, R. H. Morris, *Catal. Sci. Technol.* **2014**, *4*, 3426–3438.
- [25]a) P. Büschelberger, E. Reyes-Rodriguez, C. Schöttle, J. Treptow, C. Feldmann, A. Jacobi von Wangelin, R. Wolf, *Catal. Sci. Technol.* **2018**, *8*, 2648–2653. b) S. Sandl, F. Schwarzhuber, S. Pöllath, J. Zweck, A. Jacobi von Wangelin, *Chem. Eur. J.* **2018**, *24*, 3403–3407.
- [26]a) D. R. Anton, R. H. Crabtree, *Organometallics* **1983**, *2*, 855–859. b) S. Chaffins, M. Brettreich, F. Wudl, *Synthesis* **2002**, *2002*, 1191–1194. c) G. Franck, M. Brill, G. Helmchen, *Org. Synth.* **2012**, *89*, 55–65.
- [27]F. Chen, B. Sahoo, C. Kreyenschulte, H. Lund, M. Zeng, L. He, K. Junge, M. Beller, *Chem. Sci.* **2017**, *8*, 6239–6246.
- [28]a) G. Zhang, S. K. Hanson, *Chem. Commun.* **2013**, *49*, 10151–10153. b) G. Zhang, Z. Yin, J. Tan, *RSC Adv.* **2016**, *6*, 22419–22423. c) S. Fu, N.-Y. Chen, X. Liu, Z. Shao, S.-P. Luo, Q. Liu, *J. Am. Chem. Soc.* **2016**, *138*, 8588–8594. d) J. R. Cabrero-Antonino, R. Adam, K. Junge, R. Jackstell, M. Beller, *Catal. Sci. Technol.* **2017**, *7*, 1981–1985. e) V. G. Landge, J. Pitchaimani, S. P.

- Midya, M. Subaramanian, V. Madhu, E. Balaraman, *Catal. Sci. Technol.* **2018**, *8*, 428–433.
- [29] Examples for cobalt-catalyzed imine and quinoline hydrogenation: a) K. Kobayashi, T. Okamoto, T. Oida, S. Tanimoto, *Chem. Lett.* **1986**, *15*, 2031–2034. b) R. Xu, S. Chakraborty, H. Yuan, W. D. Jones, *ACS Catal.* **2015**, *5*, 6350–6354.
- [30] Reviews on 1,2,3,4-tetrahydroquinoline chemistry: a) A. R. Katritzky, S. Rachwal, B. Rachwal, *Tetrahedron* **1996**, *52*, 15031–15070. b) V. Sridharan, P. A. Suryavanshi, J. C. Menéndez, *Chem. Rev.* **2011**, *111*, 7157–7259.
- [31] ^2H NMR spectroscopy of the obtained H/D-cumene mixture showed on average that 20% of the methine positions and 18% of the methyl positions bear D atoms. The higher deuteration level of the methyl positions may indicate the operation of a mono-deuterium atom transfer to the alkene or possibly an H/D-exchange via benzyl radical intermediates.
- [32] Selected examples of dinuclear cobalt hydrides: a) M. D. Fryzuk, J. B. Ng, S. J. Rettig, J. C. Huffman, K. Jonas, *Inorg. Chem.* **1991**, *30*, 2437–2441. b) J. L. Kersten, A. L. Rheingold, K. H. Theopold, C. P. Casey, R. A. Widenhoefer, C. E. C. A. Hop, *Angew. Chem.* **1992**, *104*, 1364–1366. c) K. Ding, W. W. Brennessel, P. L. Holland, *J. Am. Chem. Soc.* **2009**, *131*, 10804–10805.
- [33] a) *Catalytic Hydrogenation* Ed.: L. Cervený), Elsevier, Amsterdam, **1986**. b) *The Handbook of Homogeneous Hydrogenation* (Eds.: J. G. de Vries, C. J. Elsevier), Wiley-VCH, Weinheim, **2007**. c) P. J. Chirik, *Acc. Chem. Res.* **2015**, *48*, 1687.
- [34] Selected examples of Co-catalyzed alkene hydrogenations: a) Q. Knijnenburg, A. D. Horton, H. van der Heijden, B. de Bruin, P. H. M. Budzelaar, W. A. Gal *J. Mol. Catal. A. Chem.* **2005**, *232*, 151–159. b) G. Zhang, B. L. Scott, S. Hanson, *Angew. Chem. Int. Ed.* **2012**, *51*, 12102–12106; *Angew. Chem.* **2012**, *124*, 12268–12272. c) M. R. Friedfeld, M. Shevlin, J. M. Hoyt, S. W. Krska, M. T. Tudge, P. J. Chirik, *Science* **2013**, *342*, 1076. d) R. P. Yu, J. M. Darmon, C. Milsman, G. W. Margulieux, S. C. E. Stieber, S. DeBeer, P. J. Chirik, *J. Am. Chem. Soc.* **2013**, *135*, 13168–13184. e) M. R. Friedfeld, G. W. Margulieux, B. A. Schäfer, P. J. Chirik, *J. Am. Chem. Soc.* **2014**, *136*, 13178–13181. f) M. R. Friedfeld, H. Zhong, R. T. Ruck, M. Shevlin, P. J. Chirik, *Science* **2018**, *360*, 888

5.6 Supporting Information

5.6.1 General information

All experiments were performed under an atmosphere of dry Argon using standard Schlenk techniques or an MBraun UniLab Glovebox.

Analytical Thin-Layer Chromatography: TLC was performed using aluminium plates with silica gel and fluorescent indicator (*Macherey-Nagel*, 60, UV₂₅₄). Thin layer chromatography plates were visualized by exposure to UV light (366 or 254 nm).

Chemicals and Solvents: Solvents were dried and degassed with an *MBraun SPS800* solvent-purification system. THF, diethylether were stored over molecular sieves (3 Å). *n*-hexane was stored over a potassium mirror. 1,2-dimethoxyethane was stirred over K/benzophenone, distilled and stored over molecular sieves (3 Å). Commercially available olefins, imines, and quinolines were purified by distillation (Kugelrohr) and in case of liquids dried over molecular sieves (3 Å). Amine-boranes (NH₃BH₃ (60°C, 10⁻³ mbar, NMe₂HBH₃ (25°C, 10⁻³ mbar), NMe₃BH₃ (25°C, 10⁻³ mbar) were sublimed prior to use.

Column Chromatography: Flash column chromatography with silica gel 60 from *Sigma Aldrich* (63 – 200 µm). Mixture of solvents used are described *vide infra*.

Elemental Analyses: Elemental analyses were carried out by the analytical department of the University of Regensburg

ESI-MS: ESI-MS spectra were carried out by the analytical department of the University of Regensburg, *Agilent Q-TOF 6540 UHD*

High Pressure Reactor: Hydrogenation reactions were carried out in 160 and 300 mL high pressure reactors (*Parr*TM) in 4 mL glass vials. The reactors were loaded under argon, purged with argon, sealed and the internal pressure was adjusted. Hydrogen (99.9992%) was purchased from *Linde*.

NMR spectroscopy: ¹H, ¹³C{¹H}, ¹¹B{¹H}, and ¹¹B-NMR spectra in solutions were recorded on *Bruker Avance 300* (300 MHz) and *Bruker Avance 400* (400 MHz) if not stated otherwise. These chemical shifts are given relative to solvents

resonances in the tetramethylsilane scale. The following abbreviations have been used for multiplicities: s = singlet, d = doublet, t = triplet, q = quartet, sept = septet, m = multiplet, dd = doublet of doublet, dt = doublet of triplet. Solid-state ^{11}B -NMR spectra were recorded on an *Infinity_{plus}* spectrometer (*Agilent*) operated at 7 Tesla, equipped with a 6 mm pencil CPMAS probe. The spectrum was indirectly referenced to NaBH_4 (-42.1 ppm)^[1]

Fourier-Transformations-Infrared-Spectroscopy (FT-IR): Spectra were recorded on *Agilent Cary 630 FTIR* with ATR device. All spectra were recorded at room temperature. Wave numbers are given in cm^{-1} .

Gas chromatography with FID (GC-FID): *Shimadzu GC2010plus*. Carrier gas: H_2 . Colum: Restek Rxi[®], (30m x 0.25 mm x 0.25 μm) Carrier gas: H_2 . Standard heating procedure: 50°C (2 min), 25°C/min \rightarrow 280°C (5 min). *HP6890 GC-System* with injector 7683B and *Agilent 7820A System*. Column: HP-5, 19091J-413 (30 m x 0.32 mm x 0.25 μm), carrier gas: N_2 . Calibration of substrates and products with internal standard *n*-pentadecane and analytically pure samples.

Gas chromatography with mass-selective detector (GC-MS): *Agilent 7820A GC system, mass detector 5977B*. Carrier gas: H_2 . Column: HP-5MS (30m x 0.25 mm x 0.25 μm). Standard heating procedure: 50°C \rightarrow 300°C. *Agilent 6890N Network GC-System, mass detector 5975 MS*. Column: HP-5MS (30m x 0.25 mm x 0.25 μm , 5% phenylmethylsiloxane, carrier gas: H_2 . Standard heating procedure: 50 °C (2 min), 25 °C/min \rightarrow 300 °C (5 min).

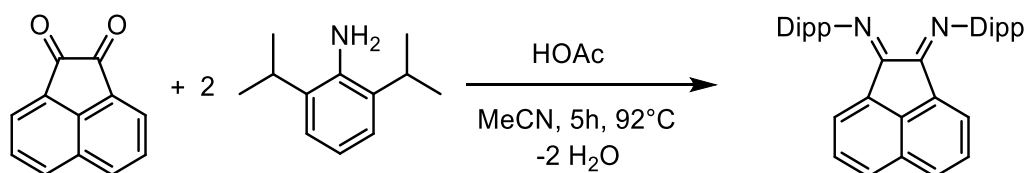
Gas evolution measurements: Gas evolution measurements were done with *Man on the Moon X103[®]* kit (supplied by Man on the moon Tech, University of Zaragoza, Facultad de Ciencias, C/Pedro Cerbuna 12, 50009 – Zaragoza, Spain; <http://www.manonthemoontech.com/>). The volume of the reaction apparatus was determined by protic hydrolysis of different amounts of zinc. Evolved hydrogen in mmol was calculated using ideal gas law. Every reaction was done under inert atmosphere.



5.6.2 Synthesis of starting materials

Synthesis of bis[*N,N'*-(2,6-diisopropylphenyl)imino]acenaphthene (DippBIAN)

DippBIAN was synthesized according to a protocol of *Fukuda* and co-workers.^[2]



Acenaphthenequinone (7.5 g, 41.2 mmol, 1.0 equiv.) was suspended in 250 mL acetonitrile and heated to reflux for one hour. 65 mL of acetic acid was added to the suspension and reflux was continued for further 30 minutes. 2,6-diisopropylaniline (18.7 mL, 99.1 mmol, 2.7 equiv.) was added dropwise over 30 min. The reaction temperature was kept for additional 4.5 hours. Then the reaction mixture was cooled to room temperature. The crude product was obtained by filtration and washed with *n*-pentane (3 x 50 mL). The solid was dissolved in 300 mL chloroform and filtered. Evaporation of the solvent yielded DippBIAN as yellow-orange powder.

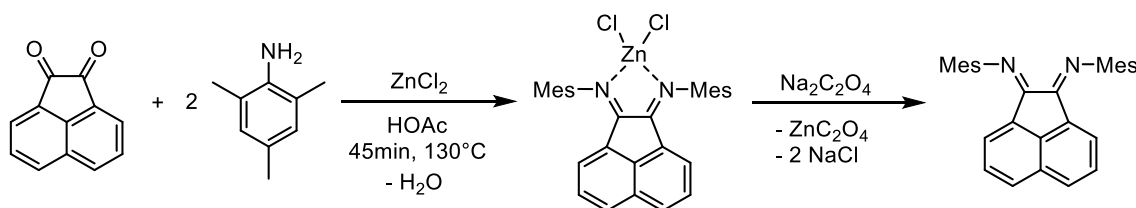
Yield: 17.0 g (34.0 mmol, 83%)

Chemical formula: $C_{36}H_{40}N_2$ (MW = 500.73 g mol⁻¹)

¹H NMR (300.13 MHz, 300 K, CDCl₃) δ [ppm]: 7.88 (d, J = 8.3 Hz, 2H, CH_{BIAN}), 7.36 (t, J = 7.8 Hz, 2H, CH_{BIAN}), 7.27 (m, 6H, CH_{Dipp}), 6.63 (d, J = 7.2 Hz, 2H, CH_{BIAN}), 3.03 (sept, J = 6.8 Hz, 4H, CH(CH₃)₂), 1.23 (d, J = 6.8 Hz, 12H, CH(CH₃)₂), 0.97 (d, J = 6.8 Hz, 12H, CH(CH₃)₂).

Synthesis of bis[*N,N'*-(2,4,6-trimethylphenyl)imino]acenaphthene (^{Mes}BIAN)

^{Mes}BIAN was synthesized according to a procedure of *Gasperini* and co-workers.^[3]



Acenaphthenone (5.5 g, 30.0 mmol, 1.0 equiv.) and zinc(II)-chloride (10.95 g, 80.3 mmol, 2.7 equiv.) were mixed in 85 mL acetonitrile and stirred for 10 minutes at 60 °C before 2,4,6-trimethylaniline (9.7 mL, 69.2 mmol, 2.3 equiv.) was added to the yellow suspension. The reaction mixture immediately turned orange and was heated to reflux for 45 min. The formed solid was filtered hot and washed with diethyl ether (3 x 50 mL). ^{Mes}BIAN-ZnCl₂ was dried in vacuo and dissolved in 500 mL dichloromethane in a separating funnel. After addition of 150 mL saturated sodium oxalate solution, the mixture was shaken for five minutes until white zinc(II)-oxalate was formed.

The organic phase was separated and dried over magnesium sulfate. After filtration, the solvent was evaporated and ^{Mes}BIAN was obtained as orange powder (9.1 g, 72.9%).

Yield: 9.1 g (21.8 mmol, 73%)

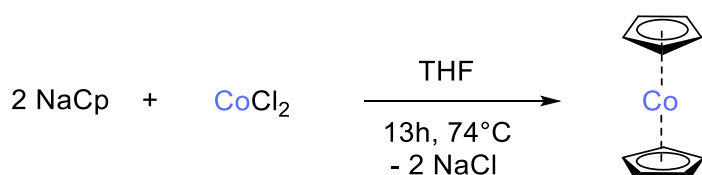
Chemical formula: $C_{30}H_{28}N_2$ (MW = 416.57 g mol⁻¹)

¹H NMR (300.13 MHz, 300 K, CDCl₃) δ [ppm]: 7.89 (d, J = 8.2 Hz, 2H, CH_{BIAN}), 7.36 (dd, J = 8.2 Hz, 7.2 Hz, 2H, CH_{BIAN}), 6.97 (s, 4H, CH_{Ar}), 6.77 (d, J = 7.2 Hz, 2H, CH_{BIAN}), 2.38 (s, 6H, *p*-CH₃), 2.38 (s, 12H, *o*-CH₃)

Synthesis of cobaltocene

Cobaltocene was synthesized according to a procedure of *King* and co-workers.^[4]

Cobalt(II)-chloride (3.0 g, 23.1 mmol, 1 equiv.) was dissolved in 70 mL THF and added dropwise to a solution of sodium cyclopentadienide (4.8 g, 46.2 mmol, 2 equiv.) in 50 mL THF. The resulting mixture was stirred at reflux for 13 h. After cooling to room temperature, the solvent was removed in vacuo. Vacuum sublimation (120°C, 10⁻³ mbar) afforded cobaltocene as purple crystals.

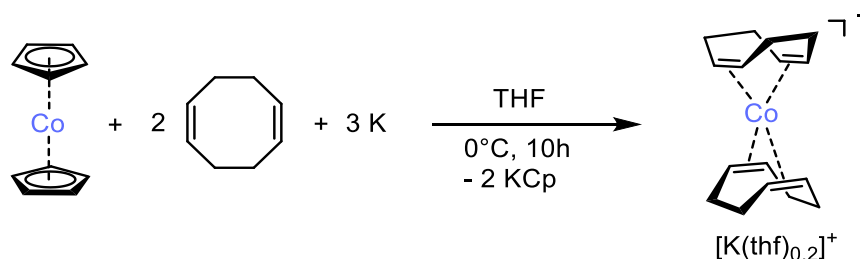


Yield: 1.83 g (9.7 mmol, 42%)

¹H-NMR (300.13 MHz, 300 K, C₆D₆) δ [ppm]: -51.74 (s, 10H, Cp)

Synthesis of potassium-bis(1,5-cyclooctadiene)cobaltate

[K(thf)_{0.2}{Co(η^4 -cod)₂}] was synthesized according to *Jonas* and co-workers.^[5]



Cobaltocene (9.0 g, 47.8 mmol, 1.0 equiv.) and distilled 1,5-cyclooctadiene (17.7 mL, 144 mmol, 3.0 equiv.) were transferred to elemental potassium (7.5 g, 191.8 mmol, 4equiv.) at 0 °C. The reaction mixture was stirred at 0 °C for 10 h with exclusion of light. The reaction mixture turned yellow-brown while stirring. The mixture was stored at -80 °C overnight. Subsequently, the suspension was filtered at -80 °C, the filtrate was concentrated and layered with diethyl ether. Dark yellow

crystals were isolated after four days at -30°C and dried *in vacuo* (7.5 g, 48.0%). The isolated compound may contain a variable amount of THF. This sample contained 0.2 THF molecules per formula unit based on elemental analysis.

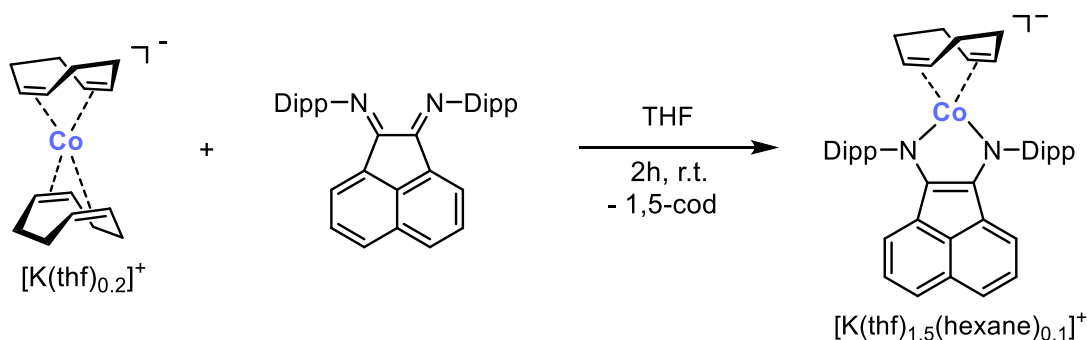
Yield: 7.5 g (22.8 mmol, 48%)

Chemical formula: $\text{C}_6\text{H}_{18}\text{BN}$ (MW = 115.03 g mol^{-1})

$^1\text{H NMR}$ (300.13 MHz, 300 K, THF- d_8) δ [ppm]: 2.20 (s, 16H, cod- CH_2), 1.88 (s, 8H, cod- CH); elemental analysis calcd. for $\text{C}_{16}\text{H}_{24}\text{Co}\cdot(\text{C}_4\text{H}_8\text{O})_{0.2}$ (328.82): C: 61.37 H: 7.85; found: C 61.44 H 7.77

Synthesis of $[\text{K}(\text{thf})_{1.5}\{(\text{DippBIAN})\text{Co}(\eta^4\text{-cod})\}]$

$[\text{K}(\text{thf})_{1.5}\{(\text{DippBIAN})\text{Co}(\eta^4\text{-cod})\}]$ was synthesized by a modified procedure from Wolf and co-workers.^[6]



A solution of DippBIAN (2.0 g, 4.0 mmol, 1.0 equiv.) in 200 mL THF was added to a solution of $[\text{K}(\text{thf})_{0.2}\text{Co}(\eta^4\text{-cod})_2]$ (1.3 g, 4.0 mmol, 1.0 equiv.) in 100 mL THF. An immediate color change to dark green was observed. After stirring the reaction mixture for two hours, the solvent was removed and the residue was washed with 100 mL *n*-hexane. The crude product was dissolved in 100 mL THF and filtered. The filtrate was concentrated and layered with *n*-hexane. Dark green crystals were obtained upon storing for one week (1.39 g, 42%). The crystals still contained 0.1 equiv. of *n*-hexane after drying the crystalline solid *in vacuo* according to $^1\text{H-NMR}$ spectroscopy.

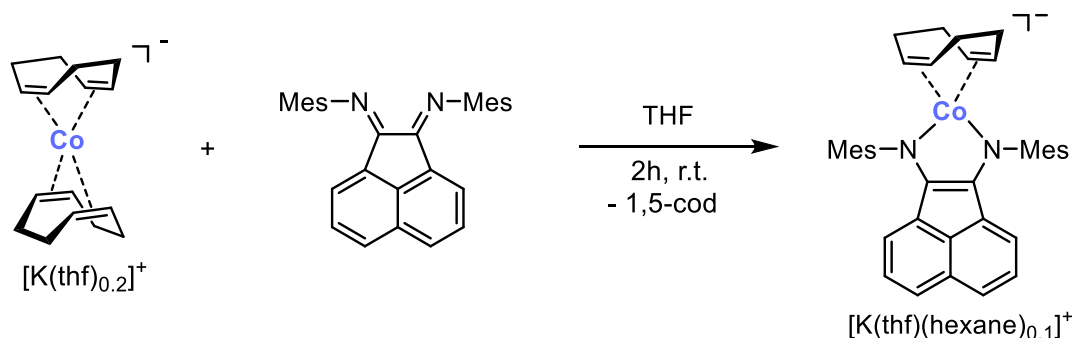
Yield: 1.39 g (1.68 mmol, 42%)

Chemical formula: $C_{44}H_{52}N_2CoK (C_4H_8O)_{1.5} (C_6H_{14})_{0.1}$ (MW = 823.7 g mol⁻¹)

¹H-NMR (300.13 MHz, 300 K, THF-d₈) δ [ppm]: 7.04 (overlapping m, 6H, CH_{Ar}), 6.28 (m, 2H, CH_{BIAN}), 6.18 (m, 2H, CH_{BIAN}), 4.88 (m, 2H, CH_{BIAN}), 4.50 (m, 4H, CH_{Dipp}), 2.91 (m, 4H, cod-CH), 2.34 (m, 4H, cod-CH₂), 1.37 (d, 12H, CH₃), 1.09 (m, 4H, cod-CH₂), 0.95 (d, 12H, CH₃)

Synthesis of [K(thf){(^{Mes}BIAN)Co(η^4 -cod)}]

[K(thf){(^{Mes}BIAN)Co(η^4 -cod)}] was synthesized by a procedure according to Wolf and co-workers.^[6]



A solution of ^{Mes}BIAN (1.15 g, 2.8 mmol, 1.0 equiv.) in 200 mL THF was added to a solution of [K(thf)_{0.2}Co(η^4 -cod)₂] (0.9 g, 2.8 mmol, 1.0 equiv.) in 100 mL THF. An immediate color change to dark green was observed. After stirring the reaction mixture for two hours, the solvent was removed and the residue was washed with 100 mL *n*-hexane. The crude product was dissolved in 40 mL THF and filtered. The filtrate was concentrated and layered with *n*-hexane. Dark green crystals were isolated after storage at room temperature upon storing for one week (0.85 g, 43%). The crystals still contained 0.1 equiv. of *n*-hexane after drying the crystalline solid *in vacuo* according to ¹H-NMR spectroscopy.

Yield: 0.85 g (1.2 mmol, 43%)

Chemical formula: $C_{38}H_{40}N_2CoK (C_4H_8O) (C_6H_{14})_{0.1}$ (MW = 703.51 g mol⁻¹)

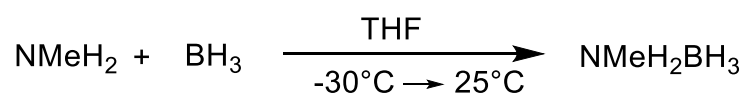
¹H NMR (300.13 MHz, 300 K, THF-d₈) δ [ppm]: 6.08 (m, 4H, CH_{Ar}), 6.28 (m, 2H, CH_{BIAN}), 6.37 (m, 4H, CH_{BIAN}), 5.21 (m, 2H, CH_{BIAN}), 2.65 (m, 4H, cod-CH), 2.45

(m, 12H, *o*-CH₃), 2.33 (m, 4H, *cod*-CH₂), 2.25 (m, 6H, *p*-CH₃), 1.02 (m, 4H, *cod*-CH₂).

5.6.3 Synthesis of amine-boranes

Synthesis of NH₂MeBH₃

N-Methylamine-borane was synthesized according to a procedure of *Fagnou* and co-workers.^[7]



A solution of borane in THF (1 M in THF, 25.0 mL, 25 mmol) was added to a solution of methylamine (2 M in THF, 12.5 mL, 25 mmol) at -30 °C. The reaction mixture was warmed to room temperature and stirred overnight. The solvent was evaporated and the white residue dried *in vacuo*. Sublimation (45 °C, 10⁻³ mbar) afforded a white crystalline solid.

Yield: 600 mg (13.4 mmol, 54%)

Chemical Formula: CH₈BN (MW = 44.92 g mol⁻¹)

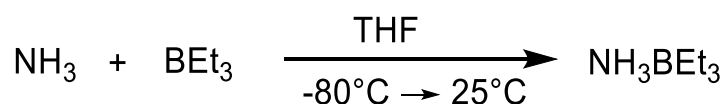
¹H NMR (400.13 MHz, 300 K, THF-d₈) δ [ppm]: 4.47 (br s, 2H, NH₂), 2.28 (t, *J* = 6.0 Hz, CH₃), 1.43 (q, *J* = 96 Hz, BH₃)

¹¹B NMR (124.6 MHz, 300 K, THF-d₈) δ [ppm]: -16.2 (s, 1B)

¹¹B{¹H} NMR (124.6 MHz, 300 K, THF-d₈) δ [ppm]: -16.2 (q, ¹*J*_{BH} = 96 Hz, 1B)

Synthesis of NH₃BEt₃

Ammonia-triethylborane was synthesized according to a procedure of *Guan* and co-workers.^[8]



A solution of triethylborane in THF (1 M, 8 mL, 8 mmol) was added to a solution of ammonia in THF (1 M, 8 mL, 8 mmol) at $-80\text{ }^{\circ}\text{C}$. The reaction mixture was warmed up to room temperature and stirred further for two hours. The solvent was evaporated and a colorless oil was obtained.

Yield: 180 mg (1.6 mmol, 20%)

Chemical formula: $\text{C}_6\text{H}_{18}\text{BN}$ (MW = 115.03 g mol^{-1})

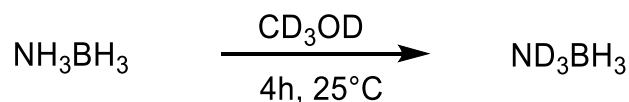
^1H NMR (400.13 MHz, 300 K, C_6D_6) δ [ppm]: 1.00 (br s, 3H, NH_3), 0.89 (t, $J = 7.8\text{ Hz}$, 9H, CH_3), 0.27 (q, $J = 7.8\text{ Hz}$, 6H, CH_2)

^{11}B NMR (93.4 MHz, 300 K, C_6D_6) δ [ppm]: -4.1 (s, 1B)

5.6.4 Synthesis of deuterated amine-boranes

a) ND_3BH_3

N-deuterated ammonia borane (ND_3BH_3) was synthesized according to a procedure of Baker and co-workers.^[9]



Ammonia borane (153 mg, 4.96 mmol) was stirred four hours in 10 mL CD_3OD . After evaporation of the solvent, the residue was dried *in vacuo*. The purity of the compound was ascertained by multinuclear NMR spectroscopy (^1H , ^2H , ^{11}B , and $^{11}\text{B}\{^1\text{H}\}$ NMR). The deuterium content was determined by ^1H NMR spectroscopy using the integrals of residual NH_3BH_3 (0.23) and comparing this with the integral of $\text{N}(\text{D}/\text{H})_3\text{BH}_3$ (2.85). Calculation: $1 - (0.23/2.85) = 0.92 = 92\%$ D-content.

Yield: 120 mg (3.5 mmol, 71%)

Chemical formula: $\text{BH}_3\text{D}_3\text{N}$ (MW = 33.88 g mol^{-1})

^1H NMR (400.13 MHz, 300 K, THF-d_8) δ [ppm]: 1.40 (q, $^1J_{\text{BH}} = 95\text{ Hz}$, 3H)

^2H NMR (400.13 MHz, 300 K, THF-d_8) δ [ppm]: 3.73 (br s, ND_3)

$^{11}\text{B}\{^1\text{H}\}$ NMR (124.6 MHz, 300 K, THF- d_8) δ [ppm]: -22.4 (q, $^1J_{\text{BH}} = 95$ Hz, 1B)

^{11}B NMR (124.6 MHz, 300 K, THF- d_8) δ [ppm]: -22.4 (s, 1B)

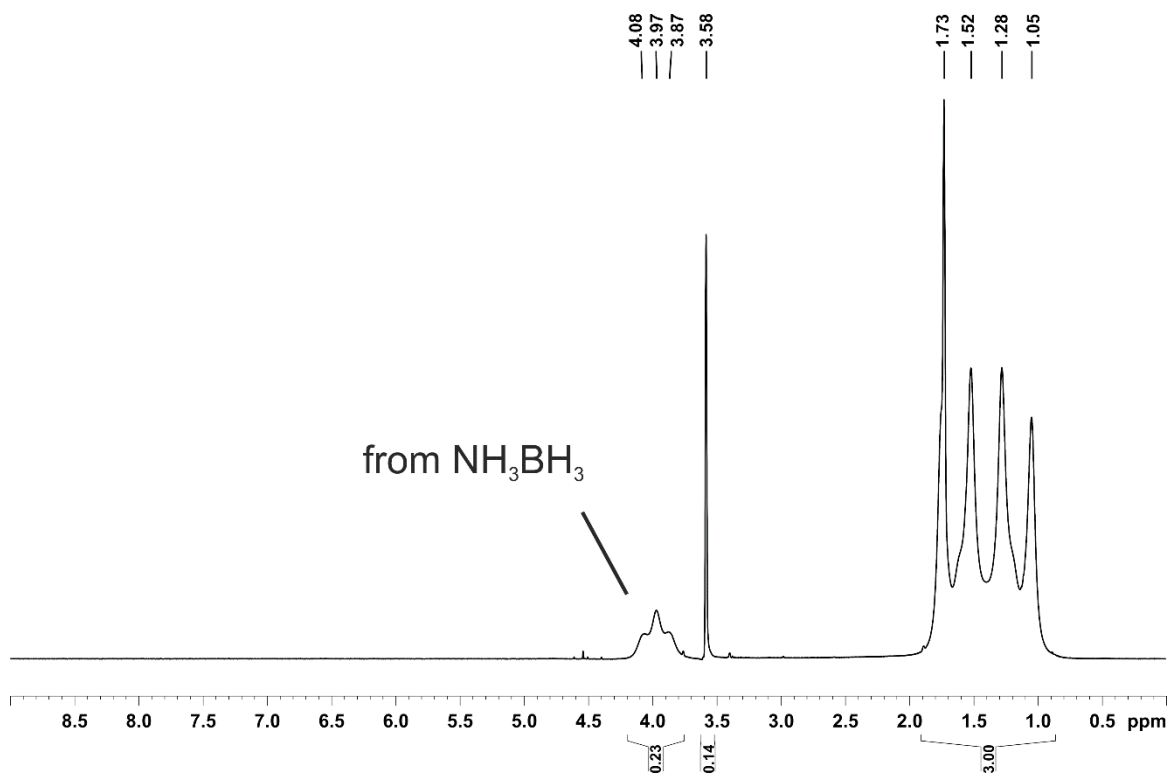


Figure 5.6.1. ^1H -NMR spectrum (400.13 MHz, 300K, THF- d_8) of ND_3BH_3 .

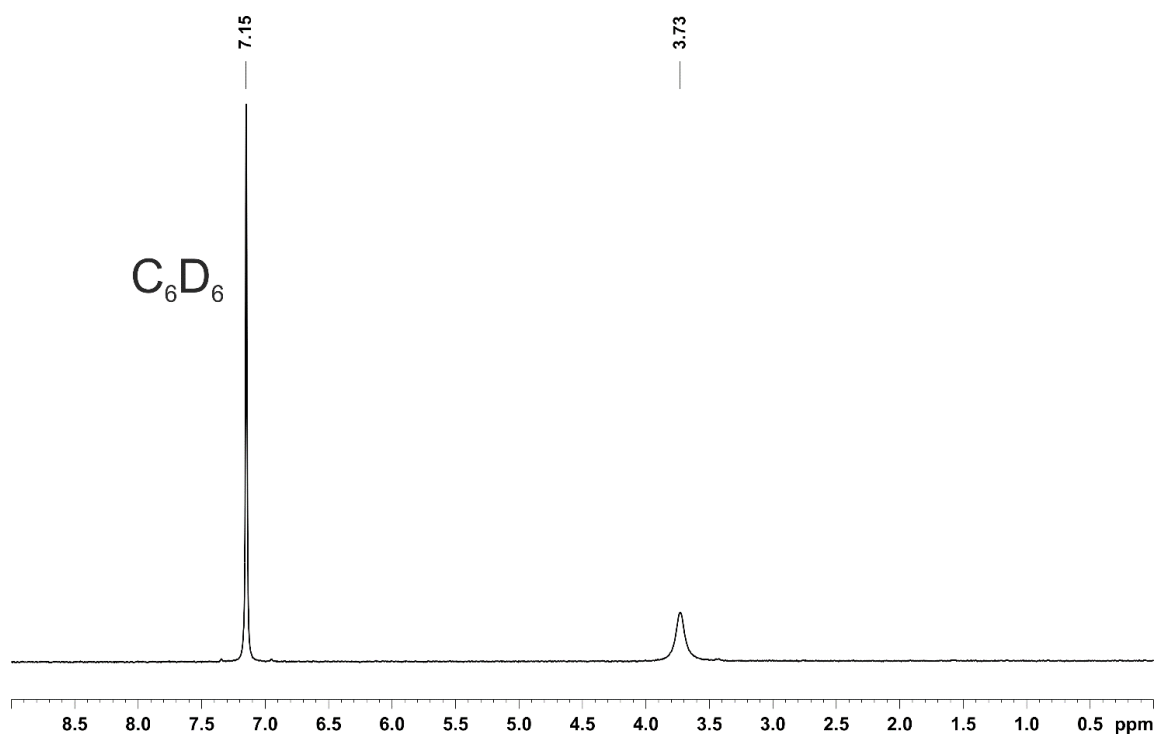


Figure 5.6.2. ^2H -NMR spectrum (128.4 MHz, 300K, THF + 10 μL C_6D_6) of ND_3BH_3 .

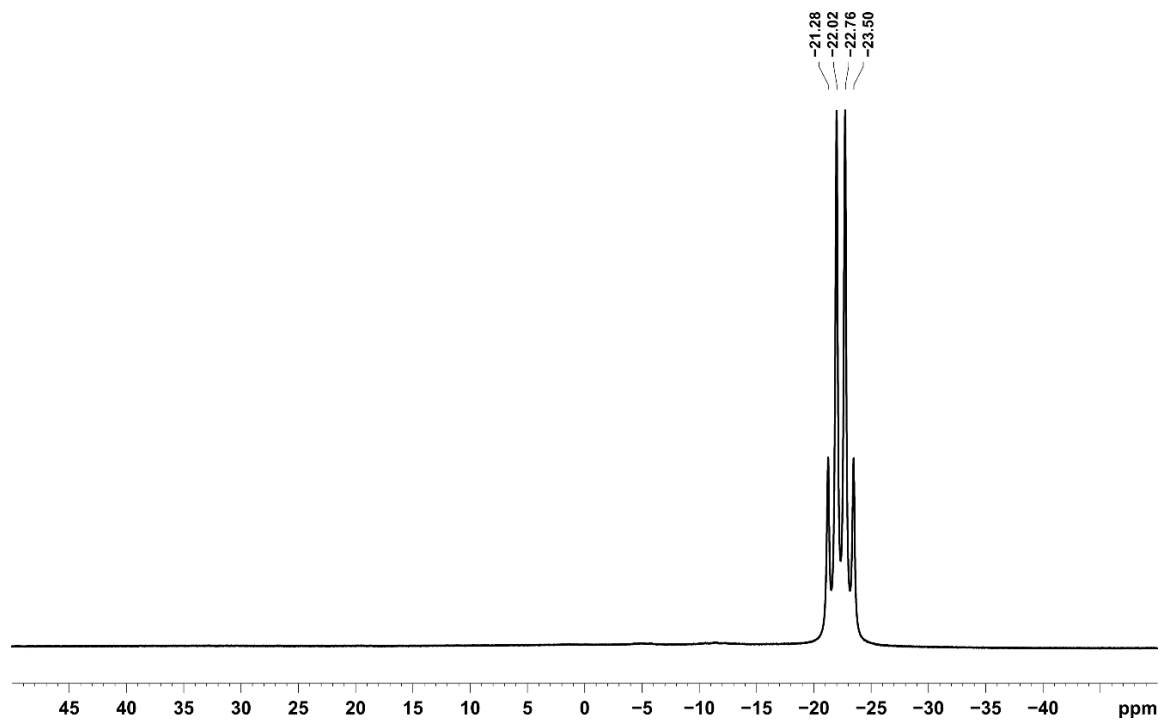


Figure 5.6.3. $^{11}\text{B}\{^1\text{H}\}$ -NMR spectrum (128.4 MHz, 300K, THF- d_8) of ND_3BH_3 .

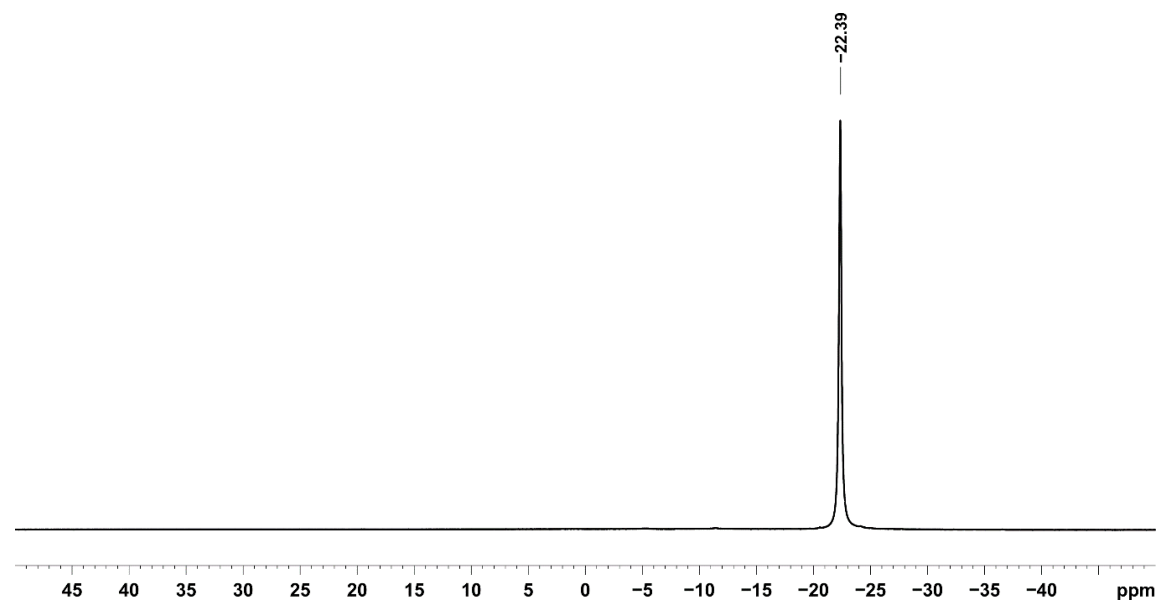
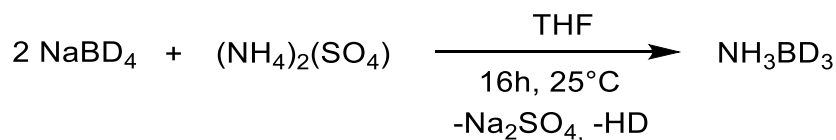


Figure 5.6.4. ^{11}B -NMR spectrum (128.4 MHz, 300K, THF- d_8) of ND_3BH_3 .

b) NH_3BD_3

B-deuterated ammonia borane (NH_3BD_3) was prepared according a procedure of *Ramachandran* and co-workers.^[10]



NaBD_4 (98%-D-content (abcr), 1.0 g, 23.8 mmol, 1.0 equiv.) and ammonium sulfate (3.2 g, 24.2 mmol, 1.02 equiv.) were mixed as solids and dissolved in THF (200 mL). The solution was stirred for 16 h at 40°C. After cooling to room temperature, the suspension was filtered and the solvent evaporated. Sublimation (60°C, 10^{-3} mbar) afforded a white solid. The deuterium content was determined by ^1H NMR spectroscopy using the integrals of residual NH_3BH_3 (0.38) and NH_3BD_3 (3.0). Calculation: $1 - (0.38/3.0) = 0.87 = 87\% \text{NH}_3\text{BD}_3$.

Yield: 300 mg (8.9 mmol, 37%)

Chemical formula: $\text{BH}_3\text{D}_3\text{N}$ (MW = 33.88 g mol⁻¹)

^1H NMR (400.13 MHz, 300 K, THF- d_8) δ [ppm]: 3.95 (m, 3H, NH_3)

^2H NMR (400.13 MHz, 300 K, THF- d_8) δ [ppm]: 1.22 (m, BD_3)

^{11}B NMR (126.4 MHz, 300 K, THF- d_8) δ [ppm]: -22.6 (s, 1B)

$^{11}\text{B}\{^1\text{H}\}$ NMR (126.4 MHz, 300 K, THF- d_8) δ [ppm]: -22.5 (s, 1B)

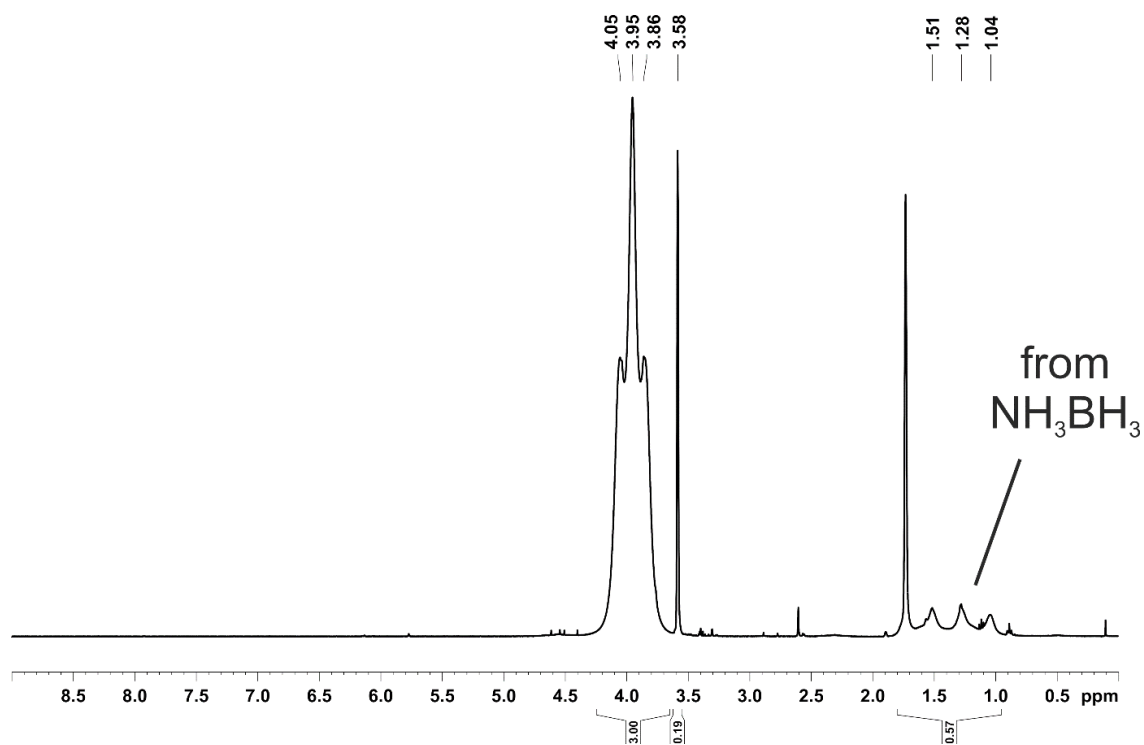


Figure 5.6.5. $^1\text{H-NMR}$ spectrum (400.13 MHz, 300K, THF-d_8) of NH_3BD_3 .

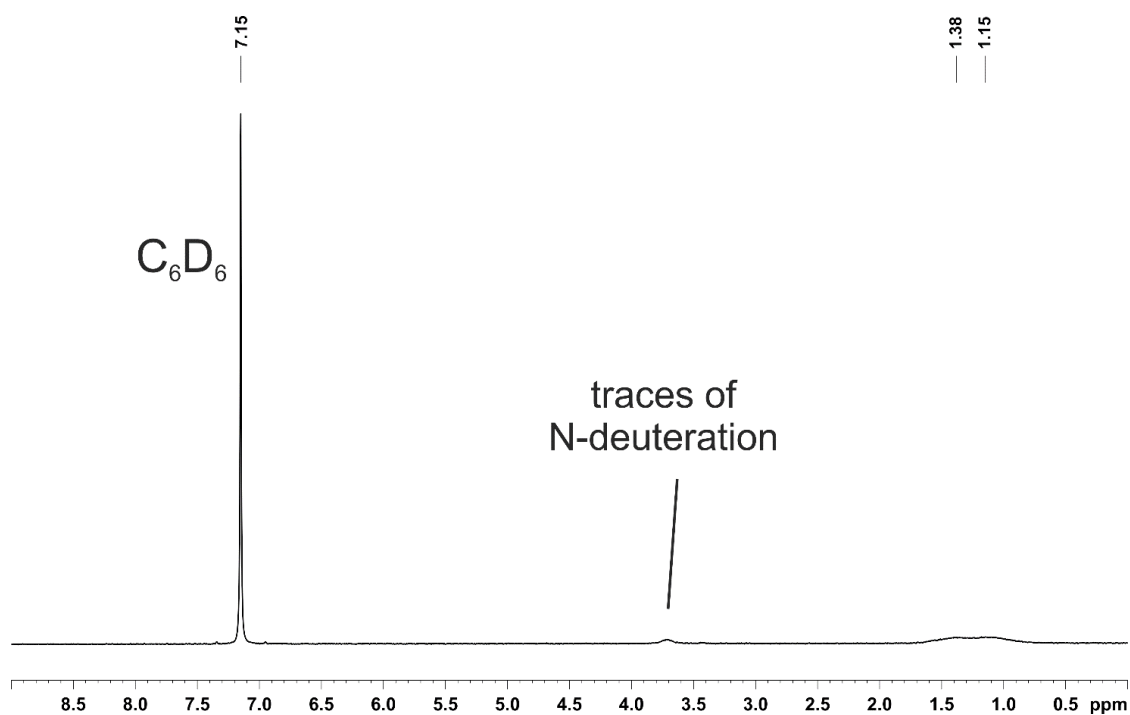


Figure 5.6.6. $^2\text{H-NMR}$ spectrum (128.4 MHz, 300K, $\text{THF} + 10 \mu\text{L C}_6\text{D}_6$) of NH_3BD_3 .

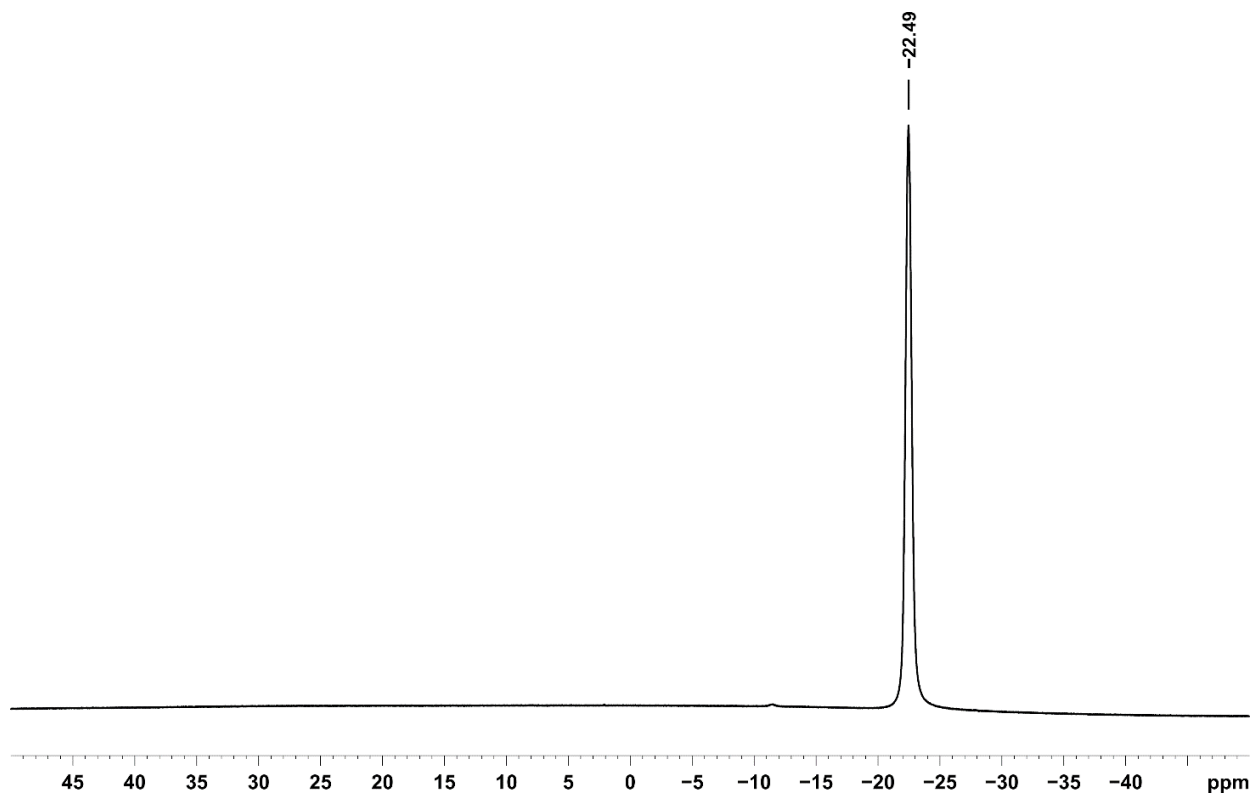


Figure 5.6.7. $^{11}\text{B}\{^1\text{H}\}$ NMR spectrum (128.4 MHz, 300K, THF-d_8) of NH_3BD_3 .

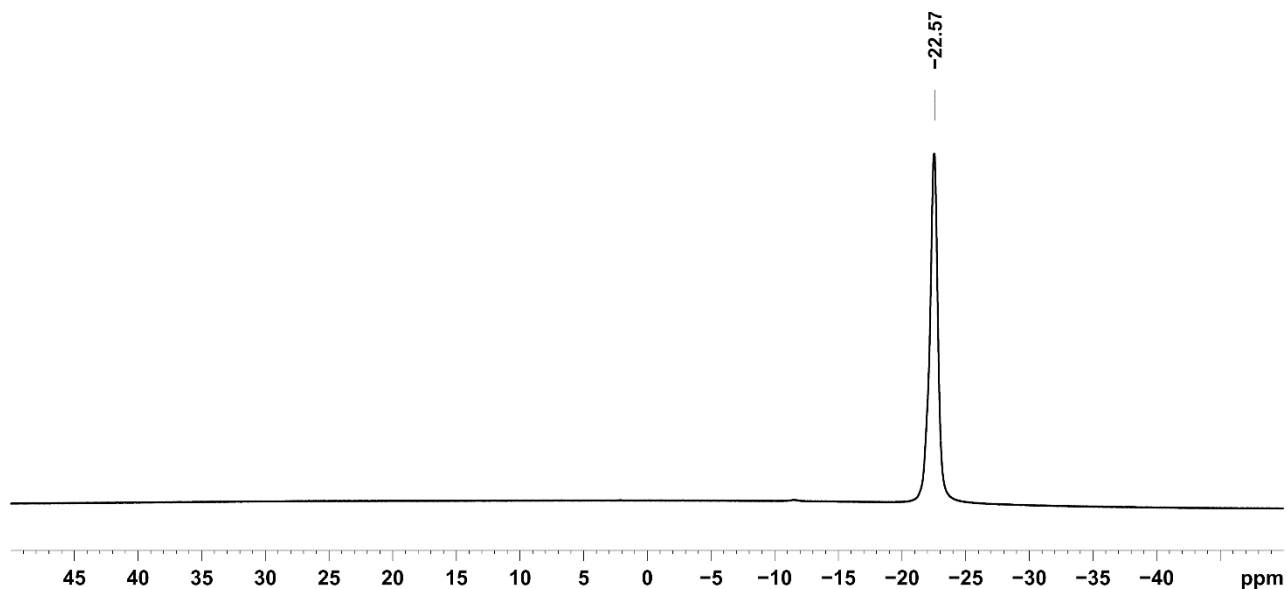
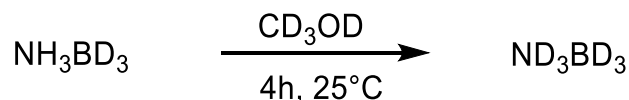


Figure 5.6.8. ^{11}B NMR spectrum (128.4 MHz, 300K, THF-d_8) of NH_3BD_3 .

c) ND₃BD₃

Fully deuterated ammonia borane (ND₃BD₃) was synthesized analogously to ND₃BH₃.^[9]



NH₃BD₃ (145 mg, 4.3 mmol, 87%-D-content) was dissolved in 10 mL CD₃OD and stirred for four hours. After evaporation of the solvent the residue was dried *in vacuo*. The purity of the compound was confirmed by multinuclear NMR-spectroscopy (¹H, ²H, ¹¹B, and ¹¹B{¹H} NMR). The deuterium content was determined by ¹H NMR spectroscopy using the integral of residual NH₃B(H/D)₃ (1.0), Figure S5 and the integral of NH₃B(H/D)₃ (0.03, Figure S5. Calculation: [(1-0.1/3)*0.87] = 0.84 = 84% ND₃BD₃.

Yield: 100 mg (8.9 mmol, 37%)

Chemical formula: BH₃D₃N (MW = 33.88 g mol⁻¹)

¹H NMR (400.13 MHz, 300 K, THF-d₈) δ [ppm]: 3.95 (m, 3H, NH₃)

²H NMR (400.13 MHz, 300 K, THF-d₈) δ [ppm]: 3.73 (br s, ND₃), 1.22 (m, BD₃)

¹¹B NMR (124.6 MHz, 300 K, THF-d₈) δ [ppm]: -22.6 (s, 1B)

¹¹B{¹H} NMR (124.6 MHz, 300 K, THF-d₈) δ [ppm]: -22.5 (s, 1B)

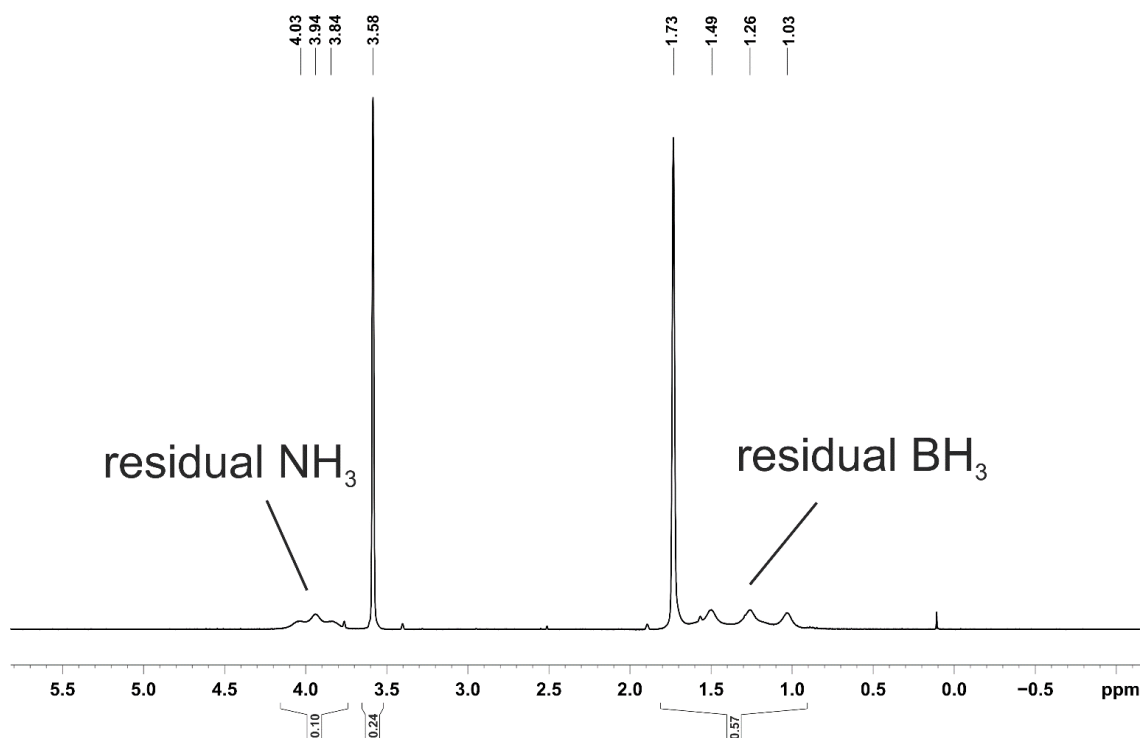


Figure 5.6.9. $^1\text{H-NMR}$ spectrum (400.13 MHz, 300K, THF-d_8) of ND_3BD_3 .

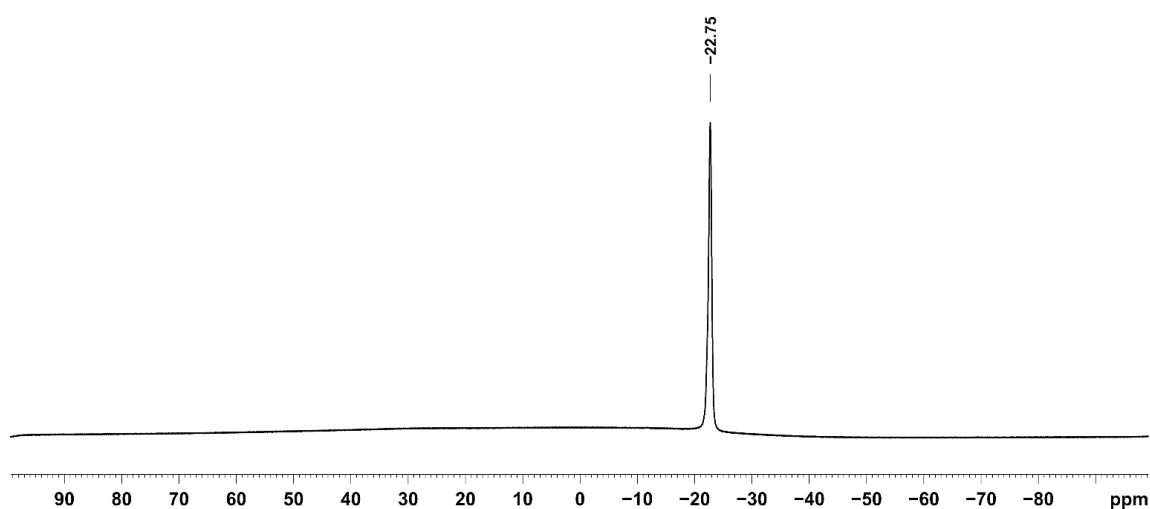


Figure 5.6.10. $^{11}\text{B-NMR}$ spectrum (128.4 MHz, 300K, THF-d_8) of ND_3BD_3 .

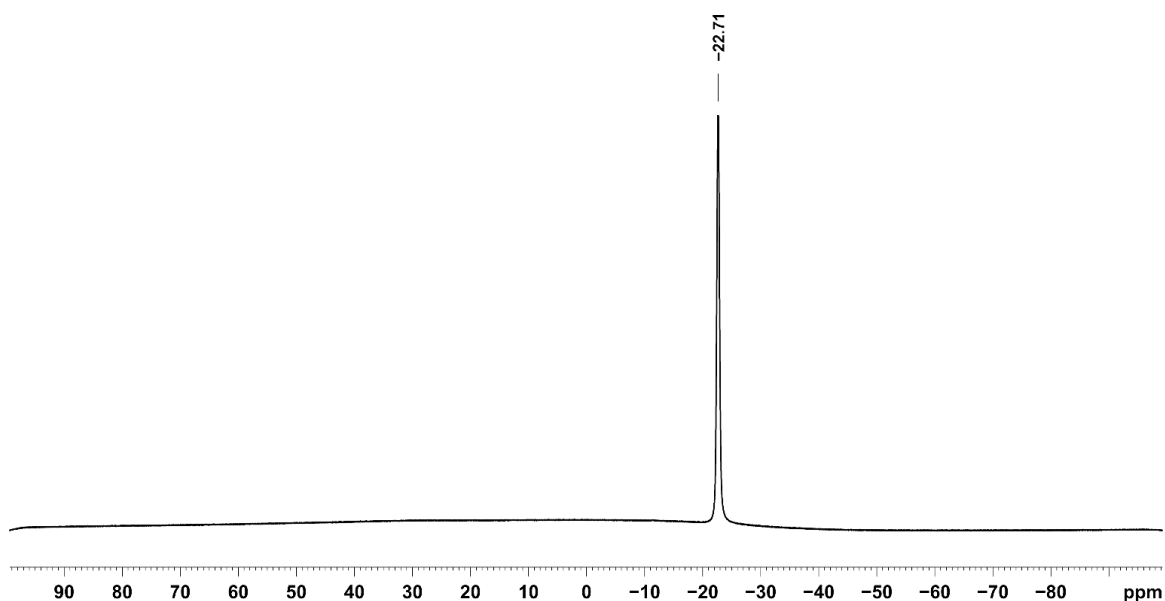


Figure 5.6.11. $^{11}\text{B}\{^1\text{H}\}$ -NMR spectrum (128.4 MHz, 300K, THF- d_8) of ND_3BD_3 .

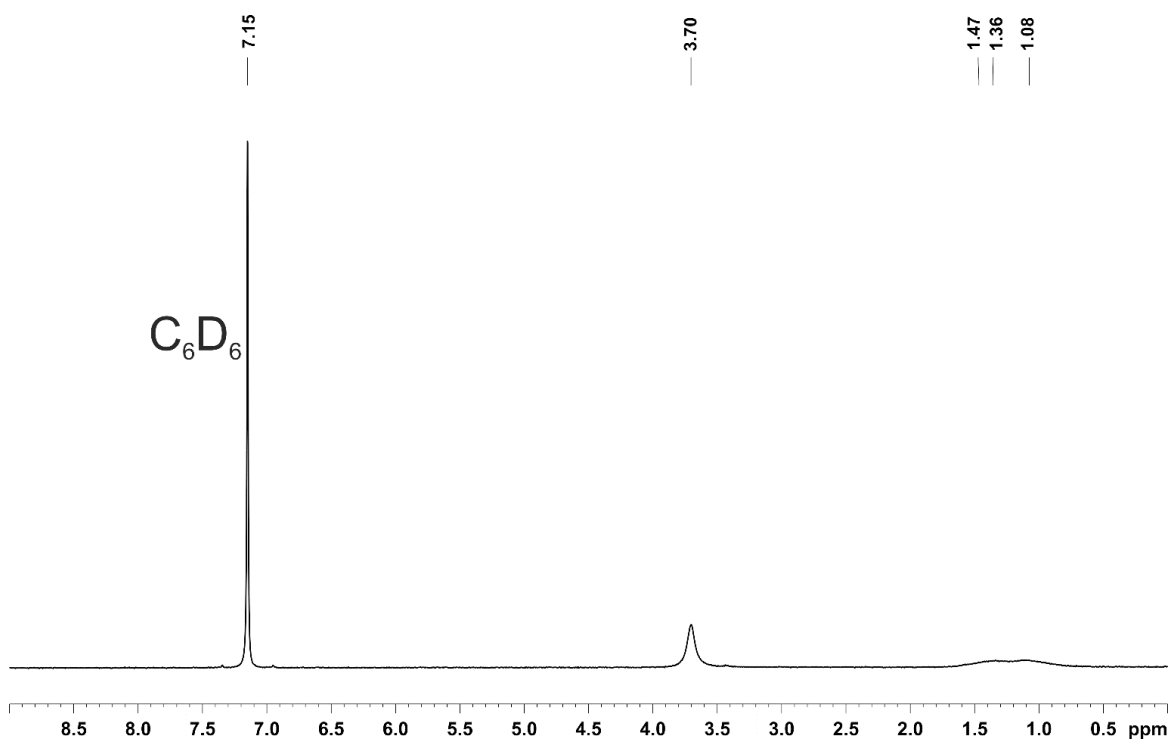


Figure 5.6.12. ^2H -NMR spectrum (128.4 MHz, 300K, THF + 10 μL C_6D_6) of ND_3BD_3 .

5.6.5 Synthesis of substrates

p- CF_3 - α -methylstyrene, *p*-OMe- α -methylstyrene, 1-phenylcyclopentene, 1-phenylcyclohexene were synthesized according to literature procedures. All

other olefinic substrates were purchased by commercial suppliers, and in case of liquids distilled prior to use.

5.6.6 Synthesis of poisoning agents

Mercury (Hg) and trimethylphosphite were received commercially. Trimethylphosphite was distilled prior to use. Both liquids were deaerated by three freeze-pump-thaw cycles. Dibenzo[*a,e*]cyclooctatetraene was synthesized in three steps according to procedures of *Wudl* and co-workers,^[11] and *Hartwig* and co-workers (step 2 & 3).^[12]

Step 1:



5-Dibenzosuberone (2.91 g, 14.1 mmol, 1.0 equiv.) was dissolved in 20 mL DCM in a 2-necked flask containing a nitrogen bubbler and a dropping funnel. Boron trifluoride etherate complex (2.67 mL, 21.0 mmol, 1.5 equiv.) was added at -10°C to the solution, which led to an immediate colour change to yellow. Trimethylsilyldiazomethane (2.0 M in diethylether, 105 mL, 21.0 mmol, 1.5 equiv.) was dissolved in DCM (25 mL) and added dropwise over 1 h at -10°C . The reaction mixture was stirred for additional 2 h at -10°C . The mixture was poured into ice and the organic phase was separated. The aqueous phase was extracted twice with DCM (100 mL) and the organic phases were combined. After washing with brine (80 mL), the organic phase was dried over MgSO_4 . The solvent was evaporated and a yellow oil was obtained. The crude product was purified by column chromatography (SiO_2 (20 cm); *n*-hexane/ethylacetate 10:1; $R_f = 0.4$). 6*H*-Dibenzo[*a,e*]cyclooctatrien-5-one was obtained as white to light yellow solid.

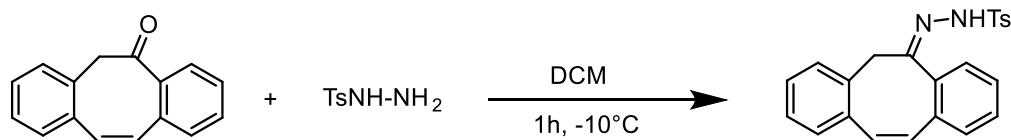
Yield: 1.60 g (7.3 mmol, 52%)

Chemical Formula: $\text{C}_{12}\text{H}_{12}\text{O}$ (MW = 220.27 g mol⁻¹)

5 Amine-Borane Dehydrogenation and Transfer Hydrogenation Catalyzed by α -Diimine Cobaltates

$^1\text{H NMR}$ (300.13 MHz, 300 K, CDCl_3) δ [ppm]: 78.29 (dd, $J = 8.0$ Hz, 1.0 Hz, 1H), 7.53-7.20 (m, 7H, CH_{Ar}), 7.05 (d, $J = 2.8$ Hz, 2H), $\text{CH}_{\text{alkene}}$), 4.08 (s, 2H, CH_2)

Step 2:

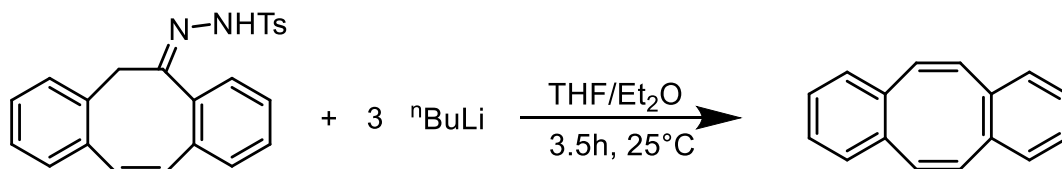


6*H*-Dibenzo[*a,e*]cyclooctatrien-5-on (0.55 g, 2.4 mmol, 1.0 equiv.) and tosylhydrazine (0.49 g, 2.6 mmol, 1.1 equiv.) were dissolved in ethanol (15 mL). After addition of 3 drops of concentrated hydrochloric acid, the suspension was stirred for 22 h. A white solid was received after filtration and dried in vacuo. This compound was used in the next step without further purification.

Yield: 1.60 g (7.3 mmol, 52%)

Chemical Formula: $\text{C}_{23}\text{H}_{12}\text{N}_2\text{O}_2\text{S}$ (MW = 388.49 g mol⁻¹)

Step 3:



The corresponding hydrazone (1.5 g, 3.9 mmol, 1.0 equiv.) was suspended in a mixture of THF/Et₂O (100 mL, 1:3). *n*-Butyllithium (2.5 M in hexane; 4.6 mL, 11.6 mmol, 3.0 equiv.) was added dropwise. The reaction mixture turned red and was stirred for 3.5 h (product formation was checked via TLC). A saturated solution of ammonium chloride (15 mL) was added to the solution, which lead to a yellow solution. After phase separation, the aqueous phase was washed with ethylacetate (2x15 mL). The organic phases were combined and dried over Na₂SO₄. A yellow oil was obtained after evaporation of the solvent. The crude product was purified by column chromatography (SiO₂ (20 cm); *n*-hexane; R_f = 0.25). Dibenzo[*a,e*]cyclooctatetraene was obtained as a white solid.

Yield: 380 mg (1.9 mmol, 49%)

Chemical Formula: C₁₆H₁₂ (MW = 204.27 g mol⁻¹)

¹H NMR (300.13 MHz, 300 K, CDCl₃) δ [ppm]: 7.17 (m, 4H, CH_{Ar}), 7.08 (m, 1H, CH_{Ar}), 6.77 (s, 1H, CH_{alkene})

5.6.7 Dehydrogenation reactions

Gas evolution measurements

Gas evolution measurements were done with *Man on the Moon X103* kit (see General Information). Every 0.3s a datapoint (time, pressure) was generated. Curves were smoothed manually.

In amine-borane dehydrogenation experiments a solution of the catalyst in THF (0.5 mL) was added with a syringe first. The pressure inside the reaction vessel was set to 0 mbar before a solution of amine-borane (0.2 mmol) in THF (0.5 mL) was added with a syringe. The resulting pressure was recorded over time.

1) Dimethylamine-borane (NMe₂HBH₃)

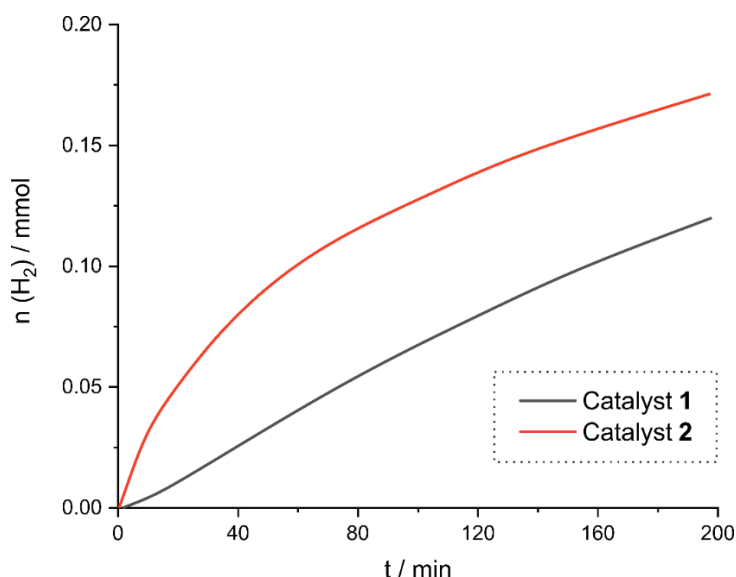


Figure 5.6.13. Time-dependent formation of H₂ from the dehydrogenation of dimethylamine-borane (200 mM) with **1** (10 mM, black curve) and **2** (10 mM, red curve).

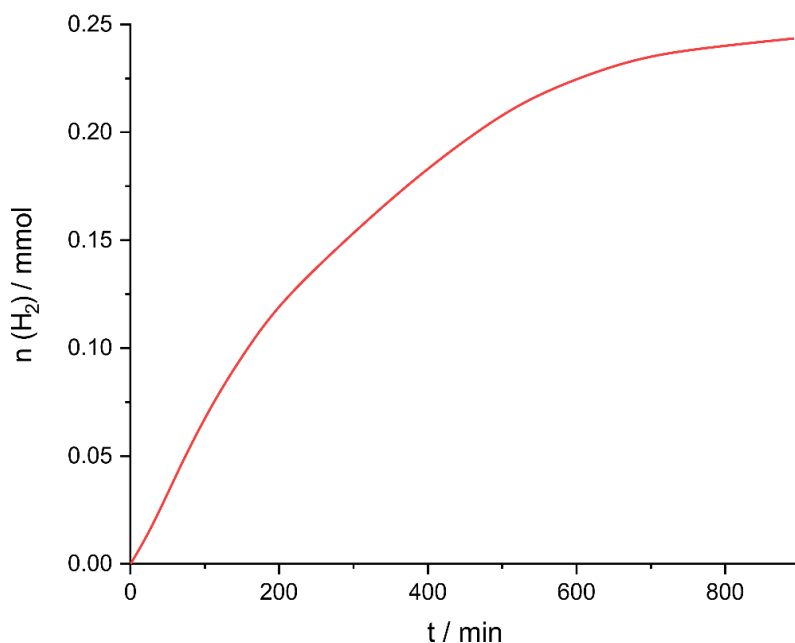


Figure 5.6.14. Time-dependent formation of hydrogenation from the dehydrogenation of dimethylamine-borane (200 mM) with catalysts 1 (10 mM).

2) Methylamine-borane (NMeH_2BH_3)

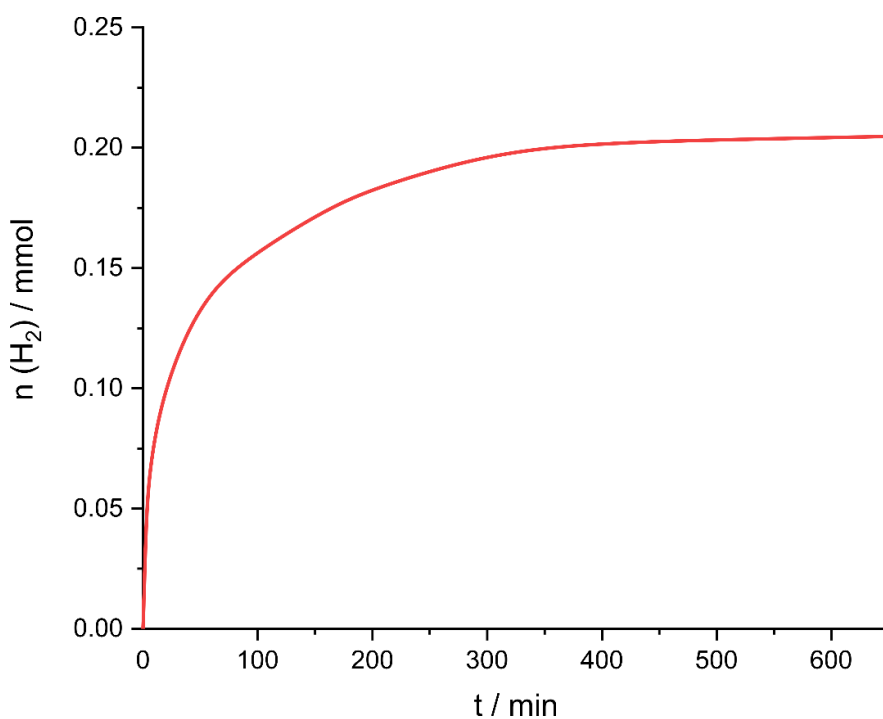


Figure 5.6.15. Time-dependent formation of hydrogenation from the dehydrogenation of methylamine-borane (200 mM) with catalyst 1.

3) Ammonia-borane (NH_3BH_3)

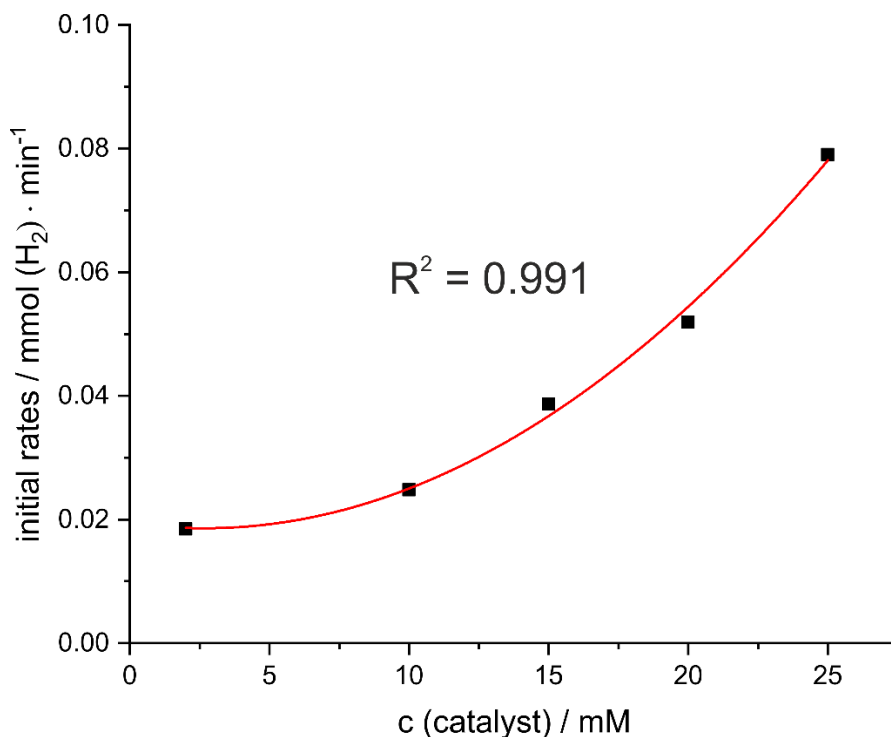


Figure 5.6.16. Initial rates of hydrogenation formation from dehydrogenation of ammonia-borane (200 mM) vs. catalyst **1** concentration.

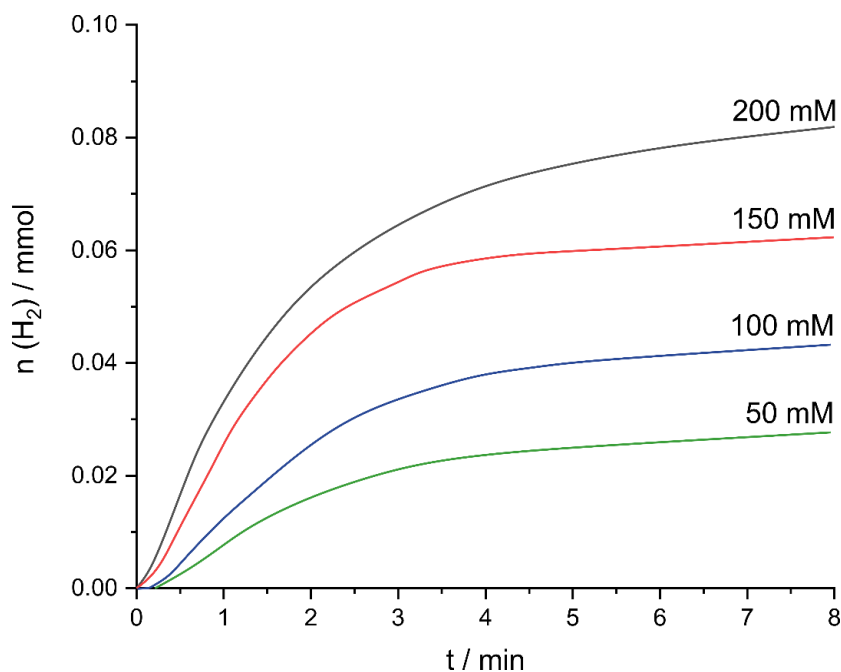


Figure 5.6.17. Time-dependent dihydrogen formation from the dehydrogenation of ammonia-borane catalysed by **1** (10 mM) and different ammonia-borane concentrations.

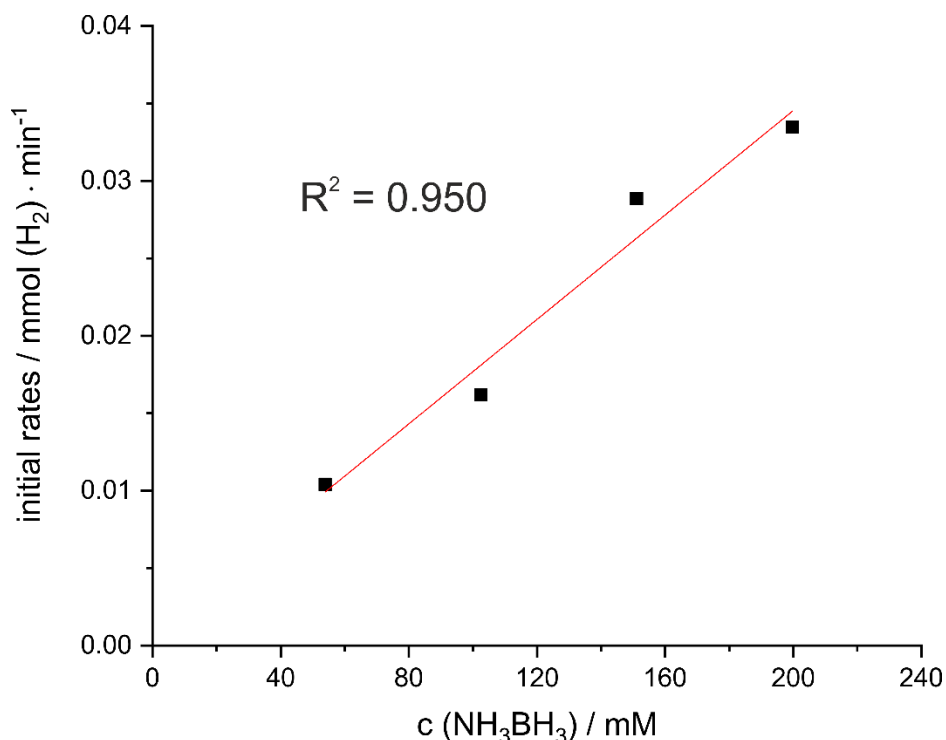


Figure 5.6.18. Initial rates of dihydrogen formation from dehydrogenation of ammonia-borane catalyzed by **1** (10 mM) vs. ammonia-borane concentration.

NMR analysis

Kinetic analysis of NMe₂HBH₃ dehydrogenation

¹¹B-NMR spectra for the kinetic analysis of the dehydrogenation of dimethylaminborane were recorded with a *Bruker 500 MHz Ascend* NMR spectrometer with a *Prodigy CryoProbe*. In an argon-filled glovebox dimethylaminborane was dissolved in 2.5 mL THF and added dropwise to a solution of the catalyst in 2.5 mL THF. The reaction mixture was stirred at room temperature. After defined times an aliquot of 0.2 mL was taken, and diluted with 0.4 mL THF, and subsequently analyzed by NMR spectroscopy.

Dehydrogenation of NⁱPr₂HBH₃

Catalyst **1** (9.7 mg, 0.012 mmol) was dissolved in 0.2 mL THF and NⁱPr₂HBH₃ (27.0 mg, 0.23 mmol) in 0.5 mL THF. The amine-borane solution was added to the catalyst. The solution was stirred for 72 h at room temperature and after addition

of a few drops C_6D_6 transferred in a quartz NMR tube and analyzed by ^{11}B -NMR spectroscopy.

Dehydrogenation of $NMeH_2BH_3$

Catalyst **1** (8.2 mg, 0.01 mmol) was dissolved in 0.2 mL THF and $NMeH_2BH_3$ (9.0 mg, 0.2 mmol) in 0.6 mL THF. The amine-borane solution was added to the catalyst. The solution was stirred for 30 h at room temperature and after addition of a few drops C_6D_6 transferred in a quartz NMR tube and analyzed by ^{11}B NMR spectroscopy.

ESI-MS analysis of $NMeH_2BH_3$ dehydrogenation

Catalyst **1** (8.2 mg, 0.01 mmol) was dissolved in 0.2 mL DME and $NMeH_2BH_3$ (9.0 mg, 0.2 mmol) in 0.6 mL DME. The amine-borane solution was added to the catalyst. The solution was stirred for 24 h at room temperature. After that the solution was filtered two times, diluted with DME, and subsequently analyzed by ESI-MS.

Units of $[-BH_2-NHMe-]_n$ from $n=4$ to $n=11$ can be observed (negative fragmentator potential -120 V). Using a positive fragmentator potential (120 V), $^{Dipp}BIAN$ (exact mass = 500.32 Da) could be identified as the main species. Addition of formic acid lead to the observation of oligomer peaks. $\Delta m/z = 43$).

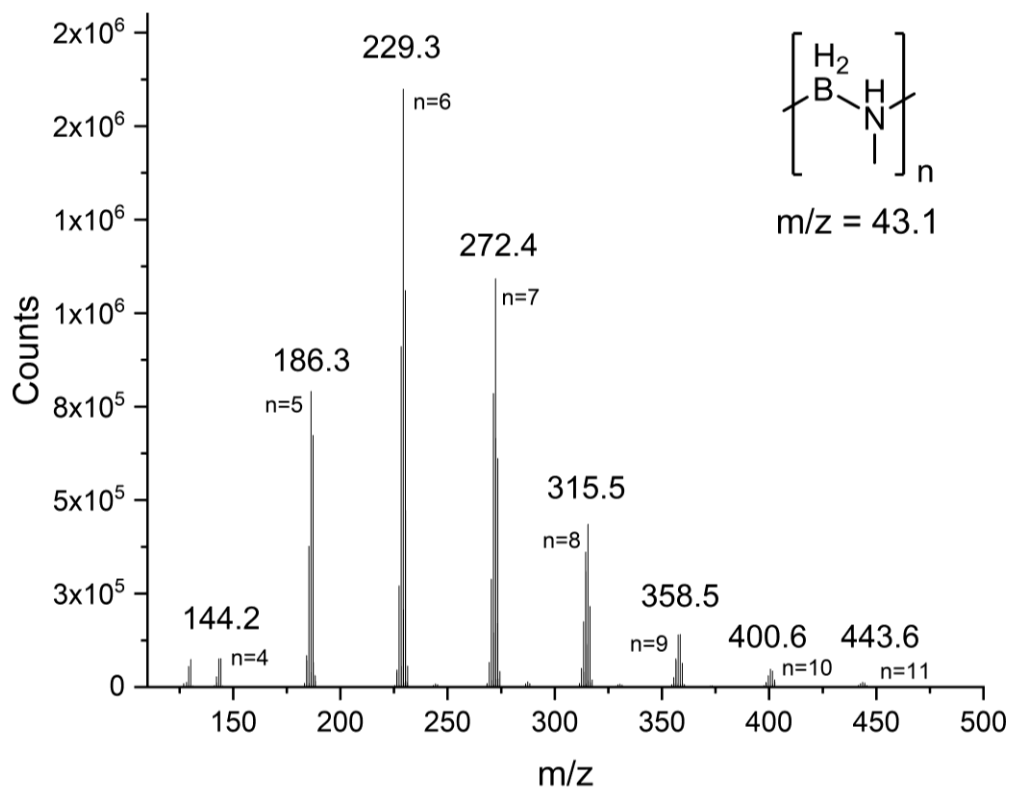


Figure 5.6.19. ESI-Scan (rt: 0.445-0.669 min, 28 scans) Frag=-120.0V.

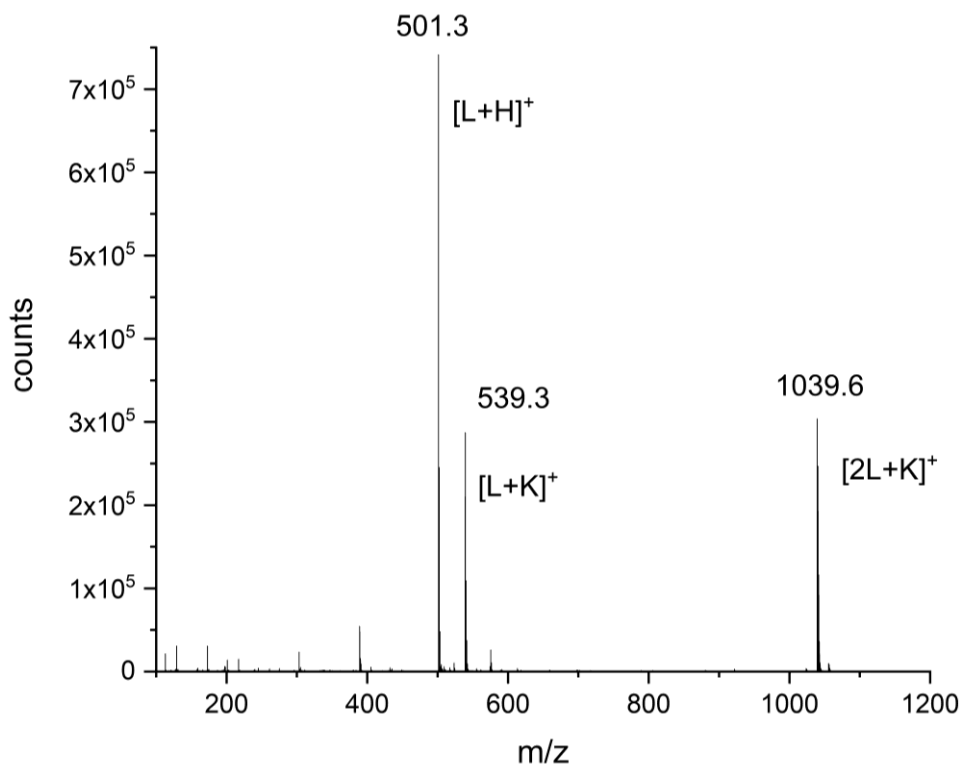


Figure 5.6.20. ESI-Scan (retention time: 0.907-1.389 min, 59 scans) Frag=+120.0V; L=ligand DippBIAN (exact mass = 500.32 Da), K = potassium.

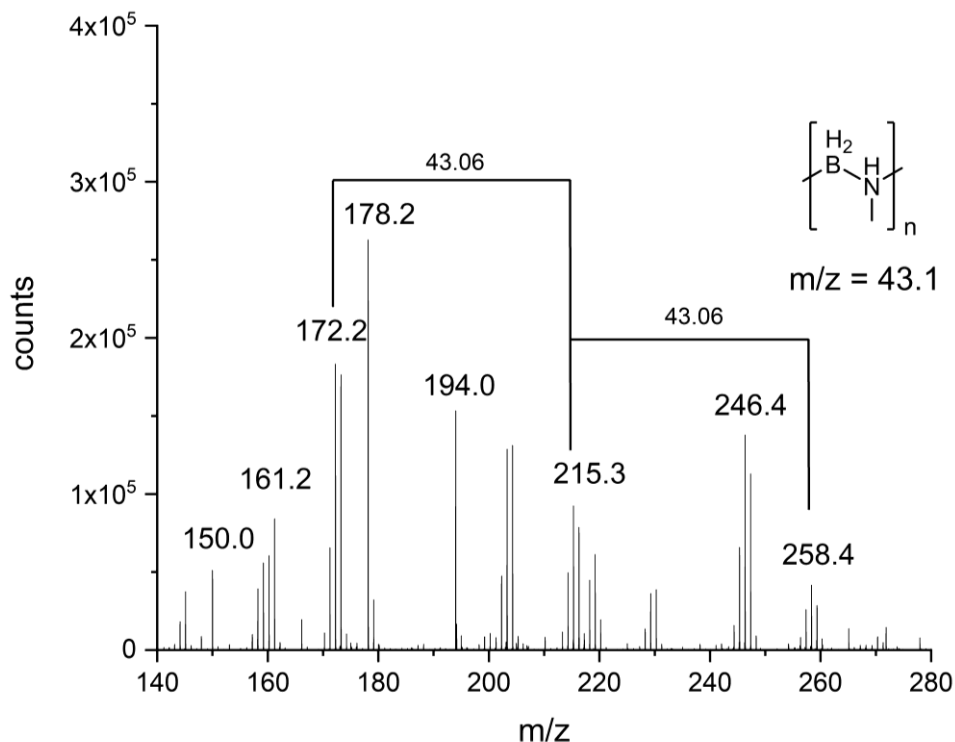


Figure 5.6.21. ESI-Scan (rt: 0.188-0.536 min, 22 scans) Frag=+120.0V, add. of 0.1% HCOOH.

Dehydrogenation of NH_3BH_3

Catalyst **1** (13.3 mg, 0.016 mmol) was dissolved in 0.3 mL THF and NH_3BH_3 (9.6 mg, 0.31 mmol) in 0.3 mL THF. NH_3BH_3 was added to the catalyst. The solution turned dark and was stirred for 40 min. After addition of a few drops of C_6D_6 , the reaction mixture was analyzed by ^{11}B -NMR spectroscopy. The signals were assigned based on the work of *Schneider* and co-workers.^[13]

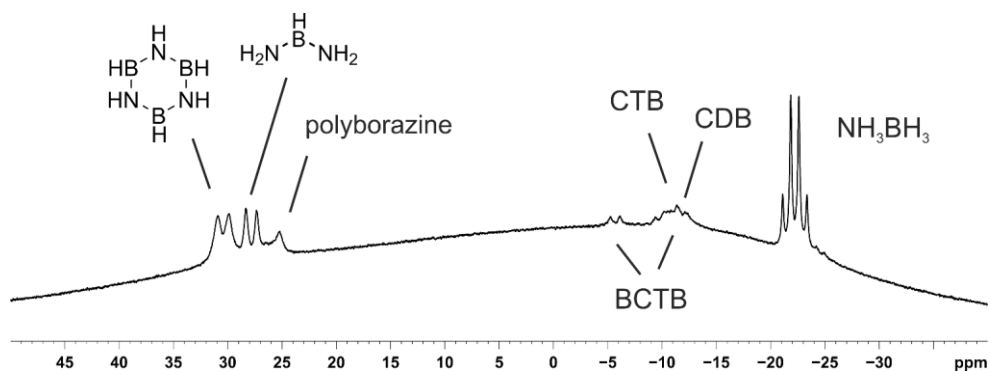


Figure 5.6.22. ^{11}B -NMR spectrum of NH_3BH_3 dehydrogenation catalyzed by **1** after 40 min (CTB = cyclotriaminoborane, CDB = cyclodiaminoborane, BCTB = $\text{H}_3\text{NBHNNH}_2$ -cyclo- $\text{B}_3\text{N}_3\text{H}_{11}$).

Catalyst **1** (13.8 mg, 0.017 mmol) was dissolved in 0.3 mL THF and NH_3BH_3 (10.6 mg, 0.34 mmol) in 0.3 mL THF. NH_3BH_3 was added to the catalyst. The solution turned dark and was stirred for 24 h. After addition of a few drops C_6D_6 , the reaction mixture was analyzed by ^{11}B -NMR spectroscopy.

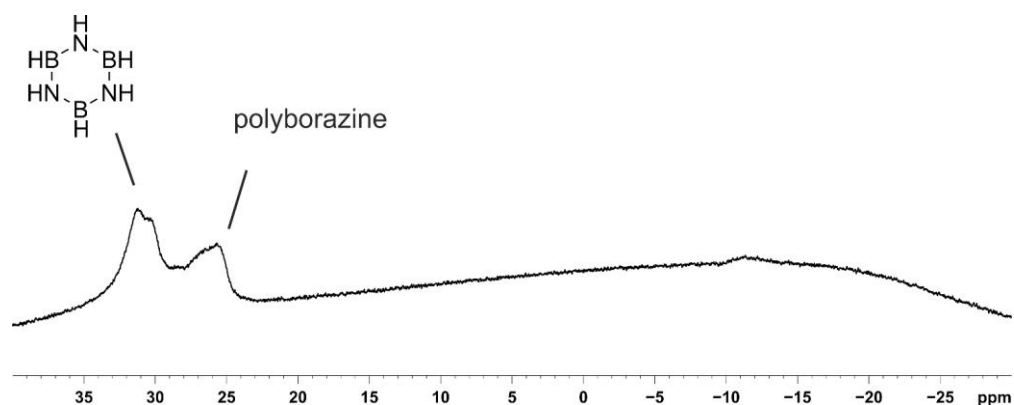


Figure 5.6.23. ^{11}B -NMR spectrum of NH_3BH_3 dehydrogenation catalyzed by **1** after 24 h.

Isolation of Polyaminoborane from NH_3BH_3 dehydrogenation

NH_3BH_3 (76.5 mg, 2.5 mmol) in 5 mL THF was added to catalyst **1** [$\text{K}(\text{Et}_2\text{O})_{0.1}\{(\text{DippBIAN})\text{Co}(\text{cod})\}$] (96.5 mg, 0.12 mmol) in 5 mL THF. During the reaction, the flask was depressurized briefly by opening the schlenk tube for a moment. After 24 h, the reaction was filtered and the black residue washed with THF, *n*-hexane, and DME. Addition of aqueous HCl lead to a colour change to white. The white residue (25 mg) was washed several times with Et_2O and dried *in vacuo*. The resulting powder was analyzed by IR-spectroscopy and ^{11}B -MAS.

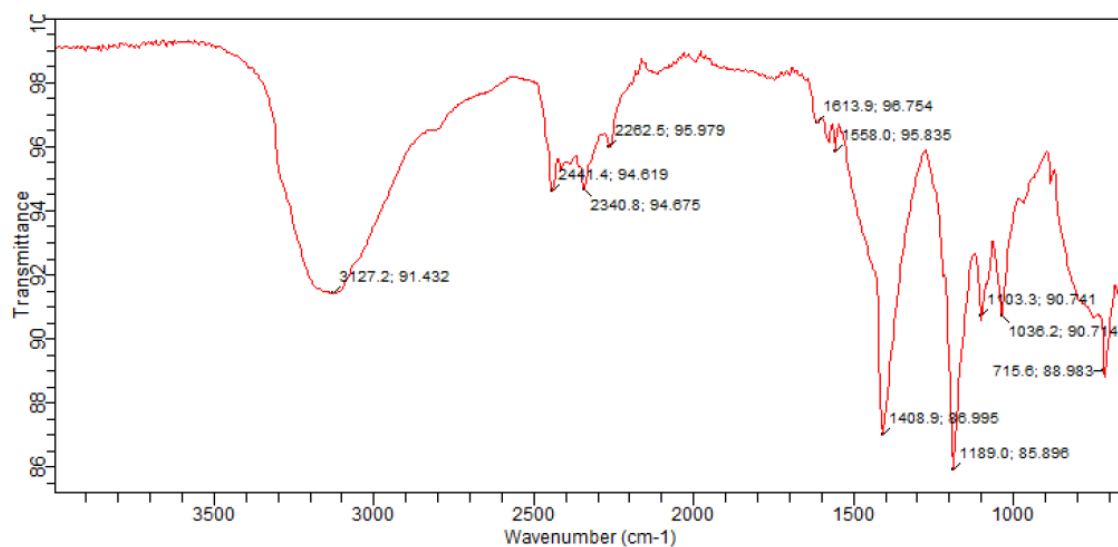


Figure 5.6.24. IR-spectra of obtained polyaminoborane.

Reaction of NMe_3BH_3 with catalyst **1** [$\text{K}(\text{thf})_{1.5}\{(\text{DippBIAN})\text{Co}(\eta^4\text{-cod})\}$]

Catalyst **1** (12.4 mg, 0.015 mmol) in 0.5 mL THF was added to NMe_3BH_3 (21.9 mg, 0.3 mmol) in 0.3 mL THF. No colour change was observed. After stirring for 19 h, and addition of a few drops C_6D_6 , the reaction mixture was analyzed by ^{11}B -NMR spectroscopy.

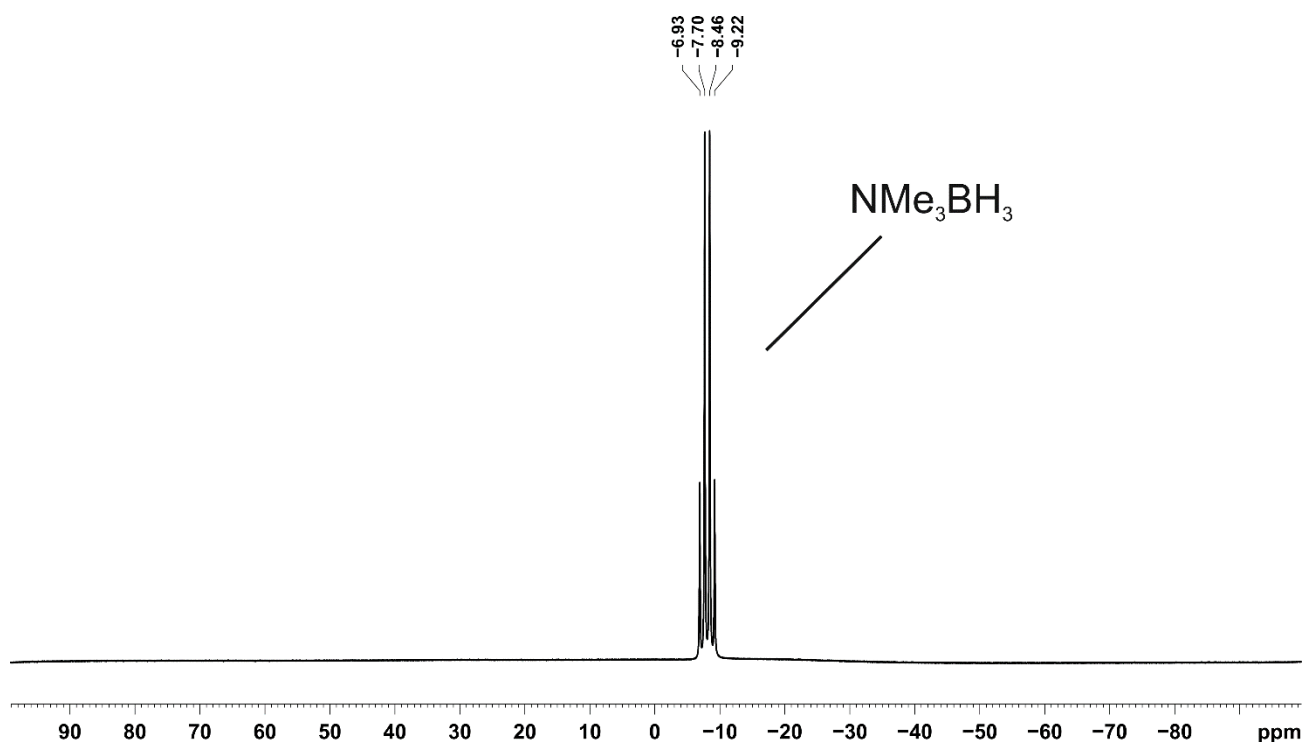


Figure 5.6.25. ^{11}B -NMR spectrum of a reaction mixture of NMe_3BH_3 and **1**.

Reaction of NH_3BEt_3 with catalyst $[\text{K}(\text{thf})_{1.5}\{(\text{DippBIAN})\text{Co}(\eta^4\text{-cod})\}]$ (**1**)

Catalyst **1** (6.2 mg, 0.008 mmol) in 0.3 mL THF was added to NH_3BEt_3 (15.2 mg, 0.13 mmol) in 0.3 mL THF. The reaction mixture slightly brownish and was stirred for further 20 h. After addition of a few drops C_6D_6 , the solution was analyzed by ^{11}B -NMR spectroscopy.

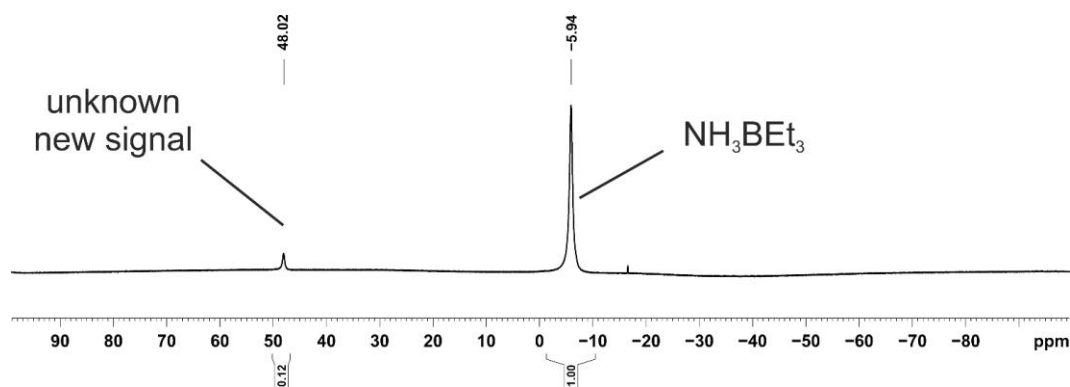


Figure 5.6.26. ^{11}B -NMR spectrum of a reaction mixture of NH_3BEt_3 and **1**.

Dehydrogenation cross experiment with NH_3BEt_3 and NMe_3BH_3

Catalyst **1** (12.4 mg, 0.015 mmol) in 0.5 mL THF was added to a solution of NMe_3BH_3 (22.1 mg, 0.3 mmol) and NH_3BEt_3 (39.0 mg, 0.34 mmol) in 0.3 mL THF. The color of the reaction turned slightly lighter. The mixture was stirred for 19 h. After addition of a few drops C_6D_6 , the solution was analyzed by ^{11}B -NMR spectroscopy.

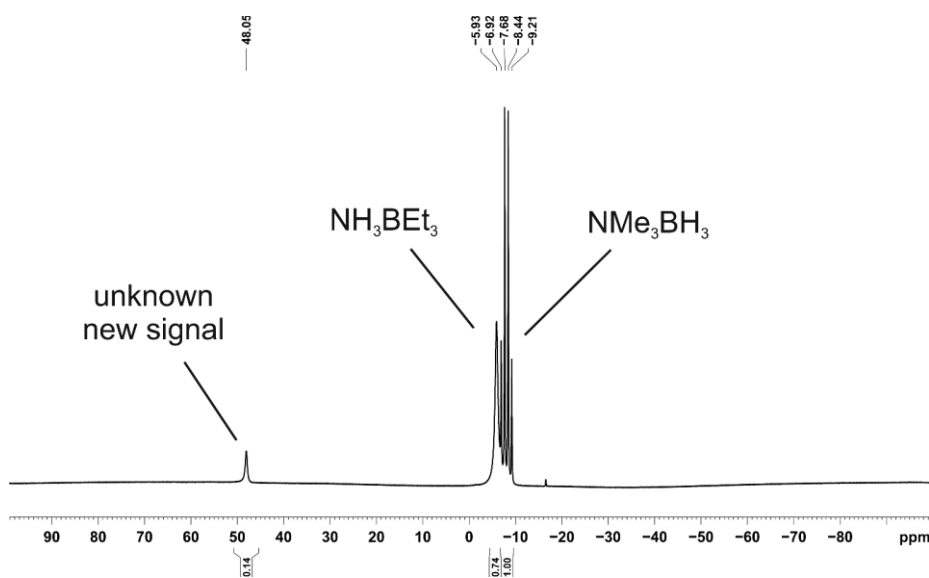


Figure 5.6.27. ^{11}B -NMR spectrum of a reaction mixture of NMe_3BH_3 , NH_3BEt_3 and **1**.

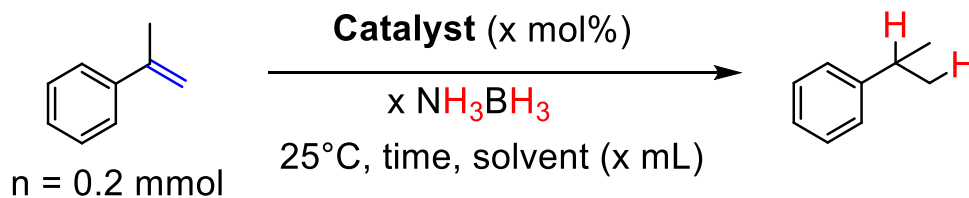
5.6.8 Transfer hydrogenation reactions

General procedure

Under an atmosphere of argon, a 5 mL screw cap vial with a PTFE septum and magnetic stir bar was charged with the catalyst ($n = 0.01$ mmol) in THF (0.5 mL), *n*-Pentadecane (20 μ L) as internal standard, and the substrate ($n = 0.2$ mmol). The ammonia borane solution ($n = 0.2$ mmol) in THF (0.5 mL) was added with a syringe through the septum. After a certain reaction time, the reaction was quenched with saturated aqueous NH_4Cl or NaHCO_3 (in case of imines or quinolines). The mixture was extracted with ethyl acetate and the combined organic layers were dried (Na_2SO_4) and filtered over a pad of silica. The pad of silica was washed with ethyl acetate for one time. The reaction mixture was analyzed by quantitative GC-FID analysis.

Some representative products (0.4 mmol, 2-fold approach) were isolated, in particular 1,2,3,4-tetrahydroquinolines. After the reaction, the solution was quenched with saturated aqueous NaHCO_3 . The crude product was purified by column chromatography (SiO_2).

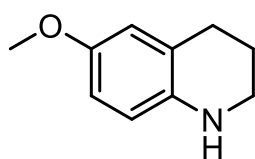
Optimization of Reaction Conditions

Table 5.6.1. Optimization of NH_3BH_3 dehydrogenation by modifying different parameters (catalyst, concentration, solvent, time).

Entry	Catalyst / mol%	NH_3BH_3 / equiv.	Time / h	Solvent / mL	Yield (Conversion) / %
1	1 (5)	0.4	16	THF (1)	57 (71)
2	1 (5)	0.65	16	THF (1)	77 (89)
3	1 (5)	1.0	16	THF (1)	91 (100)
4	1 (5)	1.0	18	THF (1)	93 (100)*
5	2 (5)	1.0	18	THF (1)	92 (100)*
6	1 (5)	1.0	16	DME (1)	93 (100)
7	1 (5)	1.5	16	THF (1)	84 (94)
8	1 (5)	1.0	2	THF (1)	71 (76)
9	1 (5)	1.0	4	THF (1)	77 (81)
10	1 (5)	1.0	6	THF (1)	81 (86)
11	1 (0.1)	1.0	16	THF (1)	2 (9)
12	1 (1)	1.0	16	THF (1)	10 (19)
13	1 (3)	1.0	16	THF (1)	36 (45)
14	1 (5)	1.0	16	THF (0.5)	83 (90)
15	1 (5)	1.0	16	THF (2)	81 (89)
16	-	1.0	16	THF (1)	0 (22)
17	1 (5)	NMe_2HBH_3 1.0	16	THF (1)	58 (70)

* 0.34 mmol substrate

Isolated products of transfer hydrogenation



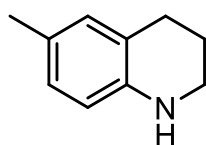
6-methoxy-1,2,3,4-tetrahydroquinoline

$C_{11}H_{15}NO$ 163.22 g mol⁻¹

slightly brownish liquid

Yield	58.4 mg (0.36 mmol, 90 %)
Solvent	From Pent:EtOAc:NEt ₃ (100:20:1) to Pent:EtOAc:NEt ₃ (100:40:1)
¹H-NMR	(400.13 MHz, 300 K, CD ₂ Cl ₂) δ [ppm]: 6.57 (m, 2H _{Ar}), 6.41 (m, 1H _{Ar}), 3.71 (s, 3H, OCH ₃), 3.64 (br s, 1H, NH), 3.24 (t, J = 5.6 Hz, 2H, CH ₂), 2.75 (t, J = 6.5 Hz, 2H, CH ₂), 1.91 (m, 2H, CH ₂)
¹³C{¹H}-NMR	(101.4 MHz, 300 K, CD ₂ Cl ₂) δ [ppm]: 152.1, 139.5, 123.1, 115.6, 115.1, 113.1, 56.0, 42.7, 27.6, 22.9
GC-MS	t_R = 9.80 min , (EI, 70 eV): m/z = 163 [M ⁺] , 148, 130, 118, 103, 91, 77, 65, 51

Analytical data were in full agreement with *Beller* and co-workers.^[14]



6-methyl-1,2,3,4-tetrahydroquinoline

$C_{10}H_{13}N$ 147.22 g mol⁻¹

slightly brownish liquid

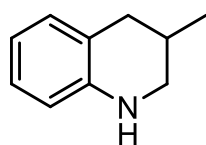
Yield	50.8 mg (0.35 mmol, 86 %)
Solvent	Pent:EtOAc:NEt ₃ (100:2:1)
¹H-NMR	(400.13 MHz, 300 K, CD ₂ Cl ₂) δ [ppm]: 6.71 (m, 2H _{Ar}), 6.37 (m, 1H _{Ar}), 3.70 (br s, 1H, NH), 3.27 (t, J = 5.6 Hz, 2H, CH ₂), 2.73 (t, J = 6.4 Hz, 2H, CH ₂), 2.02 (s, 3H, CH ₃), 1.92 (m, 2H, CH ₂)

5 Amine-Borane Dehydrogenation and Transfer Hydrogenation Catalyzed by α -Diimine Cobaltates

$^{13}\text{C}\{^1\text{H}\}$ -NMR (101.4 MHz, 300 K, CD_2Cl_2) δ [ppm]: 143.0 130.3, 127.5, 126.2, 121.8, 114.5, 42.5, 27.3. 22.9, 20.5

GC-MS $t_{\text{R}} = 8.54$ min, (EI, 70 eV): $m/z = 146$ [M^+], 132, 117, 103, 91, 77, 65, 51

Analytical data were in full agreement with *Beller* and co-workers.^[14]



2-methyl-1,2,3,4-tetrahydroquinoline

$\text{C}_{10}\text{H}_{13}\text{N}$ 147.22 g mol⁻¹

slightly yellow liquid

Yield 44.9 mg (0.31 mmol, 76 %)

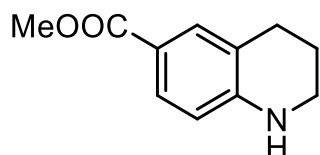
Solvent Pent:EtOAc:Net₃ (100:1:1)

^1H -NMR (400.13 MHz, 300 K, CD_2Cl_2) δ [ppm]: 6.94 (m, 2H_{Ar}), 6.58 (m, 2H_{Ar}), 6.46 (m, 2H_{Ar}) 3.93 (br s, 1H, NH), 3.28 (dq, J = 11.1 Hz, 2.0 Hz, 1H, CH), 2.78 (m, 1H, CH₂), 2.45 (m, 1H, CH₂), 2.04 (m, 1H, CH₂) 1.07 (d, J = 6.6 Hz, 3H, CH₃)

$^{13}\text{C}\{^1\text{H}\}$ -NMR (101.4 MHz, 300 K, CD_2Cl_2) δ [ppm]: 145.0, 130.0, 127.0, 121.4, 117.0, 114.0, 49.2, 35.9, 27.7, 19.2

GC-MS $t_{\text{R}} = 7.98$ min, (EI, 70 eV): $m/z = 143$ [M^+], 132, 115, 104, 89, 77, 71, 63, 51

Analytical data were in full agreement with *Beller* and co-workers.^[14]



6-methylester-1,2,3,4-tetrahydroquinoline

$\text{C}_{11}\text{H}_{13}\text{NO}_2$ 191.23 g mol⁻¹

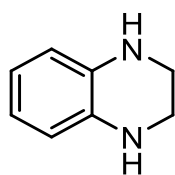
almost colourless liquid

Yield 57.0 mg (0.30 mmol, 75 %)

5 Amine-Borane Dehydrogenation and Transfer Hydrogenation Catalyzed by α -Diimine Cobaltates

Solvent	From Pent:EtOAc:Net ₃ (100:20:1) to EtOAc:Net ₃ (100:1)
¹H-NMR	(400.13 MHz, 300 K, CD ₂ Cl ₂) δ [ppm]: 7.59 (m, 2H _{Ar}), 6.40 (m, 1H _{Ar}), 4.50 (br s, 1H, NH), 3.80 (s, 3H, COOCH ₃), 3.33 (t, J = 5.6 Hz, 2H, CH ₂), 2.76 (t, J = 6.3 Hz, 2H, CH ₂), 1.90 (m, 2H, CH ₂)
¹³C{¹H}-NMR	(101.4 MHz, 300 K, CD ₂ Cl ₂) δ [ppm]: 167.6, 149.4, 131.4, 129.3, 120.3, 117.5, 112.9, 51.6, 42.0, 27.3, 21.8
GC-MS	t_R = 12.25 min, (EI, 70 eV): m/z = 191 [M ⁺], 176, 160, 144, 132, 117, 104, 89, 77, 65, 51

Analytical data were in full agreement with *Beller* and co-workers.^[14]



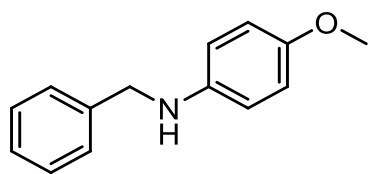
1,2,3,4-tetrahydroquinoxaline

C₈H₁₀N₂ 134.18 g mol⁻¹

slightly reddish liquid

Yield	47.8 mg (0.36 mmol, 90 %)
Solvent	From Pent:EtOAc:Net ₃ (100:1:1) to EtOAc:Net ₃ (100:1)
¹H-NMR	400.13 MHz, 300 K, CD ₂ Cl ₂) δ [ppm]: 6.50 (m, 4H, CH _{Ar}), 3.54 (br s, 2H, NH), 3.37 (s, 4H, CH ₂)
¹³C{¹H}-NMR	(101.4 MHz, 300 K, CD ₂ Cl ₂) δ [ppm]: 134.2, 118.7, 114.7, 41.7
GC-MS	t_R = 9.12 min, (EI, 70 eV): m/z = 133 [M ⁺], 119, 104, 92, 77, 66, 51

Analytical data were in full agreement with *Beller* and co-workers^[14]



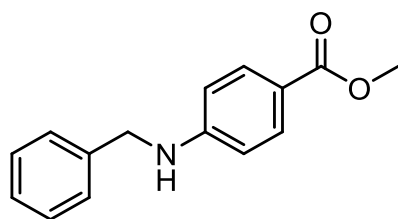
N-benzyl-4-methoxyaniline

$C_{14}H_{15}NO$ 213.28 g mol⁻¹

orange oil

Yield	74.7 mg (0.35 mmol, 88 %)
Solvent	Pent/EA: 95:5 to 90:5 (Alumina N)
¹H-NMR	(300.13 MHz, 300 K, CDCl ₃) δ [ppm]: 7.35 – 7.29 (m, 2H, CH _{Ar}), 7.24 – 7.15 (m, 2H, CH _{Ar}), 6.94 – 6.84 (m, 2H, CH _{Ar}), 6.78 – 6.70 (m, 1H, CH _{Ar}), 6.68 – 6.62 (m, 2H, CH _{Ar}), 4.27 (s, 2H, CH ₂), 4.20 – 4.00 (br s, 1H, NH), 3.82 (s, 3H, CH ₃).
¹³C{¹H}-NMR	(75.5 MHz, 300 K, CDCl ₃) δ [ppm]: 159.0, 148.2, 131.4, 129.4, 129.0, 117.7, 114.1, 113.0, 55.4, 48.0.
GC-MS	t_R = 10.12 min, (EI, 70 eV): m/z = 213.1

Analytical data were in full agreement with *Bhanage* and co-workers.^[15]



N-benzyl-4-methylesteraniline

$C_{15}H_{15}NO_2$ 241.29 g mol⁻¹

beige powder

Yield 52.3 mg (0.22 mmol, 55 %)

Solvent Pent/EA: 95:5 to 90:5 (Alumina N).

¹H-NMR (300.13 MHz, 300 K, CDCl₃) δ [ppm]:
7.91 – 7.84 (m, 2H, CH_{Ar}), 7.40 – 7.28 (m, 5H, CH_{Ar}), 7.65 – 7.56 (m, 2H, CH_{Ar}), 5.20 – 4.60 (br s, 1H, NH), 4.39 (s, 2H, CH₂), 3.85 (s, 3H, CH₃).

GC-MS t_R = 11.7 min, (EI, 70 eV): m/z = 241.1

Analytical data were in full agreement with *Yamaguchi* and co-workers.^[16]

Reaction progress analysis of TH (α -methylstyrene) with catalyst 1

Under an atmosphere of argon, a 5 mL screw cap vial with a PTFE septum and magnetic stir bar was charged with catalyst **1** (20.5 mg, n = 0.05 mmol) in THF (2.5 mL), *n*-Pentadecane (50 μ L) as internal standard, and α -methylstyrene (65 μ L, n = 0.5 mmol). The ammonia borane solution (15.5 mg, n = 0.5 mmol) in THF (2.5 mL) was added with a syringe through the septum. After certain times, an aliquot (0.1 mL) was taken, quenched with saturated aqueous NH₄Cl, filtered over silica, and extracted with ethyl acetate. The sample was analyzed by GC-FID.

TH (α -methylstyrene) with catalyst 1 in a D₂ atmosphere

Under an atmosphere of deuterium gas (99.5% deuterium content, *Sigma-Aldrich*, 1.1 bar, 0.44 mmol), a 10 mL Schlenk flask with a magnetic stir bar was charged with catalyst **1** (8.2 mg, n = 0.01 mmol), α -methylstyrene (26 μ L, n = 0.2 mmol) and C₆D₆ (8.3 μ L, n = 0.094 mmol) in THF (0.5 mL). The ammonia borane solution (6.2 mg, n = 0.2 mmol) in THF (0.5 mL) was added with a syringe through the septum. After 5 minutes an aliquote (0.1 mL) was taken and analyzed by GC-MS.

5 Amine-Borane Dehydrogenation and Transfer Hydrogenation Catalyzed by α -Diimine Cobaltates

Subsequently, the septum was removed and the Schlenk flask closed with a glass stopper. After 16 h the reaction mixture was filtered in order to remove polyaminoborane. The solution was analyzed by ^2H -NMR spectroscopy. Remaining solution (0.5 mL) was quenched with saturated aqueous NH_4Cl and the organic phase was extracted with ethyl acetate and dried over Na_2SO_4 . The sample was analyzed by GC-MS. Deuterium signals of cumene- d_x were assigned according to *Jacobi von Wangelin* and co-workers.^[17]

The amount of formed cumene- d ($\delta = 2.64$ ppm) was calculated by comparing the integral with the internal standard C_6D_6 (0.094 mmol) added before starting the reaction.

relative amount of deuterium incorporated into the methine position of the i Pr group of cumene:

$$n(\text{cumene-}\text{d}) = 0.43 \cdot 0.094 \text{ mmol} = 0.04 \text{ mmol} \rightarrow 0.04 \text{ mmol} / 0.2 \text{ mmol} = 20\%$$

relative amount of deuterium incorporated into the methyl position of the i Pr group of cumene:

$$n(\text{cumene-}\text{d}) = 2.38 \cdot 0.094 \text{ mmol} / 6 = 0.037 \text{ mmol} \rightarrow 0.037 \text{ mmol} / 0.2 \text{ mmol} = 18\%$$

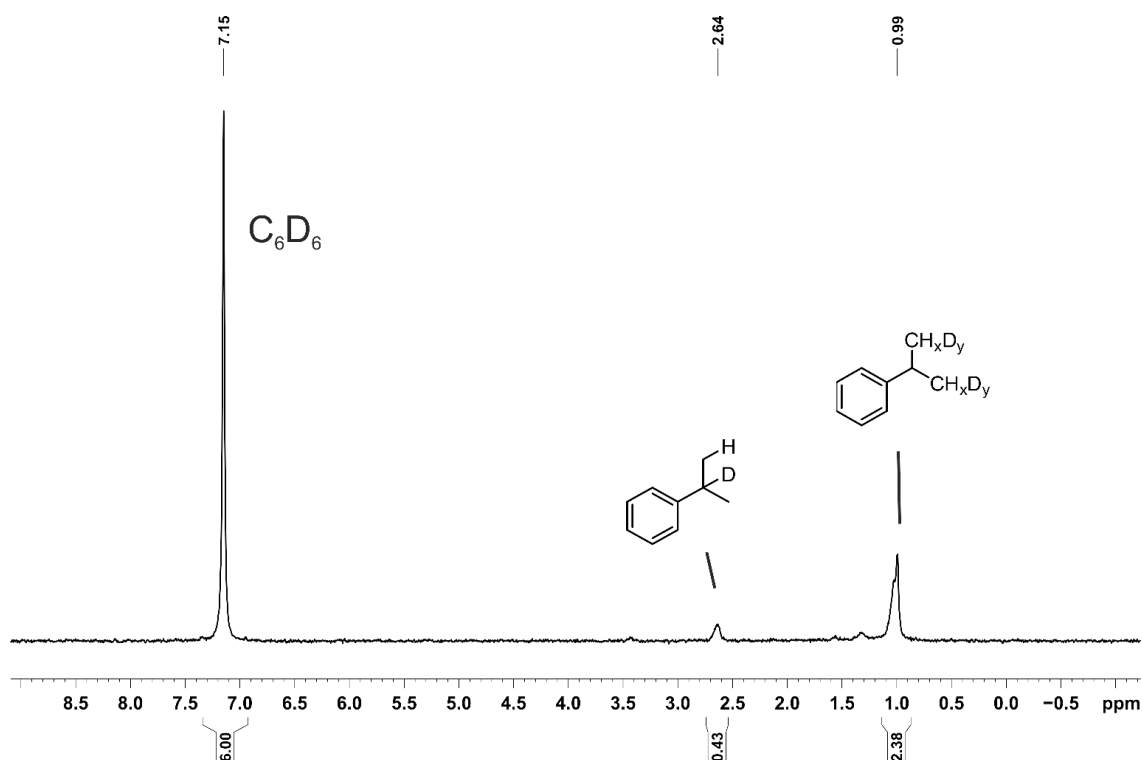


Figure 5.6.28. ^2H -NMR spectrum (61.4 MHz, 300K, THF) of reaction mixture after 16 h.

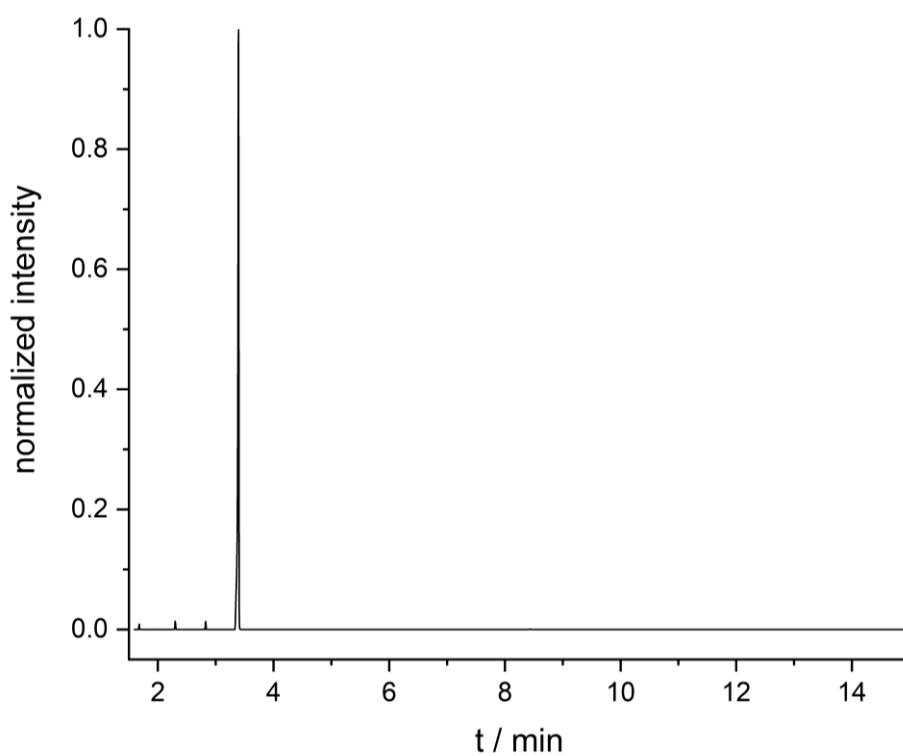
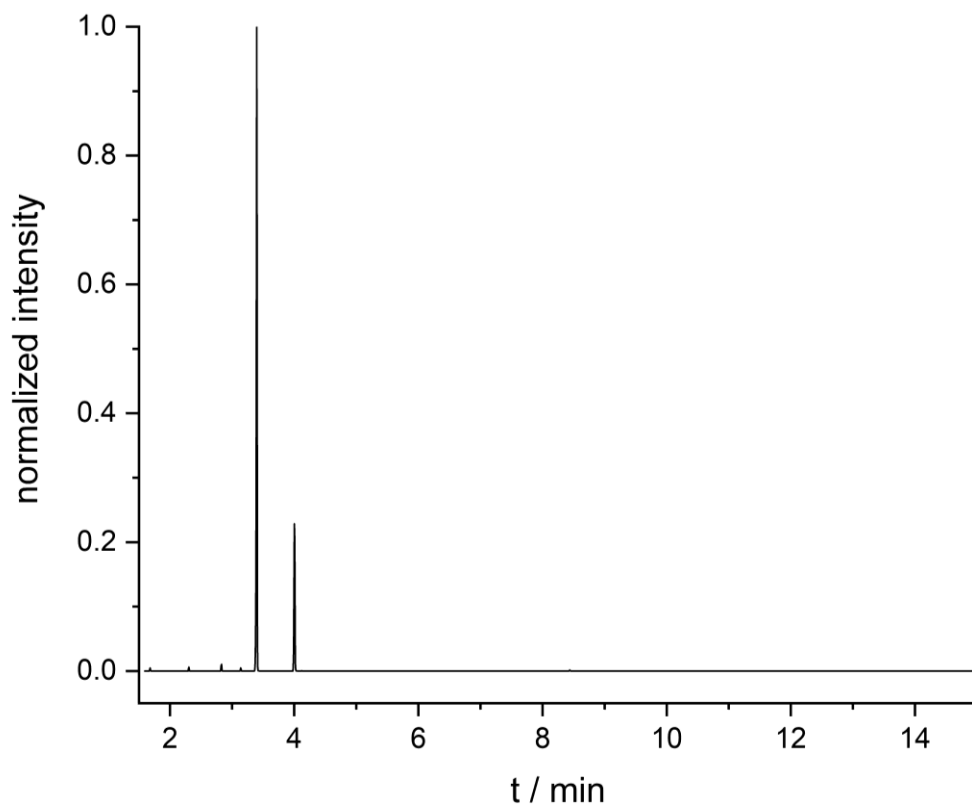


Figure 5.6.29. Chromatograms (GC-MS analysis) after 5 min (top) and 16 h (bottom); 3.39 min (cumene) and 4.00 min (α -methylstyrene).

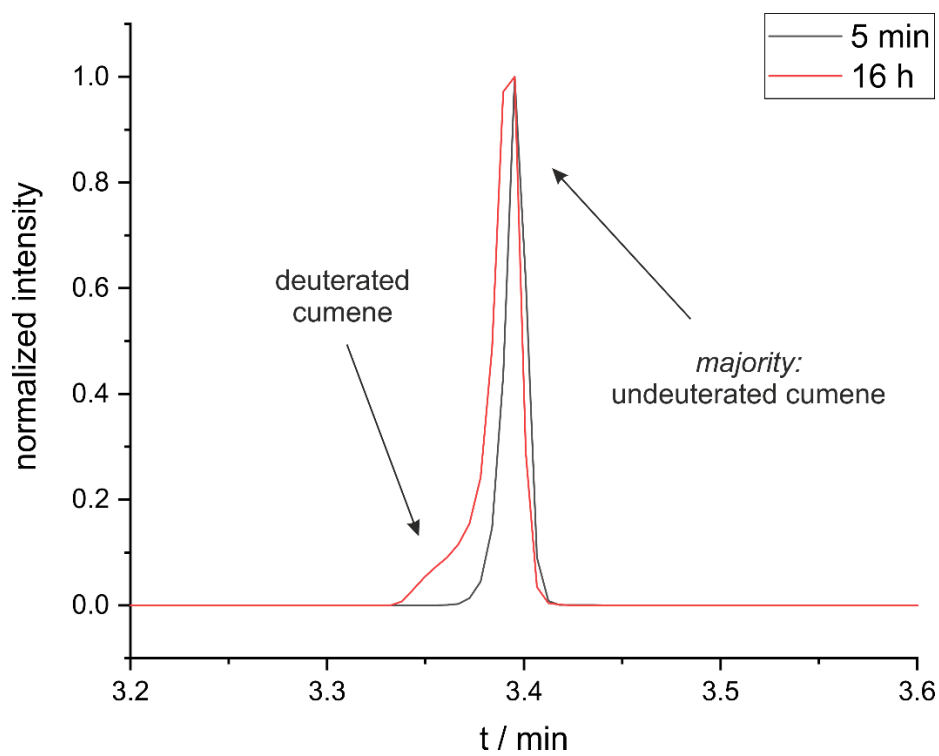
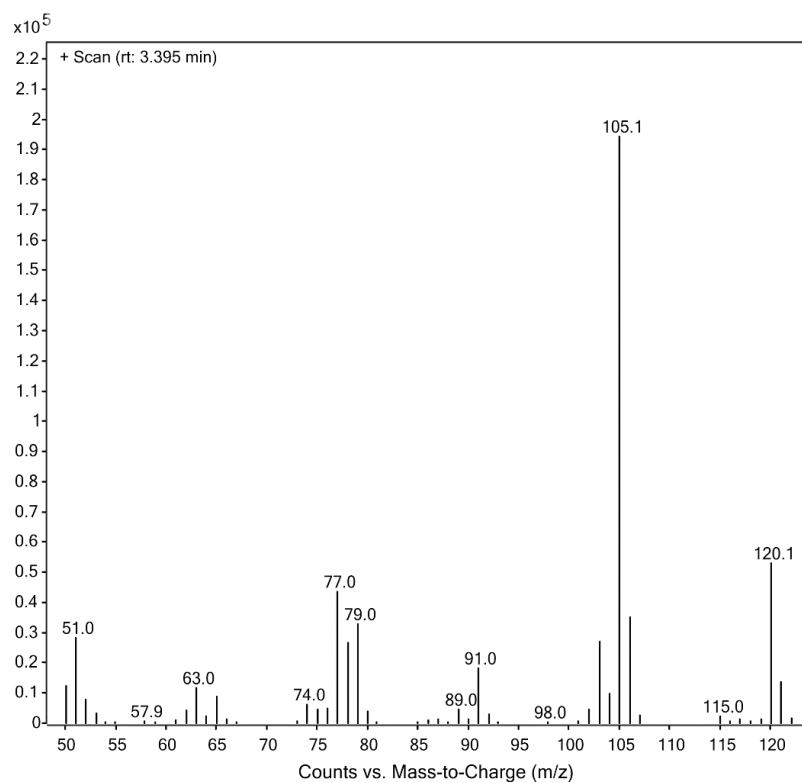
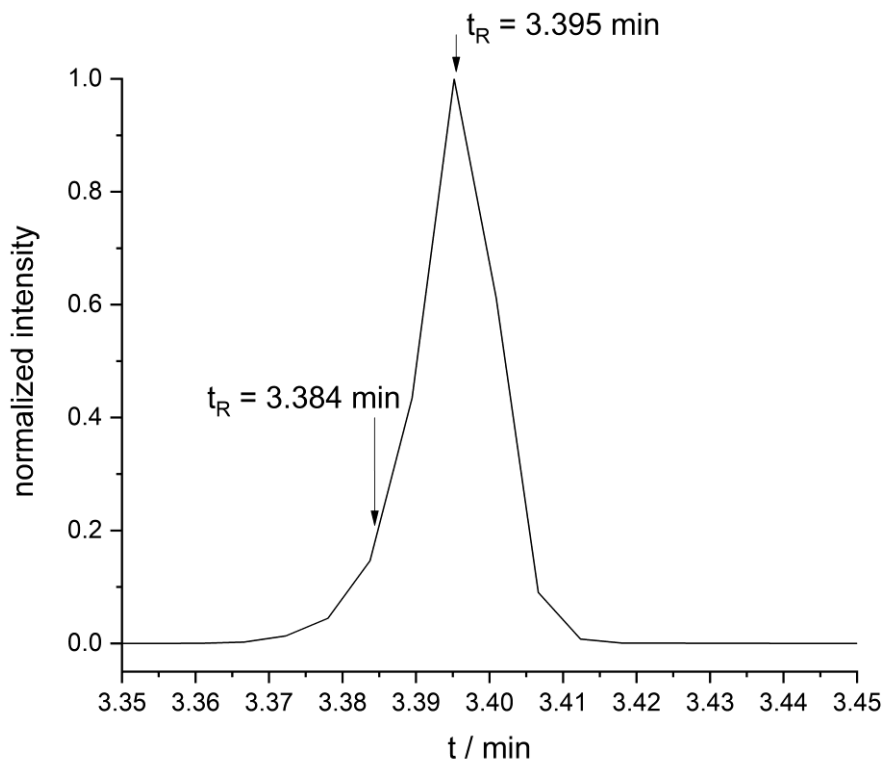


Figure 5.6.30. Comparison of cumene in chromatograms after 5 min (black) and 16 h red.

5 Amine-Borane Dehydrogenation and Transfer Hydrogenation Catalyzed by α -Diimine Cobaltates



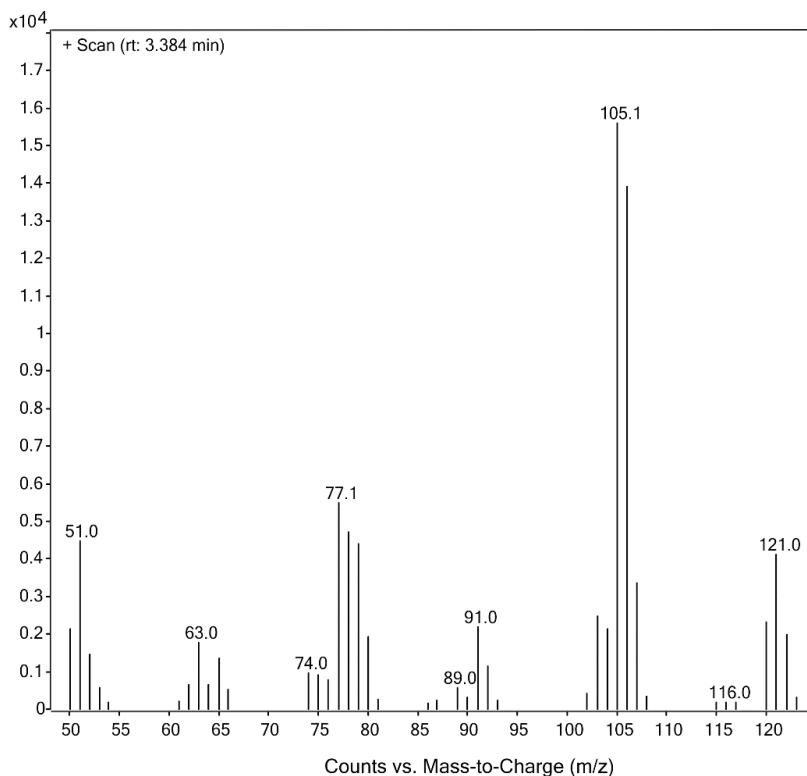
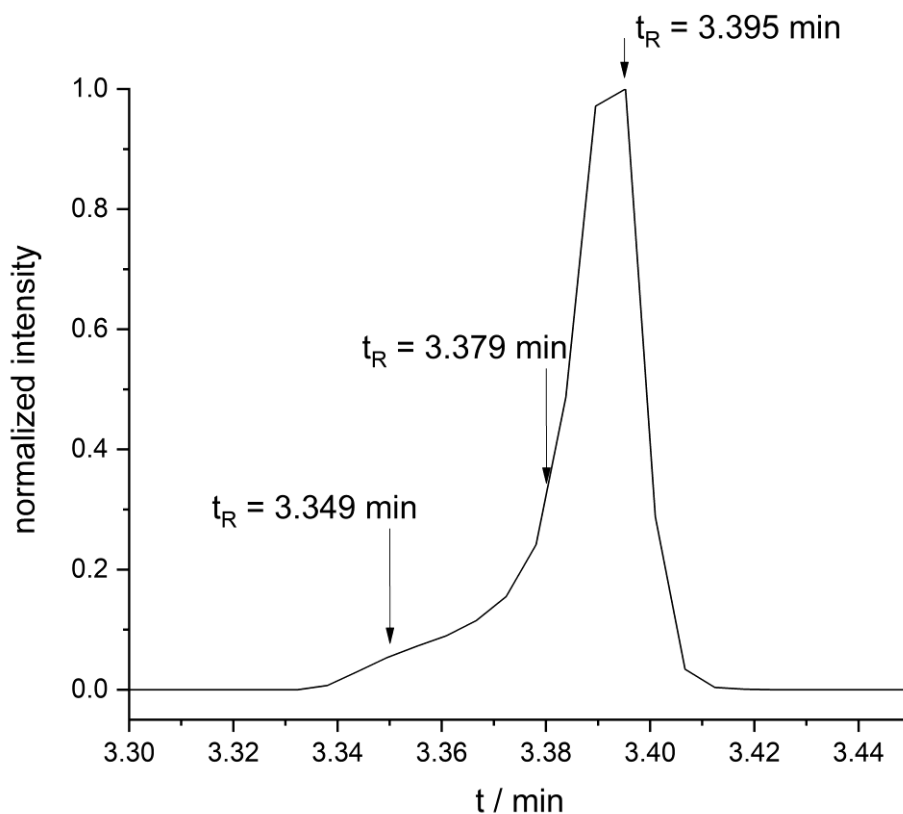
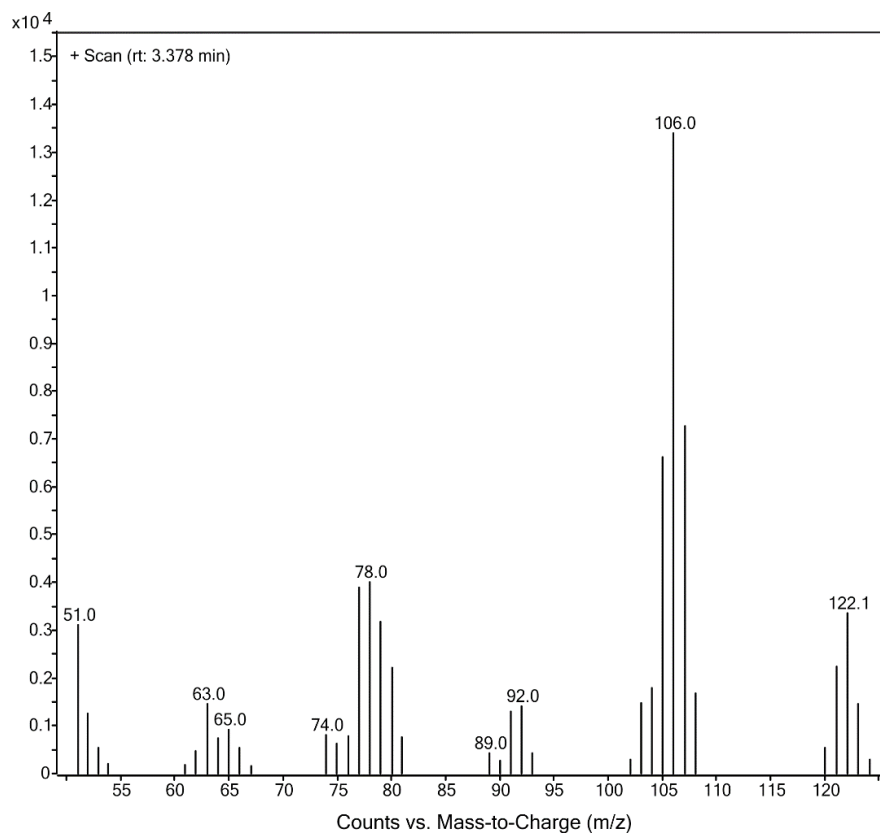
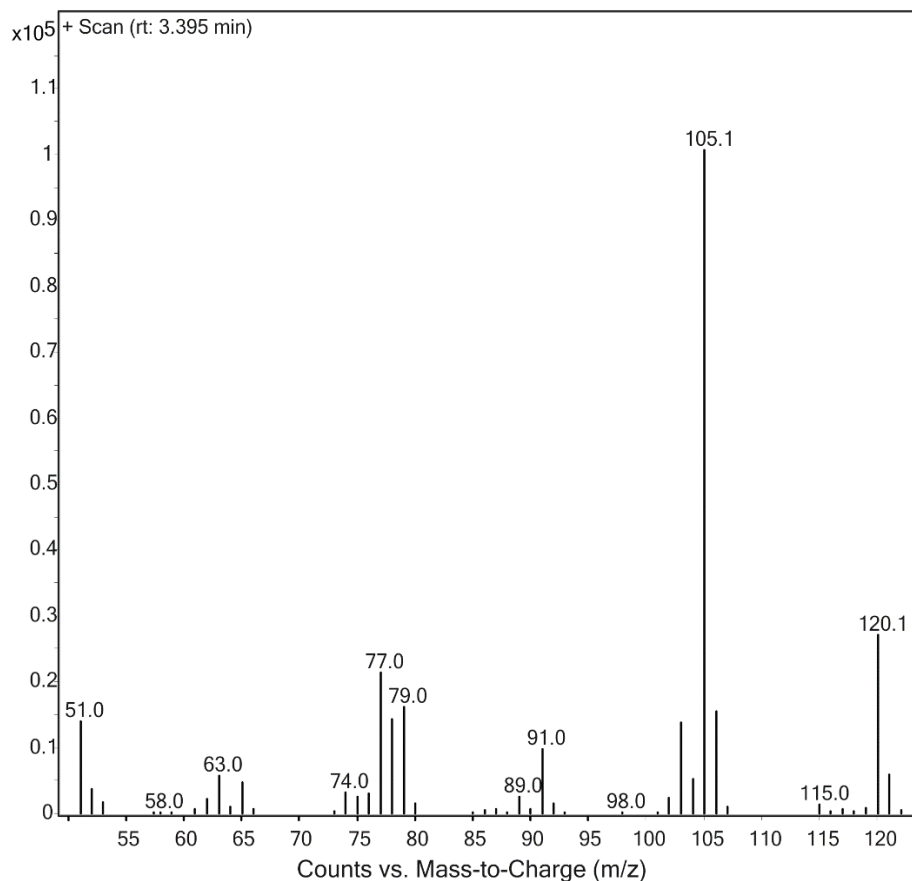


Figure 5.6.31. Zoom of chromatogram and m/z data of cumene (different retention times) after 5 min.



5 Amine-Borane Dehydrogenation and Transfer Hydrogenation Catalyzed by α -Diimine Cobaltates



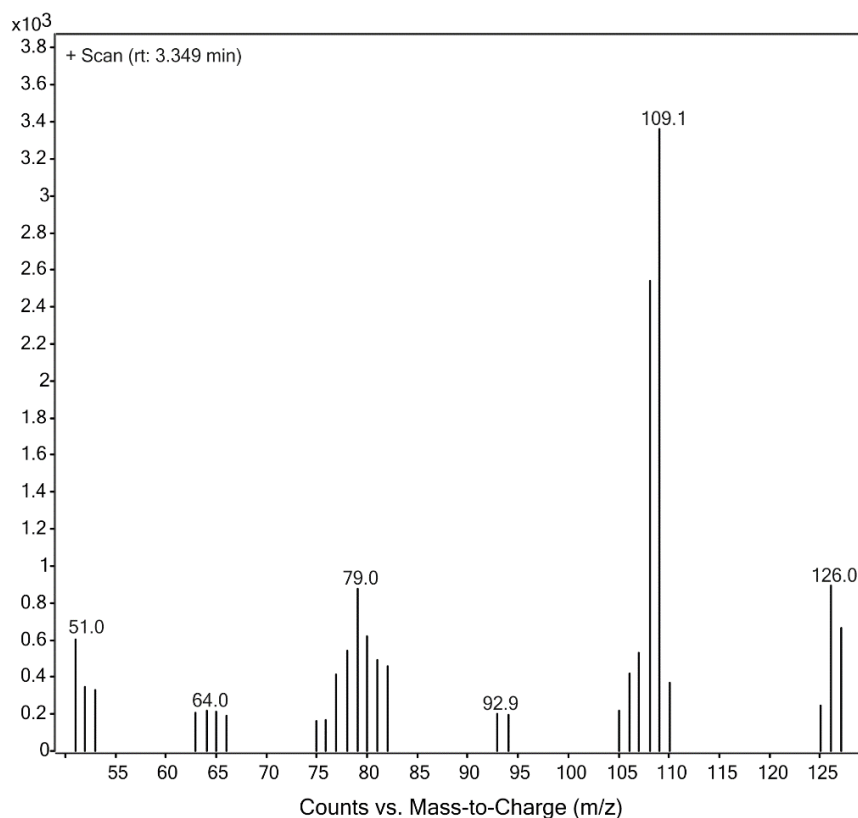


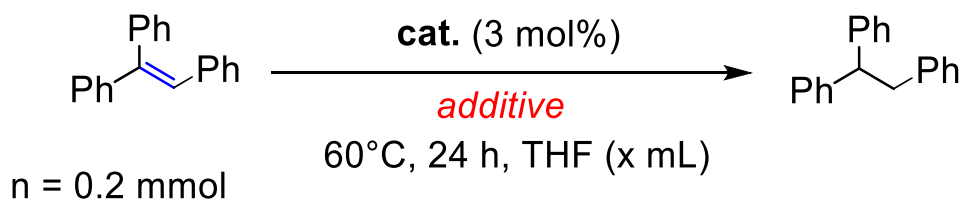
Figure 5.6.32. Zoom of chromatogram and m/z data of cumene (different retention times) after 16 h.

5.6.9 Hydrogenation reactions (autoclave)

General procedure

In an argon-filled glovebox, a flame-dried 4 mL reaction vial was charged with the substrate (0.2 mmol), n-pentadecane (50 μ L) as internal reference for GC-FID quantification and the catalyst (0.006 mmol) in THF (1 mL). A solution of NH_3BH_3 (0.06 mmol) in THF (1 mL) was added during which the color changed to dark violet and hydrogen evolution occurred. The reaction vial was transferred to a high-pressure reactor which was sealed and removed from the glovebox. The reactor was purged with H_2 (3 x 2 bar) and the reaction pressure and temperature were set. After the indicated reaction time, the vial was retrieved and the reaction mixture was hydrolyzed with a saturated aqueous solution of NH_4Cl (1 mL). The reaction mixture was extracted with ethyl acetate (3 x 1 mL), dried over Na_2SO_4 and analyzed by GC-FID and GC-MS. Procedure for substrates, which are not tolerated by the metalate (4-X-alpha-methylstyrene; X=Cl, Br, SMe): The substrate is added after addition of the NH_3BH_3 solution.

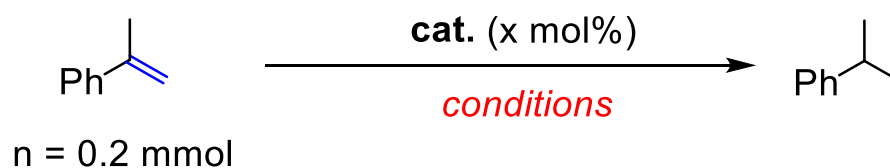
Optimization of reaction conditions

Table 5.6.2. Optimization of reaction conditions by modifying different parameters (catalyst, additive).

Entry	Catalyst / %	Additive / mol%	Yield (Conversion) / %
1	1	-	0 (13)
2	2	-	0 (11)
3	1	NH₃BH₃ (30)	95 ^[a]
4	2	NH₃BH₃ (30)	>99 ^[a]
5	1	NH ₃ BH ₃ (60)	11 (23) ^[a]
6	2	NH ₃ BH ₃ (60)	10 (19) ^[a]
7	1	NH ₃ BH ₃ (15)	90 ^[a]
8	1	Me ₂ NHBH ₃ (30)	52 (58)
9	2	Me₂NHBH₃ (30)	92
10	1	Me ₂ NHBH ₃ (15)	15 (24)
11	1	NEt ₃ (30)	0 (15)
12	2	NEt ₃ (30)	1 (13)
13	2	Pyrrolidine (30)	1 (13)
14	2	Pyridine (30)	1 (14)
15	2	Piperidine (30)	0 (12)
16	2	BH ₃ .THF (30)	2 (52)
17	2	NH₃BH₃ (30)	14 (27) ^[b]

Conditions: 0.2 mmol (0.1M) alkene in THF, 3 mol% catalyst, 20 bar bar H₂, 25 °C, 24 h. Yields (GC-FID vs. internal *n*-pentadecane); conversions in parentheses if <90%. ^[a] 10 bar; ^[b] 3 bar, 3 h.

Table S3 Hydrogenation of α -methylstyrene with catalyst **1** and **2** and different temperatures.



Entry	Catalyst / mol%	Conditions	Yield (Conversion) / %
1	1 (3 mol%)	60 °C, 20 bar, 24 h	>99 (>99)
2	2 (3 mol%)	60 °C, 20 bar, 24 h	39 (39)
3	1 (5 mol%)	25 °C, 20 bar, 13 h	- (<5)
4	2 (5 mol%)	25 °C, 20 bar, 13 h	- (<5)

Conditions: 0.2 mmol (0.1M) alkene in THF, 3 mol% catalyst. Yields (GC-FID vs. internal *n*-pentadecane); conversions in parentheses if <90%.

Note: The substitution / hydrogenation of 1,5-cyclooctadiene is presumably favored at elevated temperature, which might activate the catalyst precursor for the investigated reaction.

5.6.10 NMR spectra

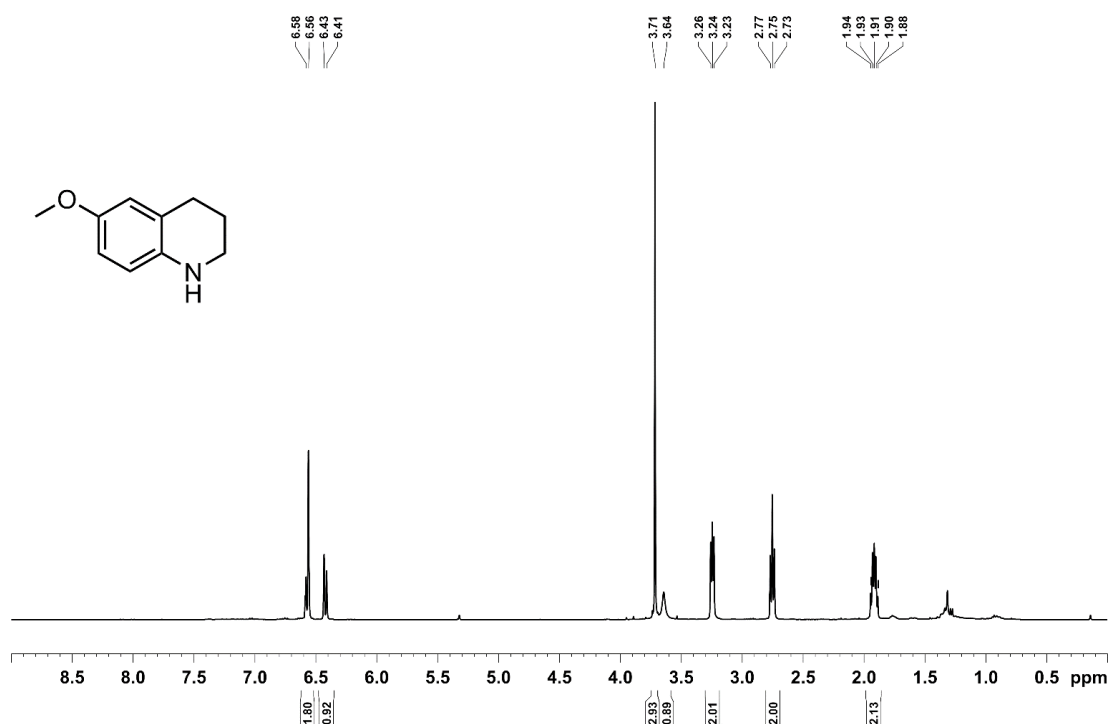


Figure 5.6.33. ^1H NMR spectrum (400.13 MHz, 300K, CD_2Cl_2) of 6-methoxy-1,2,3,4-tetrahydroquinoline.

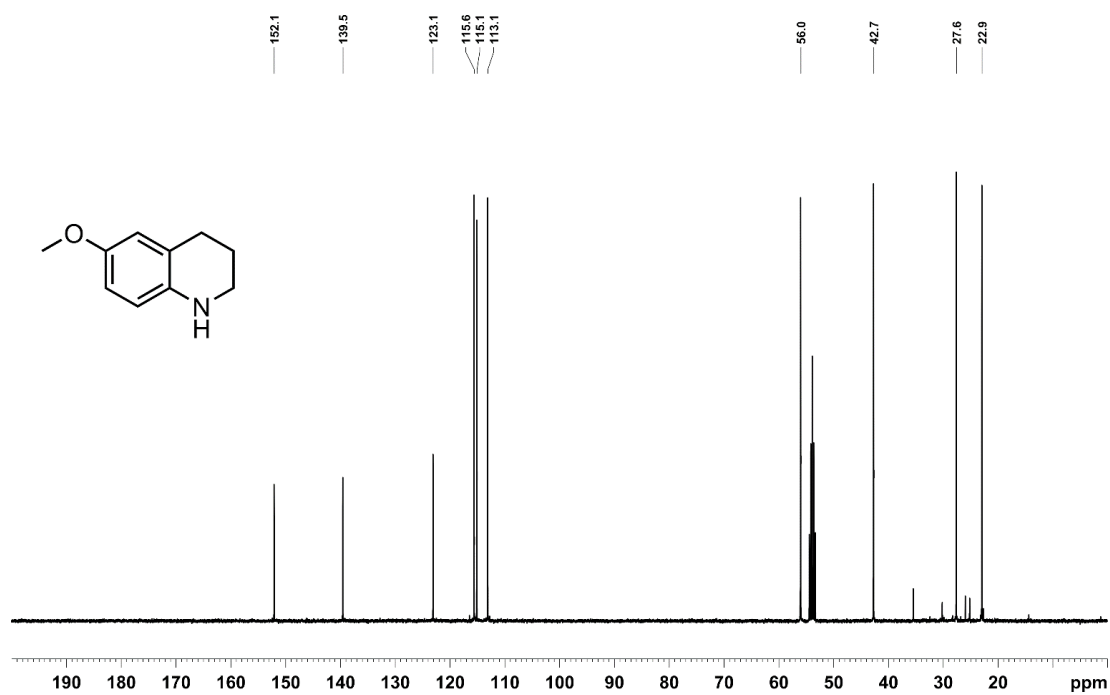


Figure 5.6.34. $^{13}\text{C}\{^1\text{H}\}$ NMR spectrum (101.4 MHz, 300K, CD_2Cl_2) of 6-methoxy-1,2,3,4-tetrahydroquinoline.

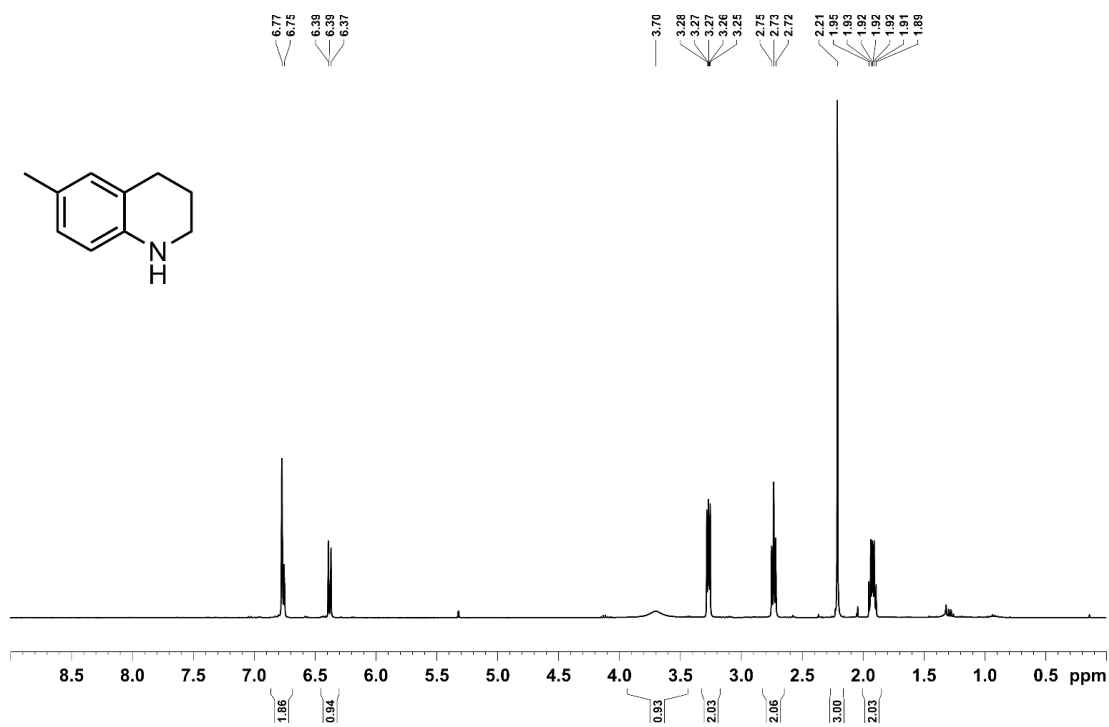


Figure 5.6.35. ¹H NMR spectrum (400.13 MHz, 300K, CD₂Cl₂) of 6-methyl-1,2,3,4-tetrahydroquinoline.

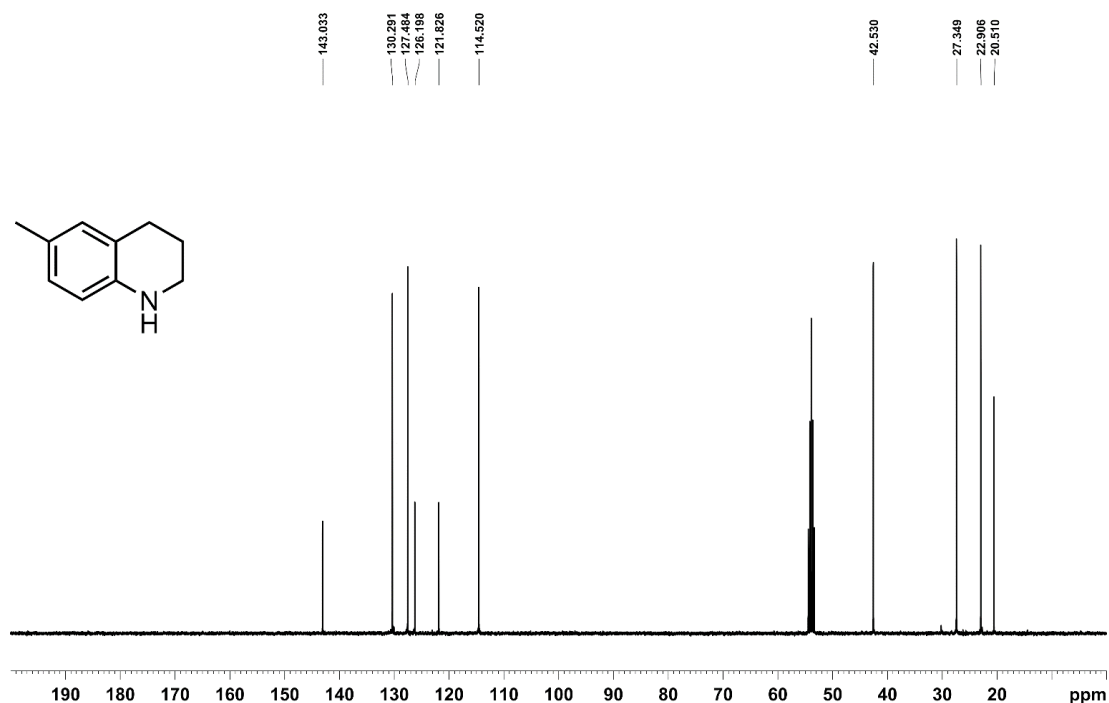


Figure 5.6.36. ¹³C{¹H} NMR spectrum (101.4 MHz, 300K, CD₂Cl₂) of 6-methyl-1,2,3,4-tetrahydroquinoline.

5 Amine-Borane Dehydrogenation and Transfer Hydrogenation Catalyzed by α -Diimine Cobaltates

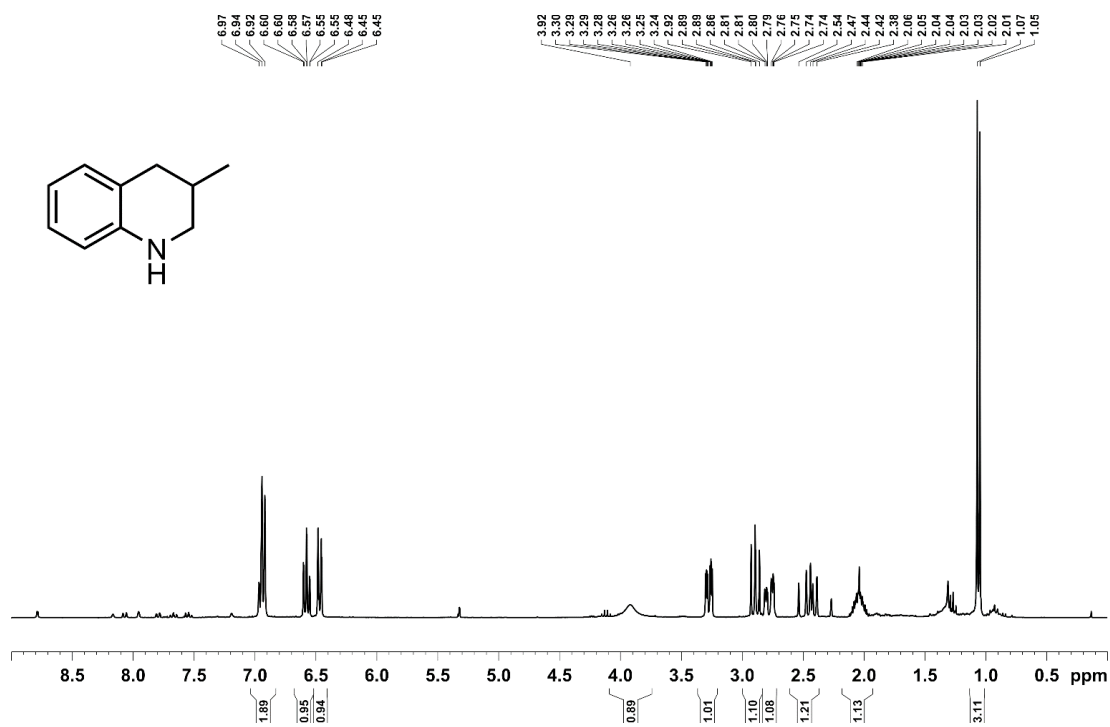


Figure 5.6.37. ^1H NMR spectrum (400.13 MHz, 300K, CD_2Cl_2) of 2-methyl-1,2,3,4-tetrahydroquinoline.

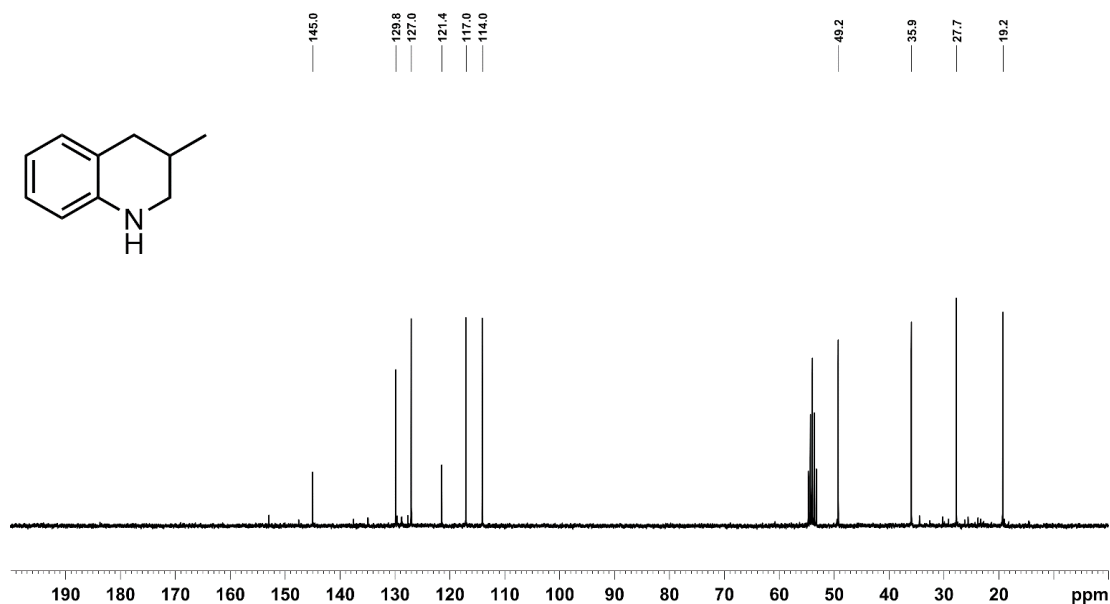


Figure 5.6.38. $^{13}\text{C}\{^1\text{H}\}$ NMR spectrum (101.4 MHz, 300K, CD_2Cl_2) of 2-methyl-1,2,3,4-tetrahydroquinoline.

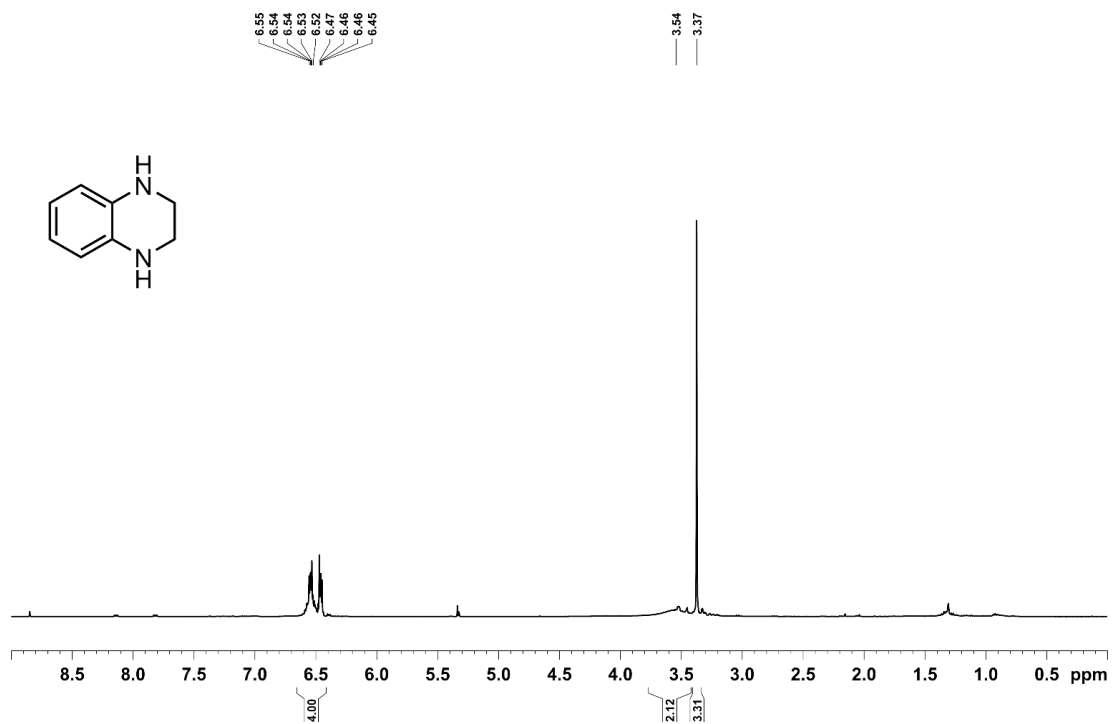


Figure 5.6.39. ^1H NMR spectrum (400.13 MHz, 300K, CD_2Cl_2) of 1,2,3,4-tetrahydroquinoxaline.

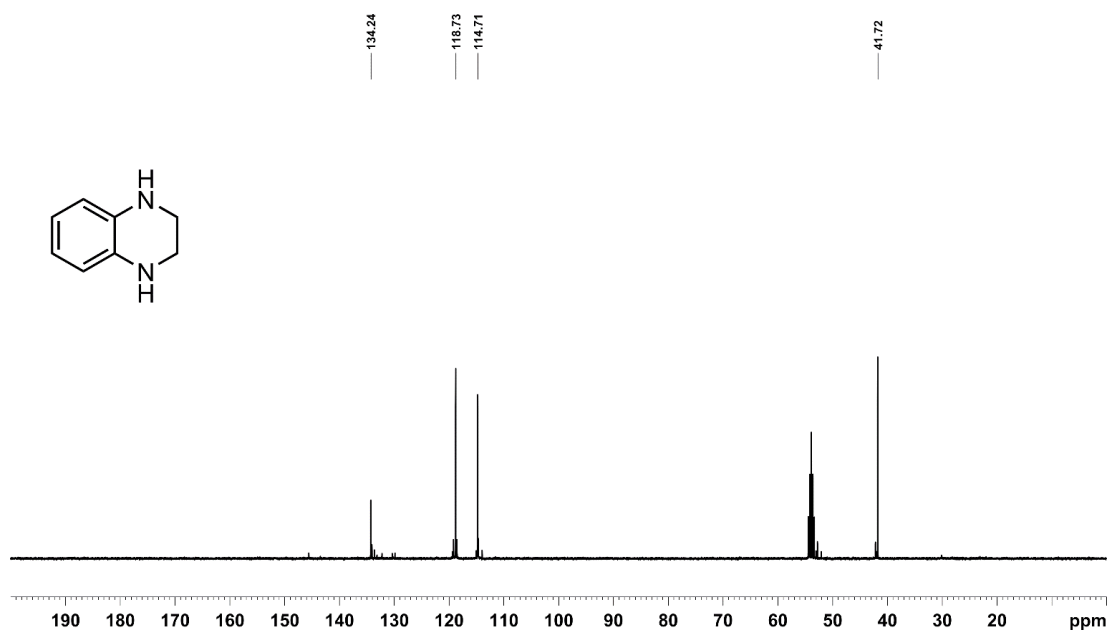


Figure 5.6.40. $^{13}\text{C}\{^1\text{H}\}$ NMR spectrum (101.4 MHz, 300K, CD_2Cl_2) of 1,2,3,4-tetrahydroquinoxaline.

5 Amine-Borane Dehydrogenation and Transfer Hydrogenation Catalyzed by α -Diimine Cobaltates

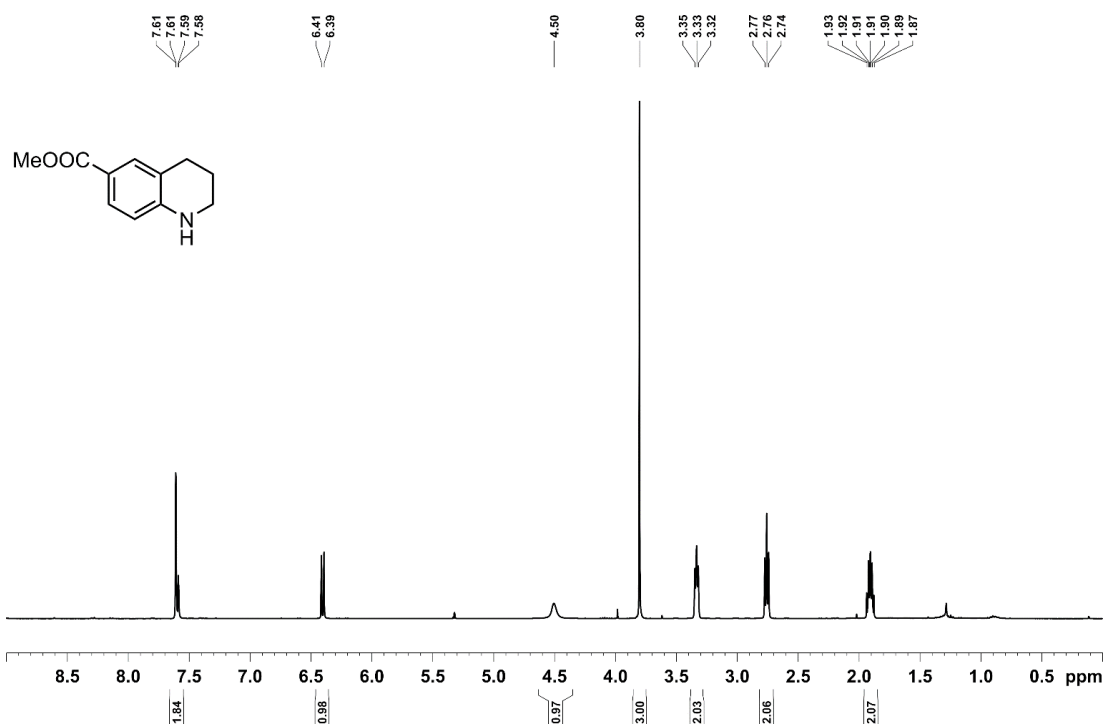


Figure 5.6.41. ^1H NMR spectrum (400.13 MHz, 300K, CD_2Cl_2) of 6-methylester-1,2,3,4-tetrahydroquinoline.

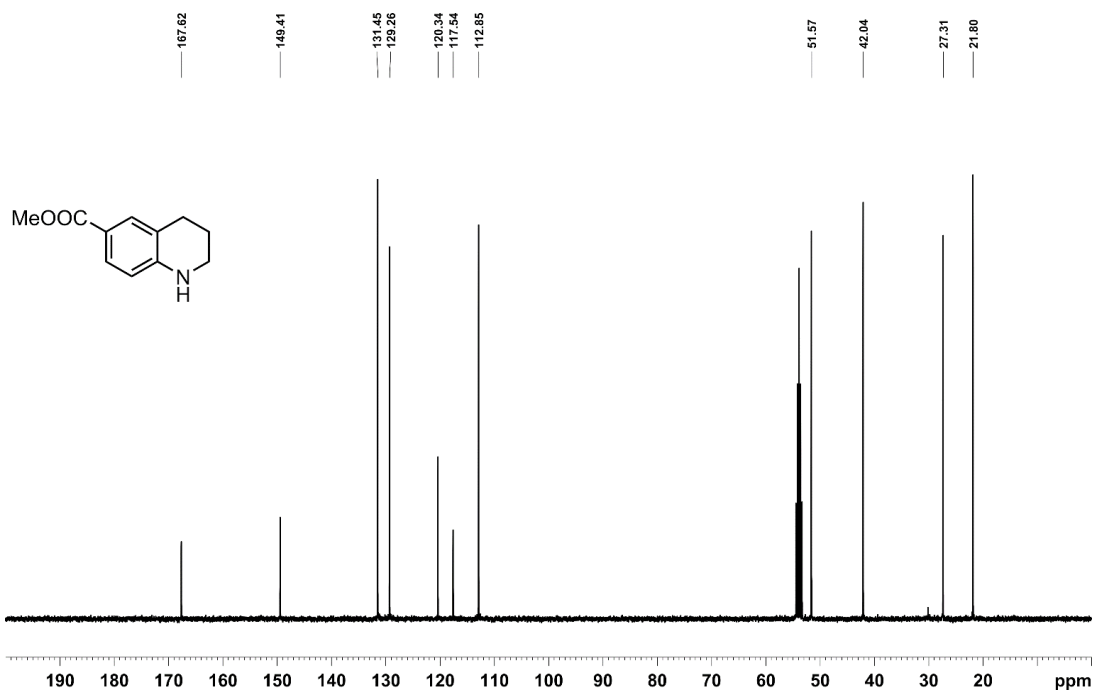


Figure 5.6.42. $^{13}\text{C}\{^1\text{H}\}$ NMR spectrum (101.4 MHz, 300K, CD_2Cl_2) of 6-methylester-1,2,3,4-tetrahydroquinoline.

5 Amine-Borane Dehydrogenation and Transfer Hydrogenation Catalyzed by α -Diimine Cobaltates

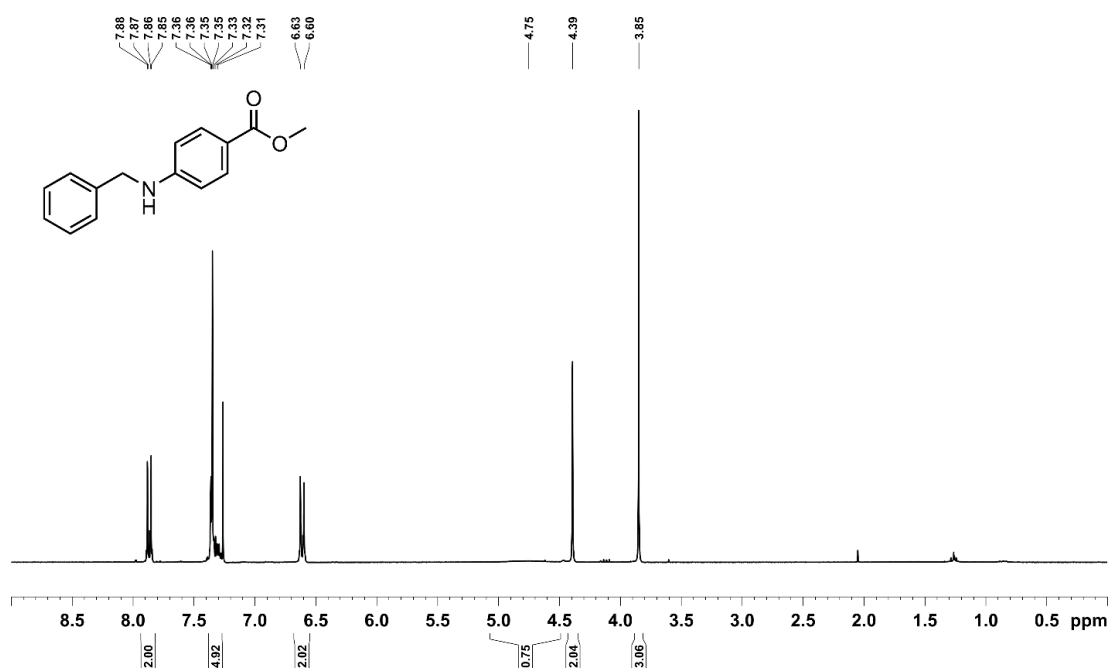


Figure 5.6.43. ¹H NMR spectrum (400.13 MHz, 300K, CD₂Cl₂) of N-benzyl-4-methylesteraniline.

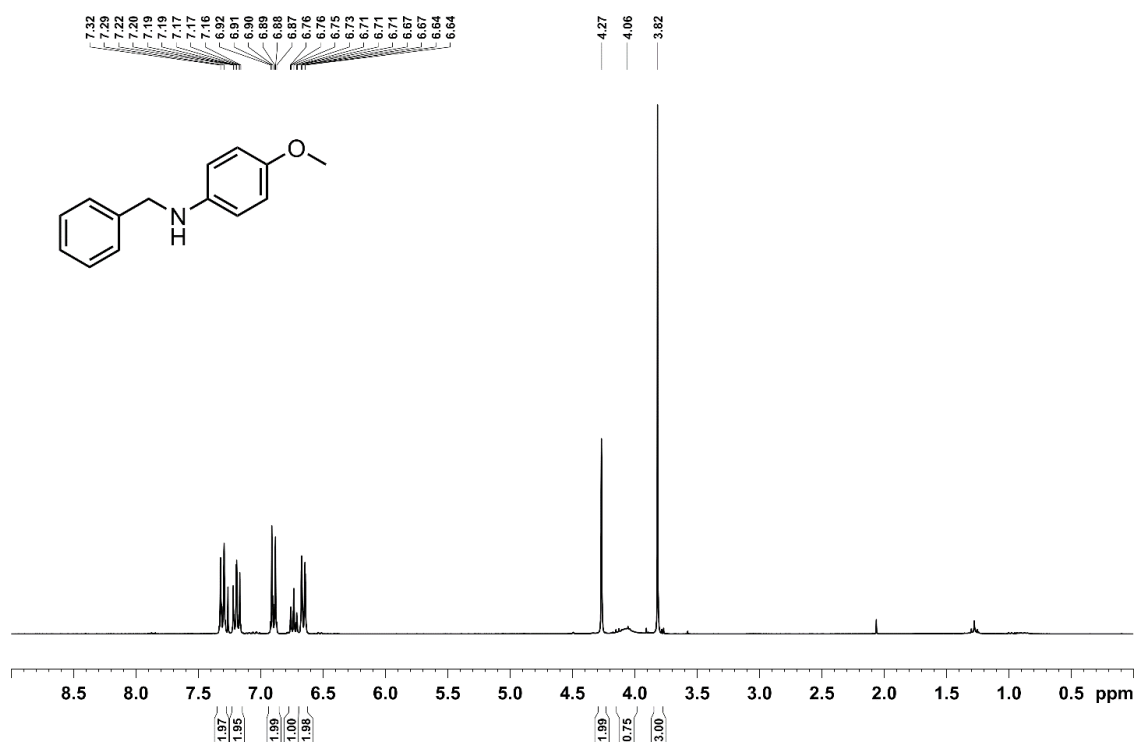


Figure 5.6.44. ¹H NMR spectrum (400.13 MHz, 300K, CD₂Cl₂) of N-benzyl-4-methoxyaniline.

5 Amine-Borane Dehydrogenation and Transfer Hydrogenation Catalyzed by α -Diimine Cobaltates

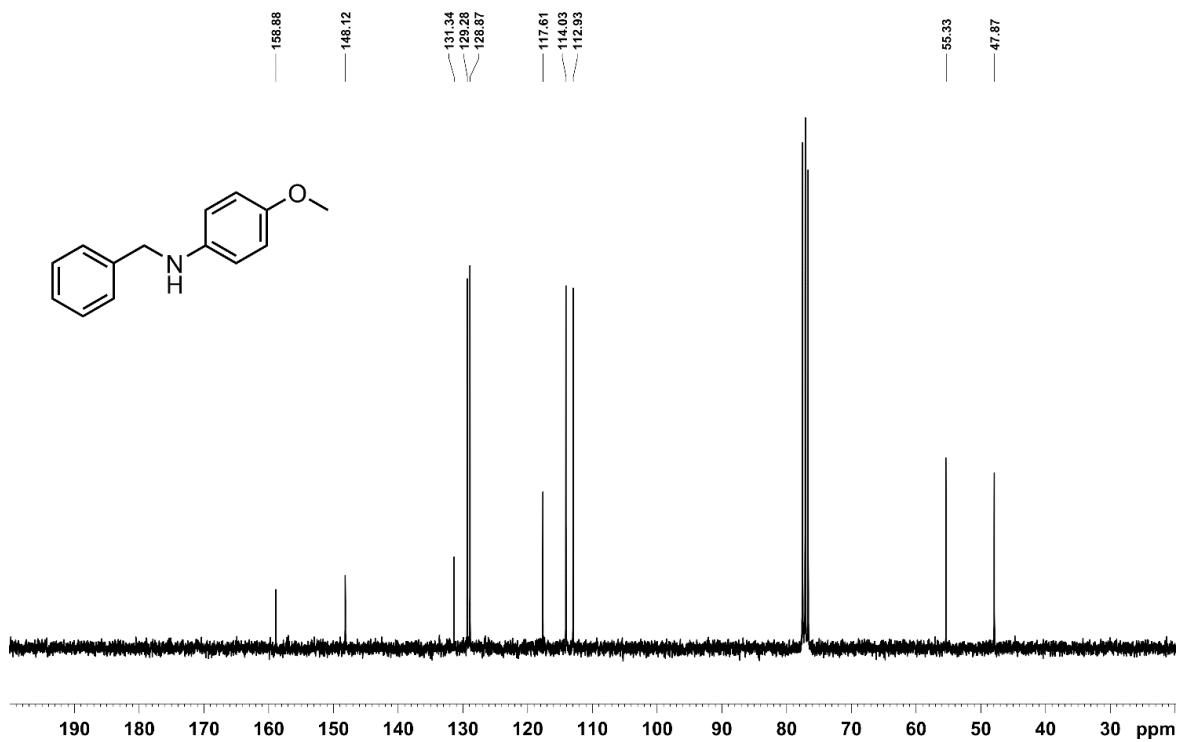
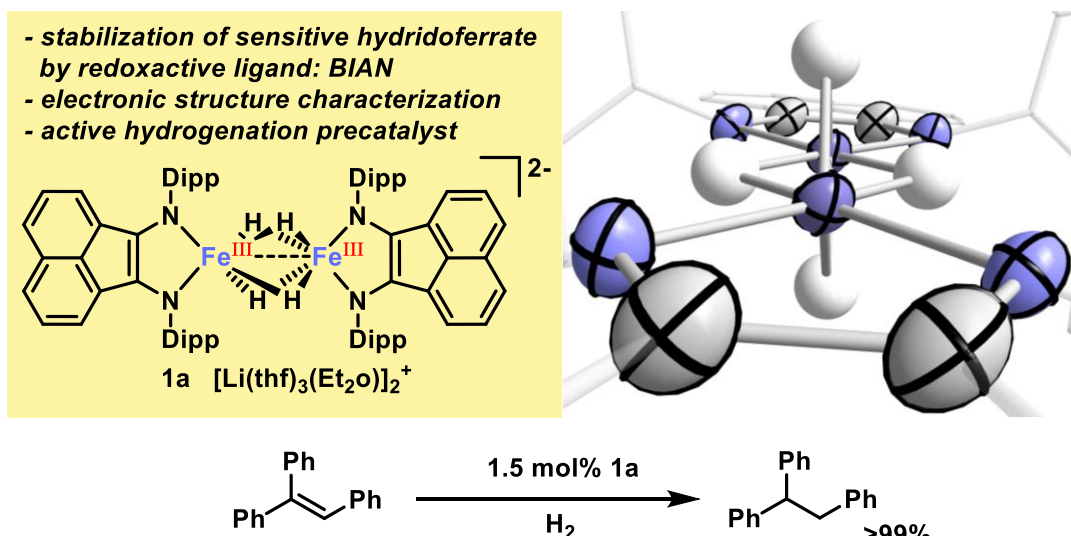


Figure 5.6.45. $^{13}\text{C}\{^1\text{H}\}$ NMR spectrum (101.4 MHz, 300K, CD_2Cl_2) of *N*-benzyl-4-methoxyaniline.

5.6.11 References

- [1] S. Hayashi, K. Hayamizu, *Bull. Chem. Soc. Jpn.* **1989**, 62, 2429–2430
- [2] A. Paulovicova, U. El-Ayaan, K. Shibayama, T. Morita, Y. Fukuda, *Eur. J. Inorg. Chem.* **2001**, 2001, 2641–2646.
- [3] M. Gasperini, F. Ragaini, S. Cenini, *Organometallics* **2002**, 21, 2950–2957.
- [4] R. B. King, M. B. Bisnette, *Journal of Organometallic Chemistry* **1967**, 8, 287–297.
- [5] a) K. Jonas, R. Mynott, C. Krüger, J. C. Sekutowski, Y.-H. Tsay, *Angew. Chem. Int. Ed. Engl.* **1976**, 15, 767–768; b) K. Jonas, R. Mynott, C. Krüger, J. C. Sekutowski, Y.-H. Tsay, *Angew. Chem.* **1976**, 88, 808–809; c) K. Jonas, US Patent 4169845 **1979**
- [6] S. Pelties, T. Maier, D. Herrmann, B. de Bruin, C. Rebreyend, S. Gärtner, I. G. Shenderovich, R. Wolf, *Chem. Eur. J.* **2017**, 23, 6094–6102.
- [7] N. Blaquiere, S. Diallo-Garcia, S. I. Gorelsky, D. A. Black, K. Fagnou, *J. Am. Chem. Soc.* **2008**, 130, 14034–14035.
- [8] P. Bhattacharya, J. A. Krause, H. Guan, *J. Am. Chem. Soc.* **2014**, 136, 11153–11161.
- [9] R. J. Keaton, J. M. Blacquiere, R. T. Baker, *J. Am. Chem. Soc.* **2007**, 129, 1844–1845.
- [10] P. V. Ramachandran, P. D. Gagare, *Inorg. Chem.* **2007**, 46, 7810–7817.
- [11] S. Chaffins, M. Brettreich, F. Wudl, *Synthesis* **2002**, 9, 1191–1194.
- [12] W. Chen, J. F. Hartwig, *J. Am. Chem. Soc.* **2013**, 135, 2068.
- [13] A. Glüer, M. Förster, V. R. Celinski, J. Schmedt auf der Günne, M. C. Holthausen, S. Schneider, *ACS Catal.* **2015**, 5, 7214–7217.
- [14] R. Adam, J. R. Cabrero-Antonino, A. Spannenberg, K. Junge, R. Jackstell, M. Beller, *Angew. Chem. Int. Ed.* **2017**, 56, 3216.
- [15] D. B. Bagal, R. A. Watile, M. V. Khedkar, K. P. Dhake, B. M. Bhanage, *Catal. Sci. Technol.* **2012**, 2, 354.
- [16] R. Kawahara, K. I. Fujita, R. Yamaguchi, *Adv. Synth. Catal.* **2011**, 353, 1161.
- [17] T. N. Gieshoff, M. Villa, A. Welther, M. Plois, U. Chakraborty, R. Wolf, A. J. von Wangelin, *Green Chem.* **2015**, 17, 1408–1413.

6 A Dimeric Iron Ate Complex with Four Bridging Hydrides: Synthesis and Reactivity^{VI}



Abstract: Sensitive hydridic ferrates display key intermediates in iron-catalyzed reduction reactions. Only few examples have been reported and characterized. Herein, we report the synthesis, characterization and reactivity of a new dimeric ferrate anion with four bridging hydrides $[\text{Li}(\text{thf})_3(\text{Et}_2\text{o})]_2\{[(^{\text{Dipp}}\text{BIAN})\text{Fe}]_2(\mu\text{-H})_4\}$ (**1a**). Isolability of **1a** was enabled by the redox-active ligand bis(imino)acenaphthene (BIAN). A doubly reduced BIAN and Fe^{III} has been observed. Remarkably, anion **1a** differs only by two hydrides to $[\text{Li}(\text{thf})_4]_2\{[(^{\text{Dipp}}\text{BIAN}^{2-})\text{Fe}^{\text{II}}]_2(\mu\text{-H})_2\}$ (**2**) and the complexes might be related by oxidative addition. **1a** is an active precatalyst in catalytic hydrogenations of alkenes and might be an intermediate for the catalytic system $[(^{\text{Dipp}}\text{BIAN})\text{FeCl}_2] / 3 \text{ LiEt}_3\text{BH}$.

^{VI} Author contribution:

S. Sandl: Syntheses and characterization of **1a**, **1b**, **2** and **3** (Scheme 6.1 and 6.2, Figure 6.2); reactivity of **1a** (Scheme 6.3); manuscript preparation.

M. Villa: Development of catalytic reaction conditions; substrate scope (Scheme 6.4) see M. Villa, *Dissertation*, Universität Regensburg, 2017.

T. Maier: Discussions and assistance in the characterization of **1a**.

D. Schaarschmidt: Cyclic voltammetry of **1a** and **3**.

R. Wolf: Valuable discussions.

A. Jacobi von Wangelin: Corresponding author.

6.1 Introduction

Transition metal hydrides display key intermediates in various synthetic^[1] and biological^[2] areas. Their biggest industrial application is the hydrogenation reaction.^[3] Recent research efforts have focused on iron as one of the more abundant late transition metals in catalysis.^{[4],[5],[6]} However, little mechanistic info is known as most of our extensive knowledge about mechanistic scenarios stems from its heavier congeners.^[7] Detailed characterization of the electronic structure and reactivities of complex iron hydrides has been rare.^[8] This might be due to the intrinsic properties of such complexes that tend to populate various spin states. The resulting vivid coordination geometry and paramagnetism (i.e. metalloradicals) hampers the isolability of such complexes and routine analysis such as nuclear magnetic resonance (NMR) spectroscopy. Decomposition and aggregation to particles is often observed under the reaction conditions. Consequently, interesting divergent reactivity pattern and properties are expected. Nevertheless, analysis of such compounds is indeed possible by sophisticated methods, such as SQUID magnetometry and Mößbauer spectroscopy. SQUID capitalizes on the paramagnetism of the complex, while the latter technique is especially useful for iron complexes.^[9] Hence, detailed characterization and reactivity assessment under relevant catalytic conditions may substantially enhance our knowledge and mechanistic understanding about iron-catalyzed hydrogenation reactions and related processes. Especially, the recent advent of sensitive organoferrates as potential active catalysts in related processes renders such complexes as highly attractive for such a study.^[10] Unfortunately, only few examples of relevant hydridoferrates have been reported and even less have been fully characterized or probed in catalysis (Figure 6.1).^{[8],[11]} An early example of a hydridoferrate was reported by Shilov and coworkers 1992.^{[8]a} However, an electronic structure characterization is not available from the publication. In 2012, Holland and coworkers reported on a related compound based on bulky β -diketiminato ligands.^{[8]d}

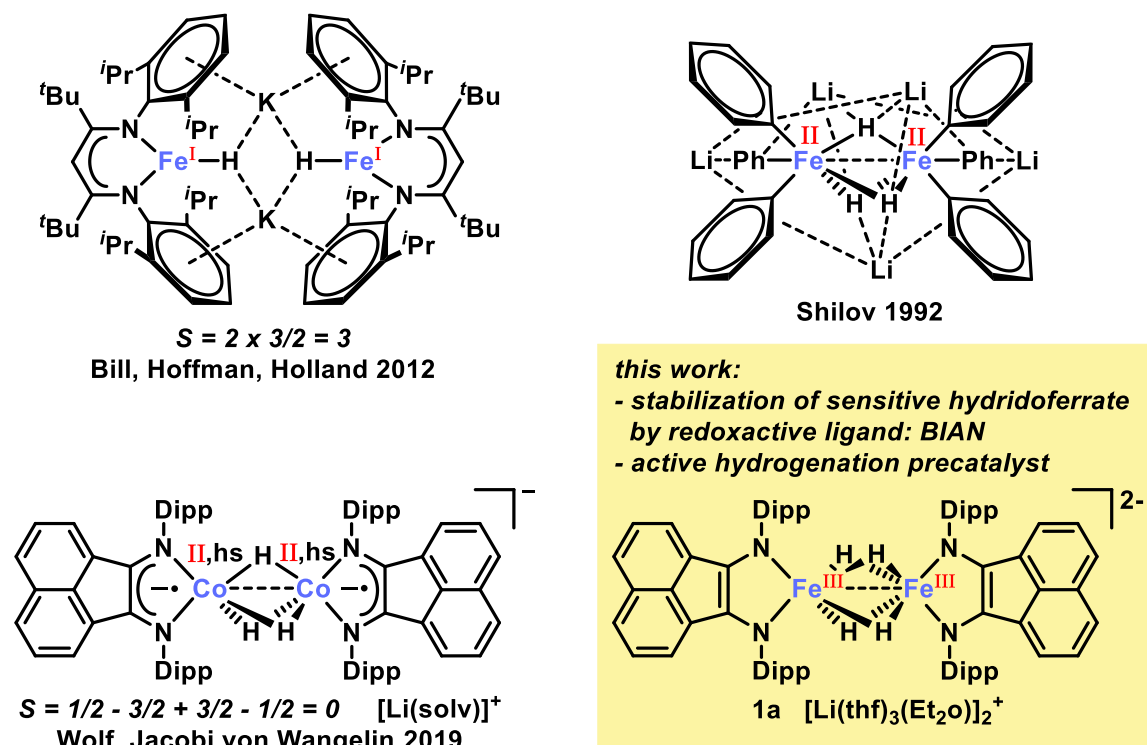


Figure 6.1. Reported dimeric hydridoferrates and -cobaltates.

We envisioned the stabilization of highly reduced ferrates by the redoxactive ligand bis(imino)acenaphthene (BIAN). BIANs can be easily synthesized from commercial precursors on multigram scales and are highly redox-active as they can harbor up to four electrons.^{[12],[13]} Recently, BIAN has been employed by our group for the synthesis of a related dimeric cobaltate with three bridging hydrides, which was an active precatalyst for the hydrogenation of alkenes.^[14] Hence, we were interested in the (i) isolability, (ii) electronic structure and (iii) catalytic reactivity of its ferrate derivative. However, oxidation state determination in complexes with redoxactive ligands is nontrivial.^[15] An eligible technique for accurate determination of the electron density at the metal is hard X-ray spectroscopy such as X-ray absorption spectroscopy (XAS), near-edge X-ray absorption fine structure (XANES) and X-ray emission spectroscopy (XES).^[16] A recent study from the Bauer and coworkers unveiled the electronic structure of a neutral hydridic iron dimer. Note, that the experimentally determined oxidation state is Fe^{II} rather than the formal oxidation state of Fe^{III}.^[17]

Herein, we report on the synthesis, (electronic structure) characterization and reactivity of the new hydridic ferrate $[\text{Li}(\text{thf})_3(\text{Et}_2\text{O})]_2[\{(\text{DippBIAN})\text{Fe}\}_2(\mu\text{-H})_4]$ (**1a**). Comprehensive electronic structure investigations are currently under progress by means of SQUID, Mößbauer spectroscopy, XRAY spectroscopy (XAS, XANES, XES) and density-functional theory calculations (DFT). **1a** is an active precatalyst in catalytic hydrogenations of alkenes.

6.2 Results and Discussion

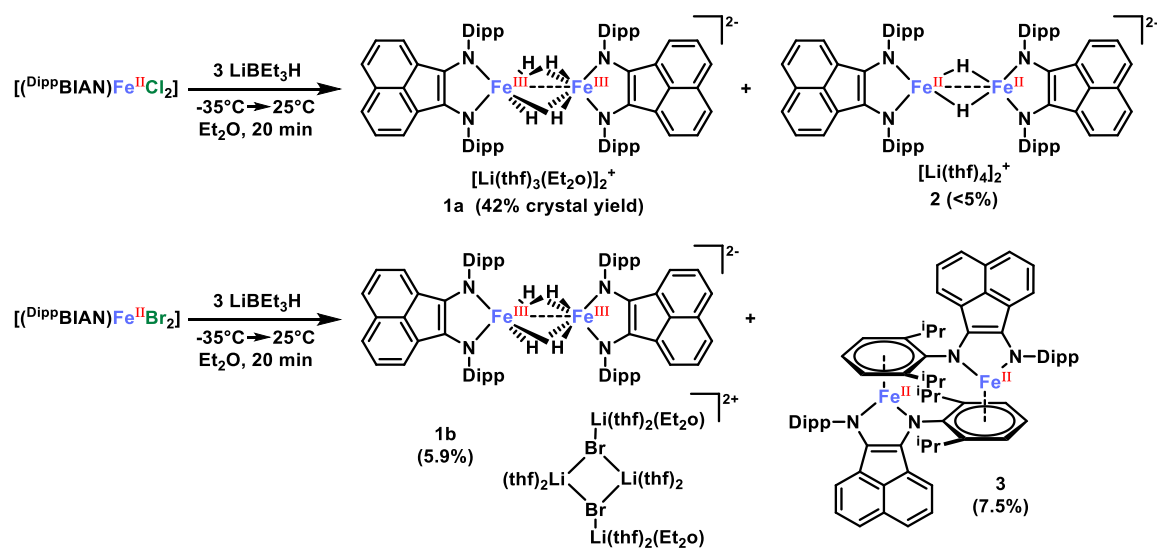
6.2.1 Synthesis and Crystallography

In an effort to synthesize hydridoferrates, we reduced the stable precursor [(^{Dipp}BIAN)FeCl₂] with 3 equiv. LiBEt₃H in Et₂O in a closed reaction vessel.^[18] Effervescence was observed during the reduction, presumably by formation of H₂. The mixture was extracted with *n*-hexane and Et₂O to afford the anionic hydridoferrate **1a** as dark green crystals in 42% yield (Scheme 6.1). Single X-ray diffraction analysis shows four hydride ligands (located in the electron density Fourier map) that bridge two (^{Dipp}BIAN)Fe units (Figure 6.2). The molecule shows pseudo *D*_{2h} symmetry and lies across an inversion center, which is located between the iron atoms. The [Li(thf)₃(Et₂O)]⁺ cation is solvent-separated. A short Fe-Fe distance (2.5286(7) Å) is observed due to the presence of four bridging hydrides and may indicate metal-metal interaction. This bond is longer than in the related complexes [(Cp*Fe)₂(μ-H)₄] (2.202(2) Å)^{[8]b} and Li₅[(Ph₃Fe)₂(μ-H)₃] (2.389(1) and 2.379(1) Å),^{[8]a} but shorter than [(NacNac)Fe(μ-H)₂] (2.624(2) Å).^{[8]c} The Fe-H bond distances are 1.60(7) Å and 1.73(11) Å. The NC=CN bond length of BIAN is significantly shortened in comparison to the neutral ligand and indicative of a dianionic BIAN (Figure 6.2; C-N 1.383(4) Å and 1.374(4) Å; C-C 1.397(4) Å; Fe-N: 1.981(2) Å; N-Fe-N: 88.26(10)°). Similar bond lengths have been recently reported by Wolf and coworkers for a related ferrate [(^{Dipp}BIAN)Fe^I(1,5-cod)]⁻ (1,5-cod = 1,5-cyclooctadiene, C-N 1.385(4) Å, C-C 1.388(5) Å, Fe-N 1.971(2) Å, N-Fe-N 82.1(1)°).^[19] **1a** proved highly sensitive as very diluted THF solutions decomposed in an Ar-filled glovebox. Hence, UV-vis analysis was not feasible.

Additional analyses of the ferrate **1a** include elemental analysis (EA) and cyclic voltammetry (THF/ [nBu₄N]PF₆; E^o = -2.53 V (ΔE_p = 84 mV, reversible oxidation); E^o = -2.19 V (ΔE_p = 123 mV, most likely reversible oxidation) vs. Fc/Fc⁺ (see SI). ¹H-NMR analysis only shows solvate signals from the cation that are indicative of paramagnetism (NMR-silent anion). The preliminary data supports a highly unusual electronic structure of the tetrahydridodiferrate anion of **1a** which is best described as [(^{Dipp}BIAN²⁻)Fe^{III}]₂(μ-H)₄. Detailed characterization of **1a** is currently under progress and will be reported soon (ESI mass spectrometry, Mößbauer

spectroscopy, SQUID magnetometry, hard X-ray spectroscopy (XAS, XANES and XES), density functional theory calculations).

During the optimization of the reaction conditions, a small fraction was isolated, which contained the related ferrate $[\text{Li}(\text{thf})_4]_2\{[(\text{Dipp})\text{BIAN})\text{Fe}\}_2(\mu\text{-H})_2\}$ (**2**, Scheme 6.1). Single X-ray diffraction analysis shows a very similar structure to **1a** which merely differs by two hydride ligands (hydrides located in the electron density Fourier map, Figure 6.2). The metrical distances are indicative of a dianionic BIAN (C-C 1.387(3) Å; C-N: 1.382(2) and 1.393(2) Å; Fe-Fe: 2.5122(5) Å; Fe-N: 1.9863(16) and 1.9890(16) Å; Fe-H 1.84(3) Å; N-Fe-N 89.00(6)°). **2** was additionally characterized by elemental analyses (EA). $^1\text{H-NMR}$ analysis only shows solvate signals from the cation that are indicative of paramagnetism (NMR-silent anion). However, synthesis optimization of **2** either lead to **1a** or decomposition. The two hydrides **1a** and **2** might be related by oxidative addition of hydrogen. Notably, the number of hydrides in the ferrates results in a different solubility: **1a** is moderately soluble in Et_2O (good solubility in toluene and THF) while **2** is only moderately soluble in THF.



Scheme 6.1. Synthesis of **1a**, **2** and **3**.

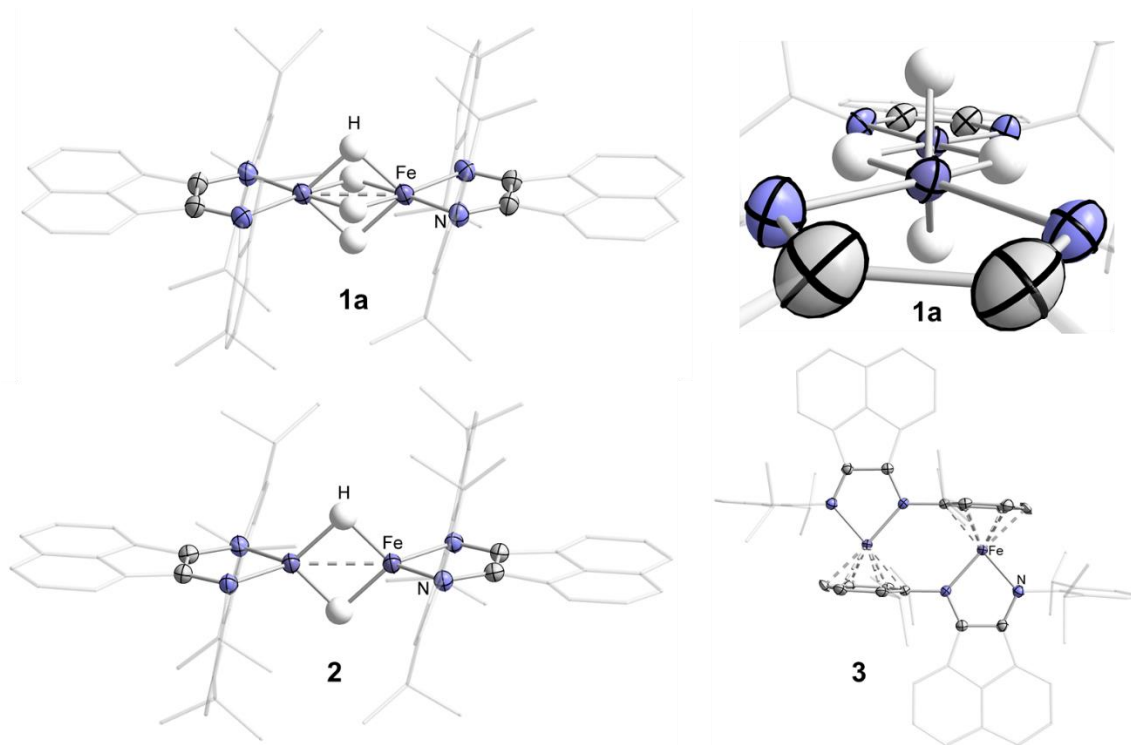


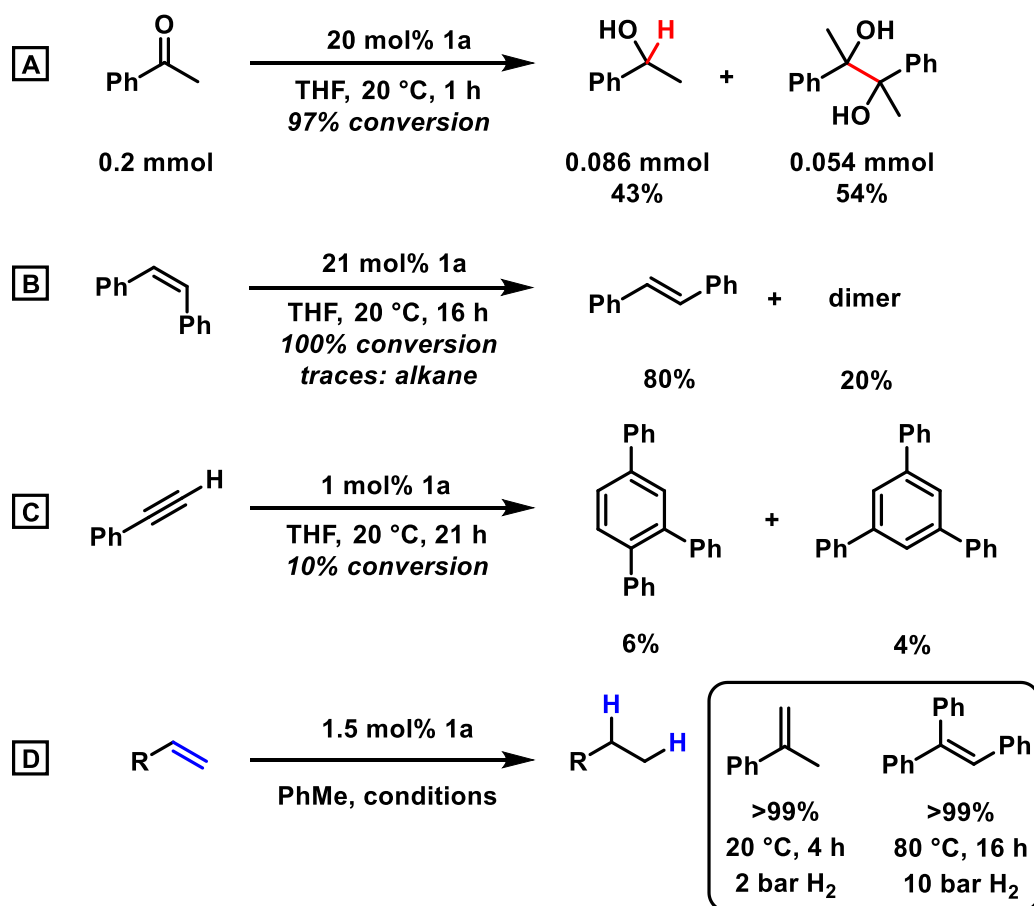
Figure 6.2. Molecular structures of **1a**, **2** and **3**. Thermal ellipsoids at the 50% probability level; minor disordered parts, non-coordinated solvents, selected H atoms, and cations omitted for clarity.

Note, that it is indispensable to use $[(\text{DippBIAN})\text{FeCl}_2]$ instead of $[(\text{DippBIAN})\text{FeBr}_2]$ to obtain **1a** in good yields. Analogous reaction with $[(\text{DippBIAN})\text{FeBr}_2]$ lead to an unselective product distribution including the related hydride $[\{\text{Li}(\text{thf})_2(\mu^3\text{-Br})\}_2\{(\kappa\text{-Br})\text{Li}(\text{thf})_2(\text{Et}_2\text{O})\}_2] [\{(\text{DippBIAN})\text{Fe}\}_2(\mu\text{-H})_4]$ (**1b**) in 5.9% yield and the neutral dimer $[(\text{DippBIAN})\text{Fe}]_2$ (**3**) in 7.5% yield (Scheme 6.1). **1b** showed similar bond distances to **1a** in the single X-ray diffraction analysis. The $(\text{DippBIAN})\text{Fe}$ units in **3** are bridged by coordination to the phenyl rings (Figure 6.2). The NCCN bond lengths of BIAN (Figure 6.2; C-C 1.405(4) Å; C-N 1.345(4) Å; 1.336(4); Fe-N: 1.928(3) Å; 1.909(3) Å; Fe- π plane: 1.5577(13) Å; N-Fe-N: 82.79(11) $^\circ$) are in good agreement with a related complex $[(\text{DippBIAN})\text{Fe}(\text{iPrC}_6\text{H}_5)]$ by Findlater and coworkers (C-C 1.405(3) Å; C-N 1.341(3) Å and 1.343(3) Å; Fe-N: 1.9137(16) Å and 1.9026(16) Å; Fe- π plane: 1.5474(9) Å; N-Fe-N: 82.72(7) $^\circ$). The authors suggested a monoanionic BIAN which is strongly antiferromagnetically coupled to a Fe^{I} center ($S = 0$).^[20] However, Fedushkin and coworkers reported on a monoanionic BIAN that is antiferromagnetically coupled to a high-spin Fe^{II} in

$[(\text{DippBIAN})_2\text{Fe}]$ (C–C 1.4234(18) Å; C–N 1.3367(15) and 1.3393(15) Å). Note, that the C–C bond length of this monoanionic BIAN is much longer than in **3**. The electronic structure ($S = 2 - 2 \cdot \frac{1}{2} = 1$ ground state) was assigned by SQUID magnetometry.^[21] Hence, an alternative description for **3** would involve a dianionic BIAN with a low-spin Fe^{II} ($S = 0$). Additional analyses of the iron complex **3** include elemental analysis (EA), ^1H nuclear magnetic resonance ($^1\text{H-NMR}$) and UV–vis spectroscopy (THF; $\lambda_{\text{max}} = 491 \text{ nm}$, $\epsilon_{\text{max}} = 32300 \text{ mol}^{-1} \text{ cm}^{-1} \text{ L}$).

6.2.2 Reactivity

To gain insight into possible applications of **1a**, initial reactivity assessment has been performed (Scheme 6.2): In the presence of acetophenone, 20 mol% **1a** reacted to 43% 1-phenylethanol and 54% hydrobenzoin (Scheme 6.2A). This may indicate competing hydride transfer and single-electron transfer from **1a**. Accordingly, Fe–H transfers 0.54 hydrides to obtain 1-phenylethanol. The formation of both products accounts for a redox economy of 81% (related to a transfer of three electrons per Fe). Olefin coordination to the hydride has been observed in the isomerization of (Z)-stilbene to (E)-stilbene (80%), which has been accompanied by cyclodimerization (20%, Scheme 6.2B). Poor performance has been detected in the cyclotrimerization of phenylacetylene (10%, Scheme 6.2C). Gratifyingly, **1a** is an active precatalyst for the hydrogenation of challenging alkenes such as triphenylethylene. It is a conceivable intermediate of our recently reported catalytic system $[(\text{DippBIAN})\text{FeCl}_2] / 3 \text{ } n\text{BuLi}$.^[22] However, kinetic comparison of both catalysts suggests **1a** as off-cycle intermediate (SI). After a reaction time of 5 minutes, turnover frequencies (TOF) of 339 h^{-1} and 144 h^{-1} were measured in the hydrogenation of α -methylstyrene (1.9 bar H_2 , 20 °C) for $[(\text{DippBIAN})\text{FeCl}_2] / 3 \text{ } n\text{BuLi}$ (3 mol%) and **1a** (1.5 mol%), respectively.

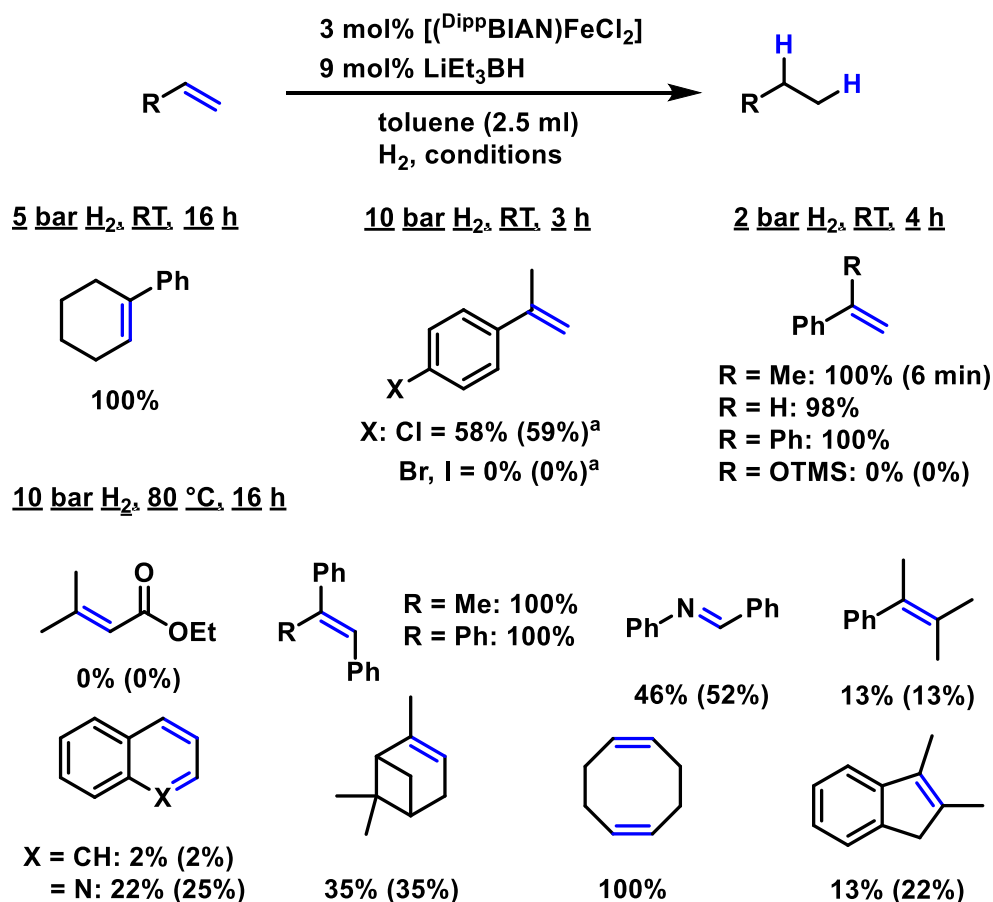


Scheme 6.2. Reactivity of **1a**; 0.2 mmol substrate; B: traces of 1,2-diphenylethane; D: see Scheme 6.3 for hydrogenation conditions.

6.2.3 Catalysis

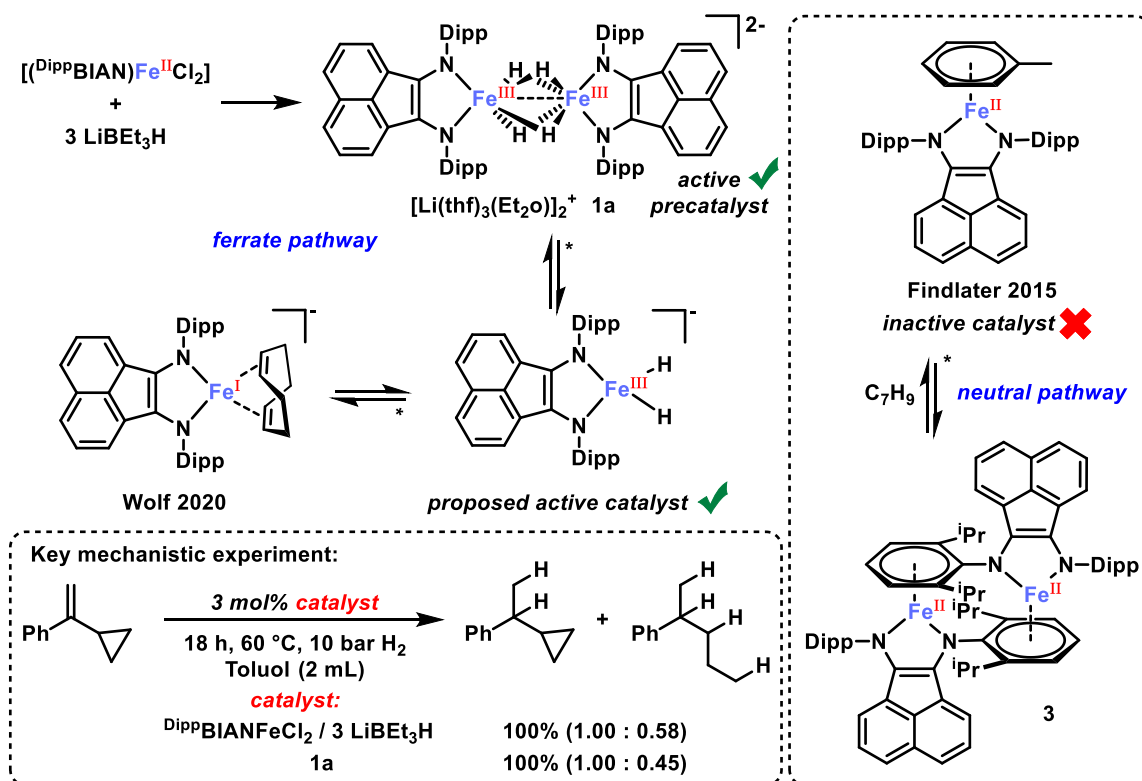
As a conceivable catalytic hydrogenation system, we used $[(^{\text{Dipp}}\text{BIAN})\text{FeCl}_2]$ and 3 equiv. LiEt_3H in toluene. Quantitative hydrogenation of alkenes under mild conditions was observed (20–60 °C, 2–10 bar). These results are similar to our previously reported catalyst $[(^{\text{Dipp}}\text{BIAN})\text{FeCl}_2] / 3 n\text{BuLi}$ (Scheme 6.3).^[22] During the optimization studies, an enhanced hydrogenation activity of catalysts that stem from $[(^{\text{Dipp}}\text{BIAN})\text{FeCl}_2]$ and a lithium-containing reductant were observed (SI). This indicates an alkali-cation effect which we recently observed for a related cobalt catalyst.^[14] One possible explanation for this effect is an attractive noncovalent cation– π interaction.^[23] Notably, a LIFDI-MS analysis of the reduced catalyst $[(^{\text{Dipp}}\text{BIAN})\text{FeCl}_2] / 3 \text{LiEt}_3\text{H}$ in toluene revealed the presence of the ferrate $\text{Li}[(^{\text{Dipp}}\text{BIAN})\text{Fe}(\text{toluene})]$ (655 m/z , SI). However, several attempts to isolate this species failed due to the formation of its related neutral complex

$[(^{\text{Dipp}}\text{BIAN})\text{Fe}(\text{toluene})]$ ($\approx 70\%$). The latter compound was found to be an inactive precatalyst for the hydrogenation of α -methylstyrene (1.9 bar H_2 , 20 °C, 3 h). This unselective catalyst formation hampered the analysis of the reaction order in Fe. Overall, this neutral iron complex is an illustrative showcase for a predominant reduced metal species that is an inactive precatalyst. Presumably, the active catalyst consists of a ferrate with a reduced BIAN ligand (Scheme 6.4). Remarkably, $[(^{\text{Dipp}}\text{BIAN})\text{FeCl}_2] / 3 \text{LiEt}_3\text{BH}$ and **1a** delivered a very similar ratio of competing alkene hydrogenation and hydrogenative ring-opening of α -cyclopropyl styrene (Scheme 6.4, inset). This key experiment indicates a closely related mechanism. However, the reduction of the iron precursor under the catalytic conditions is unselective to obtain a significantly diminished reactivity. The mere formation of $[(^{\text{Dipp}}\text{BIAN})\text{Fe}(\text{toluene})]$ is visible by the dark red color of the catalyst solution (see UV-VIS of **3** in the SI).



Scheme 6.3. Substrate scope of the iron-catalyzed hydrogenation of alkenes. Bonds in blue indicate the site of π -bond hydrogenation. 0.25 mmol of substrate,

Yields were determined by quantitative GC-FID vs. *n*-pentadecane. Conversions are given in parentheses if < 95 %; ^a traces: hydrodehalogenation.



Scheme 6.4. Proposed formation of the active catalyst for alkene hydrogenation; inset: hydrogenative ring-opening experiment with α -cyclopropyl styrene; * denotes equilibria not unambiguously established; arrows are used for illustrative purposes only.

6.3 Conclusions

In summary, synthesis and characterization of a new dimeric ferrate anion with four bridging hydrides $[\text{Li}(\text{thf})_3(\text{Et}_2\text{O})]_2\{(\text{DippBIAN}^{2-})\text{Fe}^{\text{III}}\}_2(\mu\text{-H})_4$ (**1a**) has been achieved. Significant stabilization of the sensitive hydridoferrate has been enabled by the ligand bis(imino)acenaphthene (BIAN). This redox-active ligand has been reduced to its dianionic form to keep the iron center in a stable oxidation state. Remarkably, anion **1a** differs only by two hydrides to $[\text{Li}(\text{thf})_4]_2\{(\text{DippBIAN}^{2-})\text{Fe}^{\text{II}}\}_2(\mu\text{-H})_2$ (**2**) and the complexes might be related by oxidative addition. Comprehensive electronic structure investigations of **1a** are currently under progress by means of SQUID, Mößbauer spectroscopy, XRAY spectroscopy (XAS, XANES, XES) and density-functional theory calculations (DFT). Moreover, this report suggests hydridoferrates as active catalysts in iron-catalyzed hydrogenations: **1a** is an active precatalyst in catalytic hydrogenations of alkenes. Currently, we investigate related transformations with late 3d metalates in our laboratories.

Acknowledgement

This work was funded by the Deutsche Forschungsgemeinschaft (DFG, JA 1107/6-1) and by the European Research Council (ERC) through a Consolidator grant (683150).

6.4 References

- [1] a) M. Y. Darensbourg, C. E. Ash, *Adv. Organomet. Chem.*, **1987**, *27*, 1–50; b) *Recent Advances in Hydride Chemistry* (Eds. M. Peruzzini, R. Poli), Elsevier Science Ltd, **2001**; c) S. J. C. Robinson, D. M. Heinekey, *Chem. Commun.* **2017**, *53*, 669–676; d) H. Dai, H. Guan, *Isr. J. Chem.* **2017**, *57*, 1170–1203.
- [2] Hydrogenases: a) W. Lubitz, H. Ogata, O. Rüdiger, E. Reijerse, *Chem. Rev.* **2014**, *114*, 4081–4148; b) D. Schilter, J. M. Camara, M. T. Huynh, S. Hammes-Schiffer, T. B. Rauchfuss, *Chem. Rev.* **2016**, *116*, 8693–8749.
- [3] a) *The Handbook of Homogeneous Hydrogenation*, (Eds. J. G. de Vries, C. J. Elsevier), Wiley, Weinheim, **2007**; b) *Homogeneous Hydrogenation with Non-Precious Catalysts* (Ed.: J. F. Teichert), Wiley, Weinheim, **2019**.
- [4] a) *Catalysis Without Non-Precious Metals* (Ed.: R. M. Bullock), Wiley, Weinheim, **2010**. b) P. Chirik, R. Morris, *Acc. Chem. Res.* **2015**, *48*, 2495; c) *Non-Noble Metal Catalysis* (Eds.: R. J. M. Klein Gebbink, M.-E. Moret), Wiley, Weinheim, **2018**.
- [5] a) W. M. Czaplík, M. Mayer, J. Cvengroš, A. Jacobi von Wangelin, *ChemSusChem* **2009**, *2*, 396–417; b) I. Bauer, H. Knölker, *Chem. Rev.* **2015**, *115*, 3170–3387; c) R. B. Bedford, P. B. Brenner, *Top. Organomet. Chem.* **2015**, *50*, 19–46; d) C. Cassani, G. Bergonzini, C.-J. Wallentin, *ACS Catal.* **2016**, *6*, 1640–1648; e) T. L. Mako, J. A. Byers, *Inorg. Chem. Front.* **2016**, *3*, 766–790; f) A. Piontek, E. Bisz, M. Szostak, *Angew. Chem. Int. Ed.* **2018**, *57*, 11116–11128.
- [6] P. J. Chirik, *Acc. Chem. Res.* **2015**, *48*, 1687–1695; b) G. A. Filonenko, R. van Putten, E. J. M. Hensen, E. A. Pidko, *Chem. Soc. Rev.* **2018**, *47*, 1459–1483; c) T. Irrgang, R. Kempe, *Chem. Rev.* **2019**, *119*, 2524–2549; d) Wei, C. Darcel, *Chem. Rev.* **2019**, *119*, 2550–2610; e) D. Formenti, F. Ferretti, F. K. Scharnagl, M. Beller, *Chem. Rev.* **2019**, *119*, 2611–2680; f) L. Alig, M. Fritz, S. Schneider, *Chem. Rev.* **2019**, *119*, 2681–2751.
- [7] a) C. A. Tolman, P. Z. Meakin, D. L. Lindner, J. P. Jesson, *J. Am. Chem. Soc.* **1974**, *96*, 2762–2774; b) J. Halpern, *Inorg. Chim. Acta* **1981**, *50*, 11–19; c) S. B. Duckett, C. L. Newell, R. Eisenberg, *J. Am. Chem. Soc.* **1994**, *116*, 10548–10556.

- [8] Relevant hydrides: a) $\text{Li}_5\{[\text{Ph}_3\text{Fe}]_2(\mu\text{-H})_3\}$ T. A. Bazhenova, L. M. Kachapina, A. E. Shilov, M. Y. Antipin, Y. T. Struchkov, *J. Organomet. Chem.* **1992**, *428*, 107–123; b) $\{[(\text{Cp}^*)\text{Fe}]_2(\mu\text{-H})_4\}$: Y. Ohki, H. Suzuki, *Angew. Chem. Int. Ed.* **2000**, *39*, 3120–3122. c) $[(\text{NacNac})\text{Fe}(\mu\text{-H})]_2$ J. M. Smith, R. J. Lachicotte, P. L. Holland, *J. Am. Chem. Soc.* **2003**, *125*, 15752–15753; d) $\text{K}_2[(\text{NacNac})\text{FeH}]_2$ K. P. Chiang, C. C. Scarborough, M. Horitani, N. S. Lees, K. Ding, T. R. Dugan, W. W. Brennessel, E. Bill, B. M. Hoffman, P. L. Holland, *Angew. Chem. Int. Ed.* **2012**, *51*, 3658–3662; e) A. K. Hickey, S. M. Greer, J. A. Valdez-Moreira, S. A. Lutz, M. Pink, J. A. DeGayner, T. D. Harris, S. Hill, J. Telser, J. M. Smith, *J. Am. Chem. Soc.* **2019**, *141*, 11970–11975.
- [9] E. Münck, A. Stubna, *Mössbauer Spectroscopy: Bioinorganic in Compr. Coord. Chem. II* (Eds.: J. A. McCleverty, T. J. Meyer), Elsevier, **2003**, 279–286.
- [10] a) S. B. Muñoz, S. L. Daifuku, J. D. Sears, T. M. Baker, S. H. Carpenter, W. W. Brennessel, M. L. Neidig, *Angew. Chem. Int. Ed.* **2018**, *57*, 6496; b) J. D. Sears, S. B. Muñoz, S. L. Daifuku, A. A. Shaps, S. H. Carpenter, W. W. Brennessel, M. L. Neidig, *Angew. Chem. Int. Ed.* **2019**, *58*, 2769; c) M. L. Neidig, S. H. Carpenter, D. J. Curran, J. C. DeMuth, V. E. Fleischauer, T. E. Iannuzzi, P. G. N. Neate, J. D. Sears, N. J. Wolford, *Acc. Chem. Res.* **2019**, *52*, 140–150; d) S. Sandl, A. Jacobi von Wangelin, *Angew. Chem. Int. Ed.* **2020**, 10.1002/anie.201914844.
- [11] Hydridocarbonylferrates: M. Y. Darensbourg, D. J. Darensbourg, H. L. C. Barros, *Inorg. Chem.* **1978**, *17*, 297–301; b) J. P. Collman, R. G. Finke, P. L. Matlock, R. Wahren, R. G. Komoto, J. I. Brauman, *J. Am. Chem. Soc.* **1978**, *100*, 1119–1140; c) J. J. Brunet, *Chem. Rev.* **1990**, *90*, 1041–1059; d) C. Femoni, M. C. Iapalucci, G. Longoni, S. Zacchini, *Dalt. Trans.* **2011**, *40*, 8685.
- [12] a) H. tom Dieck, A. Orlopp, *Angew. Chem. Int. Ed.* **1975**, *14*, 251–252; b) H. tom Dieck, H. Bruder, *J. Chem. Soc., Chem. Commun.* **1977**, *1*, 24–25.
- [13] a) M. W. Van Laren, C. J. Elsevier, *Angew. Chem. Int. Ed.* **1999**, *38*, 3715; b) I. L. Fedushkin, A. A. Skatova, V. A. Chudakova, G. K. Fukin, *Angew. Chem. Int. Ed.* **2003**, *42*, 3294–3298. c) F. S. Wekesa, R. Arias-Ugarte, L. Kong, Z. Sumner, G. P. McGovern, M. Findlater, *Organometallics* **2015**, *34*, 5051–5056; d) V. V. Khrizanforova, V. I. Morozov, M. N. Khrizanforov, A. N. Lukoyanov, O. N. Kataeva, I. L. Fedushkin, Y. H. Budnikova, *Polyhedron* **2018**, *154*, 77–82.

- [14] S. Sandl, T. M. Maier, N. P. van Leest, S. Kröncke, U. Chakraborty, S. Demeshko, K. Koszinowski, B. de Bruin, F. Meyer, M. Bodensteiner, C. Herrmann, R. Wolf, A. Jacobi von Wangelin, *ACS Catal.* **2019**, *9*, 7596-7606.
- [15] a) K. Ray, T. Petrenko, K. Wiegardt, F. Neese, *Dalt. Trans.* **2007**, 1552-1566. b) P. J. Chirik, K. Wiegardt, *Science* **2010**, *327*, 794–795; c) V. K. K. Praneeth, M. R. Ringenberg, T. R. Ward, *Angew. Chem. Int. Ed.* **2012**, *51*, 10228–10234; d) V. Lyaskovskyy, B. de Bruin, *ACS Catal.* **2012**, *2*, 270–279; e) O. R. Luca, R. H. Crabtree, *Chem. Soc. Rev.* **2013**, *42*, 1440–1459; f) P. Karen, *Angew. Chem. Int. Ed.* **2015**, *54*, 4716–4726.
- [16] A. Schoch, L. Burkhardt, R. Schoch, K. Stührenberg, M. Bauer, *Faraday Discuss.* **2019**, *220*, 113–132.
- [17] L. Burkhardt, C. Mueller, O. A. Groß, Y. Sun, H. Sitzmann, M. Bauer, *Inorg. Chem.* **2019**, *58*, 6609–6618.
- [18] W. W. Laxson, S. Özkar, S. Folkman, R. G. Finke, *Inorganica Chim. Acta* **2015**, *432*, 250–257.
- [19] T. M. Maier, R. Wolf, *unpublished results*.
- [20] P. J. Larson, F. S. Wekesa, A. Singh, C. R. Smith, A. Rajput, G. P. McGovern, D. K. Unruh, A. F. Cozzolino, M. Findlater, *Polyhedron* **2019**, *159*, 365–374.
- [21] I. L. Fedushkin, A. A. Skatova, N. M. Khvoynova, A. N. Lukoyanov, G. K. Fukin, S. Y. Ketkov, M. O. Maslov, A. S. Bogomyakov, V. M. Makarov, *Russ. Chem. Bull.* **2013**, *62*, 2122–2131.
- [22] M. Villa, D. Miesel, A. Hildebrandt, F. Ragaini, D. Schaarschmidt, A. Jacobi von Wangelin, *ChemCatChem* **2017**, *9*, 3203.
- [23] a) K. Grubel, W. W. Brennessel, B. Q. Mercado, P. L. Holland, *J. Am. Chem. Soc.* **2014**, *136*, 16807–16816; b) C. R. Kennedy, S. Lin, E. N. Jacobsen, *Angew. Chem. Int. Ed.* **2016**, *55*, 12596–12624; c) G. P. Connor, P. L. Holland, *Catal. Today* **2017**, *286*, 21–40; d) S. Yamada, *Chem. Rev.* **2018**, *118*, 11353–11432; e) K. T. Mahmudov, A. V. Gurbanov, F. I. Guseinov, M. F. C. Guedes da Silva, *Coord. Chem. Rev.* **2019**, *387*, 32–46.

6.5 Supporting Information

6.5.1 General

Analytical Thin-Layer Chromatography: TLC was performed using aluminium plates with silica gel and fluorescent indicator (Merck, 60, F254). Thin layer chromatography plates were visualized by exposure to ultraviolet light (366 or 254 nm) or by immersion in a staining solution of molybdato-phosphoric acid in ethanol or potassium permanganate in water.

Column Chromatography: Flash column chromatography with silica gel 60 from KMF (0.040-0.063 mm). Mixtures of solvents used are noted in brackets.

Chemicals and Solvents: Commercially available olefins were distilled under reduced pressure before use. Solvents (THF, Et₂O, *n*-hexane, toluene) were distilled over sodium and benzophenone and stored over molecular sieves (3 Å) under argon. Solvents used for column chromatography were distilled under reduced pressure prior use (ethyl acetate). LiBEt₃H (1 M in THF) was used as received from SigmaAldrich or diluted before use.

Cyclic voltammetry: Electrochemical measurements were carried out under an atmosphere of nitrogen using 0.5 mmol·L⁻¹ solutions of the analyte and [N(*n*-Bu)₄][PF₆] (0.1 mol·L⁻¹) as supporting electrolyte in tetrahydrofuran. A BASi C3 Cell stand potentiostat was applied using a glassy carbon working electrode (\varnothing = 2.5 mm), a Pt wire as counter and an Ag/AgCl reference electrode. Ferrocene was employed as internal reference; the redox potentials are given against the ferrocene/ferrocenium redox couple according to G. Gritzner, J. Kuta, *Pure Appl. Chem.* **1984**, *56*, 461–466.

High Pressure Reactor: Hydrogenation reactions were carried out in 160 and 300 mL high pressure reactors (ParrTM) in 4 mL glass vials. The reactors were loaded under argon, purged with H₂ (1 min), sealed and the internal pressure was adjusted. Hydrogen (99.9992%) was purchased from Linde.

¹H- und ¹³C-NMR-Spectroscopy: Nuclear magnetic resonance spectra were recorded on a Bruker Avance 300 (300 MHz) and Bruker Avance 400 (400 MHz). ¹H-NMR: The following abbreviations are used to indicate multiplicities: s = singlet;

d = doublet; t = triplet, q = quartet; m = multiplet, dd = doublet of doublet, dt = doublet of triplet, dq = doublet of quartet, ddt = doublet of doublet of quartet. Chemical shift δ is given in ppm to tetramethylsilane.

Gas chromatography with FID (GC-FID): HP6890 GC-System with injector 7683B and Agilent 7820A System. Column: HP-5, 19091J-413 (30 m \times 0.32 mm \times 0.25 μ m), carrier gas: N₂. GC-FID was used for reaction control and catalyst screening. Calibration with internal standard *n*-pentadecane and analytically pure samples. Non-commercial authentic samples were prepared by hydrogenation with Pd/C/H₂.

Gas chromatography with mass-selective detector (GC-MS): Agilent 6890N Network GC-System, mass detector 5975 MS. Column: HP-5MS (30m \times 0.25 mm \times 0.25 μ m, 5% phenylmethylsiloxane, carrier gas: H₂. Standard heating procedure: 50 °C (2 min), 25 °C/min \rightarrow 300 °C (5 min).

Gas-uptake reaction monitoring: Gas-uptake was monitored with a *Man On the Moon X201* kinetic system to maintain a constant reaction pressure. The system was purged with hydrogen prior use. Reservoir pressure was set to about 9 bar H₂. H₂ consumption was related to final yields by GC-FID vs. *n*-pentadecane.

Magnetic moment: Magnet susceptibility χ_M was determined by performing a NMR experiment following the procedure of *Evans*. (D. F. Evans, *J. Chem. Soc.* **1959**, 2003.)

UV-Vis-spectroscopy: UV-vis spectra of investigated solutions were recorded on a Varian Cary 50 spectrophotometer in quartz cuvettes with a layer thickness of 1 cm and a concentration of 10⁻⁴ to 10⁻⁶ mol·L⁻¹ at room temperature.

X-ray crystallography: The single crystal X-ray diffraction data were recorded on an Agilent SuperNova with an Atlas CCD detector with microfocus Cu K α radiation (λ = 1.54184 Å) or Mo K α radiation (λ = 0.71073 Å). Empirical multi-scan and analytical absorption corrections were applied to the data.

CrysAlisPro 1.171.40.18, CrysAlisPro Software System, Rigaku Oxford Diffraction, (2019).

The structures were solved with SHELXT and least-square refinements on F^2 were carried out with SHELXL.

O.V. Dolomanov and L.J. Bourhis and R.J. Gildea and J.A.K. Howard and H. Puschmann, Olex2: A complete structure solution, refinement and analysis program, *J. Appl. Cryst.*, (2009), **42**, 339-341.

Sheldrick, G.M., Crystal structure refinement with ShelXL, *Acta Cryst.*, (2015), **C27**, 3-8.

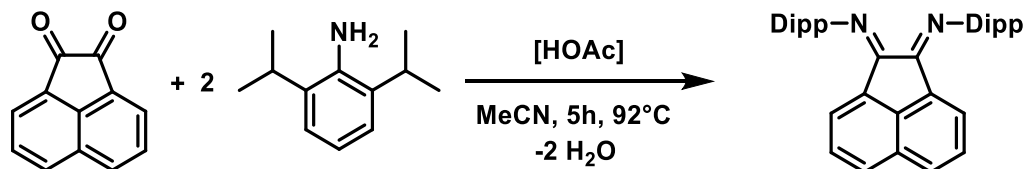
Sheldrick, G.M., ShelXT-Integrated space-group and crystal-structure determination, *Acta Cryst.*, (2015), **A71**, 3-8.

Liquid injection field desorption mass spectrometry (LIFDI-MS): The spectra were recorded by the Central Analytics Lab at the Department of Chemistry, University of Regensburg, on a LIFDI-MS from Linden connected to an AccuTOF GCX from Jeol.

6.5.2 Synthesis of complexes

Synthesis of bis[*N,N'*-(2,6-diisopropylphenyl)imino]acenaphthene (^{Dipp}BIAN)

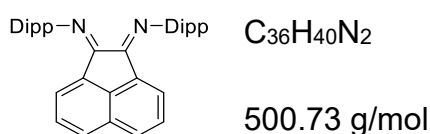
Synthesis was performed following a procedure by A. Paulovicova, U. El-Ayaan, K. Shibayama, T. Morita, Y. Fukuda, *Eur. J. Inorg. Chem.* **2001**, 2001, 2641–2646.



Scheme 6.5.13. Synthesis of ^{Dipp}BIAN.

Acenaphthenquinone (3.50 g, 19.2 mmol, 1.00 equiv.) was suspended in acetonitrile (125 mL) and refluxed at 90 °C for 1 h. After addition of 35 mL acetic acid the reaction mixture was stirred for further 30 min. During this time acenaphthenquinone was almost dissolved with a yellow to orange color. 2,6-diisopropylaniline (8.15 g, 46.0 mmol, 2.40 equiv.) was added dropwise during

which a color change to red-orange was observed. The solution was heated under reflux for 5.5 h. A yellow-orange solid was formed, filtered at room temperature and washed with *n*-pentane (5 x 20 mL). The raw material was dissolved in chloroform (300 mL), filtered and the solvent was removed under reduced pressure. After washing with *n*-pentane (2 x 100 mL) bis[*N,N'*-(2,6-diisopropylphenyl)imino]acenaphthene was isolated by drying in vacuo as orange-yellow powder.



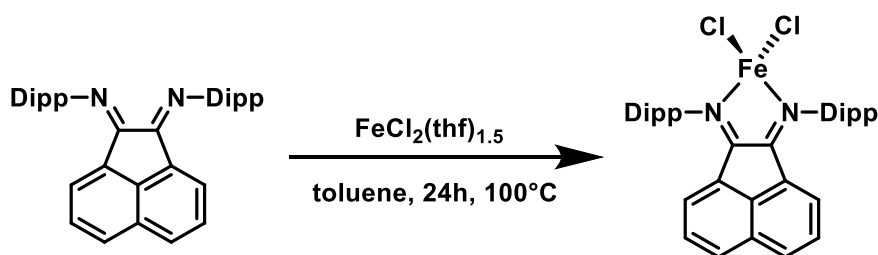
Appearance Yellow to orange solid

Yield 7.5 g, 1.9 mmol (49%)

$^1\text{H-NMR}$ (300 MHz, CDCl_3): δ 7.88 (d, $J = 8.3$ Hz, 2H, CH_{BIAN}), 7.36 (t, $J = 7.6$ Hz, 2H, CH_{BIAN}), 7.27 (m, 6H, CH_{Dipp}), 6.63 (d, $J = 7.2$ Hz, 2H, CH_{BIAN}), 3.03 (sept, $J = 6.8$ Hz, 4H, $\text{CH}(\text{CH}_3)_2$), 1.23 (d, $J = 6.8$ Hz, 12H, $\text{CH}(\text{CH}_3)_2$), 0.97 (d, $J = 6.8$ Hz, 12H, $\text{CH}(\text{CH}_3)_2$)

[^{Dipp}BIANFeCl₂]

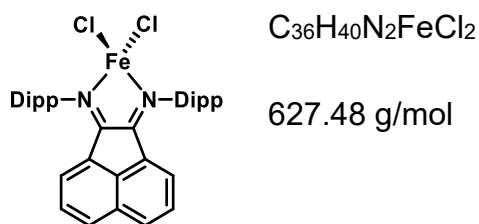
Synthesis was performed following an adapted procedure by M. Villa, D. Miesel, A. Hildebrandt, F. Ragaini, D. Schaarschmidt, A. Jacobi von Wangelin, *ChemCatChem* **2017**, *9*, 3203–3209. $\text{FeCl}_2(\text{thf})_{1.5}$ was synthesized according to F. Cotton, R. L. Luck, K.-A. Son, *Inorganica. Chimica. Acta.* **1991**, *179*, 11–15.



Scheme 6.5.14. Synthesis of (^{Dipp}BIAN)FeCl₂.

6 A Dimeric Iron Ate Complex with Four Bridging Hydrides: Synthesis and Reactivity

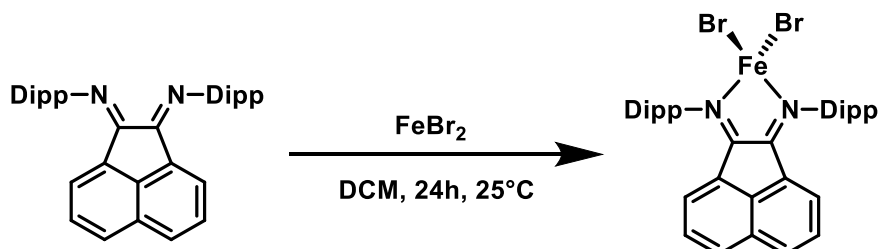
A Schlenk flask was charged with $\text{FeCl}_2(\text{thf})_{1.5}$ (4.45 g, 18.9 mmol, 1.00 equiv.) and DippBIAN (10.4 g, 20.8 mmol, 1.10 equiv.) in toluene (400 mL). The mixture was heated to 100 °C and stirred for 3 days, during which time the color changed from orange to brown-green and a precipitate formed. The mixture was cooled to room temperature and the suspension was concentrated in vacuo (200 mL). The solvent was decanted, and the green solid residue was washed with toluene (10 x 20mL). After extraction with DCM (150mL) using a P3 frit, the solvent was removed in vacuo. The product was obtained as dark green crystalline solid.



Appearance	Dark green crystals
Yield	7.27 g, 11.5 mmol (61%)
Elemental Analysis	Found (calc.): C: 68.79 (68.91); H: 6.54 (6.43); N: 4.46 (4.23)

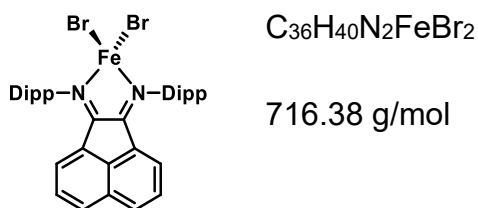
[(^{Dipp}BIAN)FeBr₂]

Synthesis was performed following an adapted procedure by M. Villa, D. Miesel, A. Hildebrandt, F. Ragaini, D. Schaarschmidt, A. Jacobi von Wangelin, *ChemCatChem* **2017**, *9*, 3203–3209.



Scheme 6.5.15. Synthesis of (^{Dipp}BIAN)FeBr₂.

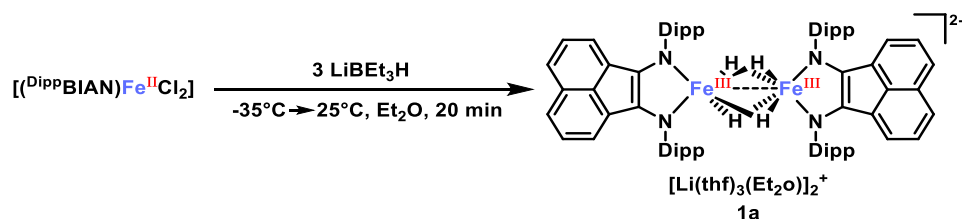
A Schlenk flask was charged with FeBr₂ (3.97 g, 18.4 mmol, 1.00 equiv.) and ^{Dipp}BIAN (9.23 g, 18.4 mmol, 1.00 equiv.) in DCM (300 mL). The mixture was stirred for 3d, during which the colour changed from orange to dark green. The solution was filtered with a Schlenk frit (P3) and concentrated in vacuo (100 mL). The raw product was recrystallised by layering with hexane (100 mL). Black needles were isolated by decantation and washed with toluene (3 x 5 mL).



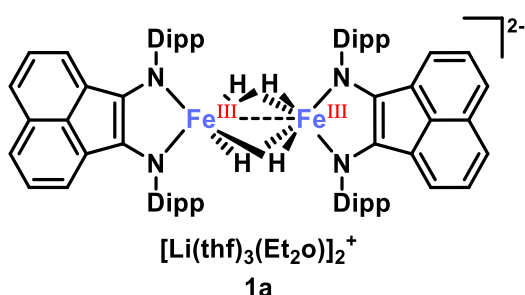
Appearance Black needles

Yield 10.6 g, 14.7 mmol, (80%).

Elemental Analysis Found (calc.): C: 60.44 (60.36); H: 5.72 (5.63); N: 3.72 (3.91)

[Li(thf)₃(Et₂O)]₂[(^{Dipp}BIAN)Fe]₂(μ-H)₄ (1a)**Scheme 6.5.16. Synthesis of 1a.**

In an argon-filled glovebox, a Schlenk flask was equipped with a suspension of [^{Dipp}BIAN)FeCl₂] (0.81 mmol) in Et₂O (20 mL) and closed with a septum. After cooling to -35 °C, the flask was taken out of the freezer and LiBEt₃H (3 equiv., 1.1M, THF, precooled to -35 °C) was added dropwise during which a color change from pale brown to dark brown, effervescence and solubilization was observed. It is very important to create an overpressure in the flask in order to obtain the product. After 20 minutes stirring, hexane (20 mL) was added and the mixture was filtered through a closed Schlenk frit (P4, gravitation). The filter cake was washed with hexane (3 x 6 mL, dark red) and extracted with Et₂O (10, 10, 5 mL, dark green). The latter fraction was crystallized at -35 °C to obtain the product as single crystals.

C₁₀₄H₁₅₂N₄Fe₂O₈Li₂

1711.91 g/mol

Appearance

Dark green blocks

Yield

291.6 mg, 0.17 mmol, (42%).

CV

$E^{\circ'} = -2.53 \text{ V}$ ($\Delta E_p = 84 \text{ mV}$, reversible oxidation); $E^{\circ'} = -2.19 \text{ V}$ ($\Delta E_p = 123 \text{ mV}$, most likely reversible oxidation) vs. Fc/Fc⁺ in THF (see below).

m.p. 204°C (decomposition).

Determination of magnetic moment μ_{eff} (THF-d₈, 293 K) = 7.9 μ_{B} .

(Evans)

Elemental analysis Found (calc. for
[Li(thf)₃(Et₂O)]₂[(^{Dipp}BIAN)Fe]₂(μ -H)₄):
C: 73.00 (72.97); H: 8.06 (8.95); N: 3.76
(3.27).

Cyclovoltammetry

Electrochemical measurements were carried out under an atmosphere of nitrogen using 0.5 mmol·L⁻¹ solutions of the analyte and [N(*n*-Bu)₄][PF₆] (0.1 mol·L⁻¹) as supporting electrolyte in tetrahydrofuran. A BASi C3 Cell Stand potentiostat was applied using a glassy carbon working electrode ($\varnothing = 2.5$ mm), a Pt wire as counter and an Ag/AgCl reference electrode. Ferrocene was employed as internal reference; the redox potentials are given against the ferrocene/ferrocenium redox couple according to G. Gritzner, J. Kuta, *Pure Appl. Chem.* **1984**, 56, 461–466.

Table 6.5.1. Cyclovoltammetry of **1a**.

Electrochemical Process	Figure	Comment
$E^{\circ} = -3.16$ V ($\Delta E_p = 235$ mV)	6.5.4	irreversible reduction
$E^{\circ} = -3.08$ V ($\Delta E_p = 228$ mV)	6.5.4	irreversible reduction
$E^{\circ} = -2.53$ V ($\Delta E_p = 84$ mV)	6.5.1–3	reversible oxidation
$E^{\circ} = -2.19$ V ($\Delta E_p = 123$ mV)	6.5.1–2	most likely reversible oxidation, large ΔE_p due to overlapping electrochemical process (might be caused by impurity)
$E^{\circ} = -1.85$ V ($\Delta E_p = 72$ mV)	6.5.5	reversible oxidation
$E^{\circ} = -1.75$ V ($\Delta E_p = 65$ mV)	6.5.5	reversible oxidation
$E_{pa} = -0.99$ V	6.5.6	irreversible oxidation
$E_{pa} = -0.33$ V	6.5.7	irreversible oxidation
$E_{pa} = 0.38$ V	6.5.8	irreversible oxidation
$E_{pa} = 0.99$ V	6.5.8	irreversible oxidation

Figure 6.5.8: irreversible oxidation of the analyte leads to decomposition accompanied with the occurrence of new electrochemical processes ($E_{pc} = -2.48$ V, $E_{pa} = -2.37$ V, $E_{pc} = -2.08$ V, $E_{pa} = -1.47$ V; $E_{pc} = -0.73$ V, $E_{pa} = -0.67$ V)

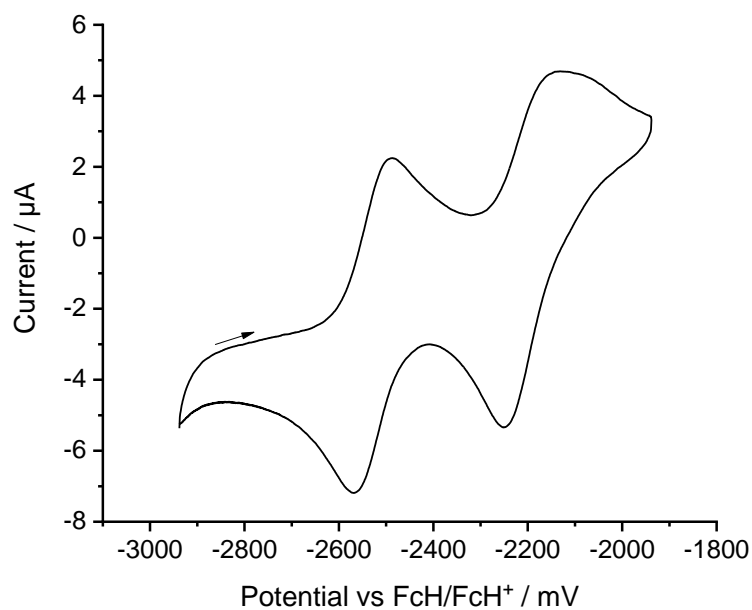


Figure 6.5.1. Cyclic voltammogram of **1a** (scan rate $100 \text{ mV}\cdot\text{s}^{-1}$).

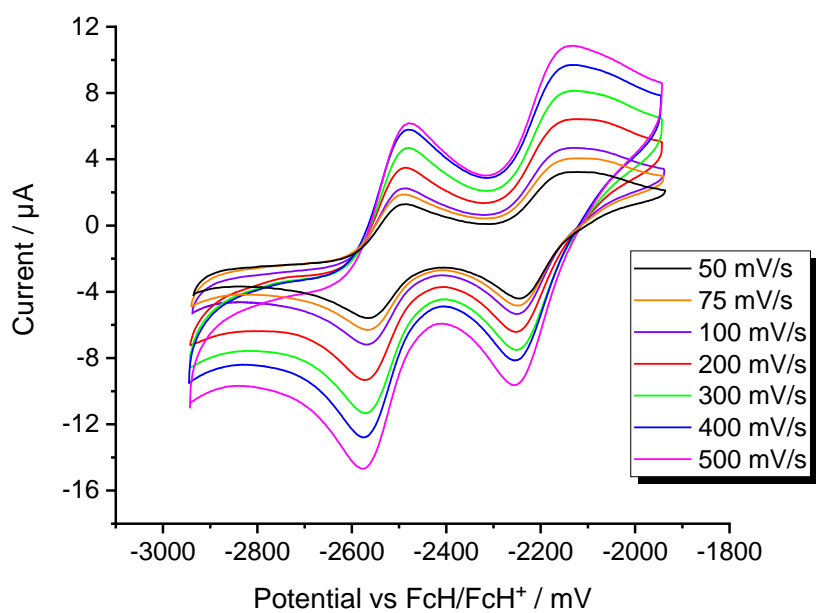


Figure 6.5.2. Cyclic voltammogram of **1a** at different scan rates.

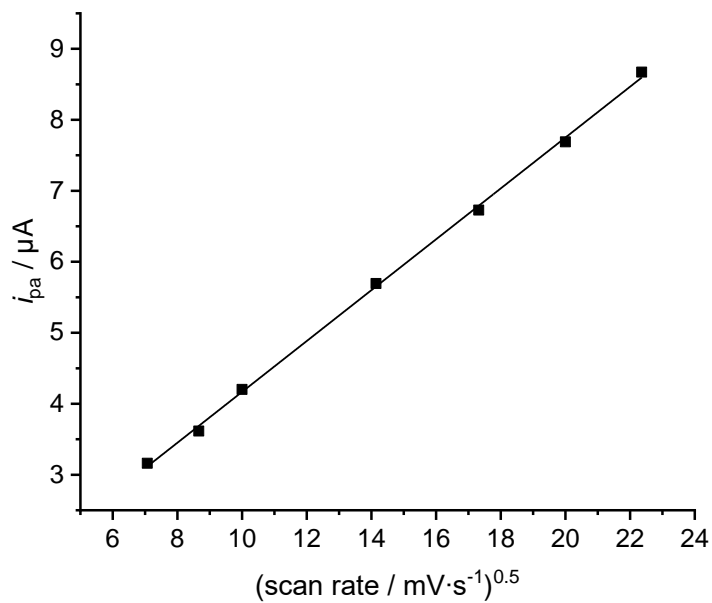


Figure 6.5.3. Anodic peak currents at different scan rates ($E^{\circ} = 2.53$ V, linear fit $R^2 = 0.99$).

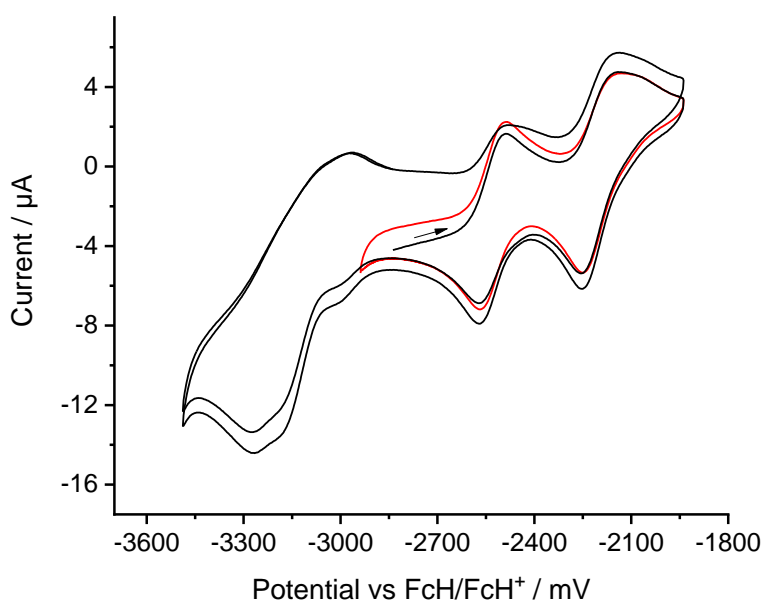


Figure 6.5.4. Cyclic voltammogram of **1a** (first two cycles are shown, scan rate 100 mV·s⁻¹).

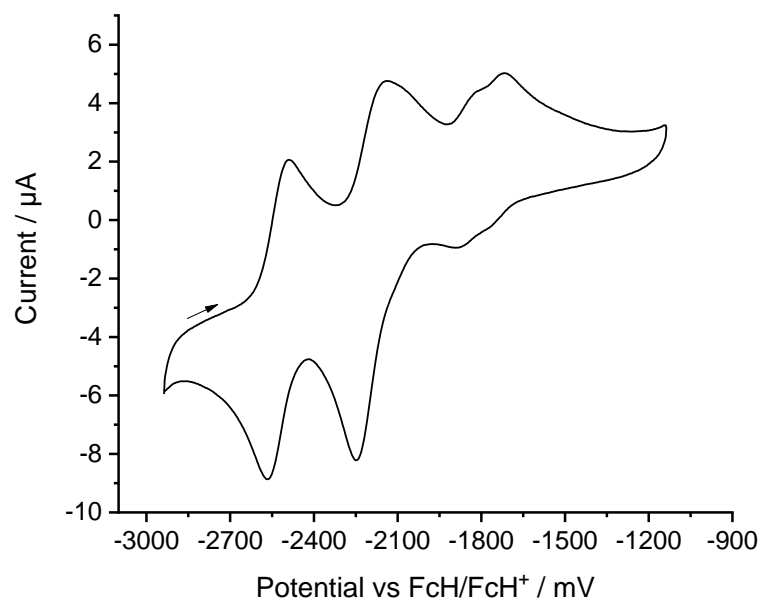


Figure 6.5.5. Cyclic voltammogram of **1a** (scan rate $100 \text{ mV}\cdot\text{s}^{-1}$).

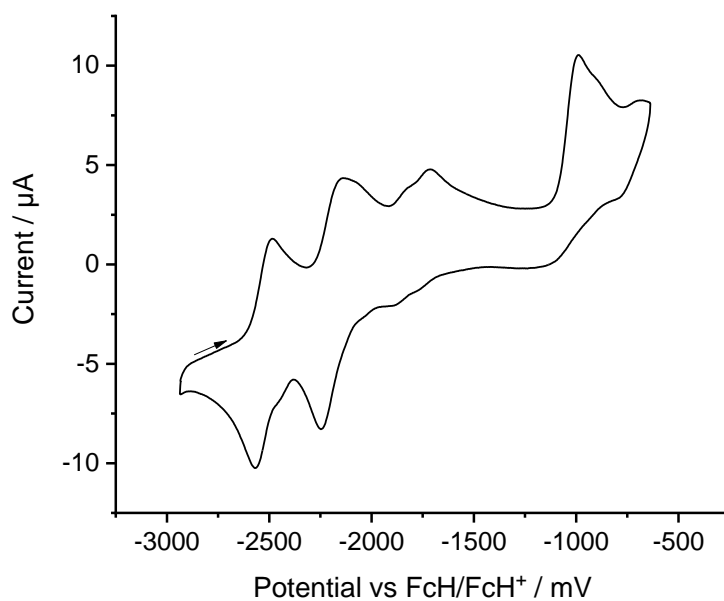


Figure 6.5.6. Cyclic voltammogram of **1a** (scan rate $100 \text{ mV}\cdot\text{s}^{-1}$).

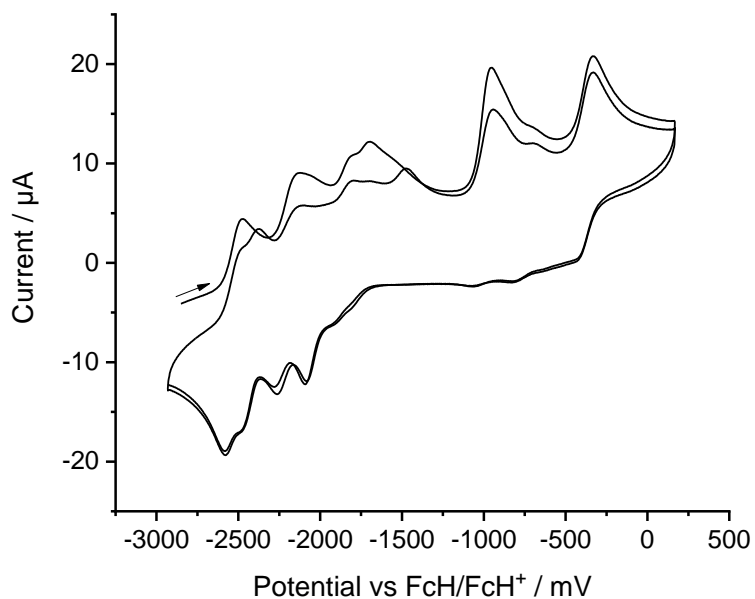


Figure 6.5.7. Cyclic voltammogram of **1a** (first two cycles are shown, scan rate $200 \text{ mV}\cdot\text{s}^{-1}$).

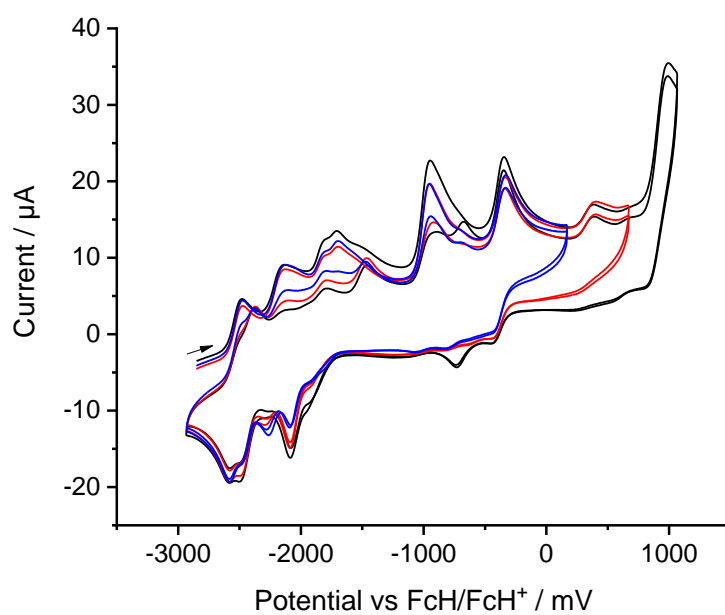


Figure 6.5.8. Cyclic voltammogram of **1a** (first two cycles are shown, scan rate $200 \text{ mV}\cdot\text{s}^{-1}$).

IR

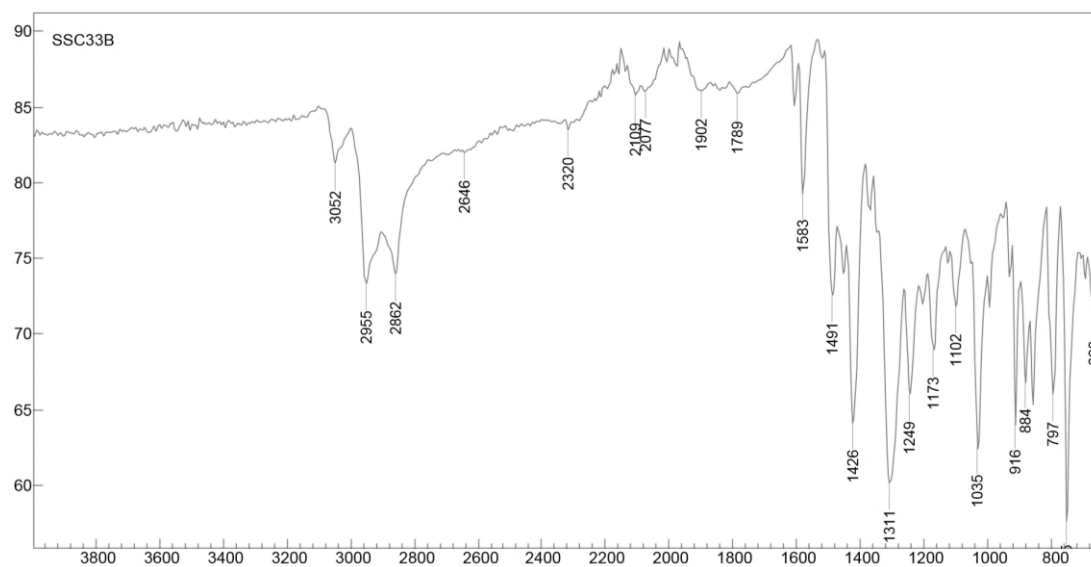


Figure 6.5.9. FT-IR of 1a.

Crystal structure

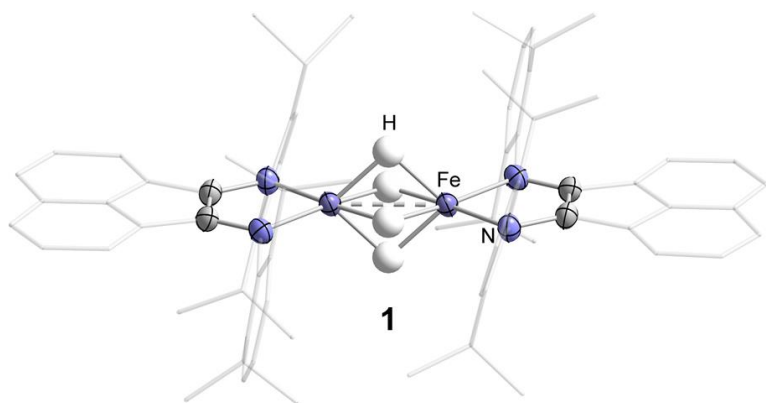


Figure 6.5.10. Solid-state molecular structure of **1a**. Minor disordered parts, non-coordinated solvents, cation and selected hydrogen atoms are omitted for clarity. Thermal ellipsoids are drawn at the 50% probability level.

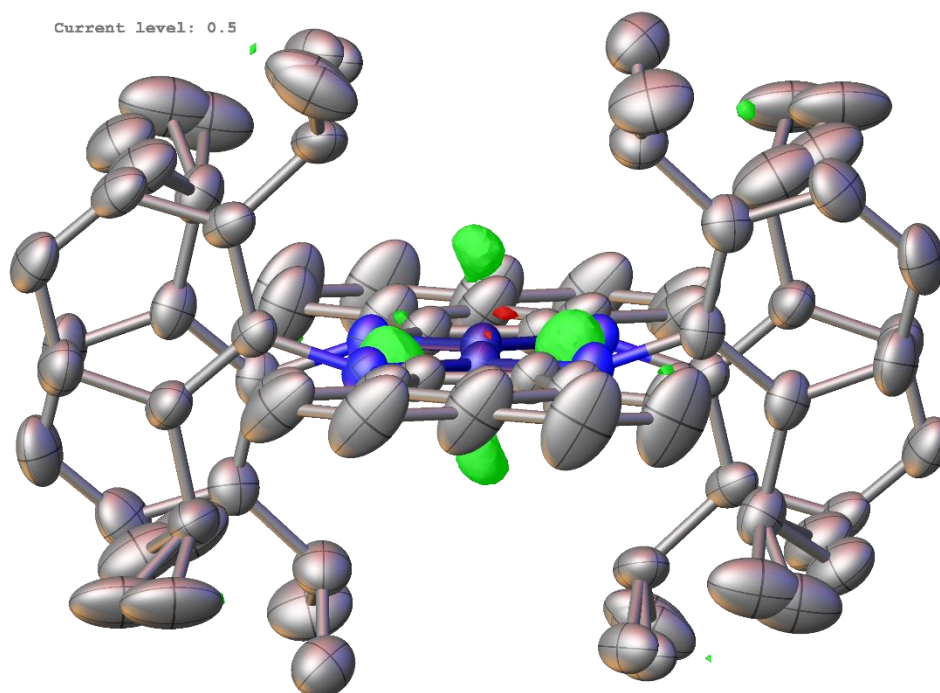
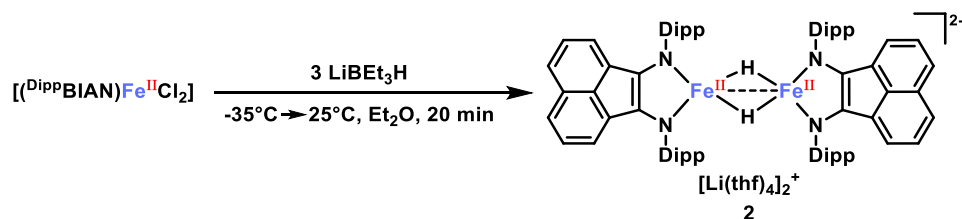


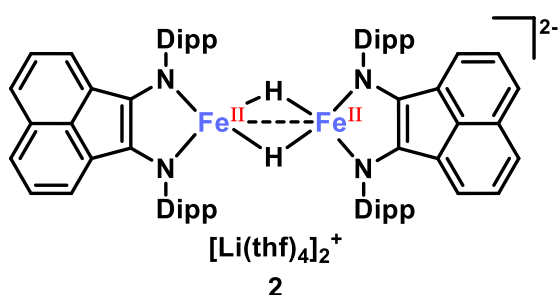
Figure 6.5.11. Residual electron density from the difference Fourier map, rendered at 0.1 Å resolution and at 0.5 e/Å³ for **1a** (hydrides removed).

Table 6.5.2. Crystal data and structure refinement for **1a**.

Identification code	SSC24D_redfilt
Empirical formula	C ₁₀₄ H _{152.97} Fe ₂ Li ₂ N ₄ O ₈
Formula weight	1712.85
Temperature/K	99.97(15)
Crystal system	monoclinic
Space group	P2 ₁ /n
a/Å	16.3569(6)
b/Å	15.6998(5)
c/Å	20.2615(7)
α/°	90
β/°	109.452(4)
γ/°	90
Volume/Å ³	4906.2(3)
Z	2
ρ _{calc} /cm ³	1.159
μ/mm ⁻¹	0.351
F(000)	1854.0
Crystal size/mm ³	0.52 × 0.417 × 0.254
Radiation	Mo Kα (λ = 0.71073)
2θ range for data collection/°	5.886 to 59.15
Index ranges	-22 ≤ h ≤ 22, -21 ≤ k ≤ 19, -28 ≤ l ≤ 28
Reflections collected	43817
Independent reflections	13613 [R _{int} = 0.0299, R _{sigma} = 0.0342]
Data/restraints/parameters	13613/1043/661
Goodness-of-fit on F ²	1.057
Final R indexes [I ≥ 2σ (I)]	R ₁ = 0.0847, wR ₂ = 0.2294
Final R indexes [all data]	R ₁ = 0.1070, wR ₂ = 0.2483
Largest diff. peak/hole / e Å ⁻³	1.21/-0.87

[Li(thf)₄]₂{[(^{Dipp}BIAN)Fe]₂(μ-H)₂} (2)**Scheme 6.5.17. Synthesis of 2.**

In an argon-filled glovebox, a Schlenk flask was equipped with a suspension of $[(^{\text{Dipp}}\text{BIAN})\text{FeCl}_2]$ (0.60 mmol) in Et_2O (20 mL) and closed with a septum. After cooling to -35°C , the flask was taken out of the freezer and LiBEt_3H (3 equiv., 1.1M, THF) was added dropwise during which a color change from pale brown to dark brown, effervescence and solubilization was observed. It is very important to create an overpressure in the flask in order to obtain the product. After 20 minutes stirring, hexane (10 mL) was added and the mixture was filtered through a closed Schlenk frit (P4, gravitation). The filter cake was washed with hexane (3 x 6 mL, dark red) and Et_2O (10, 4, 4 mL, dark green). The filter cake was washed with a THF / hexane mixture (1:1, 6 mL) and dissolved in THF (4 mL). The latter fraction was recrystallized by layering with hexane (2 mL) at -35°C to obtain the product as single crystals.

C₁₀₄H₁₃₄N₄Fe₂O₈Li₂

1693.81 g/mol

Appearance

Dark green blocks

Yield

51.4 mg, 30.3 μmol, (10%).

Elemental analysis

Found (calc. for
 $[\text{Li}(\text{thf})_4]_2\{[(^{\text{Dipp}}\text{BIAN})\text{Fe}]_2(\mu\text{-H})_2\} \cdot 2$
 THF (XRD)): C: 72.74 (72.79); H: 8.88
 (8.73); N: 3.25 (3.03).

Crystal structure

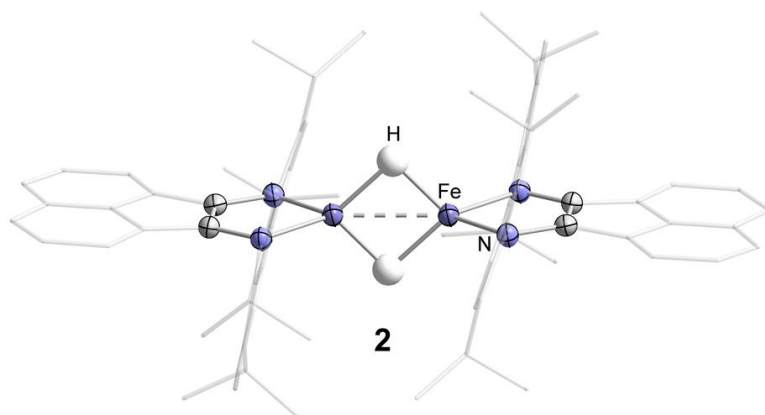


Figure 6.5.12. Solid-state molecular structure of **2**. Minor disordered parts, non-coordinated solvents, cations and selected hydrogen atoms are omitted for clarity. Thermal ellipsoids are drawn at the 50% probability level.

Current level: 0.5

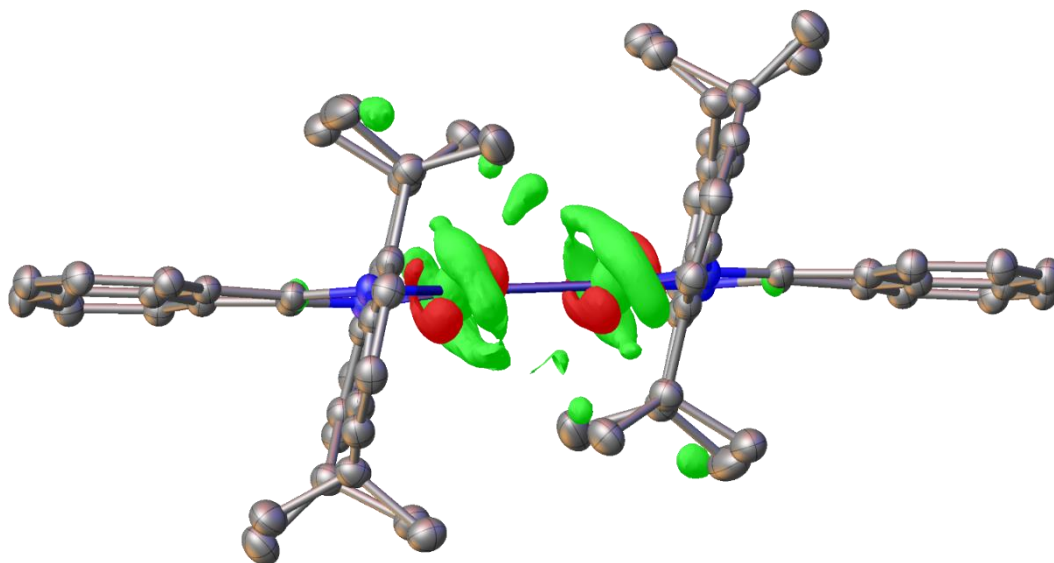
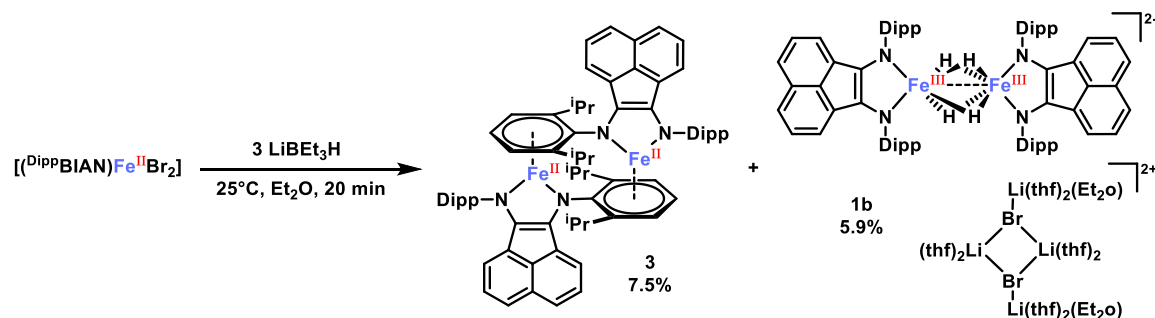


Figure 6.5.13. Residual electron density from the difference Fourier map, rendered at 0.1 Å resolution and at 0.5 e/Å³ for **2** (hydrides removed).

Table 6.5.3. Crystal data and structure refinement for **2**.

Identification code	SSC24H
Empirical formula	C ₁₁₂ H ₁₆₀ Fe ₂ Li ₂ N ₄ O ₁₀
Formula weight	1848.01
Temperature/K	99.97(15)
Crystal system	triclinic
Space group	P-1
a/Å	13.7329(5)
b/Å	14.2430(5)
c/Å	15.3872(6)
α/°	71.877(3)
β/°	67.065(3)
γ/°	71.217(3)
Volume/Å ³	2564.03(18)
Z	1
ρ _{calc} /cm ³	1.197
μ/mm ⁻¹	2.727
F(000)	998.0
Crystal size/mm ³	0.346 × 0.223 × 0.2
Radiation	Cu Kα (λ = 1.54184)
2θ range for data collection/°	6.384 to 152.362
Index ranges	-17 ≤ h ≤ 17, -17 ≤ k ≤ 17, -19 ≤ l ≤ 19
Reflections collected	53681
Independent reflections	10567 [R _{int} = 0.0435, R _{sigma} = 0.0266]
Data/restraints/parameters	10567/0/617
Goodness-of-fit on F ²	1.023
Final R indexes [I ≥ 2σ (I)]	R ₁ = 0.0530, wR ₂ = 0.1471
Final R indexes [all data]	R ₁ = 0.0565, wR ₂ = 0.1518
Largest diff. peak/hole / e Å ⁻³	1.02/-0.67

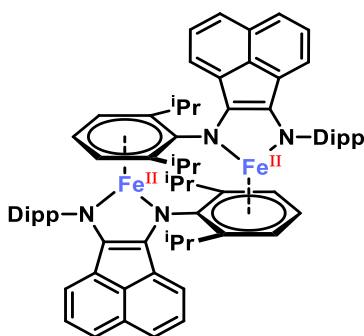
[(DippBIAN)₂Fe₂] (3) and
[{Li(thf)₂(μ³-Br)}₂{(κ-Br)Li(thf)₂(Et₂O)}₂][{(DippBIAN)Fe}₂(μ-H)₄] (1b)



Scheme 6.5.18. Synthesis of **3** and **1b**.

In an argon-filled glovebox, a Schlenk flask was equipped with a suspension of [(DippBIAN)FeBr₂] (1.47 mmol) in Et₂O (20 mL) and closed with a septum. After cooling to -35 °C, the flask was taken out of the freezer and LiBEt₃H (3 equiv., 1.1M, THF) was added dropwise during which a color change from pale brown to dark brown, effervescence and solubilization was observed. After 20 minutes stirring, hexane (20 mL) was added and the mixture was filtered through a closed Schlenk frit (P4, gravitation). The filter cake was extracted with hexane (3 x 4 mL) and Et₂O (4 x 2 mL). The hexane fraction was stored at -35°C over night during which separation was observed to a red supernatant and a dark brown slurry. The slurry was transferred to a glass pipette equipped with a filter paper (Whatman glass microfiber GF/C) and washed with hexane (3 x 4 mL) and Et₂O (3 x 4 mL) to obtain **3** as single crystals.

The Et₂O fraction was recrystallized by layering with hexane (8 mL) at -35 °C to obtain **1b** as single crystals. The crystal structure will not be published to the CCDC due to heavy disorder of the cation (see **1a** for detailed XRD analysis).



C₇₂H₈₀FeN₄
1113.16 g/mol

Appearance Dark green crystals
Yield 61.2 mg, 0.05 mmol (7.5 %)
UV-VIS THF, $\lambda_{\text{max}} / \text{nm}$ ($\epsilon_{\text{max}} / \text{L mol}^{-1} \text{cm}^{-1}$): 210 (83500), 222 (70200), 268 (29300), 325 (13100), 491 (32300).

Elemental analysis Found (calc. for $[(\text{DippBIAN})_2\text{Fe}_2]$):
 C: 77.94 (77.69); H: 5.02 (5.03); N: 7.39 (7.38).

Melting point: $>260^\circ\text{C}$

NMR spectrum

Assignment of signals was not feasible due to poor solubility in THF- d_8 (2D, ^{13}C not possible). Spectrum indicates chemical dynamics.

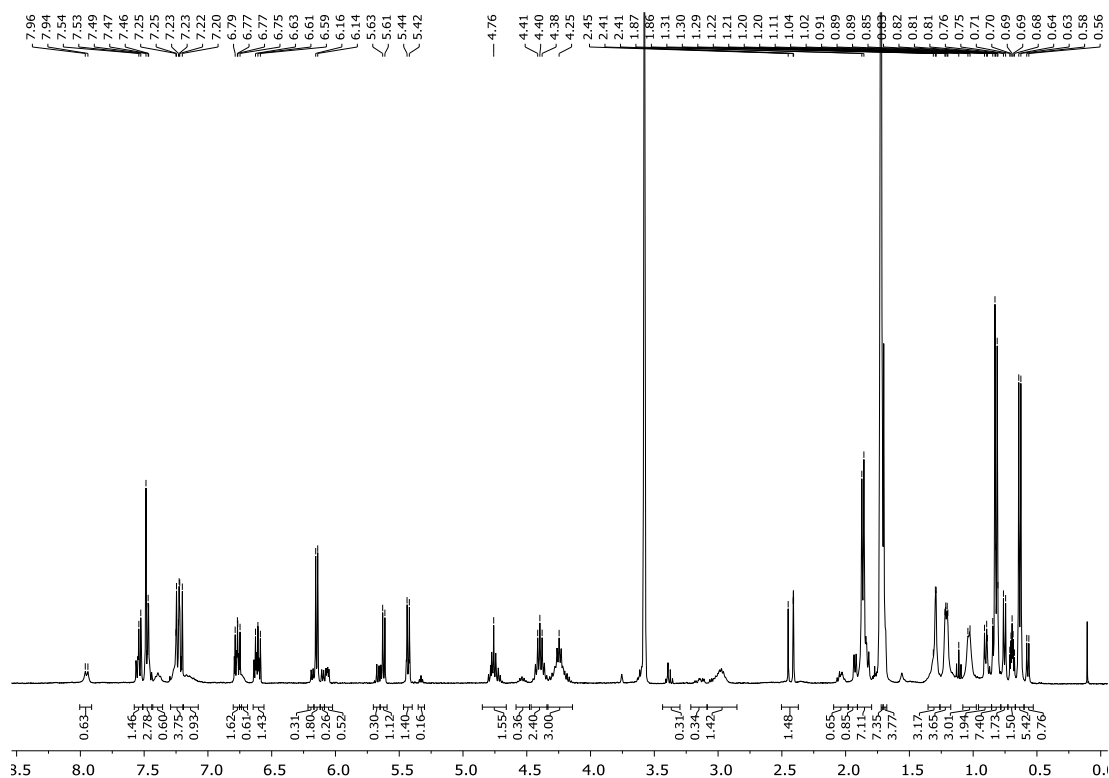


Figure 6.5.14. ^1H NMR spectra of **3** (400.13 MHz, THF, 300K).

UV-Vis spectra

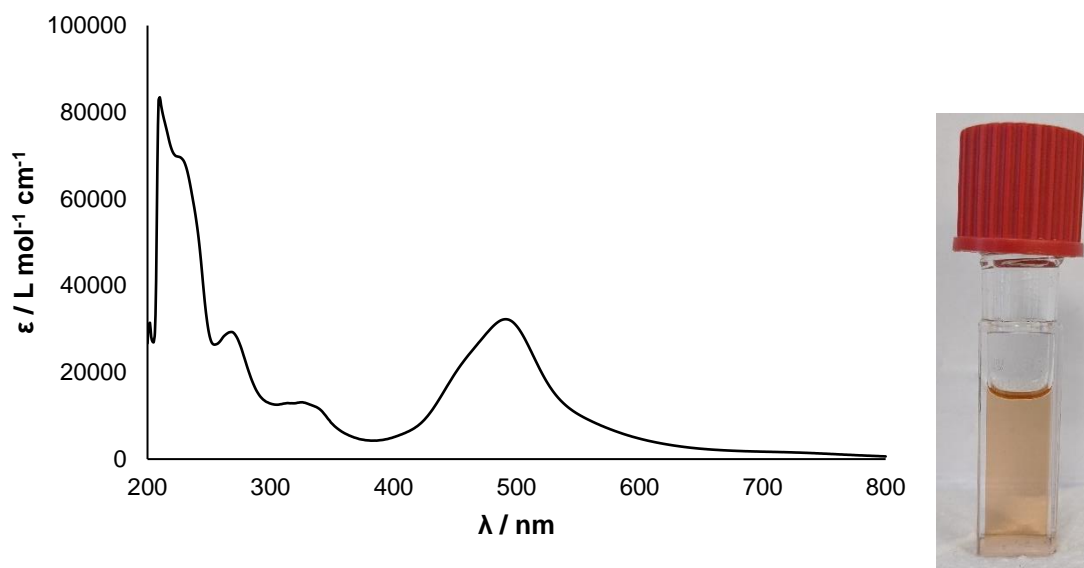


Figure 6.5.15. UV-VIS of 3.

IR

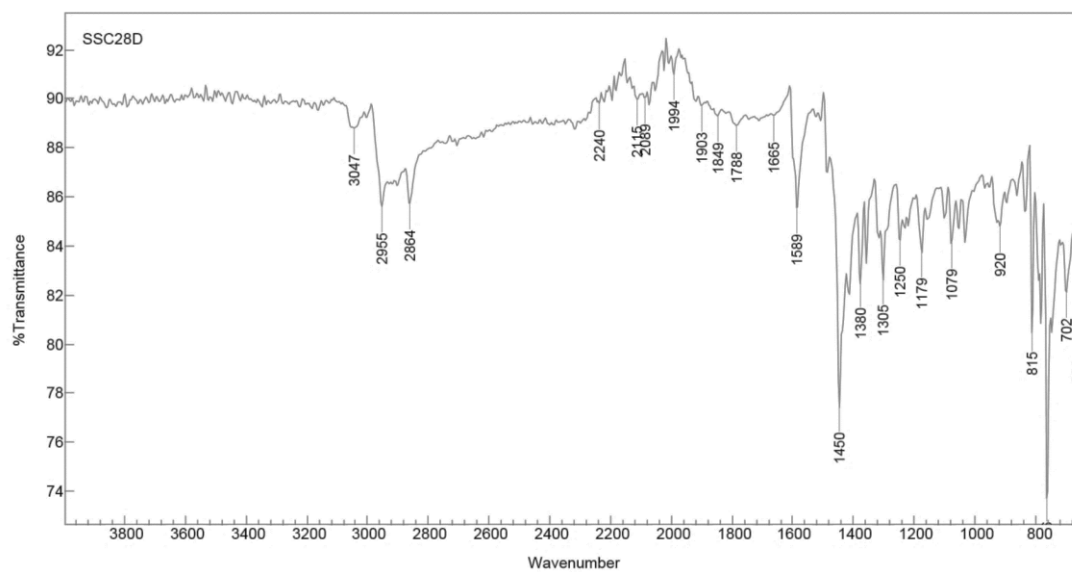
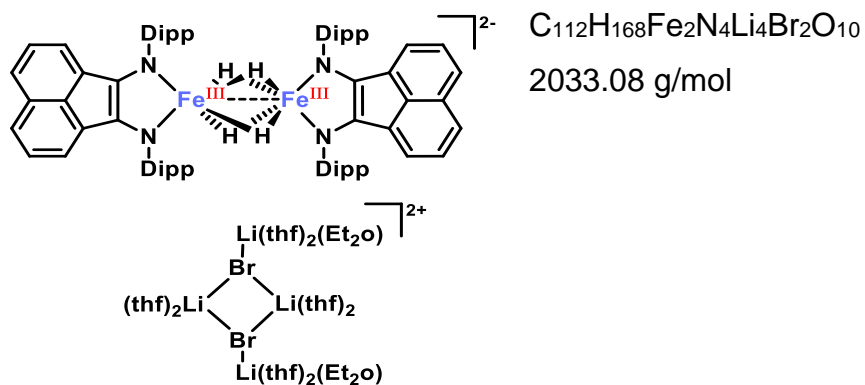


Figure 6.5.16. FT-IR of 3.

6 A Dimeric Iron Ate Complex with Four Bridging Hydrides: Synthesis and Reactivity



Appearance

Dark black blocks

Yield

87.5 mg, 0.04 mmol (5.9 %)

Elemental analysis

Found (calc. for $C_{112}H_{168}Fe_2N_4Li_4Br_2O_{10}$):
C: 66.11 (66.27); H: 8.06 (8.34); N: 2.78
(2.76).

Crystal structure

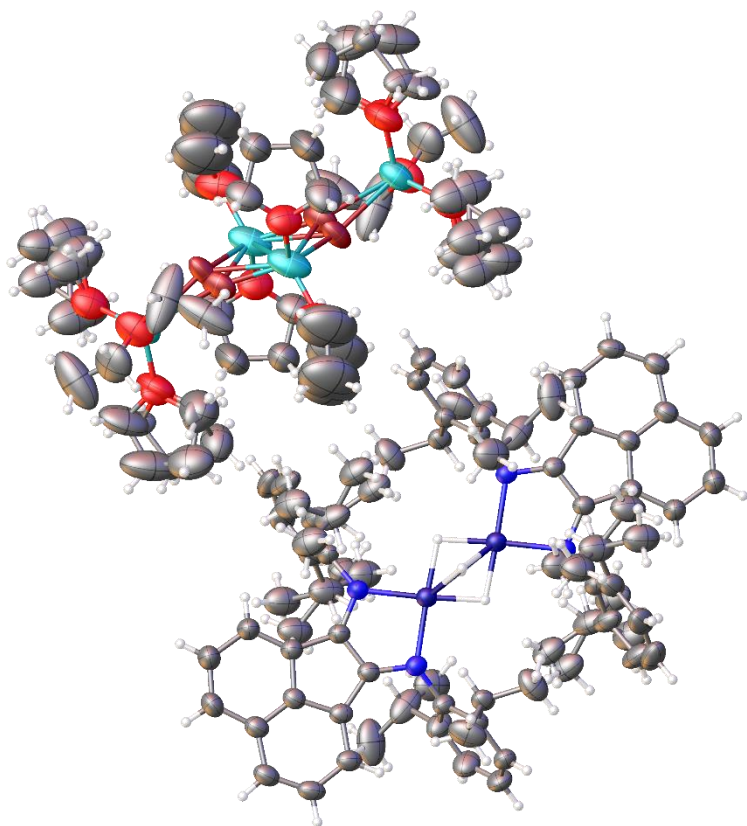


Figure 6.5.17. Solid-state molecular structure of **1b**. Thermal ellipsoids are drawn at the 50% probability level; hydrogen atoms are omitted for clarity.

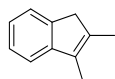
Table S19. Crystal data and structure refinement for **1b**.

Identification code	SSC28B_red
Empirical formula	C ₁₁₂ H ₁₆₈ Br ₂ Fe ₂ Li ₄ N ₄ O ₁₀
Formula weight	1941.08
Temperature/K	99.97(16)
Crystal system	triclinic
Space group	P-1
a/Å	13.2480(6)
b/Å	13.9669(5)
c/Å	16.2585(7)
α/°	83.518(3)
β/°	70.336(4)
γ/°	78.495(4)
Volume/Å ³	2772.6(2)
Z	1
ρ _{calc} /cm ³	1.163
μ/mm ⁻¹	3.371
F(000)	994.0
Crystal size/mm ³	0.225 × 0.195 × 0.147
Radiation	Cu Kα (λ = 1.54184)
2θ range for data collection/°	6.466 to 153.622
Index ranges	-16 ≤ h ≤ 16, -17 ≤ k ≤ 17, -19 ≤ l ≤ 20
Reflections collected	57238
Independent reflections	11534 [R _{int} = 0.0348, R _{sigma} = 0.0233]
Data/restraints/parameters	11534/420/757
Goodness-of-fit on F ²	1.077
Final R indexes [I ≥ 2σ (I)]	R ₁ = 0.0806, wR ₂ = 0.2424
Final R indexes [all data]	R ₁ = 0.0868, wR ₂ = 0.2523
Largest diff. peak/hole / e Å ⁻³	1.17/-1.12

6.5.3 Synthesis of substrates and hydrogenation products

2,3-Dimethyl-1H-indene

Synthesis was performed by Gieshoff, Tim, *Dissertation 2017*, Regensburg, following the procedure described by M. V. Troutman, D. H. Appella, S. L. Buchwald, *J. Am. Chem. Soc.* **1999**, *121*, 4916–4917.

C₁₁H₁₂

144.22 g/mol

Appearance

colorless liquid

Yield

1.49 g, 10.3 mmol (69%)

TLC*R_f* = 0.66 (SiO₂, *n*-pentane)**¹H-NMR**

(300 MHz, CDCl₃) δ 7.37 (dp, *J* = 7.3, 0.9 Hz, 1H), 7.31 – 7.21 (m, 2H), 7.12 (td, *J* = 7.2, 1.5 Hz, 1H), 3.31 – 3.21 (m, 2H), 2.07 (q, *J* = 1.0 Hz, 3H), 2.04 (tq, *J* = 2.1, 1.1 Hz, 3H).

¹³C-NMR

(75 MHz, CDCl₃) δ 126.05, 123.55, 122.97, 117.91, 42.46, 13.95, 10.17.

GC-MS

t_R = 6.77 min, (EI, 70 eV): *m/z* = 144 [M⁺], 129, 115, 89, 77, 63, 51.

Analytical data were in full agreement with M. G. Schrems, E. Neumann, A. Pfaltz, *Angew. Chem. Int. Ed.* **2007**, *46*, 8274–8276.

(1-cyclopropylvinyl)benzene

Synthesis was performed by Gieshoff, Tim, *Dissertation 2017*, Regensburg.

C₁₁H₁₂

144.22 g/mol

Appearance

colorless liquid

Yield

1.27 g, 8.8 mmol (80%)

TLC*R_f* = 0.53 (SiO₂, hexanes)**¹H-NMR**

(300 MHz, CDCl₃) δ 7.67 – 7.57 (m, 2H), 7.42 – 7.26 (m, 3H), 5.30 (d, *J* = 1.0, 1H), 4.95 (t, *J* = 1.2, 1H), 1.67 (ttt, *J* = 8.3, 5.4, 1.2, 1H), 0.92 – 0.79 (m, 2H), 0.61 (ddd, *J* = 6.4, 5.4, 4.1, 2H).

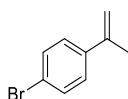
¹³C-NMR (75 MHz, CDCl₃) δ 149.47, 141.75, 128.28, 127.58, 126.25, 109.15, 77.58, 77.16, 77.16, 76.74, 15.78, 6.83.

GC-MS *t_R* = 6.31 min, (EI, 70 eV): *m/z* = 144 [M⁺], 129, 115, 103, 91, 77, 63, 51.

Analytical data were in full agreement with C. Chatalova-Sazepin, Q. Wang, G. M. Sammis, J. Zhu, *Angew. Chem. Int. Ed.* **2015**, *54*, 5443–5446.

4-Bromo- α -methylstyrene

Synthesis following a modified procedure by A. O. Terent'Ev, O. M. Mulina, D. A. Pirgach, D. V. Demchuk, M. A. Syroeshkin, G. I. Nikishin, *RSC Adv.* **2016**, *6*, 93476.



C₉H₉Br
197.08 g/mol

Appearance colorless oil

Yield 3.44 g, 17.5 mmol (83%)

TLC *R_f* = 0.67 (SiO₂, *n*-pentane)

¹H-NMR (400 MHz, CDCl₃) δ 7.50-7.40 (m, 2H), 7.36-7.28 (m, 2H), 5.39 – 5.32 (m, 1H), 5.14 – 5.07 (m, 1H), 2.13 (s, 3H).

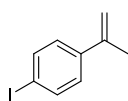
¹³C-NMR (101 MHz, CDCl₃) δ 142.2, 140.1, 131.3, 127.2, 121.3, 113.1, 21.7.

GC-MS *t_R* = 6.01 min, (EI, 70 eV): *m/z* = 197 [M⁺], 183, 171, 156, 115, 102, 91, 75, 63, 51.

Analytical data were in full agreement with T. Taniguchi, A. Yajima, H. Ishibashi, *Adv. Synth. Catal.* **2011**, *353*, 2643–2647.

4-Iodo- α -methylstyrene

Synthesis was performed by T. N. Gieshoff, U. Chakraborty, M. Villa, A. Jacobi von Wangelin, *Angew. Chem. Int. Ed.* **2017**, *56*, 3585.



C₉H₉I
244.08 g/mol

Appearance colorless solid

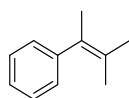
Yield 1.21 g, 4.96 mmol (71%)

TLC	$R_f = 0.84$ (SiO ₂ , <i>n</i> -pentane)
¹H-NMR	(300 MHz, CDCl ₃) δ 7.70 – 7.59 (m, 2H), 7.24 – 7.15 (m, 2H), 5.40 – 5.33 (m, 1H), 5.12 – 5.07 (m, 1H), 2.14 – 2.09 (m, 3H).
¹³C-NMR	(75 MHz, CDCl ₃) δ 142.28, 140.70, 137.27, 134.97, 127.41, 113.15, 92.88, 21.62.
GC-MS	$t_R = 7.14$ min, (EI, 70 eV): $m/z = 244$ [M ⁺], 127, 115, 102, 91, 75, 63, 50.

Analytical data were in full agreement with G. B. Bachman, C. L. Carlson, M. Robinson, *J. Am. Chem. Soc.* **1951**, 73, 1964–1965.

(3-methylbut-2-en-2-yl)benzene

Synthesis was performed by Gieshoff, Tim, *Dissertation 2017*, Regensburg, following the procedure by W. Adam, M. A. Arnold, M. Grüne, W. M. Nau, U. Pischel, C. R. Saha-Möller, *Organic Letters* **2002**, 4, 537-540.



C₁₁H₁₄

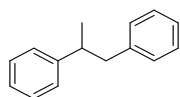
146.23 g/mol

Appearance	colorless liquid
Yield	850 mg, 5.8 mmol (39%)
¹H-NMR	(300 MHz, CDCl ₃) δ 7.36 – 7.13 (m, 5H), 1.99 (s, 3H), 1.84 (s, 3H), 1.62 (s, 3H).
¹³C-NMR	(75 MHz, CDCl ₃) δ 145.35, 130.00, 128.44, 127.94, 127.23, 125.73, 22.11, 20.85, 20.59.
GC-MS	$t_R = 5.62$ min, (EI, 70 eV): $m/z = 146$ [M ⁺], 131, 115, 103, 91, 77, 65, 51.

Analytical data were in full agreement with W. Adam, M. A. Arnold, M. Grüne, W. M. Nau, U. Pischel, C. R. Saha-Möller, *Org. Lett.* **2002**, 4, 537-540.

Hydrogenation products

Propane-1,2-diylidibenzene



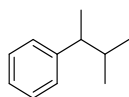
C₁₅H₁₆

196.29 g/mol

¹H-NMR	(300 MHz, CDCl ₃) δ 7.44 – 7.10 (m, 10H), 3.17 – 2.95 (m, 2H), 2.91 – 2.78 (m, 1H), 1.31 (d, <i>J</i> = 6.8 Hz, 3H).
¹³C-NMR	(75 MHz, CDCl ₃) δ 147.05, 140.88, 129.23, 128.37, 128.17, 127.11, 126.09, 125.91, 45.13, 41.96, 21.23.
GC-MS	<i>t_R</i> = 8,24 min, (EI, 70 eV): <i>m/z</i> = 196 [M ⁺], 178, 165, 152, 139, 128, 115, 105, 91, 77, 65, 51.

Analytical data were in full agreement with C. Metallinos, J. Zaifman, L. Van Belle, L. Dodge, M. Pilkington, *Organometallics* **2009**, *28*, 4534-4543.

(3-methylbutan-2-yl)benzene



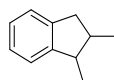
C₁₁H₁₆

148,28 g/mol

¹H-NMR	(300 MHz, CDCl ₃) δ 7.35 – 7.14 (m, 5H), 2.42 (p, <i>J</i> = 7.2 Hz, 1H), 1.77 (dp, <i>J</i> = 7.7, 6.6 Hz, 1H), 1.24 (d, <i>J</i> = 7.0 Hz, 3H), 0.94 (d, <i>J</i> = 6.7 Hz, 3H), 0.76 (d, <i>J</i> = 6.7 Hz, 3H).
¹³C-NMR	(75 MHz, CDCl ₃) δ 147.10, 128.02, 127.65, 125.68, 46.88, 34.45, 21.20, 20.20, 18.78.
GC-MS	<i>t_R</i> = 5,41 min, (EI, 70 eV): <i>m/z</i> = 148 [M ⁺], 131, 115, 105, 77, 65, 51.

Analytical data were in full agreement with V. Jurčík, S. P. Nolan, C. S. J. Cazin, *Chem. Eur. J.* **2009**, *15*, 2509-2511.

1,2-dimethyl-2,3-dihydro-1*H*-indene



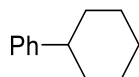
C₁₁H₁₄

146.23 g/mol

¹H-NMR	(400 MHz, CDCl ₃) δ 7.23 – 7.10 (m, 4H), 3.17 (p, <i>J</i> = 7.1 Hz, 1H), 3.04 – 2.92 (m, 1H), 2.63 – 2.53 (m, 2H), 1.15 (d, <i>J</i> = 7.2 Hz, 3H), 0.99 (d, <i>J</i> = 6.8 Hz, 3H).
¹³C-NMR	(75 MHz, CDCl ₃) δ 148.81, 142.95, 126.10, 126.04, 124.48, 123.59, 42.39, 39.39, 37.84, 15.20, 14.67.
GC-MS	<i>t_R</i> = 6.03 min, (EI, 70 eV): <i>m/z</i> = 146 [M ⁺], 131, 115, 103, 91, 77, 63, 51.

Analytical data were in full agreement with R. P. Yu, J. M. Darmon, J. M. Hoyt, G. W. Margulieux, Z. R. Turner, P. J. Chirik, *ACS Catal.* **2012**, 2, 1760–1764.

Phenylcyclohexane



C₁₂H₁₆

160.26 g/mol

¹H-NMR (300 MHz, CDCl₃) δ 7.34 – 7.25 (m, 2H), 7.24 – 7.14 (m, 3H), 2.60 – 2.39 (m, 1H), 2.00 – 1.79 (m, 4H), 1.80 – 1.73 (m, 1H), 1.51 – 1.19 (m, 5H).

¹³C-NMR (75 MHz, CDCl₃) δ 148.1, 128.3, 126.5, 125.8, 44.7, 34.52, 27.0, 26.2.

GC-MS *t*_R = 7.30 min, (EI, 70 eV): *m/z* = 160 [M⁺], 143, 129, 115, 102, 91, 77, 63, 51.

Analytical data were in full agreement with W. M. Czaplik, M. Mayer, A. Jacobi von Wangelin, *Angew. Chem. Int. Ed.* **2009**, 48, 607–610.

1,1-Diphenylethane



C₁₄H₁₄

182.27 g/mol

¹H-NMR (300 MHz, CDCl₃) δ 7.35 – 7.11 (m, 10H), 4.15 (q, *J*=7.1, 1H), 1.63 (d, *J*=7.2, 3H).

GC-MS *t*_R = 7.97 min, (EI, 70 eV): *m/z* = 182 [M⁺], 167, 152, 139, 128, 115, 103, 89, 77, 63, 51.

Analytical data were in full agreement with F. Schoenebeck, J. A. Murphy, S.-z. Zhou, Y. Uenoyama, Y. Miclo, T. Tuttle, *J. Am. Chem. Soc.* **2007**, 129, 13368–13369.

1-Cyclopropyl-1-phenylethane



C₁₁H₁₄

146.23 g/mol

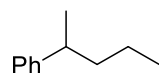
¹H-NMR (300 MHz, CDCl₃) δ 7.41 – 7.26 (m, 4H), 7.25 – 7.17 (m, 1H), 1.99 (dq, *J* = 9.2, 7.0 Hz, 1H), 1.35 (d, *J* = 7.0 Hz, 3H), 1.00 – 0.90 (m, 1H), 0.65 – 0.36 (m, 2H), 0.27 – 0.09 (m, 2H).

¹³C-NMR (75 MHz, CDCl₃) δ 147.38, 128.23, 127.00, 125.89, 44.67, 21.62, 18.56, 4.64, 4.34.

GC-MS *t_R* = 5.87 min, (EI, 70 eV): *m/z* = 146 [M⁺], 131, 117, 105, 91, 77, 65, 51.

Analytical data were in full agreement with T. N. Gieshoff, M. Villa, A. Welther, M. Plois, U. Chakraborty, R. Wolf, A. Jacobi von Wangelin, *Green Chem* **2015**, *17*, 1408–1413.

2-Pentylbenzene



C₁₁H₁₆

148.25 g/mol

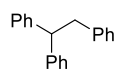
¹H-NMR (300 MHz, CDCl₃) δ 7.34 – 7.26 (m, 2H), 7.22 – 7.14 (m, 3H), 2.70 (sextet, *J* = 7.0 Hz, 1H), 1.65 – 1.45 (m, 2H), 1.35 – 1.10 (m, 5H), 0.87 (t, *J* = 7.3 Hz, 3H).

¹³C-NMR (75 MHz, CDCl₃) δ 147.9, 128.3, 127.0, 125.7, 40.7, 39.7, 22.3, 20.8, 14.2.

GC-MS *t_R* = 5.51 min, (EI, 70 eV): *m/z* = 148 [M⁺], 131, 115, 105, 91, 77, 65, 51.

Analytical data were in full agreement with R. B. Bedford, P. B. Brenner, E. Carter, T. W. Carvell, P. M. Cogswell, T. Gallagher, J. N. Harvey, D. M. Murphy, E. C. Neeve, J. Nunn, D. R. Pye, *Chem. Eur. J.* **2014**, *20*, 7935–7938.

Ethane-1,1,2-triyltribenzene



C₂₀H₁₈

258.36 g/mol

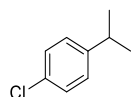
¹H-NMR (300 MHz, CDCl₃) δ 7.30 – 7.09 (m, 13H), 7.05 – 6.95 (m, 2H), 4.24 (t, *J* = 7.8 Hz, 1H), 3.37 (d, *J* = 7.8 Hz, 2H).

¹³C-NMR (75 MHz, CDCl₃) δ 144.45, 140.26, 129.08, 128.34, 128.05, 126.19, 125.88, 53.11, 42.11.

GC-MS $t_R = 10.67$ min, (EI, 70 eV): $m/z = 258$ [M^+], 167, 152, 139, 128, 115, 102, 91, 77, 65, 51.

Analytical data were in full agreement with T. C. Fessard, H. Motoyoshi, E. M. Carreira, *Angew. Chem. Int. Ed.* **2007**, *46*, 2078–2081.

1-Chloro-4-isopropylbenzene



$C_9H_{11}Cl$

154.64 g/mol

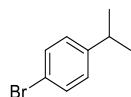
1H -NMR (300 MHz, $CDCl_3$) δ 7.25 (m, 2H), 7.21–7.09 (m, 2H), 2.89 (m, 1H), 1.23 (d, $J = 6.9$ Hz, 6H).

^{13}C -NMR (75 MHz, $CDCl_3$) δ 142.3, 131.3, 128.4, 127.8, 33.6, 23.9.

GC-MS $t_R = 5.37$ min, (EI, 70 eV): $m/z = 154$ [M^+], 139, 125, 119, 105, 89, 77, 63, 51.

Analytical data were in full agreement with S. S. Kim, C. S. Kim, *J. Org. Chem.* **1999**, *64*, 9261–9264.

1-Bromo-4-isopropylbenzene



$C_9H_{11}Br$

199.09 g/mol

1H -NMR (300 MHz, $CDCl_3$) δ 7.47 – 7.36 (m, 2H), 7.15 – 7.04 (m, 2H), 2.87 (hept, $J = 6.9$ Hz, 1H), 1.23 (d, $J = 6.9$ Hz, 6H).

^{13}C -NMR (101 MHz, $CDCl_3$) δ 147.8, 131.3, 128.2, 119.3, 33.7, 30.9, 23.8.

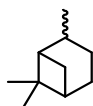
GC-MS $t_R = 6.16$ min, (EI, 70 eV): $m/z = 198$ [M^+], 185, 169, 158, 143, 119, 104, 91, 77, 63, 51.

Analytical data were in full agreement with M. A. Hall, J. Xi, C. Lor, S. Dai, R. Pearce, W. P. Dailey, R. G. Eckenhoff, *J. Med. Chem.* **2010**, *53*, 5667–5675.

Pinane

Mixture of diastereomers.

$C_{10}H_{18}$



138.25 g/mol

¹H-NMR

mixture of isomers

¹³C-NMR

(75 MHz, CDCl₃) δ 67.98, 65.88, 48.07, 47.62, 41.35, 40.88, 39.49, 38.82, 35.95, 33.96, 29.35, 28.30, 26.84, 26.54, 25.63, 24.61, 23.93, 23.83, 23.22, 23.04, 22.90, 21.61, 20.09, 15.29.

GC-MS

t_R = 4.67 min, (EI, 70 eV): m/z = 138 [M⁺], 123, 95, 81, 67, 55.

Analytical data were in full agreement with A. Stolle, B. Ondruschka, W. Bonrath, T. Netscher, M. Findeisen, M. M. Hoffmann, *Chemistry* **2008**, *14*, 6805–6814.

6.5.4 General procedures

General method for catalytic hydrogenation

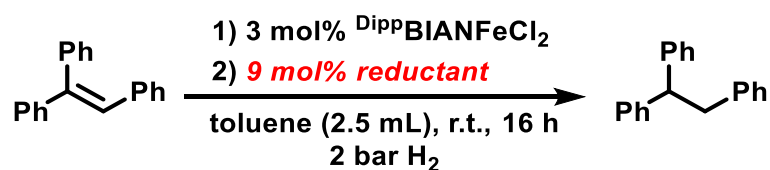
In an argon-filled glovebox a flame-dried 4 mL reaction vial was charged with DippBIANFeCl_2 (0.006 mmol), Toluene (2 mL) and *n*-pentadecane as internal reference for GC-FID quantification (0.2 mmol). The resulting suspension was reduced by dropwise addition of LiBEt_3H (0.018 mmol, 1 M, THF) with a Hamilton® syringe during which the color changed to dark red. After 10 minutes stirring, the substrate was added and the reaction vial was transferred to a high-pressure reactor which was sealed and removed from the glovebox. The reactor was purged with H_2 (3×3 bar) and the reaction pressure and temperature were set. After the indicated reaction time, the vial was retrieved and hydrolyzed with a saturated aqueous solution of NH_4Cl (1 mL). The reaction mixture was extracted with ethyl acetate (3×1 mL), dried over sodium sulfate and analyzed by GC-FID and GC-MS.

General method for kinetic examination in catalytic hydrogenation and poisoning experiments

A flame-dried 10 mL two-necked flask was connected to a *Man on the Moon X201* gas-uptake system with a reservoir pressure of 9 bar H_2 and a constant reaction pressure of 1.9 bar H_2 . After purging with H_2 , the freshly prepared catalyst solution was transferred with a syringe. The hydrogen uptake started with the addition of α -methylstyrene (0.2 mmol). After the reaction, the mixture was treated with a saturated aqueous solution of NH_4Cl and ethyl acetate. The organic phase was separated and filtered over a plug of silica and analyzed by quantitative GC-FID analysis vs. internal standard (*n*-pentadecane). The monitored hydrogen consumption was related to the yield of cumene, which was determined by GC-FID. An induction period may be not detectable since the addition by syringe through the septum creates a temporary leakage.

6.5.5 Optimization studies and catalytic application of complexes

Table 6.5.1. Catalytic optimization studies.



Entry	Reductant	Yield (%) ^a
1	<i>n</i> -BuLi	31 (31)
2	<i>i</i> -PrMgCl	51 (51)
3	LiEt ₃ BH	77 (79)
4	NaEt ₃ BH	3 (3)
5	L-selectride	62 (62)
6	N-selectride	1 (1)
7	DiBAI-H	25 (25)
8	HBPIn + KO <i>t</i> -Bu ^b	3 (3)

0.25 mmol of substrate, 3 mM solution of the precatalyst (2.5 mL). ^a quantitative GC-FID vs. *n*-pentadecane as internal reference, conversion in % in parentheses; ^b THF as solvent.

6.5.6 Mechanistic studies (ring-opening experiment, LIFDI-MS)

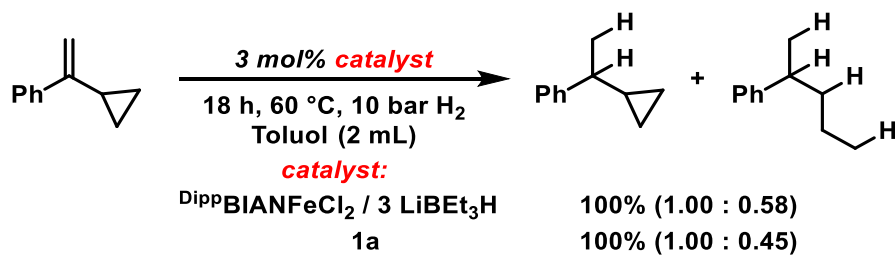
Reactivity studies of **1a**

Hydrogenations reactions were performed according to the general hydrogenation procedure.

Hydrogen-free reaction were performed as following:

In an argon-filled glovebox, the substrate (0.2 mmol) was mixed with a solution of **1a**. After the reaction, the mixture was transferred outside. Work-up and analytical investigations have been performed according to the general procedures.

Ring opening experiment with (1-cyclopropylethyl)benzene



Scheme 6.5.19. Ring opening experiment with (1-cyclopropylethylene)benzene. Yields were determined by quantitative GC-FID vs. internal *n*-pentadecane.

The hydrogenation reaction was performed according to general procedures.

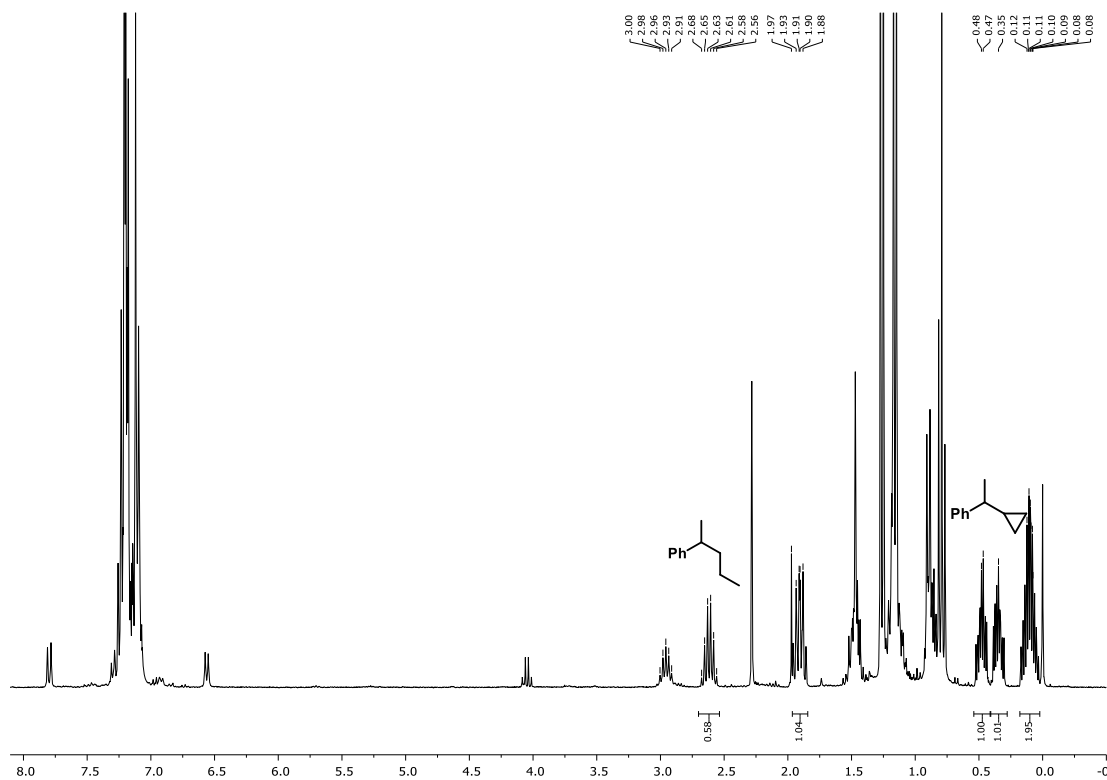


Figure 6.5.18. ¹H-NMR of the hydrogenation reaction of (1-cyclopropylethylene)benzene after work-up with DippBIANFeCl₂ / 3 LiBEt₃H.

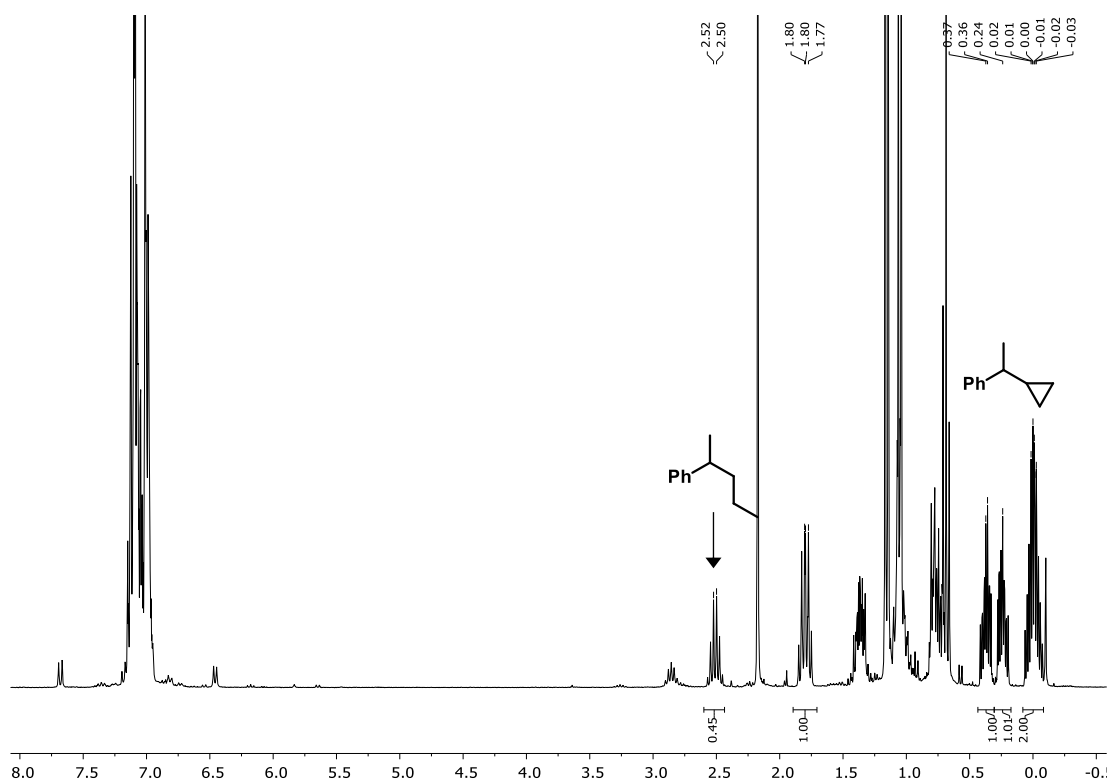


Figure 6.5.19. $^1\text{H-NMR}$ of the hydrogenation reaction of (1-cyclopropylethyl)benzene with **1a**.

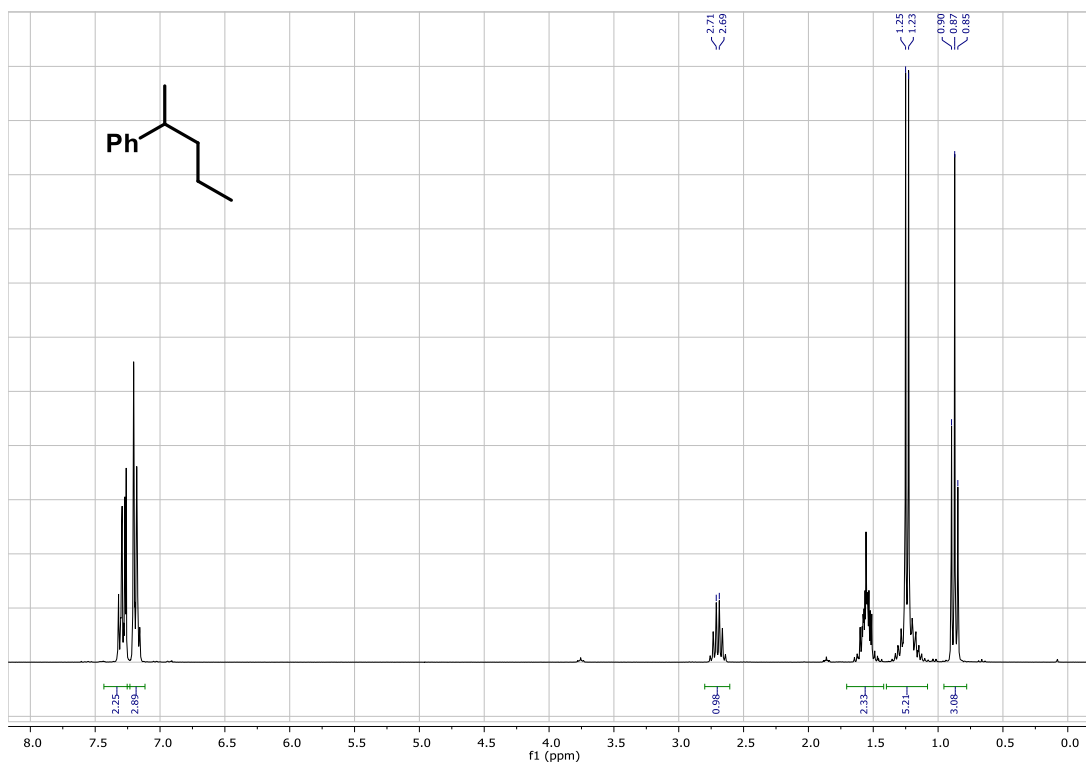


Figure 6.5.20. $^1\text{H-NMR}$ of 2-pentylbenzene.

LIFDI-MS of $\text{DippBIANFeCl}_2 + 3 \text{LiEt}_3\text{H}$ in Toluene.

In an argon-filled glovebox, a 4 mL reaction vial was charged with $[(\text{DippBIAN})\text{FeCl}_2]$ (0.1 mmol) and toluene (1 mL). The resulting pale green suspension was reduced by dropwise addition of LiEt_3H (0.3 mmol, 1 M, THF) with a Hamilton® syringe during which the color changed to red. After 10 minutes stirring, the vial was closed with a septum und removed from the glovebox. The LIFDI-MS was subsequently measured by injection through a cannula in quasi-inert conditions (vacuum).

Two major species were detected in the resulting spectrum (Figure 5-3): $[(\text{toluene})\text{Fe}(\text{DippBIAN})]$ 648 m/z ; $[(\eta^6\text{-toluene})\text{Fe}(\text{DippBIAN})]\text{-[Li]}^+$ 655 m/z .

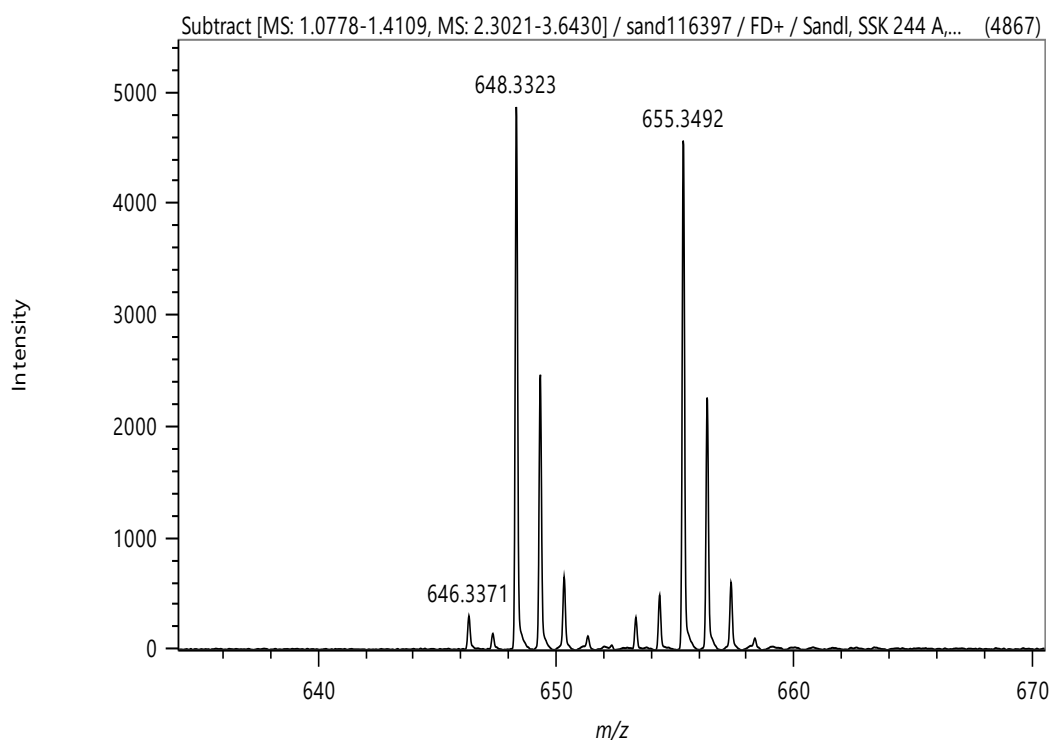


Figure 6.5.21. LIFDI-MS spectrum of reduced Fe-BIAN species.

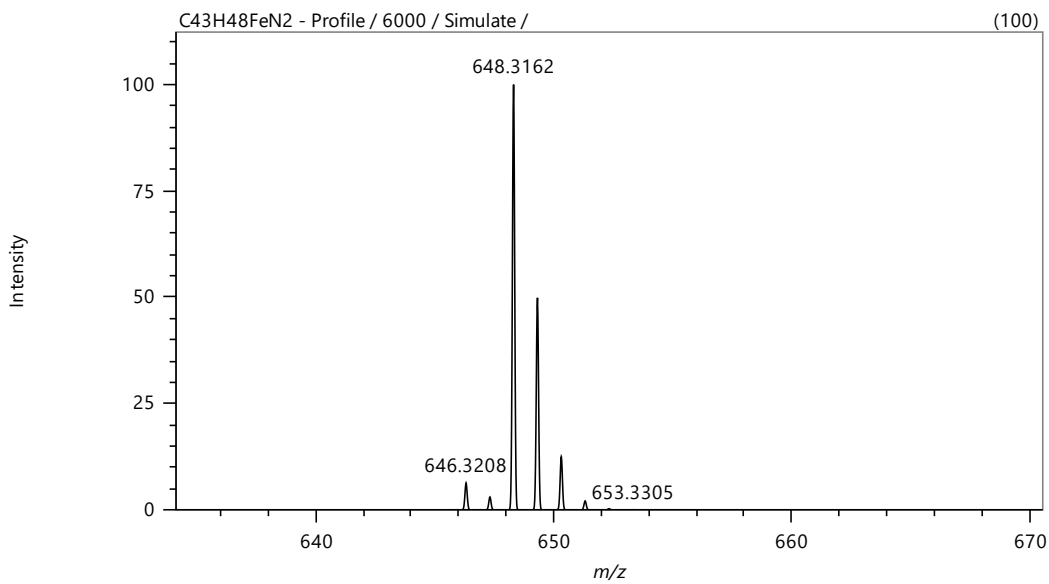


Figure 6.5.22. MS Simulation for C₄₃H₄₈FeN₂.

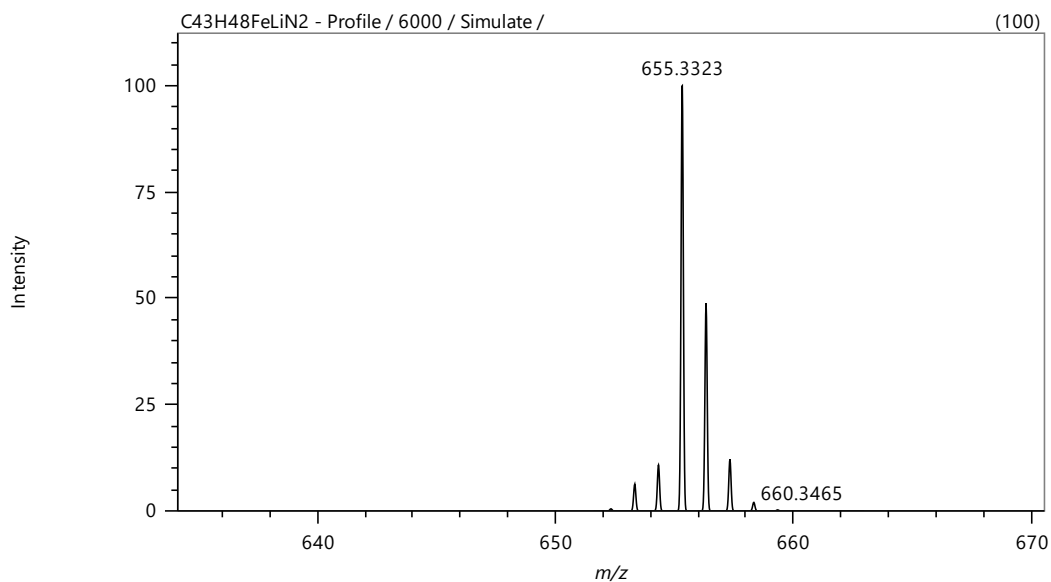


Figure 6.5.23. MS Simulation for C₄₃H₄₈FeLiN₂.

6.5.7 Reaction progress analyses

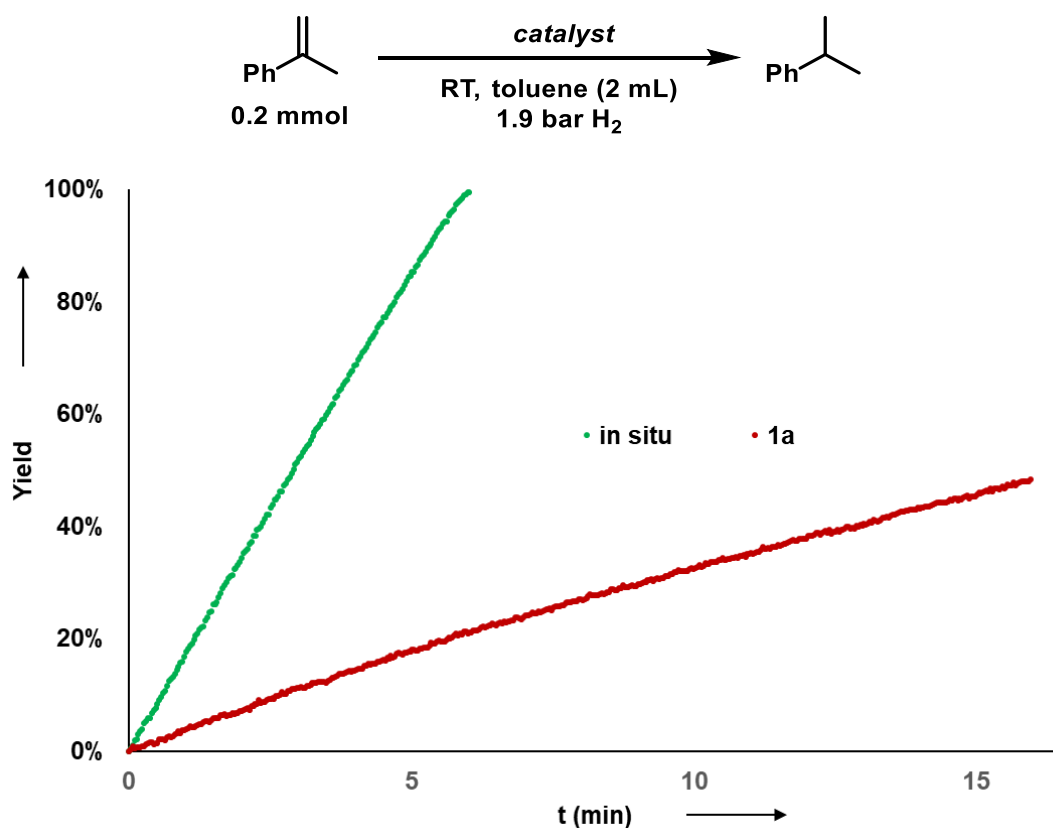
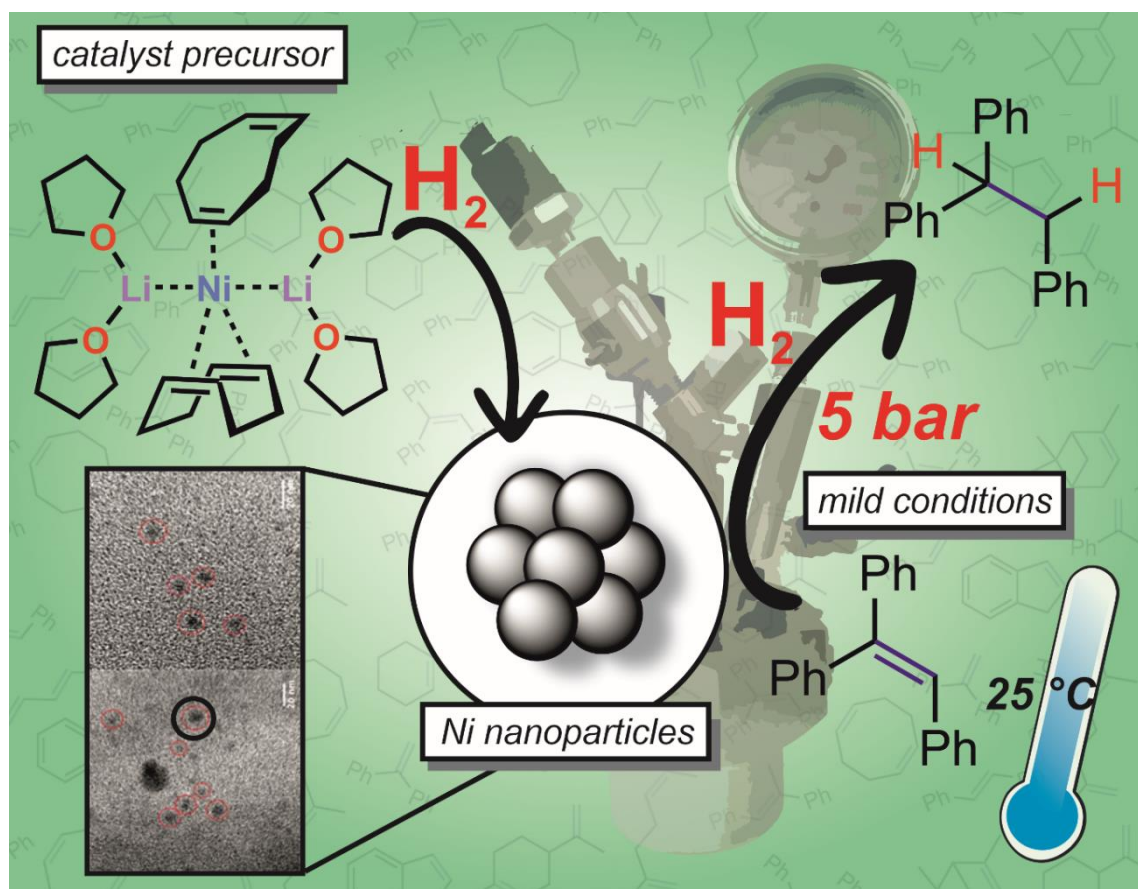


Figure 6.5.24. Reaction progress analyses: Cumene yields determined by hydrogen consumption related to final quantitative GC-FID vs. n-pentadecane.

After a reaction time of 5 minutes, a turnover frequency (TOF) of 339 h⁻¹ at a catalyst loading of 3 mol% was measured for [(^{Dipp}BIAN)FeCl₂] / 3 BuLi. For **1a**, a TOF of 144 h⁻¹ at a catalyst loading of 1.5 mol% was measured.

7 Heterogeneous Olefin Hydrogenation Enabled by a Highly-Reduced Nickel(–II) Catalyst Precursor^{VII}



^{VII} Reproduced with permission from: T. M. Maier, S. Sandl, P. Melzl, J. Zweck, A. Jacobi von Wangelin, R. Wolf, *Chem. Eur. J.* **2020**, chem.201905537. Copyright 2020 Wiley-VCH, Weinheim, schemes, figures and text may differ from published version.

Author contribution:

S. Sandl: Kinetic analyses and mechanistic investigations (Figure 7.4, Scheme 2b).

T. Maier: Development of catalytic hydrogenation reaction conditions (Scheme 7.1, Table 7.1); substrate scope (Figure 7.2 and 7.3) and mechanism (Scheme 7.2a, c-e); manuscript preparation.

J. Leitl: Cover design.

P. Melzl and J. Zweck: TEM analyses (Figure 7.5).

A. Jacobi von Wangelin: Valuable discussions.

R. Wolf: Corresponding author.

Abstract: The hydrogenation of olefins, styrenes, enoates, imines, and sterically hindered tri-substituted olefins was accomplished using the pre-catalyst dilithiumbis(cycloocta-1,5-diene)nickelate(–II) (**1**). The mild conditions tolerate hydroxyl, halide, ester, and lactone functionalities. Mechanistic studies, including reaction progress analyses, poisoning experiments, and multinuclear NMR monitoring, indicate that a heterotopic (nickel nanoparticle) catalyst is in operation.

7.1 Introduction

Olefin hydrogenation is of much industrial and academic importance as a key step in the synthesis of fine chemicals, agrochemicals, fragrances, and food additives.^[1] Precious metal catalysts (Rh, Ir, Pt, Pd, Ru) are most widely applied due to their high activity, selectivity, robustness, and ease of operation.^[2] Nevertheless, economic and environmental concern (in particular the poor crustal abundance and high cost of precious metals) have recently stimulated considerable interest in replacing noble metal catalysts by more abundant 3d metal species^[3] (e.g. with Mn,^[4] Fe,^[5] Co^[6], and Ni^{[7]–[17]}). Over the past decade, major effort has been devoted to the development of iron and cobalt compounds as catalysts for olefin hydrogenation.^{[5],[6]} Especially noteworthy are metal complexes with tridentate pincer ligands.^[5]

Nevertheless, nickel compounds have been applied in technical scale hydrogenations for many decades. Raney nickel was first reported in 1927^[7] and is still industrially used in the hardening of vegetable fats, the manufacture of vitamins, fragrances, and food additives as well as various arene functionalizations.^[8] Nickel boride (obtained from NiX₂ (X = OAc, Cl) and NaBH₄) is an effective catalyst for olefin hydrogenation.^[9] The development of more potent heterogeneous nickel catalysts continues to attract significant interest as shown by the groups of *Gómez* and *Philippot*, who reported to use of commercial [Ni(η^4 -cod)₂] (cod = cycloocta-1,5-diene) as a catalyst precursor (see Figure 7.1, **A**).^{[10],[11]} *Zhao* and co-workers demonstrated that Ni(0) nanoparticles (NPs) in ionic liquids hydrogenate α,β -unsaturated carbonyl compounds at 30 bar H₂.^[12] In addition, well-defined molecular nickel catalysts have been reported recently. The groups of *Bouwman* and *Hanson* described the hydrogenation of simple olefins with homogeneous nickel catalysts.^[13] *Hazari* and *Driess* prepared heteroleptic

7 Heterogeneous Olefin Hydrogenation Enabled by a Highly-Reduced Nickel(-II) Catalyst Precursor

carbene/silylene complexes **B** and **C**, which are very active hydrogenation catalysts.^{[14],[15]} Catalyst **D** reported by *Chirik* and co-workers constitutes the current state of the art in catalytic hydrogenations of sterically hindered tri- and tetra-substituted olefins.^[16] The active catalyst is assembled from the combination of nickel(II) bis(octanoate), pinacol borane, and an α -diimine ligand. Moreover, recent reports on asymmetric hydrogenations of dehydroamino acids catalyzed by $\text{Ni}(\text{OAc})_2$ and the chiral ligand (*S*)-binapine are noteworthy.^[17]

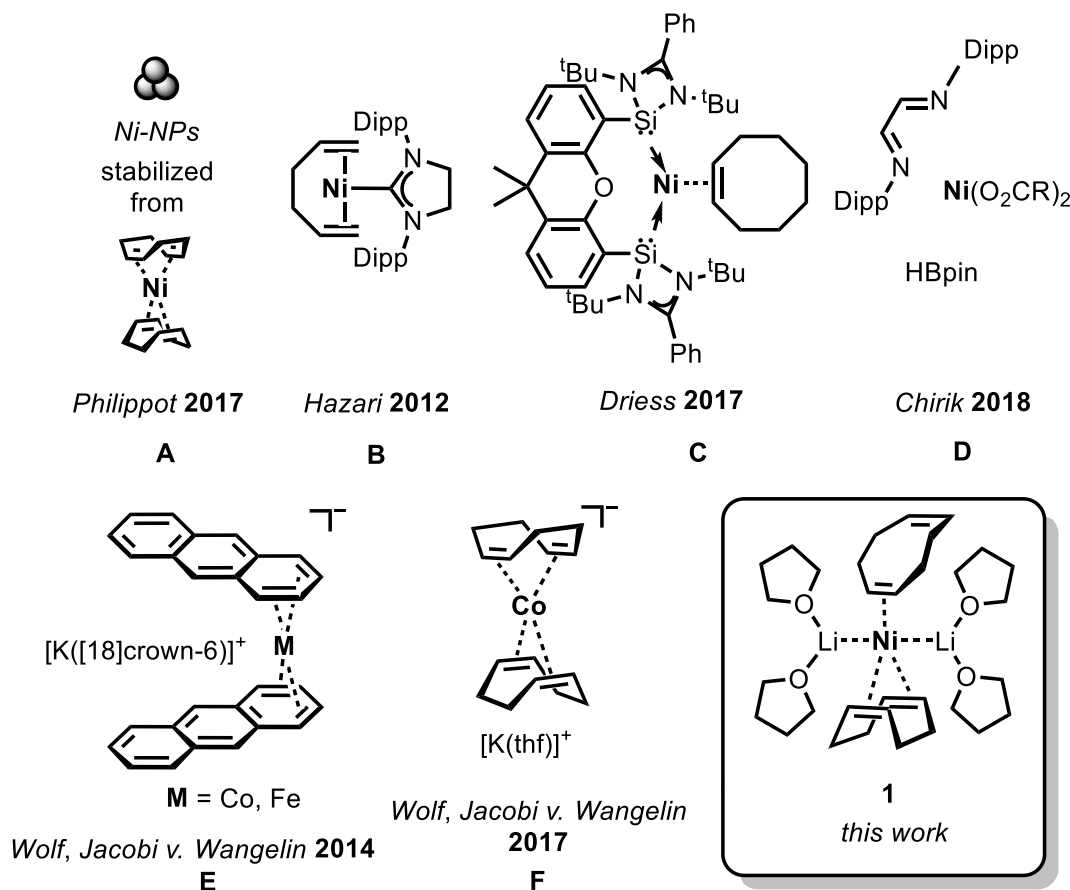


Figure 7.1 Selected examples of nickel pre-catalysts for the C=C hydrogenation (top). Low-valent anionic transition metal complexes as hydrogenation catalysts by our group (bottom). Dipp = 2,6-diisopropylphenyl.

We previously investigated low-valent ferrate and cobaltate anions $[\text{K}([\text{18}]\text{crown-6})(\text{thf})_2][\text{M}(\eta^4\text{-anthracene})_2]$ ($\text{M} = \text{Fe}, \text{Co}$), and $[\text{K}(\text{thf})_x][\text{Co}(\eta^4\text{-cod})_2]$, first synthesized by the groups of *Ellis*^{[18],[19]} and *Jonas*,^[20] as catalysts in the hydrogenation of olefins, ketones, and imines.^[6] These “quasi-naked” anionic metal species exhibited high hydrogenation activities for mono/di-substituted C=C

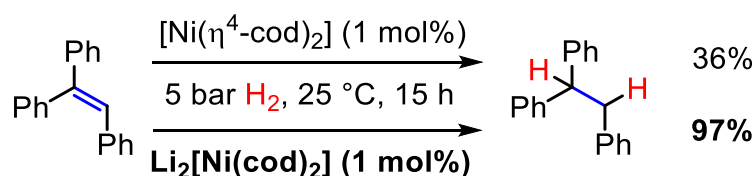
bonds but fared poorly for sterically hindered tri/tetra-substituted olefins. Due to the lability of the arene and olefin ligands, both heterogeneous and homogeneous mechanistic pathways are accessible, depending on the nature of the substrate.

Following our recent development of effective olefin hydrogenations with anionic iron and cobalt catalysts,^[6] we were interested to complement these studies with the corresponding nickelate complex $[\text{Li}_2(\text{thf})_4\{\text{Ni}(\eta^2\text{-cod})(\eta^4\text{-cod})\}]$ (**1**).^[21] This compound was first synthesized by *Jonas* and co-workers by reduction of the commercially available $[\text{Ni}(\eta^4\text{-cod})_2]$ with Li metal. **1** was only very recently structurally characterized by *Cornella* and co-workers, who also reported that **1** effectively catalyzes Kumada-Corriu cross coupling reactions.^[22] Herein, we show that **1** is a pre-catalyst for the hydrogenation of hindered olefins. We provide solid mechanistic evidence that suggests the *in-situ* formation of highly active Ni particles.

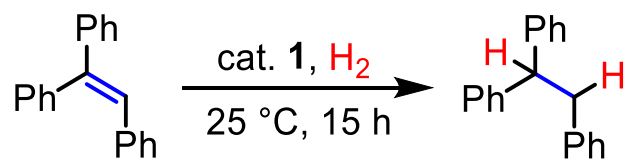
7.2 Results & Discussion

Initial optimization experiments were performed using 1,1',2-triphenylethylene as model substrate. Most importantly, the ate-complex **1** showed significantly higher activity in comparison with its oxidized counterpart $[\text{Ni}(\eta^4\text{-cod})_2]$.^[23] With $[\text{Ni}(\eta^4\text{-cod})_2]$ only a yield of 36% was achieved within 15 h, whereas full conversion to triphenylethane was observed when using anionic **1** (Scheme 7.1). The same applies for 1-phenyl-1-cyclohexene.

No conversion was observed using $[\text{Ni}(\eta^4\text{-cod})_2]$, while 74% conversion was observed with **1**. The optimized conditions for 1,1',2-triphenylethylene use 1 mol% pre-catalyst **1**, a reaction time of 15 h, and 5 bar H_2 at ambient temperature in 1,2-dimethoxyethane (DME) (Table 7.1, entries 1-3). The reaction was incomplete after 15 h, when the pressure was decreased to 1.9 bar (Table 7.1, entry 4). No conversion was observed using $[\text{Ni}(\eta^4\text{-cod})_2]$, while 74% conversion were observed with **1**. The optimized conditions for 1,1',2-triphenylethylene use 1 mol% pre-catalyst **1**, a reaction time of 15 h, and 5 bar H_2 at ambient temperature in 1,2-dimethoxyethane (DME) (Table 7.1, entries 1-3). The reaction was incomplete after 15 h, when the pressure was decreased to 1.9 bar (Table 7.1, entry 4).



Scheme 7.1. Comparison of lithium nickelate **1** and $[\text{Ni}(\eta^4\text{-cod})_2]$ as pre-catalysts in the hydrogenation of 1,1',2-triphenylethylene in DME. Yields were determined by quantitative GC-FID vs. internal *n*-pentadecane.

Table 7.1. Optimization experiments.^[a]

Entry	Catalyst ^[b]	Solvent [mL]	p (H ₂) [bar]	Yield (Conversion) [%]
1	1	THF (0.5)	5	81 (82)
2	1	DME (0.5)	5	97 (98)
3	1	DME (0.25)	5	99 (>99)
4	1	DME (0.25)	1.9	72 (74)
5	1 + exc. Hg ^[c]	DME (0.25)	5	2 (5)
6	1 + dct ^[d]	DME (0.25)	5	92 (>99)

[a] Standard conditions: Substrate (0.2 mmol), 25 °C, 15 h. Yields and conversions were determined by quantitative GC-FID vs. internal *n*-pentadecane. [b] 1 mol% catalyst. [c] large excess of Hg (one drop, 50 mg, 0.25 mmol, 125 equiv.). [d] dct (dibenzo[*a,e*]cyclooctatetraene; 0.8 mg 0.004 mmol, 2.0 equiv. per [Ni]), 21 h.

Under these optimized conditions, linear α -olefins (*trans*-4-octene, allylbenzene) and even sterically hindered olefins such as diphenylethylenes, 1-phenyl-1-cyclohexene, and cycloocta-1,5-diene were successfully hydrogenated (Figure 7.2). Myrcene was converted to 2,6-dimethyloctane after 20 h; α -pinene and (*R*)-limonene were hydrogenated under relatively mild conditions (>80% conversion at 50-60 °C). Cinnamic acid (C=C, C=O) and benzonitrile (C \equiv N) remained untouched under the standard conditions. Note that catalytic amounts of benzonitrile (5 equiv. per [Ni]) also prevented 1,1',2-triphenylethylene hydrogenation (*vide infra* and see the SI, Table S9). Precatalyst **1** is not competent for the hydrogenation of polyaromatic substrates, e.g. anthracene, naphthalene, and quinolines.

7 Heterogeneous Olefin Hydrogenation Enabled by a Highly-Reduced Nickel(-II) Catalyst Precursor

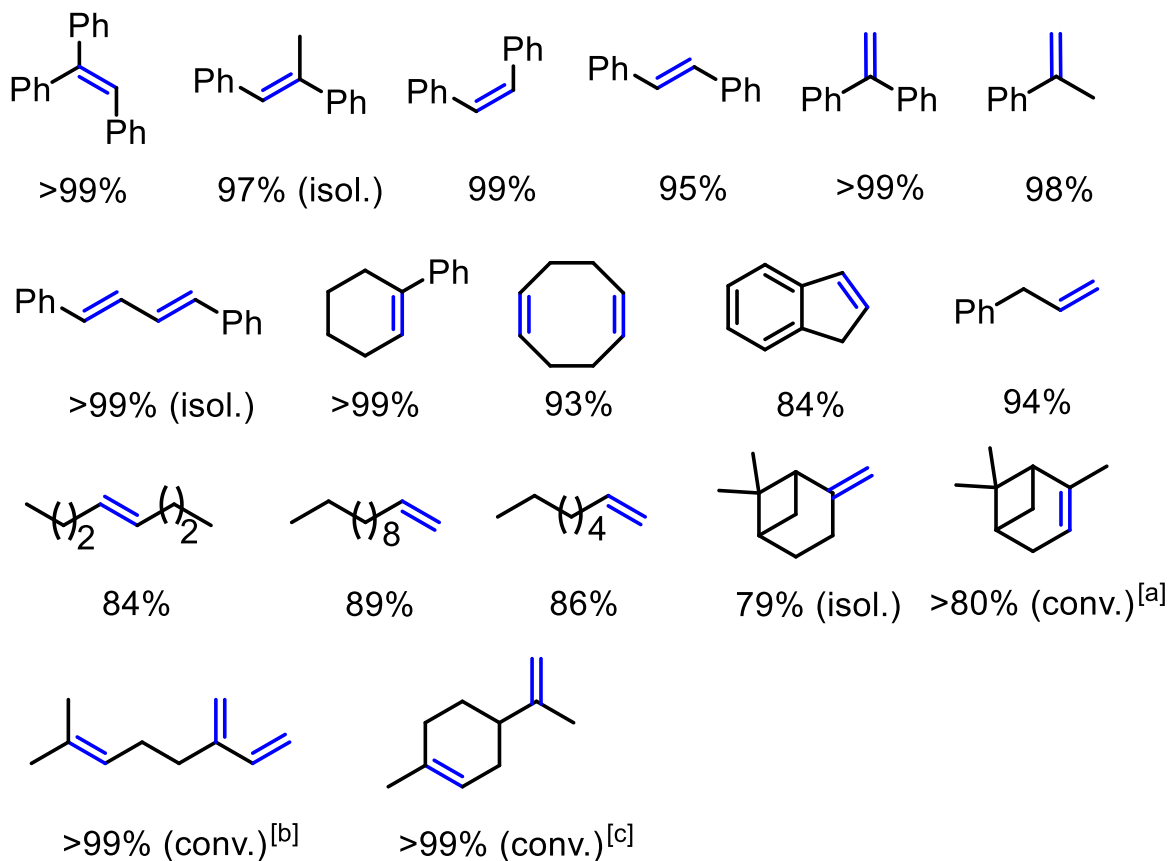


Figure 7.2. Hydrogenation of olefins with **1** (1 mol%). Standard conditions: 5 bar H₂, 25 °C, 18 h, substrate (0.2 mmol), DME (0.25 mL). Yields and conversions (conv.) were determined by quantitative GC-FID vs. internal *n*-pentadecane. Isolated products (isol.) were obtained from reactions performed on a 1.0 mmol scale in 1.25 mL DME. ^[a] 16 h, 50 °C, 50 bar H₂, DME (0.5 mL). ^[b] 20 h. ^[c] 60 °C, 25 bar H₂.

Previous reports on nickel-catalyzed hydrogenation of olefins have barely addressed functional group compatibility.^{[7]-[16]} We extended this protocol to olefinic alcohols, which are often found in bioactive molecules. Gratifyingly, olefins with phenolic as well as primary and secondary aliphatic hydroxyl functions were cleanly hydrogenated. Halogen atoms were partially tolerated. The C=C-hydrogenation of α,β -unsaturated lactones (coumarine) and esters (ethyl cinnamate) exhibited high chemoselectivities.

7 Heterogeneous Olefin Hydrogenation Enabled by a Highly-Reduced Nickel(–II) Catalyst Precursor

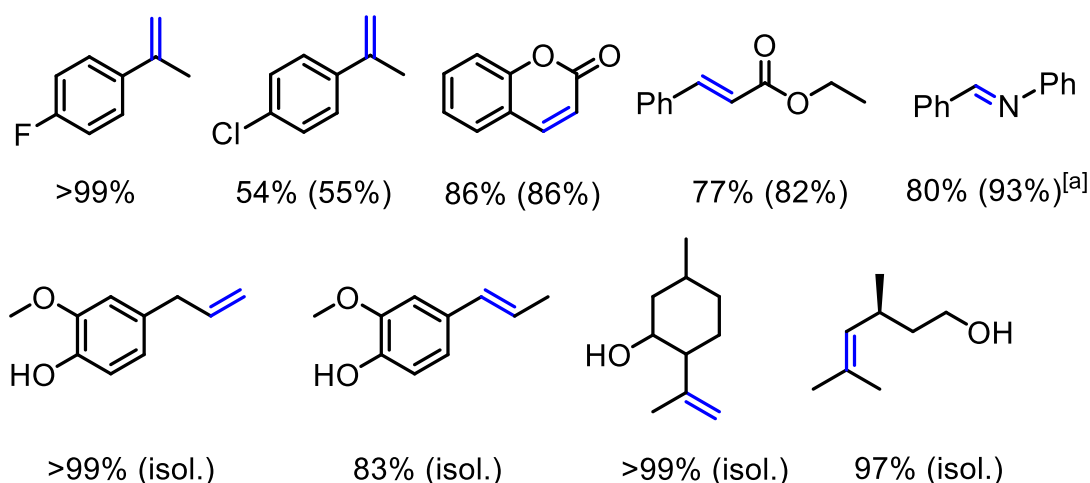


Figure 7.3. Hydrogenation of functional olefins using **1** (1 mol%). Standard conditions: 5 bar H₂, 25 °C, 18 h, substrate 0.2 mmol, DME (0.25 mL). Yields were determined by quantitative GC-FID vs. internal *n*-pentadecane if not stated otherwise. Conversions are given in parentheses. Isolated products (isol.) were obtained from reactions performed on a 1.0 mmol scale in 1.25 mL DME. ^[a] 5 mol% **1**.

A brief comparison of the catalytic properties of **1** with related anionic metalate pre-catalysts revealed that bis(η^4 -anthracene) ferrate(–I) and bis(η^4 -anthracene) cobaltate(–I) (**E**, Figure 7.1) required harsher conditions (60 °C, 2–10 bar H₂, 24 h) than **1** for the hydrogenation of α -methylstyrene and 2-octene.^[6] Bis(η^4 -cycloocta-1,5-diene) cobaltate(–I) (**F**) exhibited low functional group tolerance. However, it should be noted that the anions **E** and **F** were effective catalysts in the hydrogenation of ketones and imines.^[6]

Pre-catalyst **1** is also comparable to related Ni complexes **C** and **D** developed by *Driess* and *Chirik*, respectively (see Figure 7.1 and additionally Tables S2 and S3 of the SI).^{[14],[16]} It was reported that catalyst **C** enables the complete hydrogenation of 1-octene using 1 bar H₂ and 1.5 mol% catalyst. In comparison, **1** only gives a slightly poorer yield (86%) under the same conditions. Moreover, a similar turnover number and reaction time was observed for **D** and **1** for the hydrogenation of 1-phenyl-1-cyclohexene with H₂ (4 bar) and 0.4 mol% Ni catalyst at 50 °C (see the SI for details). Nonetheless, catalyst **D** inarguably is superior in the hydrogenation of highly challenging substrates such as tetra-substituted alkenes.^[16]

7 Heterogeneous Olefin Hydrogenation Enabled by a Highly-Reduced Nickel(–II) Catalyst Precursor

In order to study the nature of the catalytic process, simple reaction progress analyses of 1-octene, 2-(*E*)-octene, and α -methylstyrene were performed at 1.9 bar H₂ and ambient temperature using catalyst **1** (1 mol%, see the SI for details). The monitoring experiments revealed significant induction periods and sigmoidal behaviors, which are indicative of slow catalyst formation and nucleation to heterogeneous species (Figure 7.4).^[6] From these experiments, a turnover frequency (TOF) of 601 h⁻¹ can be approximated for 1-octene hydrogenation at low conversion (see the SI for details), while estimated TOFs are expectedly lower for secondary olefins 2-octene (103 h⁻¹) and α -methylstyrene (287 h⁻¹). Note that the reported values are inevitably approximate to the presence of an induction period.

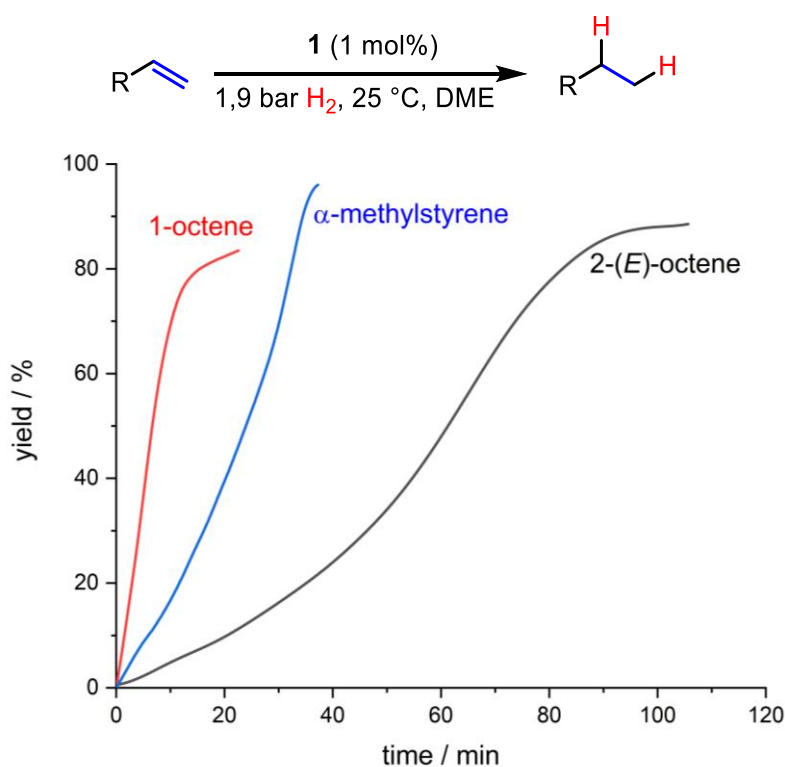


Figure 7.4. Reaction profiles of the olefin hydrogenations using **1**. Conditions: Substrate (0.2 mmol), DME (0.25 mL), 1.9 bar H₂, 25 °C. Yields determined by H₂ consumption, quantitative GC-FID vs. internal *n*-pentadecane.

The formation of heterogeneous species from the reaction of **1** and 1-phenyl-1-cyclohexene under an H₂ atmosphere was investigated by transmission electron microscopy (TEM, Figure 7.5). Particles of 10-15 nm diameter were observed alongside a few larger particles.

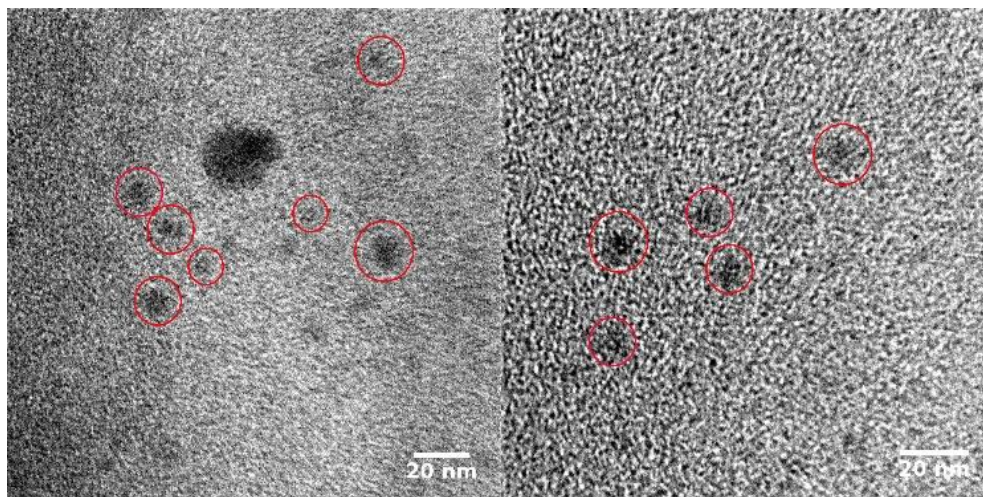


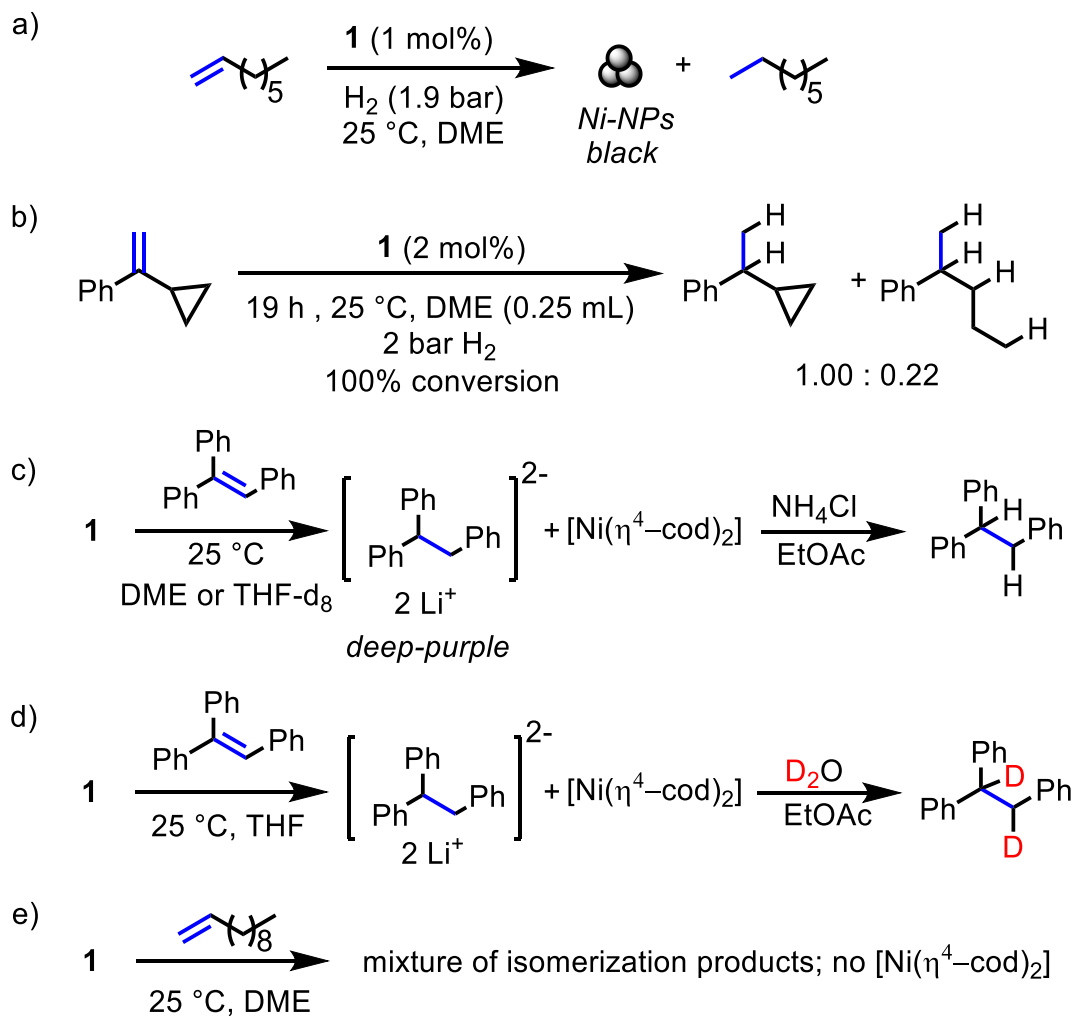
Figure 7.5. TEM images of particles formed in the hydrogenation of 1-phenyl-1-cyclohexene with **1** (particles highlighted with red circles vs. carbon film support).

Poisoning experiments were performed to corroborate the proposed heterotopic nature of the active catalyst.^[24] Addition of excess amounts of mercury led to complete catalyst inhibition in hydrogenations with **1** (Table 7.1, entry 5).^[6]^[23] By contrast, product yield was hardly affected by the presence of two equivalents of dibenzo[*a,e*]cyclooctatetraene (dct) per nickel atom (see Table 7.1, entry 6).^[25] In addition, benzonitrile (5 equiv. per Ni atom) is an efficient catalyst poison, while naphthalene only has a very minor inhibiting effect (see the SI for details). In sum, these results strongly suggest that a heterotopic catalyst is at operation.

Further mechanistic experiments were performed with the pre-catalyst **1** under reaction conditions: The rapid color change (orange to black) that was observed when treating a solution of 1-octene in DME with catalytic amounts of **1** under H₂ may indicate nanoparticle formation (Scheme 7.2a). Isomerization of allylbenzene to 1-propenylbenzene (55%) using **1** (1 mol%) proceeded in the absence of dihydrogen. Minor amounts of the ring-opening product (18%) were detected in the hydrogenation of α -cyclopropylstyrene (Scheme 2b).^[26] ¹H NMR spectra of **1** and 1,1',2-triphenylethylene in the absence of dihydrogen indicated the operation of rapid two-electron transfer from **1**. The resultant deep purple solution ($\lambda_{\text{max}} = 511 \text{ nm}$, see the SI, Figure S40) showed the characteristic signals of [Ni(η^4 -cod)₂] (Scheme 2c) Aqueous work-up afforded significant amounts of triphenylethane (see the SI). The cyclic voltammogram of the postulated triphenylethylene-dianion exhibited one irreversible reduction peak at -2.9 V vs.

Fc/Fc⁺ in THF and DME (see the SI, Figures S36, S37). This species was already detected in literature.^[27] Surprisingly, the rate of hydrogenation of 1,1',2-triphenylethylene by [Ni(η^4 -cod)₂] is significantly slower than with **1**. Deuterium experiments were performed to distinguish between H atom transfer (HAT) and ionic reactions (Scheme 2c, 2d). Reaction of **1** and 1,1',2-triphenylethylene in THF-d₈ led to no incorporation of D atoms after aqueous work-up. The same reaction in THF and subsequent work-up with D₂O furnished the formation of triphenylethane-d₂ (GC-MS, ¹H-NMR and ²H-NMR). These data strongly support an ionic mechanism. No electron transfer appeared to operate in reactions between **1** and 1-dodecene as no [Ni(η^4 -cod)₂] was observed but rather olefin isomerization products (Scheme 7.2e). In summary, the preliminary mechanistic data may suggest an electron-transfer initiation of the catalytic mechanism with reduction-sensitive substrates. Nonetheless, further mechanistic investigations are required to conclusively clarify the catalyst activation mechanism.

7 Heterogeneous Olefin Hydrogenation Enabled by a Highly-Reduced Nickel(-II) Catalyst Precursor



Scheme 7.2. Mechanistic experiments. a) Nanoparticle formation in the hydrogenation of 1-octene. b) Ring-opening of radical probe. c) Protonation and d) Deuteration of dianionic intermediate from electron transfer with 1,1',2'-triphenylethylene. e) Catalytic isomerization of 1-dodecene.

7.3 Conclusion

In conclusion, we have shown that dilithiumbis(cyclo-1,5-octadiene)nickelate (**1**) is a promising pre-catalyst for the hydrogenation of sterically hindered olefins. The catalytic hydrogenation operates under very mild conditions (5 bar H₂, 25 °C, DME as solvent). This work complements earlier studies of catalytic applications of “quasi-naked” base metal anions to olefin hydrogenations. The nickelate **1** exhibited higher catalytic activities than the related arene metalates (**E** and **F**), yet **1** was compatible with several functional groups (OH, esters, halides). Key mechanistic studies including reaction progress analyses, stoichiometric reactions, poisoning experiments, and transmission electron microscopy were conducted. These investigations support the notion of catalytically active nickel nanoparticles being operative under the reaction conditions. The catalyst formation from **1** is substrate-dependent and involves electron transfer reactions with reducible olefins (e.g. 1,1',2-triphenylethylene). This first catalytic application of a stabilized nickelate anion to olefin hydrogenations provides a firm basis for further investigations into the role of highly reduced, anionic metal catalysts as key intermediates in reductive transformations.

Acknowledgements

Financial support by the Fonds der Chemischen Industrie (fellowship to T.M.M.), the Deutsche Forschungsgemeinschaft (JA 1107/6-1, WO 1496/6-1), and the European Research Council (CoG 683150) is gratefully acknowledged. Dr. Daniel Scott is thanked for valuable comments on the manuscript.

Keywords: nickel • catalysis • hydrogenation • nanoparticles • olefins

7.4 References

- [1] a) *Catalytic Hydrogenation* (Ed.: L. Cerveny), Elsevier, Amsterdam, **1986**; b) *The Handbook of Homogeneous Hydrogenation* (Eds.: J. G. de Vries, C. J. Elsevier), Wiley-VCH, Weinheim, **2007**.
- [2] a) J. A. Osborn, F. H. Jardine, J. F. Young, G. Wilkinson, *J. Chem. Soc.* **1966**, 1711–1732; b) W. S. Knowles, M. J. Sabacky, B. D. Vineyard, D. J. Weinkauff, *J. Am. Chem. Soc.* **1975**, *97*, 2567–2568; c) H. Doucet, T. Ohkuma, K. Murata, T. Yokozawa, M. Kozawa, E. Katayama, A. F. England, T. Ikariya, R. Noyori, *Angew. Chem. Int. Ed.* **1998**, *37*, 1703–1707; d) Á. Molnár, A. Sárkány, M. Varga, *J. Mol. Catal.* **2001**, *173*, 185–221.
- [3] a) *Catalysis without precious metals* (Ed.: R. Morris Bullock), Wiley-VCH, Weinheim, **2010**; b) K. Junge, K. Schröder, M. Beller, *Chem. Commun.* **2011**, *47*, 4849–4859; c) P. J. Chirik, *Acc. Chem. Res.* **2015**, *48*, 1687–1695; d) *Non-Noble Metal Catalysis: Molecular Approaches and Reactions*, (Eds.: R. J. M. Klein Gebbink, M.-E. Moret), Wiley-VCH, Weinheim, **2018**; e) L. Alig, M. Fritz, S. Schneider, *Chem. Rev.* **2019**, *119*, 2681–2751; f) W. Ai, R. Zhong, X. Liu, Q. Liu, *Chem. Rev.* **2018**, *119*, 2876–2953; g) G. A. Filonenko, R. van Putten, E. J. M. Hensen, E. A. Pidko, *Chem. Soc. Rev.* **2018**, *47*, 1459–1483; h) L. Alig, M. Fritz, S. Schneider, *Chem. Rev.* **2019**, *119*, 2681–2751.
- [4] Selected examples for Mn a) U. Chakraborty, E. Reyes-Rodriguez, S. Demeshko, F. Meyer, A. Jacobi von Wangelin, *Angew. Chem. Int. Ed.* **2018**, *57*, 4970–4975; *Angew. Chem.* **2018**, *130*, 5064–5069; b) F. Kallmeier, R. Kempe, *Angew. Chem. Int. Ed.* **2018**, *57*, 46–60; *Angew. Chem.* **2018**, *130*, 48–63.
- [5] Selected examples for Fe: a) S. C. Bart, E. Lobkovsky, P. J. Chirik, *J. Am. Chem. Soc.* **2004**, *126*, 13794–13807; b) R. J. Trovitch, E. Lobkovsky, E. Bill, P. J. Chirik, *Organometallics* **2008**, *27*, 1470–1478; c) B. A. F. Le Bailly, S. P. Thomas, *RSC Adv.* **2011**, *1*, 1435; d) R. P. Yu, J. M. Darmon, J. M. Hoyt, G. W. Margulieux, Z. R. Turner, P. J. Chirik *ACS Catal.* **2012**, *2*, 1760–1764; e) T. N. Gieshoff, M. Villa, A. Welther, M. Plois, U. Chakraborty, R. Wolf, A. Jacobi von Wangelin, *Green Chemistry* **2015**, *17*, 1408–1413; f) M. Villa, D. Miesel, A. Hildebrandt, F. Ragaini, D. Schaarschmidt, A. Jacobi von Wangelin,

- ChemCatChem* **2017**, *9*, 3203–3209; g) J. H. Docherty, J. Peng, A. P. Dominey, S. P. Thomas, *Nat. Chem.* **2017**, *9*, 595-600.
- [6] Selected examples for Co: a) Q. Knijnenburg, A. d. Horton, H. van der Heijden, T. M. Kooistra, D. G.H. Hetterscheid, J. M. M. Smits, B. de Bruin, P. H. M. Budzelaar, A. W. Gal, *J. Mol. Catal. A* **2005**, *232*, 151–159; b) G. Zhang, B. L. Scott, S. K. Hanson, *Angew. Chem. Int. Ed.* **2012**, *51*, 12102–12106; *Angew. Chem.* **2012**, *124*, 12268–12272; c) R. P. Yu, J. M. Darmon, C. Milsmann, G. W. Margulieux, S. C. E. Stieber, S. DeBeer, P. J. Chirik, *J. Am. Chem. Soc.* **2013**, *135*, 13168–13184; d) D. Gärtner, A. Welther, B. R. Rad, R. Wolf, A. Jacobi von Wangelin, *Angew. Chem. Int. Ed.* **2014**, *53*, 3722–3726; *Angew. Chem.* **2014**, *126*, 3796–3800; e) M. R. Friedfeld, G. W. Margulieux, B. A. Schäfer, P. J. Chirik, *J. Am. Chem. Soc.* **2014**, *136*, 13178-13181; f) K. Tokmic, C. R. Markus, L. Zhu, A. R. Fout, *J. Am. Chem. Soc.* **2016**, *138*, 11907–11913; g) P. Büschelberger, D. Gärtner, E. Reyes-Rodriguez, F. Kreyenschmidt, K. Koszinowski, A. Jacobi von Wangelin, R. Wolf, *Chem. Eur. J.* **2017**, *23*, 3139–3151; h) P. Büschelberger, E. Reyes-Rodriguez, C. Schöttle, J. Treptow, C. Feldmann, A. Jacobi von Wangelin, R. Wolf, *Catal. Sci. Technol.* **2018**, *8*, 2648–2653; i) S. Sandl, F. Schwarzhuber, S. Pöllath, J. Zweck, A. Jacobi von Wangelin, *Chem. Eur. J.* **2018**, *24*, 3403–3407; j) F. K. Scharnagl, M. F. Hertrich, F. Ferretti, C. Kreyenschulte, H. Lund, R. Jackstell, M. Beller, *Sci. Adv.* **2018**, *4*, eaau1248; k) S. Sandl, T. M. Maier, N. P. van Leest, S. Kröncke, U. Chakraborty, S. Demeshko, K. Koszinowski, B. de Bruin, F. Meyer, C. Herrmann, R. Wolf, A. Jacobi von Wangelin *ACS Catal.* **2019**, *9*, 7596-7606.
- [7] M. Raney, *US patent 1628190* **1927**.
- [8] a) S. Nishimura, *Handbook of Heterogeneous Catalytic Hydrogenation for Organic Synthesis*, Wiley, New York **2001**; b) T.-K. Yang, D.-S Lee, J. Haas, *Raney Nickel, Encyclopedia of Reagents for Organic Synthesis* **2006**; c) H.-J. Arpe, *Industrial Organic Chemistry*, Wiley-VCH, Weinheim, **2010**.
- [9] a) R. Paul, P. Buisson, N. Joseph, *Ind. Eng. Chem.* **1952**, *44*, 1006-1010; b) H. C. Brown, C. A. Brown, *J. Am. Chem. Soc.* **1963**, *85*, 1005–1006; c) C. A. Brown, *J. Org. Chem.* **1970**, *35*, 1900–1904; d) C. A. Brown, V. K. Ahuja, *J. Org. Chem.* **1973**, *38*, 2226–2230.
- [10] A. Reina, I. Favier, C. Pradel, M. Gómez, *Adv. Synth. Catal.* **2018**, *360*, 3544–3552.

- [11] L. Zaramello, B. L. Albuquerque, J. B. Domingos, K. Philippot, *Dalton Trans.* **2017**, 46, 5082–5090.
- [12] Y. Hu, Y. Yu, Z. Hou, H. Yang, B. Feng, H. Li, Y. Qiao, X. Wang, L. Hua, Z. Pan et al., *Chem. Asian J.* **2010**, 5, 1178–1184.
- [13] a) I. M. Angulo, A. M. Kluwer, E. Bouwman, *Chem. Commun.* **1998**, 2689–2690; b) K. V. Vasudevan, B. L. Scott, S. K. Hanson, *Eur. J. Inorg. Chem.* **2012**, 2012, 4898–4906; c) W. H. Harman, J. C. Peters, *J. Am. Chem. Soc.* **2012**, 134, 5080–5082; d) T. J. Mooibroek, E. C. M. Wenker, W. Smit, I. Mutikainen, M. Lutz, E. Bouwman, *Inorg. Chem.* **2013**, 52, 8190–8201.
- [14] Y. Wang, A. Kostenko, S. Yao, M. Driess, *J. Am. Chem. Soc.* **2017**, 139, 13499–13506.
- [15] J. Wu, J. W. Faller, N. Hazari, T. J. Schmeier, *Organometallics* **2012**, 31, 806–809.
- [16] N. G. Léonard, P. J. Chirik, *ACS Catal.* **2018**, 8, 342–348.
- [17] a) X. Li, C. You, S. Li, H. Lv, X. Zhang, *Org. Lett.* **2017**, 19, 5130–5133; b) W. Gao, H. Lv, T. Zhang, Y. Yang, L. W. Chung, Y.-D. Wu, X. Zhang, *Chem. Sci.* **2017**, 8, 6419–6422; c) J. Long, W. Gao, Y. Guan, H. Lv, X. Zhang, *Org. Lett.* **2018**, 20, 5914–5917.
- [18] Reviews on metalate anions highlighting the pioneering work of Jonas and Ellis: a) J. E. Ellis, *Inorg. Chem.* **2006**, 45, 3167–3186; b) J. E. Ellis, *Dalton Trans.* **2019**, 48, 9538–9563.
- [19] a) W. W. Brennessel, J. Young, G. Victor, J. E. Ellis, *Angew. Chem. Int. Ed.* **2002**, 41, 1211–1215; *Angew. Chem.* **2002**, 114, 1259–1263; b) W. W. Brennessel, R. E. Jilek, J. E. Ellis, *Angew. Chem. Int. Ed.* **2007**, 46, 6132–6136; *Angew. Chem.* **2007**, 119, 6244–6248.
- [20] K. Jonas, L. Schieferstein, C. Krüger, Y.-H. Tsay, *Angew. Chem. Int. Ed.* **1979**, 18, 550–551; *Angew. Chem.* **1979**, 91, 590–591.
- [21] K. Jonas, *Angew. Chem. Int. Ed.* **1975**, 14, 752–753; *Angew. Chem.* **1975**, 87, 809–810.
- [22] L. Nattmann, S. Lutz, P. Ortsack, R. Goddard, J. Cornella, *J. Am. Chem. Soc.* **2018**, 140, 13628–13633.
- [23] For the less challenging substrate 1-dodecene, **1** and $[\text{Ni}(\eta^4\text{-cod})_2]$ showed equal activity.

- [24]a) J. A. Widegren, R. G. Finke, *J. Mol. Catal. A* **2003**, *198*, 317; b) R. H. Crabtree, *Chem. Rev.* **2012**, *112*, 1536-1554; c) J. F. Sonnenberg, R. H. Morris, *Catal. Sci. Technol.* **2014**, *4*, 3426-3438.
- [25]a) D. R. Anton, R. H. Crabtree, *Organometallics* **1983**, *2*, 855–859. b) S. Chaffins, M. Brettreich, F. Wudl, *Synthesis* **2002**, 1191–1194. c) G. Franck, M. Brill, G. Helmchen, *Org. Synth.* **2012**, *89*, 55–65.
- [26] Kinetics and mechanism of the hydrogenation of α -cyclopropylstyrene: Rate constant of the ring-opening rearrangement of the corresponding radical: $3.6 \times 10^5 \text{ s}^{-1}$ at 22°C in hexane solution. a) R. Morris Bullock, E. G. Samsel, *J. Am. Chem. Soc.* **1990**, *112*, 6886-6898; b) J. Choi, L. Tang, J.-R Norton, *J. Am. Chem. Soc.* **2007**, *129*, 234-240.
- [27]a) G. Farnia, F. Mran, G. Sandona, M. G. Severin, *J. Chem. Soc., Perkin Trans.* **1982**, *2*, 1153-1158; b) D. Suwatchara, N. V. Rees, R. G. Compton, *J. Electroanal. Chem.* **2012**, *669*, 14-20.

7.5 Supporting Information

7.5.1 General information

All experiments were performed under an atmosphere of dry Argon (Argon 4.6, Linde) using standard Schlenk techniques or a *MBraun UniLab* Glovebox.

Analytical Thin-Layer Chromatography: TLC was performed using aluminium plates with silica gel and fluorescent indicator (*Macherey-Nagel*, 60, UV₂₅₄). Thin layer chromatography plates were visualized by exposure to UV light (366 or 254 nm).

Chemicals and Solvents: Solvents were dried and degassed with an *MBraun SPS800* solvent-purification system. THF, diethylether were stored over molecular sieves (3 Å). *n*-Hexane was stored over a potassium mirror. 1,2-Dimethoxyethane was stirred over K/benzophenone, distilled and stored over molecular sieves (3 Å). Commercially available olefins were purified by distillation (Kugelrohr) and in case of liquids dried over molecular sieves (3 Å). [Ni(η^4 -cod)₂] was obtained from *Sigma-Aldrich* and used without further purification.

Cyclic Voltammetry: Cyclic Voltammetry experiments were performed in a single-compartment cell inside a nitrogen-filled glovebox using a CH Instruments CH1600E potentiostat. The cell was equipped with a platinum disc working electrode (2 mm diameter) polished with 0.05 μ m alumina paste, a platinum wire counter electrode and an Ag/AgNO₃ reference electrode. The supporting electrolyte, tetra-*n*-butylammonium hexafluorophosphate, was dried *in vacuo* at 110°C for three days. All redox potentials are reported vs. the ferrocenium/ferrocene (Fc⁺/Fc) couple.

Column Chromatography: Flash column chromatography with silica gel 60 from *Sigma Aldrich* (63 – 200 μ m). Mixture of solvents used are described *vide infra*.

High Pressure Reactor: Hydrogenation reactions were carried out in 160 and 300 mL high pressure reactors (*Parr*TM) in 4 mL glass vials. The reactors were loaded under argon, purged with hydrogen, sealed and the internal pressure was adjusted. Hydrogen (99.9992%) was purchased from *Linde*.

7 Heterogeneous Olefin Hydrogenation Enabled by a Highly-Reduced Nickel(–II) Catalyst Precursor

NMR spectroscopy: ^1H and $^{13}\text{C}\{^1\text{H}\}$ NMR spectra in solutions were recorded on *Bruker Avance 300* (300 MHz) and *Bruker Avance 400* (400 MHz) if not stated otherwise. These chemical shifts are given relative to solvents resonances in the tetramethylsilane scale. The following abbreviations have been used for multiplicities: s = singlet, d = doublet, t = triplet, q = quartet, sept = septet, m = multiplet, dd = doublet of doublet, dt = doublet of triplet.

Gas chromatography with FID (GC-FID): Shimadzu GC2025. Carrier gas: H_2 . Colum: Restek Rxi[®]-5Sil-MS, (30m x 0.25 mm x 0.25 μm) Carrier gas: H_2 . Standard heating procedure: 50°C (2 min), 25°C/min \rightarrow 280°C (5 min). Calibration of substrates and products was performed using internal *n*-pentadecane and analytically pure samples.

Gas chromatography with mass-selective detector (GC-MS): Agilent 7820A GC system, mass detector 5977B. Carrier gas: H_2 . Column: HP-5MS (30m x 0.25 mm x 0.25 μm). Standard heating procedure: 50°C \rightarrow 300°C.

Transmission electron microscopy (TEM): The particles were imaged in a FEI Tecnai F30 ST Regensburg special transmission electron microscope, equipped with a field emission gun operated at 300 kV and a super twin lens, capable of a resolution of 0.19 nm.

UV-vis spectroscopy: UV-vis spectra were recorded on an Ocean Optics Flame spectrometer (Varian Cary 50 Spectrophometer) in a Quartz cuvette with a layer thickness of 1 cm at room temperature with a concentration of 10^{-4} to 10^{-6} M.

7.5.2 Synthesis of $[\text{Li}_2(\text{thf})_4\{\text{Ni}(\eta^4\text{-cod})(\eta^2\text{-cod})\}]$ (1)

The procedure for the synthesis of $[\text{Li}_2(\text{thf})_4\{\text{Ni}(\eta^4\text{-cod})(\eta^2\text{-cod})\}]$ (1) was adapted from Jonas and co-workers^[21] and Cornella and co-workers.^[2]

$[\text{Ni}(\eta^4\text{-cod})_2]$ (1.0 g, 3.6 mmol, 1.0 equiv.) was mixed with lithium metal (0.09 mg, 13.0 mmol, 3.6 equiv.). A cooled (0 °C) THF solution was added and the suspension was stirred for seven hours under exclusion of light until no solid $[\text{Ni}(\eta^4\text{-cod})_2]$ was left. After filtration, the orange solution was concentrated to 8 mL and layered with diethylether in a 1:2 ratio. Dark-orange crystals of $[\text{Li}_2(\text{thf})_4\{\text{Ni}(\eta^4\text{-cod})(\eta^2\text{-cod})\}]$ formed after storage of the solution at –35 °C overnight. The crystals were isolated by decantation and dried *in vacuo* at –30 °C.

The complex was stored under argon at -35°C . The ^1H NMR spectrum at room temperature is in accordance with the spectrum described in literature.^[2]

Yield: 1.12 g, (1.94 mmol, 53%)

Chemical formula: $\text{Li}_2\text{NiC}_{16}\text{H}_{24} \cdot (\text{C}_4\text{H}_8\text{O})_4$ ($M = 577.37 \text{ g mol}^{-1}$)

^1H NMR (400.13 MHz, 300 K, THF-d_8) δ [ppm]: 2.28 (br s), 2.05 (br d), 2.03 (br s), 1.68 (br s).

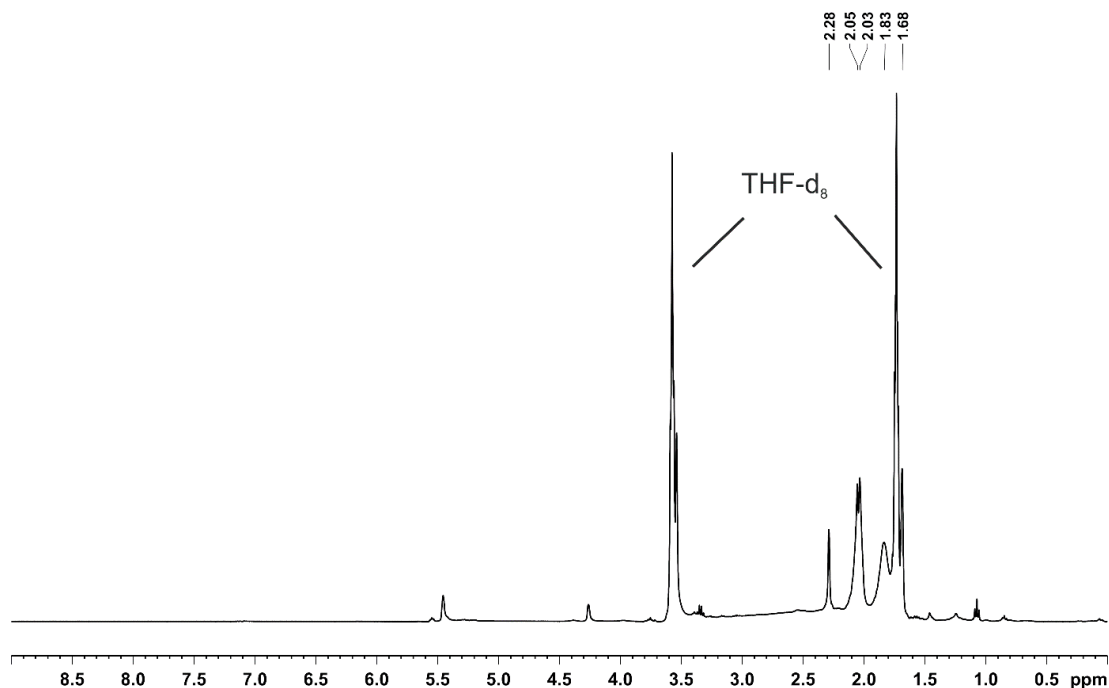


Figure 7.5.1. ^1H NMR spectrum (400.13 MHz, 300 K, THF-d_8) of **1**.

7.5.3 Hydrogenation reactions

General Procedure

In an argon-filled glovebox, a flame-dried 4 mL reaction vial was charged with the substrate (0.2 mmol) and *n*-pentadecane (20 μL) as internal reference for GC-FID quantification. The catalyst was added as a solution in DME, if not stated otherwise. The reaction vessel was transferred to a high-pressure reactor, which was sealed and removed from the glovebox. The reactor was purged with hydrogen gas (three times) and the reaction pressure and temperature were set. After the indicated reaction time, the vial was retrieved, and the reaction mixture was hydrolyzed with a saturated aqueous solution of NH_4Cl and diluted with ethyl acetate. An aliquot of the organic phase was filtered over a pad of silica, which was washed with ethyl acetate. The solution was analyzed by GC-FID and GC-MS.

7 Heterogeneous Olefin Hydrogenation Enabled by a Highly-Reduced Nickel(–II) Catalyst Precursor

After the end of the reaction the crude mixture was filtered over silica and the product isolated by solvent evaporation.

Optimization of Reaction Conditions

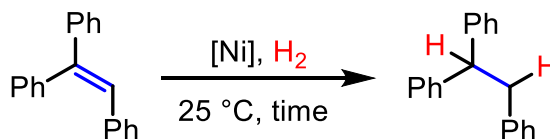


Table 7.5.1. Optimization of reaction conditions.

Entry	Catalyst ^[a]	Solvent [mL]	p (H ₂) [bar]	T [°C]	T [h]	Yield (Conversion) [%] ^[d]
1	1 ^[b]	THF (1 mL)	10	25	5	97 (100)
2	1	THF (0.5 mL)	5	25	15	81 (82)
3	1	DME (0.5 mL)	5	25	15	97 (98)
4	1	DME (0.25 mL)	5	25	15	99 (100)
5	1	DME (0.25 mL)	1.9	25	15	72 (74)
6	[Ni(η^4 -cod) ₂]	THF (0.5 mL)	5	25	15	22 (26)
7	[Ni(η^4 -cod) ₂]	DME (0.5 mL)	5	25	15	36 (38)
8	1 + Hg ^[c]	DME (0.5 mL)	5	25	15	2 (5)

[a] 1 mol%, if not stated otherwise. [b] 5 mol%. [c] Addition of an excess mercury (50 mg, 0.025 mmol, 125 equiv.) before the hydrogenation was started. [d] Yields and conversions determined by quantitative GC-FID vs. internal *n*-pentadecane.

Comparative Experiments

a) P. J. Chirik and co-workers.^[16]

Hydrogenation with Ni(OAc)₂ (1 equiv.) and HBPin (4 equiv.)

Table 7.5.2. Hydrogenation of 1-phenyl-1-cyclohexene. Yields were determined by GC-FID analysis.

Entry	Substrate	Conditions	Yield (Lit.) [%]	Yield (using 1) [%]
1	1-phenyl-cyclohexene	4 bar H ₂ , 0.4 mol%, 50 °C, 3 h	>98	>99 (after 2h)

7 Heterogeneous Olefin Hydrogenation Enabled by a Highly-Reduced Nickel(–II) Catalyst Precursor

Determination of the turnover frequency (TOF):

1-Phenyl-1-cyclohexene (catalyst **1**): t = 2 h, 0.4 mol% Ni, 4 bar H₂, 50°C; TOF = 125 h⁻¹;

1-Phenyl-1-cyclohexene (catalyst **D**, ref. [16]): t = 3 h, 0.4 mol% Ni, 4 bar H₂, 50°C; TOF = 82.5 h⁻¹

b) M. Driess and co-workers.^[4]

Hydrogenation with a nickel-silylene complex

Table 7.5.3. Hydrogenation of 1-octene. Yields were determined by GC-FID analysis.

Entry	Substrate	Conditions	Yield (Lit.) [%]	Yield (using 1) [%]
1	1-octene	1 bar H ₂ , 1.5 mol%, 25 °C, 24 h	>99	86 ^[a]

[a]: Full conversion using catalyst **1**.

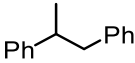
c) Unsupported [Ni(η^4 -cod)₂]

Table 7.5.4. Hydrogenation of several C=C bonds. Yields were determined by GC-FID analysis.

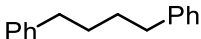
Entry	Substrate	Conditions ^[a]	Yield ([Ni(η^4 -cod) ₂]) [%]	Yield (using 1) [%]
1	1,1',2-triphenylethylene	15 h	36	99
2	1-dodecene	30 min	90	90
3	1-Ph-cyclohexene	4 h	0	74

[a] 5 bar H₂, 1 mol%, 25 °C

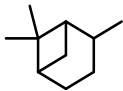
Isolated Hydrogenation Products

	1,2-diphenylpropane $C_{15}H_{16}$ 196.29 g mol ⁻¹ colorless liquid
Yield	191.8 mg (0.97 mmol, 97%)
¹H-NMR	(400.13 MHz, 300 K, CDCl ₃) δ[ppm]: 7.36–7.21 (m, 8H, CH _{Ar}), 7.16–7.14 (m, 2H, CH _{Ar}), 3.10 – 2.99 (m, 2H, CH ₂), 2.86 – 2.81 (m, 1H, CH), 1.31 (d, J = 6.8 Hz, 3H, CH ₃)
¹³C{¹H}-NMR	(100.6 MHz, 300 K, CDCl ₃) δ[ppm]: 147.1, 140.9, 129.3, 128.4, 128.2, 127.1, 126.1, 125.9, 45.2, 42.0, 21.2
GC-MS	<i>t</i> _R = 9.46 min, (EI, 70 eV): <i>m/z</i> = 196.1 [M ⁺]

Analytical data were in full agreement with those published by Pilkington and co-workers.^[5]

	1,4-diphenylbutane $C_{16}H_{18}$ 210.32 g mol ⁻¹ colorless liquid
Yield	208 mg (0.99 mmol, 99%)
¹H-NMR	(400.13 MHz, 300 K, CDCl ₃) δ[ppm]: 7.48 – 7.26 (m, 10H, CH _{Ar}), 2.76 (br s, 4H, CH ₂), 1.80 (br s, 4H, CH ₂)
¹³C{¹H}-NMR	(100.6 MHz, 300 K, CDCl ₃) δ[ppm]: 142.7, 128.6, 128.5, 128.4, 128.4, 125.8, 35.9, 31.2
GC-MS	<i>t</i> _R = 11.00 min, (EI, 70 eV): <i>m/z</i> = 210.2 [M ⁺]

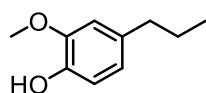
Analytical data were in full agreement with those published by Weix and co-workers.^[6]

	pinane $C_{10}H_{18}$ 138.25 g mol ⁻¹ colorless liquid
Yield	107 mg (0.77 mmol, 79%)
¹H-NMR	(400.13 MHz, 300 K, CDCl ₃) δ[ppm]: 2.31 (m, 1H), 2.13 (1H), 2.00 – 1.60 (m, 5H), 1.47 – 1.30 (m, 1H), 1.19 (br s, 3H), 1.01 (m, 2H), 0.88 – 0.82 (m, 2H)

7 Heterogeneous Olefin Hydrogenation Enabled by a Highly-Reduced Nickel(–II) Catalyst Precursor

$^{13}\text{C}\{^1\text{H}\}$-NMR	(100.6 MHz, 300 K, CDCl_3) δ [ppm]: main isomer: 48.1, 41.4, 38.8, 36.0, 34.0, 28.3, 26.6, 23.9, 23.2, 22.9; minor isomer: 47.7, 40.9, 39.5, 29.4, 26.9, 26.7, 24.6, 24.0, 23.0, 21.6, 20.1
GC-MS	t_R = two isomers 3.87 min (16.5%), 4.00 min (83.5%) (EI, 70 eV): m/z = 138.1 [M^+]

Analytical data were in full agreement with a sample obtained from *Sigma-Aldrich*.

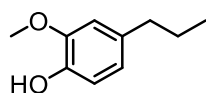


2-methoxy-4-propylphenol (from eugenol)

$\text{C}_{10}\text{H}_{14}\text{O}_2$ 166.22 g mol⁻¹

colorless liquid

Yield	163 mg (0.99 mmol, 99%)
^1H-NMR	(400.13 MHz, 300 K, CDCl_3) δ [ppm]: 6.86 (d, J = 7.8 Hz, 1H, CH_{Ar}), 6.70 (d, J = 7.9 Hz, 2H, CH_{Ar}), 5.58 (br s, 1H, OH), 3.89 (s, 3H, O- CH_3), 2.55 (t, 7.6 Hz, 2H, CH_2), 1.65 (m, 2H, CH_2), 0.97 (m, 3H, CH_3)
$^{13}\text{C}\{^1\text{H}\}$-NMR	(100.6 MHz, 300 K, CDCl_3) δ [ppm]: 146.4, 143.6, 134.7, 121.0, 114.2, 111.1, 55.9, 37.8, 24.9, 13.8
GC-MS	t_R = 7.86 min, (EI, 70 eV): m/z = 166.1 [M^+]



2-methoxy-4-propylphenol (from isoeugenol)

$\text{C}_{10}\text{H}_{14}\text{O}_2$ 166.22 g mol⁻¹

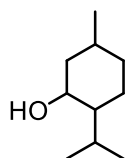
colorless liquid

Yield	136 mg (0.83 mmol, 83%)
^1H-NMR	(400.13 MHz, 300 K, CDCl_3) δ [ppm]: 6.85 (d, J = 7.8 Hz, 1H, CH_{Ar}), 6.69 (d, J = 7.9 Hz, 2H, CH_{Ar}), 5.52 (br s, 1H, OH), 3.89 (s, 3H, O- CH_3), 2.54 (t, 7.6 Hz, 2H, CH_2), 1.65 (m, 2H, CH_2), 0.96 ((t, 7.3 Hz, 3H, CH_3)
$^{13}\text{C}\{^1\text{H}\}$-NMR	(100.6 MHz, 300 K, CDCl_3) δ [ppm]: 146.3, 143.6, 134.7, 121.0, 114.1, 111.1, 55.9, 37.8, 24.9, 13.8
GC-MS	t_R = 7.86 min, (EI, 70 eV): m/z = 166.1 [M^+]

Analytical data were in full agreement with those published by Minnaard and co-workers.^[7]

2-isopropyl-5-methylcyclohexan-1-ol

7 Heterogeneous Olefin Hydrogenation Enabled by a Highly-Reduced Nickel(–II) Catalyst Precursor

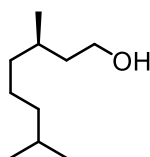


$C_{10}H_{20}O$ 156.27 g mol⁻¹

colorless liquid

Yield	155.5 mg (0.99 mmol, 99%)
¹H-NMR	(400.13 MHz, 300 K, CDCl ₃) δ[ppm]: 3.36 (s, 1H, OH), 2.16 (m, 1H), 1.93 (m, 1H), 1.70 – 1.47 (m, 4H), 1.39 (m, br s, 1H), 1.11 (m, 1H), 1.00 – 0.75 (m, 13H)
¹³C{¹H}-NMR	(100.6 MHz, 300 K, CDCl ₃) δ[ppm]: mixture of isomers: 71.8, 71.5, 67.9, 67.7, 50.1, 48.0, 45.1, 42.6, 40.1, 39.1, 35.1, 34.6, 31.7, 30.5, 29.2, 27.6, 25.8, 25.8, 24.2, 23.2, 22.4, 22.2, 21.2, 21.1, 21.0, 20.8, 20.0, 19.6, 18.1, 16.1
GC-MS	<i>t_R</i> = four isomers: 5.93 min (24%), 6.01 min (64%), 6.12 min (4%), 6.17 min (8%), (EI, 70 eV): <i>m/z</i> = 154.2 [M ⁺]

Analytical data were in agreement with those published by Krempner and co-workers.^[8]



(*R*)-3,7-dimethyloctan-1-ol

$C_{10}H_{22}O$ 158.29 g mol⁻¹

colorless liquid

Yield	153.3 mg (0.97 mmol, 97%)
¹H-NMR	(400.13 MHz, 300 K, CDCl ₃) δ[ppm]: 3.71 – 3.60 (m, 2H), 1.71 (br s, 1H, OH), 1.64 – 1.45 (m, 3H), 1.40 – 1.20 (m, 4H), 1.18 – 1.05 (m, 3H), 0.89 – 0.82 (m, 9H)
¹³C{¹H}-NMR	(100.6 MHz, 300 K, CDCl ₃) δ[ppm]: 61.1, 40.0, 39.3, 37.4, 29.5, 28.0, 24.7, 22.7, 22.6, 19.6
GC-MS	<i>t_R</i> = 6.19 min, (EI, 70 eV): <i>m/z</i> = 140.1 [M ⁺]

Analytical data were in full agreement with those published by Pilkington and co-workers.^[5]

7.5.4 Hydrogenation products: NMR spectra

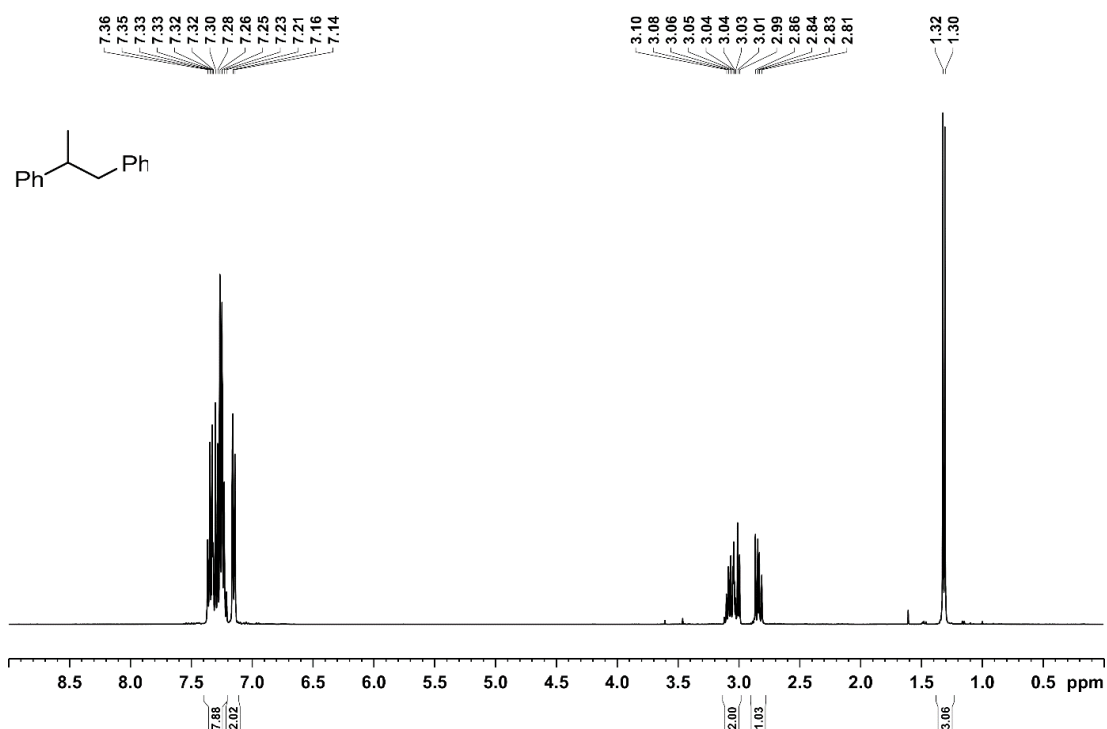


Figure 7.5.2. ¹H NMR spectrum (400.13 MHz, 300 K, CDCl₃) of 1,2-diphenylpropane.

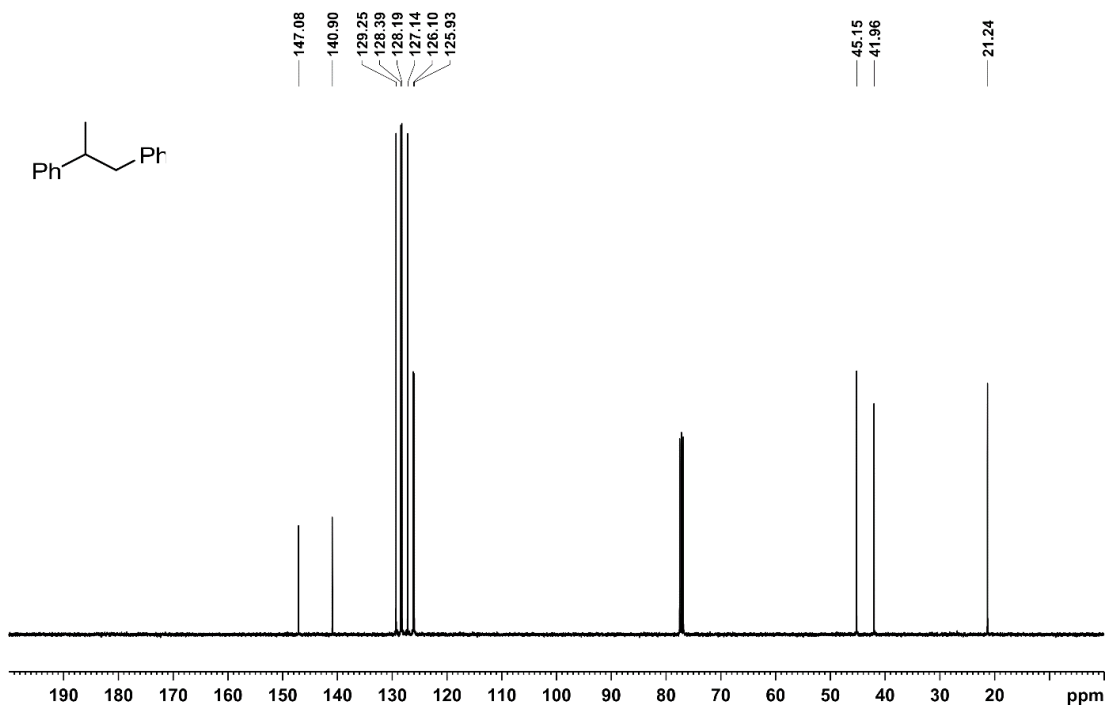


Figure 7.5.3. ¹³C{¹H} NMR spectrum (100.6 MHz, 300 K, CDCl₃) of 1,2-diphenylpropane.

7 Heterogeneous Olefin Hydrogenation Enabled by a Highly-Reduced Nickel(–II) Catalyst Precursor

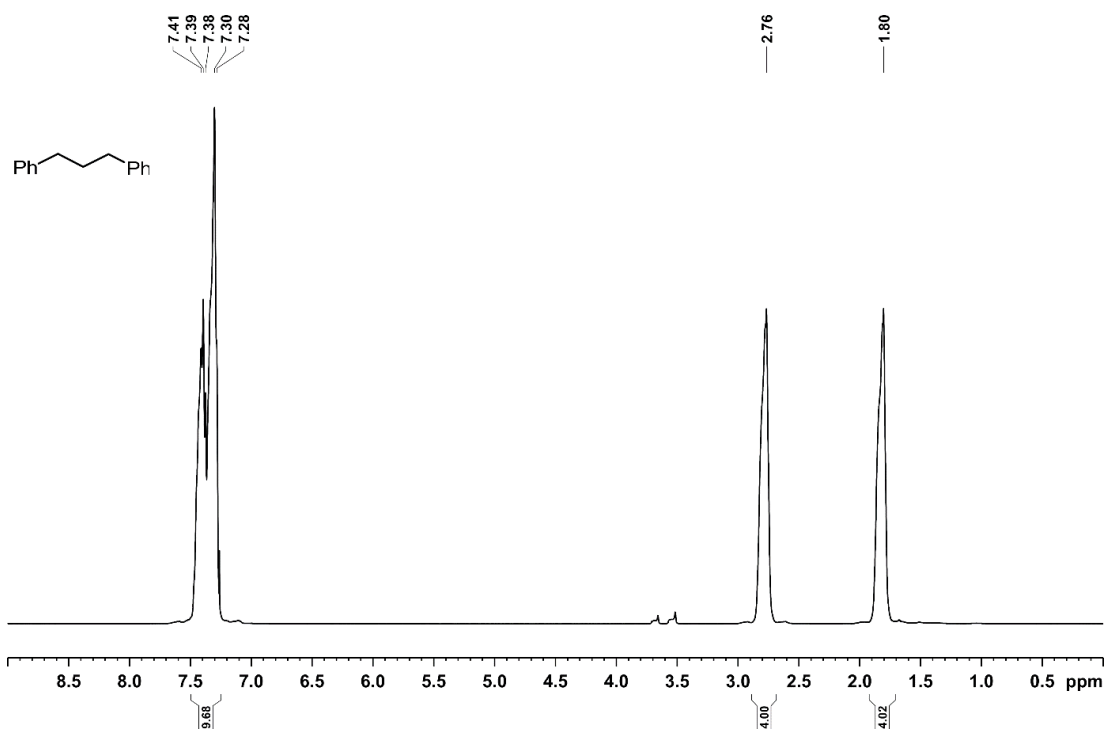


Figure 7.5.4. ^1H NMR spectrum (400.13 MHz, 300 K, CDCl_3) of 1,4-diphenylbutane.

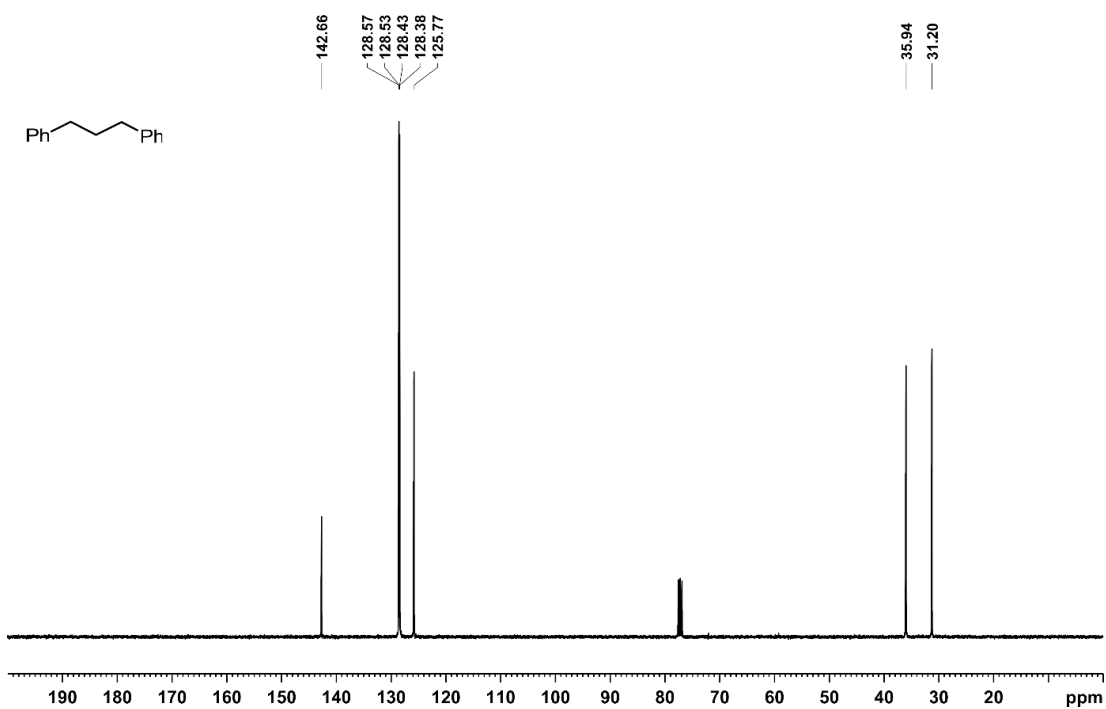


Figure 7.5.5. $^{13}\text{C}\{^1\text{H}\}$ NMR spectrum (100.6 MHz, 300 K, CDCl_3) of 1,4-diphenylbutane.

7 Heterogeneous Olefin Hydrogenation Enabled by a Highly-Reduced Nickel(–II) Catalyst Precursor

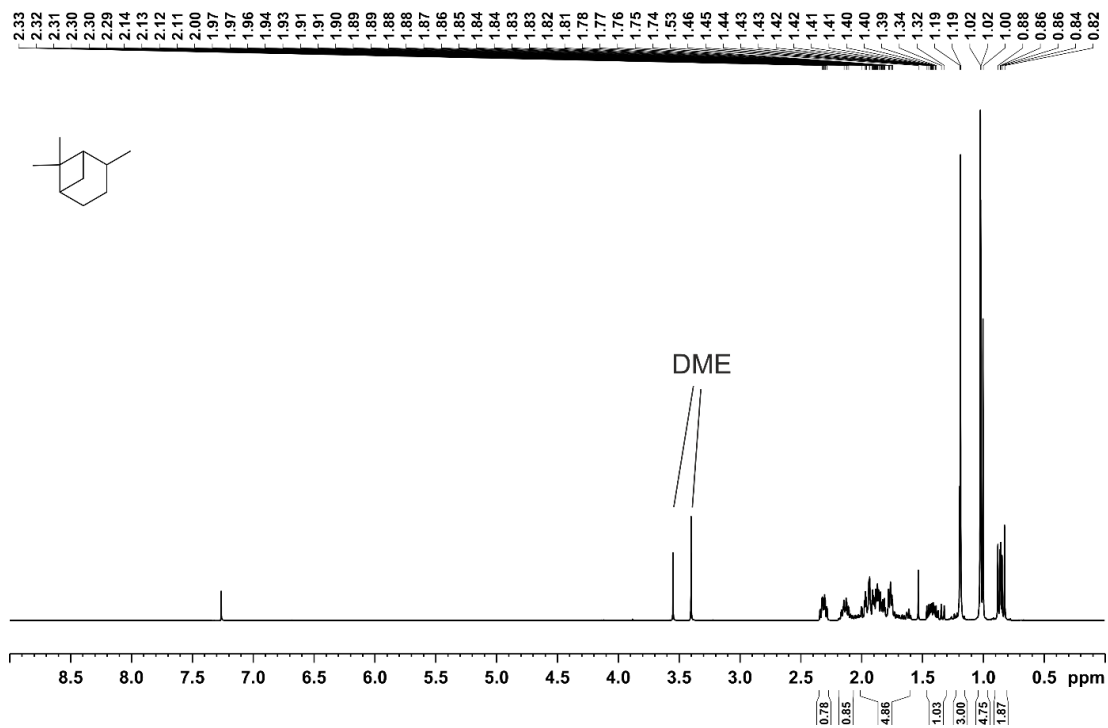


Figure 7.5.6. ^1H NMR spectrum (400.13 MHz, 300 K, CDCl_3) of pinane; small signals of residual solvent: 3.55, 3.40 (DME).

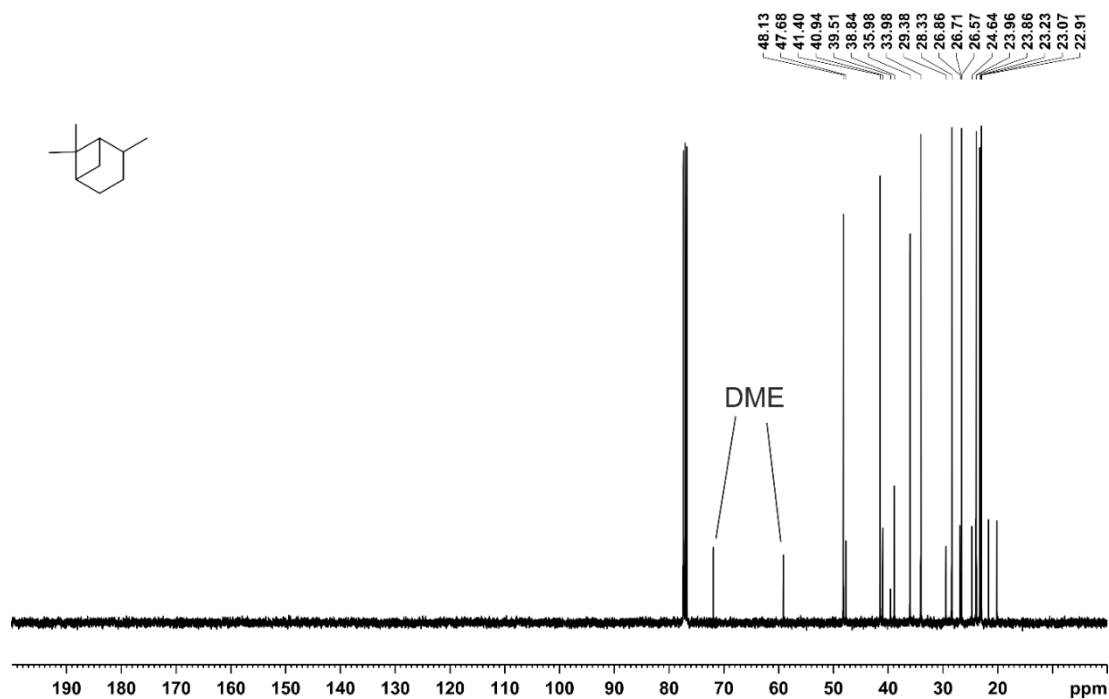


Figure 7.5.7. $^{13}\text{C}\{^1\text{H}\}$ NMR spectrum (100.6 MHz, 300 K, CDCl_3) of pinane; small signals of residual solvent: 72.6, 58.7 (DME).

7 Heterogeneous Olefin Hydrogenation Enabled by a Highly-Reduced Nickel(-II) Catalyst Precursor

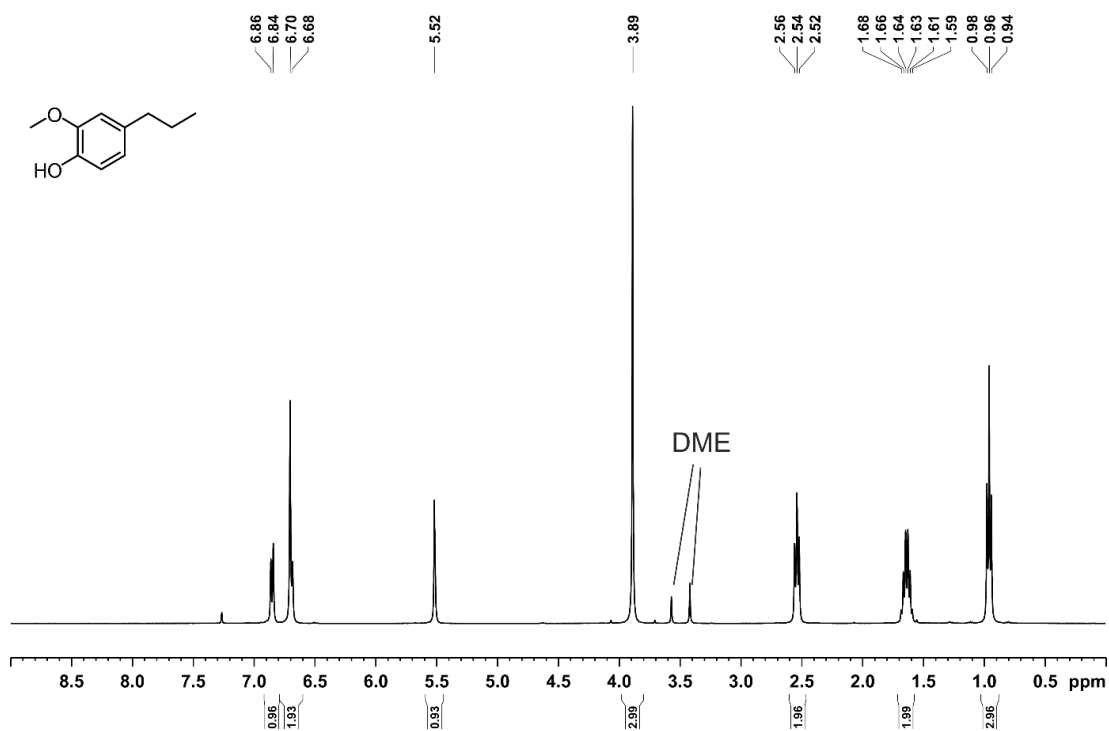


Figure 7.5.8. ^1H NMR spectrum (400.13 MHz, 300 K, CDCl_3) of 2-methoxy-4-propylphenol; small signals of residual solvent: 3.55, 3.40 (DME).

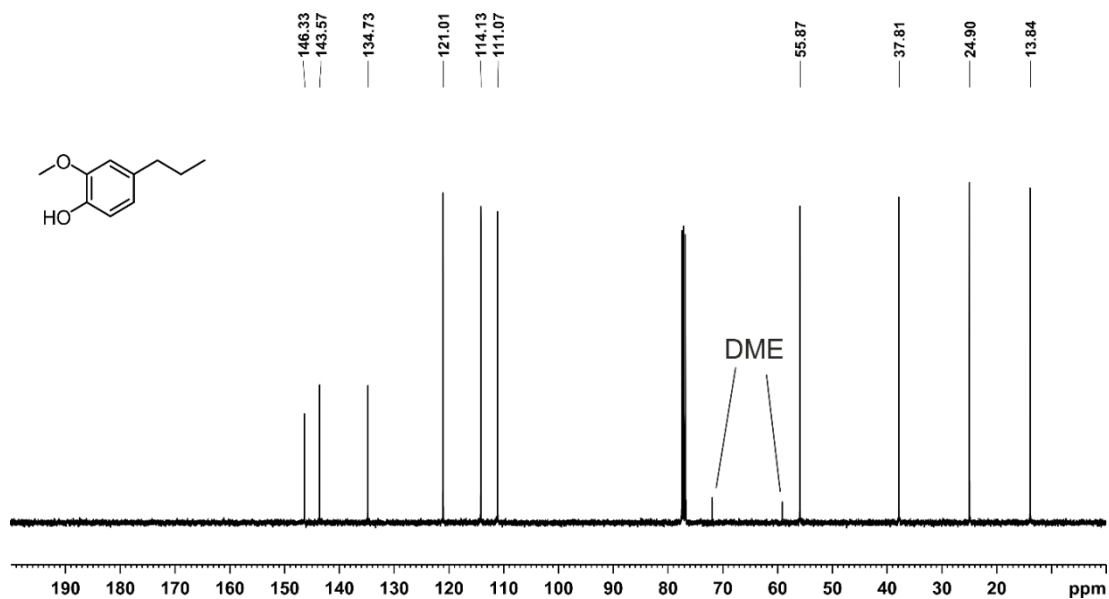


Figure 7.5.9. $^{13}\text{C}\{^1\text{H}\}$ NMR spectrum (100.6 MHz, 300 K, CDCl_3) of 2-methoxy-4-propylphenol; small signals of residual solvent: 72.6, 58.7 (DME).

7 Heterogeneous Olefin Hydrogenation Enabled by a Highly-Reduced Nickel(–II) Catalyst Precursor

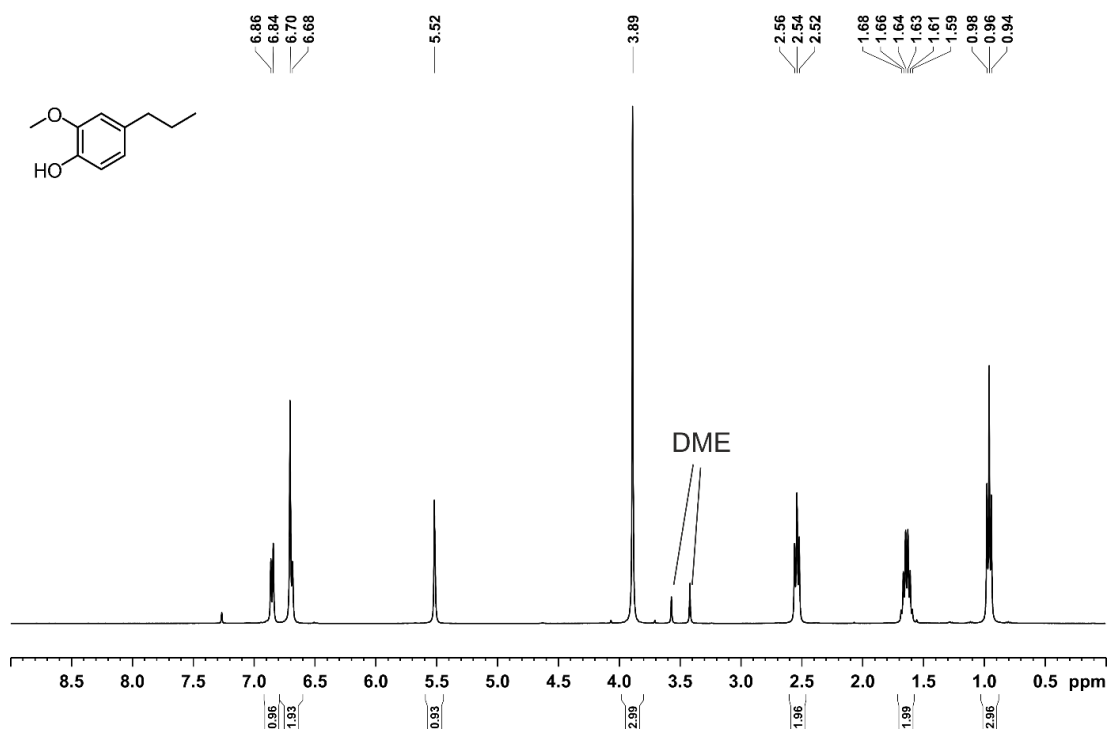


Figure 7.5.10. ^1H NMR spectrum (400.13 MHz, 300 K, CDCl_3) of 2-methoxy-4-propylphenol; small signals of residual solvent: 3.55, 3.40 (DME).

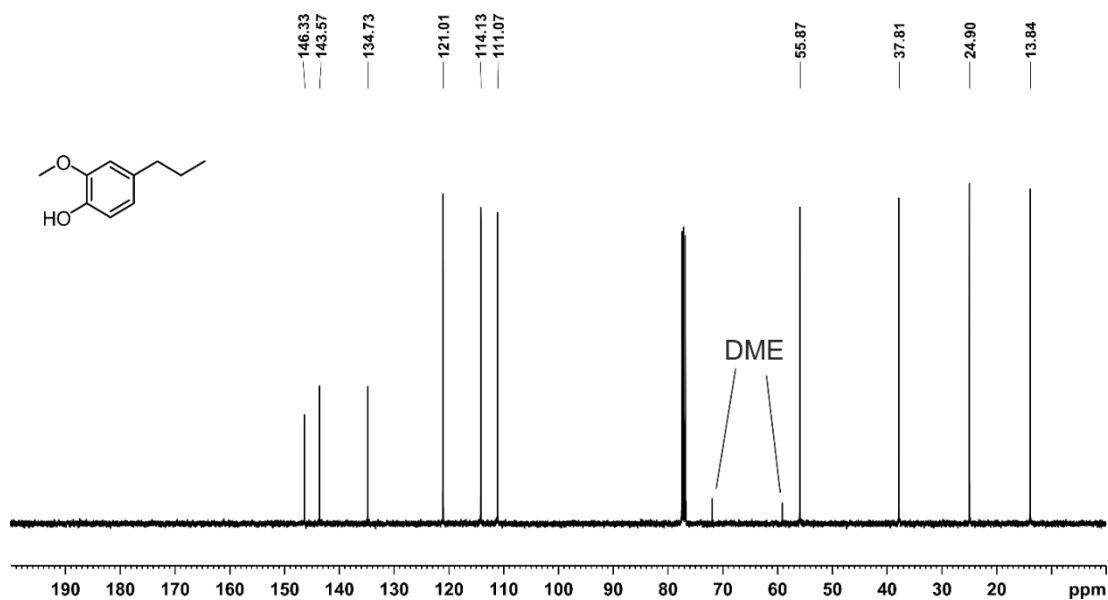


Figure 7.5.11. $^{13}\text{C}\{^1\text{H}\}$ NMR spectrum (100.6 MHz, 300 K, CDCl_3) of 2-methoxy-4-propylphenol; small signals of residual solvent: 72.6, 58.7 (DME).

7 Heterogeneous Olefin Hydrogenation Enabled by a Highly-Reduced Nickel(–II) Catalyst Precursor

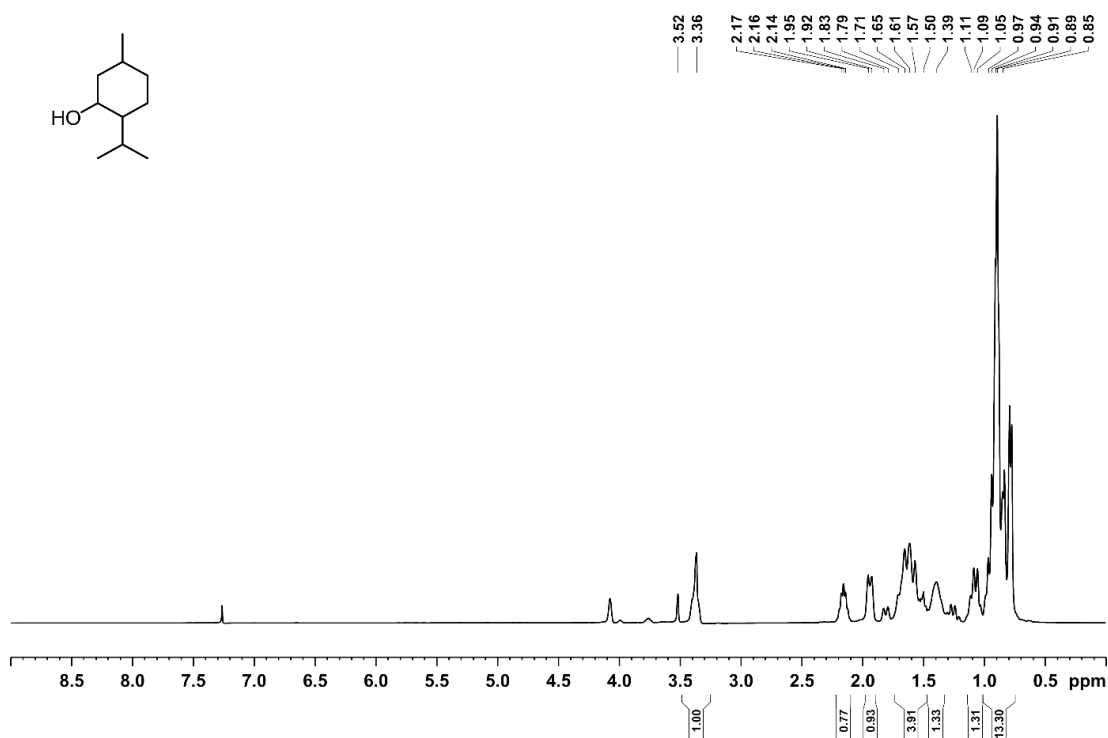


Figure 7.5.12. ¹H NMR spectrum (400.13 MHz, 300 K, CDCl₃) of 2-isopropyl-5-methylcyclohexan-1-ol; small signals of residual solvent: 3.55, 3.40 (DME).

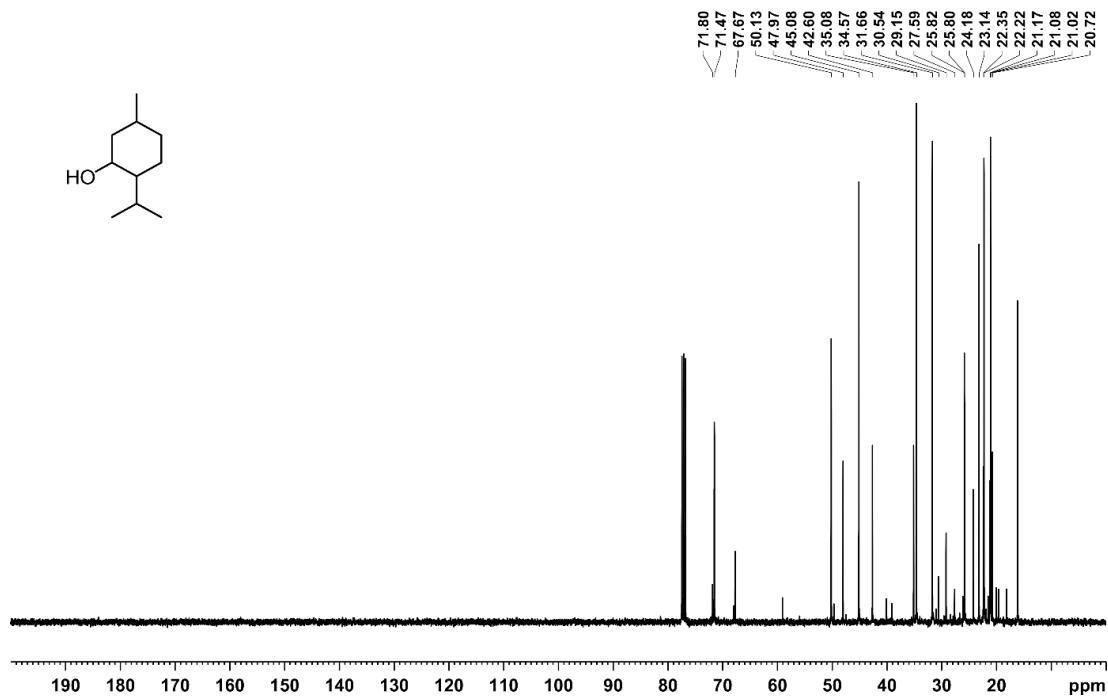


Figure 7.5.13. ¹³C{¹H} NMR spectrum (100.6 MHz, 300 K, CDCl₃) of 2-isopropyl-5-methylcyclohexan-1-ol; small signals of residual solvent: 72.6, 58.7 (DME).

7 Heterogeneous Olefin Hydrogenation Enabled by a Highly-Reduced Nickel(–II) Catalyst Precursor

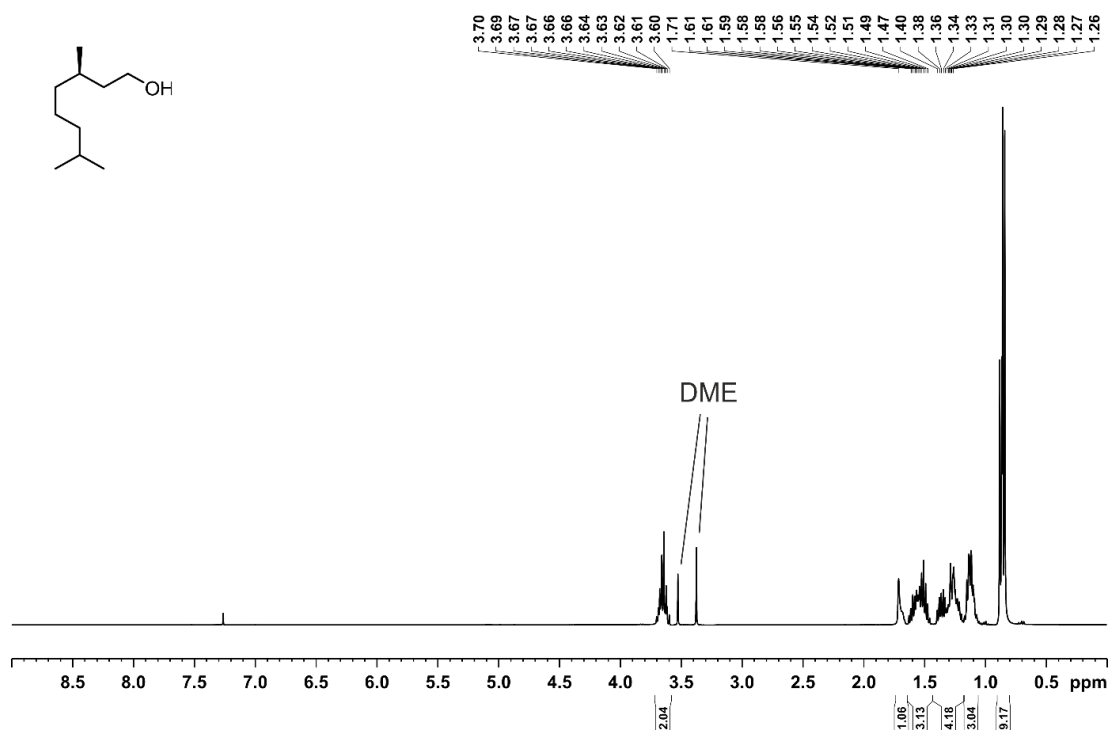


Figure 7.5.14. ¹H NMR spectrum (400.13 MHz, 300 K, CDCl₃) of 3,7-dimethyloctan-1-ol; small signals of residual solvent: 3.55, 3.40 (DME).

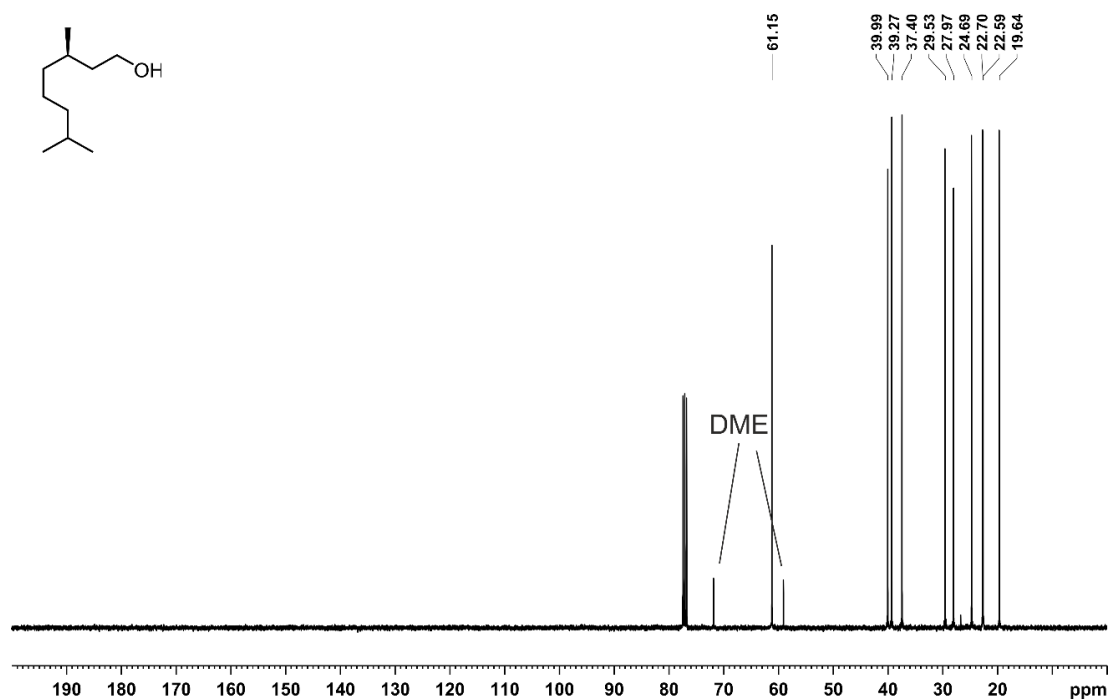


Figure 7.5.15. ¹³C{¹H} NMR spectrum (100.6 MHz, 300 K, CDCl₃) of 3,7-dimethyloctan-1-ol; small signals of residual solvent: 72.6, 58.7 (DME).

7.5.5 Hydrogenation products: GC-FID analyses

For the substrates myrcene, α -pinene, and (*R*)-limonene the peak area of the substrate and the corresponding products in the chromatogram (GC-FID) were compared in order to estimate the yield and conversion. Peak at 5.82 min corresponds to the internal standard *n*-pentadecane.

a) Myrcene

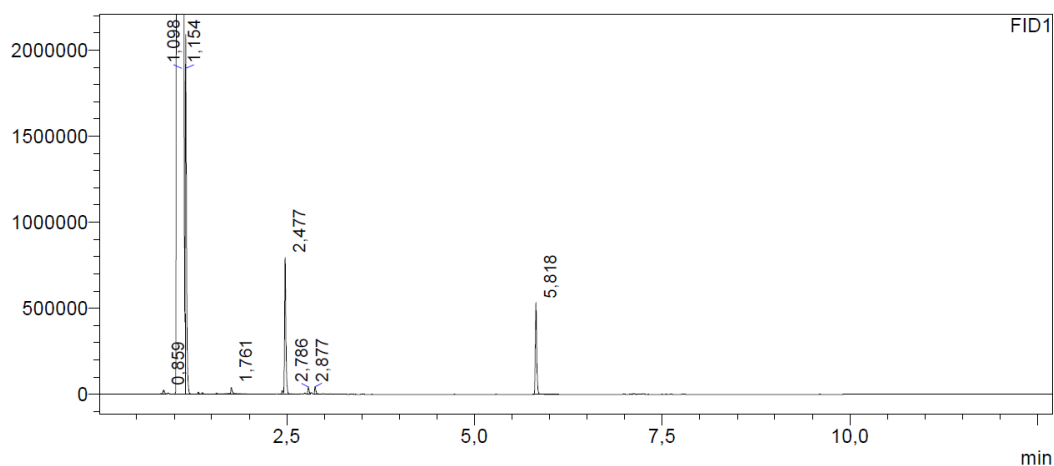


Figure 7.5.16. GC-FID chromatogram of the hydrogenation of myrcene with **1**.

Table 7.5.5. Analysis of the GC-FID chromatogram of the hydrogenation of myrcene.

Retention time [min]	Assignment	Peak area	Relative peak area [%]
2.477	2,6-dimethyloctane	972490	91
2.786	Isomer with one C=C bond	48166	4
2.877	Isomer with one C=C bond	51724	5

b) α -Pinene

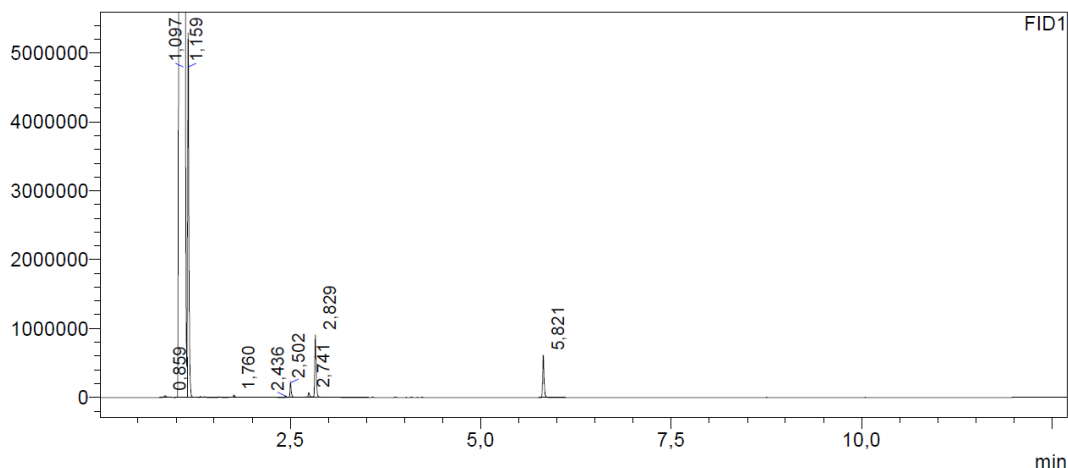


Figure 7.5.17. GC-FID chromatogram of the hydrogenation of α -pinene with **1**.

Table 7.5.6. Analysis of the GC-FID chromatogram of the hydrogenation of α -pinene.

Retention time [min]	Assignment	Peak area	Relative peak area [%]
2.791	α -pinene	240603	16
2.882	pinane	75076	5
3.076	pinane	1152099	79

c) (*R*)-Limonene

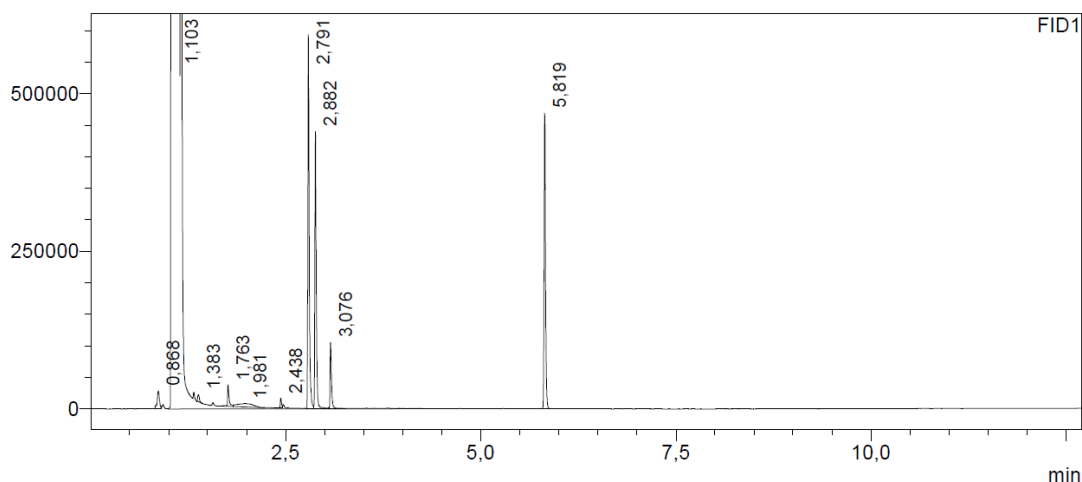


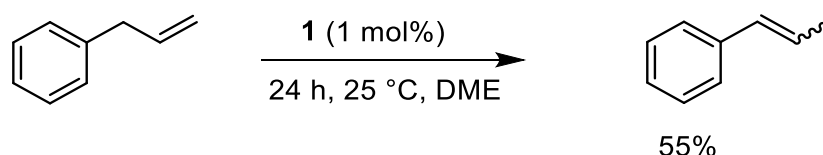
Figure 7.5.18. GC-FID chromatogram of the hydrogenation of (*R*)-limonene with **1**.

Table 7.5.7. Analysis of the GC-FID chromatogram of the hydrogenation of (*R*)-limonene.

Retention time [min]	Assignment	Peak area	Relative peak area [%]
2.502	1-isopropyl-4- methylcyclohexane	732649	54
2.741	1-isopropyl-4- methylcyclohexane	535522	38
3.076	Isomer with one C=C bond	129610	9

7.5.6 Isomerization of olefins

a) Isomerization of allylbenzene



Allylbenzene (26.5 μL , 0.2 mmol, 1.0 equiv.) was stirred for one day with a solution of **1** (1.2 mg, 0.002 mmol, 0.01 equiv.) in 0.25 mL DME and 20 L *n*-pentadecane as internal reference and analyzed by GC-FID and GC-MS after work-up (see the general information, chapter 7.5.1). According to GC-FID, 55% of allylbenzene isomerized to 1-propenylbenzene.

b) Isomerization of 1-octene



1-Octene (31.5 μL , 0.2 mmol, 1.0 equiv.) was stirred for one day with a solution of **1** (1.2 mg, 0.002 mmol, 0.01 equiv.) in 0.2 mL DME and 20 L *n*-pentadecane as internal reference and analyzed by GC-FID and GC-MS after work-up (see the general information, chapter 7.5.1). 1-, 2-, 3- and 4-octene were observed.

The GC-FID spectrum and the corresponding peak table are depicted in Figure 7.5.19 and Table 7.5.8. The assignment of the signals from 1.945 – 2.067 min being internal octenes was proven by GC-MS ($m/z = 112$) as well.

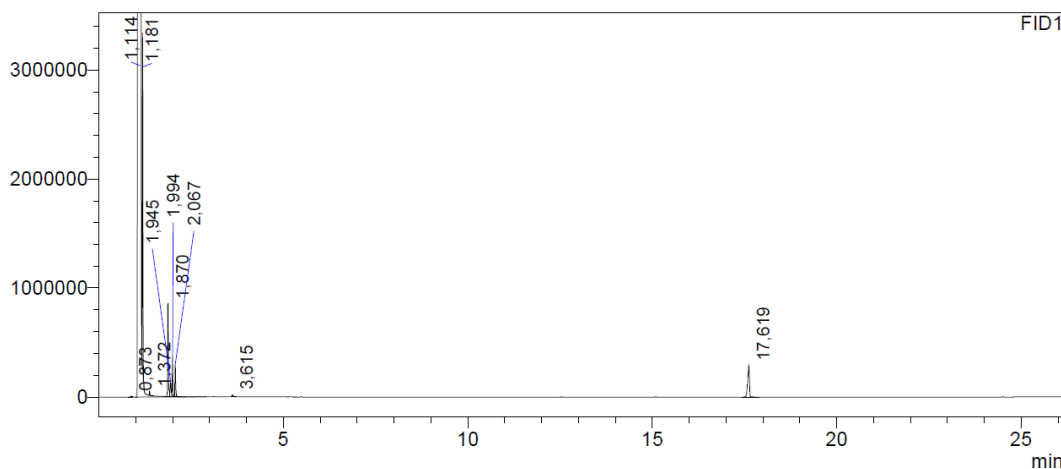


Figure 7.5.19. GC-FID chromatogram of the isomerization of 1-octene using **1**.

Table 7.5.8. Analysis of the GC-FID chromatogram of the isomerization of 1-octene.

Retention time [min]	Assignment	Peak area
1.870	1-octene	1188125
1.945	Internal octene	249948
1.994	Internal octene	494294
2.067	Internal octene	402791
17.619	<i>n</i> -pentadecane	906465

7.5.7 Ring-opening experiment with α -cyclopropylstyrene

The hydrogenation reaction was performed according to the general procedure.

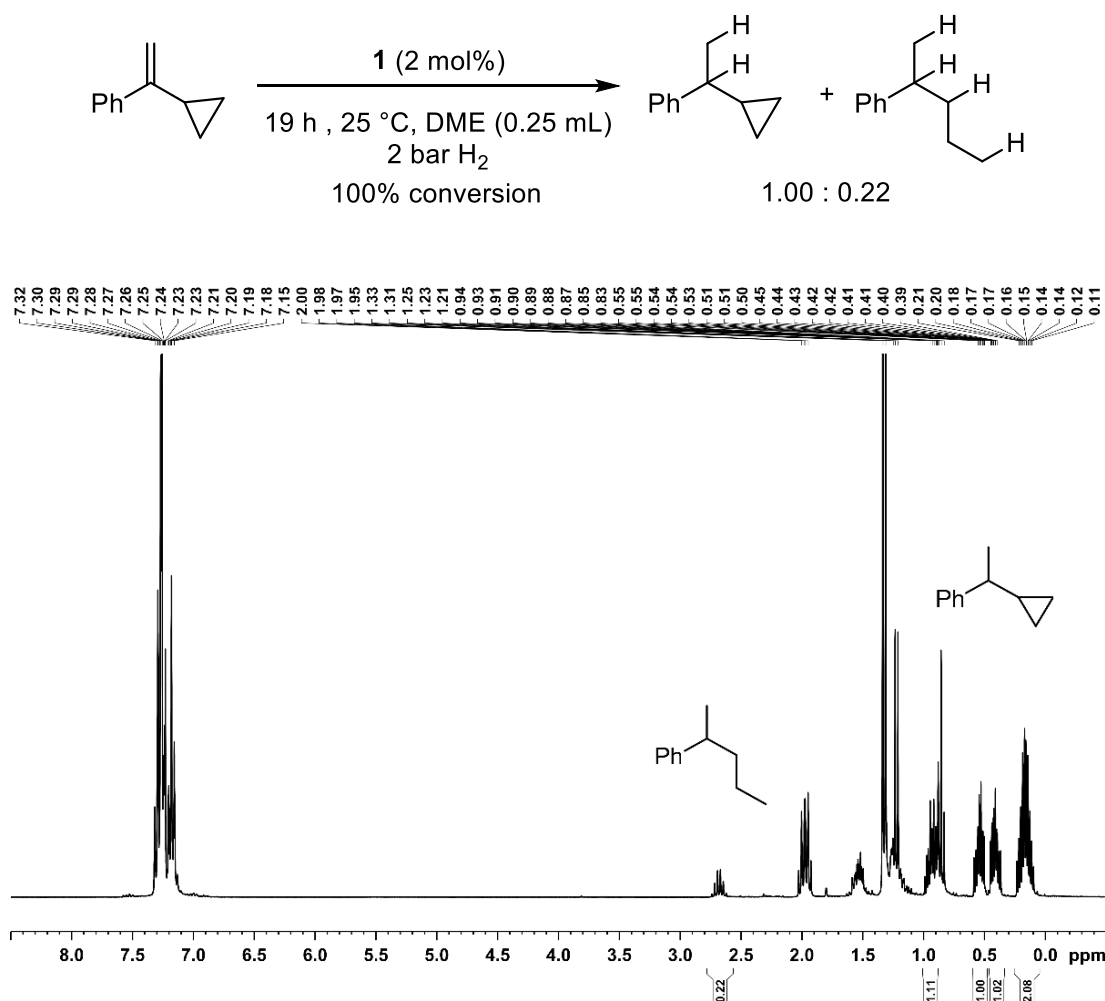


Figure 7.5.20. ¹H NMR spectrum (300 MHz, 300 K, CDCl₃) of the product mixture from the hydrogenation of α -cyclopropylstyrene using catalyst **1**.

7.5.8 Kinetic investigations

Catalyst **1** (5.8 mg, 10 μ mol, 3 mol%) was dissolved in DME (0.25 mL) and the alkene (0.2 mmol, 1.0 equiv.) was added, during which the color changed from orange to red in case of α -methylstyrene (no color change was observed for the octenes). The mixture was injected by syringe to a flame-dried 10 mL two-necked flask, which was connected to a *Man on the Moon X201 gas uptake* system (9 bar H₂, reservoir pressure 1.9 bar H₂ pressure). The hydrogen uptake started with the addition of catalyst/substrate. After the reaction, the mixture was treated with a saturated aqueous solution of NH₄Cl and ethyl acetate. The organic phases were

dried over MgSO_4 and analyzed by quantitative GC-FID analysis vs. internal standard (*n*-pentadecane). The monitored hydrogen consumption is related to the yield of product, which was determined by GC FID.

During the reaction, the dark red color slowly changed to black accompanied by formation of a black precipitate in case of α -methylstyrene. The color of the related octene/catalyst mixture immediately changed to black accompanied by formation of a black precipitate. This observation further supports an electron transfer to styrenic substrates, which is not observed for octenes (see main text, Figure 5, III). The formation of the precipitate under hydrogen atmosphere presumably accounts for the formation of nanoparticles.

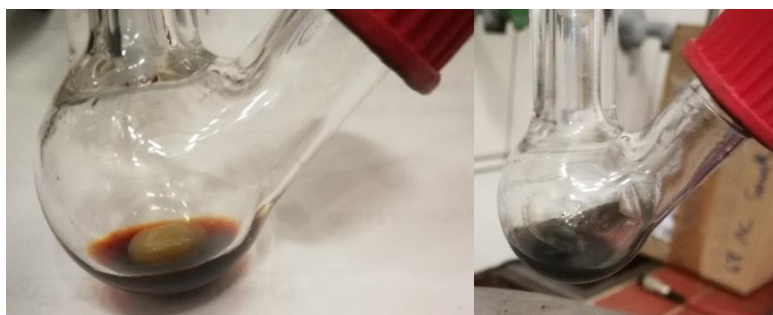


Figure 7.5.21. Selected pictures from the reaction mixture after addition of the catalyst to the flask. Left: 1-octene as substrate. Right: α -methylstyrene as substrate

7.5.9 Determination of turnover frequencies (TOFs) for selected reactions

General procedure: The TOFs were determined from reaction progress analyses (see Figure 7.4) by analysing the slope of a selected part of the reaction time profile showing a linear ascent. Note that that the resulting TOF values are necessarily approximate due to the presence of an induction period.

1-octene: $t = 4.18 \text{ min to } 4.51 \text{ min}$; $\text{TOF} = 601 \text{ h}^{-1}$;

2-octene: $t = 60.8 \text{ min to } 65.9 \text{ min}$; $\text{TOF} = 103 \text{ h}^{-1}$;

α -methylstyrene: $t = 31.2 \text{ min to } 34.3 \text{ min}$; $\text{TOF} = 287 \text{ h}^{-1}$;

7.5.10 Poisoning experiments

Poisoning experiments were performed with catalyst **1**, 1,1',2-triphenylethylene as substrate and Hg, dct (dibenzo[*a,e*]cyclooctatetraene), benzonitrile, and naphthalene as poisoning agents.

General procedure:

A solution of **1** (1.2 mg, 0.002 mmol) in 0.25 mL DME was added to the catalyst poison. The resulting solution was stirred for one minute and added to 1,1',2-triphenylethylene and *n*-pentadecane. The hydrogenation reaction and work-up was performed according to the general procedure.

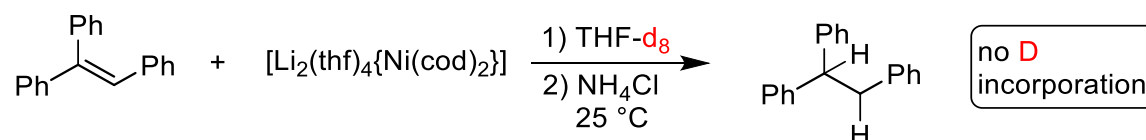
Table 7.5.9. Hydrogenation of 1,1',2-triphenylethylene in presence of selected poisoning agents.^[a]

Entry	Reagent / equiv. per [Ni]	Yield (Conversion) ^[b] / %
1	Hg (50 mg, 0.025 mmol, 125 equiv.)	2 (5)
2	Dct (0.8 mg, 0.004 mmol, 2.0 equiv.)	92 (>99) ^[c]
3	Benzonitrile (1 μ L, 0.01 mmol, 5.0 equiv.)	1 (11) ^[c]
4	Naphthalene (0.5 mg, 0.004 mmol, 2.0 equiv.)	82 (82) ^[c]

[a] Standard conditions: substrate (0.2 mmol), 25 °C, 5 bar H₂, 18 h. [b] Yields and conversions were determined by quantitative GC-FID vs. internal *n*-pentadecane. [c] 21 h.

7.5.11 Deuterium labeling experiments

a) 1,1',2-Triphenylethylene: deuterated solvent



1,1',2-Triphenylethylene (25.8 mg 0.1 mmol, 1.0 equiv.) and **1** (58.1 mg, 0.1 mmol, 1.0 equiv.) were dissolved in 1 mL THF- d_8 . The solution immediately turned deep purple upon addition of **1** to the organic substrate and was subsequently quenched with an aqueous NH_4Cl solution. After addition of *n*-pentane the organic phase was filtered over a pad of silica and dried *in vacuo*. The residue was dissolved in *n*-pentane, filtered over a pad of silica and analyzed by GC-MS. The *n*-pentane solution was dried *in vacuo* and the residue dissolved in $CDCl_3$ and analyzed by 1H NMR and 2H NMR spectroscopy.

According to GC-FID peak area comparison 55% of 1,1',2-triphenylethylene was reduced to the corresponding alkane.

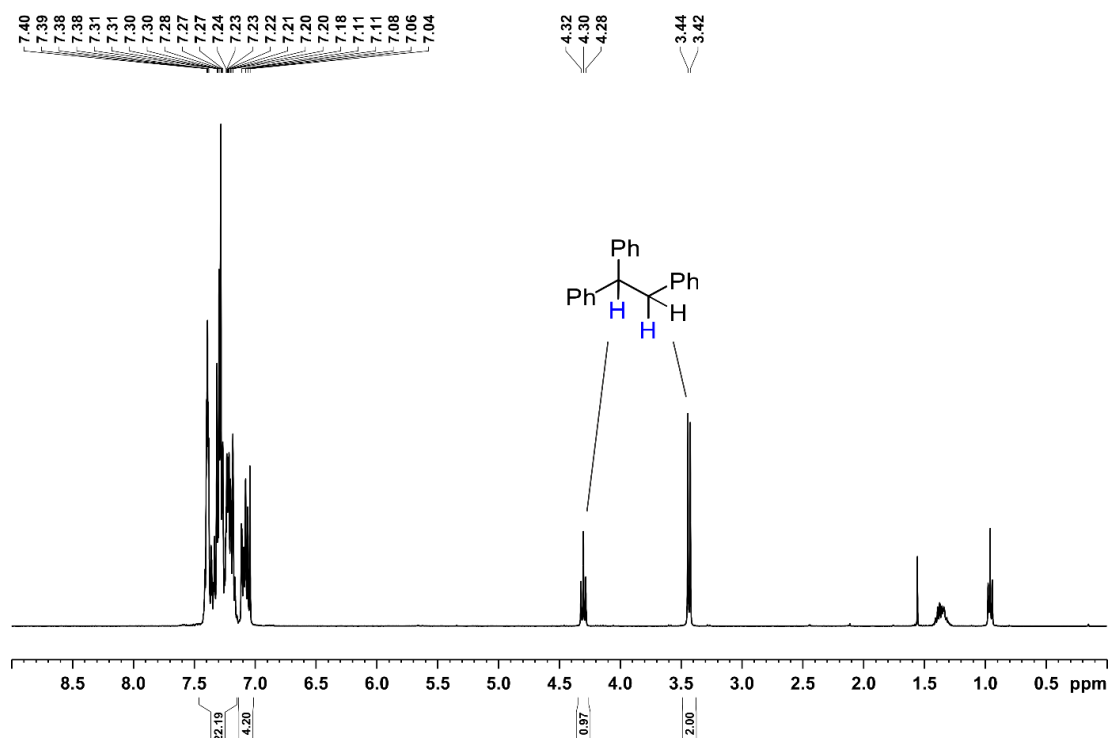


Figure 7.5.22. 1H NMR spectrum (400.13 MHz, 300 K, $CDCl_3$).

7 Heterogeneous Olefin Hydrogenation Enabled by a Highly-Reduced Nickel(–II) Catalyst Precursor

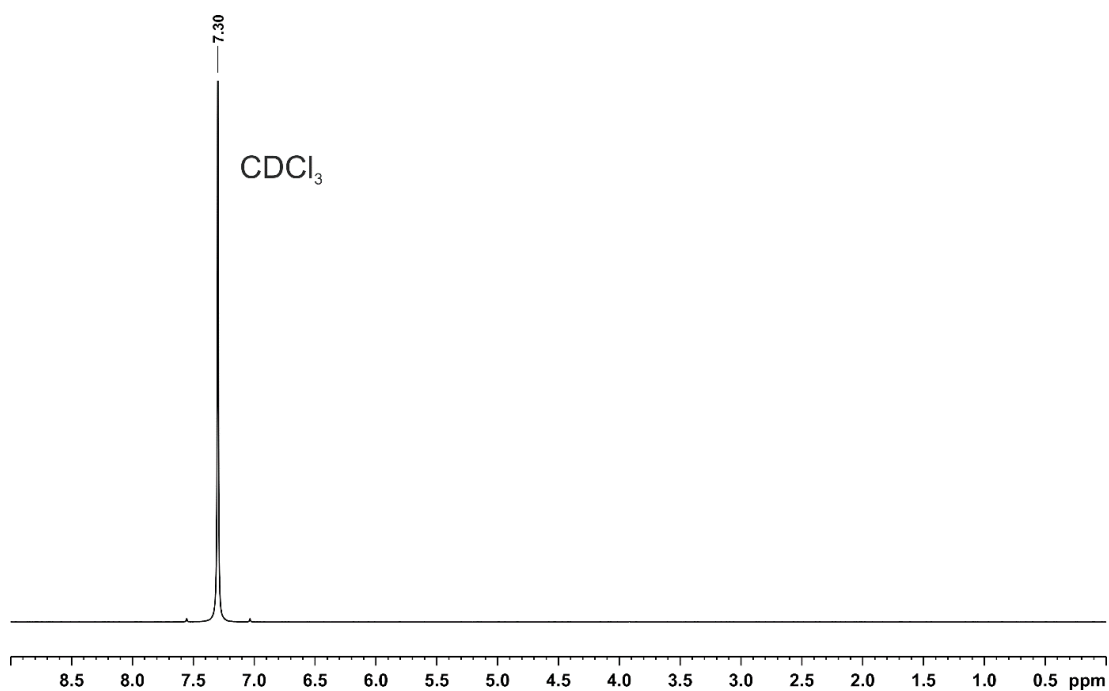


Figure 7.5.23. ^2H NMR spectrum (61.4 MHz, 300 K, CDCl_3).

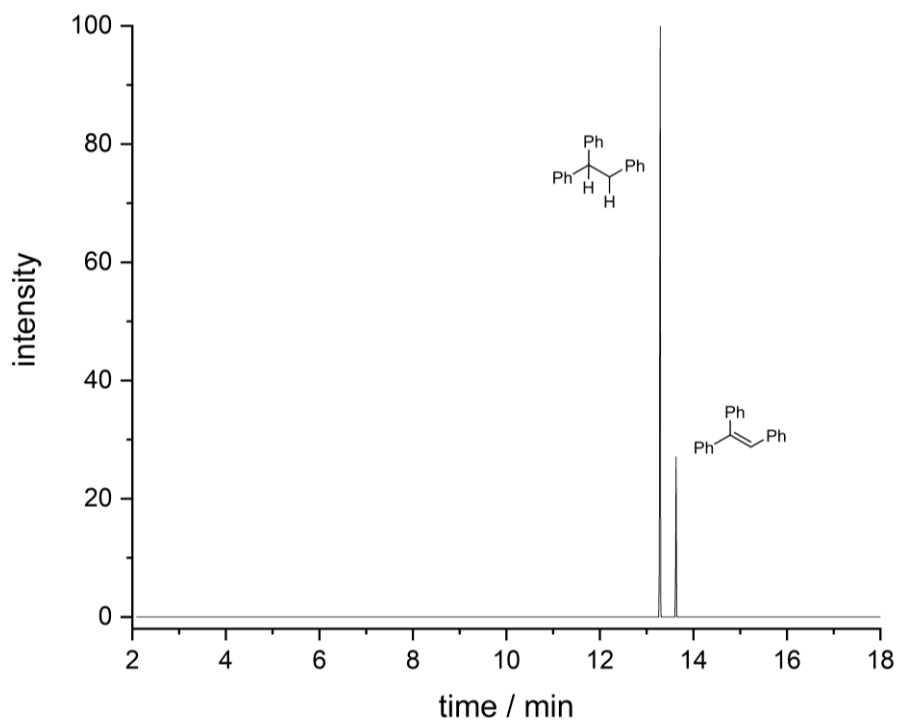


Figure 7.5.24. GC-MS chromatogram.

7 Heterogeneous Olefin Hydrogenation Enabled by a Highly-Reduced Nickel(-II) Catalyst Precursor

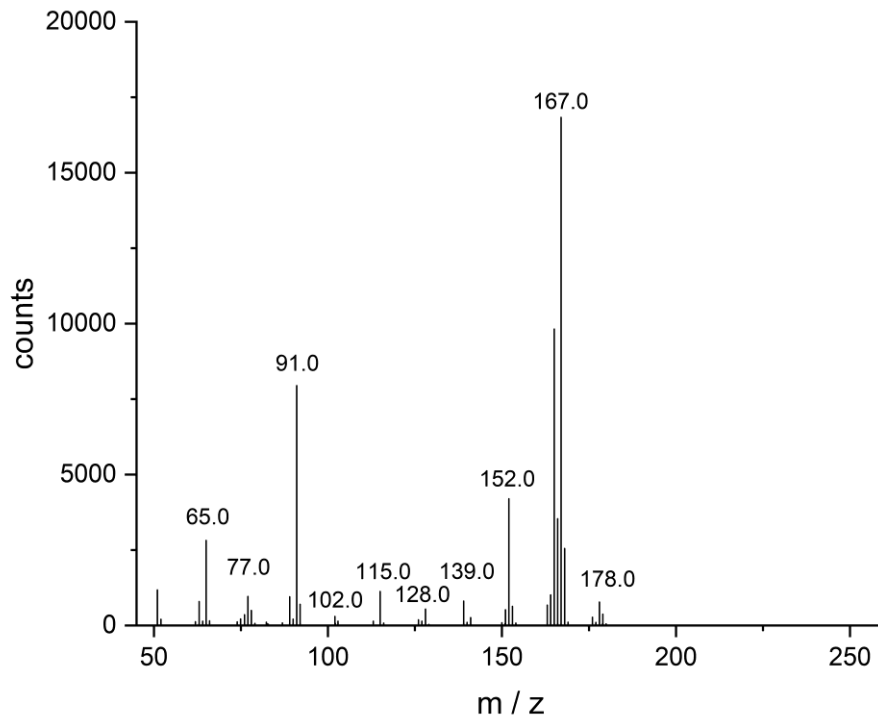
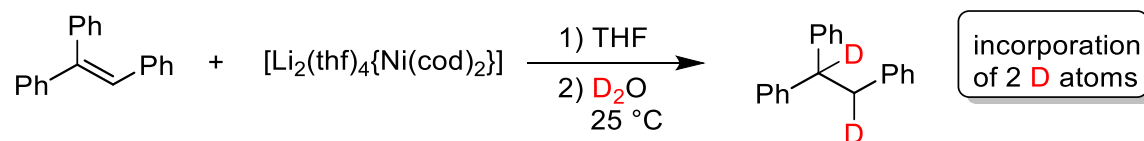


Figure 7.5.25. m/z data of peak 13.274 – 13.297 min.

7 Heterogeneous Olefin Hydrogenation Enabled by a Highly-Reduced Nickel(–II) Catalyst Precursor

b) 1,1',2-Triphenylethylene: quench with D₂O



1,1',2-Triphenylethylene (27.0 mg 0.105 mmol, 1.0 equiv.) and **1** (60.8 mg, 0.105 mmol, 1.0 equiv.) were dissolved in 2 mL THF. The solution immediately turned deep purple upon addition of **1** to the organic substrate and was subsequently quenched with 1 mL D₂O. After addition of *n*-pentane the organic phase was filtered over a pad of silica and dried *in vacuo*. The residue was dissolved in *n*-pentane, filtered over a pad of silica and analyzed by GC-MS. The *n*-pentane solution was dried *in vacuo* and the residue dissolved in CDCl₃ and analyzed by ¹H NMR and ²H NMR spectroscopy.

According to GC-FID peak area comparison 80% of 1,1',2-triphenylethylene was reduced to the corresponding alkane.

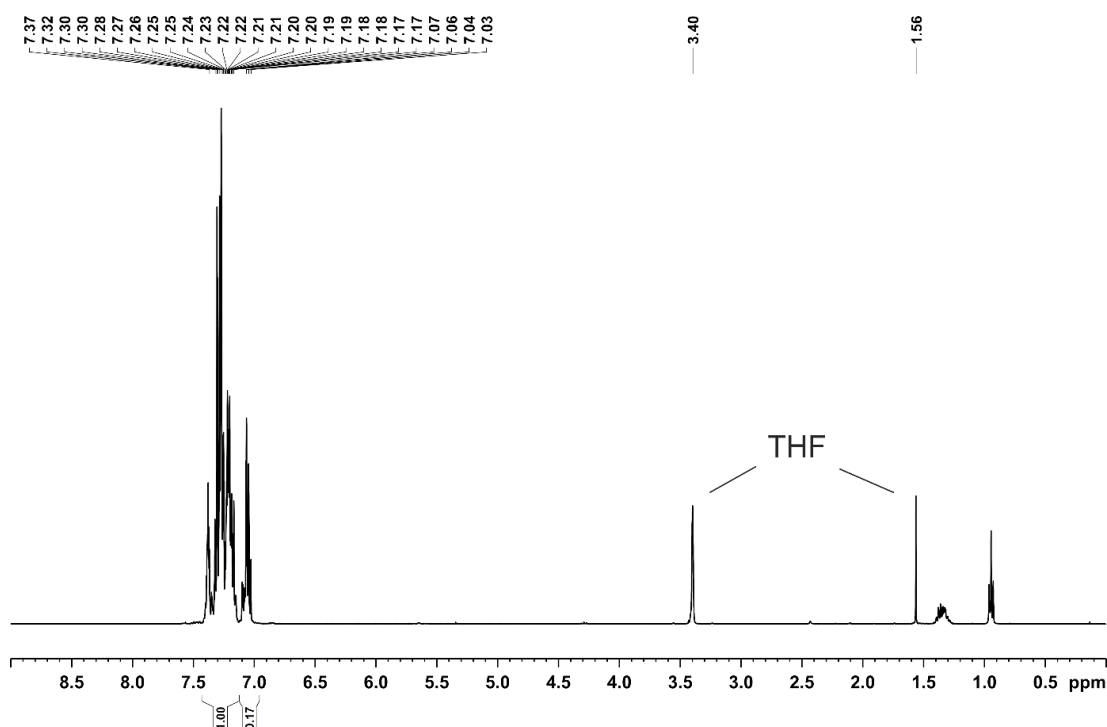


Figure 7.5.26. ¹H NMR spectrum (400.13 MHz, 300 K, CDCl₃).

7 Heterogeneous Olefin Hydrogenation Enabled by a Highly-Reduced Nickel(–II) Catalyst Precursor

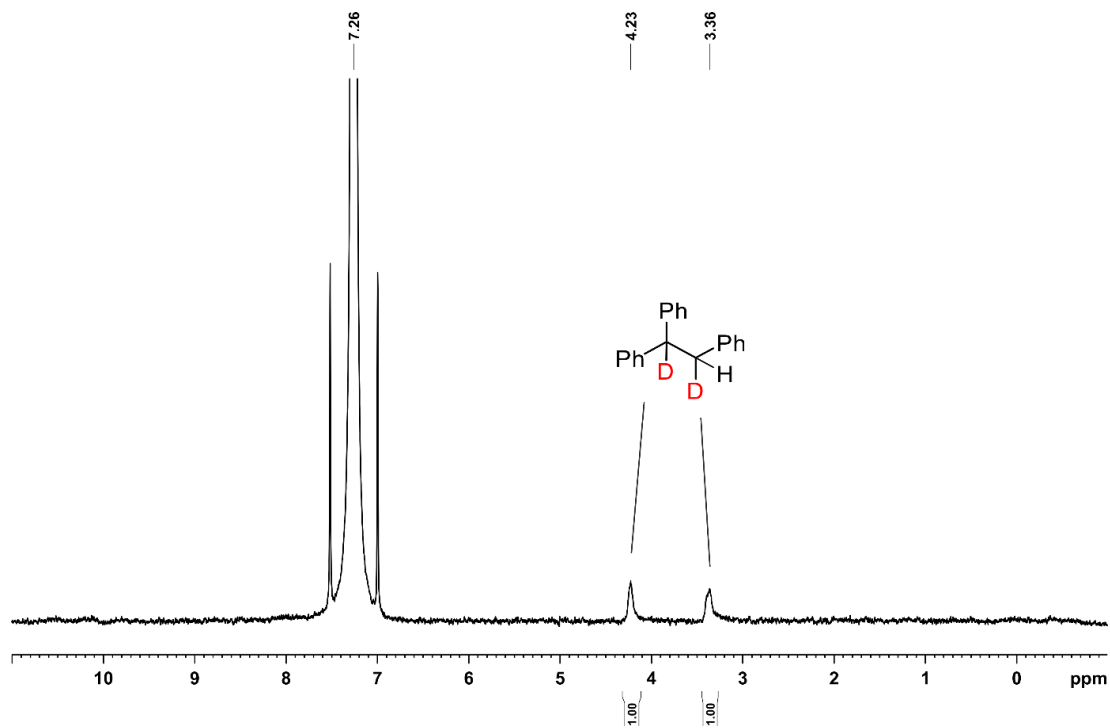


Figure 7.5.27. ^2H NMR spectrum (61.4 MHz, 300 K, CDCl_3).

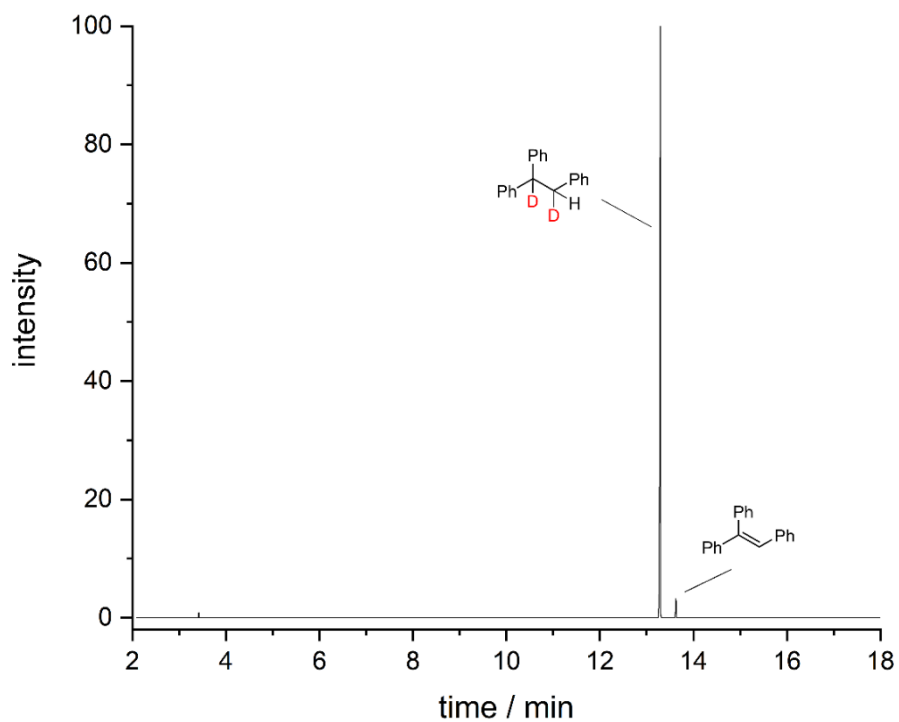


Figure 7.5.28. GC-MS chromatogram of reaction 4.1.1b.

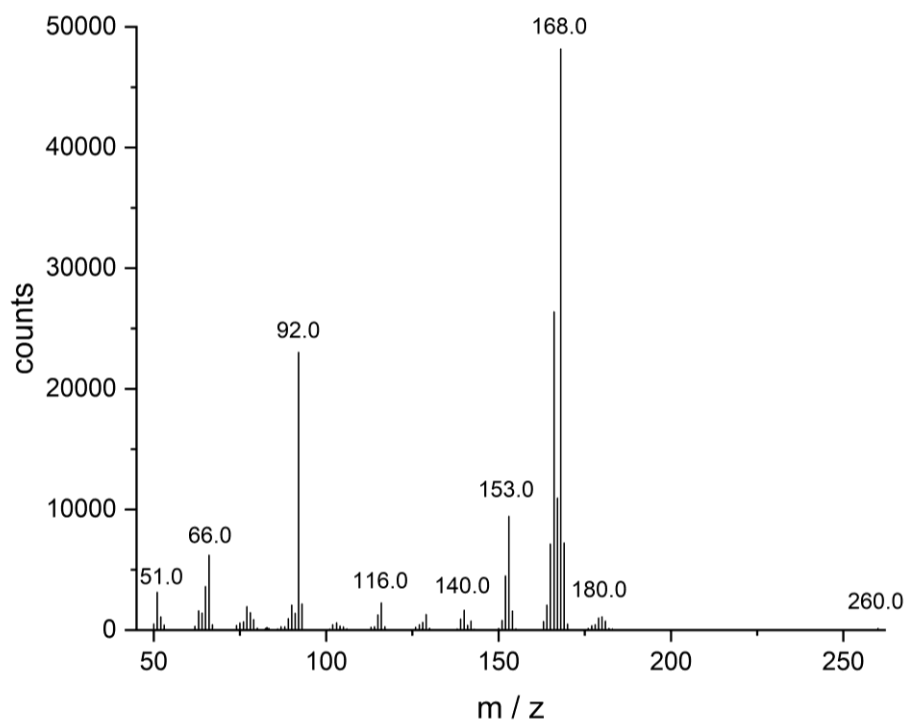
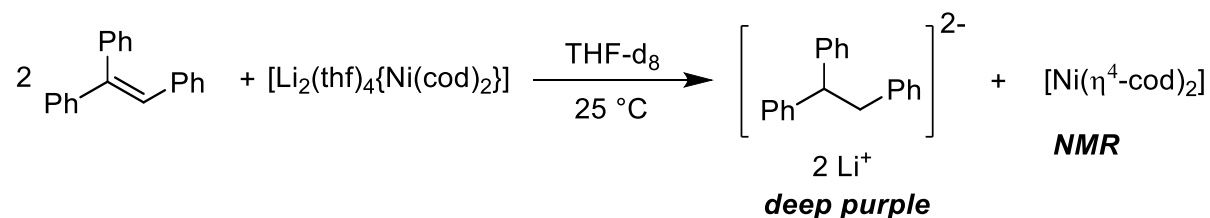


Figure 7.5.29. m/z data of peak 13.268 – 13.297 min.

7.5.12 Mechanism: Stoichiometric NMR experiments

a) 1,1',2-Triphenylethylene (2:1 reaction)



1,1',2-Triphenylethylene (6.9 mg 0.027 mmol, 2.0 equiv.) and **1** (7.8 mg, 0.0135 mmol, 1.0 equiv.) were dissolved in 0.6 mL THF-d₈. The solution immediately turned purple from red and was analyzed by ¹H NMR spectroscopy.

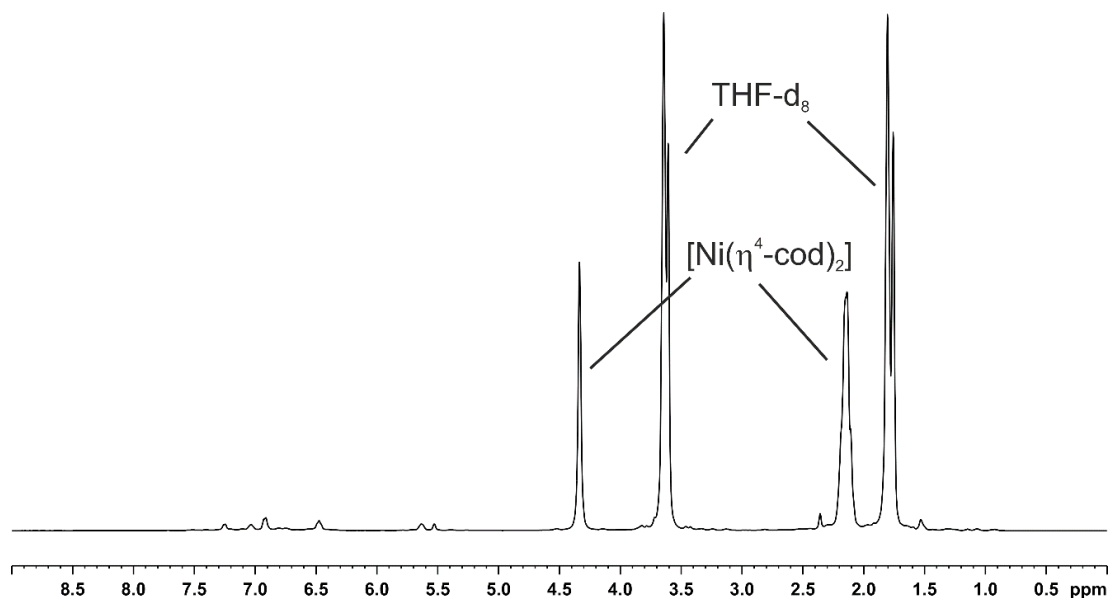
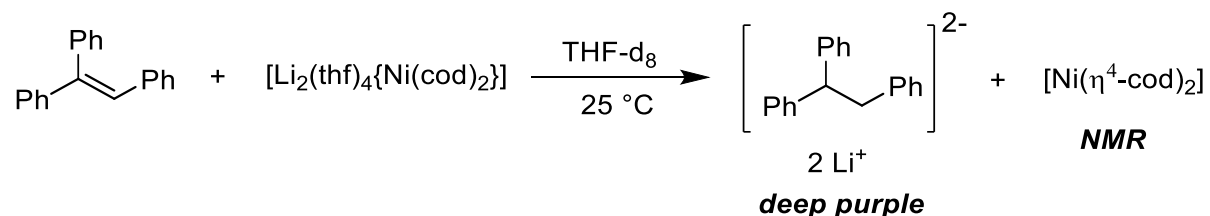


Figure 7.5.30. ^1H NMR spectrum (400.13 MHz, 300 K, THF-d_8) of **1** and 1,1',2-triphenylethylene (2 equiv.).

b) 1,1',2-Triphenylethylene (1:1 reaction)



1,1',2-Triphenylethylene (5.3 mg 0.021 mmol, 1.0 equiv.) and **1** (12.1 mg, 0.021 mmol, 1.0 equiv.) were dissolved in 0.6 mL THF-d_8 . The solution immediately turned deep purple and was analyzed by ^1H NMR spectroscopy.

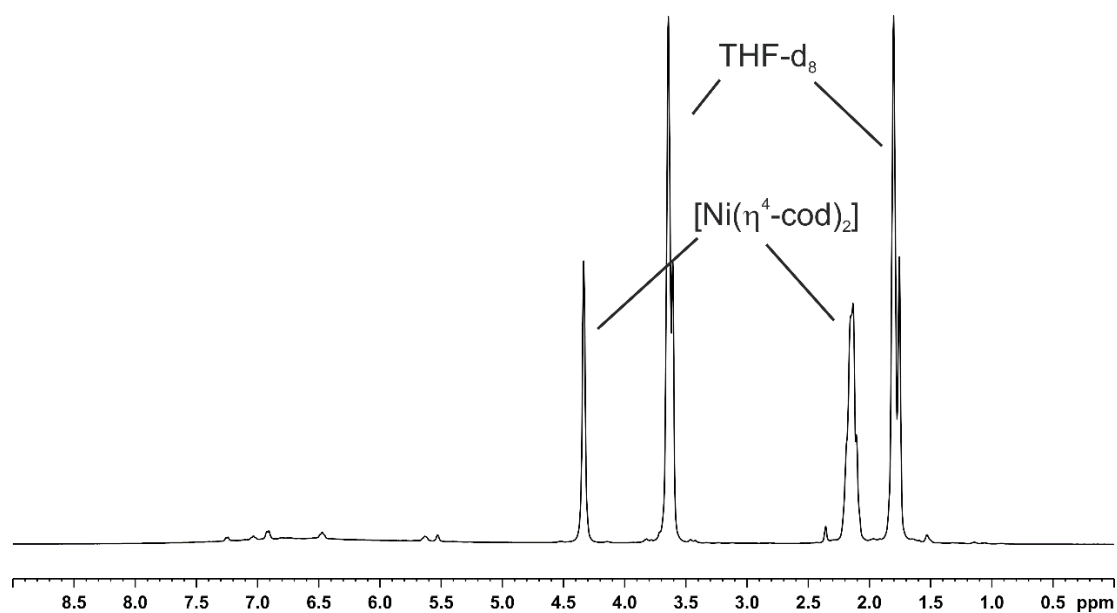
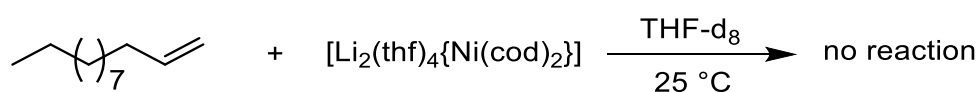


Figure 7.5.31. ¹H NMR spectrum (400.13 MHz, 300 K, THF-d₈) of **1** and 1,1',2-triphenylethylene (1 equiv.).

c) 1-Dodecene (1:1 reaction)



1-Dodecene (5 μL, 0.023 mmol, 1.0 equiv.) and **1** (13.3 mg, 0.022 mmol, 1.0 equiv.) were dissolved in 0.6 mL THF-d₈. The solution did not change the color and was analyzed by ¹H NMR spectroscopy.

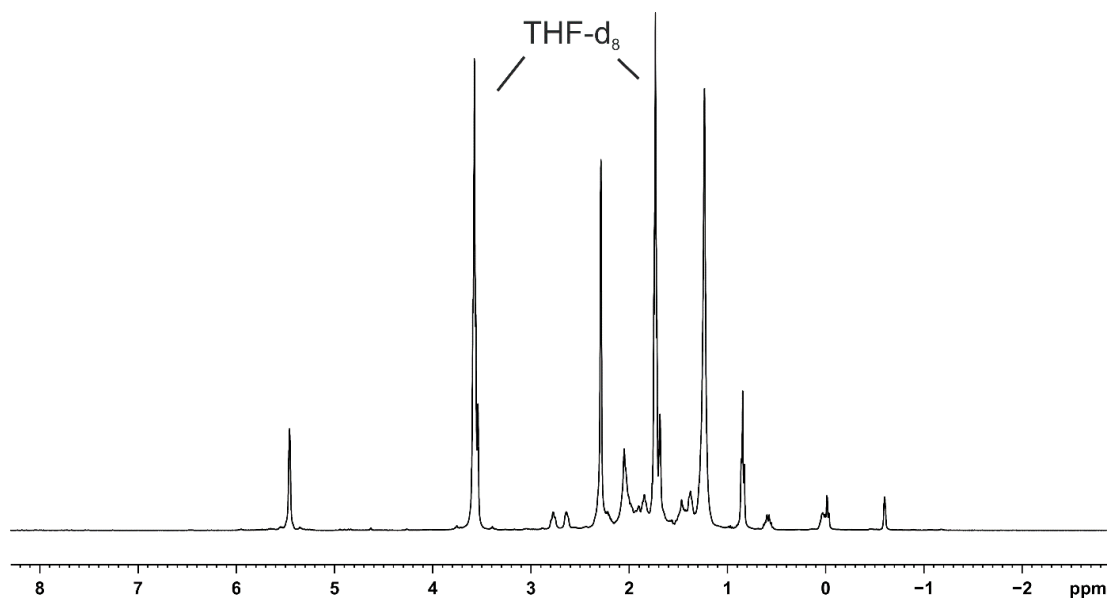
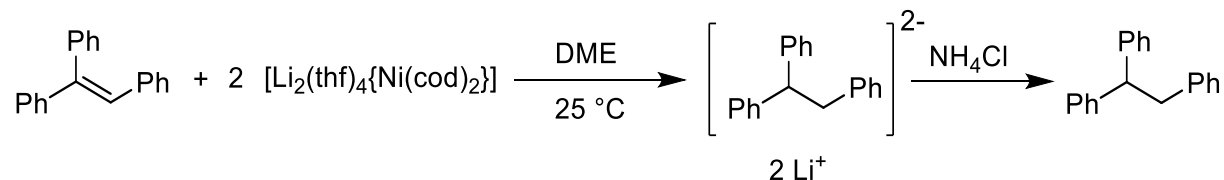


Figure 7.5.32. ¹H NMR spectrum (400.13 MHz, 300 K, THF-d₈) of **1** and 1-dodecene.

7.5.13 Mechanism: GC analyses

a) 1,1',2-Triphenylethylene (1:2 reaction)



1,1',2-Triphenylethylene (0.8 mg 0.0031 mmol, 1.0 equiv.) and **1** (3.6 mg, 0.0062 mmol, 2.0 equiv.) were dissolved in 0.5 mL DME. The solution immediately turned from red to purple and was quenched after five minutes with a saturated NH_4Cl solution and ethyl acetate. An aliquot of the organic phase was analyzed by GC-MS. A significant amount of triphenylethane was formed.

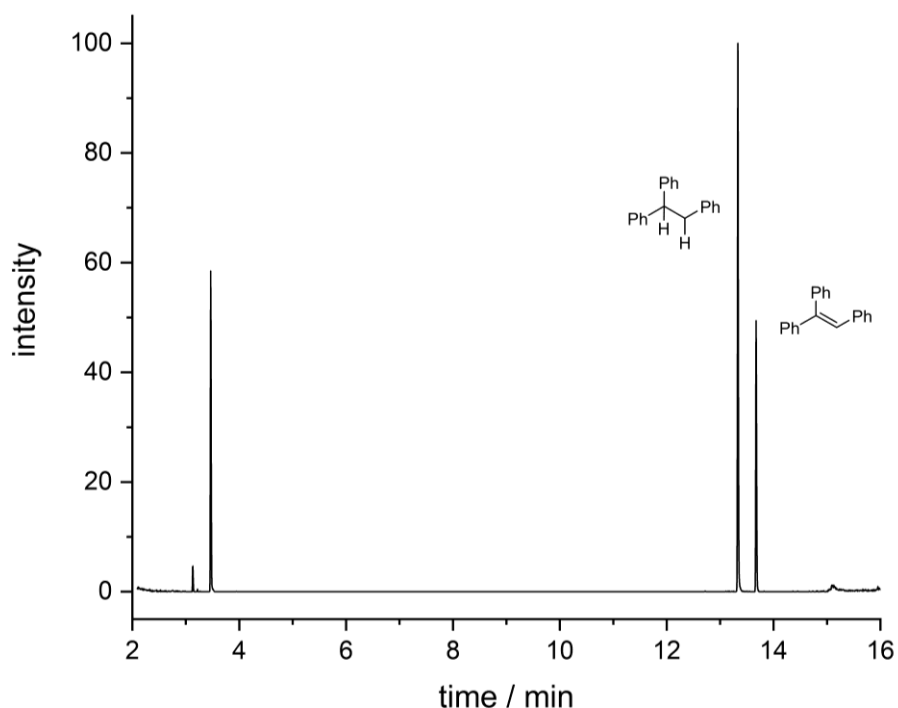
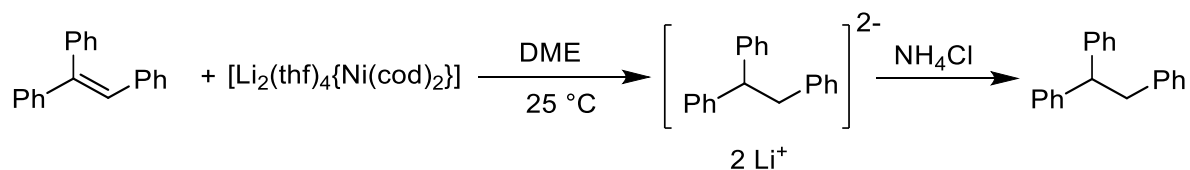


Figure 7.5.33. Chromatogram (GC-MS) from the reaction of 1,1',2-triphenylethylene with 2.0 equiv. **1**.

7 Heterogeneous Olefin Hydrogenation Enabled by a Highly-Reduced Nickel(–II) Catalyst Precursor

b) 1,1',2-Triphenylethylene (1:1 reaction)



1,1',2-Triphenylethylene (1.6 mg 0.0062 mmol, 1.0 equiv.) and **1** (3.6 mg, 0.0062 mmol, 1.0 equiv.) were dissolved in 0.5 mL DME. The solution immediately turned purple from red and was quenched after five minutes with a saturated NH₄Cl solution and ethyl acetate. An aliquot of the organic phase was analyzed by GC-MS. A significant amount of triphenylethane was formed.

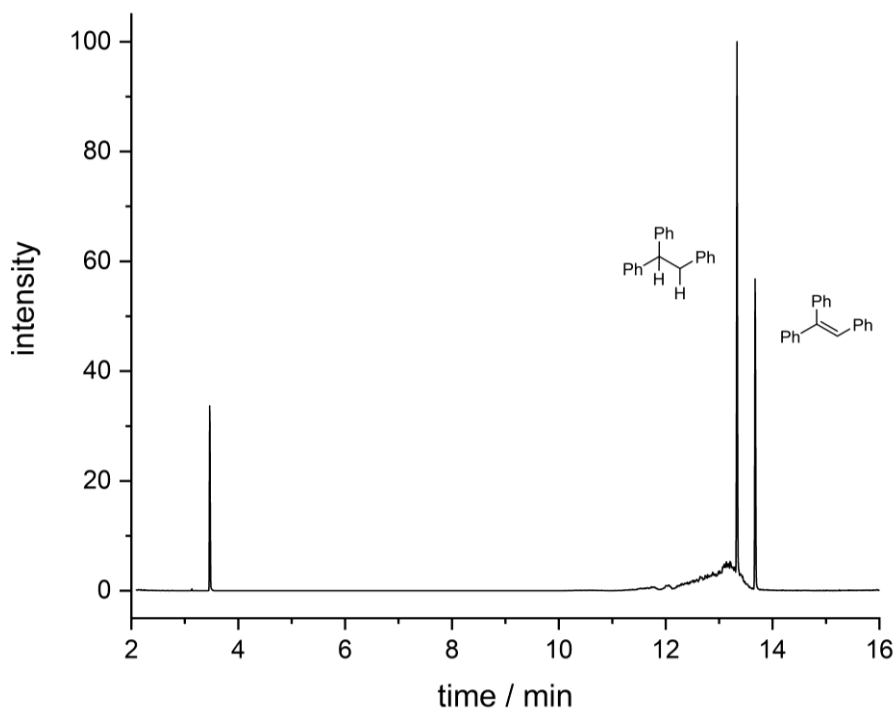
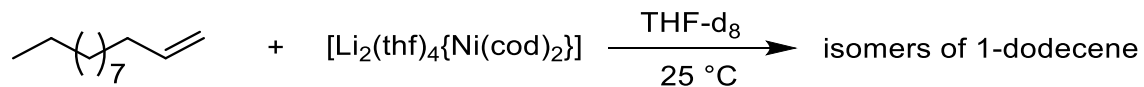


Figure 7.5.34. Chromatogram (GC-MS) from the reaction of 1,1',2-triphenylethylene with **1**.

c) 1-Dodecene (1:1 reaction)



The reaction of 4.1.1 c) was quenched after NMR spectroscopic analysis with saturated aqueous NH_4Cl solution and ethyl acetate. An aliquot of the organic phase was analyzed by GC-MS. No dodecane was observed. Instead, a significant amount of 1-dodecene isomers were detected.

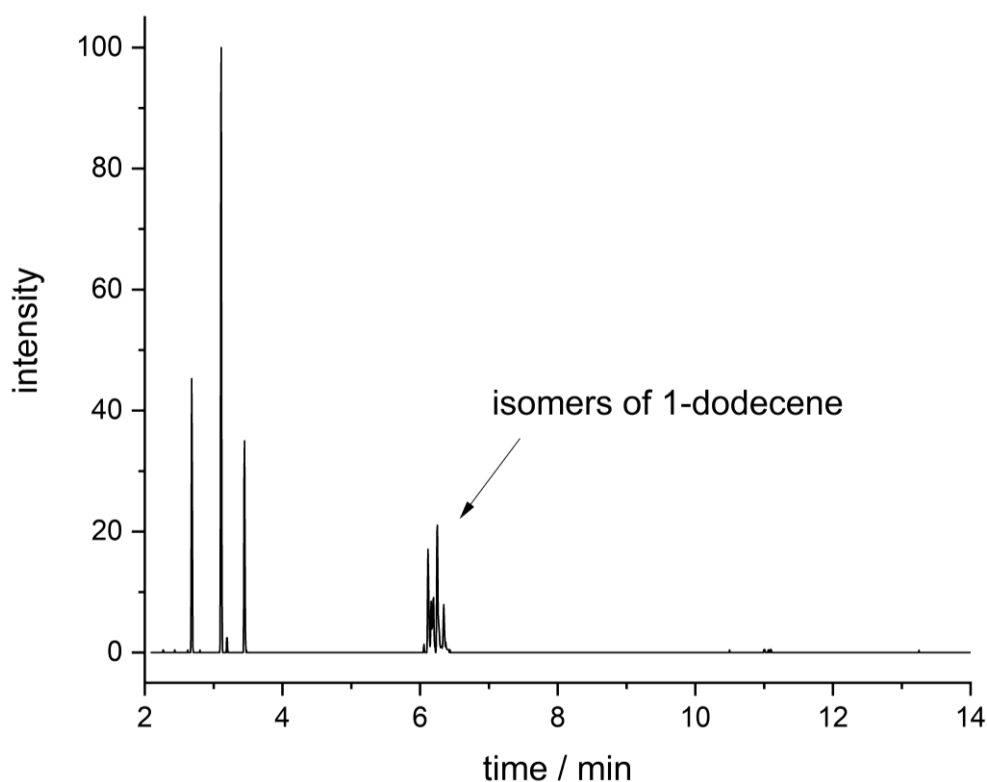
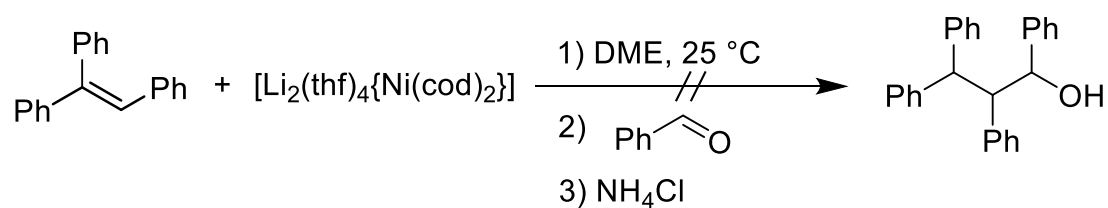


Figure 7.5.35. Chromatogram (GC-MS) from the reaction of 1-dodecene with **1**.

7 Heterogeneous Olefin Hydrogenation Enabled by a Highly-Reduced Nickel(-II) Catalyst Precursor

d) Benzaldehyde



1,1',2-Triphenylethylene (4.5 mg 0.018 mmol, 1.0 equiv.) and **1** (10.4 mg, 0.018 mmol, 1.0 equiv.) were dissolved in 0.25 mL DME each. The solution turned deep-purple upon addition of **1** to 1,1',2-triphenylethylene. The reaction was quenched with benzaldehyde (8.8 μL , 0.087 mmol, 5.0 equiv.) and became colorless. Aqueous NH_4Cl and ethylacetate was added and an aliquot of the organic phase was filtered and subsequently analyzed by GC-MS. No formation of the proposed product was observed.

This experiment supports the hypothesis that a dianionic intermediate is formed rather than a monoanionic one.

7.5.14 Mechanism: Cyclic voltammetry

The electrochemical properties of 1,1',2-triphenylethylene (TPE) were investigated by cyclic voltammetry in DME/ n Bu₄NPF₆ and THF/ n Bu₄NPF₆. The CV of complex **1** was recorded in THF/ n Bu₄NPF₆.

a) THF

1,1',2-triphenylethylene (2.5 mg, 0.010 mmol) was dissolved in a solution of n Bu₄NPF₆ (375 mg, 0.97 mmol) in 10 mL THF.

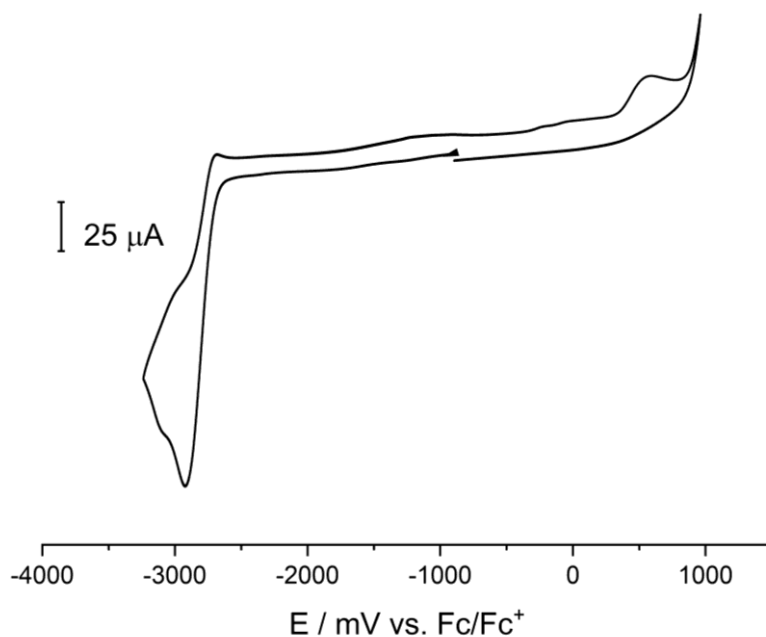


Figure 7.5.36. Cyclic voltammogram of TPE in THF/ n Bu₄NPF₆; Scan rate = 100 mV s⁻¹.

7 Heterogeneous Olefin Hydrogenation Enabled by a Highly-Reduced Nickel(-II) Catalyst Precursor

b) DME

1,1',2-triphenylethylene (3.3 mg, 0.013 mmol) was dissolved in a solution of $n\text{Bu}_4\text{NPF}_6$ (378 mg, 0.98 mmol) in 10 mL DME.

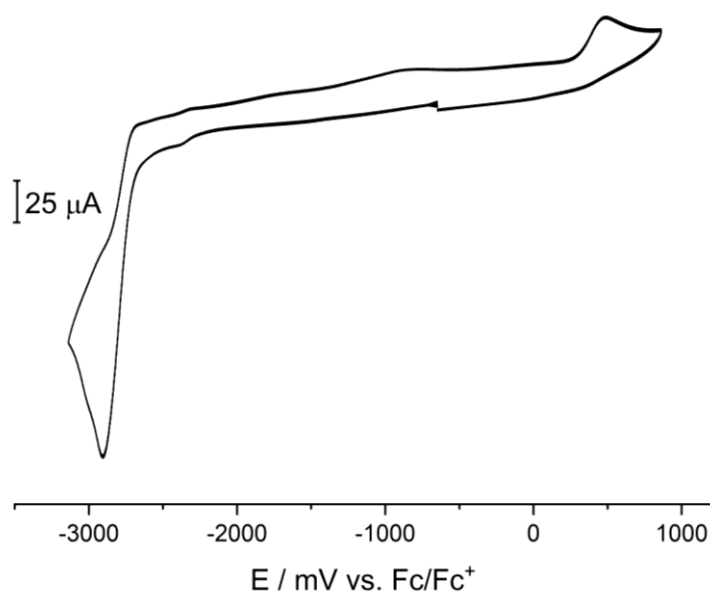


Figure 7.5.37. Cyclic voltammogram of TPE in DME. Scan rate = 200 mV s⁻¹.

c) Complex 1

Complex **1** (11.3 mg, 0.02 mmol) was dissolved in a solution of $n\text{Bu}_4\text{NPF}_6$ (380 mg, 0.98 mmol) in 10 mL THF.

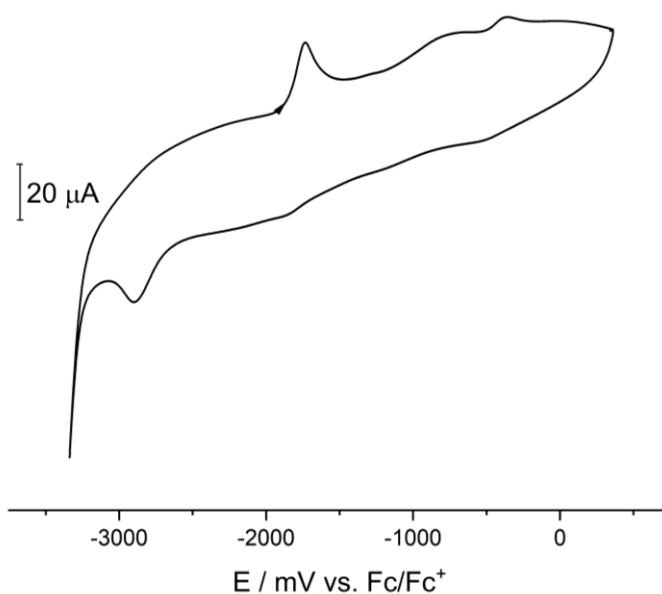


Figure 7.5.38. Cyclic voltammogram of **1** in THF. Scan rate = 200 mV s⁻¹.

7.5.15 Mechanism: UV-vis spectroscopy

a) 1,1',2-triphenylethylene

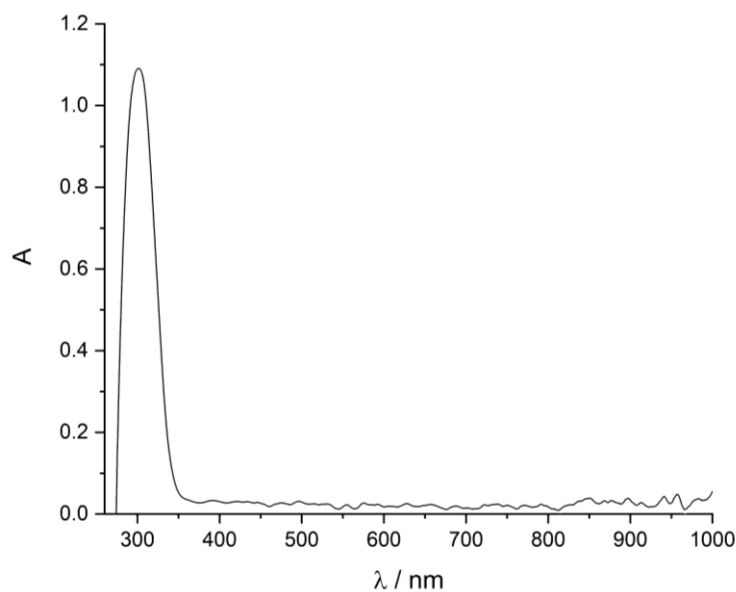


Figure 7.5.39. UV-vis spectrum of TPE with $\lambda_{\max} = 301$ nm.

b) Reaction of 1,1',2-triphenylethylene with **1**

1,1',2-Triphenylethylene (2.0 mg, 0.078 mmol) and **1** (4.3 mg, 0.0074 mmol) were both dissolved in 0.2 mL THF. The nickel complex **1** was added to the olefin solution upon colour change to deep purple was observed. So much THF has been added to the solution that the absorbance was between 0 and 1.

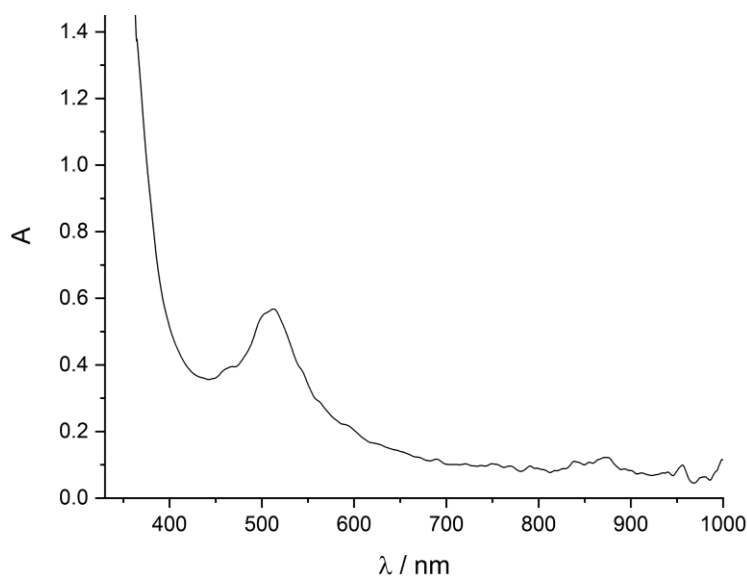


Figure 7.5.40. UV-vis spectrum of reaction of TPE and **1** with $\lambda_{\max} = 511$ nm.

7.5.16 Nanoparticle TEM analysis

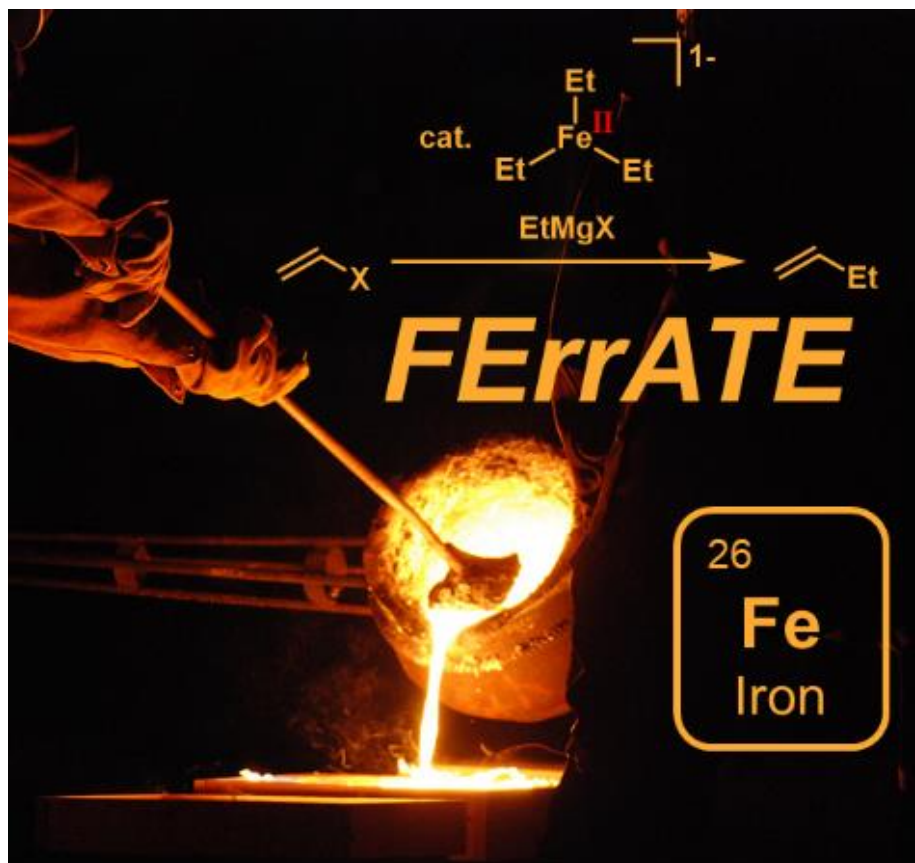
Complex **1** (1.2 mg, 0.002 mmol, 1.0 equiv.) and 1-phenyl-1-cyclohexene (31.5 μ L, 0.2 mmol, 100 equiv.) were dissolved in 0.25 mL DME. The solution was saturated with 1 bar H₂ by freeze-pump-thaw (3 cycles). Further preparation work was carried out in a Glove Box under argon to prevent any alteration of the particles. A droplet of the DME solution was transferred onto a regular, commercially available holey carbon grid. The holey carbon grid was then transferred into a special vacuum transfer holder (Gatan Inc), where the specimen can be retracted into the holder casing for protection against the atmosphere. Additionally, the holder was flooded with the inert gas from the Glove Box. After transfer of the holder, containing the sealed specimen, into the microscope, the vacuum holder was first pumped to remove the inert gas, afterwards the specimen cartridge was moved out of the sealed area, now ready for inspection by the microscope. The images were then recorded using a 1k x 1k CCD camera.

7.5.17 References

- [1] K. Jonas, *Angew. Chem. Int. Ed.* **1975**, *14*, 752-753; *Angew. Chem.* **1975**, *87*, 809–810.
- [2] L. Nattmann, S. Lutz, P. Ortsack, R. Goddard, J. Cornella, *J. Am. Chem. Soc.* **2018**, *140*, 13628–13633.
- [3] N. G. Léonard, P. J. Chirik, *ACS Catal.* **2018**, *8*, 342–348.
- [4] Y. Wang, A. Kostenko, S. Yao, M. Driess, *J. Am. Chem. Soc.* **2017**, *139*, 13499–13506.
- [5] C. Metallinos, J. Zaifman, L. Van Belle, L. Dodge, M. Pilkington, *Organometallics* **2009**, *28*, 4534-4543
- [6] M. R. Prinsell, D. A. Everson, D. J. Weix, *Chem. Commun.* **2010**, *46*, 5743-5745.
- [7] C. Smit, W. Fraaije, A. J. Minnaard, *J. Org. Chem.* **2008**, *73*, 9482.
- [8] S. Mummadi, A. Brar, G. Wang, D. Kenefake, R. Diaz, D. K. Unruh, S. Li, C. Krempner, *Chem. Eur. J.* **2018**, *24*, 16526-16531.

8 The Role of Organoferrates in Iron-Catalyzed Cross-Couplings^{VIII}

Dedicated to the pioneering work of Prof. Klaus Jonas



Abstract: Organometalates without stabilizing heteroatomic ligands constitute versatile sources of reactive metal ions. Recent ground-breaking studies have demonstrated that i) coordinatively unsaturated three-coordinate σ -alkyl-ferrates are active catalysts in Fe-catalyzed cross-couplings with Grignard reagents, ii) pronounced solvent and counterion effects dictate metalate speciation and catalyst

^{VIII} Reproduced with permission from: S. Sandl, A. Jacobi von Wangelin, *Angew. Chem. Int. Ed.* **2020**, 59, 5434–5437; *Angew. Chem.* **2020**, 132, 5474–5477. Copyright 2020 Wiley-VCH, Weinheim, schemes, figures and text may differ from published version.

Author contribution:

S. Sandl: Manuscript preparation.

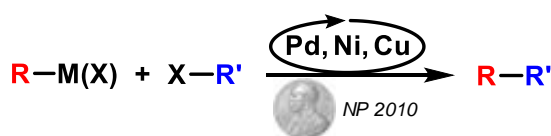
A. Jacobi von Wangelin: Corresponding author.

activity, and iii) specification of sensitive catalyst intermediates is enabled by modern spectroscopic tools.

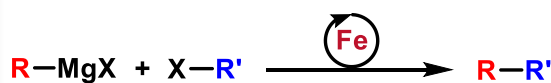
8.1 Introduction

Transition metal-catalyzed cross-coupling reactions have shaped the art of organic synthesis like no other new methodology in the past decades, with numerous applications to the preparation of fine chemicals, agrochemicals, materials, and pharmaceuticals. The high activity and versatility of conventional Pd and Ni catalysts have very recently been rivalled by the advent of effective Fe catalysts. Importantly, even the simplest commercial iron salts (e.g. FeCl₂) exhibit great catalytic activities in challenging C-C bond formations at stable organic chlorides, esters, and ethers without competition by undesired β-H elimination pathways (Scheme 1.1).^{[1],[2],[3]} Despite the success of Fe-catalyzed cross-couplings in the realm of fine chemicals synthesis, very little mechanistic insight has been available.^[2] Only recently, the groups of Fürstner, Bedford, and Neidig have contributed milestone achievements to the understanding of the structures and properties of low-valent Fe catalysts. These works have not only provided deep insight into the mechanistic scenarios of iron-catalyzed cross-coupling reactions but have ultimate ramifications on organometallic cluster syntheses and the development of advanced analytical tools.

Cross-coupling reactions:



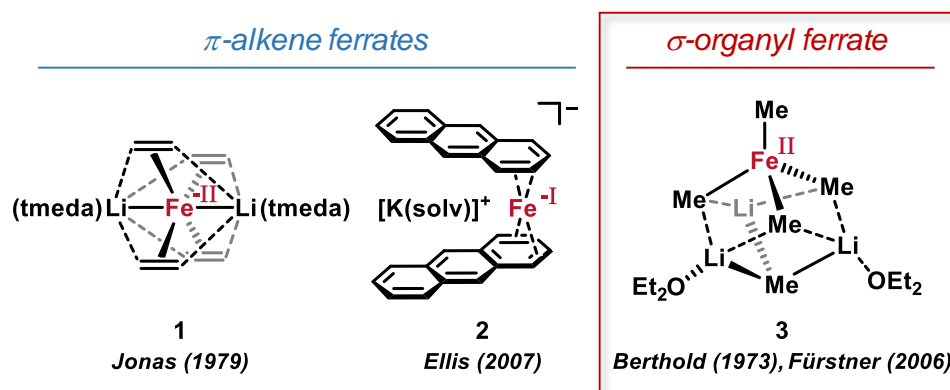
*high selectivity
numerous applications
complex ligands
mild organometallics
mechanistic knowledge*



*high reactivity
inexpensive catalyst
mostly ligand-free
strong organometallics
little mechanistic insight*

Scheme 8.1. a) Conventional cross-coupling methods; b) Fe-catalyzed cross-coupling with Grignard reagents.

Generally, the careful design, synthesis, and analysis of molecular organometallic compounds that potentially act as catalytic intermediates holds the key to the understanding of cross-coupling mechanisms. Conventional protocols employ mildly basic organometallic reagents and catalysts comprising of the late and noble transition metals (Ni, Pd, Cu) with complex ligands (phosphines, *N*-heterocyclic carbenes, amines). These framework conditions enable catalysis mechanisms which involve ligand-stabilized complexes that can be isolated or monitored with standard analytical techniques. On the contrary, iron-catalyzed cross-couplings utilize highly reactive Grignard reagents, mostly ligand-free catalysts, and operate via single-electron transfer steps which altogether impede their comprehensive mechanistic study. Very early on, the intermediacy of “naked” organoferrates was postulated, but solid mechanistic proof has been scarce.^[2] Despite the discovery of the first metalate, Na[ZnEt₃], already in 1858,^[4] the utility and versatility of such highly basic anionic organometallic reagents have been underappreciated for long. While the common view of organometallic and coordination chemistry has often considered the more stable electron-deficient metal centers and electrophilic metal complexes, the reverse scenarios of organometalates – where strongly reducing organometallic compounds are formally negatively charged and bear a cationic counterion – has only recently attracted great interest.^[5] In the past decade, the use of organic main-group and non-transition metalates [M_xR_yX_z]ⁿ⁻ (e.g. M = Mg, Zn, B, Si) has greatly expanded the scope of hydrocarbon functionalization and cross-coupling reactions.^[6] The high kinetic lability, more complex redox manifolds, paramagnetism and the lack of competent analytical tools have largely prohibited an equally rapid progress in the field of organic transition metalates.^[5] Pioneering advances were reported by the isolation of transition metalates that are devoid of any stabilizing heteroatomic ligands but merely contain labile hydrocarbons such as π-alkenes and σ-alkyl (Scheme 1.2).^{[4],[7]-[9]}

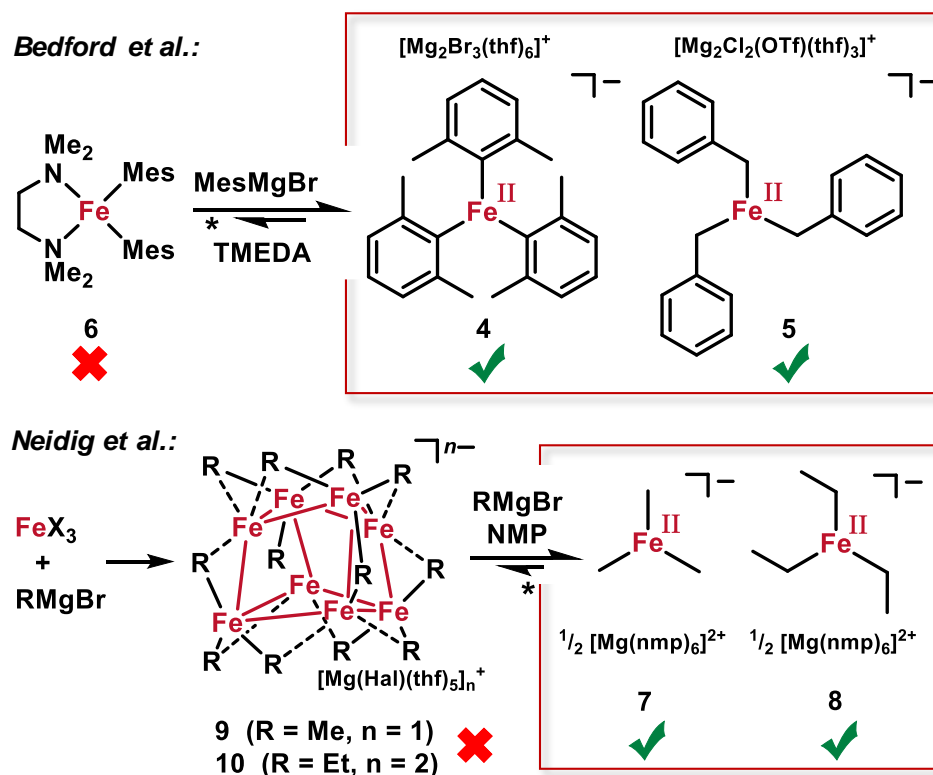


Scheme 8.2. Stabilization of ferrates by simple π - and σ -hydrocarbons.^{[7],[8],[9]}

8.2 Triorganoferrates as Active Cross-Coupling Catalysts

The isolation of the tetramethylferrate(II) complex **3** by Fürstner et al.^[9] and its observed reactivity with organic halides prompted great efforts in the search for σ -organoferrates as competent catalyst species.^[10] Bedford et al. postulated that homoleptic three-coordinate $[\text{FeR}_3]^-$ constitute the active catalysts in Fe-catalyzed cross-coupling reactions.^{[11],[12]} Such coordinatively unsaturated catalyst intermediates were isolated and characterized from reactions of $\text{FeCl}_2/\text{TMEDA}$ (tetramethyl-ethylene-1,2-diamine) with Grignard reagents (Scheme 1.3, top). Indeed, the ferrates $[\text{Mg}_2\text{Br}_3(\text{thf})_6][\text{Fe}(\text{mesityl})_3]$ (**4**) and $[\text{Mg}_2\text{Cl}_2(\text{OTf})(\text{thf})_3][\text{Fe}(\text{Bn})_3]$ (**5**) underwent rapid cross-coupling with electrophiles (Scheme 1.4). The authors further demonstrated that the proposed catalyst $[(\text{tmeda})\text{Fe}(\text{Mes})_2]$ (**6**) exhibited very low activity and rather represents an off-cycle intermediate where TMEDA acts as scavenger of non-productive Fe species.^{[11],[12]}

*Triorganoferrates $[R_3Fe]^-$: - active ✓ cross-coupling catalysts
- solvent & counterion effects*

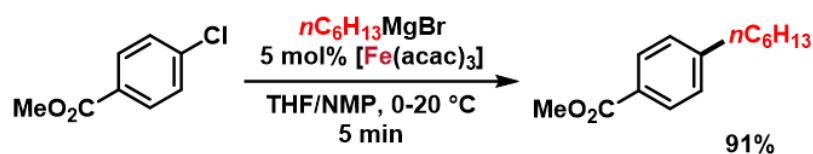


Scheme 8.3. New σ -organyl ferrates prepared by the groups of Bedford and Neidig and their relevance in catalytic cross-coupling reactions (* equilibria not unambiguously established; arrows for illustrative purposes only).

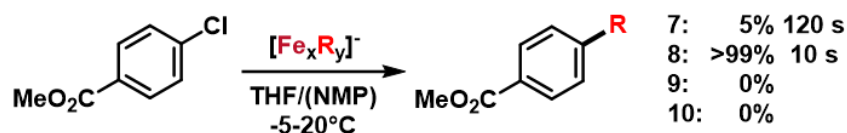
The isolation of structurally related yet more labile σ -alkyl ferrates by Neidig and coworkers constituted a milestone achievement in the mechanistic elucidation of Fe-catalyzed cross-couplings (Scheme 1.3, bottom). Reactions of FeX_3 (X = Cl, acac) with alkyl-magnesium bromides (methyl, ethyl) in THF/NMP (*N*-methyl-2-pyrrolidinone) - under conditions very similar to cross-couplings - afforded the tridentate ferrates $[Mg(nmp)_6][FeR_3]_2$ (R = Me: **7**; R = Et: **8**) in very high spectroscopic yields.^{[13],[14]} Indeed, both ferrates underwent quantitative cross-coupling with alkenyl bromide; **8** also readily reacted with 4-chlorobenzoate (Scheme 1.4).^{[13],[14]} In the absence of NMP, higher-order alkyl ferrates of the formula $[Fe_8R_{12}]^{n-}$ were isolated that contain a topologically new $[Fe_8]$ core with 12 μ_2 -alkyl groups: $[MgCl(thf)_5][Fe_8Me_{12}]$ (**9**, n = 1) and $[MgX(thf)_5][Fe_8Et_{12}]$ (**10**, n = 2, X = Cl/Br) (Scheme 1.3, bottom). **9** contains a mean oxidation state of 1.4.^{[14]-[16]} Almost 50 years after the pioneering work of Kochi on Fe-catalyzed cross-

couplings, these ferrate clusters appear to be the long-sought proof of the 1976 postulate of active Fe catalysts with an $S = \frac{1}{2}$ signature in the electron paramagnetic resonance (EPR) spectrum.^[17] However, the clusters **9** and **10** exhibited no productive coupling with electrophilic organohalides;^{[14],[15]} reaction between **9** and alkenyl bromide was only observed after addition of 1 equiv. MeMgBr (Scheme 1.4).^[15] In earlier studies by Cahiez et al., the role of NMP on the suppression of unwanted β -H-elimination in Fe-catalyzed cross-couplings with higher alkyl-Grignard reagents was discovered.^[18] This observation can now be interpreted as an effective counterion coordination that enables the formation of catalytically active monomeric ferrates.^[13] Indeed, both ethyl ferrates **8** and **10** were inert toward β -H-elimination, which is in full accord with numerous literature reports on Fe-catalyzed alkyl-couplings.^[2] The implications of these groundbreaking syntheses of hitherto unknown organometallic complexes also extend into the critical evaluation of the toolbox of analytical techniques. Neidig and coworkers have instructively demonstrated with great care that paramagnetic, redox-active, and/or thermally sensitive catalyst intermediates can indeed be investigated under catalytic reaction conditions by *in operando* spectroscopies such as EPR, magnetic circular dichroism, and Mössbauer (Scheme 1.5).^[19] These organometallic studies of metalate-catalyzed reactions have also demonstrated the opportunities for catalyst tuning by the nature of the counterion. Co-catalytic assistance of counter-ions can involve diverse modes of substrate or catalyst activations.^{[20]-[23]} Upon implementation of metal-based cations, bimetallic catalysis mechanisms can be engineered. The distinct reactivity of magnesium vs. lithium organoferrates in these studies mirror the dominance of Grignard reagents as nucleophilic components in iron-catalyzed cross-couplings.^[2]

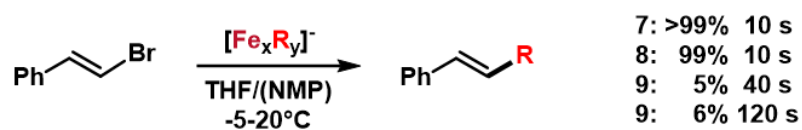
a) *In situ* catalyst system:



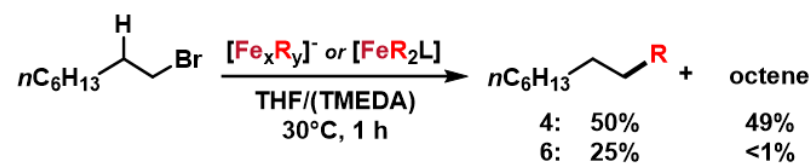
b) Alkylation of aryl chloride:



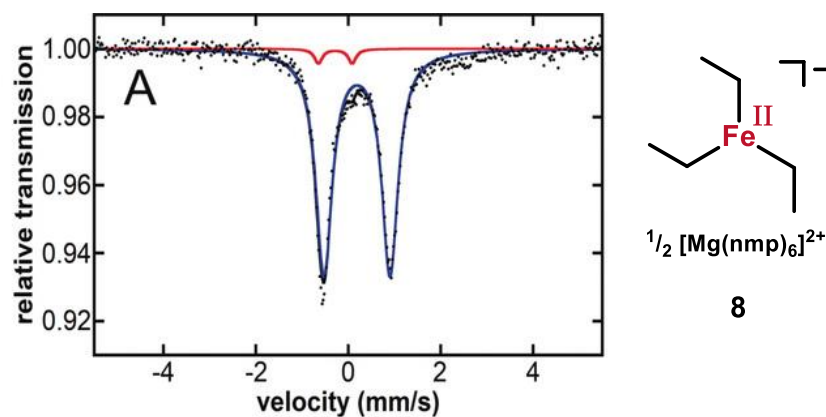
c) Alkylation of alkenyl bromide:



d) Arylation of alkyl bromide:



Scheme 8.4. Fe-catalyzed cross-coupling reactions by *in situ* formed catalyst and in the presence of organoferrates.^[1]



Scheme 8.5. Mössbauer spectrum (at 80 K) of the magnesium triethylferrate **8** formed from $\text{Fe}(\text{acac})_3$ and EtMgBr in the presence of NMP.^[14]

8.3 Conclusion

The recent studies of new σ -organyl ferrates by Fürstner, Bedford, and Neidig have greatly expanded the art of organometallic chemistry, Fe catalysis, and spectroscopic analysis of intrinsically sensitive and dynamic reactive intermediates. What are the lessons to be learned? *i)* Iron-catalyzed cross-coupling reactions have matured to a reaction class of great versatility which display distinct mechanistic features from conventional noble-metal catalyzed reactions. *ii)* Organometalates have been largely under-appreciated as reactive entities and catalyst intermediates. *iii)* Very skillful preparative organometallic synthesis has enabled the isolation of hitherto unknown, coordinatively unsaturated organoferrates $[R_3Fe]$ that are active catalysts of Fe-catalyzed cross-coupling reactions. *iv)* Pronounced solvent and counterion effects govern the aggregation of σ -organoferrates and their catalytic activity. The pioneering studies by the groups of Jonas, Ellis, Fürstner, Bedford, and Neidig have opened the door to a deeper insight into catalysis with “unusual” metalates, a general reactivity principle that may even extend to “noble metal” catalysis in cases where ligand dissociation and nanoparticle formation have been discussed so far. Lastly, these works demonstrate that successful catalysis research greatly benefits from fruitful collaborations between skilled molecular synthesis and advanced spectroscopy.

Acknowledgements

This work was generously supported by a Consolidator grant (683150) of the European Research Council (ERC).

8.4 References

- [1] a) A. Fürstner, A. Leitner, *Angew. Chem. Int. Ed.* **2002**, *41*, 609–612; b) Note, that a related NMP-free procedure gives good yields for 4-chlorobenzoate, while more challenging substrates show a significantly increased yield in presence of such ligands: E. Bisz, M. Szostak, *Green Chem.* **2017**, *19*, 5361–5366.
- [2] a) W. M. Czaplik, M. Mayer, J. Cvengroš, A. Jacobi von Wangelin, *ChemSusChem* **2009**, *2*, 396–417; b) I. Bauer, H. Knölker, *Chem. Rev.* **2015**, *115*, 3170–3387; c) R. B. Bedford, P. B. Brenner, *Top. Organomet. Chem.* **2015**, *50*, 19–46; d) C. Cassani, G. Bergonzini, C.-J. Wallentin, *ACS Catal.* **2016**, *6*, 1640–1648; e) T. L. Mako, J. A. Byers, *Inorg. Chem. Front.* **2016**, *3*, 766–790; f) A. Piontek, E. Bisz, M. Szostak, *Angew. Chem. Int. Ed.* **2018**, *57*, 11116–11128.
- [3] C. E. I. Knappke, A. Jacobi von Wangelin, *Chem. Soc. Rev.* **2011**, *40*, 4948–4962.
- [4] J. A. Wanklyn, *Liebigs Ann. Chem.* **1858**, *107*, 125–128.
- [5] a) J. P. Collman, *Acc. Chem. Res.* **1975**, *8*, 342–347; b) F. Mongin, A. Harrison-Marchand, *Chem. Rev.* **2013**, *113*, 7563–7727; c) A. Gómez-Suárez, D. J. Nelson, S. P. Nolan, *Adv. Organomet. Chem.* **2018**, *69*, 283–327.
- [6] a) R. E. Mulvey, F. Mongin, M. Uchiyama, Y. Kondo, *Angew. Chem. Int. Ed.* **2007**, *46*, 3802–3824; b) S. D. Robertson, M. Uzelac, R. E. Mulvey, *Chem. Rev.* **2019**, *119*, 8332–8405.
- [7] a) K. Jonas, L. Schieferstein, C. Krüger, Y.-H. Tsay, *Angew. Chem. Int. Ed.* **1979**, *18*, 550–551; b) K. Jonas, *Angew. Chem. Int. Ed.* **1985**, *24*, 295–311; c) The field of main group organometallic and organometalate reagents has recently been significantly expanded by new procedures, new reagents, and new applications to organic synthesis, with a major focus on cross-coupling reactions: *Handbook of Functionalized Organometallics: Applications in Synthesis* (Ed.: P. Knochel), Wiley-VCH: Weinheim, **2005**.
- [8] a) W. W. Brennessel, V. G. Young, Jr., J. E. Ellis, *Angew. Chem. Int. Ed.* **2002**, *41*, 1211–1215; b) J. E. Ellis, *Inorg. Chem.* **2006**, *45*, 3167–3186; c) J. E. Ellis, *Dalton Trans.* **2019**, *48*, 9538–9563.

- [9] a) H. J. Spiegl, G. Groh, H. J. Berthold, *Z. Anorg. Allg. Chem.* **1973**, 398, 225–230; b) A. Fürstner, H. Krause, C. W. Lehmann, *Angew. Chem. Int. Ed.* **2006**, 45, 440–444; c) A. Fürstner, R. Martin, H. Krause, G. Seidel, R. Goddard, C. W. Lehmann, *J. Am. Chem. Soc.* **2008**, 130, 8773–8787.
- [10] T. Kauffmann, *Angew. Chem. Int. Ed. Engl.* **1996**, 35, 386–403.
- [11] a) W. Seidel, K.-J. Lattermann, *Z. Anorg. Allg. Chem.* **1982**, 488, 69–74; b) R. B. Bedford, P. B. Brenner, E. Carter, P. M. Cogswell, M. F. Haddow, J. N. Harvey, D. M. Murphy, J. Nunn, C. H. Woodall, *Angew. Chem. Int. Ed.* **2014**, 53, 1804–1808.
- [12] R. B. Bedford, *Acc. Chem. Res.* **2015**, 48, 1485–1493.
- [13] S. B. Muñoz, S. L. Daifuku, J. D. Sears, T. M. Baker, S. H. Carpenter, W. W. Brennessel, M. L. Neidig, *Angew. Chem. Int. Ed.* **2018**, 57, 6496–6500.
- [14] J. D. Sears, S. B. Muñoz, S. L. Daifuku, A. A. Shaps, S. H. Carpenter, W. W. Brennessel, M. L. Neidig, *Angew. Chem. Int. Ed.* **2019**, 58, 2769–2773.
- [15] S. B. Muñoz, S. L. Daifuku, W. W. Brennessel, M. L. Neidig, *J. Am. Chem. Soc.* **2016**, 138, 7492–7495.
- [16] T. Parchomyk, S. Demeshko, F. Meyer, K. Koszinowski, *J. Am. Chem. Soc.* **2018**, 140, 9709–9720.
- [17] R. S. Smith, J. K. Kochi, *J. Org. Chem.* **1976**, 41, 502–509.
- [18] G. Cahiez, H. Avedissian, *Synthesis* **1998**, 1998, 1199–1205.
- [19] M. L. Neidig, S. H. Carpenter, D. J. Curran, J. C. DeMuth, V. E. Fleischauer, T. E. Iannuzzi, P. G. N. Neate, J. D. Sears, N. J. Wolford, *Acc. Chem. Res.* **2019**, 52, 140–150.
- [20] F. Freitag, T. Irrgang, R. Kempe, *J. Am. Chem. Soc.* **2019**, 141, 11677–11685.
- [21] S. Sandl, T. M. Maier, N. P. van Leest, S. Kröncke, U. Chakraborty, S. Demeshko, K. Koszinowski, B. de Bruin, F. Meyer, M. Bodensteiner, C. Herrmann, R. Wolf, A. Jacobi von Wangelin, *ACS Catal.* **2019**, 9, 7596–7606.
- [22] a) C. R. Kennedy, S. Lin, E. N. Jacobsen, *Angew. Chem. Int. Ed.* **2016**, 55, 12596–12624; b) S. Yamada, *Chem. Rev.* **2018**, 118, 11353–11432; c) K. T. Mahmudov, A. V. Gurbanov, F. I. Guseinov, M. F. C. Guedes da Silva, *Coord. Chem. Rev.* **2019**, 387, 32–46.
- [23] a) K. Grubel, W. W. Brennessel, B. Q. Mercado, P. L. Holland, *J. Am. Chem. Soc.* **2014**, 136, 16807–16816; b) G. P. Connor, P. L. Holland, *Catal. Today* **2017**, 286, 21–40.

9 Summary

Metal-catalyzed hydrogenations constitute one of the key chemical transformations. While dominated by noble metal catalysts, recent years have witnessed a significant increase in the use of more sustainable 3d metals. However, very little mechanistic insight has been available until recently. The present thesis deals with the development of iron group metal-catalyzed hydrogenation reactions. Specifically, catalysts have been developed at the fine borderline of homogeneous and heterogeneous catalysis. Careful analysis of the mechanism is supposed to enhance our understanding for the development of improved future catalysts.

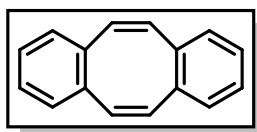
Chapter 1 advocates the use of kinetic poisoning experiments which can be easily performed in a standard laboratory and enable the distinction between homotopic and heterotopic catalysis mechanisms (Scheme 9.1). The facile transition from homogeneous to heterogeneous catalysts under reducing conditions has been a major challenge in method optimization and mechanistic understanding. While ex-situ-analyses of catalyst derivatives can be achieved by various spectroscopic techniques, their results have only limited value for the different conditions, concentrations, and complex kinetics of a real catalytic system. On the other hand, in-situ-tools usually require highly sophisticated setups aiming at the detection of fleeting intermediates.



Scheme 9.1. Distinction between homogeneous and heterogeneous catalysis by kinetic poisoning experiments.

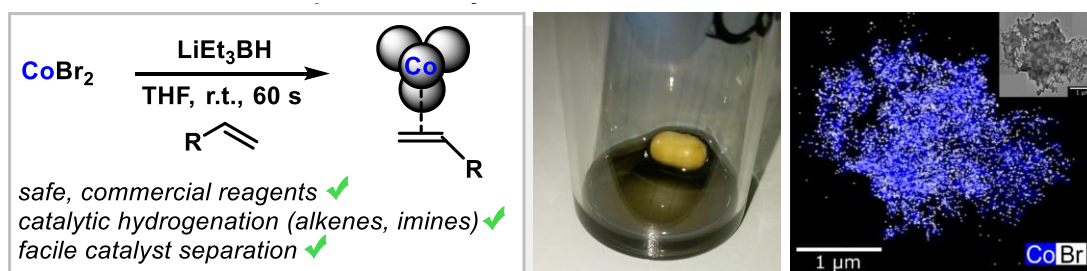
Chapter 2 reviews the selective homogeneous catalyst poison dibenzo[a,e]cyclooctatetraene (dct) (Scheme 9.2). It is a nonconjugated cyclic

diene that finds widespread use as ligand in transition metal coordination chemistry.



Scheme 9.2. Dibenzo[a,e]cyclooctatetraene (dct).

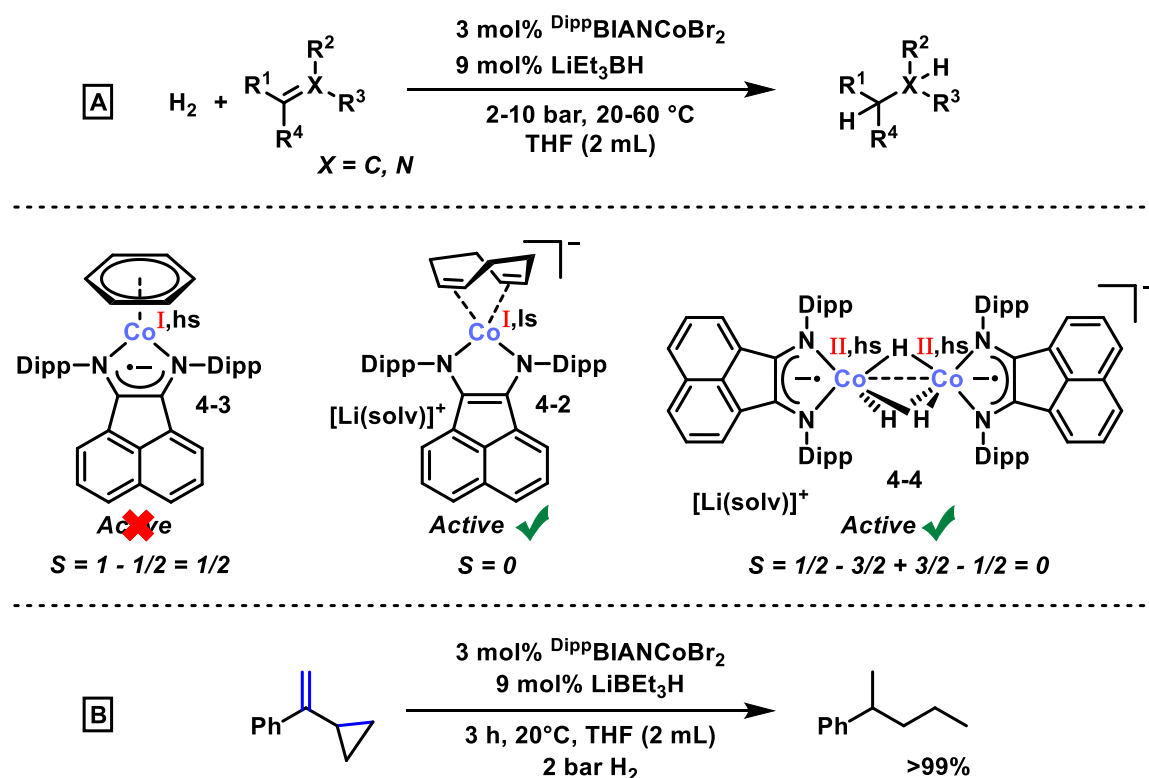
A popular concept in homogeneous metal catalysis is the combination of labile olefin ligands with strong field ligands such as phosphines for the synthesis of active, yet stable catalyst precursors. The method developed in *Chapter 3* aimed for an improvement of this concept by avoiding complex ligands, while simplifying the catalyst preparation. Specifically, cobalt salts were reduced in presence of olefinic substrates to obtain highly-active olefin-stabilized cobalt nanoparticles for the hydrogenation of challenging alkenes, carbonyls, imines, and heteroarenes at mild conditions (3 mol% cat., 2–10 bar H₂, 20–80°C, Scheme 9.3).



Scheme 9.3. Olefin-stabilized cobalt nanoparticles for C=C, C=O, and C=N hydrogenations

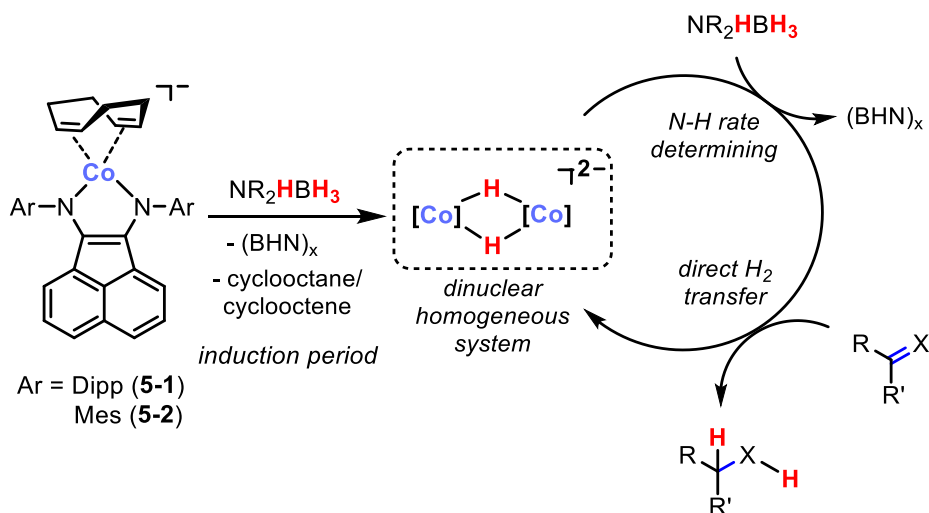
Redox-active ligands are a competent tool to moderate electron transfers within base-metal catalysts. *Chapter 4* describes the development of highly-active cobaltate complexes as hydrogenation catalysts, which are stabilized by bis(imino)acenaphthene (BIAN). Gratifyingly, sterically hindered trisubstituted alkenes, imines, and quinolines underwent clean hydrogenation under mild conditions (2–10 bar, 20–80 °C, Scheme 9.4A). Considerable reaction acceleration by alkali cations and Lewis acids was observed. Insights into the electronic structure of the catalyst has been obtained by the isolation of paramagnetic model complexes documenting the redox-activity of the ligand. [(^{Dipp}BIAN)Co^{I,hs}(η⁶-C₆H₆)]

(**9-3**) consists of a very rare high-spin d^8 configuration with the unpaired electron being primarily located at the Co center (BIAN couples antiferromagnetically). Furthermore, a unique dinuclear hydridocobaltate $[\text{Li}(\text{solv})\{(\text{DippBIAN})\text{Co}^{\text{II,hs}}\}_2(\mu\text{-H})_3]$ (**9-4**) was isolated. **9-4** represents the first cobaltate with bridging hydrides and contains the shortest $\text{Co}(\mu\text{-H})\text{Co}$ motif known to date (2.2426(3) Å). The metalloradical character of the complexes is also reflected in the catalytic hydrogenation of a ring-opening substrate (Scheme 9.4B).



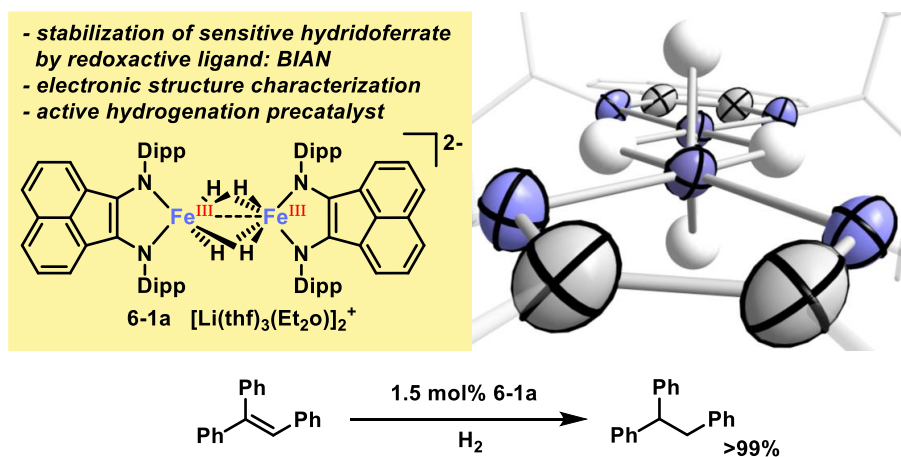
Scheme 9.4. Cobalt-catalyzed hydrogenations via Cobaltate and Hydride Intermediates.

Related cobaltate catalysts (Scheme 9.5) have been used with amine-boranes as dihydrogen surrogates in *Chapter 5* to overcome the necessity of high-pressure reaction equipment. Importantly, the dehydrogenation reaction proceeds at mild conditions (20 °C) unlike related literature precedents. Detailed mechanistic analyses of the dehydrogenation reaction unveiled (i) the operation of a homogeneous mechanism; (ii) the evolution of 1 equiv. H_2 per NH_3BH_3 ; (iii) a dinuclear active species; and (iv) participation of the protic N–H bond in the rate-determining step.



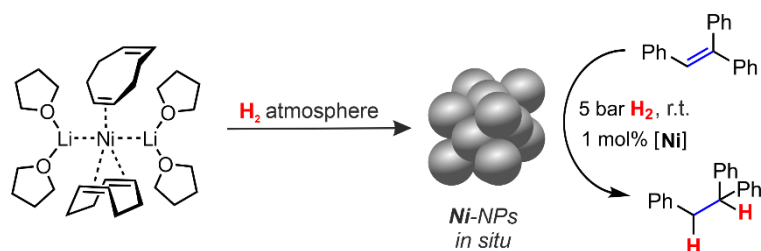
Scheme 9.5. Amine-borane dehydrogenation and transfer hydrogenation catalyzed by α -diimine cobaltates

Sensitive hydridic ferrates display key intermediates in iron-catalyzed reduction reactions. Only few examples have been reported and characterized. *Chapter 6* describes the synthesis, characterization and reactivity of a new dimeric ferrate anion with four bridging hydrides $[\text{Li}(\text{thf})_3(\text{Et}_2\text{O})]_2\{[(\text{DippBIAN}^{2-})\text{Fe}^{\text{III}}]_2(\mu\text{-H})_4\}$ (**6-1a**, Scheme 9.6). Isolability of **6-1a** was enabled by the redox-active ligand bis(imino)acenaphthene (BIAN). A doubly reduced BIAN and Fe^{III} has been observed. Remarkably, anion **6-1a** differs only by two hydrides to $[\text{Li}(\text{thf})_4]_2\{[(\text{DippBIAN}^{2-})\text{Fe}^{\text{II}}]_2(\mu\text{-H})_2\}$ (**6-2**) and the complexes might be related by oxidative addition. **6-1a** is an active precatalyst in catalytic hydrogenations of alkenes and might be an intermediate for the catalytic system $[(\text{DippBIAN})\text{FeCl}_2] / 3 \text{LiEt}_3\text{BH}$.



Scheme 9.6. A dimeric iron ate complex with four bridging hydrides.

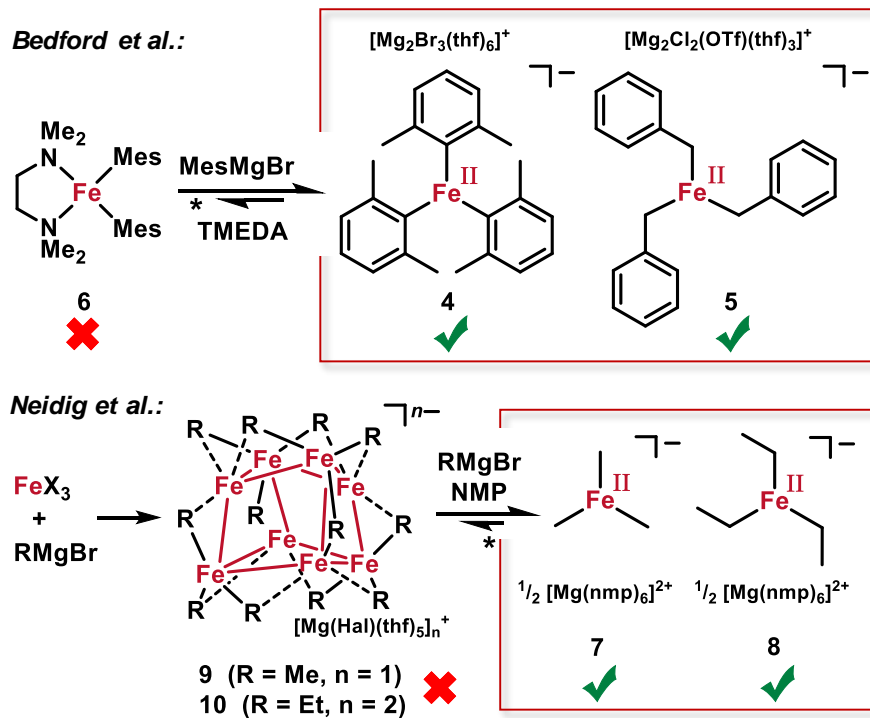
Chapter 7 reports on the nickel-catalyzed hydrogenation of olefins and imines by application of the metalate $[\text{Li}_2(\text{thf})_4\{\text{Ni}(\text{cod})_2\}]$ (Scheme 9.7). The active catalyst consists of olefin-stabilized nickel nanoparticles that are formed by hydrogenolysis. The mild conditions tolerate hydroxyl, halide, ester, and lactone functionalities. The mechanistic data contrasts earlier reports on homogeneous hydrogenation catalysts based on related homoleptic olefin ferrates and cobaltates.



Scheme 9.7. Olefin hydrogenation enabled by a Ni^{II} catalyst precursor.

Transition-metal-catalyzed cross-coupling reactions have shaped the art of organic synthesis like no other methodology in the past decades. Despite the success of Fe-catalyzed cross-couplings in the realm of fine-chemicals synthesis, very little mechanistic insight has been available. *Chapter 8* highlights recent groundbreaking studies on organoferrates (Scheme 9.8). The groups of Bedford and Neidig demonstrated that coordinatively unsaturated three-coordinate- σ -alkylferrates are active catalysts in Fe-catalyzed cross-couplings with Grignard reagents and that pronounced solvent and counterion effects dictate metalate speciation and catalyst activity. Thanks to modern spectroscopic methods, sensitive catalyst intermediates could be analyzed.

Triorganoferrates $[R_3Fe]^-$: - active ✓ *cross-coupling catalysts*
- solvent & counterion effects



Scheme 9.8. Organoferrates as active catalysts in iron-catalyzed cross-coupling reactions.

References

- Chapter 1 D. Gärtner,[†] **S. Sandl**,[†] A. Jacobi von Wangelin, *submitted* († equal contribution).
- Chapter 2 **S. Sandl**, A. Jacobi von Wangelin, *Dibenzo[a,e]cyclooctatetraene* in *e-EROS Encyclopedia of Reagents for Organic Synthesis* **2019**.
- Chapter 3 **S. Sandl**, F. Schwarzhuber, S. Pöllath, J. Zweck, A. Jacobi von Wangelin, *Chem. Eur. J.* **2018**, *24*, 3403–3407.
- Chapter 4 **S. Sandl**, T. M. Maier, N. P. van Leest, S. Kröncke, U. Chakraborty, S. Demeshko, K. Koszinowski, B. de Bruin, F. Meyer, M. Bodensteiner, et al., *ACS Catal.* **2019**, *9*, 7596–7606.
- Chapter 5 T. M. Maier, **S. Sandl**, I. G. Shenderovich, A. Jacobi von Wangelin, J. J. Weigand, R. Wolf, *Chem. Eur. J.* **2019**, *25*, 2 and 238–245.
- Chapter 6 **S. Sandl**, T. M. Maier, R. Wolf, A. Jacobi von Wangelin, *manuscript in preparation*.
- Chapter 7 T. M. Maier, **S. Sandl**, P. Melzl, J. Zweck, A. Jacobi von Wangelin, R. Wolf, *Chem. Eur. J.* **2020**, chem.201905537.
- Chapter 8 **S. Sandl**, A. Jacobi von Wangelin, *Angew. Chem. Int. Ed.* **2020**, *59*, 5434–5437; *Angew. Chem.* **2020**, *132*, 5474–5477.

10 List of Abbreviations

Ac	acetyl	min	minute
ATR	attenuated total reflection	MS	mass spectrometry
BIAN	bis(iminio)acenaphthene	NMR	nuclear magnetic resonance
Bn	benzyl	Ph	phenyl
Bu	butyl	Rf	retention factor
CCD	charge-coupled-device	rt	room temperature
d	day	SET	single-electron transfer
Dipp	diisopropylphenyl	SQUID	superconducting quantum interference device
dct	dibenzo[a,e]cyclooctatetraene	TEM	transmission electron microscopy
DiBAIH	diisobutylaluminiumhydride	thf	tetrahydrofurane
DFT	density-functional theory	TLC	thin layer chromatography
DOI	digital object identifier	TMS	trimethylsilyl
ee	enantiomeric excess	TOF	turnover frequency
EI	electron impact		
equiv.	equivalents		
ESI	electron spray ionization		
Et	ethyl		
FID	flame ionization		
FT-IR	Fourier-Transform-Infrared spectroscopy	Pr	propyl
GC	gas chromatography		
h	hour		
HR	high resolution		
Me	methyl		

11 Acknowledgments

Zuallererst möchte ich mich bei meinem Doktorvater Axel für die hervorragende Betreuung bedanken. Dank dir hatte ich die Möglichkeit beruflich und privat zu wachsen. Du hast uns zu Selbständigkeit und Kreativität erzogen. Besonders der Umzug nach Hamburg war ein Jackpot. Du warst mir ein echter Mentor.

Weiterhin möchte ich mich bei Prof. Robert Wolf für die Unterstützung, die Übernahme des Zweitgutachtens und die wertvollen Diskussionen bedanken. Besonders deine Hilfe zum Thema Vollcharakterisierung und Reproduzierbarkeit hat mir sehr geholfen.

Zudem danke ich dem Drittprüfer Prof. Manfred Scheer und Prof. Alkin Slenzka für den Vorsitz.

Ein herzlicher Dank geht an meine Kooperationspartner, die unsere Forschung in diesem Umfang ermöglicht haben. Besonders hervorheben möchte ich Thomas Maier. Das gemeinsame Arbeiten und Publizieren hat mir immer sehr viel Freude bereitet.

Meinem Arbeitskreis möchte ich für die angenehme Atmosphäre danken. Wir haben viel zusammen erlebt: Dominik Gärtner, Michal Majek, Josef Schachtner, Tim Gieshoff, Matteo Villa, Davide Brenna, Raul Perez-Ruiz, Efrain Reyes-Rodriguez, Uttam Chakraborty, Josef Bernauer, Patrik Bayer, Michael Neumeier, Pradip Gosh, Guojiao Wu, Bernhard Gregori, Jennifer Börger, Andrey Fedulin, Luana Cardinale, Javier Recio Ramos, Nils Nun, Matea Sršen und Mikhail Konev.

Ein herzlicher Dank geht auch an meine Forschungspraktikanten für die motivierte Mitarbeit: Ursula Otterpohl, Stefan Reichert, Hannes Sterzel und Martin Eisenhofer.

Ich danke den Abteilungen der Analytik und Werkstätten an beiden Universitäten. Ein besonderer Dank geht an Michael Bodensteiner, Sabine Stempfhuber, Birgit Hischa, Michaela Lutz und Veronica Scheidler für ihre Arbeit.

Bei meinen Studienkollegen bedanke ich mich für eure Unterstützung während meiner Studienzeit: Daniel, Marlene, Verena, Claudia, Veronika, Nele und Julia.

Ein Herzlichen Dank geht an meine Hamburger Freunde vom Hochschulruderverein und von der Big Band. Ihr habt mir einen sehr angenehmen Start ermöglicht und so konnte ich das Leben sehr genießen. Hier habe ich meine Liebe zur Musik endlich wiederentdeckt (Paul und Gideon).

Zuletzt danke ich meiner Familie und allen meinen Freunden für den grenzenlosen Rückhalt in meinem Leben! Danke.

12 Curriculum Vitae

Sebastian Sandl

Chemistry Ph.D. Candidate
 University of Hamburg
 D-20146 Hamburg
 Email: sebastian.sandl@chemie.uni-hamburg.de
 Telephone: +49 40 42838-3107

Education & Research Experience

Ph.D. Studies at University of Hamburg / Regensburg, DE 11/2016-present
Advisor: Prof. Axel Jacobi von Wangelin
 Research topic: Iron Group Metal-Catalyzed Hydrogenation Reactions

Master Thesis at University of Regensburg, DE 01/2016-09/2016
Advisor: Prof. Axel Jacobi von Wangelin
 Research Topic: Iron-Catalyzed Cross-Coupling Reactions with Aryl Ethers and Aryl Magnesium Compounds (1.3, "very good")

Master Studies at University of Regensburg, DE 10/2014-12/2015
 Inorganic Chemistry, Organic Chemistry, Physical Chemistry (majors, 1.2, "very good")

ERASMUS Visiting Scholar: University of St. Andrews, UK 01/2015-04/2015
Advisor: Dr. Matt Clarke
 Research topic: Enantioselective Rhodium and Palladium Catalysis

Industrial Internship at Kelheim Fibres GmbH, DE 08/2012-09/2012
 Analytical Chemistry: European Pharmacopoeia Laboratory

Bachelor Studies at University of Regensburg, DE 10/2011-09/2014
 B.Sc. Chemie (2.2 "good")
 Bachelor thesis: Iron-Catalyzed Cross-Coupling Reactions with Alkenyl Acetates and Alkyl Magnesium Compounds (1.0, "very good")

Scholarships

ERASMUS Visiting Scholar: University of St. Andrews, UK 01/2015-04/2015

Teaching Experience

Mentor of 2 master students and 4 bachelor students 2017-present
Teaching assistant Integrated Synthesis Laboratory 2017-present
Tutor Exercises Inorganic Chemistry 1 Winter 2014

Language skills

German	Native
English	Business fluent
French	Basic

IT skills

MS office	Word, Excel, Powerpoint: Advanced
Crystallography	Rigaku, CrysAlis, Olex2, Diamond: Advanced
Chemistry	ChemDraw, Mestrenova (NMR, MS), Topspin (NMR): Advanced Orca (DFT): Basic
Databases	SciFinder, Web of Science, Cambridge Crystallographic Database, Mendeley: Advanced

Scientific Skills

- Reaction analyses by gas chromatography (quantitative: GC-FID, qualitative: GC-MS)
- Work under exclusion of air and moisture (Schlenk technique, glovebox)
- High-pressure reactions (autoclave)
- Kinetic investigations & mechanism (UV-Vis, CV, (paramagnetic) NMR spectroscopy, IR)
- Crystallography (Rigaku, CrysAlis, Olex2)
- Maintenance and move of gloveboxes (MBraun), maintenance of autoclaves (Parr).

Publications

9. **Sandl, S.**; Jacobi von Wangelin, A. The Role of Organoferrates in Cross-Couplings. *Angew. Chem. Int. Ed.* **2020**, *59*, 5434–5437; *Angew. Chem.* **2020**, *132*, 5474–5477.

8. Maier, T. M.; **Sandl, S.**; Melzl, P.; Zweck, J.; Jacobi von Wangelin, A.; Wolf, R. Olefin Hydrogenation Enabled by a Nickel(–II) Catalyst Precursor. *Chem. - Eur. J.* **2020**, 10.1002/chem.201905537 (hot paper and cover picture).

7. **Sandl, S.**; Maier, T. M.; van Leest, N. P.; Kröncke, S.; Chakraborty, U.; Demeshko, S.; Koszinowski, K.; de Bruin, B.; Meyer, F.; Bodensteiner, M.; Herrmann, C.; Wolf, R.; Jacobi von Wangelin, A. Cobalt-Catalyzed Hydrogenations via Olefin Cobaltate and Hydride Intermediates. *ACS Catal.* **2019**, *9*, 7596–7606.

6. **Sandl, S.**; Jacobi von Wangelin, A. Dibenzo[a,e]cyclooctatetraene. *Encyclopedia of Reagents for Organic Synthesis*; Wiley-VCH, **2019**.

5. Maier, T. M.; **Sandl, S.**; Shenderovich, I. G.; Jacobi von Wangelin, A.; Weigand, J. J.; Wolf, R. Amine-Borane Dehydrogenation and Transfer Hydrogenation Catalyzed by α -Diimine Cobaltates. *Chem. - Eur. J.* **2019**, *25*, 238–245 (hot paper and cover picture).

4. **Sandl, S.**; Schwarzhuber, F.; Pöllath, S.; Zweck, J.; Jacobi von Wangelin, A. Olefin-Stabilized Cobalt Nanoparticles for C=C, C=O, and C=N Hydrogenations. *Chem. - Eur. J.* **2018**, *24*, 3403–3407 (hot paper).

3. Gärtner, D.;[†] **Sandl, S.**;[†] Jacobi von Wangelin, Homogeneous vs. Heterogeneous: Insights into Iron Group Metal-Catalyzed Reduction Reactions by Kinetic Poisoning Experiments. *submitted* († equal contribution).

2. Chakraborty, U.; Demeshko, S.; Weinert, B; **Sandl, S.**; Meyer, F.; Dehnen, S; Jacobi von Wangelin, A. Planar and Non-Planar Mn_nFe (n = 4,5) Molecular Nanoalloys, *ready to submit*.

1. **Sandl, S.**; Otterpohl, U.; Maier, T. M.; Herrmann, C.; Wolf, R.; Jacobi von Wangelin, A. A Dimeric Iron Ate Complex with Four Bridging Hydrides: Synthesis and Reactivity, *manuscript in preparation*.

Conference Contributions

12. Poster: *WIFO 2019 (Wissenschaftsforum: German Chemical Society)*, Aachen, DE.

11. Oral: *EUCOMC 2019 (European Conference on Organometallic Chemistry)*, Helsinki, FIN.

10. Poster: *Wöhlertagung 2018 (Wöhler Society of Inorganic Chemistry, German Chemical Society)*

9. Poster: *Wöhlertagung 2018 (Wöhler Society of Inorganic Chemistry, German Chemical Society)* Regensburg, DE.

8. Oral: *Rigaku-User-Meeting 2018 (Crystallography)*, Regensburg, DE.

7. Oral: *NDDK 2018 (Northern-German PhD student colloquium)*, Braunschweig, DE.

6. Poster: *Gordon Conference on Organometallic Chemistry 2018*, Rhode Island, USA.

5. Attendee: *Olex2-Workshop 2018 (Crystallography)*, Karlsruhe, DE.

4. Poster: *WIFO 2017 (Wissenschaftsforum: German Chemical Society)*, Berlin, DE.

3. Poster: *MPI-CEC (Max-Planck-Institute for Chemical Energy Conversion) Summer School 2017: Electronic Structure & Spectroscopy of Transition Metal Complexes*, Gelsenkirchen, DE.

2. Poster: *EUCOMC 2017 (European Conference on Organometallic Chemistry)*, Amsterdam, NL.

1. Poster: *ORCHEM 2017 (German Society of Organic Chemistry)*, Weimar, DE.

Professional Associations

German Chemical Society, Inorganic & Organic Division

Hobbies

Administration and management of music ensembles, saxophone and rowing.

13 Eidesstattliche Versicherung

- (1) Ich erkläre hiermit an Eides statt, dass ich die vorliegende Arbeit ohne unzulässige Hilfe Dritter und ohne Benutzung anderer als der angegebenen Hilfsmittel angefertigt habe; die aus anderen Quellen direkt oder indirekt übernommenen Daten und Konzepte sind unter Angabe des Literaturzitats gekennzeichnet.
- (2) Bei der Auswahl und Auswertung haben mir die in den jeweiligen Kapiteln aufgeführten Personen in der beschriebenen Art und Weise unentgeltlich geholfen.
- (3) Weitere Personen waren an der inhaltlich-materiellen Herstellung der vorliegenden Arbeit nicht beteiligt. Insbesondere habe ich hierfür nicht die entgeltliche Hilfe eines Promotionsberaters oder anderer Personen in Anspruch genommen. Niemand hat von mir weder unmittelbar noch mittelbar geldwerte Leistungen für Arbeiten erhalten, die im Zusammenhang mit dem Inhalt der vorgelegten Dissertation stehen.
- (4) Die Arbeit wurde bisher weder im In- noch im Ausland in gleicher oder ähnlicher Form einer anderen Prüfungsbehörde vorgelegt.

Regensburg, den 04.05.2020